

Power Electronics and Power Systems

Marija Ilić
Le Xie
Qixing Liu *Editors*

Engineering IT-Enabled Sustainable Electricity Services

The Tale of Two Low-Cost Green Azores
Islands

EXTRA
MATERIALS
extras.springer.com

 Springer

Series Editors:

M.A. Pai

Alex M. Stankovic

For further volumes:

<http://www.springer.com/series/6403>

Marija Ilić • Le Xie • Qixing Liu
Editors

Engineering IT-Enabled Sustainable Electricity Services

The Tale of Two Low-Cost Green Azores
Islands



Courtesy of Stephen Connors, M.I.T.

Editors

Marija Ilić
Electrical and Computer Engineering (ECE)
and Engineering Public Policy (EPP)
Carnegie Mellon University
Pittsburgh, Pennsylvania, USA

Le Xie
Department of Electrical
and Computer Engineering
Texas A&M University
College Station
Texas, USA

Qixing Liu
Carnegie Mellon University
Pittsburgh
Pennsylvania, USA

Additional material to this book can be downloaded from <http://extras.springer.com>

ISBN 978-0-387-09735-0 ISBN 978-0-387-09736-7 (eBook)

DOI 10.1007/978-0-387-09736-7

Springer New York Heidelberg Dordrecht London

Library of Congress Control Number: 2013936068

© Springer Science+Business Media New York 2013

This work is subject to copyright. All rights are reserved by the Publisher, whether the whole or part of the material is concerned, specifically the rights of translation, reprinting, reuse of illustrations, recitation, broadcasting, reproduction on microfilms or in any other physical way, and transmission or information storage and retrieval, electronic adaptation, computer software, or by similar or dissimilar methodology now known or hereafter developed. Exempted from this legal reservation are brief excerpts in connection with reviews or scholarly analysis or material supplied specifically for the purpose of being entered and executed on a computer system, for exclusive use by the purchaser of the work. Duplication of this publication or parts thereof is permitted only under the provisions of the Copyright Law of the Publisher's location, in its current version, and permission for use must always be obtained from Springer. Permissions for use may be obtained through RightsLink at the Copyright Clearance Center. Violations are liable to prosecution under the respective Copyright Law.

The use of general descriptive names, registered names, trademarks, service marks, etc. in this publication does not imply, even in the absence of a specific statement, that such names are exempt from the relevant protective laws and regulations and therefore free for general use.

While the advice and information in this book are believed to be true and accurate at the date of publication, neither the authors nor the editors nor the publisher can accept any legal responsibility for any errors or omissions that may be made. The publisher makes no warranty, express or implied, with respect to the material contained herein.

Printed on acid-free paper

Springer is part of Springer Science+Business Media (www.springer.com)

*To our families, mentors and students
May your inspiration, patience and hard
work continue to make tales come true...
Marija, Le and Qixing*

Preface

This book is motivated by the rapidly growing challenges and opportunities on the road to the sustainable energy services. Present efforts toward integrating clean and efficient resources are often not aligned with the objectives of the end users nor with the business strategies needed to make these technologies affordable. The role of “smart grids” as enablers of such integration remains fuzzy. The main premise in this book is that the information technology (IT) in its broadest sense of the word could play a major role in overcoming these problems and in integrating these new resources according to the consumers’ specifications. The design of IT architectures to support the functionality of given electric grids for aligning the characteristics of the existing and new resources with the demand needs is the key challenge. The trade-off between the IT complexity and the cost relative to the potential benefits is a major underlying question. To the best of our knowledge this is the first comprehensive model-based treatment demonstrating through systematic simulations that the existing and new resources could be integrated for meeting users’ needs according to their preferences and within the prespecified cost ranges for electricity service. As such, the book represents first-of-its-kind proof-of-concept that it is, indeed, possible to utilize very diverse resources in alignment with customers’ preferences while meeting prespecified societal goals. The mathematical treatment for the proposed concepts is not extensive. Mathematical problem formulations are used only to the extent needed to pose the new approach and to contrast it with the currently used approaches. The objective is, instead, to briefly summarize the concepts and then illustrate the potential game-changing outcomes using as realistic data gathered for the electric energy systems in the Azores Islands of Portugal.

The vision put forward is a result of the efforts by the team of over dozen researchers who, at one point of time or the other, have worked closely with the coeditors of this book. The three coeditors themselves have collaborated for nearly one decade. They hope to convince the reader that green future electric energy systems cannot be determined by looking solely at the coarse capacity estimates and the characteristics of individual technologies. Instead, a systems approach to enhancing today’s planning and operating practices is required to begin to utilize the hidden potential of many distributed clean resources. If done right, this would

lead to achieving much higher system-level efficiency than it is currently achieved even in systems with conventional and fully controllable technologies.

The new technologies considered are small hydro-, geothermal-, wind-power plants, photovoltaics (PVs), electric vehicles (EVs), and fast controllable storage, like flywheels and stationary batteries. When equipped with the embedded model-based sensing, communications, and decision-making algorithms, these new resources can be coordinated with the adaptive load management (ALM) automation on the customers' side to provide just-in-time (JIT) and just-in-place (JIP) value directly contributing to flexible and efficient asset utilization. One good measure of system-level efficiency is the system load factor which is defined as the ratio of average energy consumed and the peak demand. It is demonstrated in this book that the achievable system load factor by means of IT-enabled flexible asset utilization is significantly higher than today's system load factor. To the contrary, if new technologies are deployed as mandated by the regulators without enhancing today's operating and planning industry practices it will be very difficult to manage the new resources efficiently and reliably.

This book reports on our work in progress toward IT-enabled electricity services. The concepts are demonstrated by simulating electric power systems in two Azores Islands, Flores and Sao Miguel. We are truly encouraged by the results obtained as they demonstrate that it is possible to manage uncertainties created by the intermittent resources, such as wind power and PVs, without relying on excessively large amounts of expensive storage and on expensive and polluting diesel fuels currently used on these islands. Perhaps the most important message in this book is that it is not effective to pre-commit to the deployment of certain fixed capacity of renewables without understanding the characteristics of the existing resources and the demand characteristics and customers' preferences. Targets like deployment of prespecified capacity of renewable resources could become difficult to justify without designing new methods for their integration. As with everything else, it is necessary to assess long-term potential costs and benefits which may be brought about by the new resources. Unique to the electric energy systems, the cost/benefit analysis is critically dependent on the operating methods for utilizing these resources. In this book we present a possible framework for assessing possible technologies, for designing IT to enable their effective utilization and, notably, for utilizing efficiency brought about by the interdependence of various technologies. The emphasis is on potential savings from deploying predictive look-ahead decision methods under uncertainties and on the multi-temporal risk management.

The most effective solutions are nonunique. Possible trade-offs between complex software methods (predictions and look-ahead decision making for managing future uncertainties dynamically), on the one side, and the novel adaptive hardware technologies for managing imbalances created by the intermittent resources, on the other side, are truly striking. The need for expensive fast-responding storage can be greatly offset by predicting wind fluctuations and scheduling slower, less expensive resources. The complexity of JIT and JIP system operations and planning by the single utility is likely to become overwhelming. Instead, it is envisioned in this book that an interactive IT-enabled framework could facilitate flexible system

management; much distributed intelligence is embedded into system users and minimal coordination is required by the utility system operators. This change of operating paradigm requires fast automation to prevent extremely fast instabilities following forced equipment outages, as well as to make the dynamic system response robust with respect to various uncertainties. In order to achieve this, it becomes critical to establish new mathematical models, analysis, and control design. Qualitatively different methods for managing fast small wind power fluctuations are needed than when managing fast large wind power surges or large prolonged wind power deviations from the predicted levels. While relatively small flywheels or batteries can be used to reduce wear and tear of the slow mechanically controlled generators, it becomes necessary to rely on power-electronically controlled equipment for managing large wind surges of short duration; finally, to compensate imbalances created by the prolonged wind power deviations it becomes necessary to use larger flywheels and storage. Moreover, the control capacity required to manage these imbalances during the time window needed for the more conventional slower resources to respond greatly depends on the sensing, communications, and control logic used for automatic control.

We close by pointing out that we are at the very cusp of what promises to be a major era of IT innovations for future electric energy systems. As one of our industry friends pointed out, we are in the midst of once-in-fifty-years opportunity to make major innovations in today's electric energy industry. This must be done with clear sense of how systems work today and with a real appreciation of the fact that the most effective solutions are likely to be the result of many diverse technologies, software and hardware, complementing each other for meeting complex customers' preferences. These are no longer just needs for uniform uninterrupted electricity service. Customers differ in so many ways with respect to both their needs and preferences, as well as with respect to their ability to respond to the technical and economic signals. We have had fun testing otherwise highly theoretical concepts using realistic data from the Azores Islands. We are grateful for the opportunity given to us by having this information to illustrate recent concepts from our research on how much cleaner Azores Islands could become without increasing the actual cost and with full awareness of customers' characteristics.

On behalf of all authors Marija Ilić wishes to thank Professors Jose' M.F. Moura and Ernest J. Moniz for suggesting to study Azores islands. She also thanks her colleagues Joao A.P. Lopes, Stephen Connors and Dan Spang for sharing early on what they knew about various data sources. This book would have not happened without the help by Filipe R.G. Mendonça and António J. L. A. Furtado from Electricite de Azores (EDA). May the tale of the beautiful Azores Islands always warm all of our hearts.

Pittsburgh, PA, USA
College Station, TX, USA
Pittsburgh, PA, USA

Marija Ilić
Le Xie
Qixing Liu

Prologue

This book is a first example of what may become possible when one combines physical infrastructures, like complex electric energy systems and their power grids, with on-line information technologies, such as widespread sensing, communications, and control. The book demonstrates how data-driven distributed decisions with minimal coordination among generation, electricity users, electric power grid, and the operators and planners, offer choice and system-level social benefits at the same time.

To illustrate this potential, the authors introduced end-to-end models of two test bed electric power grids in the Azores Islands in a form that is appropriate for information technology design and that enables the desired analysis of the performance of these systems. The data provided and made available by the Electricidade dos Aores (EDA) is greatly appreciated. Having now these data and models, one can begin a systematic approach to IT and cyber design and compare different proposed solutions.

Looking forward, I see at least three major challenges:

First, the eternal challenge of how to further validate the concepts proposed in the book with test beds with hardware in the loop. This will better prepare the ground for technology transfer of the dynamic monitoring and decision systems (DYMONDS) framework presented in this book. One way could be working during long summer days in the EDA control center to further test what is proposed here. The path to deploying systems solutions is not well plowed and learning from the experts who operate the system and comparing their actions with what IT-based methods suggest is invaluable. At the same time, it is important to show practitioners how embedded IT can be used and is useful. This is no small step.

Second, now that a first proof-of-concept is available, how can one proceed and generalize the framework to other islands? As shown in the book, the need for hardware and software enhancements to support sustainable electricity services

is system conditions dependent. It is not optimal in any respect to deploy a pre-specified capacity of renewable resources. How much is needed, where and how should it be integrated into the legacy power system is not the same for every island. In addition, perhaps, the methodology for finding answers to these questions can be generalized. Having a formal approach for assessing and utilizing the best mix of technologies by all minimally coordinated stakeholders to meet the desired performance is potentially very powerful.

Finally, would it be possible to use the same framework to enhance the performance of continental power systems, and if so what types of improvements are possible and how to find the most effective hardware and software methods? The fundamentally distributed interactive approach put forward in this book offers the beginning of a framework that has the potential to scale to large power interconnected electric grids such as those of the US, China, Europe.

This project is a first seed that explores the potential of making electricity services in the Azores Islands sustainable by means of flexible data-driven embedded IT. Hopefully, the end-to-end models and data described in this book can be used by other researchers to grow the IT and software infrastructures to further improve the performance of the electric grid.

This project is a partnership between Carnegie Mellon and Instituto Superior Técnico through the Carnegie Mellon—Portugal Program. The Carnegie Mellon—Portugal Program partners Carnegie Mellon University and nine Universities in Portugal. It is managed by the Information and Communications Technologies Institute (ICTI), www.cmuportugal.org. The Carnegie Mellon—Portugal Program is supported by the Fundação para a Ciência e a Tecnologia (FCT), Portugal. We acknowledge the support of FCT to the Program that made this project possible.

Carnegie Mellon University
Philip and Marsha Dowd University Professor
Director, ICTI@CMU

José M.F. Moura

Contents

Part I The Tale of the Low-Cost Green Azores Islands

1	The Case for Engineering Next-Generation IT-Enabled Electricity Services at Value	3
	Marija Ilić	
2	The Tale of Two Green Islands in the Azores Archipelago.....	47
	Marija Ilić	

Part II The Electrical Systems Characteristics of Two Azores Islands: Flores and São Miguel

3	Electrical Networks of the Azores Archipelago	99
	Masoud Honarvar Nazari	
4	Generation and Demand Characteristics of the Islands of Flores and São Miguel	119
	Jonathan Donadee, Jhi-Young Joo, Remco Verzijlbergh, and Marija Ilić	

Part III Wind and Load Power Prediction: Look-Ahead Dispatch for the Efficient Use of Available Resources

5	Conventional Generation Dispatch Methods in Systems with Intermittent Resources	151
	Paulo D.F. Ferreira, Pedro M.S. Carvalho, and Luis A.F.M. Ferreira	
6	Multi-scale Models for Decomposing Uncertainties in Load and Wind Power	171
	Noha Abdel-Karim and Marija Ilić	

7	Look-Ahead Model-Predictive Generation Dispatch Methods	209
	Le Xie, Yingzhong Gu, and Marija Ilić	
8	Assessing the Ability of Different Types of Loads to Participate in Adaptive Load Management	225
	Jhi-Young Joo, Jonathan Donadee, and Marija Ilić	
9	Look-Ahead Model-Predictive Generation and Demand Dispatch for Managing Uncertainties	247
	Jhi-Young Joo, Yingzhong Gu, Le Xie, Jonathan Donadee, and Marija Ilić	
10	Counterexamples to Commonly Held Assumptions on Unit Commitment and Market Power Assessment	261
	Wolfgang Gatterbauer and Marija Ilić	
11	The Role of Electric Vehicles in Making Azores Islands Green	273
	R.A. Verzijlbergh, M.D. Ilić, and Z. Lukszo	

Part IV Efficient and Viable Power Delivery During Normal System Conditions

12	Optimal Placement of Wind Power Plants for Delivery Loss Minimization	295
	Masoud Honarvar Nazari	
13	Toward an Extended AC OPF-Based Approach to Wind Power Integration and Pricing	305
	Marija Ilić and Jeffrey H. Lang	

Part V Enhanced Methods for Intra-dispatch Automated Balancing of Hard-to-Predict Wind Power Fluctuations

14	Modeling and Control Framework to Ensure Intra-dispatch Regulation Reserves	345
	Nipun Popli and Marija Ilić	
15	Stabilization and Regulation of Small Frequency Fluctuations by Means of Governor and Flywheel Control	371
	Qixing Liu, Milos Cvetković, and Marija Ilić	
16	The Role of Enhanced Voltage Control in Stabilizing Dynamics of Electric Energy Systems	409
	Qixing Liu, Milos Cvetković, and Marija Ilić	
17	Small-Signal Stability Analysis of Electric Power Systems on the Azores Archipelago	445
	Masoud Honarvar Nazari	

**Part VI Corrective Adjustments and Transient Stabilization
for Ensuring Reliable Operations During Large Wind
Disturbances and Equipment Outages**

18 Toward Reconfigurable Smart Distribution Systems for Differentiated Reliability of Service	475
Siripha Junlakarn and Marija Ilić	
19 Transient Stabilization in Systems with Wind Power	491
Milos Cvetković, Kevin Bachovchin, and Marija Ilić	
Part VII Methods for Investing in New Technologies Under Uncertainties	
20 Generation Planning Under Uncertainty with Variable Resources ...	535
Audun Botterud, Noha Abdel-Karim, and Marija Ilić	
Index	553

Part I

**The Tale of the Low-Cost Green Azores
Islands**

Chapter 1

The Case for Engineering Next-Generation IT-Enabled Electricity Services at Value

Marija Ilić

1.1 Introduction

This chapter recognizes that it is not sufficient to have abundant energy resources; it is equally if not more important to have a system in place that manages them and distributes them reliably and efficiently. Given the overall complexity of today's physical electric energy systems, it is suggested that IT could play a key role in having such a system in place. However, the computer methods and automation in today's electric energy industry are generally viewed as having second-order effects on the quality and cost of electricity service. Investment planning and operations target the building of sufficient capacity to ensure long-term adequacy for the forecast system demand, and at the same time, to serve customers reliably and securely, without affecting them adversely even during the worst-case forced equipment outages. Assuming accurate system demand forecast, and typical economies of scale supporting the building of central large power plants and large-scale transmission and distribution (T&D) infrastructure to reduce long-term cost, it is easy to understand the overall lack of relying on on-line measurements and control. The main value of these technologies, generally referred to as IT, comes from providing flexible, just-in-time (JIT) adaptation to the changing system conditions and also from enabling economies of values from multiple usage of the same hardware, known as economies of scope. The industry is risk averse and will build more and have a slightly larger operating reserve, just in case conditions are not as anticipated, instead of relying on JIT and multiple use of the same equipment.

Perhaps an additional reason for the electric power industry not having relied on automation extensively in the past is the complexity of its design needed to

M. Ilić (✉)

Department of Electrical and Computer Engineering, Carnegie Mellon University,
5000 Forbes Ave, Pittsburgh, PA 15213, USA
e-mail: milic@ece.cmu.edu

guarantee its performance. It is hard for power engineers to trust automation and not have direct control of their assets in an environment in which synchronized monitoring is not in place, manufacturers' data is hard to test, and the physical laws governing complex geographically vast interconnected power networks generally lead to untractable, non-closed form models. At the same time, the very complexity of forecasting system demand and scheduling generation so that power can be delivered to the right, often distant, geographical locations (at the right time to maintain synchronism) has led to the gradually increased use of computer software and automation in today's utilities over the past several decades. The software tools have become invaluable to system operators in control centers and planners in their daily decision-making. Reconciling this complexity of designing the right software for predictable performance, with the growing needs for software that helps manage the complexity of the physical system, is not an easy balance to strike. Deciding what to leave to the operators and what to automate is an equally if not more difficult problem than deciding which new equipment to build and use.

The challenge of deploying the right IT has recently taken on a new importance with the efforts to make the most out of the available energy resources in sustainable ways. Moreover, there are pressures to utilize all system assets, both existing and new, as efficiently as possible. As these efforts are being pursued, it is becoming exceedingly difficult to directly relate any technical innovation, hardware or software, to quantifiable performance improvements. Yet, it is clear that new models, communications, sensors, computer software, and automation will be needed to integrate and utilize many diverse energy resources; in this book we refer to these technologies in a general way as IT.

To help overcome the inherent complexity of designing IT for well-understood performance, we first briefly review how the grid is operated today and highlight what are the implied assumptions and related hidden inefficiencies. Once this is understood, it becomes more straightforward to identify the limitations of the computer algorithms and automation used by the industry today, which were developed to support given industry practice.

In this chapter, one possible approach to reviewing today's industry practice is taken by stating the overall operations and planning objective of today's industry and by formulating this objective as a mathematical problem first. Once this formulation is stated, it becomes possible to discuss the fundamental roots of the complexity. Of course, the power grid was not designed by solving this overly complex problem. It has, instead, evolved, almost mushroomed, over a very long time by adding new utility-specific assets needed to solve subproblems as they surfaced. When it was predicted that demand would grow, more power plants were built, and the T&D system was built to enable power delivery. Operations were also relatively simple as the scheduling of slow plants was done first, and these plants stayed on while some faster power plants had to adjust their power output as the system load varied in real time. This is sometimes referred to as "horizontal scheduling (over time)."

In this chapter it is shown how starting from the single operations and planning problem one can decompose this complex problem into several operations and planning subproblems. Furthermore, it is discussed how the single operations

subproblem can be thought of as comprising several operations tasks commonly performed by utilities today using separate stand-alone computer applications. This decomposition process is done by making many implied assumptions in practice for simplification purposes. These assumptions are identified with the goal of proposing what can be enhanced, and why as more IT becomes available, it is needed to manage increasingly complex industry problems.

The modeling and analysis of today's operating and planning practice, and identifying its hidden inefficiencies related to implied assumptions, is the first step to posing formally the evolving changes in future systems with unconventional energy resources—renewable power and demand response, in particular. The material in this chapter is basic to explaining why it is becoming increasingly important to support the operations of the physical system with a carefully designed IT system. A full treatment of this subject is, of course, a huge undertaking and far beyond the objectives of this chapter. Nevertheless, it is essential to understand these questions at least conceptually in order to establish the link between the potential technical problems in systems with a high penetration of wind and solar power and the basic enhancements needed to overcome these potential problems. New technologies should be deployed with a good sense of what their potential benefits are, and at choice.

This chapter is written with the goal in mind of discussing what needs innovation and why, and it is organized as follows. In Sect. 1.2 we summarize today's industry approach to balancing generation and demand. This is done by considering the multi-temporal characteristics of system demand and by reviewing currently used power generation planning, scheduling, and automated control methods for supplying system demand. In Sect. 1.3 we review the problem of secure and reliable delivery of power. We mathematically pose the notion of a secure operating region by using a general model which has the form of high-order coupled differential algebraic equations (DAE) obtained by subjecting the system demand and power plant dynamics to basic electric network laws. Generation can be delivered by a complex electric power grid as long as there is no “network congestion,” namely, as long as the system states remain within the secure operating region. Computing a secure operating region exactly is a very complex problem and it is typically not done by the utilities. Instead different engineering assumptions are made when assessing the security of the grid. These assumptions help approximate the computation of the secure region. One of the most frequent approximations used for assessing whether the system will be secure is by reformulating the constrained DAE model as a constrained DC power flow model; the approximations leading to a DC power flow representation of a secure region are briefly summarized. Understanding these assumptions and their implications is key to identifying what needs to be changed, why, and how. In particular, it is illustrated in Chap. 2 how some possible unique characteristics of future candidate technologies could play a major role in enabling more efficient system operations within the secure region by making it possible to relax the assumptions leading to hidden inefficiencies.

We next formally pose the single operations-planning problem in today's power industry in Sect. 1.4 as a complex stochastic optimization problem subject to the

constraint that the solution be in a secure and reliable operating region. This is followed in Sect. 1.5 by the discussion of how, under certain assumptions, this problem can be decomposed into operations and planning stochastic optimization subproblems. In Sect. 1.5.1 we discuss the objectives of short-term scheduling for optimizing available generation. This must be done by operating securely as defined in Sect. 1.3. We then show in Sect. 1.5.2 how further simplification of the short-term scheduling problem leads to the commonly used deterministic DC optimal power flow (DC OPF) problem for scheduling the least-cost generation. In Sect. 1.5.3 we pose the generation and transmission investment subproblem and review notions of long-run marginal cost in the context of optimal investments. In Sect. 1.5.4, we specifically review the problem of optimal generation investment and optimal technology selection. We review in Sect. 1.7 the evolution of computer methods and automation currently used for planning and operations. Finally, in Sect. 1.8, we stress the need for relaxing some key assumptions and the relevance of their relaxation in enabling sustainable electric energy services at value in future electric energy systems and set the basis for introducing our dynamic monitoring and decision systems (DYMONDS) framework for next-generation IT in future electric energy systems. The approach is formalized in Chap. 2 as a possible approach to overcoming the key assumptions made in today's industry and the basis for an interactive IT-enabled platform which lends itself to supporting sustainable socio-ecological energy systems (SEESs) [4].

1.2 Operations and Planning Approach in Today's Electric Energy Systems

In preparation for stating mathematically later in this chapter a single overall objective of electric energy systems operations and planning, we first briefly review the multi-temporal characteristics of system demand and the key role of generation planning, scheduling, and control in today's industry. While both operations and planning have been done with the single objective of supplying demand reliably and as inexpensively as possible, the actual methods used are much simpler than solving the complex single problem, and they draw on the multi-temporal separation of generation supplying system demand.

1.2.1 *Multi-temporal Characterization of System Demand*

One way of explaining how the single planning and operations problem is decomposed into several subproblems and is implemented by the industry is by looking at the characteristics of system demand. System demand is an aggregate composition of many diverse loads, spanning industrial, commercial, and residential customers.

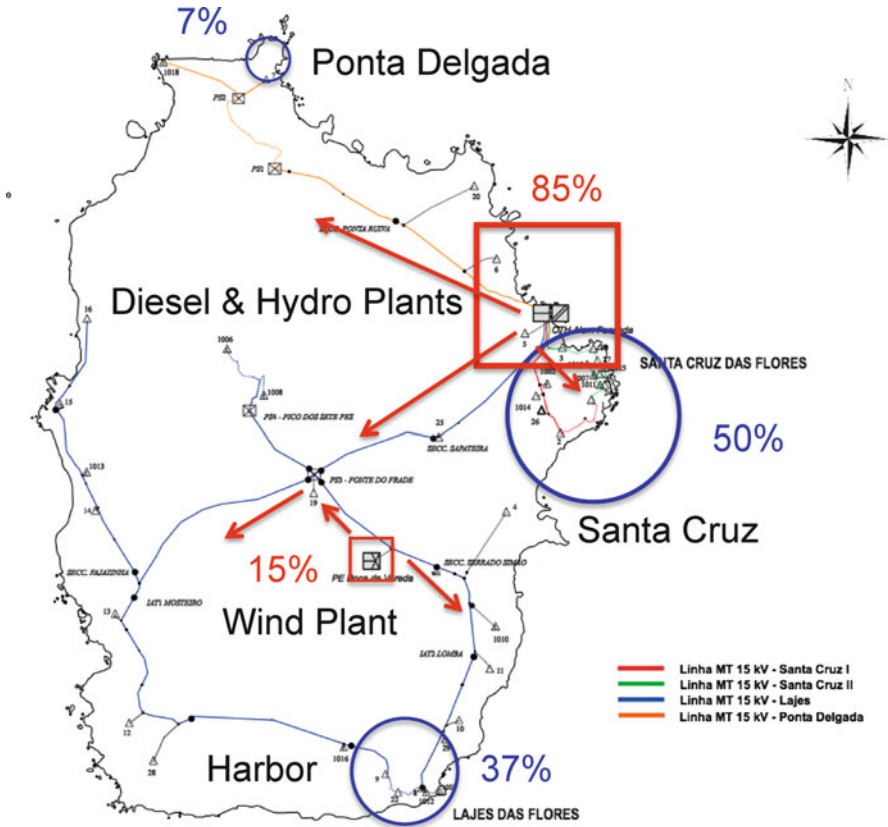


Fig. 1.1 A sketch of interconnections of power plants and main loads on Flores [8], Chap. 3

At present, utilities do not monitor accurately the temporal profiles of individual loads. Instead, methods are used to forecast the entire system load, which is assumed to be geographically distributed roughly according to the historic peak loads. Shown in Fig. 1.1 is a sketch of the power grid interconnecting geographically distant major loads to the power plants on Flores [8], Chap. 3. It can be seen that the major system load on Flores is distributed at several geographical locations and that there are many small loads connected to many more nodes in the network.

The system load has multi-temporal components which are predictable with high accuracy, multi-temporal hard-to-predict components, and continuous fast fluctuations superimposed on top of discretized load components. Predictable system load components typically exhibit several periodic patterns. Shown in Figs. 1.2 and 1.3 are the annual and daily system demand variations on Flores [8], Chap. 4. These are drawn from representative days of the year and may vary considerably with the day selected.

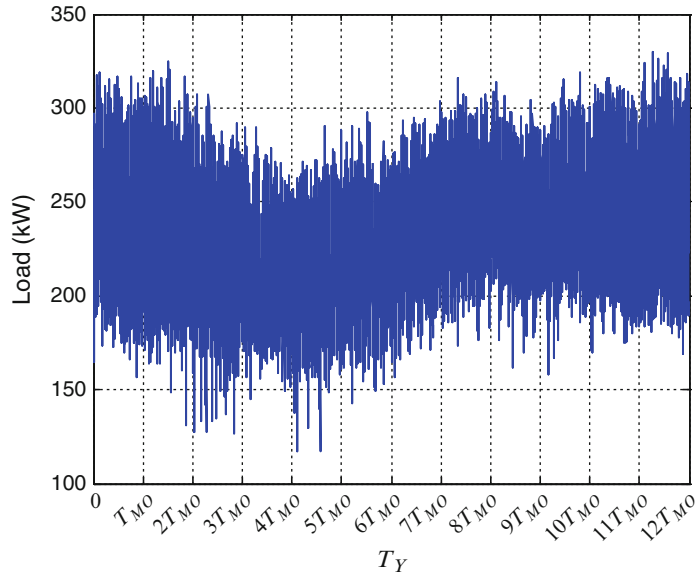


Fig. 1.2 Typical annual system load on Flores [8], Chap. 4

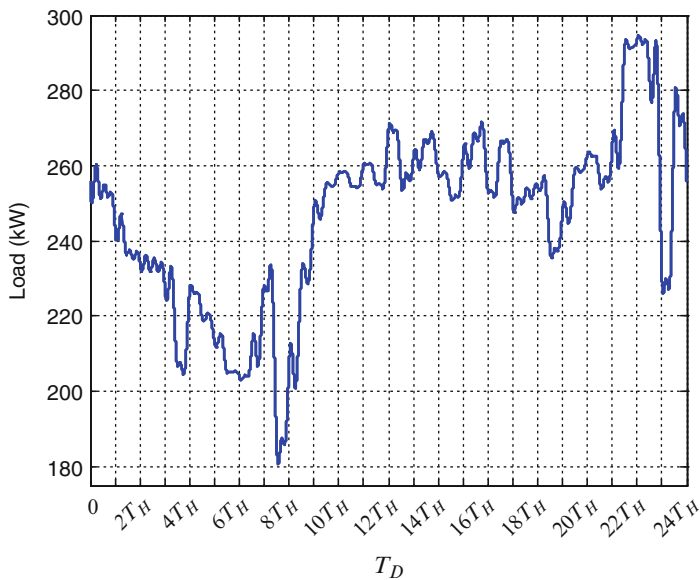


Fig. 1.3 Typical daily system load on Flores [8], Chap. 4

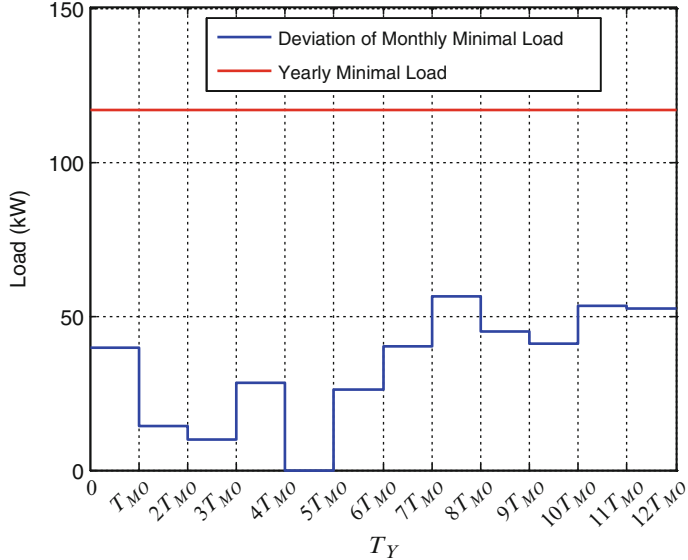


Fig. 1.4 Discretization of the annual system demand on Flores

For operations simplification system demand is usually thought of as being decomposed into several temporal components. Shown in Fig. 1.4 is the same annual system demand on Flores as in Fig. 1.2, discretized into minimum monthly components.

Similarly, shown in Fig. 1.5 is the same daily load on Flores as shown in Fig. 1.3, now discretized into hourly and 10-min minimum values. It is indicated that the predictable real power demand variations can be represented as comprising forecast annual component $\hat{P}_d[Y * T_Y]$, forecast daily component $[D * T_D]$ changing at each $[D * T_D]$, hourly component $\hat{P}_d[H * T_H]$ changing every $[T_H]$, and/or forecast 10-min $[M * T_M]$ component $\hat{P}_d[M * T_M]$. The discretization of the annual system demand can be refined into seasonal, monthly, and even weekly components. For illustration purposes, we show only the monthly discretization. For planning purposes utilities often characterize their system demand using load duration curves; these represent the number of intervals of interest when the system demand is low, medium, and high, respectively.

Hard-to-predict system demand components are superimposed on the predictable components. These deviations are minute-by-minute power fluctuations $\Delta P_d[m * T_m]$ and/or second-by-second power fluctuations $\Delta P_s[s * T_s]$. In today's industry these are not monitored in real-time operations. Shown in Fig. 1.6 is a sample hourly predictable component $[M * T_M]$ and in Fig. 1.7 a discretization of the actual $[M * T_M]$ load component into its hard-to-predict minute $[m * T_m]$ and second $[s * T_s]$ components within each $[M * T_M]$ 10-min intervals.

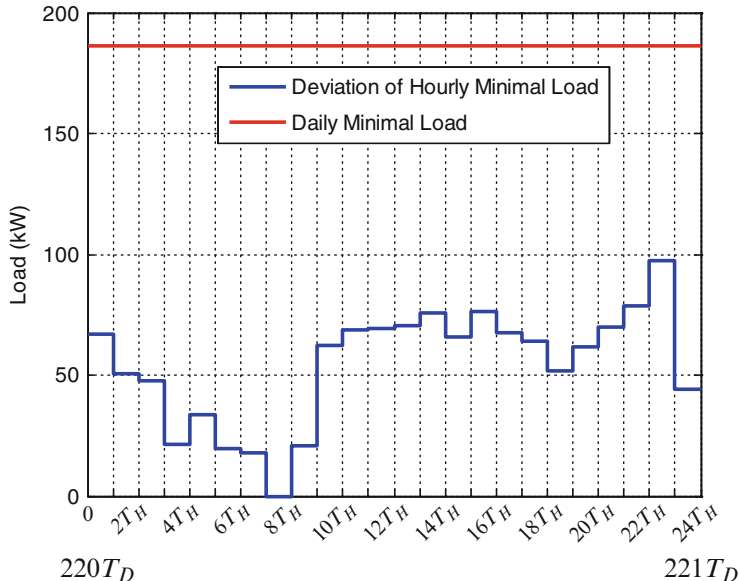


Fig. 1.5 Discretization of the daily system demand on Flores

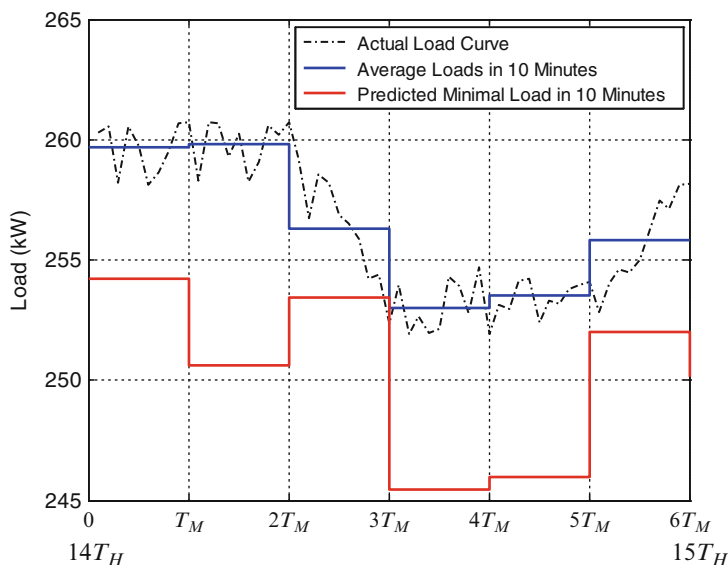


Fig. 1.6 Typical hourly system demand on Flores

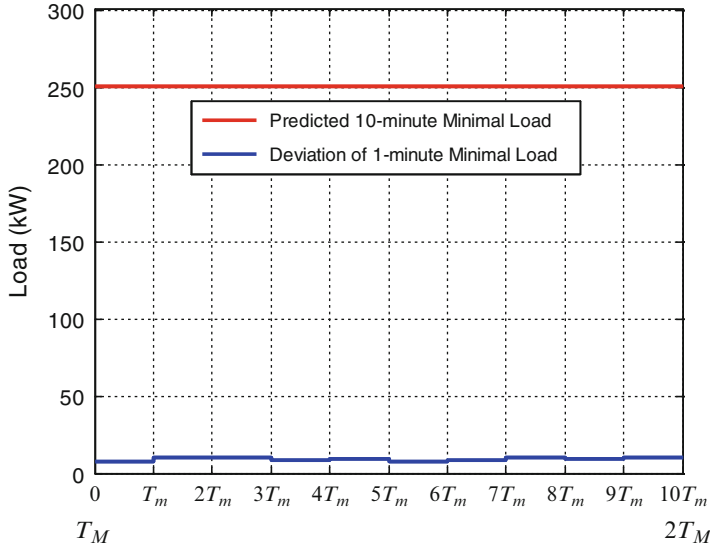


Fig. 1.7 Discretization of the 10-min system demand on Flores

Based on this multi-temporal decomposition, one can express system demand as follows¹:

$$\begin{aligned} P_d(t) = & \hat{P}_d[Y * T_Y] + \hat{P}_d[H * T_H] + \hat{P}_d[M * T_M] + \Delta P_d[m * T_m] \\ & + \Delta P_d[s * T_s] + w(t) \end{aligned} \quad (1.1)$$

Today's computer applications and automation assume that predictable system demand components (.) can be forecasted with relatively high accuracy and that the components $\Delta(\)$ are hard to predict; component $w(t)$ represents the difference between the continuous system demand and all its discretized components, predicted and hard to predict; this is typically a white noise around the combined discretized forecast components and hard-to-predict components. In what follows we use this temporal decomposition as the basis for the simplifications made in today's operations and planning industry practice.

1.2.2 Basic Generation Planning, Operations, and Control

In today's industry the demand is primarily balanced by controlling the real power generation output P_G and the terminal voltage of power plants V_G . Every

¹Depending on the potential system demand use, more detailed annual, seasonal, monthly, and weekly forecasts can be made. Here, for simplicity and without loss of generality, only the annual, hourly, and 10-min forecast components are modeled.

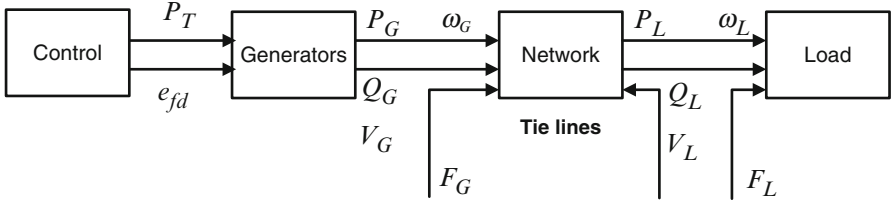


Fig. 1.8 Generator-turbine-governor system in conventional power plants [9], Chap. 6

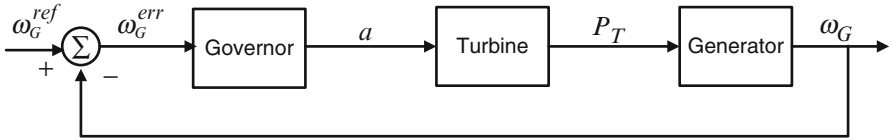


Fig. 1.9 Generator-turbine-governor system in conventional power plants [9], Chap. 6

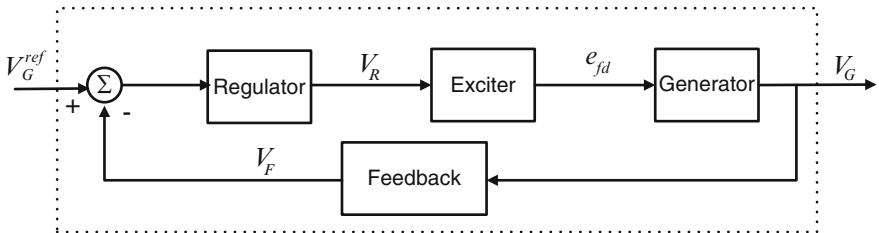


Fig. 1.10 Automatic voltage regulator in conventional power plants [9], Chap. 6

conventional power plant is equipped with a governor that controls real power sent to the system, and with a rotor excitation system that controls the terminal voltage of a power plant. Shown in Fig. 1.8 is the basic sketch of the structure of the generators, interconnected via the T&D power grid to the loads. It can be seen that both the governors and automatic voltage regulators (AVRs) are the local primary controls of generators.

Shown in Figs. 1.9 and 1.10 are sketches of a generator-turbine-governor (G-T-G) and an AVR as the primary controllers responsible for balancing today's electric power grid [9]. The governor controls the valve position a which, in turn, lets more or less steam pass through and converts it to mechanical power which, when applied to the generator rotor, is converted into electric power generation P_G . Similarly, an AVR is a local feedback which responds to deviations in the terminal voltage of the generator from its set point and attempts to keep it as given. This is done by applying more or less excitation to the rotor coils of generator e_{fd} .

1.2.3 Multi-temporal and Multi-spatial Complexity of Managing Today's Electric Energy Systems

Today, the computer applications and automation for balancing generation and demand during normal operations are organized hierarchically with respect to both time and geography/space. The objective of a hierarchical approach is to make the problem more manageable.

It is important to understand, in order to identify the future need for IT in electric energy systems, that today's system is never at an equilibrium. Both the supply-demand imbalance and the resulting frequency and voltage changes are driven by the constantly changing demand at different rates as shown in (1.1). Recall from Figs. 1.4 and 1.5 that system demand has several natural periodicities: hourly, diurnal, weekly, and seasonal. This sets the basis for viewing system operations as a process which repeats at different rates as the demand forecast becomes more accurate closer to real time. The complex operation and planning to balance supply and demand at a near-real-time rate requires annual investment decisions, generation scheduling decisions, and automation. To manage the overwhelming temporal complexity, hierarchical simplifications are made with respect to both time and space [9]. To manage inter-temporal complexity, a single operations and planning problem is usually decomposed into operations and long-term investment subproblems as described in Sect. 1.4 below. The operations problem is further decomposed into several tasks, as described in Sects. 1.7 and 1.8 later in this chapter.

The geographical/spatial complexity in large-scale electric grid interconnections which span over several states is twofold: (1) the horizontal complexity of coordinating utilities in different countries for regional- and interconnection-level efficient use of resources while respecting the sub-objectives of the utilities and countries and (2) the vertical complexity within each country and its utility of coordinating the EHV/HV transmission system sub-objectives with the sub-objectives of the MV/LV distribution systems.

The hierarchical approach to managing temporal complexity is discussed next. This is followed by a discussion of today's approach to managing spatial/geographical complexity.

1.2.4 Multi-temporal Approach to Balancing Generation and Demand

Basically, short-term generation scheduling assumes a given demand forecast, while automation responds to small frequency and voltage deviations caused by hard-to-predict demand fluctuations around the short-term demand forecast. Accordingly, generation scheduling is done in a feed-forward way to supply predictable demand components ($\hat{\Delta}$), while demand deviations $\Delta(\cdot)$ are balanced with automated feedback such as automatic generation control (AGC) and primary stabilization.

Least-cost generation scheduling in today's industry evolves around balancing forecast demand components (\cdot). This is done by adjusting governor set points $\omega_G^{\text{ref}}[H * T_H]$ and/or $\omega_G^{\text{ref}}[M * T_M]$ of the dispatchable power plants so that the least-cost generation balances the forecast system demand an hour ahead $[H * T_H]$ and/or 10 min ahead of time $[M * T_M]$, as the system demand becomes known with higher accuracy.

Understanding these temporal simplifications is key to identifying what needs to be changed, why and how, as well as what the possible unique characteristics are of future candidate technologies for enabling system operations within a secure region without having to resort to strong separation between the feed-forward and feedback designs.

1.2.5 Generation Scheduling

There are common simplifications made in operations when attempting to balance supply and demand closer to real time. Generation unit commitment and planned maintenance are done weekly and seasonally. The least-cost generation dispatch of ramp-rate-limited plants which are already up and running is done hourly each $[H * T_H]$ time interval for $H = 1, 2, \dots$. Some utilities adjust their fast-responding power plants even closer to real time each 10 min $[M * T_M]$, where $M = 1, 2, \dots$. Given forecast demand $\hat{P}_d[[H * T_H]]$ a ramp-rate limited dispatch is done to adjust the least-cost real power generation at hour $[H * T_H]$ so that the supply meets the forecast demand and that the system is secure in the sense of power flow constraints (equality constraints) and equipment inequality constraints being met at each time step $[H * T_H]$. The results of the economic dispatch are implemented by adjusting the set points of dispatchable power plants $\omega_{Gi}^{\text{ref}}[H * T_H]$ to control generated power $P_G[H * T_H]$ as desired. While there is no knob on the G-T-G system to directly control the real power generated, it can be shown that there is a one-to-one relationship between the set point of the governor and the power generated. Strictly speaking, this relationship is a three-way relationship, known as a G-T-G droop characteristic; however, as long as the system frequency is close to nominal, this relationship is unique [9].

1.2.6 Regulation and Stabilization

At present, very fast fluctuations in frequency and voltage are stabilized in a feedback automated manner by means of governor controllers, as well as by means of AVR and power system stabilizers (PSSs) [2, 10]. Recently, flexible AC transmission systems (FACTS) have become more common for stabilizing these fluctuations. Most of today's power plants have both governor and AVR stabilizers, and some have PSSs. Today's automation is based on primary- and secondary-level

control of the governors and AVR_s. Shown in Figs. 1.6 and 1.7 is a sketch of hard-to-predict deviations around demand forecast $\Delta(\cdot)$. Depending on the time interval over which forecast is made and on the type of forecast methods used, the amplitude of these deviations may vary. The better the forecast, the less need for feedback control and fast storage.

Feedback must be designed to compensate very quickly the effects of these disturbances in AC power networks. AGC and automatic voltage control (AVC) regulate quasi-stationary minute-by-minute power imbalances by means of the participating power plants adjusting their governor set points $\omega_{Gi}^{\text{ref}}[m * T_m]$ and AVR set points $V_G^{\text{ref}}[m * T_m]$, respectively. Similarly, the primary controllers, governors, and AVR_s are expected to stabilize fast frequency deviations $\omega_{Gi}[s * T_s]$ and voltage deviations $V_G[s * T_s]$ away from the quasi-stationary values $\omega_{Gi}^{\text{ref}}[m * T_m]$ and $V_G^{\text{ref}}[m * T_m]$, respectively. Today's frequency standard is such that the power imbalance between two consecutive dispatch intervals $[M * T_M]$ and $[(M + 1) * T_M]$ crosses zero at least once [3]. The implied assumption is that the system dynamics fully settle to the frequency and voltage set points of the governors and AVR_s in between the scheduling intervals $[M * T_M]$.

At present AGC is used to adjust the set points of the governor controllers on fast power plants by responding to the second-by-second frequency deviations caused by the total supply-demand imbalance. The implementation of AGC requires a supervisory control data acquisition (SCADA) system. Smaller systems, typically islands and stand-alone micro-grids, do not have AGC. Instead a few of their fast power plants have proportional-integral (PI) governor controllers; the integral control is capable of controlling steady-state error around the nominal frequency. Some systems only have proportional governor controllers and resort to the system operator curtailing demand to maintain frequency if/when it exceeds prepecified industry standards.

1.3 Objectives of Secure Operations in Today's Industry

In actual operations it is essential to ensure that power can be delivered to the right locations and that sufficient power is generated to supply, almost instantaneously, the demand given in (1.1). This is because today's power systems have very little storage and are operated as AC systems in which no major supply-demand imbalances are allowed. To introduce a mathematical notion of secure operations, we briefly summarize a general dynamical model of today's power systems next.

1.3.1 *Dynamical Model of an Interconnected Power System*

The dynamics of a conventional power system can be modeled by a set of coupled DAEs [7,9]. This model is obtained by combining the dynamics of turbine-generator

dynamics with the dynamics of the primary generator controllers (the governors and AVR). Each turbine-generator-governor-AVR plant can be modeled as a set of differential equations whose states are the local states of power plants x_{Gi} and the states of their local controllers. Currently used controllers of power plants sense the deviations in local output variables y_{Gi} away from the set point values of these output variables y_{Gi}^{ref} and stabilize these deviations back to zero.

Specific generation technologies have different states x_{Gi} and parameters P_G . Independent of particular technology, the closed-loop dynamics of each power plant can be expressed in terms of the plant's own states, the set points of the directly controlled local output variables and the interaction variables z_{Gi} between the power plant and the rest of the system. In later chapters of this book, particularly in Chaps. 14–17, specific models of the power plants on Flores and São Miguel are derived and analyzed. For now, we mention that typically controlled output variables y_{Gi}^{ref} in conventional power plants are the set point frequency of a governor ω_{Gi}^{ref} and the terminal voltage V_G^{ref} , respectively. Typical coupling variables z_{Gi} between the power plant and the network are the direct and quadrature axis generator currents $i_{G,di}$ and $i_{G,qi}$. Using this notation, a dynamical model of a single power plant independent of technology can be expressed as

$$\frac{dx_{Gi}(t)}{dt} = f_{Gi}(x_{Gi}(t), z_{Gi}(t), y_{Gi}^{\text{ref}}(t), P_G(t)) \quad (1.2)$$

This dynamic is subject to the network real power and reactive power balancing equations at all nodes known as the power flow equations [9] resulting in a set of DAEs that represent a model of the interconnected power system as follows²:

$$\frac{dx(t)}{dt} = f(x(t), z(t), y^{\text{ref}}(t), p_G(t)) \quad (1.3)$$

$$g(x(t), z(t), d(t), p_{\text{grid}}(t)) = 0 \quad (1.4)$$

with

$$f(x(0), z(0), d(0), p_{\text{grid}}(0), 0) = 0 \quad (1.5)$$

The notation without subscripts is used to denote a vector of variables in the entire system. This model is used in the next subsection to mathematically pose a general notion of secure operations.

²Observe that specific grids have different topologies and line parameters $p_{\text{grid}}(t)$. For a more detailed derivation of the DAE model of today's electric power system, see [9], Chap. 4.

1.3.2 Secure Operating Region

Secure operation in today's industry is generally characterized in terms of available transfer capability (ATC). The ATC can be formulated by defining a set of vector quantities $\theta(t) = [x(t), z(t), d(t)]$ for each of which the power network satisfies all quasi-stationary and transient operational requirements both for the existing network topology and for the set of contingency-degraded network topologies [7]. The system response to changes is defined by the DAE model given in (1.3)–(1.5) above. To define and compute a secure operating region, even for small systems, normally requires a sequence of simulations which vary the generation level until it becomes impossible to meet the security constraints.

However, most utilities do not compute the secure region on-line. Instead, off-line studies are performed to screen for the worst-case critical contingencies. These critical contingencies can be caused by a combination of complex nonlinear phenomena such as (1) the nonexistence of a system equilibrium as topology and grid parameters p_{grid} vary; (2) transient stability problems caused by not being able to move from the normal equilibrium to the new equilibrium if a disturbance lasts longer than the so-called critical clearing time; and/or (3) a non-robust, small-signal unstable equilibrium following the disturbances. For detailed analysis of these typical operating problems in a small two-bus system [9], see Chap. 4, pp. 198–210. For an introduction to the concepts and structure of comprehensive power system dynamics in large-scale systems, see [9], Chap. 7, pp. 391–497.

A detailed treatment of operating problems caused by nonlinear system dynamics, including voltage-related problems, is far beyond the objectives of this chapter. Mathematical models for Flores and São Miguel islands are derived and analyzed in Chaps. 15, 16, 17, and 19 of this book. For the purposes of identifying often hidden assumptions made in today's industry practice, it is important to keep in mind the major step made in replacing computation of secure operating regions by the conservative constraints as defined in [7], Chap. 2, and the typical DC power flow constraints used to monitor system congestion when dispatching power. Utilities pressed hard to make the most out of their T&D systems have begun to consider more accurate computation of secure regions by performing transient stability assessment and dynamic security analysis.

We stress that these methods are analysis-oriented and are not capable of identifying the most effective corrective actions and/or change of automation logic as conditions vary. Reviewed in Chap. 2 are the potential effects of optimized corrective actions and carefully designed automation methods which would contribute to a broader range of secure operating conditions over which generation scheduling can be done. These are illustrated in Chap. 13 and 18 for the islands of Flores and São Miguel.

1.3.3 Approximate Approach to Ensuring Secure Operations

Assuming that AGC, AVC, and system stabilization during normal conditions respond as expected, it becomes possible to further simplify the objective of ensuring secure operations. Instead of keeping track of the entire dynamics starting at a given time $t = 0$, typical least-cost scheduling is done today in an entirely static manner.

This is to say that a power system operates in a secure region where everything is stable at each scheduling instant $t = [H * T_H]$ and/or each $[M * T_M]$. The quantity $x(t)$ is the dynamic equations state vector (machine and load dynamics and the primary control), while $z(t)$ is the power flow state vector (real power P and reactive power Q injections, voltage magnitudes V and voltage phase angles δ , real power flows P_l , and reactive power flows Q_l in each line l). The vector $d(t)$ stands for the disturbance and parameter vector which, in its most general form, can be assumed to represent all bus load model parameters as well as all fault and contingency data, machine parameters, and any other system parameters. Equations (1.3)–(1.5) model the AC power flow and the system dynamics for the existing topology and for all possible contingency network topologies and system dynamics as well. The disturbance vector $d(t)$ describes all disturbances including faults, load changes ($w(t)$ in (1.1)), and outages during which the system must remain stable. In addition to the stability requirements, the system variables must satisfy a number of quasi-stationary operational inequalities in line flows, voltage, and frequency limits. Both the steady-state and the stability requirements can be expressed in the form

$$h(x(t), z(t), d(t), t) \leq 0 \quad (1.6)$$

Then the security region S can be defined as the set of quasi-stationary states $\theta[H * T_H] = [x[H * T_H], z[H * T_H], d(t)]$ which satisfy (1.3)–(1.6) for the set of disturbances defined by $d(t)$, within each scheduling interval $[H * T_H] \leq t \leq [(H + 1) * T_H]$, namely,

$$S = \left\{ \theta \mid \frac{dx(t)}{dt} = f(\theta(t), t); h(\theta(t), t) \leq 0 \right\} \quad (1.7)$$

Throughout this book modeling and simulations are done for Flores and São Miguel to test whether during certain disturbances the system remains in a secure region. Parts IV–VI, in particular, present a detailed modeling of the system dynamics in the electric power systems on these islands. Of particular interest is the design of the scheduling and automation to ensure that for given disturbances the system remains in a secure operating region.

Available transmission capacity can be thought of as the maximum power transfer limit within the requirements of the security region, and it can be defined by

$$TC([H * T_H]) = \max_{\theta \in S} TC(\theta[H * T_H]) \quad (1.8)$$

Equations (1.3)–(1.5) take on the form

$$f(x([H * T_H]), z[H * T_H], d[H * T_H]) = 0 \quad (1.9)$$

$$g(x[H * T_H], z[H * T_H], d[H * T_H]) = 0 \quad (1.10)$$

and

$$h(x[H * T_H], z[H * T_H], d[H * T_H]) \leq 0 \quad (1.11)$$

The dynamics of power plants (1.3) are approximated by so-called unit ramp rates R which state that power generated by a particular power plant can change within certain range per hours, namely

$$|[P_G[H + 1] * T_H] - P_G[H * T_H]| < R \quad (1.12)$$

It is discussed later in this chapter how the basic functionalities of today's computer applications and automation can be understood by combining the demand representation shown in (1.1) with (1.3)–(1.6). Given the initial condition at time $t = 0$, any secure state must satisfy the DAE model defining system response to these disturbances, the inequality constraints specific to hardware such as generation limits, the thermal line flow limits, and the equipment voltage limits.

1.3.4 The Most Frequent Characterization of a Secure Operating Region

As explained above, it is routinely assumed when performing real power economic dispatch that the system frequency has settled back to the nominal conditions and that it has become possible to directly relate power generation output $P_G[H * T_H]$ by adjusting the set point of governor $\omega_{Gi}^{\text{ref}}[H * T_H]$. This leads to the problem of computing constrained nonlinear equations (1.3)–(1.5) on-line to ensure a secure operating region at each scheduling instant $[H * T_H]$. At present, there are hardly any effective methods for computation of these equilibria for realistic size electric power grids. It is more frequent to compute the AC power flow equations. However, over wide operating ranges and for different grid topologies, even computing AC power flow solutions is prone to numerical problems. Because of this, further major simplifications are typically made when scheduling generation for the forecast demand. These simplifications are reviewed next.

To start with, when scheduling real power generation, it is assumed that the schedule does not significantly affect voltages $V G^{\text{ref}}[K * T_H]$; it is assumed that these are maintained at their nominal values (typically 1 pu) by means of the AVR. This assumption, together with linearization of the real power flow equations, results in DC power flow equations. These are routinely used when screening for the critical

equipment outages which may violate the secure region requirements and create grid “congestion.”

As a result, an overly simplified characterization of the secure operating region is derived using real power line flow sensitivities with respect to power injections $F_l(P_G(t) - P_{di}(t))$ so that: (1) the total real power generated should supply total forecast system demand, (1.13); (2) the real power line flows should be smaller than the proxy line flow limit determined using off-line stability studies, (1.14); and (3) the real power generation should be within its capacity limits (1.15).³ The real power line flow sensitivities with respect to power injections are known as the distribution factors and are easily computed using network parameters and topology.

$$\sum_i P_G(t) = \sum_i P_{Di}(t) \quad (1.13)$$

and

$$F_l(P_G(t) - P_{Di}(t)) \leq K_{l,\text{proxy}}^T \quad (1.14)$$

and

$$P_G(t) \leq K_{Gi}^G i \quad (1.15)$$

$P_G(t)$ and K_{Gi}^G denote the real power generated by power plant i and its maximum capacity, respectively. $P_{Di}(t)$ is the real power load at bus i . $F_l(t)$ and $K_{l,\text{proxy}}^T$ denote the real power flow in line l at time t and the proxy line flow capacity of line l at time t , respectively.

Ensuring that dispatched power can be delivered without congestion is done primarily by dispatching real power within the real power proxy line limits $K_{l,\text{proxy}}^T$ obtained by off-line studies to ensure no voltage- or stability-related problems. These assumptions underlie today’s security-constrained unit commitment (SCUC) and security-constrained economic dispatch (SCED) software, used by system operators in control centers for implementing secure dispatch during normal conditions. Hidden inefficiencies inherent in this software are discussed next.

1.3.5 The Key Hidden Inefficiency: Replacing Thermal Line Flow Limits with Proxy Line Flow Limits

Observing (N-1) reliability criteria amounts to an approximate screening of all possible equipment failures, one at a time, and finding the critical ones. Some utilities perform on-line screening of all contingencies to find those which are likely to violate the proxy line flow limits. AC power flow analysis is done next only for these critical contingencies to ensure that they are implementable. If they are not, the thermal line limits are modified and the proxy limits determined to ensure that there will be no power flow problems in the actual operations. SCUC and SCED are done

³For this derivation, see [5].

to dispatch real power within these proxy limits. Utilities are gradually recognizing the conservativeness of defining proxy limits in terms of the worst-case contingency and observing them in operations. They are beginning to deploy new software that enables the maximization of transfer limits by computing corrective actions to be taken in case a contingency occurs. Corrective actions are generally based on an operator's knowledge of the system, and are implemented adjusting the real power generation of a few key power plants. As a rule, no voltage schedules of controllable T&D equipment, generators' AVR settings, nor reactive power/voltage settings on the demand side are optimized to support most economic real power delivery. As a result, thermal line flow limits are often replaced by these proxy limits because the latter ensure stable and secure operations during both normal and equipment outage conditions.

In the remainder of this chapter we use the constrained DC power flow equations which are obtained through the approximations described above. It is critical for identifying the major inefficiencies in today's industry practice to recognize that this use of constrained DC power flow equations when scheduling generation to meet forecast system demand subject to observing the proxy limits is fundamentally conservative. Instead of designing corrective actions for adjusting the set points of voltage- and flow-controllable equipment, as well as the power outputs of other available power plants, to support the secure operation of the system as a whole, the worst-case approach is taken that the state is not allowed to enter a region which is not secure without relying on corrective actions. The implications of using a worst-case DC power flow-based approach to try to ensure secure operations are far reaching. It is illustrated throughout this book how this assumption can be relaxed by means of enhanced IT.

Under the same assumptions discussed above, the constrained DC power flow is generally written in its static form and used to dispatch the least-cost real power generation at each dispatch interval $[H * T_H]$. Equations (1.13)–(1.15), therefore, hold under the assumptions made for each time $[H * T_H]$ and are restated here for purposes of further discussion in this chapter and in the book as

$$\sum_i P_G[H * T_H] = \sum_i P_{Di}[H * T_H] \quad (1.16)$$

and

$$F_l(P_G[H * T_H] - P_{Di}[H * T_H]) \leq K_{l,\text{proxy}}^T[H * T_H]^4 \quad (1.17)$$

and

$$P_G[H * T_H] \leq K_{G_i}^G \quad (1.18)$$

⁴Observe that the proxy line limit generally varies with the operating conditions; at present, there are no on-line computations of this proxy line flow limit.

For purposes of further discussion, we refer to the real power generated at times $[H * T_H]$ for $H = 1, 2, \dots$ as the quasi-stationary sequence of power dispatched on an hourly basis.⁵

1.3.6 Multi-spatial Approach to Balancing Generation and Demand

A typical interconnected T&D power grid is very complex. Its voltages span from 765 kV to 110 V in US regions. The power plants and diverse loads are made by different manufacturers, and their parameters are not standardized. This makes the on-line monitoring and management of a typical regional power pool, or even of a large utility, a very difficult task. In particular, as generation is scheduled to supply time-varying demand while the network topology constantly varies for one reason or the other, the task of ensuring that the power can be delivered securely and reliably is hard. Because of this, complex interconnected networks are decomposed both horizontally and vertically, in much the same way as multi-temporal decompositions are done to simplify the problem of balancing supply and demand. The horizontal decomposition is mainly based on the organizational boundaries between the different utilities, while the vertical decomposition is done between the EHV/HV and MV/LV transmission and distribution networks, respectively.

Monitoring and managing horizontally organized utilities within a given large electric interconnection is not done systematically in today's industry. There has been an ongoing effort both in the USA and Europe to coordinate the monitoring and management of electrically interconnected utilities in different states and/or countries for reliability reasons. Many blackouts over the decades can be traced back to this problem of poor on-line coordination of electrically interconnected systems. More recently, there has been a major industry effort in the USA to coordinate the "seams" between different control areas for a more efficient utilization of available resources.

The problem of horizontal boundaries within an interconnected electric system has taken on a qualitatively new meaning as different investors in renewable technologies ask to connect to the existing utility-owned grid. Questions arise regarding both the most efficient technical integration and also the economic and policy incentives.

Both the horizontal and vertical decomposition of an interconnected power grid require approximate models of grid parts not of direct interest. The technical and economic implications of actual, often implied, approximations made could be very complex and far reaching. The network constraints in (1.4) state that both the real and also the reactive power balance must balance at each node in the given power grid.

⁵In traditional electric power systems literature a constrained DC power flow is often written without any reference to time, as each time sample $[H * T_H]$ is viewed as the power flow static steady-state solution.

1.3.7 *Hidden Inefficiency Caused by Uncoordinated Objectives of EMS and DMS Control Centers*

In today's industry, there exists a major separation between the energy and distribution management systems (DMS). When an EHV/HV energy management system (EMS) schedules generation to supply a forecast system demand, only the load at the substation level is estimated. Because of this, variations within the distribution network system, including the distribution system topology, distributed energy resources (DERs), and demand response, are not visible to the EMS operator. Similarly, when a DMS operates the distribution network equipment and resources, it is assumed that anything connected to the substation is an infinite power source. Feed-forward ramp-rate-limited economic dispatch by the EMS centers is performed at the pool level, generally comprising several utilities.⁶ AGC is performed at each control area (utility) level with the intent of balancing the slow hard-to-predict demand fluctuations $\Delta P_d[m * T_m]$. This level is referred to in the European literature as the secondary-level system balancing. Finally, very fast demand fluctuations $\Delta P_s[s * T_s]$ are compensated for by local primary controllers, mainly governors and AVR.

The DMS centers are currently being implemented in the USA. In Europe these exist, but no near-real-time SCADA information is used for corrective actions within the distribution network systems. It is described in Chap. 2 and illustrated throughout this book that DMS-coordinated demand response and use of DERs will become key to efficient and reliable electricity services. Learning customer profiles, accounting for the effects of DERs, and communicating both these things to the EHV/HV system operators will become the basic means for implementing both reliable and more efficient electricity services with active demand participation at value.

1.4 Operations and Planning as a Single Decision-Making Problem

A possible mathematical formulation of the single operations and planning problem in the regulated electric power industry can be found in [12, 15]. This formulation is reviewed here as the basis for discussing state-of-the-art methods and also changes in industry objectives leading to a new problem formulation in Chap. 2. It is suggested that this problem can be posed as a composite decision-making problem under uncertainties. It comprises an annual decision-making problem regarding investment in new generation capacity at location i and of type a K_{ia}^G ,

⁶Control areas have recently been restructured and are managed by a single Independent System Operator (ISO) in areas where power is provided competitively. Conceptually, the same ramp-limited dispatch is performed as in the existing power pools.

investment in new transmission line l of thermal capacity $K_{l,\text{thermal}}^T$, as well as near-real-time decision making on how much existing generation i of technology type a to schedule P_{ia} so that the total long-term expected cost to customers is minimized. This optimization must observe all physical network constraints and enable secure operations. A mathematical formulation of this problem is restated next for completeness and for identifying necessary enhancements in the changing industry.

Neither the computer applications currently used by the system operators and planners nor today's automation were implemented with this complex objective in mind. They have, instead, evolved slowly over time on an as-needed basis while making many simplifying assumptions. A summary of the IT evolution that has led to today's electric power industry is given later in this chapter, in Sect. 1.7. To identify key simplifications which should be relaxed as the next-generation software and IT are designed, we start by posing the complex overall industry objective first. We refer frequently in this chapter and throughout the book to this single operations and planning objective as the industry performance benchmark.

Notation

- $K_l^T(t)$ is the amount of installed transmission capacity for line l .
- $K_{ia}^G(t)$ is the amount of installed generation capacity for technology a at node i .
- $I_l^T(t)$ is the rate of investment in transmission capacity for line l .
- $I_{ia}^G(t)$ is the rate of investment in generation capacity for technology a at node i .
- $C_l^T(K_l^T, I_l^T, t)$ is the cost of investment i in line l .
- $C_{ia}^G(K_{ia}^G, I_{ia}^G, t)$ is the cost of investment in technology a at node i .
- $P_{ia}(t)$ is the production with technology a , at node i , during period t .
- $c_{ia}(t)$ is the cost of this production, excluding capacity costs.
- r_i is a random variable reflecting the uncertainty of demand consumption.
- $U_i(P_{di}(t), r_i(t))$ represents the utility function of consuming power $P_{di}(t)$ at node i during period t .
- $F_l(P_{ia}(t) - P_{di}(t))$ represents the flow on line l for the given vector of net injections $P_i(t)$.
- ρ is a discount rate.

1.4.1 Problem Formulation

Social welfare is defined as the difference between the consumers' utility and the production cost. The cost function includes both transmission costs and generation costs. The problem can be stated as follows [13]:

$$\begin{aligned}
& \max_{I_l^T, I_{ia}^G, P_{ia}} \mathcal{E} \sum_i \int_{t_0}^T e^{-\rho t} U_i(P_{di}(t), r_i(t)) dt \\
& - \sum_{i,a} \int_{t_0}^T e^{-\rho t} (c_{ia}(t, P_{ia}(t)) + C_{ia}^G(K_{ia}^G(t), I_{ia}^G(t), t)) dt \\
& - \sum_l \int_{t_0}^T e^{-\rho t} (C_l^T(K_l^T(t), I_l^T(t), t)) dt
\end{aligned} \tag{1.19}$$

subject to:

$$\frac{dK_l^T}{dt} = I_l^T(t), K_l^T(t_0) = K_l^T t_0$$

$$\frac{dK_{ia}^G}{dt} = I_{ia}^G(t), K_{ia}^G(t_0) = K_{ia}^G t_0$$

$$I_l^T(t) \geq 0$$

$$I_{ia}^G \geq 0$$

$$P_{ia}(t) \in S(P_d(t)) \tag{1.20}$$

The initial capacity of the lines and generation are $K_{l,\text{thermal}}^T(0) = K_{l,\text{thermal},0}^T$ and $K_{ia}^G(0) = K_{ia,0}^G$, respectively. In this formulation we differentiate between the systems-limited secure line capacity K_l^T and the line capacity itself. It is the lower of the thermal- and systems-limited capacity of the line which is observed when performing the optimization given in (1.19).

The optimization period is T and it corresponds to the longer of the two time intervals over which the generation or transmission investments are valued. $K_{ia}^G(t)$ and $K_l^T(t)$ are state variables. The variables are the rate of investment in transmission capacity, the rate of investment in generation capacities, and the injection of power at each node. The utility function parameters and forecast load $P_{di}(t)$ are the disturbance inputs. The control is bounded by the set of constraints described above. A set of Lagrange multipliers is associated with each set of constraints.

This problem formulation, despite its apparent complexity, captures many well-known trade-offs relative to the efficiency of the power industry. First, the discount rate reflects the time value of money. Everything being equal, it is better to spend money now than later. Thus, the investment timing balances the trade-off between the costs and benefits over time. Second, this formulation shows that different technologies at different locations can be used to produce power. Thus, for a given load duration curve, the ratio between variable costs and capacity costs for each of these generation resources determines the optimal pattern and mix of generation. Third, generation capacity can be substituted for transmission capacity. The trade-off between saving on generation costs and investing in transmission capacity is also encapsulated in the problem. The level of transmission capacity is not based on the maximum yearly flow. A trade-off between the costs of congestion and the costs of transmission capacity must be considered. Finally, the problem stated above

is an uncertain problem. The stochastic formulation reflects the value in flexible investment under uncertainties.

This optimization problem given in (1.19)–(1.20) is a very complex multi-temporal stochastic control problem; while investment decisions are made less frequently and long into the future, the economic dispatch of available generation is done closer to real time. This single operations-planning problem is hardly ever solved. Instead, it can be used by the regulators after the fact to evaluate how well the utilities have performed, and how they should be rewarded in the future. This formulation can be used to select an “optimal” investment as a break-even point between the capital cost in new investment, on the one hand, and the cumulative inefficiency which will result if the investment is not made, on the other hand [1,11,12]. This notion of optimal investment is a powerful means of selecting among different investment options in the electric energy industry, as discussed in Chap. 2 and illustrated throughout this book.

To relate this complex performance objective to the role of different computer applications used by today’s electric power industry, we explain next how under certain assumptions this single operations-planning problem can be decomposed into operations and planning subproblems. We stress that it is possible to systematically derive reduced-order models for solving the short-term optimization subproblems key to generation operation and maintenance (O&M) cost minimization, assuming a given generation and transmission capacity; similarly, it is possible to make investment decisions using coarser reduced-order models. In [15] two subproblems are introduced, and they are restated here because of their fundamental relevance to understanding the major causes of economic and technical problems that are cropping up as more intermittent resources are being deployed within the existing system.

We note that the benchmark optimum formulation requires perfect information about the demand, resource characteristics, and T&D topology and parameters. The main problem is that such information does not exist *ex ante* when the decisions have to be made. As a consequence, the actual operating and investment cost after the fact is generally much higher. We will describe in Chap. 2 how enhanced IT, which is used to make better predictions and to make model-based look-ahead decisions, could contribute significantly to reducing the overall cost of uncertainties. We review next how a single operations-planning is decomposed into two subproblems.

1.5 Decomposing a Single Operations-Planning Problem into Two Subproblems

The single operations-planning problem stated above can be interpreted as a stochastic optimal control problem for a dynamic model in a standard discrete-time singularly perturbed form

$$\min_{u_f, u_s} J_T(u_f, u_s, d) \quad (1.21)$$

subject to

$$\frac{dx}{dt} = g(x, u_s, d) \quad (1.22)$$

and

$$u_f \in S(u_s, u_f, x, d) \quad (1.23)$$

where $x = [K^G \ K^T]$ is the capacity state, $u_f = [P_G]$, and $u_s = [I_l^T \ I_i^G]$.

The process of scheduling supply to meet demand in operations typically happens much faster than the rate at which investment decisions are made. This observation is the basis for solving the two subproblems as if they were decoupled. To formally introduce these two subproblems, assume without loss of generality that the short-term (daily or hourly) decisions are made each hour $[H * T_H]$ and that investment decisions are made each year $[Y * T_Y]$, and $Y = 0, 1, \dots$, where $T_H = \frac{T_Y}{8640}$. The problem defined in (1.19)–(1.20) and Sect. 1.3 can then be restated as an optimization problem subject to multi-rate discrete-time processes. The objective function (1.19) takes on the form⁷

$$\begin{aligned} \min_{I_l^T[Y*T_Y], I_i^G[Y*T_Y], P_l[H*T_H]} & \mathcal{E} \left\{ \sum_i \sum_{k=0}^{\frac{T}{T_H}} e^{-\rho[Y*T_Y]} (c_i(kT_H, P_l[H*T_H], [H*T_H])) \right. \\ & + \sum_i \sum_{n=0}^{\frac{T}{T_Y}} e^{-\rho[Y*T_Y]} C_i^G(K_i^G[Y*T_Y], I_i^G[Y*T_Y], [Y*T_Y]) \\ & \left. + \sum_l \sum_{n=0}^{\frac{T}{T_Y}} e^{-\rho[Y*T_Y]} C_l^T(K_l^T[Y*T_Y], I_l^T[Y*T_Y], [Y*T_Y]) \right\} \end{aligned} \quad (1.24)$$

subject to

$$\begin{aligned} K_l^T[(Y+1)T_Y] &= K_l^T[Y*T_Y] + I_l^T[Y*T_Y]T_Y \\ K_i^G[(Y+1)T_Y] &= K_i^G[Y*T_Y] + I_i^G[Y*T_Y]T_Y \\ I_l^T[Y*T_Y] &\geq 0 \\ I_i^G &\geq 0 \\ P_l[H*T_H] &\in S[H*T_H] \end{aligned} \quad (1.25)$$

⁷Strictly speaking, discretization of the continuous time problem defined in (1.19) and Sect. 1.3 can only be done as long as there are no dynamic problems in transitioning from the state at $[H*T_H]$ to $[(H+1)*T_H]$. As discussed above, in today's industry, ensuring no dynamic problems amounts to replacing the thermal line flow limits by more conservative proxy line flow limits. Power-electronically controlled FACTS and fast storage are shown in Chap. 19 to have major potential for ensuring no transient stability problems and for contributing to a larger security region.

Observe that the slow and fast variables are coupled primarily through load demand (disturbance) dynamics $P_D[H * T_H]$ and through the requirement that scheduled power be in secure operating region S for each $[H * T_H] \leq t \leq [(H + 1) * T_H]$. The multiple periodicity of the load demand sets the basis for the separation of planning and operations objectives in today's industry. Planning is the process of controlling the rate of investments in transmission and generation, $I_l^T[Y * T_Y]$ and $I_i^G[Y * T_Y]$, respectively, so that load demand evolving over longer-term horizons (years and longer) is served at the lowest possible cost. Similarly, controlling the use of available generation $P_G[H * T_H]$ in real-time operations (hourly and shorter) is done to meet the anticipated hourly demand at the lowest possible cost.

The ultimate objective is to minimize the combined cost of both investments and operations while meeting the uncertain system load demand $P_d(t)$ given in (1.1). Theoretical conditions under which the two subproblems are separable and the implications for suboptimality of the single operations-planning objective defined over long time horizon $T J_T$ have never been studied rigorously in the context of the electric energy industry. It is explained in Chap. 2 why understanding their interdependencies will become important in the context of industry changes. In what follows, we first describe the zeroth order (decoupled) short-term and long-term stochastic control subproblems for the regulated industry.⁸

Much the same way as with any other composite control design for singularly perturbed systems, one must study the conditions under which solving the two subproblems makes sense. Moreover, inherent in solving the slow control problem is the optimal solution of the expected fast control problem over the entire time horizon. The point is made that, by viewing the composite operations/planning problem as one and decomposing it into simpler, systematically derived dynamic decision subproblems under relatively unrestrictive conditions, a near-optimal investment may be possible. This problem formulation is qualitatively different from the entirely static economic dispatch problem; we discuss this difference next.

1.5.1 Short-Term Coordinated Scheduling: Fast Decision-Making Subproblem

The composite operations/planning problem formulation is used next to pose the objectives of short-term transmission operations and planning as two decoupled near-optimal subproblems evolving at significantly different rates. Assuming that the network and generation are given over the entire T , a zeroth order fast control subproblem becomes a decision-making process regarding which units to turn on and off and how to adjust the power generated in short-term operations.

⁸Shown in [12] is that much-debated nodal pricing as a proposed means of short-term congestion pricing is a result of solving the fast control subproblem in near-optimal composite control of the coupled operations/planning problem. System λ is the short-term spot electricity price.

This sub-problem formulation directly follows from the composite optimization problem under the assumption that $\frac{T_H}{T_Y} \ll 1$. The network topology and parameters, $K_l^T[Y * T_Y]$, as well as the generation plants, $K_i^G[Y * T_Y]$, are given. Assuming furthermore that the daily economic dispatch process is a moving equilibrium at optimum clearing price $\lambda[H * T_H]$), a short-term operating optimization subproblem is formulated as follows:

$$\min_{P_l[H * T_H]} \mathcal{E} \sum_{H=0}^{H=\frac{T}{T_H}} \sum_{i=1}^n c_i(P_i[H * T_H], P_d[H * T_H]) \quad (1.26)$$

subject to the constraints:

$$\sum_{i=1}^{n+nd} H_{li} (P_i[H * T_H] - P_{di}[H * T_H]) \leq K_l^T[Y * T_Y] : \mu_l[H * T_H] \quad (1.27)$$

$$P_l[H * T_H] \leq K_i^G[Y * T_Y] : \sigma_i[H * T_H]$$

$$\lambda[(k+1)T_H] = \lambda[H * T_H] + c_{\text{spot}}(\sum_{i=1}^n P_i[H * T_H] - \sum_{j=1}^{nd} P_{dj}[H * T_H]) \quad (1.28)$$

The term λ represents the price of power at an arbitrarily chosen (slack) node. H is the matrix of the distribution factors [14] and transmission losses are neglected. Observe that the value of the H matrix is dependent on the choice of a slack (reference) bus. The term $\sum H_{li} \mu_l$ reflects the locational differences in optimal prices. Even though μ_l is always positive by definition, the term $\sum H_{li} \mu_l$ can be positive or negative. The value of λ and the distribution factors matrix depend on the choice of the arbitrary slack bus. However, the value of nodal prices p_i and of the μ_l are independent from this choice. The term μ_l represents the marginal value of the existing transmission capacity of line l . In other words, it represents the increment in social welfare that would result from a unit transmission capacity upgrade. This value is equal to zero, as long as the line is not congested and becomes strictly positive when the flow on line l is equal to capacity K_l . These formulae provide the basis for so-called nodal or locational marginal pricing (LMP) in spot electricity markets where these markets exist.

It is important to recognize that this problem is also a stochastic control problem; a fast control (decision) variable is the controllable power injected into individual network nodes in response to the forecast fast random fluctuations in load demand given in (1.1). This problem is a dynamic control problem that can be solved using various computing methods. Deterministic approximations are presently used for short-term operations; these approximations are static tools. When deterministic assumptions are made, it is not possible to co-optimize the investment and scheduling decisions; thus, there could be significant suboptimality due to such approximations.

1.5.2 Security-Constrained Economic Dispatch: DC Optimal Power Flow (DC OPF)

The short-term optimization problem given in (1.26)–(1.28) is typically solved as a static optimization problem each $[H * T_H]$ assuming a given $P_d[(k + 1)T_H]$ for the next hour and optimizing generation, $P_G[(H + 1)T_H]$, to meet it at the lowest possible cost.

$$\min_{P_G, P_d} \sum_{i=1}^n C_i(P_{Gi}) - U_i(P_{di})$$

subject to the constraints:

$$\sum_{i=1}^n P_i = 0 ; \sum_{i=1}^n H_{li}(P_G - P_{di}) \leq K_l$$

Here, a simplified DC load flow approximation is used to express line flow constraints. Observe that the value of the H matrix is dependent on the choice of a slack bus. The solution to this constrained optimization problem takes the following form:

$$p_i = \frac{dC_i}{dP_i} = \lambda - \sum_{l=1}^L H_{li}\mu_l \quad (1.29)$$

We note here that the static single-step optimization currently done is suboptimal relative to the short-term optimization formulated in (1.26) when subject to the unit ramp rates defined in (1.12). This is because the latter enables one to incorporate predictions and look-ahead decision methods and therefore to manage uncertainties more efficiently than the static single-step DC OPF. This observation is the basis for proposing the new model-based predictive look-ahead economic dispatch that accounts for ramp rate limits in Part III of this book.

1.5.3 Long-Term Coordination: Optimal Investment Subproblem

Assuming that real-time optimization can be decoupled from the investment problem, we consider the more complex, less studied, issue of optimal investments. Generally speaking, the notion of investment is inherently inter-temporal. By investing a fixed amount of money today, the centralized utility reduces its costs

over time. For this reason, uncertainty issues are at the heart of investment theories. The basic existence of risk is taken into account through the choice of the discount rate ρ : the more uncertain future payoffs are the higher the discount rate and the lower the optimal investments. To pose the investment problem as an active risk management problem, we view it here as a slow optimal control subproblem of the coupled operations/planning problem given in (1.19)–(1.20) as follows:

$$\min_{I_l^T[Y*T_Y], I_i^G[Y*T_Y]} \mathcal{E} \left\{ \sum_i \sum_{H=0}^{\frac{T}{T_H}} e^{-\rho[H*T_H]} (c_i[*T_H], P_l[H*T_H]) + \sum_i \sum_{Y=0}^{\frac{T}{T_Y}} e^{-\rho[Y*T_Y]} C_i^G(K_i^G[Y*T_Y], I_i^G[Y*T_Y], [Y*T_Y]) + \sum_l \sum_{Y=0}^{\frac{T}{T_Y}} e^{-\rho[Y*T_Y]} C_l^T(K_l^T[Y*T_Y], I_l^T[Y*T_Y], [Y*T_Y]) \right\} \quad (1.30)$$

subject to

$$\begin{aligned} K_l^T[(Y+1)T_Y] &= K_l^T[Y*T_Y] + I_l^T[Y*T_Y]T_Y \\ K_i^G[(Y+1)T_Y] &= K_i^G[Y*T_Y] + I_i^G[Y*T_Y]T_S \\ I_l^T[Y*T_Y] &\geq 0 \\ I_i^G[Y*T_Y] &\geq 0 \end{aligned} \quad (1.31)$$

The first term in (1.29) represents cumulative annual dispatch cost; this cost generally gets optimized using the short term optimization problem described above on daily basis. It is possible to take into consideration the dependence of this operating cost by running short-term optimization for candidate generation and transmission investments; this results in short-run annual cost $SRAC(K_l^T[Y*T_Y], K_i^G[Y*T_Y])$. This function gets replaced into (1.29) and then long-term optimization is done over capital cost investments by taking into consideration different effects of investments on cumulative annual dispatch cost. This is perhaps the most straightforward way of decomposing the complex stochastic planning-operations problem into two subproblems while accounting for their interdependencies.

It is generally assumed in today's industry that future demand and supply functions are known with perfect certainty. This setup leaves very little room for active risk management. Relaxing this assumption will be essential in the future electric energy industry. Nevertheless, to review the notion of an “optimal investment” that assumes perfect knowledge, we consider next the problem of generation investments.

1.5.4 Optimal Generation Investment Problem

Power is produced using different technologies a . They differ in their marginal cost c_a and their unit cost of capacity C_a^G that we assume to be constant. The total installed capacity for technology a is denoted K_a^G . We assume that the demand curves for different periods are elastic and known with perfect certainty. Let us denote by $P'(P_d^1, \dots, P_d^T)$ the demand function for period t . It is assumed to be a function of the consumption quantities for all periods in order to take into account cross-temporal interdependencies. A simpler presentation would make it dependent on P_d only.

We analyze the investments in generation capacity from a long-term perspective. Thus, contrary to the economic dispatch problem, the optimal investment problem considers the total amount of installed capacity as an optimization variable. It is stated as the following mathematical problem [1]:

$$\max_{P_a^t, P_d^t, K_a^G} \sum_t \int_0^{(L^1, \dots, P_d)} P_d(y^1, \dots, y^T) dy - \sum_{t,a} c_a P_a^t - \sum_a C_a^G K_a^G$$

subject to

$$\begin{aligned} P_a^t &\leq K_a^G : \sigma_a^t \\ \sum_a P_a^t &= P_d^t : \lambda_t \end{aligned}$$

The Lagrangian associated with this problem is

$$\sum_t \int_0^{(L^1, \dots, P_d)} P_d(y^1, \dots, y^T) dy - \sum_{t,a} c_a P_a^t - \sum_a C_a^G K_a^G + \sum_t \left(\sum_a P_a^t - P_{di} \right) + \sum_{a,t} \sigma_a^t (P_a^t - K_a^G)$$

The necessary optimality conditions are obtained by stating that the first derivative of the Lagrangian with respect to P_a^t, P_d^t, K_a^G is equal to zero, resulting in

$$\begin{aligned} P^t &= \lambda^t \\ \sum_t \sigma_a^t &\leq C_a^G; K_a^G \left(\sum_t \sigma_a^t - C_a^G \right) = 0 \\ \lambda^t - \sigma_a^t &\leq c_a; P_a^t (\lambda^t - \sigma_a^t - c_a) = 0 \\ \sigma_a^t &\geq 0; \sigma_a^t (K_a^G - P_a^t) = 0 \end{aligned}$$

This formulation shows that, consistent with the economic dispatch methodology, the inexpensive generators are dispatched first and the resulting price P^t is set equal to the short-run marginal cost.

Moreover, a combination of the second and third equations shows that the difference between the price and the cost of dispatched generators σ_a^t , when accumulated over several periods, is equal to the cost of the installed generation capacity:

$$\sum_t \sigma_a^t P_a^t = C_a^G K_a^G \quad (1.32)$$

Thus, the price paid by consumers reflects the cost of capacity and can be interpreted as a long-run marginal cost. We should note that this result is a direct consequence of putting ourselves in a deterministic world. For an interpretation of these conditions in an uncertain environment, see [12]. Thus, the peak-load pricing theory, by optimizing with respect to installed transmission capacity, makes the long-run and cumulative short-run marginal costs equal. The mathematical condition given in (1.32) defines the optimal investment condition. Any investment with a capital cost the same as the cumulative cost due to inefficient existing generation utilization over time T is a nonunique optimal generation investment candidate. As unconventional candidate technologies a become available, the cumulative inefficiency of supply meeting demand without such technology is harder to evaluate. It becomes necessary to account for the value of flexibility of new candidate technologies, such as storage. Evaluating the potential benefits from such flexibility is a complex, yet doable challenge.

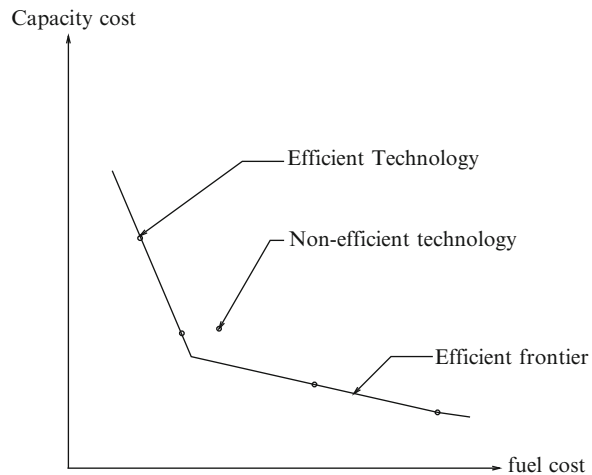
Several important results follow from the above formulation of the optimal generation mix.

First, the introduction of several technologies contributes to increasing the total social welfare since we optimize over a wider range of variables. Moreover, this increase will be strictly positive due to several effects:

- *Cost reduction:* By spreading demand over several technologies, fewer of the most expensive technologies will remain idle during off-peak periods. This gain may not be completely offset by the higher fuel cost during peak periods.
- *Pricing effect:* By charging a different price for different periods, this scheme provides better economic incentives. Consumers may decrease their consumption at different rates or transfer it to another period.

However, even though introducing more technologies increases the total social welfare, it may be the case that the optimal installed capacity is zero for one specific technology and that, consequently, the associated increase in total welfare is null. An obvious example is the introduction of a new technology with the same cost of capacity but a higher fuel cost. This enables the introduction of an efficient frontier of generators on the c_a, C_a^G plane. This efficient frontier is downward sloping since a higher fuel cost must be compensated for by a lower capacity cost. This frontier is also convex, since for any linear combination of two existing technologies to be implemented, a new technology must have a lower capacity cost, fuel cost being equal to the composite technology, to be efficient (Fig. 1.11).

Fig. 1.11 The generation peak-load pricing efficiency frontier



1.6 The Challenge of Operating and Planning Future Electric Energy Systems

As one attempts to propose new computer methods and software for managing energy resources and demand efficiently and to embed automation in the process for enhanced performance, it is important to understand that today's industry approach has evolved over time as the complexity of the power grids has increased.

There has not been one single industry approach to assessing the trade-offs between what is built and how the assets are utilized. Instead, as reviewed above, operations and planning have been considered two separable problems, often managed by different departments within the same utility. Planning is generally done to decide among "proven" technologies, typically generation and T&D lines, to ensure that sufficient generation and transmission capacity is in place to serve the long-term forecast system demand. Planning is done to ensure that the peak load is served at all times and that "one day in ten years" uninterrupted service to customers is ensured. Generation has been considered to be the main means of supplying demand, and there has not been much differentiation between controllable and passive T&D equipment and the demand side when deciding how to enforce the T&D grid in order to deliver power at all times from the generators.

1.6.1 Overcoming Inefficiencies Related to Approximations of Secure Operating Regions

As discussed above, planning is generally done by optimizing generation investments, and T&D equipment is generally considered to be an order of magnitude less costly than generation investments, and it is often designed redundantly very often

in order to ensure secure delivery. As a result of this worst-case planning approach, utilities have had considerable generation and T&D reserves; the generation reserves are not estimated over time; instead, they are defined as the difference between the generation capacity available and the peak-load expected. As reviewed in Sect. 1.3, the ability of T&D to deliver power, known as the ATC, is complicated to measure because it depends on the actual power line flow patterns. It is common to find statistics documenting the ratio of the average line flow and its thermal rating as the line utilization. This number is very low, often 30%. However, we stress that looking at the line's utilization is a very misleading metrics. Nevertheless, it is important to stress that the so-called system load factor, defined as the ratio of the peak load and the average annual load, is very small, under 50% in the United States. Except for a very small number of electric power systems worldwide, this load factor is typical and has been decreasing recently.

1.6.2 The Challenge of Implementing Flexible Asset Utilization

The above numbers point to the conclusion that there exists a considerable discrepancy between the available resources measured in terms of capacity, and their actual use in operations. It is important to keep in mind this distinction as new technologies present themselves in future electric energy systems and societal objectives change. The fundamental role of IT is to make the most out of the available assets by adjusting to the ever-changing demand and system conditions. To help understand the potential of IT in enabling more efficient utilization, we have reviewed the objective of today's industry planning and operations as a single complex problem. Based on this review, and on the implied underlying assumptions, it can be concluded that it would be possible to enhance its performance solely by means of a carefully designed next-generation IT. Given the sheer complexity of electric grids and the diverse generation and demand components connected to them, it is fundamentally impossible, using today's methods, to make effective investment decisions under uncertainties while accounting for the effects of JIT and JIP technologies, in particular.

Depending on how advanced modeling and decision-making tools are overlayed with the physical operations of the system, the actual asset utilization will vary significantly. There are two possible paths forward:

- Identify the most critical assumptions made by today's EMS and DMS centers and introduce an approach which systematically relaxes these assumptions,
- Engage in a fundamentally new paradigm that is based on embedding decision-making tools into (groups of) system users with a significant ability to manage uncertainties and inter-temporal dependencies at the distributed level; the information from the system users is exchanged with the EMS and DMS centers responsible for ensuring secure grid operations.

In what follows we summarize the major challenges which must be overcome to bring about more efficient long-term industry performance measured in terms of the long-term social welfare given in (1.19). In Chap. 2 we introduce a possible change of paradigm that we have named DYMONDS.

1.6.3 The Challenge of Managing Low-Probability High-Impact Events Efficiently

Perhaps the biggest challenge is the management of power grids when forced large equipment failures occur. Most widespread blackouts have been triggered by such events. In order to prevent widespread disruption of service during such events, today's industry mandates that the system to be designed and operated according to $(N - 1)$ or at times even $(N - 2)$ reliability criteria. These criteria require that sufficient generation and T&D reserve be available in standby mode all the time just in case a forced outage occurs. The typical approach has been to build and operate the system so that even when what is considered to be the worst-case forced outage takes place, customers do not get interrupted for at least 30 min following the event. Many utilities do not rely on adjustments of other available resources during forced outages. Instead, the utilities have on-line reserve ready to be used.

In this book, we stress that as more stochastic resources get deployed, it is going to become very hard to assess the worst-case contingency and have sufficient standby reserves without experiencing major efficiency loss. It is with this in mind that we stress the need for new computer algorithms capable of drawing on other key available resources following a forced outage and which do require the same amount of standby reserve as today. Notably, consumers need to become responsive to the changing system conditions, and the old concept of viewing system demand as predictable with high accuracy, and only needing automation to manage zero mean disturbances during normal conditions, will have to be rethought. Finally, the behavior of only ensuring that the system is transiently stable during forced outages by not operating the system closer to stability boundary during normal conditions is clearly going to have to be modified. It will become necessary to implement power electronically controlled fast storage in order to stabilize system response transiently, on the rare occasions when potentially destabilizing outages occur. We suggest in this book that a careful cost–benefit analysis should be done to assess if and when operating conservatively on the off chance a forced outage may occur and should be relaxed by relying on fast nonlinear control and communications.

1.7 The Evolution of IT and Its Use in Today's Industry

The short-term decision-making formulation given in (1.26)–(1.28) and Sect. 1.3 is the least-cost short-term dispatch problem subject to generation being in secure region S . The overall objective of operating electric energy systems is organized hierarchically over time as follows:

- Feed-forward computer applications in support of dispatch, unit commitment, and power dispatch functions that balance predictable demand components ($\hat{\Delta}$)
- Feedback automation to ensure that the system operation is stable and within the quasi-stationary operating conditions when small, hard-to-predict deviations from forecast demand $\Delta(\cdot)$ occur
- The management of low-probability high-impact equipment outages

1.7.1 *The Need to Enhance Operations*

Individual utilities have long operated their systems with a human operator in the loop according to predefined rules (nomograms) that are specific to each utility. However, as utilities have interconnected for economic and reliability reasons, it has become increasingly difficult for system operators to coordinate their interactions with neighboring utilities and to manage the effects of the electrical interconnections on their own systems. The first response to this challenge was to introduce computer applications capable of scheduling the least-cost available real power generation to supply the forecast demand while also agreeing to exchange power with the neighboring utilities. The power grid interconnection evolved to share the burden of standby reserves by means of several electrically interconnected utilities. Only at later stages did tie lines begin to be used for economic trades between the utilities. Over time, other computer applications were introduced to screen for the worst equipment outages, often referred to as “contingencies,” and to help system operators set the required reserve that would ensure uninterrupted service to customers even when bad equipment failures occurred. This has resulted in computer methods for SCED and SCUC. These applications are currently routinely used today by many utilities when scheduling generation to supply the forecast demand. Some utilities also use computer algorithms to minimize T&D delivery losses by adjusting the settings of voltage-controlled reactive power equipment, such as on-load tap changing transformers (OLTCs) and capacitor banks (CBs). The current obstacles to implementing loss minimization are lack of accurate on-line reactive power load and voltage data, as well as the convergence problems of nonlinear optimization software. Consequently, today’s electric power grids are typically not optimized for voltage support. Instead, on-line power flow analysis is performed to test how much power can be transferred without creating voltage-related technical problems. Once the power flow software fails, the grid is unable to deliver more real power generation.

While the generation dispatch software supporting the optimization of generation to supply forecast demand has become more or less standardized, today's power grid automation responding to hard-to-predict disturbances is much less so. When it comes to automation, the current situation is as follows. All major power plants have governor and excitation controllers for fast frequency and voltage stabilization. This control is known as the primary control, and it responds to local deviations of frequency and voltage from the set values of these controllers. The primary control does not adapt to the changing conditions. It is, instead, tuned to stabilize local disturbances caused by a worst-case equipment outage in the rest of the system.

To avoid utility-level minute-by-minute frequency drift away from nominal frequency that is caused by load deviations from load forecast, two solutions are practiced at present: (1) equipping several fast power plants with proportional-integral (PI) primary controllers, and/or (2) relying on an automatic generation control (AGC) scheme known as the secondary-level control. The AGC responds to a system-level power imbalance known as the area control error (ACE), which is a linear combination of frequency deviations and net deviations of power flow exchanged with the neighboring utilities. The ACE is communicated by the control center to the power plants participating in the AGC, and these respond in an automated feedback way by compensating for a prespecified percent of ACE. Using local PI controllers is simpler and does not require communications between the plants participating in the AGC and the control center. As a matter of fact, in small stand-alone island systems control centers are not always in place. Frequency is regulated by a few proportional-integral (PI) governor controllers and/or by manual load interruptions when frequency drops exceed the prespecified industry specifications.

Several large utilities in Europe have implemented utility-level AVC schemes, often referred to as Secondary Voltage Control; conceptually, these are similar to the AGC scheme. They are implemented to ensure that voltage deviations remain within the prespecified industry standards when the reactive power load deviates from its forecast, much the same as how AGC is a utility-level scheme for frequency regulation. To avoid complexity, only several critical, pilot-point, load voltages are monitored and they are regulated to remain constant by adjusting the voltage set points of the participating power plants in response to hard-to-predict deviations in reactive power consumption. When the pilot points are selected systematically, the other load voltages will follow the pilot-point voltages, which remain unchanged even when reactive power disturbances occur.

Both the primary and secondary controls in today's utilities are intended to regulate small, relatively slow deviations in frequency and voltage during normal conditions. No automation is presently in place that can respond to forced large equipment outages. Near-real-time, communications-intensive, synchronized measurements are not used at present for transient stabilization or for the prevention of voltage collapse during large sudden system changes. Except for sporadic deployment of wide-area measurement systems (WAMS)-based special protection schemes (SPSs), which attempt to manage the well-understood effects of frequently

occurring and severe equipment outages, no system-level automation has been built that ensures transient stabilization and prevents voltage collapse. The main consequence of this lack of automation is an operator's inability to use assets efficiently during normal operations. To ensure that customers are not affected during these outages, today's practice is to have sufficient fast spinning generation reserve and to operate at lower transfer limits in case a worst-case outage occurs. As the use of power grids continues to develop into something significantly different from the use for which the grids were initially built, it is becoming increasingly difficult to operate systems reliably based on the worst-case off-line calculations and preparations. This all indicates that ultimately a more powerful fast automation, that can enable the response of many available resources during large outages, will be needed.

1.7.2 Recent Technological Breakthroughs

Developing an IT that efficiently utilizes assets by means of flexible operations and planning represents a major theoretical and practical challenge. To start with, there is, at present, very little that has been done in terms of modeling electric power system dynamics for operating over very broad ranges of conditions. It is discussed in Chap. 2 what is needed and why in terms of establishing formal and systematic models for designing adaptive transient stabilization. We point out here that the existing models are intended for analysis and do not lend themselves to systematic adaptive control design for complex dynamic systems. Parameter identification in these complex models is the second major challenge on the way to powerful automation. Given the extreme time criticality, the models must be carefully derived to represent the phenomena being controlled; the effectiveness of adaptive and nonlinear control in the event of large disturbances is often very sensitive to the accuracies of models and parameters used.

Very recent breakthroughs in deploying synchronized near-real-time measurements at the system level have created unprecedented opportunities for qualitatively new ways of managing the effects of large outages in the future. Conceptually, model verification and parameter identification in complex power systems can be pursued without disrupting operations; system dynamics can be monitored over broad ranges of conditions and key parameters can be identified. More than anything else, confidence in the models can be developed.

The recent North American Synchrophasor Initiative (NASPI) is an attempt to overcome this major lack of fast synchronized data and provide coordinated WAMS. The overall small reliance on automation is a result of poor observability of system-wide dynamic states in the power grid. Major actions are undertaken, based on off-line studies of the most severe unexpected equipment failures known, by a human-in-the-loop. The availability of synchronized fast measurements using synchrophasors gives promise for the first time to system-level WAMS-based automation. This, in turn, requires rethinking of how this data would be useful for enhanced operations and control. The broad expectation is that better knowledge

of near-real-time changes in the system, together with carefully designed software and automation, will ultimately enable more efficient and reliable utilization of any given system. The major challenge lies in understanding how a given system operates today and how to introduce systematically but phased-in software to support humans decisions and also necessary automation. As with deploying hardware, there are major trade-offs depending on the solutions selected.

To sum up, today's operations and control paradigm is at its crossroads. Both because of new societal needs and also advances in IT, communications, and sensing, we need to rethink what is being done and where the major payoffs would be from possible enhancements. In today's industry the only adjustments—feed-forward to manage forecast conditions and/or automated feedback in response to small frequency and voltage fluctuations—are made by the conventional power plants. There is very little on-line adjustment by the demand or T&D equipment. Also, it is important for identifying future needs when considering enhanced IT tools that the dispatch tools not be solely static and deterministic. The AGC is based on steady-state concepts of frequency being the same everywhere in the system; AGC is, therefore, not capable of differentiating the effects of electrically distant controllers. Moreover, the primary stabilization tools, such as governors and AVR_s, are tuned locally one at a time, while representing the rest of the system as a static Thevenin equivalent. Fundamental problems with using automation of this type in systems with large, intermittent resources have been discussed throughout this chapter. We have considered the problem of power system operations and planning for future electric energy systems by first defining the overall problem for today's industry and then discussing further the implied assumptions made in computer applications and automation. We have suggested that some of these assumptions must be revisited, and enhanced computer applications must be designed that support efficient and reliable operations and long-term performance of future electric energy systems. In Chap. 2, we review the potential role and importance of IT in the energy-strapped islands of the Azores Archipelago.

1.8 The Need for Enhancing Computer Methods and Automation

Here we revisit computer algorithms currently used by industry operators to schedule resources for feed-forward dispatch and unit commitment (operations Task 1), minimize delivery losses (Task 2), and make power delivery for forecast conditions feasible (Task 3). We then point out that the automated feedback control for frequency and voltage regulation and stabilization must be designed more systematically in order to meet prespecified frequency and voltage quality standards in systems with many hard-to-predict resources (Task 4). Third, we consider computer methods needed to ensure reliable service during large unexpected wind gusts and during equipment failures (Task 5) as an important IT-enabled alternative to costly overdesign [7].

The line between the feed-forward and feedback functions is not always easy to define. It critically depends on the accuracy of the forecast, as well as on the operating practices, namely, on how well the forecast conditions are managed. In Chap. 2 we explain that there exist major trade-offs between building capacity for forecast conditions, on the one hand, and developing an IT that efficiently balances supply and demand using automation, on the other. This observation could be viewed as an un-necessary detail, but it is in fact the major rationale behind the fundamental need to enhance the, just-in-time (JIT), just-in-place (JIP), and just-in-context (JIC) functionalities brought about by IT and fast storage [4]. Relying on JIT and JIP functionalities is likely to become one of the major means by which future electric energy systems will be operated both reliably and efficiently. In this book, we illustrate this claim multiple times by comparing what is doable with and without such functionalities, all else being equal.

Today's operations and planning industry approach could be thought of as comprising at least five major distinct tasks [7], Chap. 2. In the past, we have found this classification to be particularly useful for understanding how the electric power grid is operated and what role specific computer applications play. Based on this experience, we proceed by starting from the same operations task classification.⁹

Task 1 concerns the Unit Commitment (UC) and Economic Dispatch (ED) of generation to meet forecast demand \hat{P}_d . The basic UC approach uses a 24-h or longer system demand forecast to select the units that should be on and capable of generating power. While this forecast is not perfect, it is needed to support UC, namely, the selection of power generation units which need to be up and running in preparation for economic dispatch closer to real time. The industry practices and software used are often system specific and not fully standardized. We consider UC/ED Task 1 to be the basic supply and demand balancing problem because it recognizes that different power plants can only increase or decrease their power generation output at a certain ramp rate; no network constraints are observed. This, in turn, implies that very slow base-load units, such as nuclear and coal power plants, cannot turn on/off very quickly. Therefore, they cannot follow rapid demand variations nor fast wind power changes. These problems require software which proactively utilizes multi-temporal predictions and optimizes in a look-ahead way with the best possible predictions. In particular, it becomes necessary to enhance today's static SCUC with optimization tools capable of computing when even slower plants need to be turned on and help balance uncertainties multi-temporally.

Task 2 concerns transmission and distribution (T&D) delivery loss compensation for the forecast system demand. Because of delivery losses, it is generally necessary to produce more generation than the forecast demand; and there are many computer methods for estimating system losses and for scheduling the generation needed to compensate them. At present this function is performed in the EMS control centers which estimate losses and schedule extra power to compensate for these estimated

⁹This classification was initially introduced to align physical system operations with the electricity market design rules.

losses. In the future, qualitatively different methods of compensating for delivery losses, such as distributed resources compensating for their own losses close to the end users, are likely to be deployed. It is plausible to perform loss compensation in a distributed way and also to place future distributed resources at locations that reduce the losses created [6].

Task 3 concerns the delivery feasibility of the generation scheduled to supply forecast demand. Network constraints are often accounted for closer to real time, say 1 h or 10 min ahead; the generation power output from the plants that are already up and running as a result of performing Task 1 is adjusted to ensure that power delivery is feasible. For purposes of understanding the necessary evolution that will lead to future electric energy systems, it is important to observe here that system limitations to delivering the most economically and environmentally desirable power are quite complex. We illustrate in this book the importance of relaxing often conservative system delivery limits (the line proxy limits introduced earlier in this chapter) by implementing near-real-time corrective actions and by designing the automated control so that it stabilizes system dynamics based on fast synchronized measurements and communications. We explain and illustrate in specific chapters of this book how this change from observing the worst-case operating limits to performing on-line corrective actions and automation enables a much more efficient utilization of the available transmission and distribution (T&D) assets than is currently possible.

Task 4 takes into consideration system dynamics and concerns automation that ensures system-wide stability and an acceptable frequency and voltage quality of electricity provided to the end users. The hard-to-predict wind power fluctuations ΔP_{WG} around the forecast component are generally compensated for by using automatic generation control (AGC) of several fast-responding power plants that respond to the frequency deviations. Past industry practice has assumed fast and small near-zero mean demand fluctuations around the system demand forecast.

As more wind power is deployed, it is no longer going to be possible to make this assumption. As a matter of fact, how much and which type of stabilizing and regulating resources will be needed in the future will be heavily determined by how accurate the prediction models are used for feed-forward decision-making and how efficiently the forecast demand is supplied. The remaining power imbalance will have to be corrected quickly to prevent instabilities using the automated feedback control of often expensive storage. We suggest that trade-offs between the wear and tear of more conventional resources used to provide frequency and voltage stabilization and regulation, and the cost of power-electronically controlled fast storage and FACTS, will have to be assessed carefully as different technological solutions to the problem of persistent wind power fluctuations are being considered.

Task 5 concerns the secure operations of the complex grid during hard-to-predict equipment failures. Qualitatively new tools are needed for supporting decisions regarding corrective adjustments on settings of controllable equipment during non-time critical faults and/or large wind power deviations; introducing such tools could go a long way toward ensuring reliable service in systems with large wind penetrations. In this book we illustrate the potential benefits from such corrective

actions that adjust voltage-controllable T&D equipment and that reduce demand enough to ensure viable operation.

Finally, software is needed in support of new planning paradigms for investing in new technologies. We point out that it is particularly important the interdependence of most effective technologies and the operating protocols for utilizing selected technology in actual operations. Because decisions must be made in a highly uncertain environment, it is important to have well-defined interactive protocols for information exchange and for computing the financial incentives for managing uncertainties. A systematic combination of highly accurate short-term wind prediction models for economic dispatch and not very accurate long-term wind prediction models for investment decisions that account for the cumulative short-term payoffs from candidate technologies are needed to define the best investments. It is discussed in this book, and illustrated using the Flores and São Miguel island systems, how long-run marginal bids (LRMB) for deploying the best candidate technologies in support of wind power integration can be created by the candidate investors themselves. Long-term decisions by the investors and by the system operators and regulators must be supported by new software that enables interactive dialogue and decision-making for selecting and utilizing the best candidate technologies. Since much of the payoff of different fast technologies (fast storage, communications, sensing, and computing and control, in particular) comes from just-in-time (JIT), just-in-place (JIP), and just-in-context (JIC) adjustments, one of the major challenges concerns the financial incentives at the investment decision stage needed to value flexibility brought about by such adjustments that are unique to each given technology. In other words, a fast load following power plant has a higher value when it comes to compensating for wind power fluctuations, but it is not currently differentiated from base-load plants. Even more complex is the challenge of deploying an amount of fast storage that carefully reflects the break-even point of the capital cost and the cumulative value brought to the system as a whole. At present, fast-responding energy storage is not compensated for by the deferral of standby large reserves, but this must be done if a convincing business case is to be made for otherwise expensive storage. Moreover, as mentioned earlier, the actual amount and type of storage needed will critically depend on how well wind power is predicted and also on how dispatch is done under uncertainties based on this prediction. The better this is done, the less need there will be for very expensive storage, and, consequently, the lower the overall cost of electricity services in systems with wind power will be. Much the same way as it is both challenging and necessary to carefully assess the value of fast-responding hardware, it is essential to assess the value of the needed analytics and IT to support their deployment and use. At present IT is not an explicit part of the financial assessments when planning new investments. Given the potential major enhancements in both the reliability and efficiency of electricity services by means of systematically designed IT, we suggest that considerations of new IT as a means of solving problems of interest should be made equally important as the consideration of hardware such as fast storage, in particular.

In summary, it is becoming quite clear that various controllers, placed throughout the T&D grid, in power plants, and embedded into specific loads of power consumers, can fundamentally reduce the delivery limits currently imposed on the existing power grid. It is therefore essential to deploy and utilize the next-generation IT methods for both feed-forward decision-making and for automation. The complexity of IT-enabled electricity services requires a major rethinking of the fundamentals of operating and planning future energy systems.

1.9 Chapter Summary

In this chapter we revisit the overwhelming complexity underlying planning and operations in today's electric energy systems. We provide a short summary of how today's system is managed and identify common simplifications for managing the necessary decision processes in a timely manner. We next propose that the operations and planning of future electric energy systems will become much more complex than they are in the present or have been and that data-driven knowledge about system changes will become essential. Both industry objectives and available technologies are such that the current industry paradigm needs rethinking. We claim that to integrate and utilize new technologies according to the well-understood objectives and at value, it will become essential to engineer IT-enabled electricity services. The importance of systems thinking in setting the goals of Information Technology (IT) design for evolving electric energy systems is discussed by taking a look at the objectives of today's operations and planning and the type of software and automation used to reach these objectives today. We make an assessment of the underlying assumptions and their implications for achievable reliability and efficiency, and use the findings to define the need for new and enhanced IT-enabled operations and control tools for managing evolving system complexity.

Acknowledgements The ideas presented in this chapter draw in part on joint early work with Professor Francisco Galiana from McGill University in Canada. The ideas have also evolved as a result of many research efforts with several graduate students, notably Benoit Lecinq and Jean-Pierre Leotard. The author fondly remembers many hours of working together and acknowledges the input. The joint early work is cited to the best of the author's ability.

References

1. M. Crew, P. Kleindorfer, *The Economics of Public Utility Regulation* (Macmillan, London, 1986)
2. F.P. DeMello, C. Concordia, Concepts of synchronous machine stability affected by excitation control. *IEEE Trans. Apparatus Syst.* **88**, 316–328 (1968)
3. S. Hoffman, H. Illian, Control performance criteria, in *Proceedings of the American Power Conference*, Chicago, IL, 1996

4. M. Ilić, Dynamic monitoring and decision systems for enabling sustainable energy services. Proc. IEEE **99**, 58–79 (2011)
5. M. Ilić, *Smart Grids and Future Electric Energy Systems*. ECE Course, Lecture notes Carnegie Mellon University, Spring 2012
6. M. Ilić, R. Cordero, On providing interconnected operations services by the end user: case of transmission losses, in *Proceedings of the NSF Conference on Unbundled Power Quality Service*, Key West, FL, 1996, pp. 28–38
7. M. Ilić, F.D. Galiana, L. Fink (eds.), *Electric Power Systems Restructuring: Engineering and Economics* (Kluwer, Boston, 1998)
8. M. Ilić, L. Xie, Q. Liu (eds.), *Engineering IT-Enabled Electricity Services: The Case of Low-Cost Green Azores Islands* (Springer, Berlin, 2012)
9. M.D. Ilić, J. Zaborszky, *Dynamics and Control of Large Electric Power Systems* (Wiley Interscience, New York, 2000)
10. E.V. Larsen, D. Swann, Applying power system stabilizers: Parts I-III. IEEE Trans. Power Apparatus Syst. **100**, 3017–3046 (1981)
11. B. Lecinq, M. Ilić, Peak-load pricing for transmission access, in *Proceedings of the Hawaii International Conference on System Sciences*, Maui, HI, January 1997, pp. 624–633
12. J.-P. Leotard, Transmission pricing and incentives for investments under uncertainty in the deregulated industry. TPP (Civil Engineering), MIT Master Thesis, February 1999
13. J.-P. Leotard, M. Ilić, On the objectives of transmission pricing under open access, in *Proceedings of the IEEE Power Engineering Society Winter Meeting*, New York, NY, February 1999
14. D. Shirmohammadi, H.W. Hong, A. Semlyen, G.X. Luo, A compensation-based power flow method for weakly meshed distribution and transmission networks. IEEE Trans. Power Syst. **3**, 753–760 (1988)
15. C.N. Yu, J.-P. Leotard, M. Ilić, Dynamic transmission provision in competitive electric power industry, in *Discrete Event Dynamic Systems: Theory and Applications*, vol. 9 (Kluwer, Boston, 1999), pp. 351–388

Chapter 2

The Tale of Two Green Islands in the Azores Archipelago

Marija Ilić

2.1 Introduction

This chapter concerns the next-generation computer methods and automation for future electric energy systems. In Chap. 1 we have identified the major assumptions in today's operations and planning that make the management of complex electric energy systems possible. As explained, some of these often hidden assumptions present major roadblocks to the reliable and efficient integration of new resources and to the seamless participation of electric energy users. These simplifications are embedded in today's computer methods and automation, and as such, they indirectly make it hard to operate unconventional resources. We describe one possible new IT-enabled framework that supports the relaxing of these hidden sources of inefficiencies; we refer to this approach as dynamic monitoring and decision systems (DYMONDS). We show how this approach can be used as the basis for a paradigm shift toward more data-driven operations and planning in future electric energy systems.

We start in Sect. 2.2 by briefly summarizing the main motivation for this book, namely, the challenge of making the electric energy systems of two islands as green as possible without increasing the long-term service cost. We describe the characteristics of the electrical power grids, energy resources, and demand characteristics on the islands of Flores and São Miguel in the Azores Archipelago. We highlight how electric energy is provided today on these islands and the basic challenges and opportunities in front of these islands as they consider the evolution of their electric energy systems.

M. Ilić (✉)

Department of Electrical and Computer Engineering, Carnegie Mellon University,
5000 Forbes Ave, Pittsburgh, PA 15213, USA
e-mail: milic@ece.cmu.edu

We put forward the major premise that it would indeed be possible to transform their current electric energy systems into sustainable, low-cost systems by means of a systematic deployment of IT-enabled methods and automation. Illustrating this premise is the subject of our entire book. To do this, we first summarize our vision for sustainable socio-ecological energy systems (SEESs) in Sect. 2.3. We next highlight in Sect. 2.4 the key role of IT-enabled operations and planning in transforming future electric energy systems into sustainable SEESs. We explain how a carefully designed IT, and a man-made physical network, can enable the relaxing of several major assumptions causing hidden inefficiencies in today's operations and planning.

In particular, we explicitly relate the role of “smart grids” in the aligning of temporal, spatial, and contextual resource and user characteristics within a given governance system. This relation for the first time makes an explicit connection between the multiple objectives of SEESs and smart grid design principles. We point out that this general relation can be applied to designing smart grids for any given electric energy system. The solutions are nonunique, path-dependent, and ultimately driven by the sustainability multi-objectives and their tradeoffs. However, the basic idea of aligning the temporal, spatial, and contextual characteristics of both the energy resources and the users within a given governance system, in order to enable sustainability by means of carefully-designed IT, is common to any SEES.

The complexity of the models and principles of IT and automation design needed to induce sustainability requires a systematic approach. One possible way of proceeding is to identify how better temporal, spatial, and contextual alignments of resources and users can be achieved by enhancing today's operations and planning industry practice, as introduced in Sects. 2.5–2.8. This is basically the approach taken in this book. In this chapter, we summarize in Sect. 2.10 the methods proposed for achieving this. Our emphasis is on the enhancements of specific computer applications and automation made and on explaining how the proposed solutions fit into the broad framework of smart grid design in support of sustainable SEESs. We discuss the explicit dependence of sustainable electricity service on data driven predictions, computer-supported decisions, and automation. The major new concepts in each chapter contributed to this book are briefly summarized.

We illustrate the key findings reported throughout the book as the first proof-of-concept IT framework for sustainable SEES. We briefly discuss how these concepts jointly contribute to a possible IT-enabled implementation of electricity service at choice reliably while meeting environmental objectives by deploying more wind and solar power, in particular—and all without an excessive cost increase for electricity services. Finally, in Sect. 2.11, we briefly describe the first data repository of real-world data (found in the DVD of this book) as the supporting source behind the claims made in this book. We close in Sect. 2.12.

2.2 The Tale of Two Low-Cost Green Azores Islands

As a more specific illustration of the potential for enabling future electric energy systems with a man-made physical grid and its IT, we consider next two representative islands of the Azores Archipelago. These islands are presently supplied by very expensive fuels shipped from faraway places. This makes the energy supply very expensive and precious. At the same time, the islands are in wind-rich places and quite sunny. Therefore, their situation begs the question of whether it would be possible to replace the currently used expensive and polluting fuels with natural renewable resources, such as wind, solar, geothermal, and hydropower. Being small, they are potentially great test-beds for what can and cannot be done since cause and effect in their systems is much more transparent than in the large continental electric energy systems; the effects of supply and demand imbalance fluctuations on the quality of frequency and voltage in the electricity services provided are quite pronounced, and it is conceptually possible to model and analyze these effects.

The above are some of the reasons that have motivated us to use the islands as real-world test-beds for demonstrating our basic premise that it is fundamentally possible, through management with IT, and without increasing the long-term cost of electric energy services, to deploy much more renewable energy than is currently done. In this book, we have chosen two islands: the largest island in the Azores Archipelago, São Miguel, and the very small Flores. Flores already has some wind power plants and has deployed one fast storage flywheel for balancing the intermittent wind power. Flores also has a small amount of precious controllable hydropower, which is a clean, large storage capable of compensating for wind power changes over time.

We challenge ourselves in this book with the question of how much more wind power capacity does it make sense to deploy on Flores and São Miguel, and why and how should the new plants be integrated and operated such that they offset the use of diesel power plants. To begin answering these questions, one needs a systematic framework with clearly defined performance objectives. Viewed over longer time horizons, there are multiple performance metrics and they are not always aligned. In particular, it is important to quantify the expected annual variable fuel cost, annual emissions cost, annual T&D power delivery loss, unserved load cost, the cost of wear and tear in power plants following demand variations, the cost of poor quality of electricity service, and lastly, the capital cost of new investments and the sunk cost of existing assets if these are to be replaced by the new ones. A qualitatively new aspect of the changing electric energy industry is that the cost listed above is much more complicated to assess when deploying large-scale equipment than in the case of capacity-based worst-case designs. Outcomes are sensitive to how well economies of scope are extracted and to what the tradeoffs are between investing in hardware versus increasing short-term asset utilization; smart grids are the key to increasing short-term asset utilization, all else being equal, and as such could contribute to relatively low-cost solutions which offset the investments in high-cost hardware.

These vastly different costs indicate the need for integrated cost management, in which coordinated decisions by policy makers, system planners, operators, and the respective island community should be made to nurture the long-term evolution of sustainable electric energy services. Methods are needed to compare the long-term tradeoff between (1) the significant capital cost of investing in wind power plants, small household- and/or neighborhood-level photovoltaic (PV) panels, efficient technologies for energy users, plug-in electric vehicle infrastructure, and the IT infrastructure necessary to keep it all together, and (2) the cumulative long-term savings from replacing expensive and polluting fuels with renewable energy. It is clear that this assessment cannot be done with the deterministic capacity-based cost-benefit analysis currently used by the industry and regulators.

One of the major messages throughout this book is that the tale has a happy ending if/when one begins to view future electric energy systems as complex SEESs in which many small effects contribute to solving big problems [4, 15]. Our main vision is that economies of scope can be achieved by enabling assets with unique functionalities [16]. Instead of building capacity to ensure unconditional use of electricity by the customers, it should be built to enable customers to choose at value, assessed by themselves, if/when it would be beneficial to modernize their electric energy loads, including a switch to electric vehicles, to respond just-in-time (JIT) and just-in-place (JIP) to the availability of intermittent power and be rewarded for doing that. These preferences should be communicated to the policy makers and to the local utilities that are ultimately responsible for providing the electricity service.

In this environment carefully designed IT tools could become invaluable for processing collected data for supporting long-term decisions to participate proactively in greening the islands and for enabling near-real-time adaptations as short-term energy resources change their power availability. This is needed because it is hard to be flexible without IT. Highly complex domain-specific specialized sensing, communications, and control automation are needed to ensure that complex electric energy systems operate reliably and safely and at the same time utilize existing assets efficiently.

The key challenge is to design a systematic framework for IT-enabled adaptation, within a complex electric energy system, to the availability of power and well-understood customer preferences. In this book we contrast what can be done when considering wind power as a negative load with what can be done when wind is carefully forecasted and system users adjust to the predicted variations ahead of time. We contrast further what can be done by combining wind forecast with controllable hydro available on Flores, with what can be done on São Miguel where there is no controllable hydropower. On São Miguel one can justify more reliance on demand response since this is one realistic means of balancing the forecast wind power; there is no controllable hydropower on São Miguel. To coordinate the available power with customers it is essential to have systematic protocols for information exchange at value [3]. We show how much can be achieved by preprogramming the electric energy use of large users capable of doing this on São Miguel longer into the future. These common-sense ideas are modeled, simulated, and illustrated for the first time in this book.

Notably, what can and cannot be achieved on the two islands critically depends on how efficiently and reliably power is delivered and what the cost of delivery infrastructure is. Here again, different computer algorithms, software, and automation can be put in place to facilitate power delivery. To start with, we show that the actual location of the wind power plants can make the difference in how much power is lost in electric wires when delivering the wind power. Once the plants are in place, one could ask the question about where to place very small dispersed PVs and clusters of electric vehicles to further minimize delivery losses from faraway larger wind and conventional power plants. Moreover, the complexity of automation for balancing hard-to-predict wind power fluctuations away from the forecast output greatly depends on the relative locations and electrical distances between the large loads, the power plants, and the newly placed renewable resources.

We discuss in this chapter and illustrate throughout the book the dependence of the IT infrastructure complexity level on the accuracy of the models and parameters used for designing the automation. In short, embedded DYMONDS are needed not only for actuating the response to changing system conditions but for identifying parameters and updating models in an online environment for fault-tolerant automation. A related issue concerns the complexity resulting from the required coordinated system-level communications and control assuming the models and parameters are known and accurate. The robustness of fast storage control for preventing blackouts and/or managing major brownouts during large wind gusts and equipment outages depends to a large extent on the accuracy of the models and parameters used.

In this chapter we summarize the main approaches we take to design the JIT and JIP automation that allows our tale of two islands to end happily. For now, we point out that a deployment of more renewable resources on the islands could lead to skyrocketing electric energy infrastructure costs unless a systematic framework is used to assess what can and should be done, with a clear understanding of the long-term costs and benefits.

Making islands green without escalating long-term costs requires careful consideration of the possible nonunique technology portfolio. An in-depth knowledge of their unique functionalities is needed to design JIT- and JIP-embedded DYMONDS capable of balancing supply and demand efficiently and reliably. Much the same way as it is necessary to have a systematic way of deciding which future hardware assets to build, it is equally important to proceed with an IT infrastructure based on a quantifiable understanding of the information to be exchanged and its value.

Low-cost electric energy systems for green islands cannot be achieved by considering one single “best” energy resource, one single “best” computer application, or one “best” storage type. None of these solutions work by themselves since their value materializes only when they are used at the same time as other technologies. For example, stand-alone storage has very little value unless it is used to compensate for hard-to-predict power imbalance. Otherwise, a much less costly base load energy resource can be used. Economies of scope come into major play.

Perhaps the most difficult challenge is to have a design of a framework for supporting an ongoing evolution of the electric energy systems, with well-understood innovation objectives. The objectives of future electric energy systems are much beyond strictly technical and economic. They will evolve as the societies become more aware and accepting of the needs for sustainable SEESs [15].¹ The tale will never end as the societal needs evolve and as new candidate technologies present themselves over time. The tradeoffs are often hidden depending on time over which the objectives are attempted.

Instead of policy makers setting goals for deploying specific technologies over a predefined time horizon, we suggest that it is much more sustainable to consider dynamic innovative investments over time [12, 17]. Nonunique solutions may emerge depending on the time frame over which the innovations are made, indirectly biasing the technology choice. The technological breakthroughs in making small resources efficient make it possible to evolve today's electric energy systems, which rely on conventional generation following demand, into systems in which generation, consumers, and T&D jointly contribute to sustainable future electric energy services. The promise of such change presents us with both challenges and opportunities. The challenge inherent in enhancing today's operations and planning paradigm is to facilitate this transformation to an SEES in which the electricity users are equally as active in the decision making as the producers. Engineering T&D and its IT-enabled smarts to support such interactive decision making is the main topic of this book. The really exciting opportunity is to create long-term sustainable SEESs. We briefly present our vision of SEESs next.

2.3 Sustainable SEESs

One of the main premises in this chapter and in the entire book is that the objectives of a smart grid should be closely related to the objective of enabling sustainable energy services. Given the characteristics of the energy resources and the energy users, and of the governance system (core variables [15]), the design and operation of the man-made energy delivery system greatly impact how well the characteristics of the resources and users will be matched. A possible qualitative and quantitative approach to conceptualizing the role of smart grids is motivated by the concepts put forward in seminal work as a socio-ecological systems (SES) framework for sustainability analysis [15]. In particular, the idea of introducing a common set of variables key to identifying factors that may affect the likelihood of a particular policy to enhance sustainability in one type and size of resource system and not in other types is extremely appealing when tackling the problem of the

¹A happy tale of two Azores islands is the one which provides a “development that meets the needs of the present without compromising the ability of future generation to meet their own needs.” The quote is the working definition of sustainability by the US National Academies.

RESOURCE SYSTEM (RS)	RESOURCE UNITS (RU)	GOVERNANCE SYSTEM (GS)	USERS (U)
SIZE	MOBILITY	COLLECTIVE CHOICE RULES	NUMBER
PRODUCTIVITY			LEADERSHIP
PREDICTABILITY			SOCIAL NORMS
			SES KNOWLEDGE

Fig. 2.1 Key core- and second-order variables of an SES [15]

governance required to support sustainable electric energy systems as they undergo their evolution. Sustainability fundamentally means a careful balancing of multiple objectives such as emissions, cost (O&M and capital), and the business stability of innovating hardware and software technologies at value [8]. Policies determining these tradeoffs are critical to both the short- and long-term ability of an SES to sustain itself [8].

Shown, for the sake of completeness, in Fig. 2.1 is a summary of the core- and second-order variables characterizing any SES that are believed to affect its sustainability characteristics most critically, as proposed in the Nobel Prize-winning framework for water SES [4, 15]. The sustainability of an SES is represented by the characteristics (second-order variables) of the core variables, and it depends on (1) the size, productivity, and predictability of the overall resource system; (2) the mobility of the resource units; (3) the governance system that is in place, in particular on having collective choice rules; and (4) on the number, leadership, social norms, and overall knowledge of the system users concerning the characteristics of the resource system, resource units, and governance system characteristics.

To briefly review our notion of a SEES, consider the simple electric power system diagram shown in Fig. 2.3. We observe that each energy system, independent of specific architecture, has the same core variables as the one shown in Fig. 2.1; here the resource system and units are the generators, the users are the loads (consumers), and the governance system is a set of operations, planning and economic rules for managing the resources and users.

We have recently proposed that viewing any future energy system in terms of its core-, second-, and deeper-order variables, and designing the man-made grid and IT to induce these variables to lend themselves in the best possible way to sustainability, is one possible approach to aligning the characteristics of the energy resources, electric power grid, IT, and policy [4]. The smart grid becomes consequently a means of implementing the man-made physical power grid and

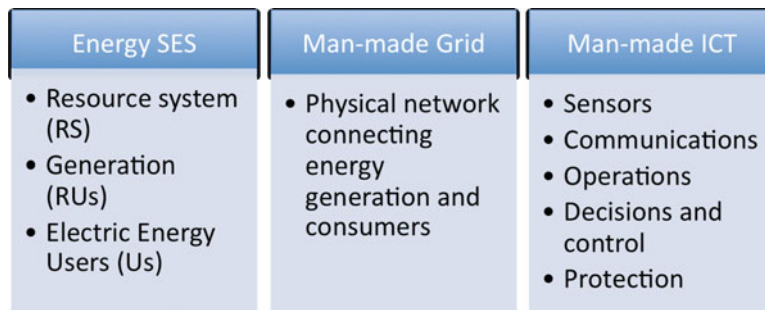


Fig. 2.2 Electric power grid and IT as enablers of sustainable socio-ecological energy systems (SEESs) [4]

its IT in support of a sustainable energy SES. Specific to the energy systems, shown in Fig. 2.2 are the key core- and second-order variables whose characteristics determine how sustainable a SEES can be, based on the characteristics of the resources, users, and governance system.

We stress that how well the characteristics of the resources and users are matched in time determines the basic quality of service (QoS), efficiency, and environmental impact of any given SEES. To start with, there exists a very real mismatch between, for example, the most efficient energy production by specific resources, on one side, and their typical utilization, driven by the users' needs and the ability to deliver the energy to the right place, on the other; this leads to a gross underutilization of individual generators when performing economic dispatch within an interconnected power grid, for example. This mismatch highlights the need for caution when assessing system efficiency based on the attributes of individual components; it is generally not possible to attain a full efficiency of individual components due to temporal and spatial network-level constraints.

Similarly, because of the often vast geographical distances between the components within an SEES, it is generally difficult to deliver energy from the most desirable energy resources to the users. In reference to Fig. 2.1, energy systems generally do not have many mobile resources, and this makes their sustainability sensitive to how well the man-made electric power grids and other energy delivery means align the production and consumption. Delivery-related constraints often contribute to significant underutilization of otherwise highly attractive energy resources. Finally, we point out that mutual temporal and spatial interdependencies themselves may sometimes also be pronounced within an SEES, and because of this, it is not possible to manage them separately.

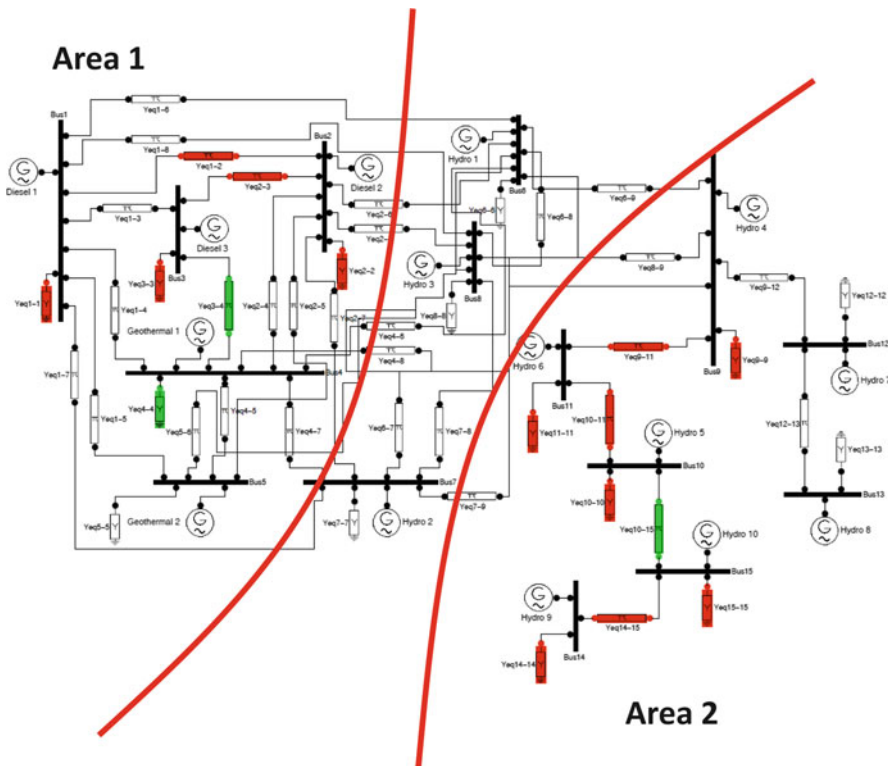


Fig. 2.3 Two electrically-distant areas on the Island of São Miguel, [13], Chap. 15

2.4 The Key Role of IT in Enabling Sustainable SEESs

Conceiving, designing, and implementing effective IT solutions for enabling sustainable SEESs is not a matter of simply adding on or making minor modifications, to the existing operating and control practices. Instead, doing it right requires an in-depth understanding of the electric power systems as complex dynamical systems and a strong background in the key areas essential for creating an evolutionary sensing, monitoring, and control design while also keeping in mind the changing requirements in future electric energy systems. Much must be done to design a systematic IT that enables the effective integration of large-scale wind power, for example.

The necessary sensing, communication, and control hardware is already available and quite cost-effective. Missing are the concepts for embedding intelligence into such hardware so that the components, by optimizing their own sub-objectives, help meet the overall goals of the system. These goals are no longer the traditional cost

minimization subject to many complex physical constraints. Instead, the grid must serve as an enabler that allows the implementation of multiple tradeoffs ranging from reliability and QoS to economics and environmental goals.

By assessing the second-order characteristics of the core variables in any SES, such as a water or energy system, it becomes possible to define how sustainable the given system is likely to be. The more aligned the temporal, spatial, and contextual characteristics of the core variables (the resources, users, and governance system) are, the more sustainable any given SES will be.

In this section, we review how this notion can be used to define sustainable SEESs as a particular complex system of interest. We suggest that the man-made electric power network and its IT play the key role in empowering the resources, users, and the governance system with the monitoring, sensing, prediction, learning, and adjustment tools for changing conditions necessary to contribute jointly to sustainable electric energy services. We then suggest a possible DYMONDS framework with supporting software, as a means of aligning the characteristics of the energy resources, users, and governance system and making the SEES more sustainable. Therefore, IT plays a fundamental role in inducing the sustainability of electric energy systems. We further conjecture that one of the key objectives in the transformation of today's energy systems to smart systems capable of meeting short- and long-term future needs must be to develop methods for the better understanding and matching of broad SEES attributes, the properties of physical grids, and the characteristics of both the IT and the governance system.²

To pose the problem of smart grid design and operation, one should start by first characterizing the energy resources, user preferences, and governance system much the same way as water systems were characterized using the SES framework in [15]. This general framework for assessing the sustainability of any SES can be applied to future energy systems and, in particular, to forming one possible basis for understanding the role of smart grids and IT in shaping the sustainability of those systems. Shown in Fig. 2.2 is an energy system viewed as a SES, augmented by a man-made grid and man-made IT. For any given SEES, the man-made grid and its IT must be designed so that they induce the core- and second-level variables, listed in Fig. 2.1, that lend themselves best to an overall sustainable SEES. Our basic approach is for the system users to internalize the system constraints as much as possible and transform them into the explicit sub-objectives of a complex dynamical system. The power grid users, resources, and consumers can adjust to the changing conditions and/or communicate with the others to align their needs and preferences with the system-level objectives [10].

²For understanding several qualitatively different architectures of energy systems and the necessary architecture-specific design of the IT that makes the best use of the available resources, see [4]. Notably, since the starting SEES of each representative architecture is qualitatively different, the design of the man-made grid and the IT for each one must be different.

2.5 SES-Based Modeling Framework for Sustainable SEESs

Much the same as in the seminal SES work and its recent applications to water systems, we are concerned with the creation of a design model for a sustainable SEES. Relevant models and IT design for sustainable performance strongly depend on the type of SEES. In order to create an IT design framework for smart grids, it is essential to establish a sufficiently accurate, yet not too complex, modeling framework that captures the interdependencies between the SEES, physical grid, IT, and governance system. We point out that the choice of the key variables depends on the type of architecture and on the questions the modeling framework is attempting to answer.

2.5.1 *The Need to Model Deeper-Level Variables*

In order to induce sustainable just-in-place (JIP) electric energy services by means of smart grids and their IT, it becomes necessary to extend the concepts of the general SES sustainability framework to include spatial interdependencies. This can be done only if the mathematical models capture significant interactions among the spatially distant resources and users. Therefore, it becomes necessary to model the spatial interactions between different clusters of delivery system users across a very large interconnected bulk man-made power grid. It is here that modeling the physical processes underlying man-made power systems becomes crucial to smart grid management design for sustainability.

To elaborate, we recall the mathematical models derived in the engineering literature, with an eye to assessing qualitatively and quantitatively the highly complex, nonlinear interdependencies among the multiple variables used to characterize electric energy systems [1, 2, 9]. In particular, the physical interaction variables reflecting the electrical distances between different portions of a large man-made grid become good candidates for deeper-level variables within an overall SEES and its man-made grid [2]. It is important to understand that these variables can only be modeled by careful model reduction of an otherwise very complex electric grid. Shown in Fig. 2.3 is the island of São Miguel; line connections colored red, green and white are strong, medium and weak strength lines shown in Fig. 2.4 are the interaction variables created by a disturbance located in one part of two electrically distant areas on the island [13], Chap. 15. Interaction variables colored in blue and green are those of areas 1 and 2, respectively. Matching different patterns of users and resources in these two electrically distant areas efficiently will require sensing and control of this interaction variable.

It should be somewhat intuitively clear that the characteristics of second- and deeper-level variables for hybrid and fully distributed architectures are very different than the characteristics of these variables in the bulk energy systems reviewed in Chap. 1 of this book. Consequently, the type of IT that will induce sustainable performance in these systems is very different. In particular, since these systems will

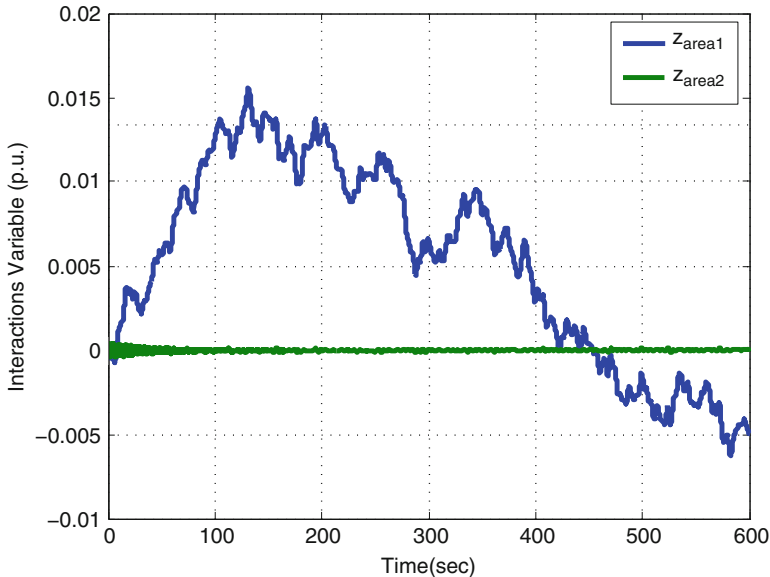


Fig. 2.4 Power exchange between two electrically distant areas on São Miguel, [13], Chap. 15

have a significant penetration of small hard-to-predict core variables IT paradigms supporting peer-to-peer communications and decision making by self-organizing highly proactive users are likely to support sustainable services with the right governance in place. Many technologies recognized as smart distribution system technologies (smart meters and advanced meter infrastructures (AMIs) in particular) become key to sensing and adapting in a highly distributed way. According to the general principles of sustainable SEESs, technologies such as distributed storage, electric vehicles, wind power, and solar power all lend themselves to being highly capable of becoming part of a sustainable eco-energy system.

Modeling relevant interactions for other than fully regulated large-scale SEES represents a major R&D future challenge. Even the aggregation of distributed users and resources is an open question. For example, it is possible to aggregate system users that have similar temporal characteristics but are dispersed throughout an electric power grid. It is also possible to aggregate system users that are located in the same parts of the electric power grid but have vastly different temporal characteristics. Qualitatively different challenges to IT and DYMONGS design complexities would arise when attempting to make an SEES sustainable in these two different situations.

However, given the aggregation of small system users into portfolios of one or the other type, it is fundamentally possible to generalize the notion of interaction variables and deeper-order variables for these new architectures as well. More specifically, a vector of variables internal to the aggregated portion of the system

is generally a function of its internal states and the decision making that is in place. The interaction variables, by definition, cannot be affected by internal actions unless a subsystem is connected to the rest of the system. While this definition is analogous to the definition for today's bulk power systems, much work is needed to understand how the interactions are affected by the new technologies being deployed.

Missing at this time are governance mechanisms which value the just-in-time (JIT), just-in-place (JIP), and just-in-context (JIC) contributions of these technologies to a high quality of sustainable energy services. For example, integrating large amounts of wind power will require highly responsive demand. The power mismatch between a portfolio of wind and inelastic demand is qualitatively different from the power mismatch between a portfolio of wind and price-responsive demand, as they create qualitatively different needs for power produced by the conventional power plants. In the first case, the need for fast large fluctuations by the natural gas plants is significantly larger than in the case when demand and intermittent wind power are coordinated within a single portfolio subsystem. It is not hard to conclude that the IT design and DYMONGDS embedded to implement price-responsive demand contribute significantly to the sustainability of the overall SEES. Dispatching conventional power plants in a sustainable way requires the monitoring and control of a portfolio of wind power and responsive demand.

These are only some of the first examples illustrating the importance of deeper-order interaction variables within an SEES. To our knowledge, relating the sustainability of an SEES to the interaction variables within the complex electric power grid was attempted for the first time in [4]. More work is needed to develop formal models for the evolving architectures. Also, the deeper-order variables can be used to assess inefficiencies caused by a lack of coordination. Actual system data should be used to assess at least order of magnitude inefficiencies.

2.6 Toward an Approach to Designing and Operating Smart Grids for Sustainable Energy Services

The premise we put forward is that for any given particular type of energy resource system, the operations and planning engineering practices must ensure that the deeper-level variables of the man-made electric power grid are such that they align both the resource and the user characteristics. In simple terms, the interaction variable needs to be sensed and communicated to the right controllers to induce a good spatial and temporal matching of resources and users. This requires careful engineering and governance design. Only then will the likelihood of having a sustainable complex man-made electric energy grid embedded within the natural energy resource system be high. This conjecture, recently presented for the first time in [4], is directly motivated by the work in [15]. We pose the design of a man-made

electric power grid within the ecological energy resource system as the problem of inducing the properties of second-level variables in the resource system that are most likely to be sustainable. To us, this is an exciting novel link that one could use to carefully design man-made systems in order to make the most out of the available natural resources [4]. We emphasize that the desired properties can be induced by starting with models that represent the core- and second-level variables and then by introducing deeper-level variables specific to the energy systems that capture the nonlinear interdependencies within the overall system.

Designing a man-made power grid, and accompanying IT, to induce sustainability using these models amounts to designing a symbiotic energy SES and a man-made grid-IT system which, jointly, are most likely to have sustainable properties. Based on this, our proposed approach to modeling and designing the man-made power grid and its IT for sustainable service becomes basically a three-step process [4]:

Step 1—Start with the core- and second-level variables to characterize a given SEES.

Step 2—Define and model deeper-level variables to capture the interdependencies between the SEES, physical grid, IT, and governance system.

Step 3—Design the physical grid, IT, and governance system to induce sustainability by sensing and controlling the interaction (deeper-level) variables so that the closed-loop system has good JIT, JIP, and JIC functionalities.

Notably, a general SES framework helps define the most adequate IT design needed for the core subsystem characteristics and their second-level variables to enable the man-made electric power grid with the functions needed to obtain an overall sustainable SEES. The actual IT design needs to be done with a clear understanding of this purpose. A better understanding of the SEES-electric power grid-IT complex system is key to enhancing both the physical grid and its intelligence to support SEES in long-term sustainable energy provision.

Using the language of SES, we conclude that the main purpose of IT is to align the attributes of the resource system, resource units, and users. This is no small task given the spatial and temporal complexities of near-real-time power balancing. We illustrate in this book that identifying the predictability of system users' characteristics by means of IT techniques is particularly important to the system design. To enable both choice and system-level performance, temporal and spatial information must be exchanged about the second-order and deeper-order variables of the core variables within an SEES. The closer these characteristics are aligned, the more likely the system is to be long-term sustainable. To us, this has been a guiding light to revisiting the modeling, decision-making software, SCADA, and automation in today's industry, and to identifying the principles enhancing their performance as new resources are being added.

2.6.1 *The Role of Smart Grids and IT for Sustainable Energy Delivery*

Somewhat unique to the energy systems in which energy is transported via an electric power grid is the problem of sustainable electric power delivery, since electric energy resources are generally not mobile. An interactive multilayered IT framework with much embedded intelligence at all layers (resources and users) with minimal coordination among the layers could enable a large penetration of wind, in coordination with responsive demand and other distributed technologies, without requiring any new large investments in conventional generation or transmission [8]. This is contrary to many estimates and predictions that associate clean sustainable energy service with unavoidable, unacceptably high-energy tariffs. Shown in the same work is a comparison between what is achievable with today's IT in place (which relies on old industry rules for bulk power systems) and what is doable by implementing JIT and JIP energy services. If predictions are used, the volatility is even further reduced. The interactions are the deeper-level variables discussed above. There is much research to be done on modeling, communications, and control design in all types of SEES architectures. We refer to this interactive paradigm as DYMONDS, which is described in this chapter as a possible IT solution that supports sustainable energy utilization.

2.7 The Impact of Hidden Inefficiencies on the Sustainability of SEESs

Recall from Chap. 1 that today's operations rely on at least five major tasks that are being performed on line at different rates. In Chap. 2 of [6] system operations was described as comprising these five basic tasks. We have found this classification to be particularly useful over the years, and in this book we start with this exact operations task classification.³ Recall that these operations tasks are:

- *Task 1:* Economic dispatch of ramp-rate-limited power plants to supply forecast demand
- *Task 2:* Delivery loss minimization of dispatched power to the right consumer locations
- *Task 3:* Ensuring that power can be delivered without creating network congestion, given the expected equipment status (normal conditions)

³This classification has been particularly useful when relating physical system operations to electricity market problems.

- *Task 4:* Ensuring that frequency and voltage are maintained within prespecified industry standards during hard-to-predict small demand fluctuations
- *Task 5:* Ensuring reliable service to customers even during forced large equipment outages

It is described in Chap. 1 of this book how, by making assumptions about the hierarchical separation of intertemporal dependencies, one can start from a single operations-planning industry objective and decompose it into operations and planning subproblems. The operations subproblem is further decomposed into the five operations tasks listed here. The reasons for these simplifications are both historic and out of necessity to manage an otherwise extremely complex problem.

We next discuss the effects of these simplifications on the achievable sustainability of a given SEES. To formalize these interdependencies we recall from Sect. 2.3 above that the more temporally, spatially, and contextually the characteristics of the resources and the users are aligned given the rules of the governance system, the more sustainable an SEES will be.

2.7.1 *The Role of the Governance System*

The governance system generally defines the performance objectives of the industry as a whole by requiring a certain QoS and by allowing certain ranges of service tariffs. Given an SEES and the second-order variables of its resources and users, different governance systems will lead to qualitatively different sustainability over time. For example, if the governance system monitors the performance of the service providers after the fact and does not take into consideration the effects of inevitable uncertainties at the time of investing or scheduling the existing resources, the expected performance will be overly optimistic when compared to what is achievable in practice. Both short- and long-term uncertainties have a huge impact on which technologies will be deployed and how efficiently the resources and users are aligned. Moreover, the choice of time horizon over which service providers are evaluated also has a major impact on long-term sustainability.

Governance systems which rely more on proactive decision making by the resources and users than on the centralized coordination for managing intertemporal dependencies under major uncertainties support very different technologies and outcomes, because risks are managed in a distributed way over many resources and users and over time as decisions for managing risks are not over prespecified time for all. Understanding these fundamental interdependencies of core- and second-order variables is challenging and cuts across many disciplines. It has only been recently that it has become more critical to assess sustainability of electric energy systems. With this comes a difficult challenge of crossing discipline boundaries. Here we are specifically interested in the aspects of the interdependencies which could help identify how enhancing IT for future SEES could help more sustainable performance. This more modest task is discussed next.

2.8 The Key Role of IT for Relating Planning and Operations Industry Objectives

In the past, integrated resource planning to invest in large equipment was done for “proven” technologies only. The industry standards have traditionally been based on capacity-based thinking in order to ensure acceptable QoS even during very large equipment failures. The decision making has been largely based on deterministic worst-case performance thinking. Innovative technologies capable of enabling more efficient service have routinely gone unconsidered. This amounts to the planning process being a scenario analysis for finding the worst conditions and overbuilding just in case such an event takes place. In contrast, there has been some sporadic academic research on optimizing investments by managing of resources more efficiently in the actual operations; only a handful of utilities have done any planning with such an approach.

Consequently, significant extra capacity has had to be built to have sufficient standby reserve for full service during large equipment failures without having to resort to on-line corrective management of other equipments during the emergency. Using the SES framework, one can see, after the fact, that the load factor (the ratio of the average load to the peak load) and the generation utilization factor (the ratio of the energy used to the capacity rated energy) are generally low. These are possible quantifiable measures of a lack of alignment between the characteristics of the resources and the users. Shown in Figs. 2.5 and 2.6 are sketches of typical load factors for the islands of Flores and São Miguel.

The basic challenge facing new IT methods is how to increase both the load factor and generation utilization.

2.9 The Key Role of IT for Enabling More Efficient Operations

The five operations tasks listed above can be made more efficient by inducing a closer temporal, spatial, and contextual alignment of resources and users within a given governance system. We first assess these five tasks assuming a fully regulated governance system. Only the effect of enhanced IT on performance, without any change in the regulatory rules, is discussed next.

In a nutshell, the separation of operations Tasks 1, 4, and 5 generally leads to inefficiencies caused by poor knowledge of the intertemporal dependencies. The more accurate the predictions, the less need there is for fast-responding generation, automation, and expensive storage. In addition, relaxing the worst-case deterministic requirement for standby reserve, and relying instead on just-in-time corrective management by means of other available resources, generally contributes to major improvements of the load factors and generation utilization factors. Ensuring efficient spatial alignment by delivering just-in-place generally brings

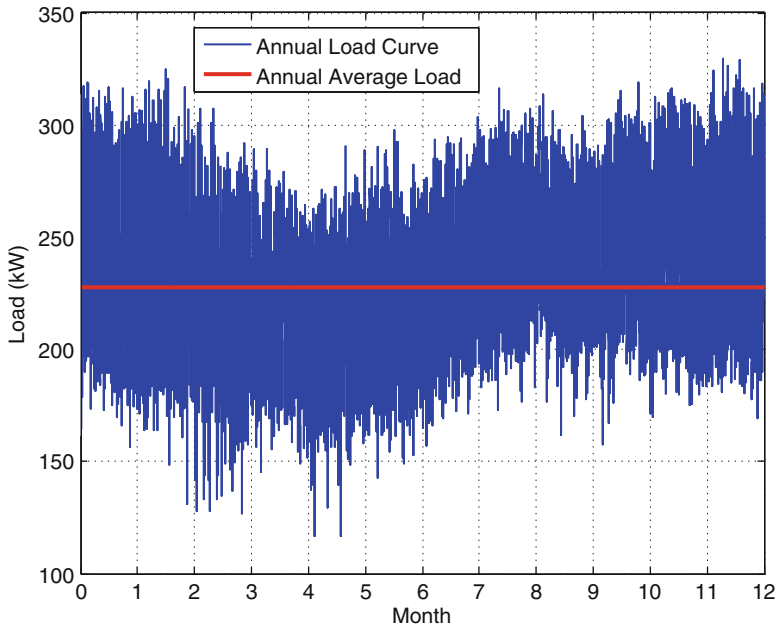


Fig. 2.5 Annual load profile for Flores, with load factor 0.69 [13], Chap. 4

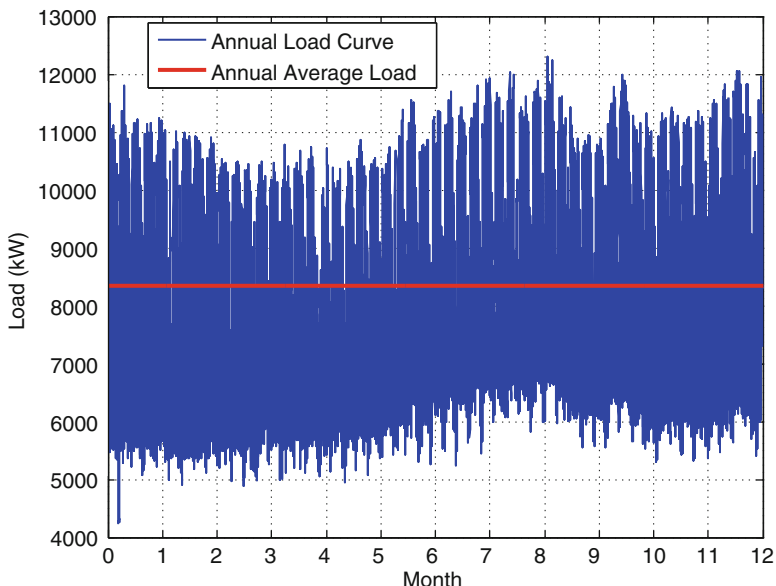


Fig. 2.6 Annual load profile for São Miguel, with load factor 0.6772 [13], Chap. 4

about considerable efficiencies in Tasks 2 and 3. Lastly, eliminating spatial network congestion requires a robust response to disturbances. Because of this, the major challenge is to design the IT so that both complex spatial inefficiencies and temporal inefficiencies are reduced.

2.9.1 DYMONDS Approach to Designing IT for Sustainable SEESs

An IT infrastructure complexity based on the attempt to re-bundle for sustainability in a centralized way is likely to become explosive as new technologies foreign to system operators connect to the existing grid. These technologies could connect in large numbers in the form of small dispersed renewable generation and responsive demand, and it will become excessively hard for the system operator to know technology-specific characteristics and to utilize them efficiently and reliably in synchrony with conventional resources.

To manage this unprecedented temporal and spatial complexity, we have proposed a multilayered approach to (1) internalizing decision making under uncertainties by the core components of the SEES (resources, users, governance system) and (2) exchanging information that aligns their temporal and spatial characteristics (the second-order and deeper-order variables). Resources, users, and governance system can either align their characteristics locally in a distributed way or rely on the others within the SEES to help. The complexity of information exchange and of the local decision making greatly depends on how much is done locally. A deployment and utilization of a handful of small distributed energy resources (DERs) generally does not require much information exchange or coordination with the rest of the system. The most difficult questions in future electric energy systems concern orderly scaling up of DERs without creating problems in operations. Using the language of traditional power industry, protocols for interconnecting DERs to the existing electric power grid must be introduced so that these resources are utilized efficiently and reliably. Our general approach is to design local IT that manages temporal and spatial complexities and uncertainties in a distributed model-predictive manner, and to require minimal coordination of the interaction variables that aligns the characteristics of the resources, users, and governance system that are not already aligned locally. This is the basis for our envisioned DYMONDS framework. Shown in Fig. 2.7 is our commonly used sketch of embedded DYMONDS within a complex SEES. As computational complexity is distributed into different groups of system users and the T&D system, the alignments of spatial and temporal second-level variables among the core variables of the once fully regulated governance system begin to occur by internalizing the intertemporal and the interspatial uncertainties given the predictions about the second-order and deeper-level variables. This internalization of the sub-objectives by the groups of core variables shapes the second-order and deeper-order variables.

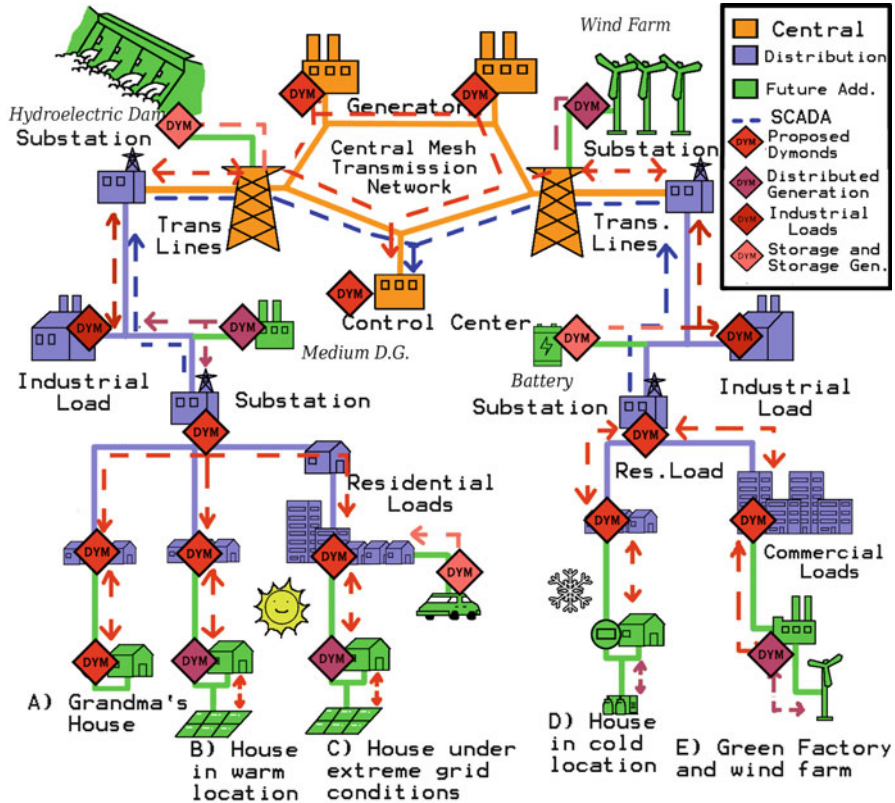


Fig. 2.7 DYMONDS architecture of electric energy future systems [4]

The information about these variables is exchanged interactively, and a minimal coordination of preferences, expressed by the core components in terms of their second- and deeper-level variables, is carried out in order to align these with the objectives of the SEES.

2.9.2 IT-Enabled Governance System Evolution for Sustainable SEESs

This framework ultimately leads to a new IT-enabled governance system in which the core variables make more complex decisions and have embedded automation for implementing their own sub-objectives, using a deep detailed knowledge about their own characteristics and preferences. Learning about the likely system conditions expressed in terms of second-order and deeper-order variables occurs in a

distributed way. The look-ahead, model-predictive decision making and automation occur when the groups of core components define their own ranges of choice for acceptable solutions. Minimal coordination at the SEES level takes place to align the ranges of choice by selecting the one which best aligns all the core variables according to the sustainability of the SEES as a whole. This somewhat abstract process underlies our DYMONDS framework. Different degrees of distribution for managing complex temporal and spatial uncertainties require different IT and automation.

Further work is needed to prove how the evolution of a governance system into distributed proactive core components, interacting among themselves and minimally coordinated at the SEES level, results in as optimal solution as possible for such a complex systems. It is important to recognize that this concept does not assume perfect information, after the fact, for assessing the performance of the SEES. Instead, information about the environment is sensed and processed by the core components for future predictions and decisions about the characteristics of the second- and deeper-order variables that need minimal coordination. The more transparent this information about the core components is and further into the future, the more likely the overall system will be sustainable for the ranges of choice given by the core variables [3].

This SES interpretation of the fundamentally different benefits from IT-enabled management of future energy systems can be supported by the formal mathematical derivation of the bounds on achievable performance created by interactive decision making within a complex system. The qualitatively new challenge is the design of adequate IT and automation that makes the most out of the given core variables within an SEES. This theoretical challenge is far beyond the scope of this chapter. It will keep the research community busy for some time to come, as it poses questions to learning in complex network systems while accounting for the multiple temporal, spatial, and contextual properties of the core variables embedded in the components of such systems.

In the next section we provide a guided tour of our book by offering sample IT methods for managing temporal and spatial interdependencies. Of particular interest is an explanation of how the computer algorithms and automation methods proposed present some common-sense IT enhancements and why they fundamentally support more sustainable performance of an SEES as a whole while enabling choice. The book organization is discussed as it evolves around the ideas of interactive re-bundling of the five operations tasks and the planning problem into a single operations-planning task under uncertainties.

2.10 Book Organization

We have organized this book in seven parts. Part I comprising Chaps. 1 and 2 introduces the basic thinking about the role of IT in making future electric energy systems more sustainable. Part II has two chapters that describe the two island

systems used in the book to illustrate the potential of the proposed concepts. Chapter 3 describes the overall electrical system characteristics of Flores and São Miguel islands in the Azores Archipelago. Chapter 4 provides data about today's generation and system demand characteristics for the two islands. Also, the wind power data for Flores is described and included. This information is used in all the other chapters to illustrate and compare the various concepts proposed. Use of the same system data throughout the book contributes to a highly unified information flow among the groups of otherwise different coauthors.

The remaining parts of the book mainly describe the enhanced IT methods and automation that are proposed to support the five operations tasks more sustainably and at choice. The last part of the book revisits the difficult question of rebundling the objectives of operations and investment planning subproblems under uncertainties in order to enable long-term sustainable use of available resources. We describe how the proposed architecture represents an evolutionary outgrowth of today's operations and planning practice by a careful relaxation of key hidden assumptions. Ultimately, the vision for enhancing IT in support of sustainable energy services becomes computationally less complex than the one employed by the industry today, but it requires an interactive information exchange infrastructure among the different industry groups of core components. A more specific tangible description of what these concepts mean is summarized next. The emphasis is on illustrating a few key performance improvements. The details of how this is done are presented in the specific chapters and parts of the book.

2.10.1 Part III: Predictions and Model-Predictive Look-Ahead Scheduling for Temporal Alignment in Operations

Part III concerns qualitatively new ways of performing unit commitment in future energy systems with many intermittent resources and actively participating demand. These methods are related to Task 1 of the operations methods for balancing supply and demand, in systems with intermittent resources, without explicitly considering the network delivery limitation.

2.10.1.1 Economic Dispatch and Unit Commitment Enhancements

Task 1 is the so-called unit commitment (UC) and economic dispatch (ED) task.⁴ The basic UC approach uses the 24-h or longer system demand forecast to select units which should be on and capable of generating power. While this forecast is not perfect, it is needed to support UC, which is the selection of power generation units that need to be up and running in preparation for economic dispatch closer to

⁴Operations tasks are based on [6], Chap. 2.

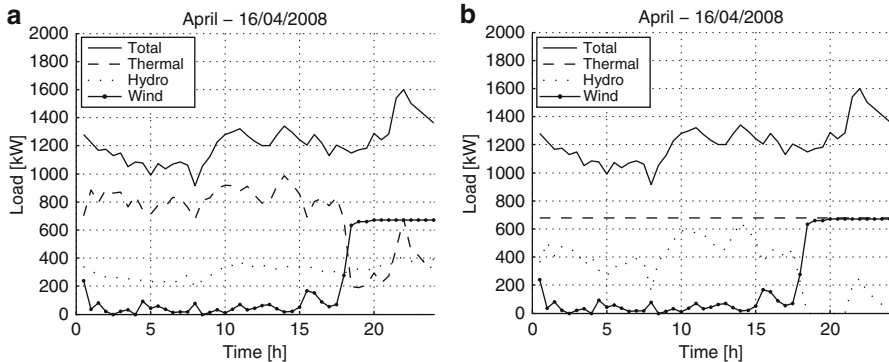


Fig. 2.8 Flores – Comparison, for the same day, assuming that there is (a) hydro generation with a reservoir and (b) hydro generation without a reservoir. It is assumed that there are 2 wind turbines in the system. (a) With the possibility of using hydro resources for peak shaving, diesel generation keeps steady throughout the day. (b) Without the possibility of using hydro resources for peak-shaving, diesel generation maintains the balance between demand and generation. The wind power profile plotted refers to the wind power available, not necessarily the wind power injected into the grid

real time. The industry practices and software used are often system-specific and not fully standardized. Part III concerns possible enhancements based on the predictions and look-ahead model-predictive dispatch.

It is important to understand today's hidden inefficiency when performing static economic dispatching in light of the system's inability to align the temporal characteristics of power plants with the temporal characteristics of users. This inability to align the temporal characteristics of resources and users generally leads to excessive use of fast and expensive load-following units, gas power plants in particular. Enhancing the ramp-rate-limited dispatch by relying on predictions and look-ahead dispatch overcomes the need for expensive resources, with IT supporting predictions and model-predictive dispatch enabling less expensive resources to supply varying the demand forecast.

In Chap. 5, unit commitment and economic dispatch are performed based on the computer methods typically used at present. The objective of this chapter is to provide a benchmark assessment of the impact of wind penetration on the generation O&M cost. Of particular interest is how much wind power must be “spilled” in order to balance the supply and demand, given the system demand profile for the islands studied. It is assumed that the system operator has full knowledge and control of the generation resources and system demand. Shown in Fig. 2.8 is a representative simulation of generation dispatch on Flores with seven wind power units [13].

Several follow-up chapters in this part of the book introduce novel ways of balancing supply and demand in systems with large uncertainties. To start with, in Chap. 7, we illustrate the use of model-predictive generation dispatch assuming given system load. A mathematical formulation of look-ahead model-predictive economic dispatch observes the ramp rates and utilizes the knowledge of predicted

Fig. 2.9 Generation based on static dispatch (method 1) on Flores for Apr 16 [13], Chap. 7

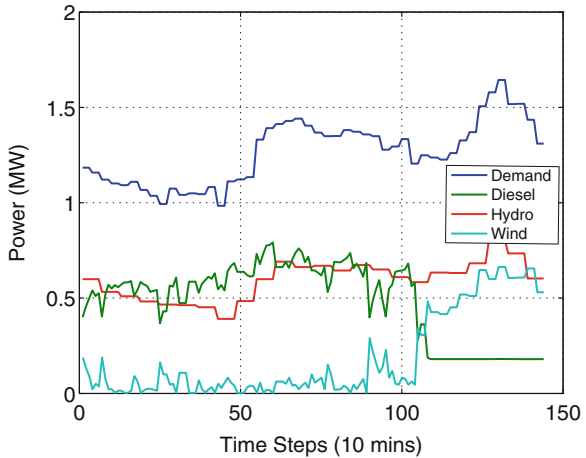
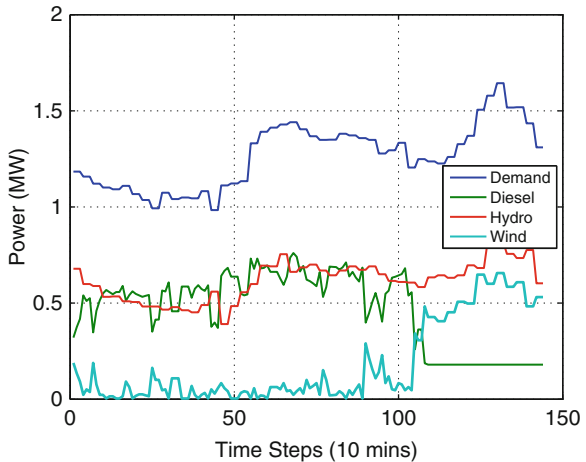


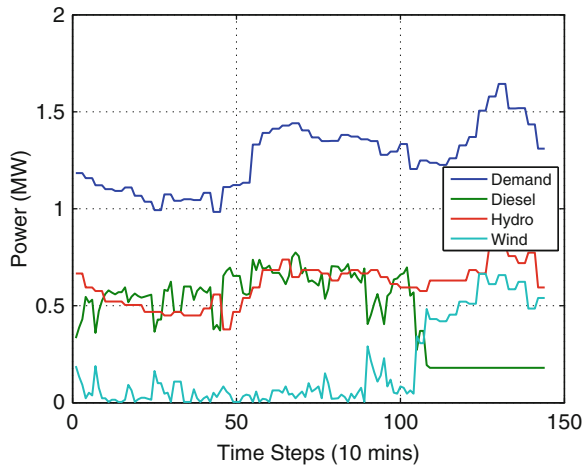
Fig. 2.10 Generation based on (method 2) look-ahead dispatch (method 2) on Flores for Apr 16 [13], Chap. 7



maximum wind power generation. For the small island of Flores it is shown that optimizing hydropower to balance the varying wind forecast enables a more economic utilization of the overall generation and results in less use of expensive and polluting diesel power on the island. This is shown for illustration purposes in Figs. 2.9 and 2.10, in which a comparison of conventional economic dispatch and look-ahead economic dispatch is seen. It can be concluded from these two figures that by predicting the wind power and by optimizing over longer time horizons, it becomes possible to schedule even slower resources, like hydropower on Flores, and, consequently, require less fast-responding expensive and polluting diesel power generation.

Figure 2.11 compares generation dispatch by distributed model-predictive look-ahead dispatch with centralized model-predictive economic dispatch. An important distinction between centralized model-predictive UC/ED and model-

Fig. 2.11 Generation based on distributed look-ahead dispatch (method 3) on Flores for Apr 16 [13], Chap. 7



predictive distributed decision making by the system users (the generators and consumers) is that in the latter the intertemporal constraints, the ramp rates in particular, are internalized in a distributed way. A comparison of the two dispatch methods is illustrated in Table 2.1. It can be seen that the simulations show that the two approaches, namely, the complex centralized look-ahead unit commitment by all the power plants, performed by the system operator, and the distributed UC/ED by the system users, result in an almost identical optimum (modulo small duality gap) [12, 13], Chap. 7. Nevertheless, there remain interesting and potentially relevant alternatives to using distributed UC/ED. These alternatives are presented in Chap. 10.

2.10.1.2 The New Role of IT-Enabled Demand Participation in Scheduling

The follow-up Chaps. 8 and 9 explore the potential of demand participation in balancing highly varying wind and hydropower. Chapter 8 in particular provides an assessment of candidate consumers on Flores and São Miguel whose loads may be able to participate proactively in balancing supply and demand. It is explained why refrigeration and air-conditioning on Flores have relatively small potential to affect the imbalance created by the wind variations (Figs. 2.12 and 2.13). On the other hand, a more industrial and commercial part of São Miguel could contribute quite significantly to longer-term, seasonal and annual scheduling (Fig. 2.14). A particular emphasis is on the relation between the time scale at which demand participates (multi-annual planning by the regulators and utilities that count on demand participation and reward the participants accordingly; seasonal agreements with utilities at well-defined and quantifiable time-of-use (ToU) rates; day-ahead (DA) and/or real-time (RT) (10 min) dispatch; direct load control (DLC) in emergencies).

Table 2.1 Daily dispatch cost comparison (\$) for Flores [13], Chap. 7

Date	Method 1	Method 2	Method 3
Jan 16	4,017.11	3,953.94	3,970.28
Apr 16	4,676.08	4,604.45	4,633.94
Jul 16	8,287.53	8,257.15	8,290.98
Oct 15	8,890.01	8,890.01	8,890.01

Fig. 2.12 Air-conditioning load based on day-ahead dispatch for July 16, 2008, on São Miguel [13], Chap. 9

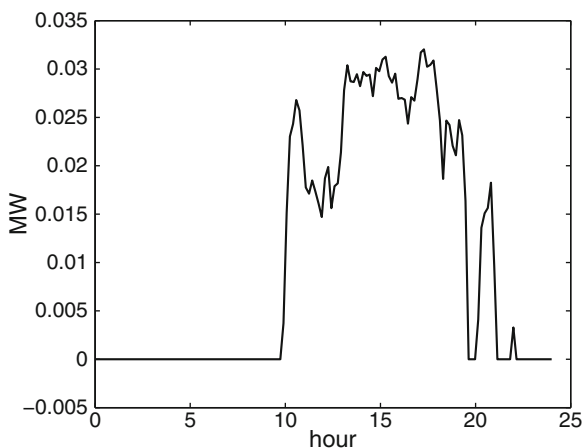
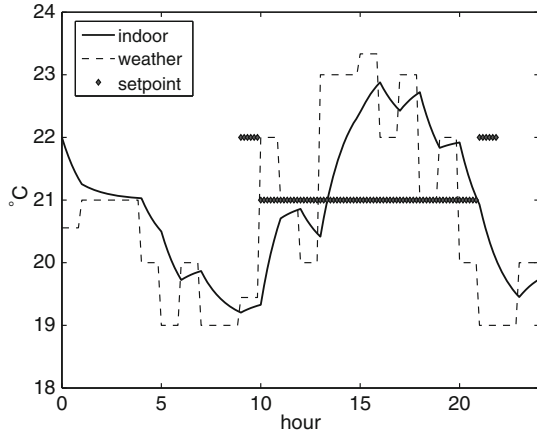


Fig. 2.13 Temperature inside the mall assuming air-conditioning load dispatch under day-ahead scheduling for July 16, 2008, on São Miguel [13], Chap. 9



The relationship between customers' tariffs, their energy needs and preferences, and the IT-enabled participation in energy balancing are discussed.

Chapter 8 summarizes the concept of adaptive load management (ALM) which is qualitatively different from a more typical DLC. The consumers internalize their own physical characteristics and preferences for the anticipated electricity prices and offer simple bids to the system operator regarding how much and at which hours they would need electricity and how much they are willing to pay for the services. These bids are binding, and the system operator can count on demand response to help compensate for wind deviations, for example, at mutually agreed-

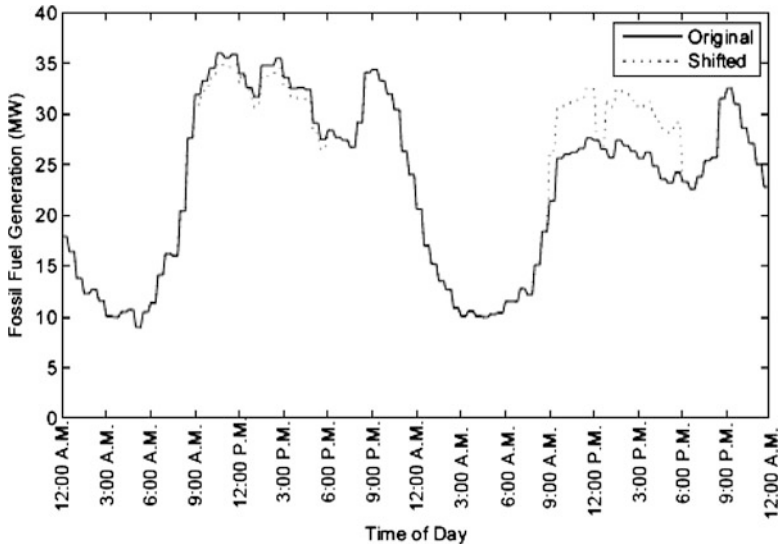


Fig. 2.14 Original and shifted fossil fuel for a Friday and Saturday [13], Chap. 8

upon prices. An important point is made that such agreements could be defined for time-of-use (TOU) instead of only day or hour ahead. ALM is an important concept that facilitates both choice by the consumers and selection by the system operator of the demand bids that will help most to balance the supply.

2.10.1.3 IT-Enabled Efficient Scheduling of Electric Vehicles

Finally, in Chap. 11, the potential of electric vehicles for balancing wind power deviations on the island of Flores is assessed. Two key observations follow from this chapter: first, for the islands which burn a great deal of very expensive diesel fuel, one can make the case that the cost of the infrastructure necessary to implement electric vehicles would pay off even without accounting for the environmental costs. Second, the assessment of electric vehicle potential must be done against an incremental cost that includes the capital cost, rather than just using short-term marginal cost (Fig. 2.15). The value of EVs compensating for wind power and displacing the use of very expensive diesel fuel is sufficiently high that it would make sense to allow wind power to be charging such an incremental (levelized) cost. This way, a combined investment in wind power plants to replace diesel plants, and in EVs as the key storage needed to manage volatile wind in a feed-forward way, becomes a viable subsidy-free business arrangement. Shown in Fig. 2.16 are typical charging patterns of EVs relative to predicted wind power patterns. It can be seen that significant cost savings are possible with a smart distributed look-ahead scheduling of wind power and EVs. Shown in Tables 2.2 and 2.3 are the estimated cost savings and emission impacts if such new IT-enabled scheduling were in place.

Fig. 2.15 Long-run marginal cost (LRMC) curve based on the marginal cost of diesel generators, the expected amount of produced energy, and the value of loss of load [13], Chap. 11

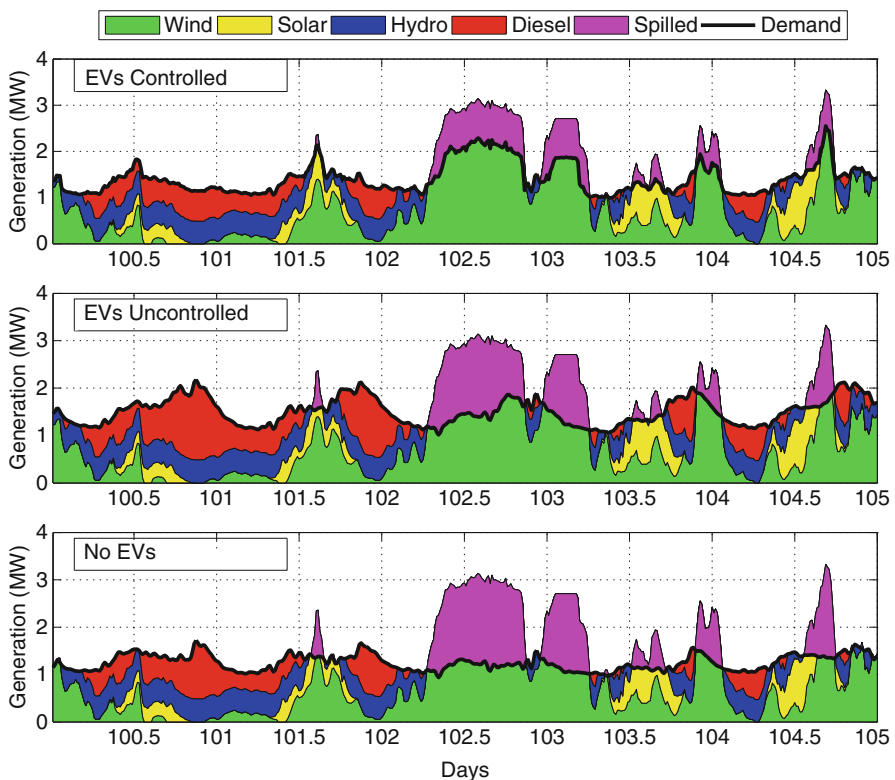
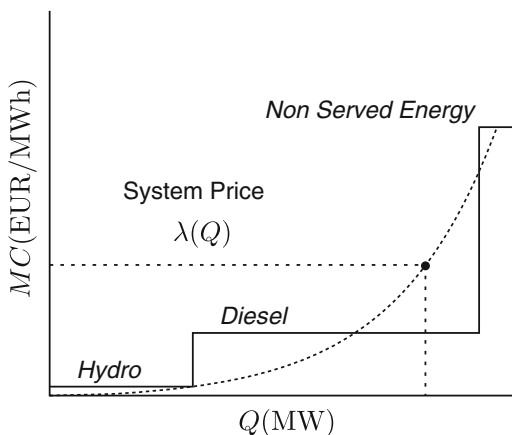


Fig. 2.16 Use of different generation types for a period in spring with 1000 EV scenario when there is moderate wind and solar power available [13], Chap. 11

Table 2.2 Total (electricity generation + vehicle emissions) yearly CO₂ emissions in kton for different scenarios [13], Chap. 11

Electricity scenario	Vehicle scenario				
	All diesel	50 % EVs uncont.	50 % EVs cont.	100 % EVs uncont.	100 % EVs cont.
ICE					
Current generation mix	8.38	8.08	8.06	7.80	7.76
Moderate wind and solar	6.18	5.37	4.65	4.26	3.05
Aggressive wind and solar	5.52	4.42	3.29	3.13	1.29

Table 2.3 Percentage of spilled renewable generation (wind + solar) for different scenarios

Electricity scenario	Vehicle scenario				
	50 % No EVs	50 % EVs uncont.	50 % EVs cont.	100 % EVs uncont.	100 % EVs cont.
ICE					
Current generation mix	0	0	0	0	0
Moderate wind and solar (%)	28	21	10	23	8
Aggressive wind and solar (%)	49	42	30	45	29

Recall that the amounts of installed renewables are larger in the case with 100 % EVs by approximately 20 % [13], Chap. 11

2.10.1.4 DYMONDS-Enabled Azores Islands

In closing, we refer to the prediction and model-predictive look-ahead algorithms described in Part III that are to be embedded into the distributed decision makers (the resources and demand), combined with the supporting IT-enabled information exchange with the system operator, as the DYMONDS modules shown in Fig. 2.7 above [11]. We have illustrated how this framework enables both choice on the part of the system users, wind power plants, conventional power plants, responsive demand, and EVs, and also the alignment of all of these with the system operators and planners responsible for ensuring system-wide performance. The IT signals needed for the centralized, on the one hand, and distributed, on the other, alignment of second-order temporal variables between the core variables and the system operator are qualitatively different. Fundamentally, more processing, sensing, and decision making takes place at the core variable level when using DYMONDS, thus requiring minimal information exchange about their second- and deeper-level variables. In a centralized industry, the control centers require major computer-intensive algorithms and centralized SCADA and make decisions on behalf of the core components within an SEES.

2.10.1.5 IT-Enabled Predictions of Temporal Characteristics

The above recently proposed model-predictive look-ahead economic dispatch critically depends on accurate short-term 10-min wind prediction and load

prediction [11,12]. It is with this importance in mind that Chap. 6 derives a family of multi-temporal predictive wind power models using data from Flores. An innovative approach to decomposing the historic wind power data into their slow, medium, and fast components, and deriving predictive models for each component separately, is described. It is illustrated how this approach provides much higher accuracy than when predicting wind power without such decomposition. The models derived range from short-term 10-min predictions to 1-h-ahead and 24-h-ahead predictive models that are needed for data-driven feed-forward look-ahead dispatch. Shown in Figs. 2.17 and 2.18 is the temporal decomposition of the wind power and load power signals for the island of Flores [13], Chap. 6. Alternatively, Markov model-based decision trees are derived for both short- and long-term probabilistic decision making; an illustration of such a decision tree, this one indicating short-term load states, is shown in Fig. 2.19. In this chapter long-term predictive models are also derived, and these can be used for formulating the planning problems for systems with wind power as discussed in Chap. 20 of this book.

2.10.2 Part IV: Efficient and Feasible Power Delivery During Normal Operating Conditions

The complexity of balancing the multiple objectives of system operations with corrective resource management of various equipment is a major challenge that needs to be assessed in light of SEES sustainability objectives. In Part III, enhanced IT methods that schedule real power to balance supply and demand by aligning the temporal characteristics of resources and users within an SEES are introduced. It is often not possible for the T&D power grid to deliver this optimal power schedule. The difficulties of aligning resources and users spatially are reflected in a reduced efficiency of economic dispatch, caused by either delivery losses or the inability of the physical grid to deliver to the right locations.⁵

Task 2 concerns delivery loss compensation for the forecast system demand. Because of delivery losses, it is generally necessary to produce more generation than the forecast demand. Over the years, many centralized computer methods for estimating system losses, and for scheduling the generation needed to compensate for them, have been proposed. In Chap. 12 we illustrate how careful placement of DERs can reduce delivery losses (operation Task 2) significantly. In operations, optimizing the set points of voltage-controllable T&D and generation equipment can contribute to delivery loss reduction. Shown in Chap. 12 is a method for minimizing transmission losses by DER placement and/or by optimizing T&D and generation voltage-controllable equipment. These methods are illustrated using the islands of Flores and São Miguel. Notably, as the industry paradigm shifts, it may become

⁵This is not a common way of thinking about T&D losses and/or power grid congestion. However, we find it extremely useful, since it directly provides a measurable way of relating how efficiently the resources can provide energy to the users.

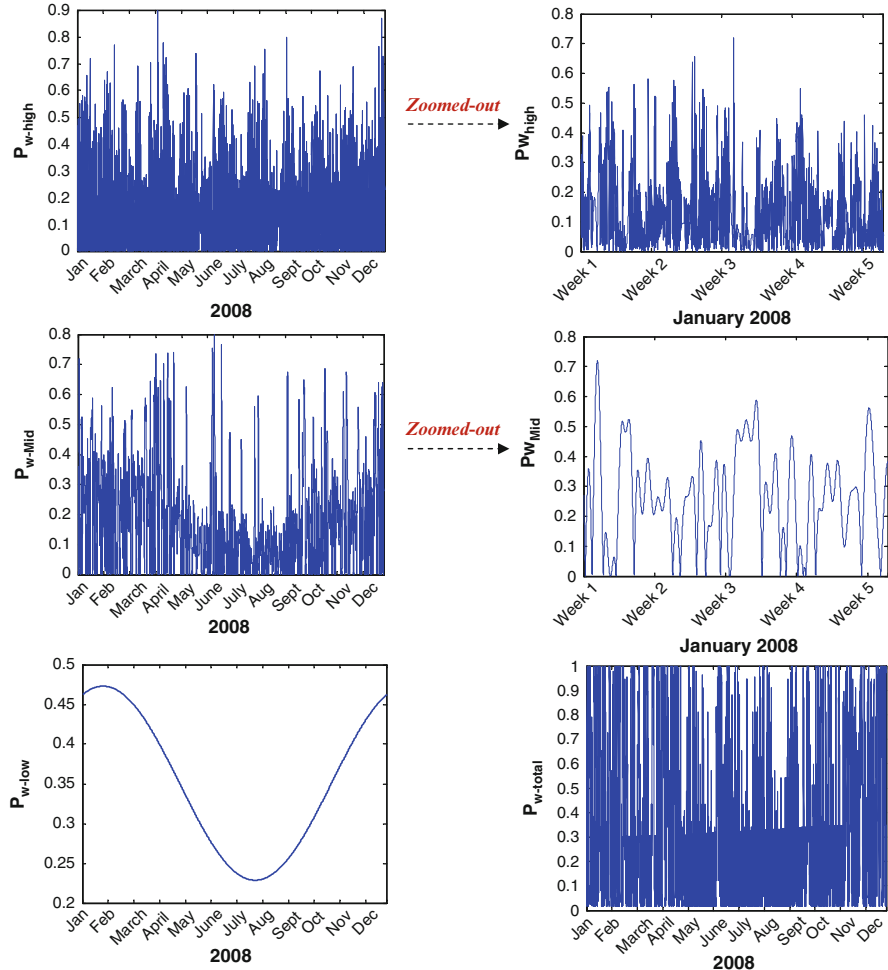


Fig. 2.17 Low- medium- and high-frequency components of normalized wind power in Flores (330 KW capacity) [13], Chap. 6

possible to implement approximate loss compensation by means of the power plants themselves estimating their contribution to delivery losses and then each of them producing a bit more real power, without relying on the system operator and the complex inaccurate allocation of losses.

Task 3 concerns the feasibility of the generation scheduled supplying the forecast demand. The network constraints are often accounted for closer to real time, say 1 h or 10 min ahead of time. For purposes of understanding the evolution that will be necessary in future electric energy systems, it is important to observe here that the system limitations to delivering the most economically and environmentally

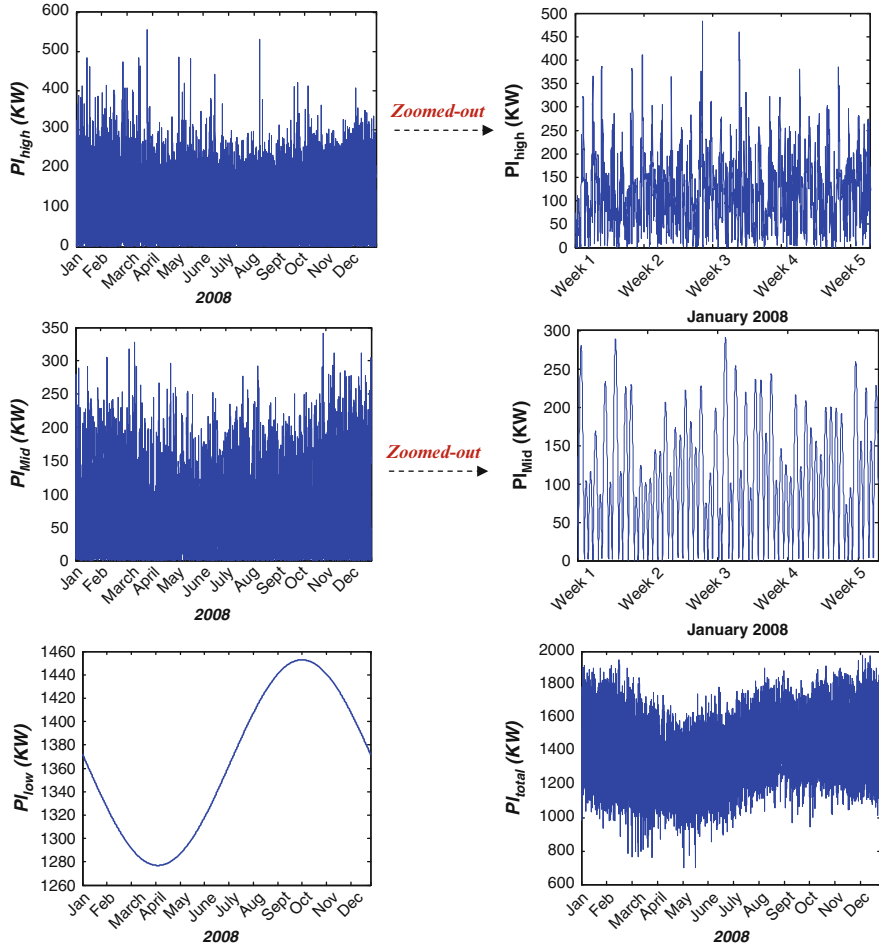


Fig. 2.18 Low-, medium-, and high-frequency components of load power in Flores [13], Chap. 6

desirable power are quite complex.⁶ We illustrate in this chapter the importance of relaxing often conservative system delivery limit⁷ by implementing an IT-enabled optimization of the set points on the controllable equipment. This is achieved primarily by enlarging the feasible region of power delivery through an active optimization of the most effective equipment settings. In Chap. 13, we illustrate the potential of an AC extended optimal power flow (AC OPF) to be a basic

⁶Task 3 (optimization of the voltage controllable T&D, generation and demand equipment) can be interpreted, in light of sustainable SEES IT design, as being particularly important for aligning the spatial characteristics of the core variables.

⁷Recall the notion of proxy line flow limit, Chap. 1.

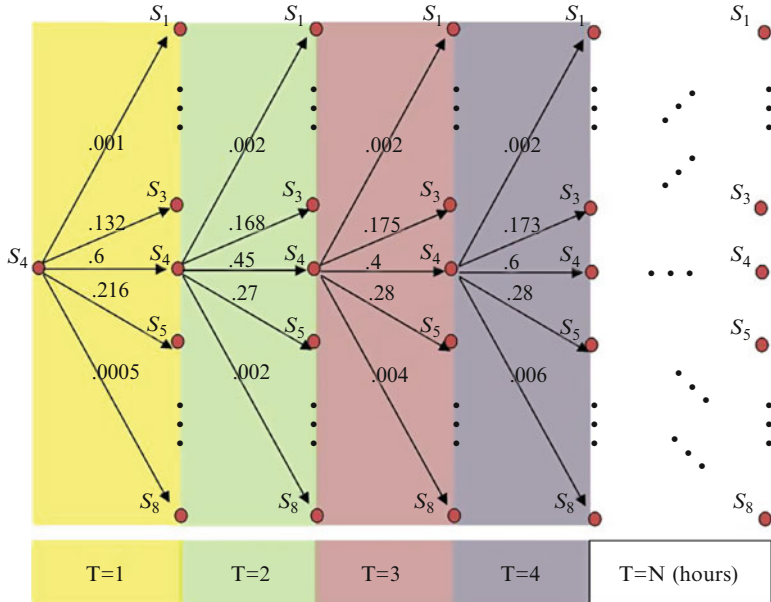


Fig. 2.19 Load power short-term uncertainty/decision tree [13], Chap. 6

means of implementing corrective resource management in future electric energy systems [7, 14]. We illustrate how such near-real-time corrective actions contribute significantly to the efficiency of the power delivery. It is shown in this chapter that a systematic optimization of voltages as real power generation dispatch is done can be beneficial for managing both thermal and voltage-related system congestion. This voltage optimization can be implemented by adjusting the set points of the generator controllers and the set points of T&D controllable equipment such as onload tap-changing transformers (OLTCs) and capacitor banks. In the future, the set points of voltage-controllable DERs could become an important means of managing voltage. In Chap. 13 we illustrate the potential of AC OPF to bring about less costly dispatch and power delivery in both Flores and São Miguel.

2.10.3 Part V: Enhanced IT Methods for Intra-dispatch Automated Frequency and Voltage Regulation and Stabilization

Part V concerns the challenge of balancing supply and demand during normal conditions within the intervals when UC/ED is done, operations Task 4 [2]. It is assumed that the ED is performed every 10–30 min and that intra-dispatch power deviations are hard-to-predict. In today's industry intra-dispatch balancing is done by means of automatic generation control (AGC), which responds to

frequency deviations caused by power imbalances around the forecast demand. Smaller power systems, such as islands, may not have AGC; they have, instead, a few fast-responding units, whose governors are Proportional Integral (PI) controllers that correct for the time error resulting from the cumulative frequency deviations around the nominal frequency. Automated voltage control (AVC), which responds to voltage deviations due to reactive power imbalances in major loads, is much less frequently used, except in Europe. This is particularly true since, at present, even the feed-forward scheduling of controllable reactive power resources is not a common practice.

Both AGC and AVC differ fundamentally from the feed-forward dynamic scheduling of resources since they are both automated schemes reacting to frequency and voltage deviations caused by inaccurate feed-forward schedules. Their design rests on the assumption that power imbalances are zero mean around the forecast values. However, in future electric energy systems with a large presence of hard-to-predict and hard-to-control DERs, the nature of deviations around the forecast and look-ahead schedules is likely to change in fundamental ways. Notably, the deviations may have a significant nonzero mean and would, therefore, require different methods for balancing intra-dispatch imbalances.

In Chap. 14, we pose the problem of intra-dispatch load following, frequency regulation, and stabilization as a temporally interdependent design problem. Instead of using the static notion of ramp rate, it becomes critical to understand the dynamic capabilities of the different technologies to respond to imbalances at certain rates. Examples from Flores and São Miguel are used to illustrate different candidate technologies. In this chapter we begin to differentiate between the load-following function and the frequency regulation function. The load-following function is the slower of the two, and it ensures that sufficient mechanical power is produced and available for balancing load deviations and for frequency regulation. For example, if UC/ED is performed each half hour, the load-following function could be performed every 10 min, and the frequency regulation would have the objective of ensuring frequency quality within 10 min.

Notably, the novel load-following model in this chapter has power generated as explicit states and is therefore capable of tracking which power plant contributes how much to ensuring intra-dispatch frequency quality. This has been hard to do with presently used AGC models, since the steady-state frequency is almost identical throughout the entire system. One more distinct advantage of working in the extended state space where phase angles are replaced by the power generated as states [5] is that new, stationary resources, such as batteries in particular, are easier to characterize in terms of their power generated. This model is an alternative to the conventional quasi-stationary power-balancing approach that compensated for the area control error (ACE) without accounting for the electrical characteristics of the power grid. Shown in Figs. 2.20 and 2.21 is the locational effect of wind power disturbance (Fig. 2.22) for a power plant placed at two different locations on São Miguel. The effect on the regulation power required and the resulting frequency quality are very different, indicating that the locational effects in systems with electrically distant connections should be modeled and controlled. In addition, depending on which power plant follows the wind disturbance, and which is the

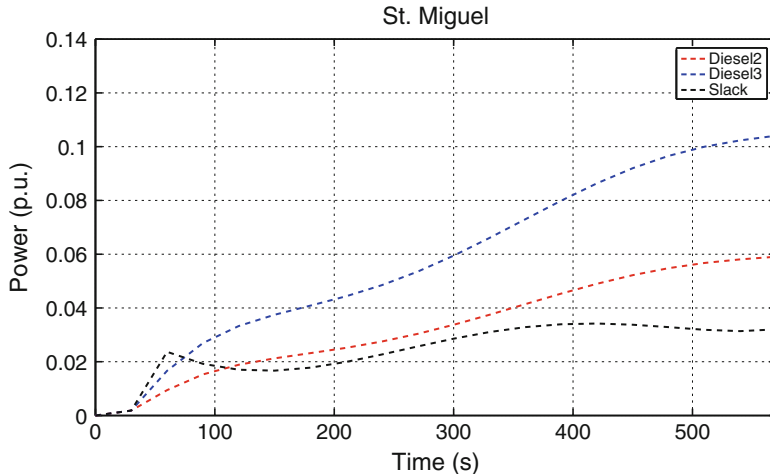


Fig. 2.20 Wind farm placed at Bus-4 on São Miguel [13], Chap. 14

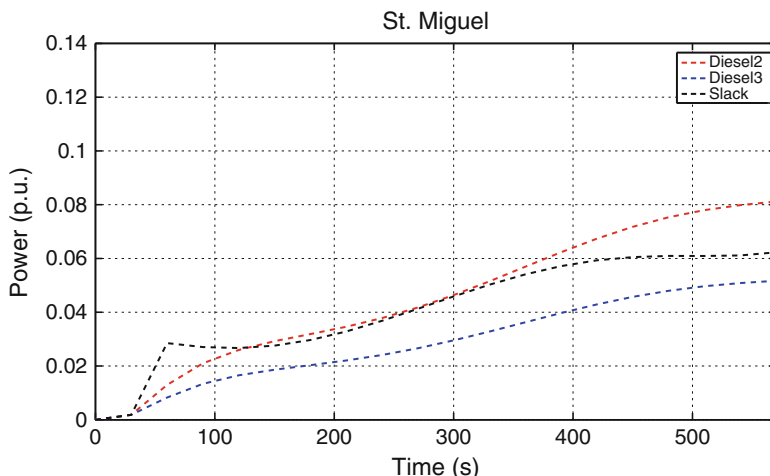


Fig. 2.21 Wind farm placed at Bus-15 on São Miguel [13], Chap. 14

slack generator, the load-following cost differs qualitatively as shown in Fig. 2.23. More generally, based on studies in Part V of this book, we arrive at a general conclusion that the smarter the IT can be in enabling the use of slower technologies first, the lower the overall cost of managing the system will be.

In Chap. 15, we revisit the objectives of frequency stabilization and frequency regulation and design criteria needed to ensure that the frequency remains stable and that it remains within the prespecified industry standards in future electric energy systems characterized by persistent dynamically fluctuating wind perturbations. We point out that the steady-state notion of AGC will no longer be adequate to

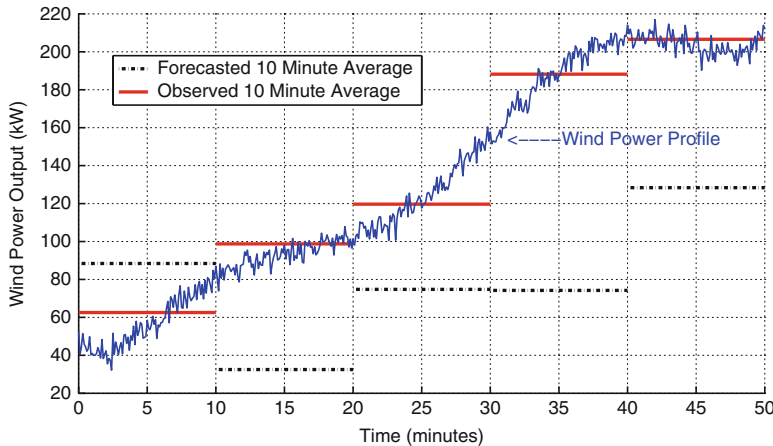


Fig. 2.22 A 10-min-ahead wind power forecast and actual [13], Chap. 14

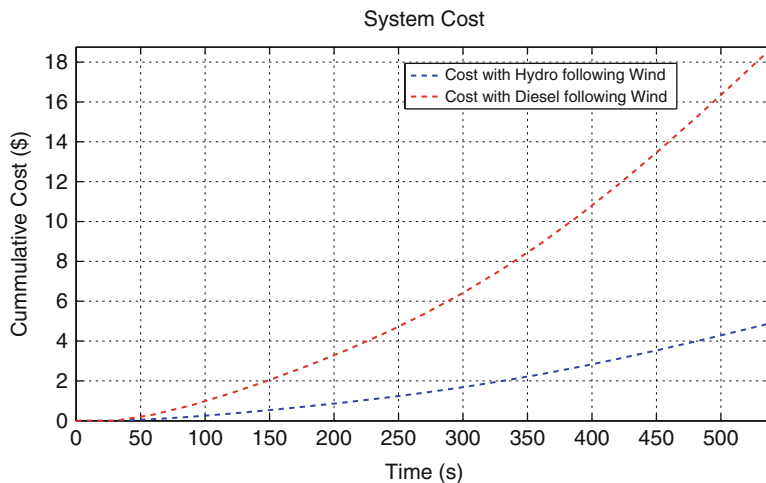


Fig. 2.23 Comparison of cumulative 10 min cost [13], Chap. 14

regulate frequency in such systems, and we propose, as an alternative, a framework for assessing potential instabilities and systematic methods to stabilize and regulate frequency. The means to regulate frequency come in the form of the governors of conventional power plants and, when necessary, fast energy storage devices, flywheels in particular. The results of this new framework are illustrated using the Flores and São Miguel island systems. It is concluded, ironically, that the wear-and-tear costs to the conventional power plants whose governors participate in frequency stabilization and regulation would become excessive, and it is with this in mind that “when necessary” the devices—flywheels—are proposed as the main alternative.

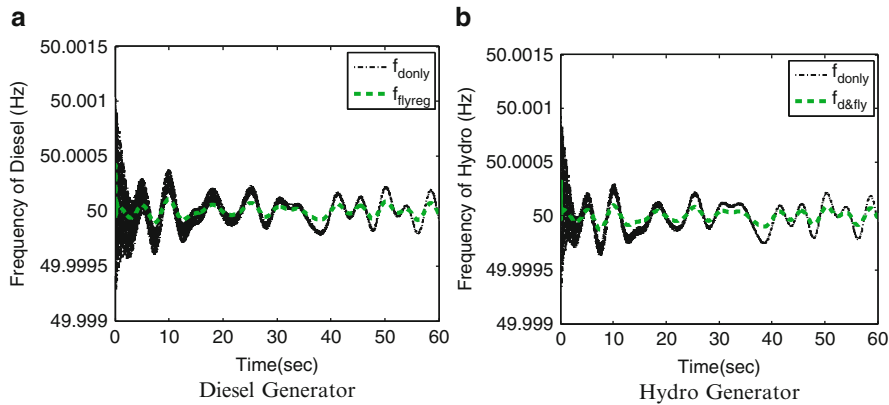


Fig. 2.24 Time response of frequency on Flores island, system with negative load wind generator [13], Chap. 15

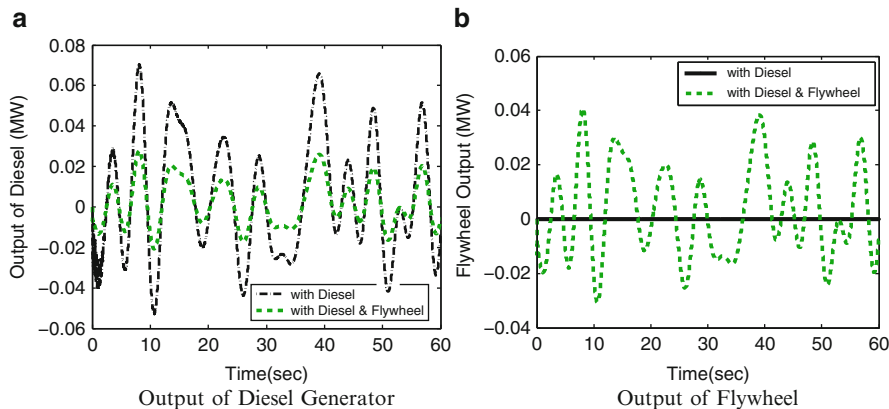


Fig. 2.25 Output of diesel and flywheel in response to frequency deviations, system with negative load wind generator [13], Chap. 15

The use of synchrophasors as sensors of fast measurements is critical for implementing this enhanced frequency stabilization and regulation control. In Fig. 2.24 the time responses of diesel and hydro generators' frequency with/without flywheels participating in frequency control are compared. Improvement in frequency quality can be seen when flywheels are coordinated so that they compensate for wind power disturbances and enable prespecified frequency quality. We further compare the wear and tear to conventional power plants before and after flywheels are utilized. It is shown in Fig. 2.25 that the diesel generators contribute much less to the balancing of disturbances after flywheels begin to participate. Therefore, we see that the wear and tear, caused by fast disturbances, on conventional generators can be reduced.

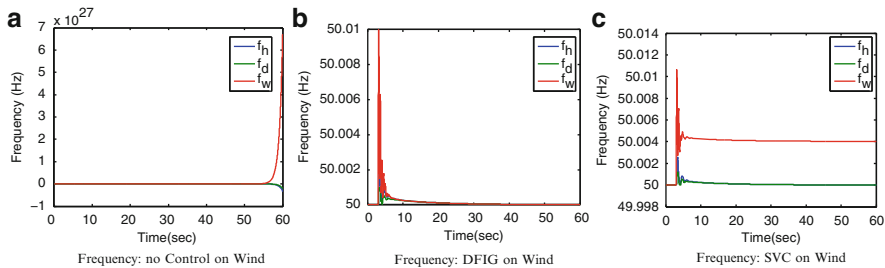


Fig. 2.26 Time response of the system with wind induction generator, large electrical distance [13], Chap. 16

Next, in Chap. 16, we explore the possibility of using the excitation control and advanced power system stabilizers (PSSs) of conventional power plants to stabilize system dynamics excited by persistent fast wind power fluctuations. This can be done by designing the control of the electromagnetic energy stored in the rotor windings to stabilize the electromechanical power imbalances responsible for the frequency fluctuations. Therefore, there is a need to derive and use a coupled real power-voltage model for such a control design. To fill this need, a new modeling and control design for the interconnected system is introduced, and this alternative is illustrated using Flores system. A coupled linearized real power-voltage model of the interconnected system in standard state space form, with the phase angle as the key state to be measured and controlled, is derived for the first time here and combined with the complex model of the wind power plant [5].

When the electrical distance between the wind and the main power grid is large, it is essential to have sufficient local wind control. Otherwise, the system becomes small-signal unstable, even with the excitation control of diesel and hydro power plants as shown in Fig. 2.26 for the island of Flores. We compare the effects of power electronics control of the wind power plant (DFIG) and the grid FACTS device (SVC), as shown in Fig. 2.26.

Finally, in Chap. 17, in order to analyze possible instabilities in future electric energy systems, we introduce a different state-space model, an extended state-space-based model in which real power generation is an explicit state. It is shown how this modeling approach helps to analyze the effect of electrical interactions between the stable stand-alone dynamic components. Sufficient conditions for deciding the minimum electrical distance between the power plants are illustrated to ensure that the plants' interactions do not become unstable. The dynamics of Flores and São Miguel are studied, and it is shown that the decoupled real power-frequency model may indicate that the interconnected system remains stable when the individual dynamic components are stable. However, the coupled extended state-space-based real power-voltage model could exhibit small-signal instability for certain governor gains. The extended state-space model of São Miguel exhibits interesting network-wide interactions since some parts of the system are strongly

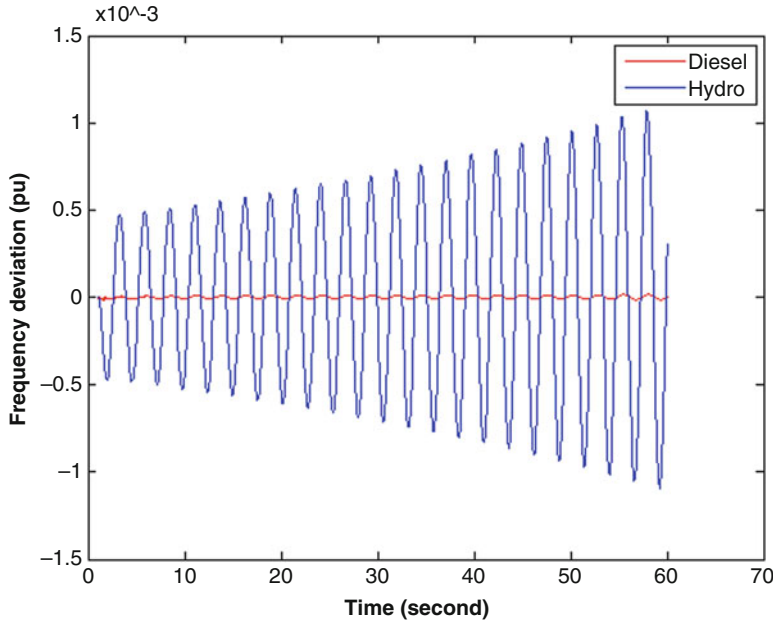


Fig. 2.27 Unstable frequency response to a small wind power disturbance [13], Chap. 17

coupled and others are weakly coupled. Notably, when new wind power generation is placed at the locations determined by the loss minimization criteria in Chap. 12, the interconnected electric power system may exhibit instabilities due to swings created through the dynamic interactions of power plants. The use of extended state space indicates that the power generated contributes directly to the power swings between the different generators and, ultimately, to unstable operations (Figs. 2.27 and 2.28).

This part of the book provides the reader with a family of models and control/communications designs that might be needed to ensure acceptable dynamic performance in future electric energy systems within the intra-dispatch intervals. Based on the simulation results, we conclude that the modeling must be done systematically to represent sufficiently accurately the subprocesses evolving at time scales of interest, without neglecting the effects of other subprocesses in the reduced-order models. Moreover, since this part of the book concerns both analysis and control design, the models used are in so-called standard state-space form; generally, the dynamics of state variables are determined by the state variables, control input, and disturbances. All models used in this part of the book represent models of the interconnected power grid. As such, they lend themselves to systematic communications and control design that meets desirable dynamic performance, as opposed to models that are primarily concerned with analysis of system response during different scenarios.

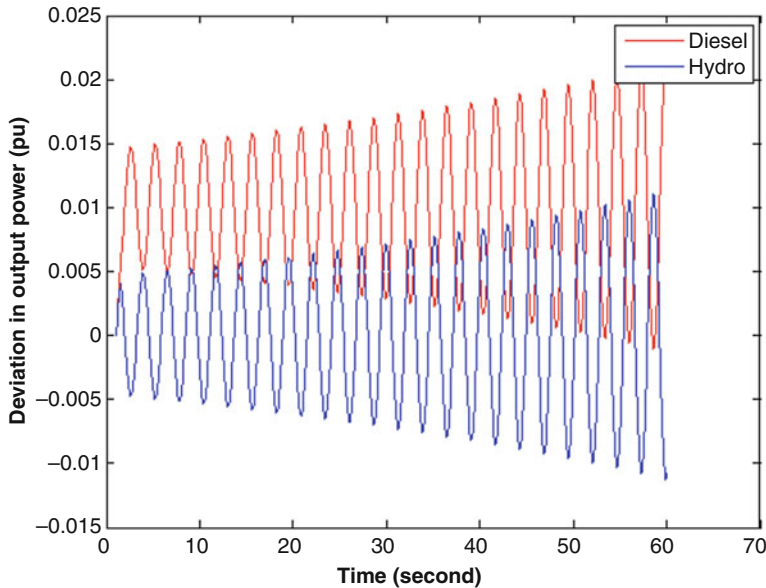


Fig. 2.28 Unstable power output changes in response to a small wind power disturbance [13], Chap. 17

2.10.4 Part VI: IT-Enabled Corrective Resource Management for Transient Stabilization and Reliable Operations During Contingencies

Next, Part VI of this book concerns how to ensure that service is not interrupted and remains reliable, during forced low-probability high-impact equipment outages. We observe that ensuring uninterrupted service in systems with a large penetration of hard-to-predict and hard-to-control resources presents the industry with a major new challenge. This is fundamentally the case because all industry reliability standards are currently designed to ensure that during the “worst-case” equipment failure customers do not get interrupted in major ways. This is generally achieved by carrying out detailed off-line simulations and finding the worst-case scenarios, accumulating standby reserve, and operating preventively even during normal conditions just in case a large equipment outage takes place. This preventive approach generally results in a dispatch of more expensive generation during normal conditions; the estimated inefficiencies in some large US utilities are on the order of 20 % of the generation O&M cost.

Relying on more on-line monitoring, and on more flexible and adaptive adjustments of other available equipment during major equipment failures, could bring about the most benefits. We describe the cumulative costs associated with preventive and nonadaptive operations that are currently done for the sake of

reliability. We strongly recommend that the state-of-art IT be such that it is possible to implement on-line adjustments for many non-time-critical changes in generation output and equipment status. We illustrate the potential savings from optimizing the settings of voltage-controllable generation and T&D equipment, such as automatic voltage regulators (AVRs), OLTCs, and shunt capacitors (SCs). We show, using the examples of the electric systems on Flores and São Miguel, how feed-forward corrective actions in combination with corrective actions during non-time-critical equipment failure can be used to ensuring reliable services and reduce the amount of standby reserve (and therefore the cost associated with it) considerably.

In Chap. 18 we consider the idea of reducing standby central generation reserve in distribution systems with reconfiguration of normally open switches (NOSs) and of normally closed switches (NOCs) during faults. A very recent algorithm that utilizes active switching of connection to serve customers according to prespecified priorities is discussed using distribution power grid on Flores. A detailed analysis is able to illustrate potential differentiated reliability of service that minimizes the liability cost paid by the Electricite de Azores (EDA) in case customers have to be interrupted. A cost-benefit estimate of reconfiguration infrastructure deployment on Flores is presented. To our knowledge, this is the first analysis of its kind. Having a systematic method for assessing the cost of reconfiguration infrastructure that enables differentiated use of DERs in distribution systems is likely to become critical to implementing differentiated reliability at choice made by the users. Notably, remote fast communications and control between the control center and the major substations and DERs will become the staple of future reconfigurable smart distribution systems.

Next in Chap. 19 we introduce the concept of transient stabilization in systems with wind power by means of power-electronically controlled fast storage. We suggest that this type of automation will become critical for the prevention of stability problems in moments when sudden large-amplitude short duration or large-amplitude persistent deviations of wind power around the predicted outputs occur. There have already been many occurrences of major electricity service interruptions in parts of the world where there is a major dependence on wind power. Hard-to-predict wind gusts are likely to become more frequent as more intermittent wind power is being deployed. Typical wind gust disturbances are shown in Fig. 2.29. Short-term high-magnitude wind power perturbation is simulated using a tenfold increase in the mechanical power input on the wind generator. Figure 2.30 shows a comparison of the mechanical frequencies of generators (a) without control on the SVC and (b) with control on the SVC. The frequency is unstable in the uncontrolled case, while advanced control on the SVC improves the stability of the system.

Today's approach to managing such events is to drastically reduce power transfers from the wind power plants to major load centers and avoid transient stability problems by ensuring that there is sufficient transfer capacity for the worst-case scenarios. Some other alternatives to managing transient stability problems are to build new transmission, preferably DC lines. The current state of the art of FACTS does not lend itself well to ensuring the transient stability of the interconnected system, as the tuning of FACTS control logic and gain is most frequently done

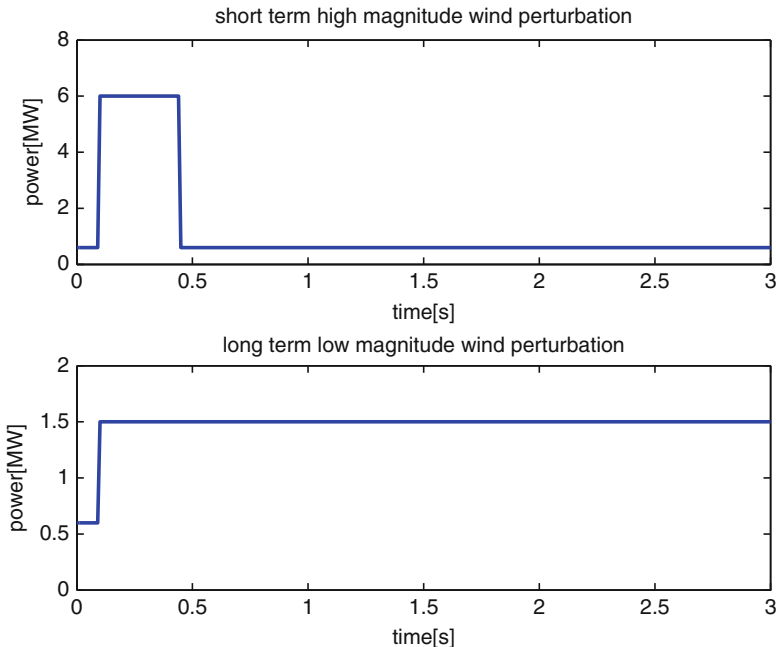


Fig. 2.29 Wind disturbances simulated in the Flores example [13], Chap. 19

by representing the rest of the system as an equivalent static Thevenin equivalent. This, in turn, makes it impossible to model the power swings caused by dynamic interactions between parts of the system that are spatially far away from each other. Moreover, today's FACTS control is generally a linear constant gain control that does not lend itself to provable stabilization of nonlinear system dynamics excited by large faults or large sudden wind power output variations. This approach to managing large disturbances that cause transient instability is therefore one of the major obstacles to replacing conventional generation with wind power.⁸

We propose an alternative design for power-electronically controlled fast storage to ensure that the interconnected system remains transiently stable, in the case of a very long wind power failure, until some slower standby resources get on line and start producing power. We suggest that major savings could be achieved

⁸The interconnection standards that require, for example, 9 ms ride-through of wind power plants without disconnecting themselves are fundamentally not implementable. The ability to meet this standard is system-specific and cannot be guaranteed without testing the wind power plant against the dynamics of the specific power grid to which the wind power plant would be connected. Even more fundamental is the problem of excessive requirements for high-gain power electronics design to fully decouple the closed-loop dynamics of a wind power plant from the rest of the power system. Of course, this is simple but very costly and often unnecessary. There are no similar requirements set on conventional power plants when these are interconnected to the power grid.

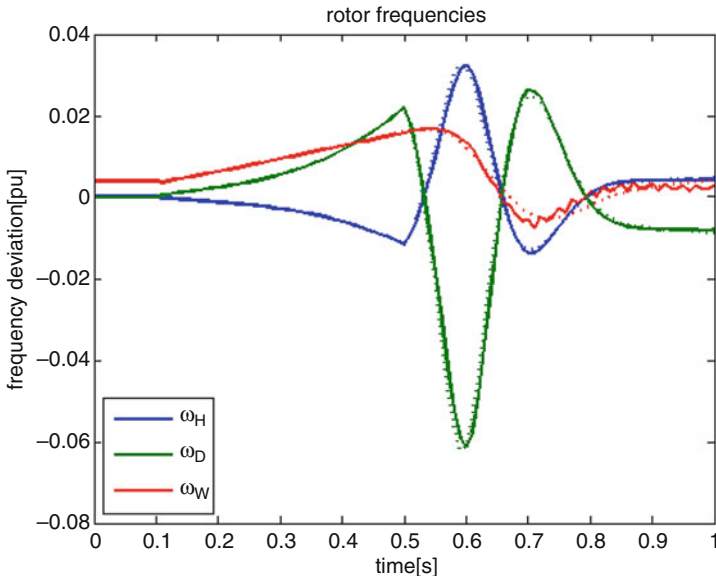


Fig. 2.30 Mechanical frequency of all generators in the system during a short-term high-magnitude wind perturbation; (a) dashed: without control on the SVC, (b) solid: with control on the SVC [13], Chap. 19

by considering a power-electronically based control design of fast storage that is system-specific and intended to manage certain types of disturbances in transiently stable manner. The proposed FACTS-type control design requires dynamic management of the reactive energy stored in reactive devices, capacitors, and inductors. Transient stabilization and/or other fast control of devices capable of storing real energy remains by and large an open R&D area. The economic implications of how FACTS control is designed are major and it is with this in mind that we illustrate the issues and possible control design options and their comparisons. We also propose using flywheels to manage large prolonged wind gust disturbances. The full diagram of connecting the flywheel to the power system on Flores island is depicted in Fig. 2.31. With this diagram and flywheels utilized by means of sliding mode control, the frequency of the hydro, diesel, and wind generators, as well as of the flywheel, is shown in Fig. 2.32. It can be seen that the frequency on all the generators can be stabilized by controlling the flywheel.

In closing, Part VI of this book is most exploratory since it suggests a qualitatively new approach to ensuring reliable operations while it attempts to use the least-expensive cleanest resources in normal operations. It is illustrated how non-time-critical large changes can be managed by adjusting the settings of many other controllable resources as the major changes occur. The time-critical events that threaten the transient response, and therefore could potentially lead to sudden voltage collapse and/or a loss of synchronism, should be managed

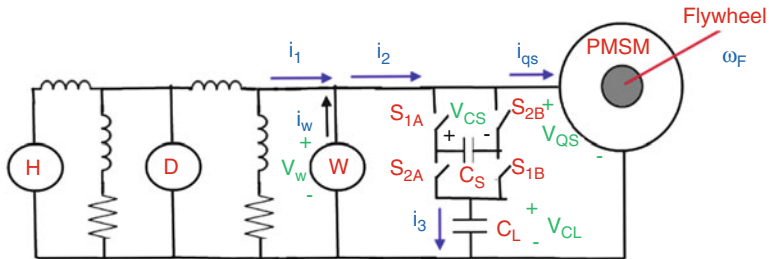


Fig. 2.31 Full diagram connecting the flywheel to Flores [13], Chap. 19

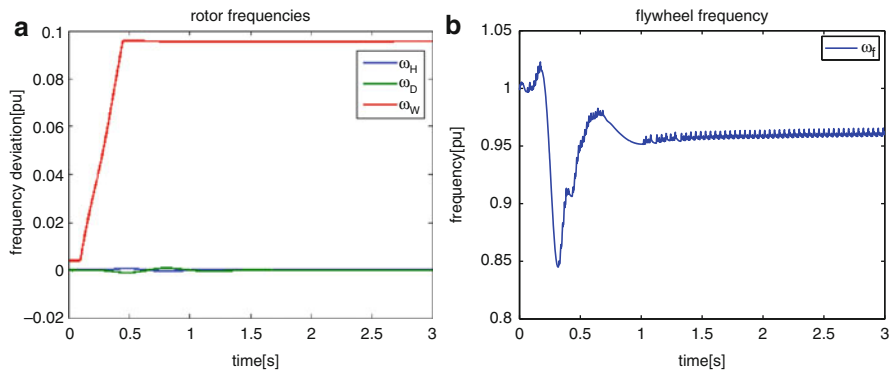


Fig. 2.32 Frequency of (a) the hydro, diesel, and wind generators, and (b) the flywheel, in the Flores system [13], Chap. 19

with power-electronically controlled fast storage, both FACTS and flywheels. The time-critical faults can also be managed by smart reconfiguration in distribution systems. We believe that major breakthroughs are required in the movement toward modeling the complex fast nonlinear dynamics of the interconnected system and that they must be followed by a systematic design for nonlinear control and fast communications support.

2.10.5 Part VII: IT-Enabled Methods for Investing in New Technologies Under Uncertainties

Finally, Part VII considers methods for ensuring sufficient long-term capacity for the reliable and efficient provision of electricity services in future electric energy systems. Planning has become a much more challenging problem than in the past, given several new sources of major uncertainty. In operations, there is major uncertainty because the power generated by the intermittent resources is hard-to-predict and control. Moreover, given the major potential for responsive demand

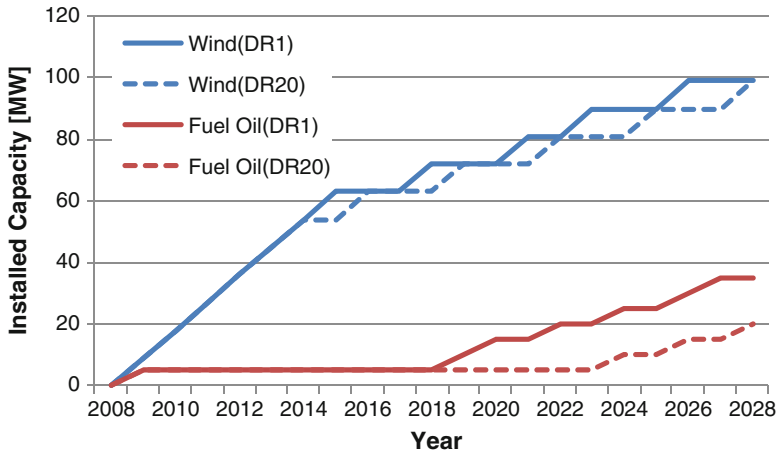


Fig. 2.33 Optimal expansion of wind power and fuel oil capacity with 1% (DR1) and 20% (DR20) demand response, 2008–2028 [13] Chap. 20

and no direct control of the consumers' load, system operators are facing serious related risks in addition to better understood long-term load uncertainties and forced outages. Planning criteria have become multi-objective, and there are major tradeoffs between planning for long-term reliability, for efficiency, and for meeting environmental goals. Planning is no longer a matter of utility planners projecting long-term load growth and building sufficient capacity to meet the highest projected load peak and having the standby capacity to ensure uninterrupted service during the failure of the largest power plant. Operations in future electric energy systems will rarely be limited by generation capacity. Instead, it will be mainly affected by these new uncertainties in operations, as well as by the transmission and distribution system's inability to deliver the power to the right places. Longer-term reliability goals will be affected by environmental and electricity market rules.

It is therefore no longer possible for the system planner to guess various uncertainties in a top-down way and then plan centrally. Instead, it will become essential to engage in interactive planning so that investors in different candidate technologies internalize various risks and offer well-defined bids to system planners on how much they are willing to build, at which long-run marginal cost and under which system integration conditions. Without such information exchange the risk will be asymmetric and it will be practically impossible to plan for a sustainable utilization of assets [3]. In Chap. 20 we illustrate a possible dynamic investment method under uncertainties for investing in wind power. A stochastic decision-making process weighs the likely payoffs from operations against the capital cost of investing. An optimal investment is based on finding the break-even point between the expected cumulative payoffs and the capital investment cost. Shown in Figs. 2.33 and 2.34 are the results of this investment decision method. The results

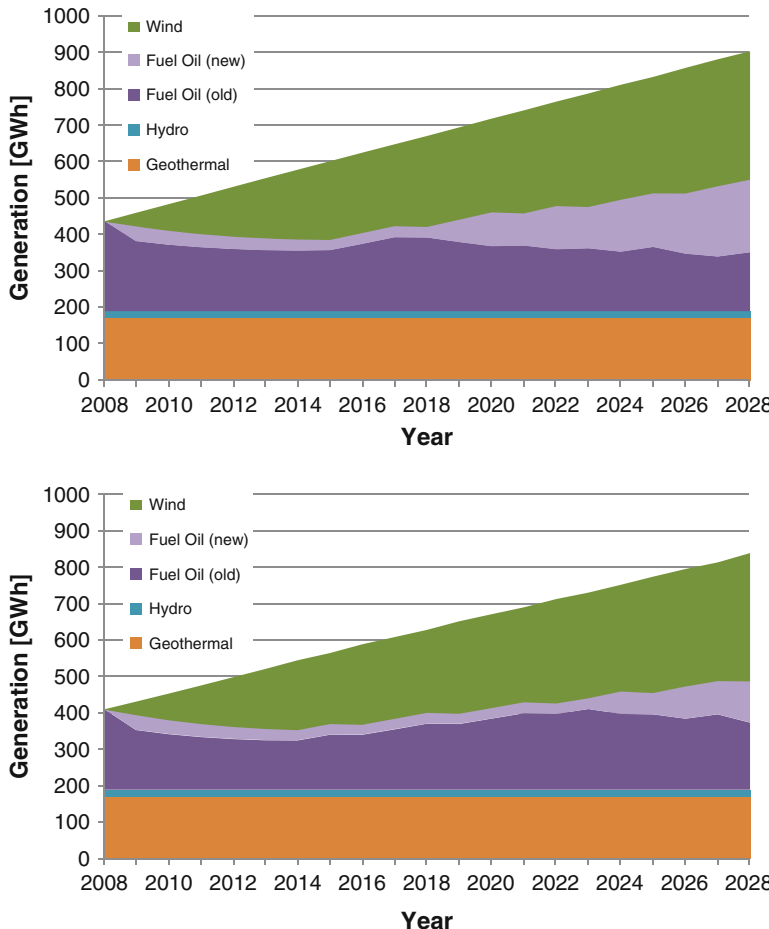


Fig. 2.34 Expected annual generation dispatch with 1% (*upper*) and 20% (*lower*) demand response, 2008–2028 [13], Chap. 20

are the optimal expansion of wind and fuel oils and the expected optimal dispatch, respectively.

Computer methods that rely on both short- and long-term predictive modeling must be developed for assessing these payoffs with certain confidence. The complexity of managing multiple risks and their tradeoffs easily becomes overwhelming when done in a centralized way. In this book we propose that multi-temporal decisions under uncertainties could be internalized by the candidate investors themselves. The risks related to the integration rules for scheduling future assets in a reliable way could be managed by the system operators and planners. In order to facilitate the integration of new technologies at value in a highly uncertain environment, it is essential to have well-defined protocols for IT-enabled bidding

information exchange and distributed risk management over time and across various industry stakeholders.

2.11 Data Repository for Flores and São Miguel Islands

The input data necessary for the Flores and São Miguel modeling and simulations presented in this book is made available in the on-line. The data repository has been designed in such a way that each folder is self-contained and corresponding to specific chapters. In the data folder for Chap. 3, the steady-state characteristics of buses, loads, generators, and branches for the electric power system of Flores and São Miguel are described. The data set is in standard PSS/E v.23 format. More detailed steady-state characteristics of generation cost, generator parameters, wind speed, and wind generation power data are described in Chaps. 4, 5, and 7, which is associated with simulation presented in Chaps. 4, 5, and 7. Wind power and load forecast data necessary for Chap. 6 is provided in Chap. 6. The cost input data for demand and generation dispatch are described in Chaps. 8 and 9 (in support of the simulations in Chaps. 8 and 9); each demand and generation entity uses this data in order to calculate their bids to the system operator. The electric vehicle and solar power generation data necessary for Chap. 11 is presented in Chap. 11. The dynamical data necessary for the simulations in Parts IV–VI are described in Chap. 13. The power flow-based system equilibrium used for deriving the linearized models in Chaps. 15 and 16 is described in a joint Chaps. 15 and 16. The final Chap. 20 contains the planning parameters used in Chap. 20. In this folder the discrete distributions for short-term uncertainties in wind power and load used are provided.

2.12 Chapter Summary

Motivated by the specific problem of enabling the electric energy systems of small islands to become more sustainable, we start with the more general objective of making SES sustainable, as introduced by the Nobel Prize winner Elinor Ostrom. We explain how our extension of this powerful concept of sustainable SEESs helps identify the key enabling role of a man-made electric power grid and its supporting IT infrastructure. Notably, the definitions of core-order, second-order, and deeper-order variables help us pose an IT engineering design for a given man-made electric energy system according to well-defined quantifiable multi-objectives and their tradeoffs. These somewhat abstract concepts are related to the enhancements needed in today's electric power industry operations and planning practices (identified in Chap. 1). We propose one such possible systematic IT-enabled enhancement which we refer to as the DYMONDS framework. Finally, we discuss how this approach could enable clean low-cost electricity provision to two islands in the Azores Archipelago. We illustrate the basic ideas in this book in light of such a design

and highlight a few key results by analyzing our simulations of this framework that we ran based on sample electric energy system data for these islands. We describe the first proof-of-concept results based on novel software and automation that we consider to be essential for providing these islands, electricity services with a clear understanding of differentiation according to the desired QoS and minimized cost and environmental impact. The role of energy consumers is highlighted.

Acknowledgements This work was supported by the US National Science Foundation Award 0931978 and by the Semiconductor Research Corporation (SRC) Smart Grid Research Center (SGRC) at Carnegie Mellon University. The ideas of our book that have been reviewed in this chapter have evolved as a result of many research efforts, with several current and former graduate students coauthoring book chapters. The author fondly remembers many hours of working together and acknowledges the input.

References

1. M. Ilic, Automating operation of large electric power systems over broad ranges of supply, demand and equipment status, in *Applied Mathematics for Restructured Electric Power Systems*, chap. 6, ed. by J. Chow, F. Wu, J. Momoh (Kluwer, Dordrecht, 2005), pp. 105–137. ISBN 0-387-23470-5
2. M. Ilić, From hierarchical to open access electric power systems, in Proceedings of IEEE, *Special Issue on Modeling, Identification, and Control of Large-Scale Dynamical Systems*, ed. by S. Haykin, E. Mouines, vol. 95, No. 5, 2007
3. M. Ilic, 3Rs for power and demand. Public Utilities Fortnightly Magazine, December 2009
4. M. Ilic, Dynamic monitoring and decision systems for enabling sustainable energy services. Proc. IEEE **99**, 58–79 (2011)
5. M. Ilic, Q. Liu, Toward sensing, communications and control architectures for frequency regulation in systems with highly variable resources, in *Control and Optimization Methods for Electric Smart Grids*, chap. 1, ed. by A. Chakrabortty, M.D. Ilić (Springer, New York, 2011), pp. 3–34
6. M. Ilic, F.D. Galiana, L. Fink (eds.), *Electric Power Systems Restructuring: Engineering and Economics* (Kluwer, Boston, 1998)
7. M. Ilić, J. Lang, X. Luo, E. Litvinov, The critical role of computationally robust optimal AC power flow in reliable and efficient voltage/reactive power dispatch, in *Proceedings of the 2006 Power Systems Conference and Expo*, Atlanta, GA, October 2006
8. M. Ilić, J.-Y. Joo, L. Xie, M. Prica, N. Rotering, A decision making framework and simulator for sustainable electric energy systems. IEEE Trans. Sustain. Energ. **2**(1), 37–49 (2010)
9. M.D. Ilić, J. Zaborszky, *Dynamics and Control of Large Electric Power Systems* (Wiley Interscience, New York, 2000)
10. M.D. Ilic, L. Xie, U.A. Khan, J.M.F. Moura, Modeling, sensing and control of future cyber-physical energy systems. IEEE Trans. Syst. Man Cybern. Syst. Hum. **40**(4), 825–838 (2010)
11. M.D. Ilic, L. Xie, J. Joo, Efficient coordination of wind power and price-responsive demand - Part I: theoretical foundations. IEEE Trans. Power Syst. **26**(4), 1875–1884 (2011)
12. M.D. Ilic, L. Xie, J. Joo, Efficient coordination of wind power and price-responsive demand - Part II: case studies. IEEE Trans. Power Syst. **26**(4), 1885–1893 (2011)
13. M. Ilic, L. Xie, Q. Liu (eds.), *Engineering IT-Enabled Sustainable Electricity Services: The Tale of Two Green Low-Cost Azores Island* (Springer, 2013)
14. J.-P. Leotard, M. Ilic, On the objectives of transmission pricing under open access, in *Proceedings of the IEEE Power Engineering Society Winter Meeting*, New York, NY, February 1999

15. E. Ostrom et al., A general framework for analyzing sustainability of social-ecological systems. *Science* **325**, 419 (2009)
16. J.C. Panzar, R.D. Willig, Economies of scope. *Am. Econ. Rev.* **71**, 268–272 (1981)
17. M. Prica, M. Ilić, J. Ilić, On the fundamental importance of relating operating and planning objectives in the changing electric power industry, in *Proceedings of the North American Power Symposium*, Starkville, MI, 4–6 October 2009

Part II

The Electrical Systems Characteristics of Two Azores Islands: Flores and São Miguel

Chapter 3

Electrical Networks of the Azores Archipelago

Masoud Honarvar Nazari

3.1 Introduction

The Azores Archipelago consists of nine islands located in the middle of the North Atlantic Ocean. The western group consists of Flores and Corvo islands; the central group consists of Graciosa, Terceira, São Jorge, Pico, and Faial islands; and the eastern group consists of São Miguel and Santa Maria islands (<http://en.wikipedia.org/wiki/Azores>). In this chapter, the electrical network of each island is briefly described. The main focus is on Flores and São Miguel. Therefore, their electrical networks are explained in detail.

3.1.1 Flores Island

Flores Island is one of the smaller islands of the Azores Archipelago. The population is approximately 4,000 inhabitants, and its area is around 143 km² ([http://en.wikipedia.org/wiki/Flores_Island_\(Azores\)](http://en.wikipedia.org/wiki/Flores_Island_(Azores))). Figure 3.1 is a satellite image of the island.

The electrical network of Flores consists of a 15 kV radial distribution network with 45 nodes and 44 branches. The total demand of the island is around 2 MW. More than 50 % of the demand is concentrated in the town of Santa Cruz; around 37 % of the load is situated in the vicinity of the harbor (Lajes Das Flores); approximately 7 % of the load is located in the town of Ponta Delgada, and the rest (2–3 %) is dispersed throughout the rest of the island. Figure 3.2 illustrates the schematic of the distribution network of Flores Island.

M. Honarvar Nazari (✉)

Department of Engineering and Public Policy, Carnegie Mellon University,
5000 Forbes Ave, Pittsburgh, PA 15213, USA

e-mail: mhonarva@andrew.cmu.edu

Fig. 3.1 Satellite image of Flores Island

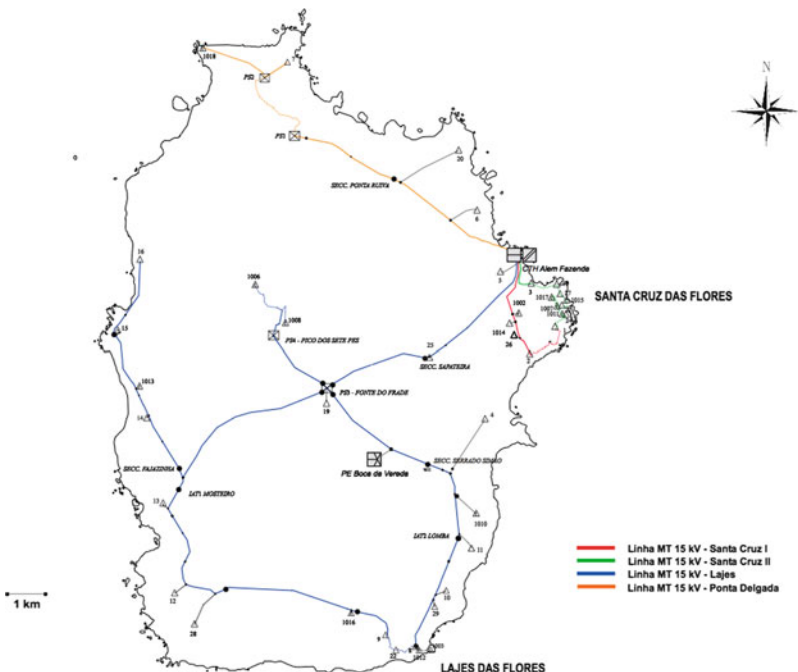


Fig. 3.2 Electrical network of Flores Island [1]

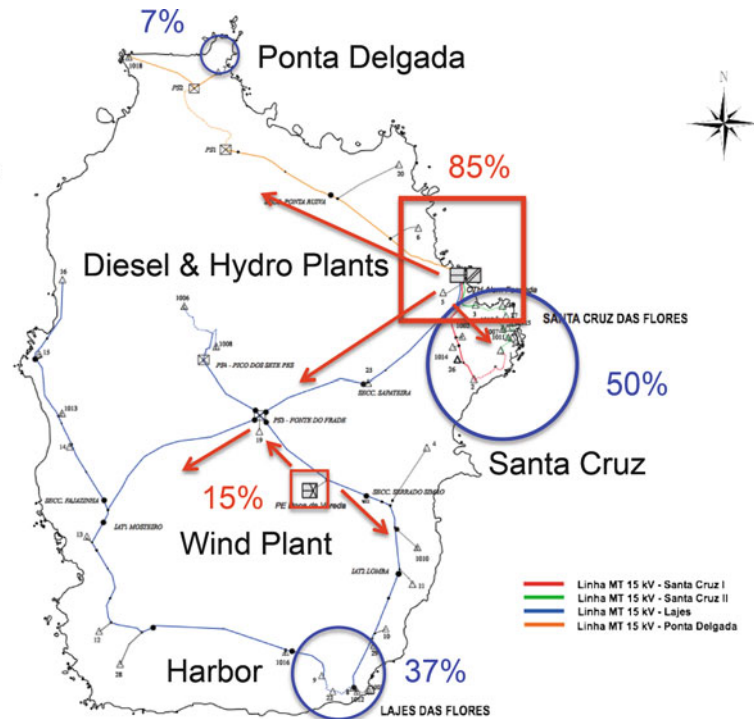


Fig. 3.3 Illustrating the location of large loads and power plants and how real power flows

Three small power plants supply the electrical demand. More than 50 % of the electricity is provided by four diesel generators whose total capacity is 2.5 MW. Around 35 % of the demand is supplied by four hydropower plants with an overall capacity of 1.65 MW. Two synchronous wind power plants with a total capacity of 0.65 MW provide the rest of the demand (15 %). The hydro plants and diesel generators are located next to the town of Santa Cruz, and the wind plants are located in the middle of the island far from the major load centers [1]. Figure 3.3 demonstrates where the large loads and power plants are located and how real power flows in the distribution system of the island. In Appendix A, the steady-state characteristics of the nodes, loads, generators, and branches of Flores Island are presented in PTI 23 standard format [1].

Since the electrical network of the island is an AC system, active power needs to be balanced almost instantaneously. The hydro generator is a reservoir hydro plant with the ability to store energy. However, the hydro plant has slow dynamic response and cannot balance active power instantaneously. The synchronous wind power plant has no governor control and cannot regulate frequency. The diesel plant, as the only fully controllable power plant, balances demand and supply. The diesel plant also compensates for active and reactive losses occurring in the system.

Table 3.1 Critical lines of Flores Island

Ponta Delgada	Vicinity of harbor
Lines 1–41	Lines 1–17
Lines 41–42	Lines 17–18
Lines 42–43	

There is no control center on Flores Island. Therefore, the diesel generator regulates frequency locally. It is shown in Chap. 17 that using a diesel generator for frequency regulation has major drawbacks for the system, such as increased pollution, higher operating costs, and the problem of wear and tear. Alternative solutions are needed. The parameters of the dynamic model of generators are presented in Appendix B.

On Flores Island, distribution lines have been over built. Hence, contingencies due to the reaching of thermal limits are unlikely to occur. However, due to the strong interaction between the electromagnetic and electromechanical parts of the generators, small-signal instability can occur on the island. This is modeled in Chap. 17.

One of the major flaws of the electrical network on Flores is the lack of (N-1) reliability criteria. Due to the radial structure of the distribution network, if the line connecting the diesel plant to the center of the island (Fonte de Frade) is disconnected, a local blackout occurs in the central and southern parts of the island. Similarly, if the line connecting the diesel plant to the north of the island (Ponta Delgada) is disconnected, a local blackout occurs in the northern part. The critical lines are presented in Table 3.1.

In order to improve reliability, we suggest that new wind power plants be installed in the central and northern parts of the island. Implementing normally open switches to connect the southern part of the island to the town of Santa Cruz, where the diesel and hydro plants are installed, could enhance reliability in the south. Since the harbor of Flores is located in the south, it is essential to improve reliability at least in the vicinity of the harbor.

3.1.2 Corvo Island

Corvo Island is the smallest island of the Azores Archipelago. The population is approximately 468 inhabitants (http://en.wikipedia.org/wiki/Corvo_Island). Figure 3.4 is a satellite image of the island.

Corvo has a very small electrical network consisting of a single-line distribution network with a voltage level of 15 kV. The total demand of the island is approximately 250 kW. There are no renewable energy resources on Corvo. A diesel generator with 4 small units provides the electrical demand of the island. The total capacity of the diesel generator is 536 kW. The generator is located close to the town of Corvo, the only load center on the island. Figure 3.5 shows the

Fig. 3.4 Satellite image of Corvo Island

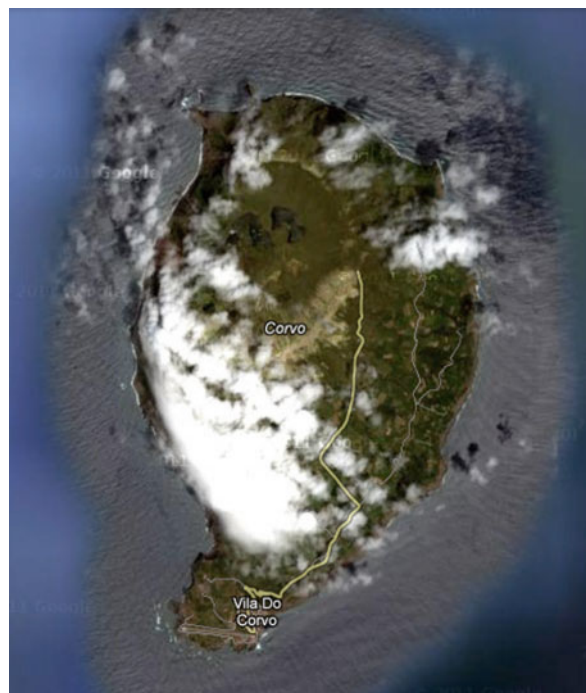


Fig. 3.5 Electrical network of Corvo Island [1]

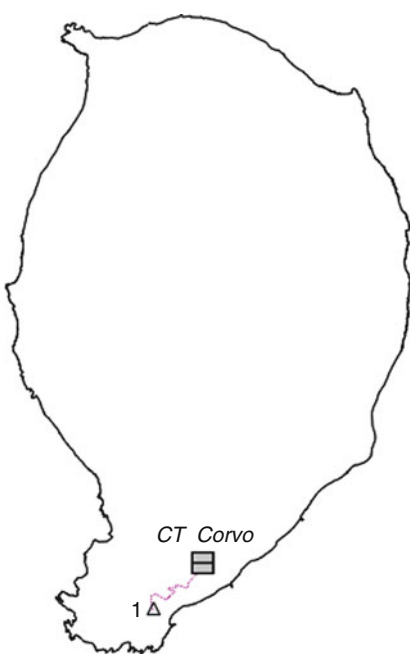




Fig. 3.6 Satellite image of Graciosa Island

schematic of the distribution network of Corvo. The diesel plant balances active and reactive power in the system, compensating for losses occurring in the system and regulating frequency. If the line connecting the diesel plant to the town of Corvo is disconnected, a blackout will occur on the island. This implies that the (N-1) reliability criteria are not satisfied on Corvo.

3.1.3 Graciosa Island

Graciosa Island is the northernmost of the central group of the Azores Archipelago. The island has an area of 60.65 km^2 and its population is approximately 4700 inhabitants (<http://en.wikipedia.org/wiki/Graciosa>). Figure 3.6 is a satellite image of Graciosa.

Graciosa Island has a 15-kV ring distribution network. The overall demand of the island is around 2.5 MW, and two generators supply this demand. Around 68 % of the electricity is provided by a diesel generator. The diesel plant is composed of 6 smaller units with an overall capacity of 3.43 MW. The rest of the electrical demand (approximately 32 %) is supplied by a wind power plant consisting of 4

smaller units. The overall capacity of the wind plant is 0.8 MW. Figure 3.7 shows the schematic of the distribution network of Graciosa Island (<http://en.wikipedia.org/wiki/Azores>).

Graciosa Island, like most of the smaller islands of the Azores Archipelago, has no control center for coordinating dispatch on-line. The diesel generator is the only controllable generator on the island; it balances demand and supply, compensates for active and reactive power losses, and regulates frequency.

3.1.4 *Terceira Island*

Terceira Island is one of the larger islands of the Azores Archipelago, with a population of approximately 56,000 inhabitants in an area of 396 km² (http://en.wikipedia.org/wiki/Terceira_Island). Figure 3.8 shows a satellite image of Terceira.

The electrical network of Terceira Island is composed of a small transmission network with a voltage level of 30 kV and a large ring distribution network with a voltage level of 15 kV. The total demand of the island is approximately 36 MW. Three small power plants supply the demand.

More than 90 % of the electricity is produced by a large diesel generator consisting of 10 smaller units. The full capacity of the diesel plant is 61 MW. Around 6 % of the electricity is provided by a wind plant with three smaller units. The overall capacity of the wind plant is 4.5 MW. The rest of the electricity (around 4 %) is supplied by three hydro plants with a full capacity of 1.4 MW. Figure 3.9 shows the schematic of the distribution network of Terceira Island (<http://en.wikipedia.org/wiki/Azores>).

Terceira has an advanced control center that handles both generation control and distribution management. The control center provides the most economical dispatch for the generators by minimizing the operating costs of the system. It also regulates frequency by means of automatic generation control (AGC). The advanced control system helps the island to manage system operations during off-peak hours with a very large penetration of wind power [2].

3.1.5 *São Jorge Island*

São Jorge Island is a relatively long thin island with a population of approximately 10,500 inhabitants. The east to west length of the island is 53 km and its north to south width is 8 km; its area is 237.59 km² (http://en.wikipedia.org/wiki/S%C3%A3o_Jorge_Island). Figure 3.10 shows a satellite image of the island.

São Jorge Island has a 15-kV radial distribution network. The overall demand of the island is around 4.7 MW, and two generators supply this demand. Approximately 86 % of the electricity is generated by a diesel generator consisting of 7 smaller units. The full capacity of the diesel plant is 7.09 MW. The rest of the electrical demand (around 14 %) is supplied by 7 small wind plants with an overall capacity

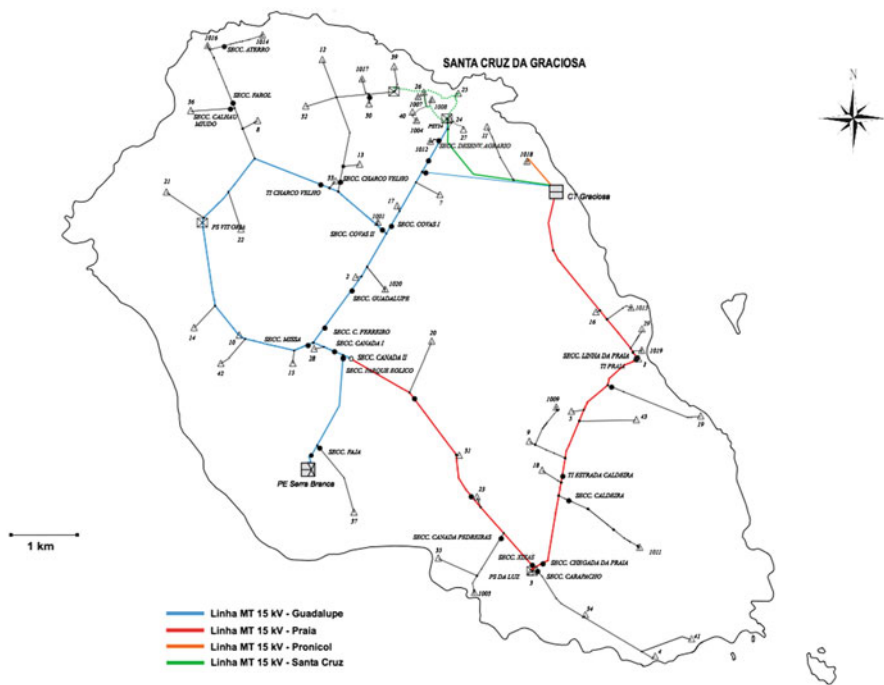


Fig. 3.7 Electrical network of Graciosa Island [1]



Fig. 3.8 Satellite image of Terceira Island

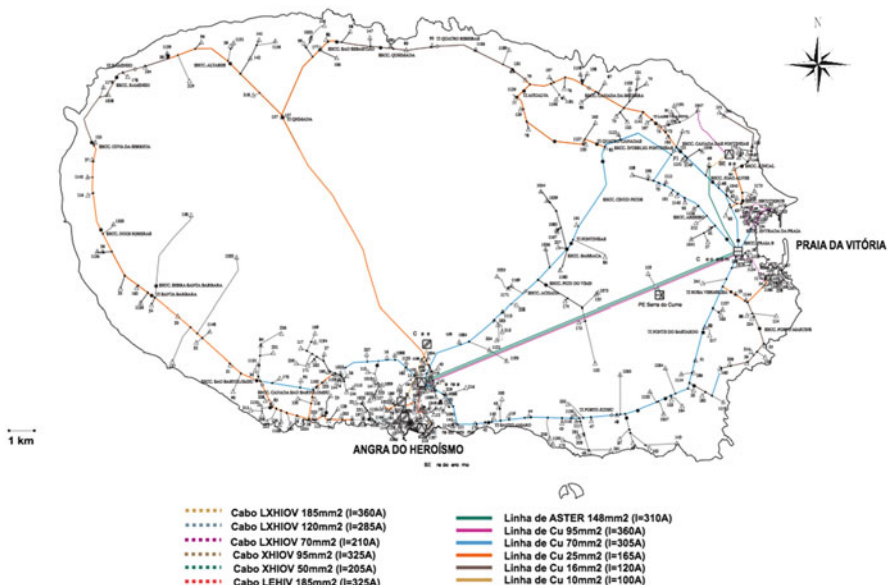


Fig. 3.9 Electrical network of Terceira Island [1]



Fig. 3.10 Satellite image of São Jorge Island

of 1.15 MW. Figure 3.11 shows the schematic of the distribution network of São Jorge (<http://en.wikipedia.org/wiki/Azores>).

Due to the long radial structure of the distribution system of São Jorge, voltage drops across the distribution system. This leads to voltage problems, especially

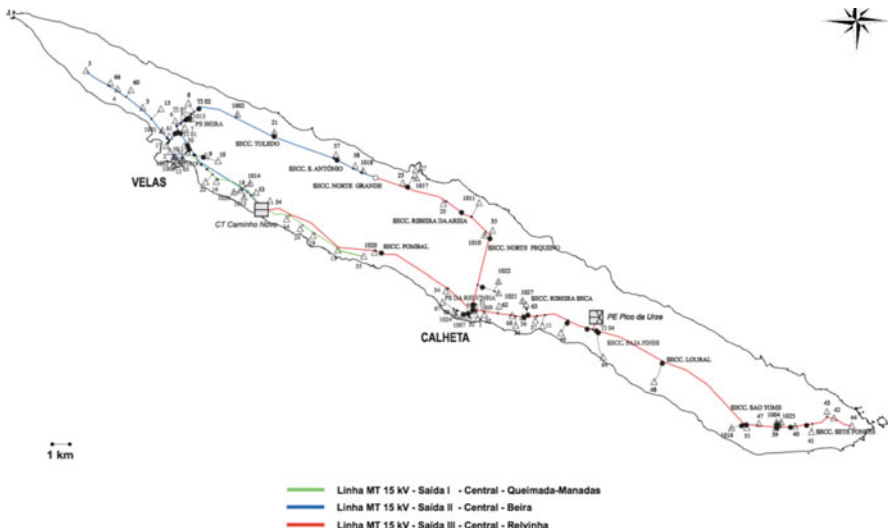




Fig. 3.12 Satellite image of Pico Island

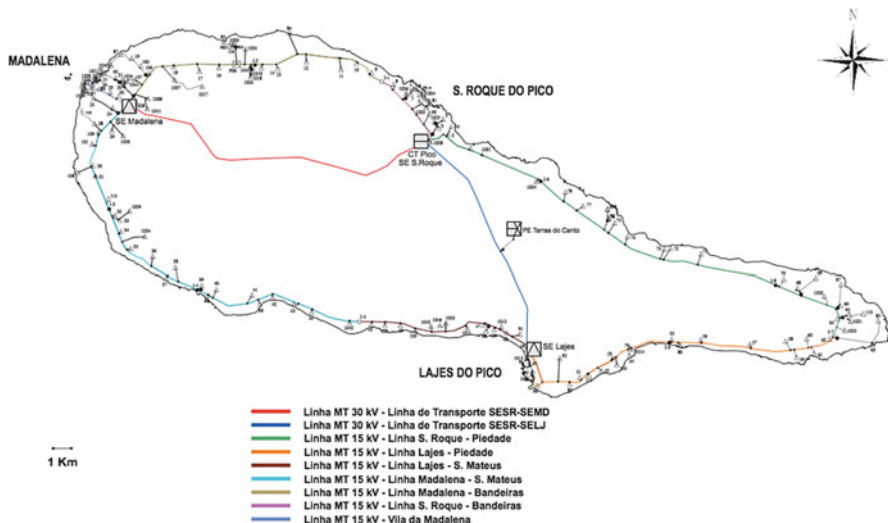


Fig. 3.13 Electrical network of Pico Island [1]

3.1.7 Faial Island

Faial Island is in the central group of the Azores Archipelago. Its population is around 14,900 inhabitants and its area is 173.06 km² (http://en.wikipedia.org/wiki/Faial_Island). Figure 3.14 shows a satellite image of Faial (http://en.wikipedia.org/wiki/Faial_Island).

The island has a 15-kV ring distribution network. The total electrical demand of the island is around 9 MW, and six generators supply the demand. Around 89 %

of the electricity is generated by four diesel generators. The full capacity of the diesel plants is 17 MW. Approximately 9.4% of the electricity is produced by a wind plant with a full capacity of 1.8 MW. The rest of the electrical demand (around 1.6%) is supplied by a small hydro plant with a total capacity of 0.32 MW (<http://en.wikipedia.org/wiki/Azores>). Figure 3.15 shows the schematic of the distribution network of Faial Island.

3.1.8 São Miguel Island

São Miguel Island is the capital, and the largest, island of the Azores Archipelago. The population of this island is approximately 140,000 inhabitants and the area of the island is 744.55 km² (http://en.wikipedia.org/wiki/S%C3%A3o_Miguel_Island). Figure 3.16 shows a satellite image of São Miguel.

The electrical system of São Miguel consists of a 60-kV transmission network, situated in the middle of the island, which connects the large power plants to large loads. Figure 3.17 illustrates how real power flows in the transmission network. As shown in Fig. 3.17, two large diesel generators located in the middle of the island (close to the large loads) produce 75% of the electrical demand. Two large geothermal plants provide more than 20% of the demand. The rest comes from seven small hydro plants with run-of-the-river hydropower (<http://en.wikipedia.org/wiki/Azores>). The capital of the island (Ponta Delgada) is the largest load.

There is a 30-kV and a 10-kV ring distribution network located along the coastal area. Figure 3.18 shows the schematic of the distribution network of the island and where the largest loads are located. In Appendix C, the steady-state characteristics of the nodes, loads, generators, and branches of São Miguel Island are presented in PTI 23 standard format.

Like the other islands of the Azores Archipelago, São Miguel has an all-AC electrical system. This requires an almost instantaneous balancing of active power. On São Miguel, the hydro and geothermal plants are noncontrollable generators, so they provide base-load power only. It falls on the diesel plants to balance demand and supply almost instantaneously. In addition, the diesel generators compensate for active and reactive power losses occurring in the system. The parameters of the dynamic model of the generators are presented in Appendix D.

São Miguel Island has an advanced control center. The control center provides generation control and regulates frequency by communicating with the AGC of the diesel plants. The control center also provides the most economical dispatch for the diesel generators by minimizing their operating costs. The advanced control system helps the island to manage system operations during peak hours.



Fig. 3.14 Satellite image of Faial Island

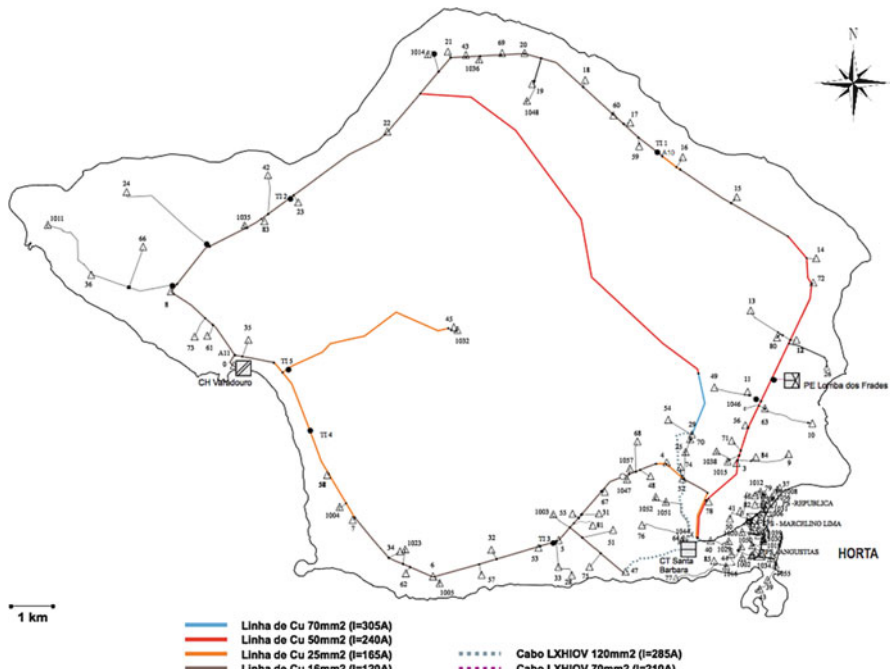


Fig. 3.15 Electrical network of Faial Island [1]



Fig. 3.16 Satellite image of São Miguel Island

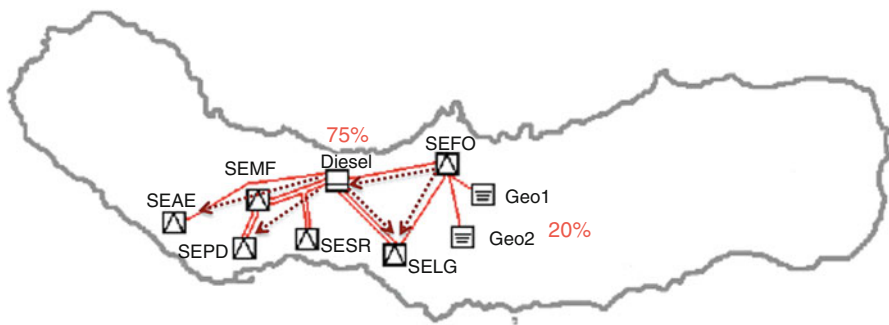


Fig. 3.17 Transmission network of São Miguel Island [1]

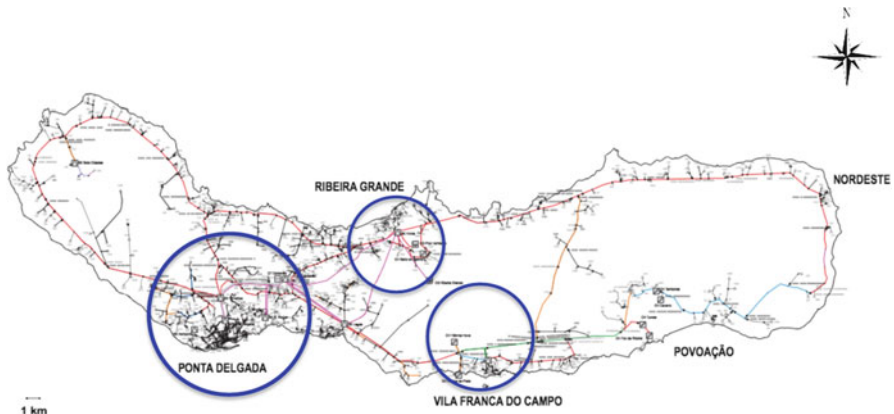


Fig. 3.18 Distribution and transmission network of São Miguel Island [1]



Fig. 3.19 Satellite image of Santa Maria Island

3.1.9 *Santa Maria Island*

Santa Maria Island is one of the eastern group of the Azores Archipelago. The population is around 5,600 inhabitants and the area of the island is 96.89 km^2 (http://en.wikipedia.org/wiki/Santa_Maria_Island). Figure 3.19 shows the satellite image of the island.

The electrical network of Santa Maria consists of a ring distribution network with a voltage levels of 6 and 10 kV. The total demand of the island is around 3.5 MW, and two generators supply this demand. More than 85 % of the electricity is provided by a diesel generator, consisting of five smaller units, with a total capacity of 5.68 MW. The rest of the electrical demand (around 15 %) is supplied by a wind farm with three wind plants. The full capacity of the wind farm is 0.9 MW [1]. Figure 3.20 shows the schematic of the distribution network of Santa Maria.

Appendix A

Appendix A includes the steady-state characteristics of the electric power system of Flores in PSS/E v. 23. The data is available in the CD attached to the book.

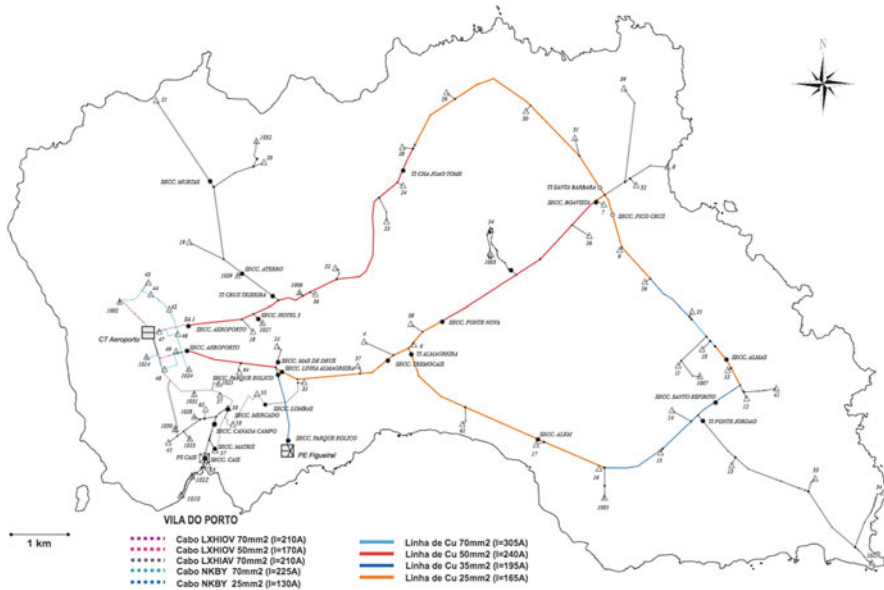


Fig. 3.20 Electrical network of Santa Maria Island [1]

Table B.1 Electromechanical parameters of the diesel plant

M_d (MJ/Hz)	D_d (MW/Hz)	T_2 (s)	K_2 (pu)	R_d (pu)	C_d (pu)
0.216	0.005	0.6	40	0.03	1
KI (pu)	Cc (pu)				
10	1				

Table B.2
Electromechanical
parameters of the wind plant

M_w (MJ/Hz)	D_w (MW/Hz)	Kp_w (pu)
0.089	0.002	2

Appendix B

Electromechanical and electromagnetic parameters of the power plants on Flores are presented in Tables B.1–B.6. These parameters are estimated based on the data set provided by Professor Pecas Lopes from INESC Porto [4] and based on the models used in [3]. The original data set is available in the CD attached to the book. The bases are $S_{base} = 1 \text{ MVA}$, $V_{base} = 0.4 \text{ kV}$, and $f_{base} = 50 \text{ Hz}$.

Table B.3 Electromechanical parameters of the hydro plant

M_h (MJ/Hz)	D_h (MW/Hz)	K_d (pu)	K_w (pu)	T_f (s)	r_h (pu)
0.2749	0.02	2.78	1.52	-3.6	7
T_q (s)	T_w (s)	T_e (s)	T_s (s)	r_p (pu)	
0.72	4	2	0.06	0.06	

Table B.4 Electromagnetic parameters of the diesel plant

Ta_d (s)	Tf_d (s)	Td_d (s)	Ka_d (pu)	Xd_d (pu)	$X'd_d$ (pu)
0.2	0.65	2.35	25	8.1479	0.5917
R_d (pu)	Te_d (s)	Ke_d (pu)	Se_d (pu)		
0.000	0.6544	1	0.105		

Table B.5 Electromagnetic parameters of the wind plant

Td_w (s)	Xd_w (pu)	$X'd_w$ (pu)	Rw (pu)
0.661	28.161	3.052	0.0002

Table B.6 Electromagnetic parameters of the hydro plant

Ta_h (s)	Tf_h (s)	Td_h (s)	Ka_h (pu)	Xd_h (pu)	$X'd_h$ (pu)
0.05	0.9	3.5	400	2.399	0.3609
R_h (pu)	Te_h (s)	Ke_h (pu)	Se_h (pu)		
0.000	0.9	1	0.035		

Table B.7 Characteristics of the plants in Flores Island

Node number in the original system	Capacity (MW)	Type of plant
1	2.5	Diesel
1	1.5	Hydro
19	0.6	Wind

Appendix C

Appendix C includes the steady-state characteristics of the electric power system of São Miguel in PSS/E v.23. The data is available in the CD attached to the book.

Appendix D

Electromechanical parameters of the power plants in São Miguel are presented in Tables D.1–D.15. These parameters are estimated based on the data set provided by Professor Pecas Lopes from INESC Porto and Professor Pedro Carvalho from IST Lisbon and based on the models used in [3]. The bases are Sbase = 100 MVA and fbase = 50 Hz.

Table D.1 Electromechanical parameters of the first diesel plant

M_{d1} (MJ/Hz)	D_{d1} (MW/Hz)	T_{d1} (s)	K_{d1} (pu)	R_{d1} (pu)	C_{d1} (pu)
5.853	0.704	1.07	40	0.03	1
KI_1 (pu)	Cc_1 (pu)				
10	1				

Table D.2 Electromechanical parameters of the second and third diesel plants

M_{d2} (MJ/Hz)	D_{d2} (MW/Hz)	T_{d2} (s)	K_{d2} (pu)	R_{d2} (pu)	C_{d2} (pu)
6.473	0.352	1.25	40	0.03	1
KI_2 (pu)	Cc_2 (pu)				
10	1				

Table D.3 Electromechanical parameters of the first geothermal plant

M_{geo1} (MJ/Hz)	D_{geo1} (MW/Hz)
2.653	0.298

Table D.4 Electromechanical parameters of the second geothermal plant

M_{geo2} (MJ/Hz)	D_{geo2} (MW/Hz)
2.331	0.262

Table D.5
Electromechanical
parameters of Hydro 1

M_{h1} (MJ/Hz)	D_{h1} (MW/Hz)
0.2038	0.0036

Table D.6
Electromechanical
parameters of Hydro 2

M_{h2} (MJ/Hz)	D_{h2} (MW/Hz)
0.162	0.0122

Table D.7
Electromechanical
parameters of Hydro 3

M_{h3} (MJ/Hz)	D_{h3} (MW/Hz)
0.1849	0.0033

Table D.8
Electromechanical
parameters of Hydro 4

M_{h4} (MJ/Hz)	D_{h4} (MW/Hz)
0.1424	0.0106

Table D.9
Electromechanical parameters of Hydro 5

M_{h5} (MJ/Hz)	D_{h5} (MW/Hz)
0.1424	0.0106

Table D.10
Electromechanical parameters of Hydro 6

M_{h6} (MJ/Hz)	D_{h6} (MW/Hz)
0.1424	0.0106

Table D.11
Electromechanical parameters of Hydro 7

M_{h7} (MJ/Hz)	D_{h7} (MW/Hz)
0.0285	0.00051

Table D.12
Electromechanical parameters of Hydro 8

M_{h8} (MJ/Hz)	D_{h8} (MW/Hz)
0.1216	0.0022

Table D.13
Electromechanical parameters of Hydro 9

M_{h9} (MJ/Hz)	D_{h9} (MW/Hz)
0.1217	0.0022

Table D.14
Electromechanical parameters of Hydro 10

M_{h10} (MJ/Hz)	D_{h10} (MW/Hz)
0.1217	0.0022

Table D.15 Characteristics of the plants in the electric power system of São Miguel

Node number in the original system	Capacity (MW)	Type of the plant
932	32.688	Diesel 1 (SLACK)
933	32.688	Diesel 2
934	32.688	Diesel 3
963	14.8	Geothermal 1
1049	13	Geothermal 2
1666	0.67	Hydro 1
1669	0.8	Hydro 2
1672	0.608	Hydro 3
1675	0.553	Hydro 4
1676	0.553	Hydro 5
1677	0.553	Hydro 6
1680	0.094	Hydro 7
1683	0.4	Hydro 8
1686	0.4	Hydro 9
1687	0.4	Hydro 10

Acknowledgments The author greatly acknowledges Professor Jeffrey Lang and Professor Marija Ilić for helping to prepare the input data of São Miguel Island in PTI 23 format. The author also appreciates the help of the EDA in providing technical data for the Azores Islands. Last but not least, the author greatly appreciates his earlier discussions during his stay at MIT with Mr. Stephen Connors and Doctor Edward Spang regarding the Green Island Project. Financial support for this work was provided by the Portugal-Carnegie Mellon joint program under Grant 18396.6.5004458.

References

1. EDA, Informação Estatística, Electricidade dos Açores, *Monthly Information Reports for 2005–2009* (2009). Available on website: http://www.google.com/url?sa=t&rct=j&q=&esrc=s&source=web&cd=3&cad=rja&ved=0CEAQFjAC&url=http%3A%2F%2Fpaginas.fe.up.pt%2F~ee02072%2Fdocs%2Fcare_eda_2009_2010_03_31.pdf&ei=cEAmUdCbKIhs8wTDpoHoDw&usg=AFQjCNFLLQgM_37AokB5t9oo3VGPiXeeSw&sig2=r-6tom2CXHRd07B2Dvn88Q&bvm=bv.42661473,d.eWU
2. N. Hatziargyriou, G. Contaxis, M. Papadopoulos, B. Papadias, E. Nogaret, G. Kariniotakis, J.A. Pecas Lopes, M. Matos, J. Halliday, G. Dutton, P. Dokopoulos, A. Bakirtzis, A. Androutsos, J. Stefanakis, A. Gigantidou, Control of isolated power systems with increased wind power generation. Med. Power 98, Lefkosia, Cyprus, 16–18 Nov 1998
3. J. Cardell, M. Ilić, R.D. Tabors, *Integrating Small Scale Distributed Generation into a Deregulated Market: Control Strategies and Price Feedback*, Laboratory for Electromagnetic and Electronic Systems, Massachusetts Institute of Technology, 1998
4. M. Angelo and P. Lopes, *Simultaneous Tuning of Power System Stabilizers Installed in DFIG-Based Wind Generation*, Power Tech Proceedings, Lausanne, Switzerland, July 2007

Chapter 4

Generation and Demand Characteristics of the Islands of Flores and São Miguel

Jonathan Donadee, Jhi-Young Joo, Remco Verzijlbergh, and Marija Ilić

4.1 Introduction

This chapter describes electrical energy consumption and generation resource data for two of the Azores islands, namely, Flores and São Miguel. The data presented here is used as input data in other chapters, which analyze various methods for the operation of electrical grids. It was important that all simulations in the monograph use the same basic data so that valid comparisons can be made between the results of different methods. Energy consumption is described by patterns in the system load, as well as the composition of the load. The structure of retail electricity tariffs on the Azores islands is also summarized. Energy supply is described by the composition of installed generation equipment and their estimated leveled costs of energy (LCOE). The availability of existing and potential renewable energy resources is also described. The majority of the primary data and information was provided by the local regulated utility, Electricity of the Azores (EDA).

J. Donadee (✉) • J.-Y. Joo • M. Ilić

Department of Electrical and Computer Engineering, Carnegie Mellon University, 5000 Forbes Ave, Pittsburgh, PA 15213, USA

e-mail: jdonadee@andrew.cmu.edu; joo@andrew.cmu.edu; milic@ece.cmu.edu

R. Verzijlbergh

Energy and Industry Group, Delft University of Technology, P.O. Box 5015, 2600 GA Delft, the Netherlands

e-mail: R.A.Verzijlbergh@tudelft.nl

4.2 Load Data

This section describes the source of electrical energy consumption data for each island and the data's characteristics. Seasonal differences in load profiles are analyzed. Other general statistics about consumption on the islands of Flores and São Miguel are presented as well.

4.2.1 Load Data Preprocessing

Demand for electric energy on Flores and São Miguel islands was derived on a 10-min timestep using generation output data. Average power output data was provided by the local regulated utility, EDA, on a half-hour timestep for all generators for the year of 2008 [1]. The sum of the output across generators is used as an approximation for system load. In many instances, data for one or more generators was missing. These instances might be the result of outages or maintenance. In these cases, aggregate load from another day in the same month and of the same day of the week is used to replace corrupted data. Because some of the simulations conducted in later sections investigate physical dynamics on a timescale faster than half an hour, load data is adjusted to be on a 10-min timestep. System power consumption is assumed to be constant across the three 10-min timesteps that compose each half-hour timestep. We made this assumption because we have no other information about the system load on faster timescales.

4.2.2 Seasons in the Azores

In order to analyze seasonality in electrical energy consumption we define four seasons in the Azores islands. Based on average daily high temperatures [2], we grouped months into seasons as shown below in Fig. 4.1: winter consists of January, February, and March; spring consists of April, May, and June; summer consists of July, August, and September; and autumn consists of October, November, and December.

4.2.3 Flores Island Load

For the year 2008, the total electrical energy produced in Flores was 11.6 GWh. Energy consumption can be allocated by consumer type as shown below in Fig. 4.2 [3]. EDA statistics show that residential customers used roughly 4.5 GWh of energy. The load duration curve of our data for Flores Island in 2008 is plotted below

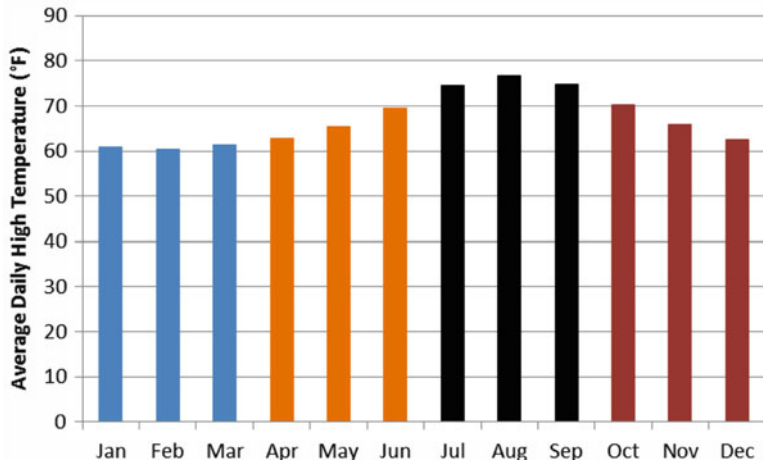
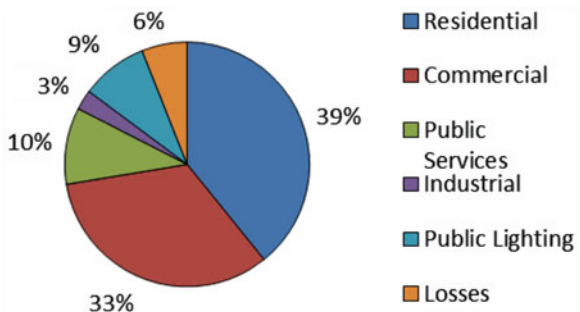


Fig. 4.1 Monthly average of daily high temperatures for the Azores islands

Fig. 4.2 Energy consumption by consumer type for the island of Flores, 2008



in Fig. 4.3. Figure 4.3 shows that the system load is between 1,800 and 1,000 kW for the vast majority the time. The system reaches a maximum of 1,978 kW and a minimum of 701 kW.

Plots below show the annual averaged system load pattern, as well as the averaged seasonal system load patterns for Flores Island. The plots are stratified into weekdays, Saturdays, and Sundays. A sample day load profile is also plotted for each season. These Plots (Figs. 4.4–4.12) show that the system load pattern is dependent on the day of the week. The difference between the load patterns mainly occurs during working hours between 8 a.m. and 6 p.m.

For these hours, the load is lowest on Sundays and highest on weekdays. There are also seasonal variations in the load pattern. The peak load occurs before 9 p.m. during winter and autumn, but occurs after 9 p.m. in spring and summer. Spring has the lowest peak load, while autumn has the highest peak load.

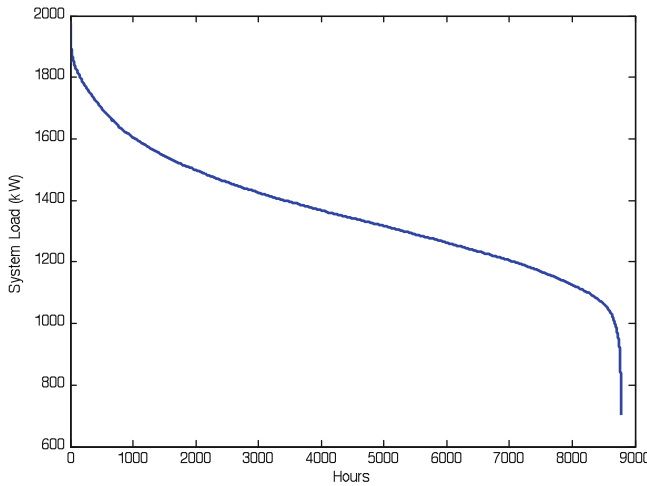


Fig. 4.3 Flores Island system load duration curve

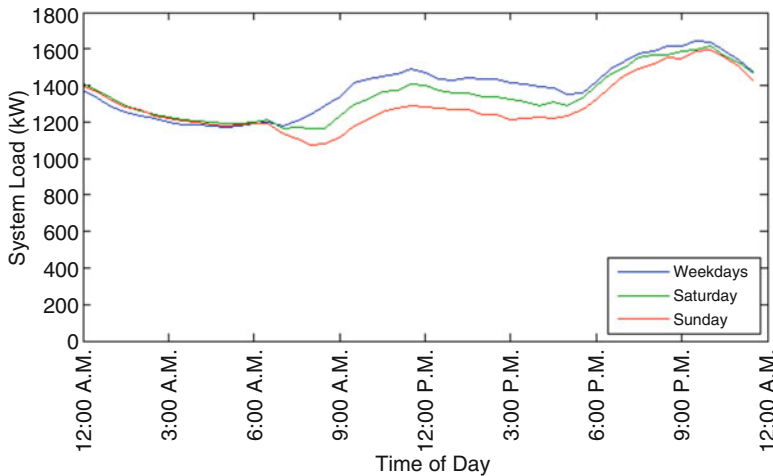


Fig. 4.4 Annual system load profiles for Flores Island

4.2.4 São Miguel Load

For the year 2008, total electrical energy produced in São Miguel was 441 GWh. Energy consumption can be allocated by consumer type as shown below in Fig. 4.13 [3]. EDA statistics show that residential customers used roughly 132 GWh of energy. The load duration curve of our data for São Miguel Island in 2008 is plotted below in Fig. 4.14. The vast majority of the hours have loads between 70 and 30 MW. The system reaches a maximum load of 73.9 MW and a minimum of 25.4 MW.

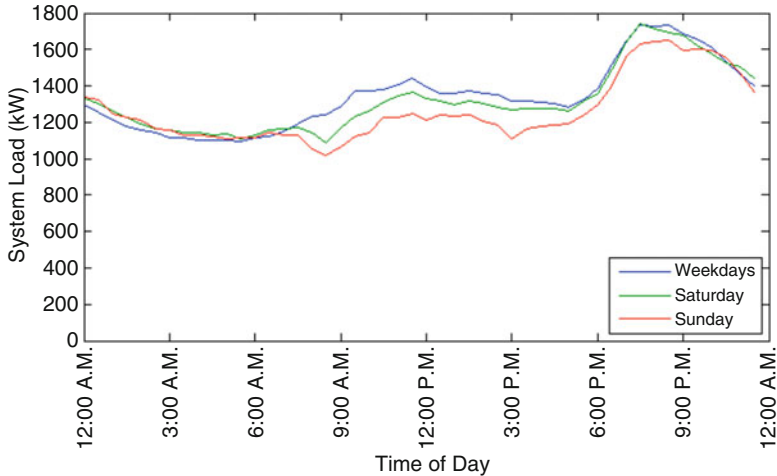


Fig. 4.5 Winter system load profiles for Flores Island

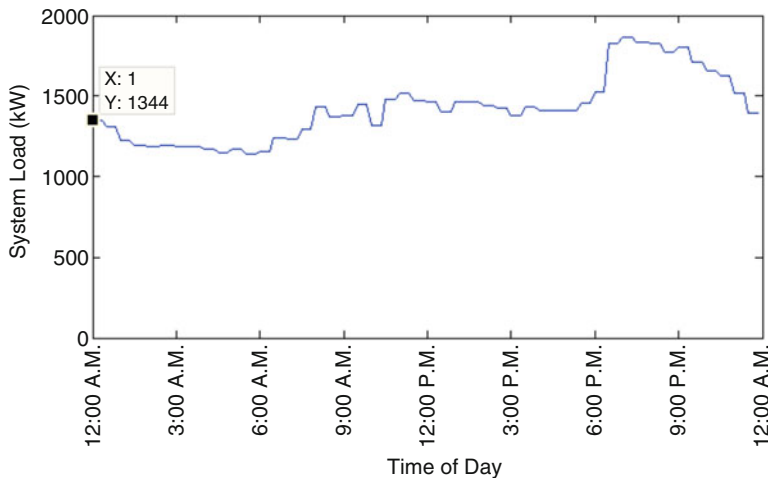


Fig. 4.6 Flores Island system load for Jan 16, 2008

Figures 4.15–4.23 show the annual averaged system load pattern, as well as the averaged seasonal system load patterns for São Miguel Island. The plots are stratified into weekdays, Saturdays, and Sundays. A sample day load profile is also plotted for each season. The plot of the annual average system load profile, Fig. 4.15, shows a very flat system load with three peaks on weekdays and two peaks on weekends. The three-weekday peaks show up in late morning just before noon,

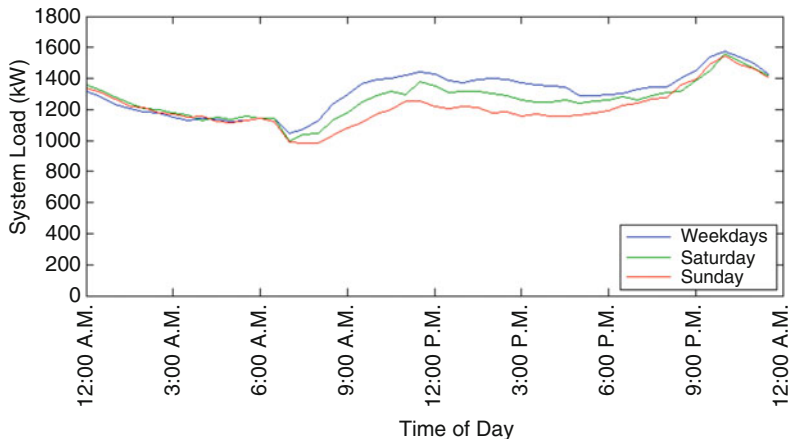


Fig. 4.7 Spring system load profiles for Flores Island

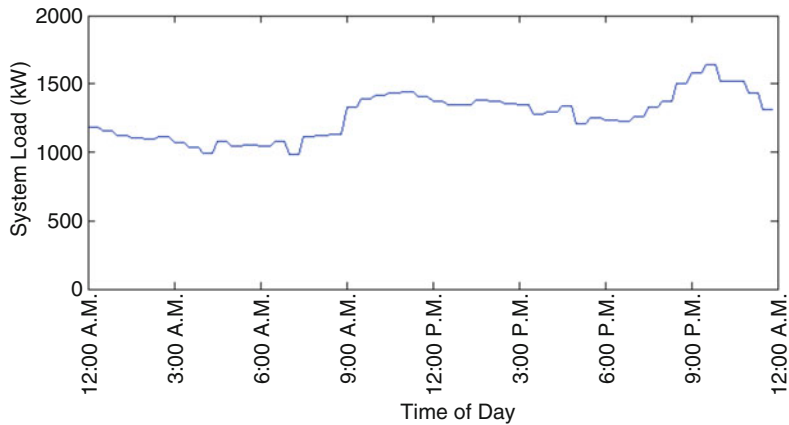


Fig. 4.8 Flores Island system load for Apr 16, 2008

between 1 and 3 p.m., and again in the evening after 6 p.m. The peaks shift with the seasons as shown in the plots below. In winter and autumn, the evening peak is highest and occurs well before 9 p.m. In spring and summer, the late morning peak is highest and the evening peak occurs well after 9 p.m. The charts also show that the load on São Miguel is much higher on weekdays than weekends. The difference is most prominent between the hours of 6 a.m. and midnight. The highest demands of the year occur in the late mornings of summer (Figs. 4.20 and 4.21).

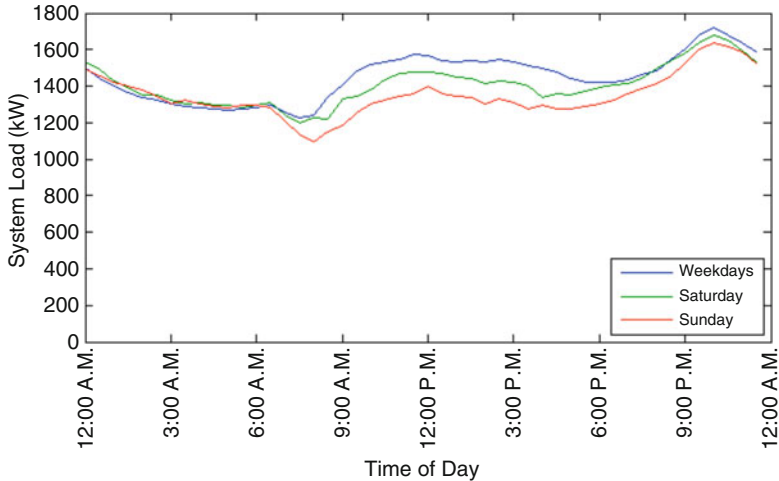


Fig. 4.9 Summer system load profiles for Flores Island

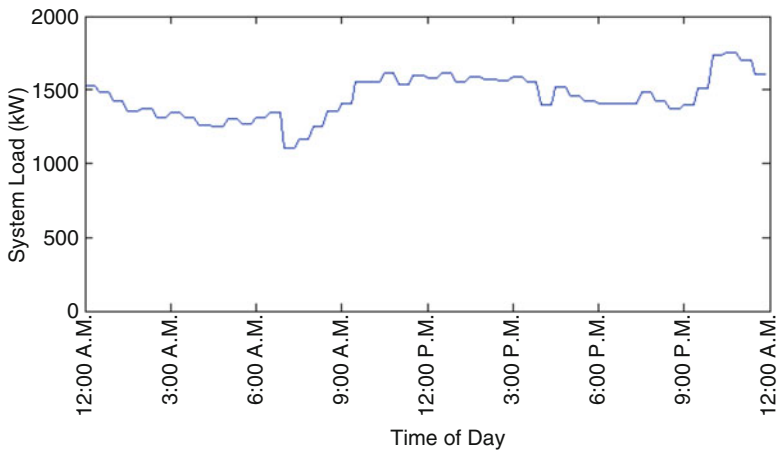


Fig. 4.10 System load profile for Flores Island, July 16

4.3 Electricity Generation

Each island in the Azores has its own unique features and resources for energy generation. This section describes the installed energy generation equipment on each island as well as potential renewable energy resources. Costs and dynamic properties of generators are discussed as well as important characteristics of historical dispatch of the equipment. Generation from wind power is analyzed in detail in Sect. 4.4.

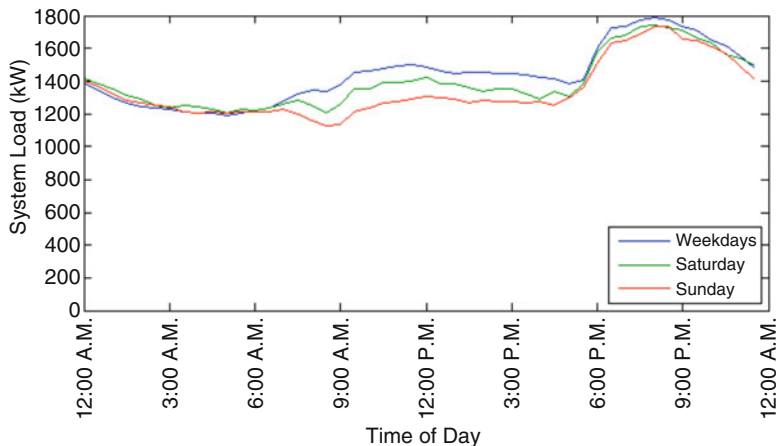


Fig. 4.11 Autumn system load profiles for Flores Island

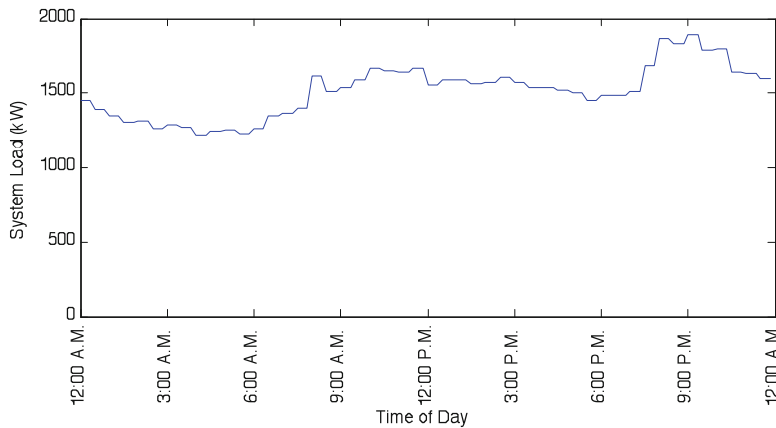


Fig. 4.12 System load profile for Flores Island on Oct 15, 2008

4.3.1 Generation on Flores Island

Flores Island is powered by a fleet of diesel, hydropower, and wind generators. Table 4.1 shows the power capacity, minimum output, and fuel type of individual generators installed on Flores Island. In 2008, 52% of energy was produced from diesel, 31% from hydropower, and 17% from wind power. The energy available from hydropower and wind power changes significantly by season. Monthly averages of the daily profile of hydropower output on Flores are plotted below in Fig. 4.24. Duration curves of hydropower and wind are also shown in Figs. 4.25

Fig. 4.13 Energy consumption by consumer type for the island of São Miguel, 2008

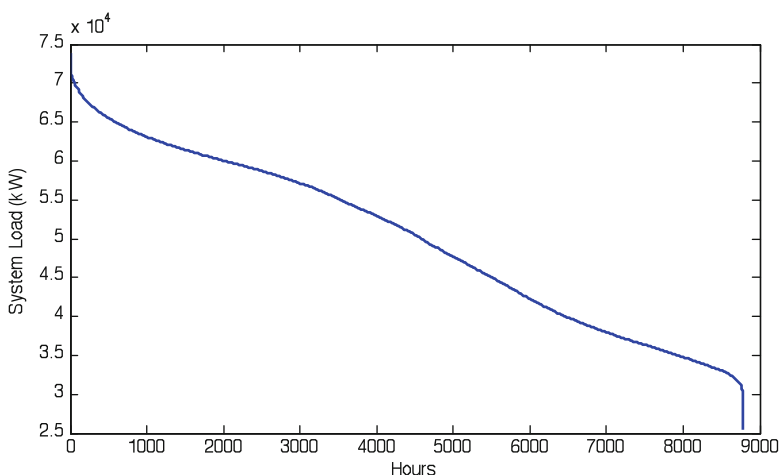
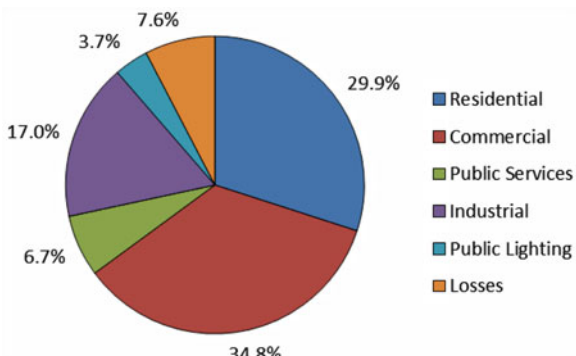


Fig. 4.14 São Miguel Island system load duration curve for 2008

and 4.26 for the different seasons as defined in Sect. 4.2.2. Wind power generation on Flores is analyzed in detail in Sect. 4.4.2.

Figures 4.24 and 4.25 show the seasonal variation in availability of hydropower on Flores Island. November through March appear to have the most hydropower availability, while the summer months have lower availability. Hydro output in the summer is below 400 kW for the majority of the hours, while staying between 300 and 800 kW for the vast majority of the winter.

Figure 4.26 below shows the variation in seasonal availability of wind power. Summer clearly has the lowest wind resource. During the summer there are only 6 h at maximum output, and the majority of hours have output below 100 kW. The other 3 seasons achieve maximum output for roughly 200 h. Winter and autumn appear to have the best wind resource availability.

Costs must be derived for planning and operational analyses conducted in this monograph. The two main costs of power generation can be described as either

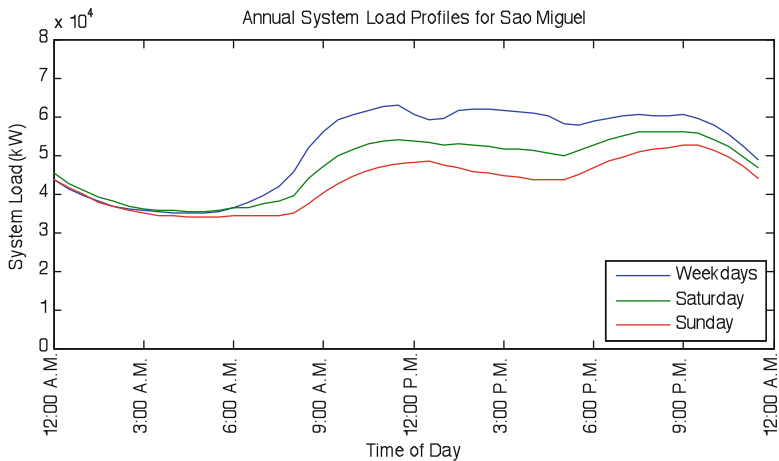


Fig. 4.15 Averaged annual system load profiles for São Miguel Island

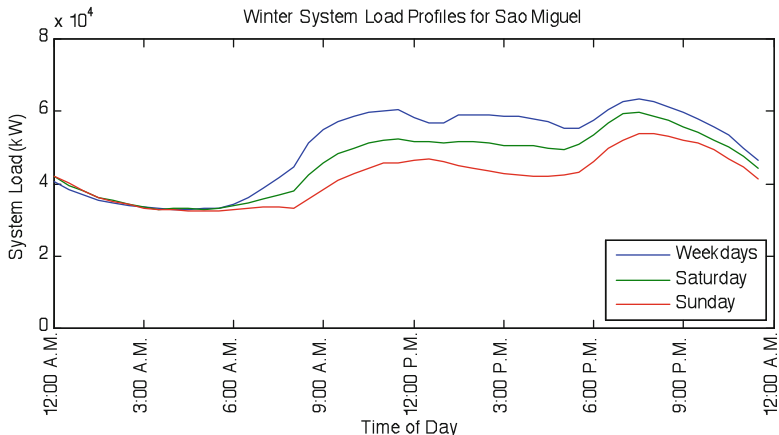


Fig. 4.16 Winter system load profiles for São Miguel Island

operations and maintenance cost (O&M) or capital costs. O&M costs consist of fuel costs and maintenance costs and are dependent on the amount of energy produced or the number of operating hours. Capital costs are simply the fixed purchase cost of the equipment. In a regulated energy system, such as in the Azores, unit commitment and economic dispatch of generators only considers O&M costs and temporal dynamic constraints, while combined O&M and capital costs must be considered for planning purposes. If generators operate in a deregulated environment, they must receive prices high enough to recover both capital and O&M costs in order to stay in business. If the marginal cost of generation is higher than the average cost of

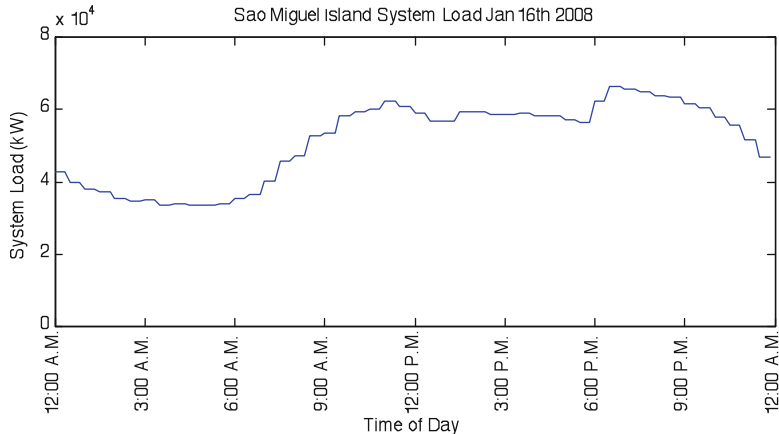


Fig. 4.17 System load profile for São Miguel Island on Jan 16, 2008

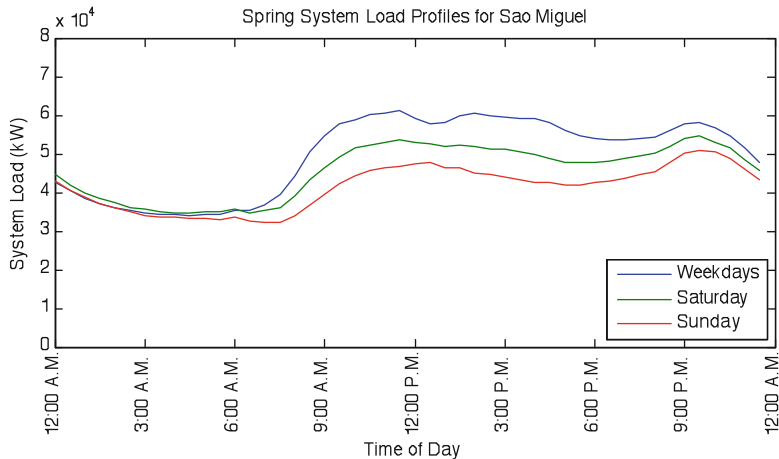


Fig. 4.18 Spring system load profiles for São Miguel Island

generation, and no generator has market power, then economic theory predicts that generators would bid their marginal cost. In the case of the Flores Island, UC or ED could be done simply minimizing the amount of diesel generation used to supply the load. Diesel fueled generators operate with a constant heat rate and therefore constant marginal cost per kWh. Hydro- and wind power have no fuel cost and very low O&M costs compared to diesel. Because of these characteristics of the generators, because energy generation in the Azores is regulated, and because we have not obtained detailed information on maintenance costs for hydropower and wind power, the marginal cost of hydropower and wind power is irrelevant for economic dispatch or unit commitment in this research.

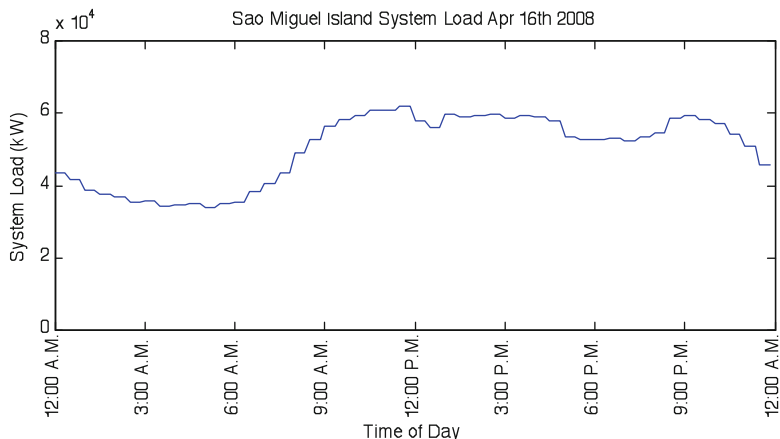


Fig. 4.19 System load profile for São Miguel Island on Apr 16, 2008

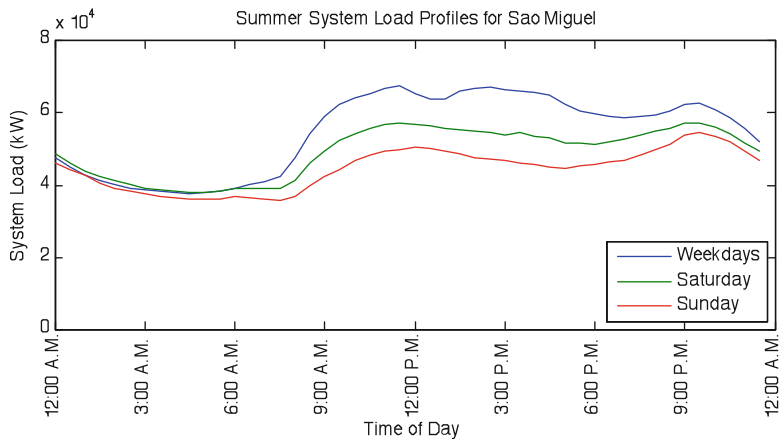


Fig. 4.20 Summer system load profiles for São Miguel Island

In the tables below we derive relevant costs for the power plants on Flores Island. For diesel fueled generation, a constant cost per kWh is calculated using recent spot market prices for fuel [4], cumulative annual energy generated by diesel, and cumulative annual fuel consumption [3]. LCOE is the cost for hydro and wind that is most relevant to this study, especially for planning. An annuity cost is calculated for each technology using equipment purchase and installation cost [5], assumed lifetimes for equipment, and an assumed interest rate of 5%. The annuity is divided by expected annual energy production to calculate LCOE (Tables 4.2–4.4).

Another critical piece of information is the maximum rate at which generator output can change. The ramp rates used in ED and UC simulations are given below in Table 4.5. Diesel generation is fast enough that power plants can be started and throttled to maximum power output within a single minute (Personal

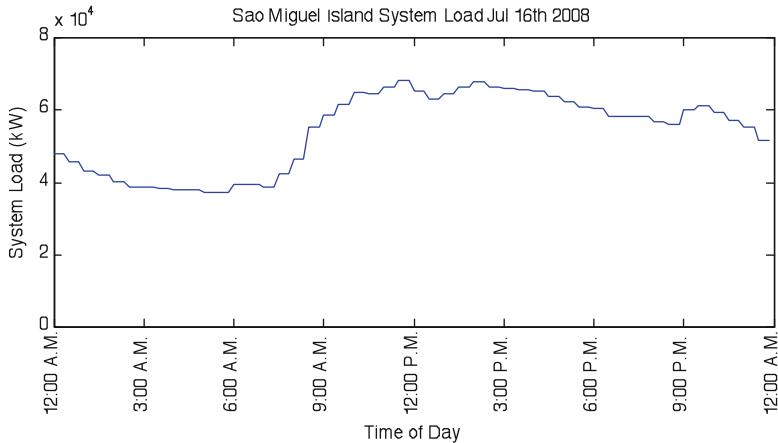


Fig. 4.21 System load profile for São Miguel Island on Jul 16, 2008

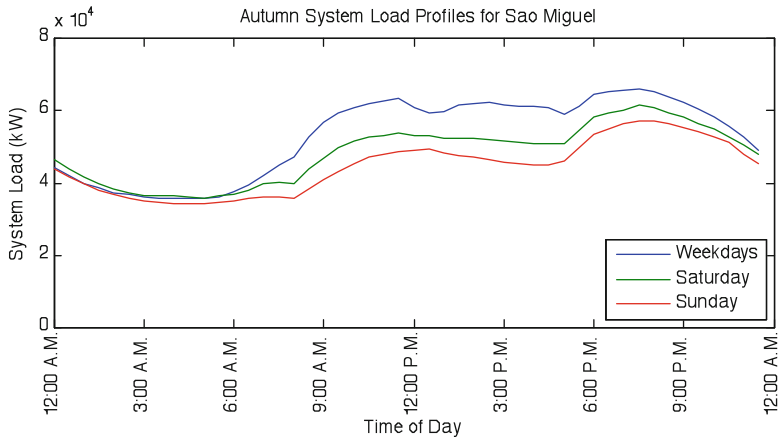


Fig. 4.22 Autumn system load profiles for São Miguel Island

communication with a representative of Cummins Diesel, Aug 2011). Wind power plants can also be controlled to change power output quickly, but the maximum power, of course, depends on the prevailing wind speed (Personal communication with a former employee of GE Wind, Aug 2011). The hydropower ramp rate was found from historical dispatch data for Flores Island. Differences were calculated between sequential dispatch points, yielding a maximum absolute difference of 5.1% of installed capacity.

A number of simplifying assumptions are made about generation equipment in simulations throughout the later chapters. Start-up and shutdown cost data was not available for use in unit commitment, so these costs are ignored. Also, some analyses treat groups of generators as a single unit.

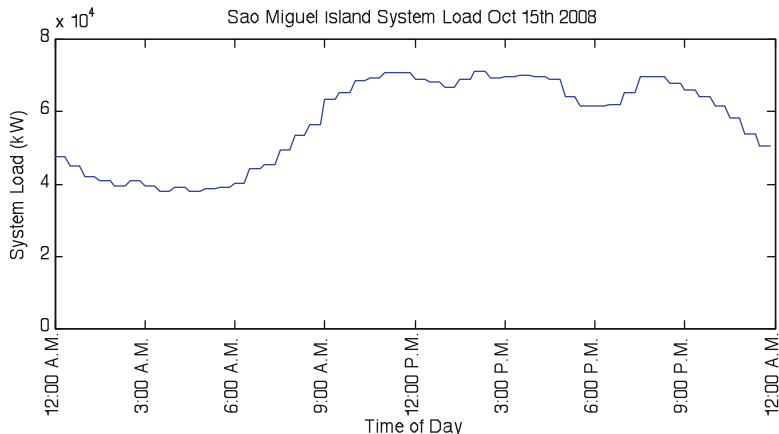


Fig. 4.23 System load profile for São Miguel Island on Oct 15, 2008

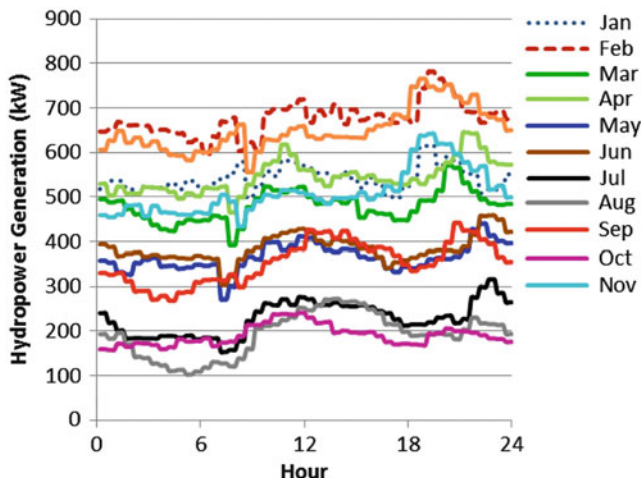


Fig. 4.24 Monthly average hydropower generation profiles for Flores Islands

4.3.2 *Generation on São Miguel*

São Miguel currently has no wind power installed and gets only 4.5% of its energy from hydropower. However, São Miguel obtains nearly 40% of its energy from geothermal power plants. The remainder of São Miguel's energy is generated from heavy fuel oil [3]. Potential wind power for São Miguel is discussed in Sect. 4.4.3.

Seasonal duration curves of geothermal power output are shown below in Fig. 4.27. This plot shows the sum of the output from São Miguel's two geothermal

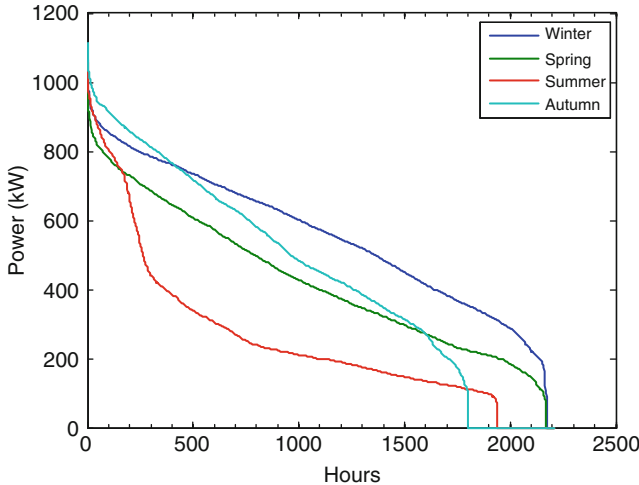


Fig. 4.25 Seasonal duration curves for hydropower on Flores Island

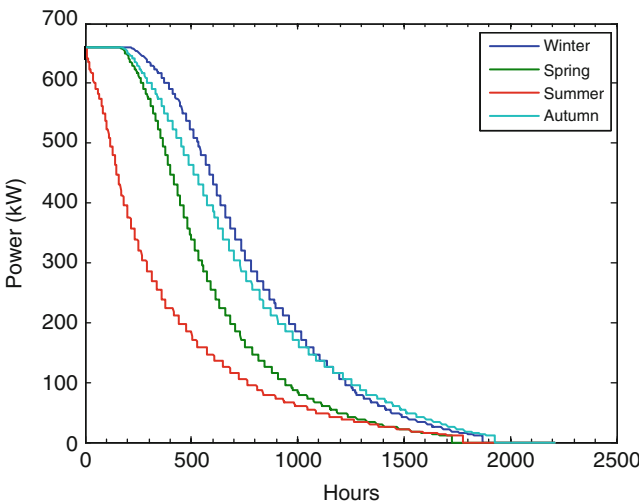


Fig. 4.26 Seasonal duration curves for wind power on Flores Island

power plants. During winter, spring, and summer, the power plants consistently produce over 18 MW. Autumn has the weakest resource availability, yet output is greater than 20 MW half of the time.

The generation equipment installed on São Miguel is shown below in Table 4.6.

Similar to diesel generators on Flores, heavy fuel oil generators have a constant heat rate and constant marginal cost of \$0.185 per kWh as calculated by an MIT student researcher [6]. Because of the same arguments made in Sect. 4.3.1, we

Table 4.1 Data for installed energy generation equipment on the island of Flores as of 2008

Power plant	Type	P_{\min} (MW)	P_{\max} (MW)
Além-Fazenda	Diesel	0.18	0.5
		0.18	0.5
		0.18	0.5
		0.28	0.7
Boca da Vereda	Wind	0.33	
		0.33	
Além-Fazenda	Hydro	0.371	
		0.371	
		0.371	
		0.76	

Table 4.2 Data for calculation of marginal cost of diesel generation

Diesel market price (\$/l)	0.867
Annual consumption (l)	1,807,879
Annual energy produced (kWh)	6,006,856
Constant marginal cost (\$/kWh)	0.261

Table 4.3 Data for calculation of LCOE for wind

Lifetime (years)	15
Expected annual production (MWh)	22,500
Installation cost (€)	14,500,000
\$/€	1.42
Interest rate	5%
LCOE (\$/kWh)	0.088

Table 4.4 Data for calculation of LCOE for hydropower generation

Lifetime (years)	50
Expected annual production (MWh)	5,120
Installation cost (€)	5,700,000
\$/€	1.42
Interest rate	5%
LCOE (\$/kWh)	0.087

Table 4.5 Flores Island maximum generator ramp rates

	Ramp rate (% P_{\max} /min)
Diesel	100
Hydro	5.1
Wind	67

consider only LCOE of hydro-, geothermal, and wind power. The LCOE of wind and hydro on São Miguel is assumed to be the same as on Flores in Sect. 4.3.1, although in reality it would depend on the specific project and realized power output. Data for the calculation of LCOE of geothermal is shown below in Table 4.7.

Geothermal, which operates at a near constant output; hydropower, which might not be controllable; and biomass generation, which is very small are considered as negative load. Historical dispatch data for these power plants is used as negative

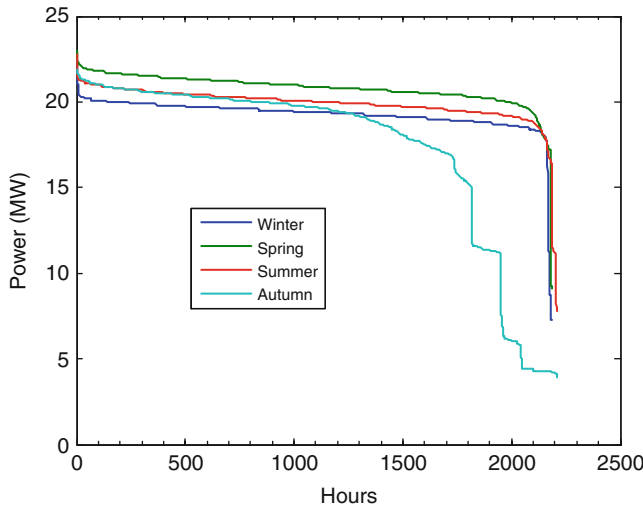


Fig. 4.27 Seasonal power duration curves of geothermal power on São Miguel Island

Table 4.6 Data for installed energy generation equipment on the Island of São Miguel as of 2008

Power plant	Type	P_{\min} (MW)	P_{\max} (MW)
Caldeirão	Fuel oil	3.848	7.5
		3.848	7.5
		3.848	7.5
		3.848	7.5
		8.41	18.165
		8.41	18.165
		8.41	18.165
		8.41	18.165
Agraçor	Biomass	0.4	
		0.4	
Túneis	Hydro		1.658
Tambores			0.094
Fábrica Nova			0.608
Canário			0.4
Ribeira Quente			0.8
Ribeira da Praia			0.8
Faiã Redonda			0.67
Pico Vemelho	Geothermal		13
Ribeira Grande			14.8

load in the later chapters for UC and ED analyses, although the chapters may make slightly different assumptions. Again, as on Flores, start-up and shutdown cost data was not available for use in unit commitment, so these costs are ignored. Also, some analyses treat groups of generators as a single unit. Fuel oil generators have

Table 4.7 Data for calculation of LCOE for geothermal generation

Lifetime (years)	50
Expected annual production (MWh)	83,000
Installation cost (€)	30,000,000
\$/€	1.42
Interest rate	5%
LCOE (\$/kWh)	0.0281

Table 4.8 Maximum generator ramp rates

	Ramp rate (%P _{max} /min)
Fuel oil (7.5 MW)	27
Fuel oil (18 MW)	17

slower cold start-up ramp rates when they transition from off to on, but this level of complexity is not considered in our simulations. Fuel oil generators are assumed to have ramp rates shown below as derived by a student researcher [6] (Table 4.8).

4.4 Wind Data

This section describes the sources and methods used to create the data set of wind power used for various analyses throughout this monograph. First we describe our source of raw meteorological wind speed data, how it is corrected for missing data, and then how it is extrapolated to wind turbine hub height. The wind turbine manufacturer's data sheets are then used to convert wind speed to wind power. The wind power is then normalized for use in numerous simulations. Finally we describe wind power daily profiles, output duration curves, and sample daily profiles for Flores and São Miguel Islands.

4.4.1 Wind Data Preprocessing

A 10-min normalized wind power data set was created for use in dispatch analyses in Chaps. 5, 7–9 and for prediction analyses in Chap. 6. Raw wind speed data is converted to normalized power output for the Enercon E33 330 kW and Enercon E101 3 MW wind turbines. These models were chosen for our analyses because 2 E33 turbines are already installed on Flores Island, and because the larger E101 would be more appropriate for installation on the island of São Miguel, which has a system base load of approximately 30 MW. Wind speed data for Flores and São Miguel Islands was gathered from Instituto de Meteorologica (Portugal Meteorological Institute), <http://www.meteo.pt>. Ten minute averaged wind speed data was measured at a height of 6.8 m at meteorological stations on the two islands. This data was corrected for missing data, filling in missing data with the average of neighboring points. The wind data was also adjusted to account for the fact that wind

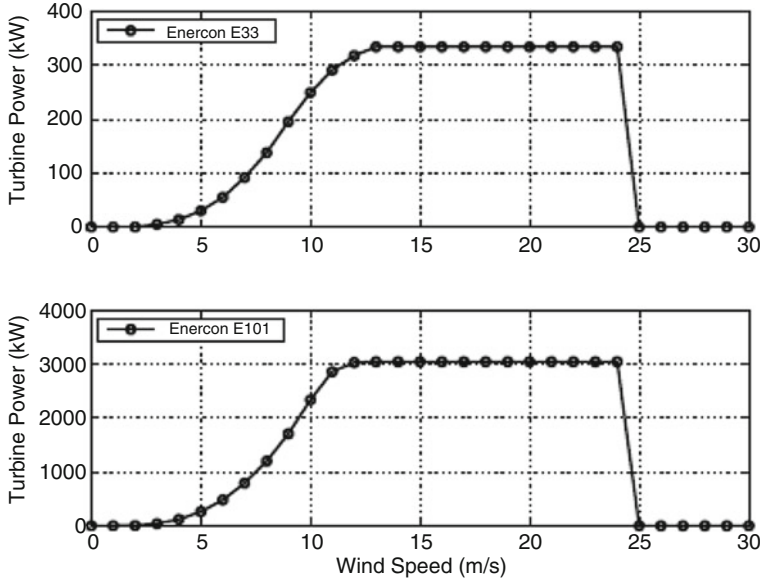


Fig. 4.28 Power curves for the two types of wind turbines under consideration

speeds are faster at the higher wind turbine heights. The vertical profile of horizontal wind speed is often described with the following logarithmic relation (see, e.g., [7]):

$$U(z) = \frac{v^*}{k} \ln \left(\frac{z}{z_0} \right) \quad (4.1)$$

U denotes the friction velocity, k the Von Karman constant, and z_0 the surface roughness length. The relation between the wind speed at measurement height z_m and the wind turbine hub height z_h is then given by

$$U(z_h) = U(z_m) \frac{\ln(\frac{z_h}{z_0})}{\ln(\frac{z_m}{z_0})} \quad (4.2)$$

For example, using a surface roughness length of $z_0 = 0.1$ m corresponding to a terrain, $z_h = 44$ m for the Enercon 33 model, and $z_m = 6.8$ m for the measurement location, Equation (4.2) reduces to

$$U(z_h) = U(z_m) \cdot 1.44 \quad (4.3)$$

Wind speed is mapped to wind power using the wind speed to wind power curve on the manufacturer's datasheets [8]. The curves are shown below in Fig. 4.28. The data is then normalized by dividing each time series of power by the maximum power output of the matching wind turbine, resulting in data ranging from 0 to 1.

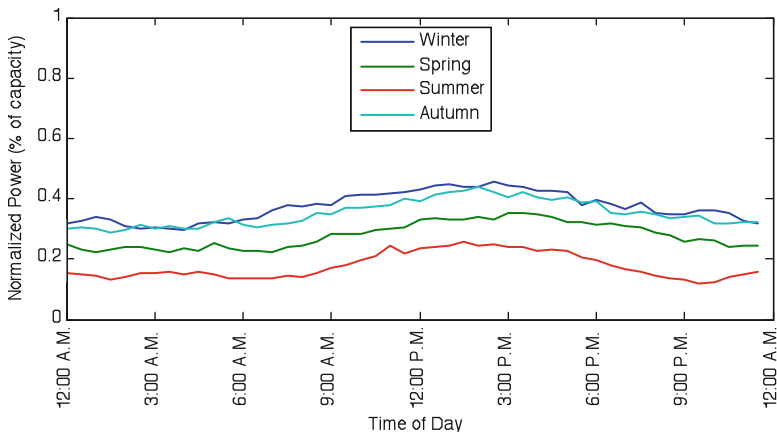


Fig. 4.29 Flores Island seasonal average wind power profiles normalized for the E33 wind turbine

The Enercon E33 wind turbine specifications were used to create a normalized data set for Flores Island, while Enercon E101 specifications were used for the island of São Miguel. When this data is used for simulations in the other chapters, it can simply be multiplied by the scenario's installed wind generation capacity to yield the appropriate wind power time series.

4.4.2 *Flores Island Wind Data*

A series of plots is presented below showing the final normalized wind power data for an Enercon E33 turbine on Flores Island. Figure 4.29 shows seasonal averages of the daily wind power profile. Wind power is generally lowest in the summer months and highest in the winter months. A diurnal pattern is also apparent, smoothly reaching a maximum in the afternoon. We can see that there is no hour during any season where wind power averages over 50% or below 10% of installed capacity. Figure 4.30 shows the output duration curve of the normalized power. The plot shows that we assume an E33 turbine would generate electricity near maximum output for 580 h and have no output for nearly 1,500 h in a year.

Figure 4.31 through Fig. 4.34 show normalized wind power profiles for four sample days. These profiles show the volatility of wind power on the island. Output on the January day is mostly high, with a period of quick drops and rises. The April day in Fig. 4.32 shows a fast transition from a sustained period of low output to a sustained period of high output. The July day in Fig. 4.33 shows a sustained period of near-zero output. Figure 4.34 shows wind power quickly transitioning back and forth between high and low output over the course of a day.

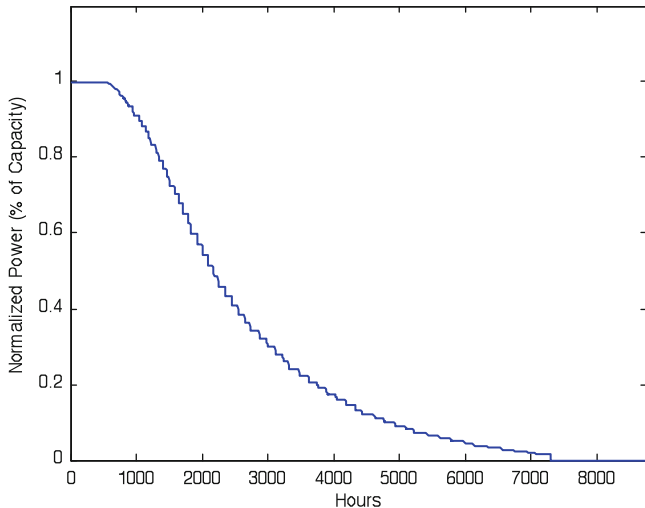


Fig. 4.30 Flores Island normalized wind power duration curve for the E33 wind turbine

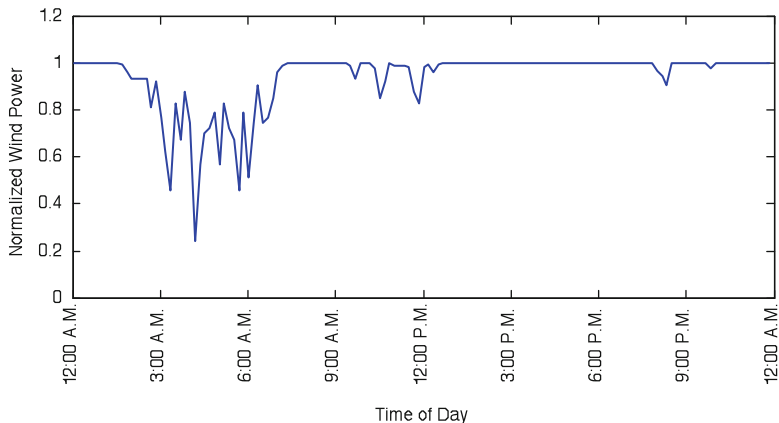


Fig. 4.31 Wind power profile for Flores Island on Jan 16, 2008, normalized to the maximum output of the E33 wind turbine

4.4.3 São Miguel Island Wind Data

A series of plots is presented below showing the final normalized wind power data for an Enercon E101 on São Miguel Island. Figure 4.35 shows seasonal averages of the daily wind power profile. Wind power is generally lowest in the summer months and highest in the winter months. A diurnal pattern is also apparent, smoothly reaching a maximum in the afternoon. We can see that the output on winter afternoons averages over 60% of installed capacity, while output on summer nights averages between 20% and 30% of installed capacity.

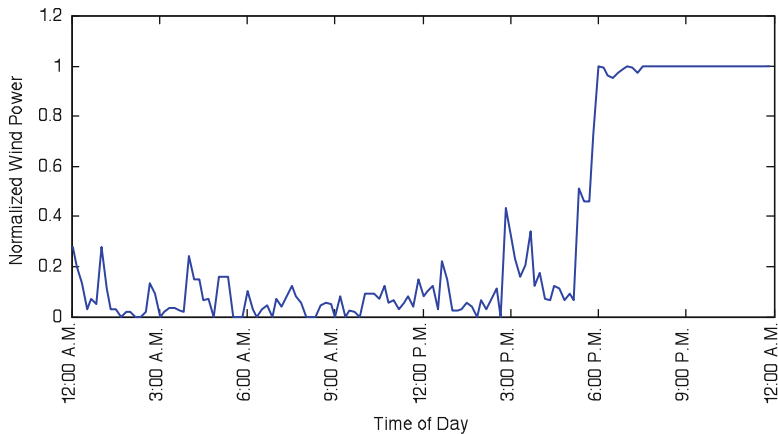


Fig. 4.32 Wind power profile for Flores Island on Apr 16, 2008, normalized to the maximum output of the E33 wind turbine

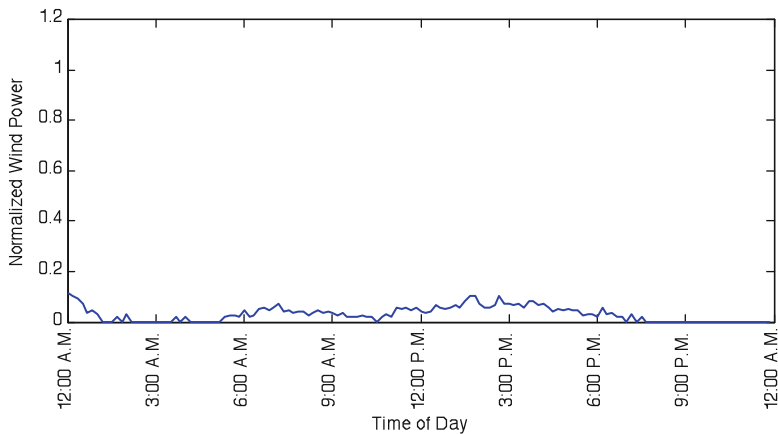


Fig. 4.33 Wind power profile for Flores Island on Jul 16, 2008, normalized to the maximum output of the E33 wind turbine

Figure 4.36 shows the output duration curve of the normalized power. The plot shows that we assume an E101 turbine would generate electricity near maximum output during 1,500 h and have no output for only 360 h in a year. Figure 4.37 through Fig. 4.40 show normalized wind power profiles for four sample days. These profiles show the volatility of wind power on the island. Figure 4.37 shows wind

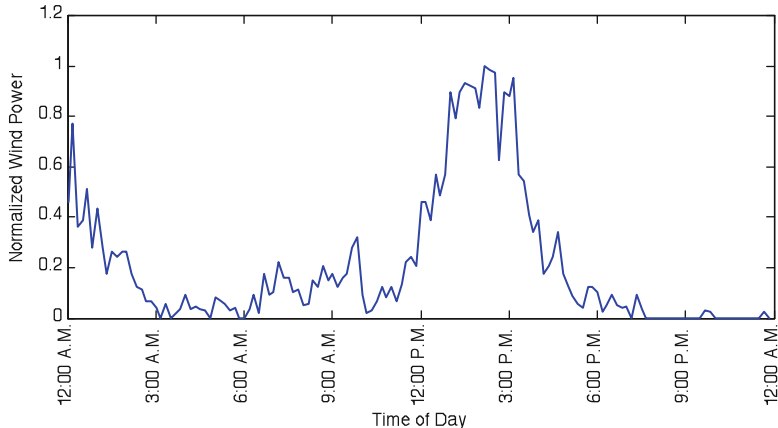


Fig. 4.34 Wind power profile for Flores Island on Oct 15, 2008, normalized to the maximum output of the E33 wind turbine

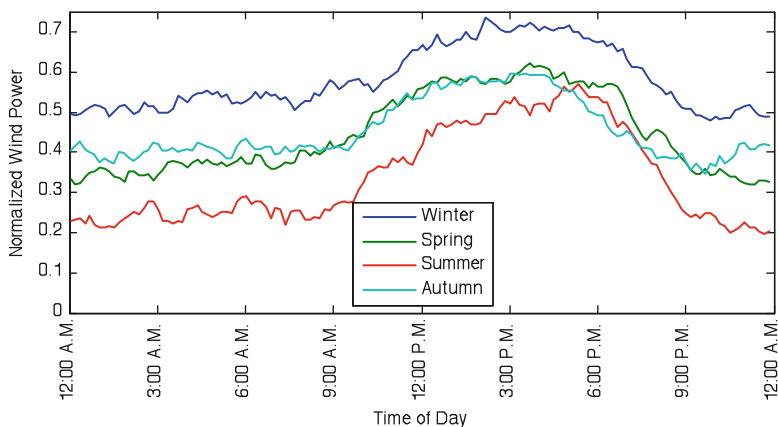


Fig. 4.35 São Miguel Island seasonal average wind power profiles normalized for the E101 wind turbine

power fluctuating from near maximum output down to 20% in the morning when energy demand is typically increasing. Figure 4.38 shows a day where wind power is near maximum output for a large portion of the day, but still has fluctuations of 30% of output within an hour between 9 a.m. and noon. Figure 4.39 shows wind power spiking up many times, but very briefly, over the course of the day. Figure 4.40 shows a daily profile where there is very little wind power available.

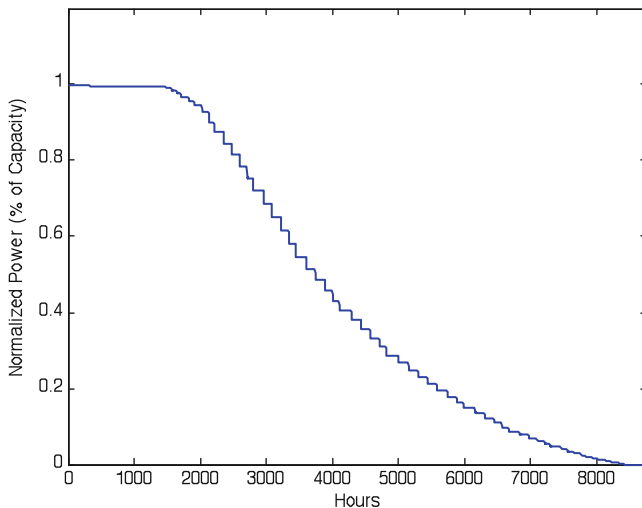


Fig. 4.36 São Miguel Island normalized annual wind power output duration curve for the E101 wind turbine

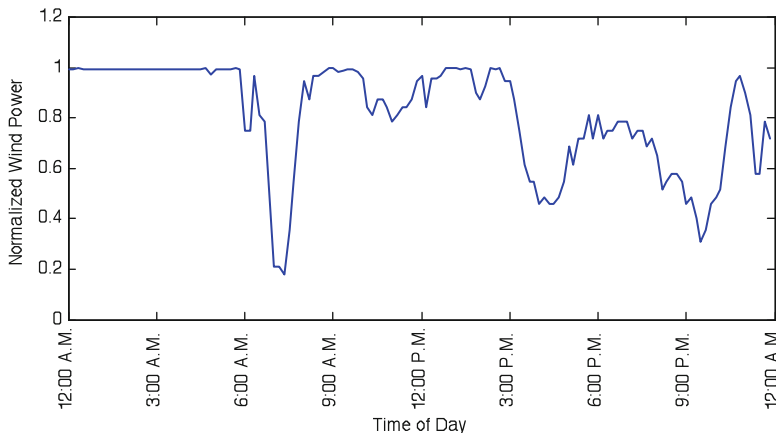


Fig. 4.37 Wind power profile for São Miguel Island on Jan 16, 2008, normalized to the maximum output of the E101 wind turbine

4.5 Electricity Pricing In The Azores

Electricity of the Azores offers two different tariffs depending on the distribution voltage levels: medium voltage (Média Tensão, MT) and low voltage (Baixa Tensão, BT). BT is again divided into two different pricings of low voltage normal (Baixa Tensão Normal, BTN) and low voltage special (Baixa Tensão Especial, BTE). All of these tariffs offer a fixed rate of price within each of the two to four different blocks

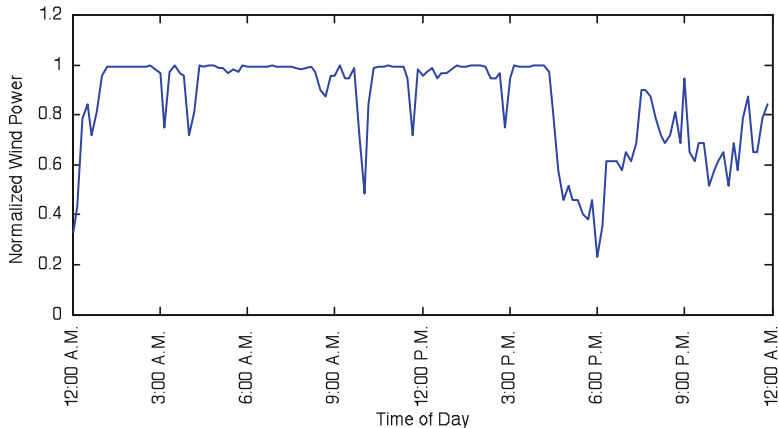


Fig. 4.38 Wind power profile for São Miguel Island on Apr 16, 2008, normalized to the maximum output of the E101 wind turbine

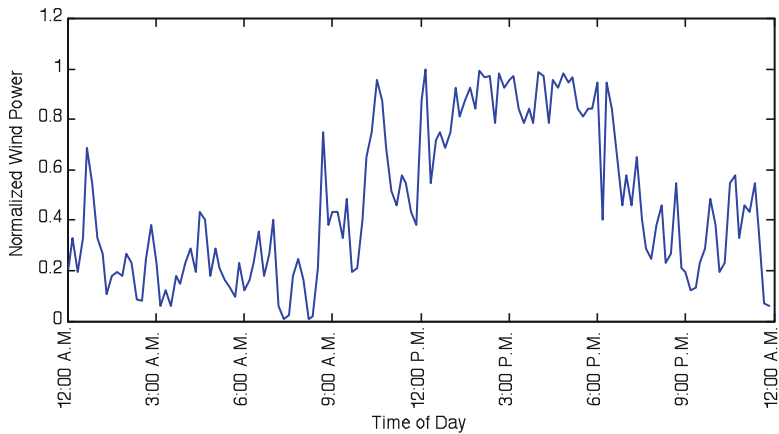


Fig. 4.39 Wind power profile for São Miguel Island on Jul 16, 2008, normalized to the maximum output of the E101 wind turbine

within a day (Tables 4.9 and 4.10). This is a type of time-of-use (TOU) pricing. MT is applied to the commercial service, public service, industrial, public lighting, and self-generation sectors of the consumers. All the residential users pay in BT, along with some users in all of the other sectors mentioned [9]. Apparent power consumption levels further subdivide the tariffs of BTN.

Table 4.11 shows the BTN tariffs for consumers with a power level greater than 17.25 kVA. A consumer sector defined as “organizations” with 17.25 kVA and “other consumers” pay by the same structure of this tariff, but with slightly different rates. BTN consumers within the power level of 2.3 and 17.25 kVA have three different tariff structures: simple, two-block and three-block tariffs. Simple tariff

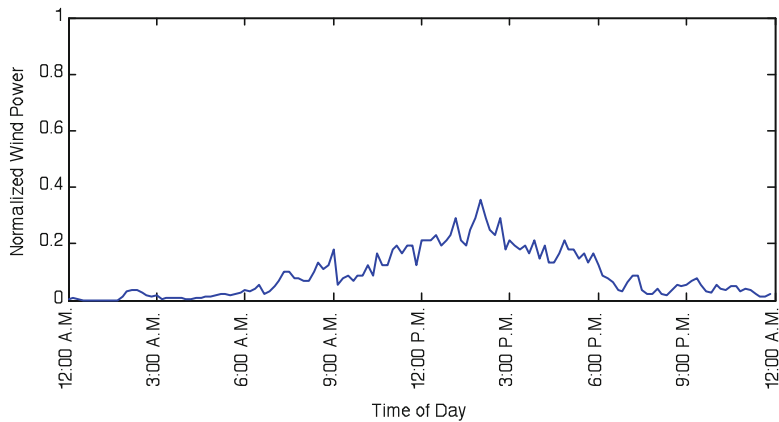


Fig. 4.40 Wind power Profile for São Miguel Island on Oct 15, 2008, normalized to the maximum output of the E101 wind turbine

Table 4.9 Retail prices in four-block MT (medium voltage), 2011

Fixed term	€	1.4401
Capacity	€/kW·day	
	Peak hours	0.2725
	Contracted	0.0369
Active energy	€/kWh	
Periods I, IV	Peak hours	0.1099
	Shoulder hours	0.0861
	Normal off-peak hours	0.0534
	Super off-peak hours	0.0499
Periods II, III	Peak hours	0.1134
	Shoulder hours	0.0879
	Normal off-peak hours	0.0555
	Super off-peak hours	0.0516
Reactive energy	€/kVarh	
	Provided	0.0191
	Received	0.0141

charges a flat rate for any time of the day, which applies to most residential users. Two-block tariff charges different rates during the peak hours and the others. Three-block tariff has peak, mid-peak, and off-peak hours. The users with less than 2.3 kVA pay by a simple tariff with a capacity charge of 1.15€/day and active energy charge of 0.1188€/kWh. This implies that the small residential users are not yet exposed to dynamic pricing, but are incented to lower their peak consumptions.

The hour blocks for both MT and BT are shown in Table 4.12. All the data shown in this subsection is obtained and translated from tariff brochures issued by EDA in January 2011. There are some interesting points regarding the tariffs of EDA. First, EDA charges not only for energy, but also for capacity in most tariffs. Second, for MT (medium voltage) and BTE (low-voltage special), they also

Table 4.10 Retail prices in four-block BTE (low-voltage special), 2011

Fixed term	€	0.6531
Capacity	€/kW· day	
	Peak hours	0.5689
	Contracted	0.0365
Active energy	€/kWh	
	Peak hours	0.1246
	Shoulder hours	0.0967
	Normal off-peak hours	0.0591
	Super off-peak hours	0.0551
Reactive energy	€/kVarh	
	Provided	0.0224
	Received	0.0168

Table 4.11 Retail prices in three-block BTN (low-voltage normal) (>17.25 kVA), 2011

	Capacity	€/kW· day
Three-block tariff	20.7	0.9354
	27.6	1.2328
	34.5	1.5302
	41.4	1.8276
	55.2	2.4224
	69.0	3.0172
	103.5	4.5042
	110.4	4.8016
	138.0	5.9912
	172.5	7.4782
	207.0	8.9652
	215.0	9.3100
Active energy	€/kWh	
Three-block tariff	Peak hours	0.2670
	Shoulder hours	0.1350
	Off-peak hours	0.0708

Table 4.12 Daily cycle for all the supplies in the Azores, 2011

Standard time period in winter		Standard time period in summer	
Peak	9:30 a.m.–11:00 a.m.	Peak	9:00 a.m.–11:30 a.m.
Shoulder	8:00 a.m.–9:30 a.m.	Shoulder	8:00 a.m.–9:00 a.m.
Normal off-peak	5:30 a.m.–8:00 a.m.	Normal off-peak	5:30 a.m.–8:00 a.m.
Super off-peak	1:30 a.m.–5:30 a.m.	Super off-peak	1:30 a.m.–5:30 a.m.

charge for reactive power both supplied and received. Third, the time blocks are determined very specifically and in detail. It would be interesting to explore how the MT customers respond to this complex dynamic pricing, for example, what technologies they use to optimize their energy bills. Also, one can see that winter has the highest rate due to the climate and the available generation resources by season (Fig. 4.41).

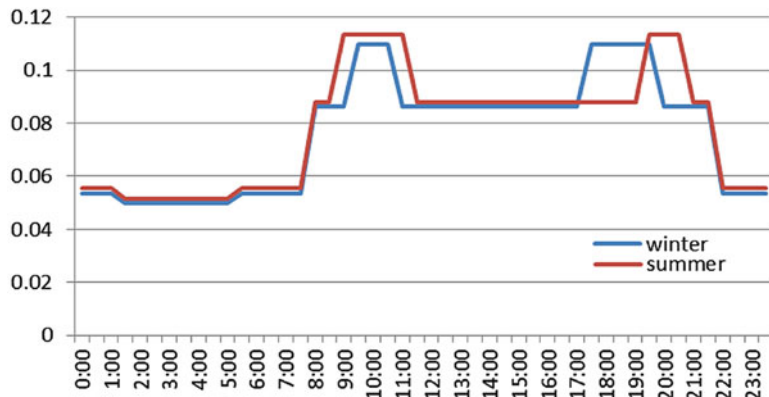


Fig. 4.41 MT tariff within a day

4.6 Concluding Remarks

Chapter 4 has provided an overview of the electrical energy system on the islands of Flores and São Miguel. These islands are small isolated systems with large amounts of renewable energy already in place. The islands also rely on very expensive diesel and heavy fuel oil thermal generation. Later chapters will investigate methods of planning and operating these electric grids with the goal of minimizing costs, emissions, and inefficiencies.

Acknowledgments Support for this research was provided partly by the Fundação para a Ciência e a Tecnologia (Portuguese Foundation for Science and Technology) through the Carnegie Mellon Portugal Program, and partly by Semiconductor Research Corporation (SRC) Energy Research Initiative (ERI) for Smart Grid Research Center (SGRC) Task 2111.001 Adaptive Load Management.

References

1. EDA, All Islands Electricity Data Half Hourly Production 2006–2009, provided by MIT Portugal Green Islands Project, January 2011
2. Wikipedia, Azores Climate. <http://www.en.wikipedia.org/wiki/Azores> Climate. Accessed 4 Aug 2011.
3. EDA, Informação Estatística da Electricidade dos Açores, Monthly Information Reports for 2005–2009 (2009). Available at <http://www.eda.pt>, Accessed 4 Aug. 2011
4. EIA, Spot prices for oil and other petroleum products. http://www.eia.doe.gov/dnav/pet/pet_pri_spt_s1_w.htm, data for New York, NY. Accessed 4 Aug 2011
5. EDA, Plano de Investimentos da EDA em Energias Renováveis, EDA Informa, No. 120/121 (July–August 2008)

6. Parness, Max. Dispatch Model Data (in .xls format) provided by MIT Portugal Green Islands Project (2011)
7. J.F. Manwell, J.G. McGowan, A.L. Rogers, *Wind Energy Explained: Theory, Design and Application* (Wiley, Chichester, 2002)
8. Enercon, Enercon Wind Energy Converters Product Overview, Tech. Rep., 2010
9. EDA, Informação Estatística (June 2011). Available at <http://www.eda.pt>, Accessed 4 Aug 2011

Part III

Wind and Load Power Prediction:

Look-Ahead Dispatch for the Efficient Use

of Available Resources

Chapter 5

Conventional Generation Dispatch Methods in Systems with Intermittent Resources

Paulo D.F. Ferreira, Pedro M.S. Carvalho, and Luis A.F.M. Ferreira

5.1 Problem Formulation

5.1.1 Mathematical Formulation

The Unit Commitment problem is solved in order to minimize the generation costs while balancing the supply and demand. Given the cost parameters associated with different generators (wind being cheapest), the idea is to dispatch the resources available in a way that minimizes diesel production, allowing more wind power injection into the grid.

The problem is formulated as

$$\min_{P_{G_i}, u} \sum_{k=1}^{48} C_{D_i}(P_{G_i}(k), x(k), u(k)) \quad (5.1)$$

subject to

$$x(k) = f(x(k-1), u(k)) \quad (5.2)$$

where $C_{D_i}(k)$ is the total cost of diesel generation at time step k , defined as a function of power output $P_{G_i}(k)$, generator state $x(k)$, and decision $u(k)$. The generator state at time step k is a function of the actual decision, $u(k)$, and is restricted by its own situation at previous time step $(k-1)$. $f(k)$ is a resource function described by a state transition diagram for the resource.

P.D.F. Ferreira (✉) • P.M.S. Carvalho • L.A.F.M. Ferreira
Instituto Superior Técnico, Technical University of Lisbon, 1049–001 Lisbon, Portugal
e-mail: pdff@ist.utl.pt; pcarvalho@ist.utl.pt; lmf@ist.utl.pt

The problem could be simplified as

$$\min_{P_{G_i}} \sum_{k=1}^{48} \alpha \cdot P_D(k) \quad (5.3)$$

subject to

$$\sum_{k=1}^{48} P_H(k) = A(k) \quad (5.4)$$

$$P_D(k) + P_H(k) = D(k) - \hat{P}_{G_w}(k) - P_{G_g}(k) - P_{Hnc}(k) \quad (5.5)$$

$$|P_D(k+1) - P_D(k)| \leq R \quad (5.6)$$

where $P_D(k)$ is the diesel power production at time step k , $P_H(k)$ is the controllable hydro production, $P_{Hnc}(k)$ is the noncontrollable hydro production, $\hat{P}_{G_w}(k)$ is the wind production, $P_{G_g}(k)$ is the geothermal production (if available), and $D(k)$ is the demand. $A(k)$ is the power production assigned to controllable hydro plants and R is the maximum power change allowed to diesel units.

If there are no controllable hydro plants, then $A(k) = 0$. The details of power production assignment to controllable hydro plants are in Sect. 5.1.1.2.

This simplified model can be solved through linear programming but does not consider thermal dynamics. To get more accurate results the UC problem is solved including the restrictions associated with thermal units. These restrictions are described in Sect. 5.1.1.1.

The UC with thermal dynamics cannot be solved with linear programming; the solution is provided instead through dynamic programming.

5.1.1.1 Thermal Dynamics

Thermal units have several constraints that make this model more complex.

The output power that a thermal unit can supply is defined by a non-continuous function:

$$P_{G_i\text{out}} = \{0\} \cup [P_{G_i}^{\min}, P_{G_i}^{\max}] \quad (5.7)$$

with $P_{G_i}^{\min} > 0$.

Also, there are restrictions associated with *minimal downtime*, since the generator needs some time to shut down. These restrictions can be defined by the following function:

If $x(k) = 0 \& \mu(k) = 0$, then $x(k+1) = 0$

$x(k) = 0 \& x(k-1) = 0 \& x(k-2) = 0 \& x(k-3) = 0 \& \mu(k) = 1$,

then $x(k+1) = 1$

$x(k) = 0 \& \{x(k-1) \neq 0 || x(k-2) \neq 0 || x(k-3) \neq 0\} \& \mu(k) = 1$,

then $x(k+1) = 0$

5.1.1.2 Controllable Hydro Dynamics

For the Unit Commitment decision process it is assumed that the outflow/output power relation of the hydro generation is linear, starting from zero. Based on the available historical data, it is assumed that the available hydro power output has a monthly pattern. This monthly pattern allows us to determine the average amount of power available for each day, which will be applied to peak-shaving. Since there is no significant change in load behavior for the different days of the week, the limitations on power production are assumed to be the same.

5.1.1.3 Interruptions

The need for preprogrammed maintenance or the occurrence of unexpected failure, in hydro, wind, and geothermal production has an impact on the total energy produced by fuel-powered plants, as well as on the ideal number of *green* resources for the system.

The study of the impact of generation interruption is done by randomly generating interruptions in a chronological simulation, with an average number of *interruptions per year* and an average *duration*.

5.1.2 Data

5.1.2.1 Wind and Load

UC for Flores and São Miguel was run on load and wind data described in Chap. 4.

The load data has three profiles (Wednesday, Saturday and Sunday) for every month, with a 30-min resolution.

Both Flores and São Miguel data have a 30-min resolution for every day between January 2008 and December 2008. Detailed data specification is available in the chapter on the input data.

5.1.2.2 Hydro Constraints

Flores has a hydro plant with a $50,000 \text{ m}^3$ reservoir. The daily restrictions on energy production (Table 5.1) were set based on the average monthly production between 1996 and 2004.

Table 5.1 Flores hydro plant-restrictions on daily production

Month	Energy per day [kWh]
January	10.500
February	10.200
March	10.800
April	10.900
May	9.300
June	8.700
July	7.200
August	6.000
September	6.100
October	6.300
November	7.200
December	8.400

5.2 Simulations

5.2.1 Flores

5.2.1.1 Results

Flores has a small power system in which hydro resources contribute significantly. However, water flow depends on the season, so there is a typical generation pattern along the course of the year. Figure 5.1 illustrates how this affects the system—in this case, the lack of water flow is compensated for through the increase in diesel production.

The thermal dynamics is also depicted. In Fig. 5.2c, at hour 11, the hydro and wind production is enough to supply the demand. However, diesel production is not set to zero due to the fact that at least one generator is always needed to compensate for wind power fluctuations. Because the thermal units cannot be kept running and set to zero output power (Sect. 5.1.1.1), in some situations there might exist more power available than the demand. This leads to some power to be spilled out—typically the wind power is spilled.

The operational challenge of (1) controlling all hydro resources, (2) intermittent wind power availability, and (3) nonzero thermal units minimum output creates several difficulties for the integration of noncontrollable renewable resources. Excess of wind turbines in a small power system will cause wind spill, leading to a reduction on return of investment. Figure 5.3a illustrates the wind spill due to an increase in wind turbines in the power system. Figure 5.3b illustrates the duration curves of diesel production along the course of the year. The increase in wind turbines reduces the power supplied by diesel-powered generators but this power amount is never set to zero.

Flores has some hydro resources with reservoirs. This allows the operator to use them for peak-shaving and/or keeping water on windy days, allowing more wind

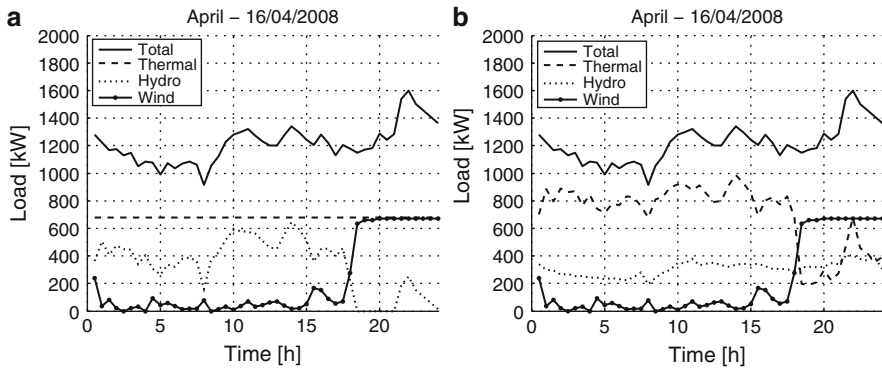


Fig. 5.1 Flores – Comparison, for the same day, assuming that there is (a) hydro generation with a reservoir and (b) hydro generation without a reservoir. It is assumed that there are 2 wind turbines in the system. (a) With the possibility of using hydro resources for peak shaving, diesel generation keeps steady throughout the day. (b) Without the possibility of using hydro resources for peak-shaving, diesel generation maintains the balance between demand and generation. The wind power profile plotted refers to the wind power available, not necessarily the wind power injected into the grid

power to be integrated into the grid. The balance between generation and demand kept by hydro resources allows for savings in diesel operation. Figure 5.1 illustrates how hydro resources can be used for peak-shaving. Tables 5.2 and 5.3 show the cost reduction to diesel operation associated with hydro peak-shaving.

The inclusion of wind turbines in Flores power system is expected to reduce the costs related to diesel operation. However, due to the impossibility of shutting down all diesel generators, a significant increase in wind turbines does not mean an equivalent reduction on diesel costs. Table 5.2 and Fig. 5.3 show that there is a cost reduction on diesel-powered energy; however, the cost converges to a nonzero value.

Figure 5.4b and 5.5b illustrates the grid limit for absorbing wind power generation—the relation between the number of turbines and the wind energy injected into the grid is not linear.

5.2.1.2 Results Impact of Interruptions

The results presented do not consider the impact of interruptions in hydro and wind production due to either the need for preprogrammed maintenance or to unexpected faults. To assess the impact of unit interruptions on the cost, Fig. 5.6 compares several scenarios:

- No faults [0 – 0]
- Four interruptions/year with an average duration of 10 h [4 – 10]
- Eight interruptions/year with an average duration of 10 h [8 – 10]

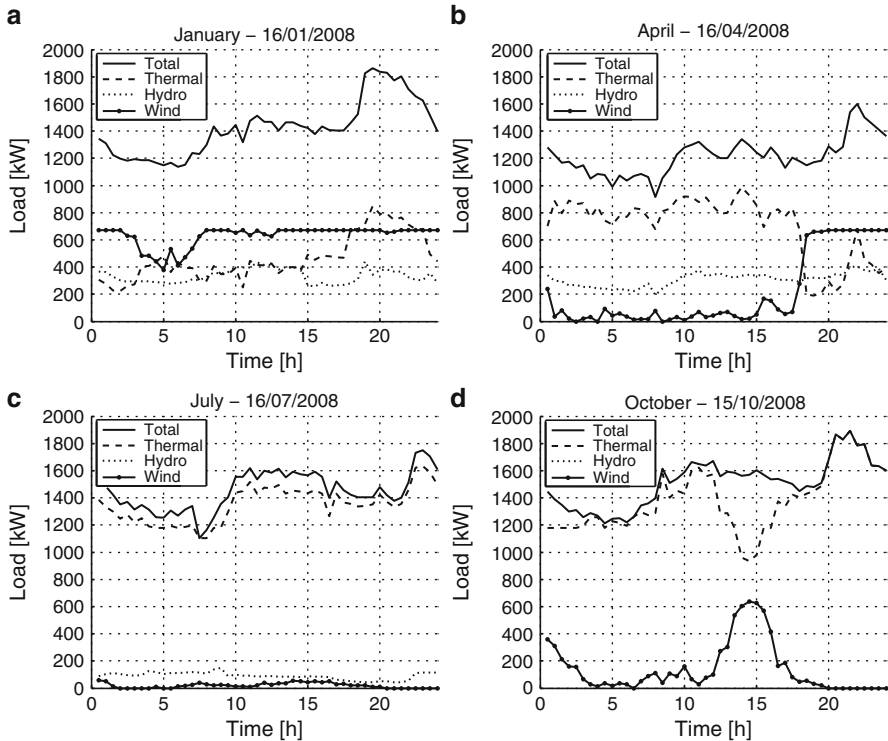


Fig. 5.2 Typical load diagram of Flores for each season of the year, considering 2 wind turbines available on the grid. The wind profile plotted refers to the wind power available, not necessarily the wind power injected into the grid. The lack of water flow in summer is compensated for through an increase in diesel production. In Fig. 5.2c, at hour 7, the hydro and wind production is enough to supply the demand, but diesel production is not set to zero due to thermal dynamics; this, as described above, eventually leads to wind spill

The interruptions ratio is applied individually to each generator.

Figure 5.6 shows that the impact of interruptions is residual for annual wind spill, unless under very extreme conditions (Figure 5.5, [60-10] scenario). The increase in diesel production needed to compensate for the lack of other resources is less than 7 %. Since we use wind spill as a criterion to determine the ideal number of wind turbines for the grid, one can conclude that the impact of faults on the system does not need to be considered.

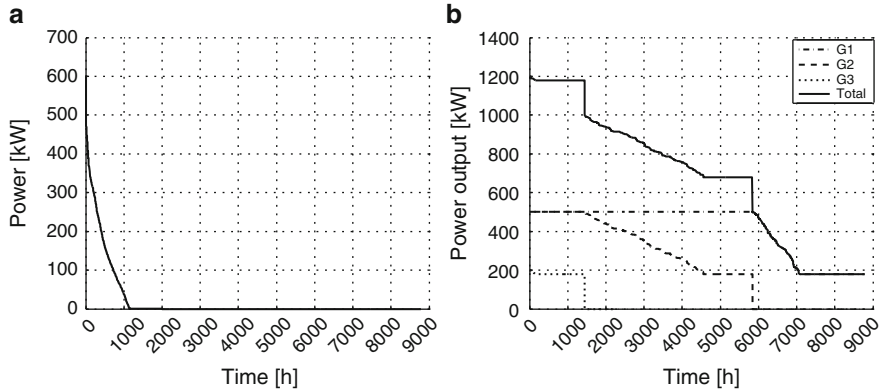


Fig. 5.3 Duration curves on Flores, considering 4 wind turbines available on the grid as well as hydro resources with a reservoir. **(a)** Total wind spill. The total energy spilled by all four turbines, in this scenario, is about 6% of all energy expected to be produced for the course of 1 year. **(b)** Duration curve associated with diesel production. The *solid line* represents the sum of all the generators. As expected, the total diesel power never goes to zero, as diesel generation is never shut down

Table 5.2 Flores – Total diesel costs—2008

No. wind turb.	Total energy produced [MWh]		Cost [USD]	
	Reservoir	No reservoir	Reservoir	No reservoir
1	8,063	9,884	2,104,300	2,579,600
2	7,238	8,991	1,889,200	2,346,500
3	6,458	8,235	1,685,400	2,149,300
4	5,955	7,708	1,554,300	2,011,900
5	5,585	7,331	1,457,600	1,913,400
6	5,293	7,025	1,381,600	1,833,600
7	5,039	6,769	1,315,400	1,766,600

Comparison between the scenarios where (1) hydro resources have a reservoir and (2) no reservoir is available. All groups are assumed to have 26.10 c/kWh. There is a reduction in the cost and the power supplied by diesel units (columns 2 and 4) when the number of wind turbines increases, but that cost converges to a nonzero value

5.2.2 São Miguel

5.2.2.1 Results

São Miguel also has a small power system, although it is bigger than Flores.

Figure 5.8 illustrates the typical generation diagram of São Miguel. In this scenario 10 wind turbines are considered to be existent in the system. There is geothermal generation that has steady output power, with very little capacity to

Table 5.3 Flores Diesel costs—May to October

No. wind turb.	Total energy produced [MWh]		Cost [USD]	
	Reservoir	No reservoir	Reservoir	No reservoir
1	2,821	3,953	736,150	1,031,700
2	2,406	3,537	627,960	923,100
3	2,081	3,149	543,130	822,000
4	1,914	2,913	499,450	760,300
5	1,787	2,769	466,360	722,900
6	1,689	2,656	440,820	693,300
7	1,606	2,558	419,130	667,500

Comparison between the scenarios where (1) hydro resources have a reservoir and (2) no reservoir is available. All groups are assumed to have 26.10 c/kWh. There is a reduction in the cost and the power supplied by diesel units (columns 2 and 3) when the number of wind turbines increases, but that cost converges to a nonzero value

Table 5.4 São Miguel Total oil costs—2008

No. wind turbines	Total energy produced [MWh]		Cost [USD]
	produced [MWh]	Cost [USD]	
1	290,090.0	53,667,000.0	
5	243,010.0	49,570,000.0	
10	193,740.0	35,843,000.0	
15	167,260.0	30,943,000.0	
20	152,810.0	28,827,000.0	
25	146,380.0	26,525,000.0	
30	136,390.0	25,231,000.0	

All groups are assumed to have 18.5 c/kWh. There is a reduction in the cost and the power supplied by diesel units (columns 2 and 3) with an increase in the number of wind turbines, but that cost converges to a nonzero value

adjust. As with Flores, the variations between the demand and the generation profile are compensated for through diesel generation.

5.2.2.2 Costs

Similarly to Flores, the introduction of wind turbines into São Miguel power system is expected to reduce the costs related to diesel operation. As on Flores, due to the impossibility of shutting down all diesel generators, a significant increase in wind turbines does not mean an equivalent reduction in diesel costs. However, since São Miguel has a bigger power system than Flores, it is able to handle more wind turbines with more nominal power.

Table 5.4 and Fig. 5.9a present the cost reduction with respect to energy produced by diesel generation. Figure 5.9b illustrates the grid limit for absorbing wind power generation on São Miguel.

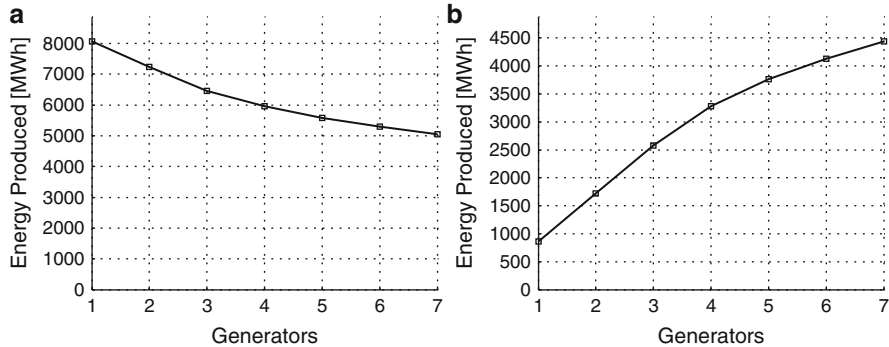


Fig. 5.4 Flores (a) Total energy produced by diesel units for different numbers of wind turbines available on the grid. The diesel production does not converge to zero as it is impossible to shut down all thermal units. (b) Total energy produced by wind generators for different numbers of wind generators available on the grid. Since there is no possibility of shutting down all diesel generation, and due to the small size of the power system, an increase in the number of wind turbines means an increase in wind spill

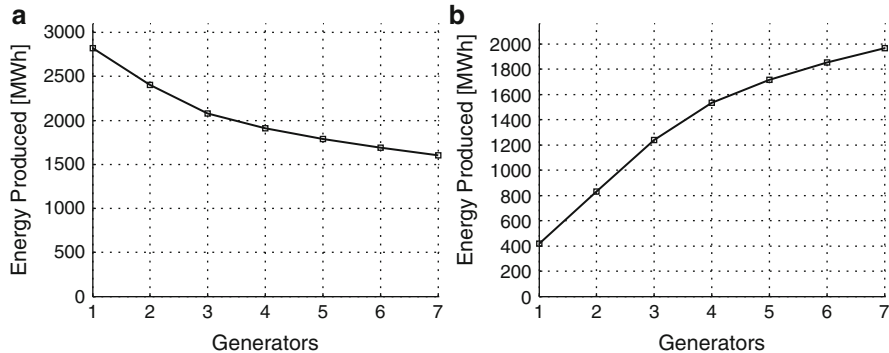


Fig. 5.5 Flores (a) Increase of energy by diesel generators due to failure of wind or hydro resources. The [60–10] fault is included to compare the effect of different fault magnitudes on the system. (b) Wind spill considering several interruption scenarios. Since the fault regime is severe, the wind spill drops due to the lack of wind power

5.2.2.3 Results Impact of Interruptions

Similarly to the results presented in Sect. 5.2.1.2, Fig. 5.10 compare several scenarios:

- No faults [0 – 0]
- Four interruptions/year with an average duration of 10 h [4 – 10]
- Eight interruptions/year with an average duration of 10 h [8 – 10]

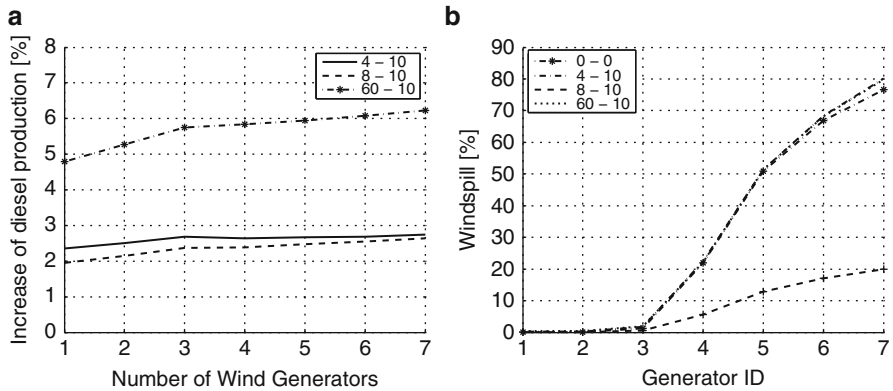


Fig. 5.6 (a) Total energy produced by diesel units for different numbers of wind turbines available on the grid on Flores. The diesel production does not converge to zero since it is impossible to shut down all thermal units. The X-axis starts from 1 turbine. (b) Total energy produced by wind generators for different numbers of wind generators available on the grid. Since there is no possibility of shutting down all diesel generation, and due to the small size of the power system, an increase in the number of wind turbines means an increase in wind spill. The X-axis starts from 1 turbine

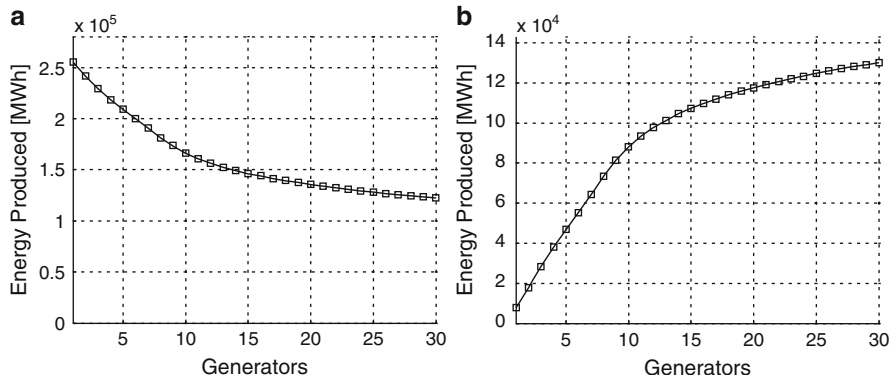


Fig. 5.7 (a) Total energy produced by diesel units—May to October. (b) Total energy produced by wind generators—May to October. The pattern is similar to the annual results

For wind turbines the interruptions ratio is applied individually to each generator.

Figures show that on São Miguel the impact of interruptions is residual for annual wind spill. The increase in diesel production to compensate for a lack of other resources is less than 4% for low impact interruptions scenario and less than 6% for more severe scenario (20-20). Again, since wind spill is used as a criterion to determine the ideal number of wind turbines for the grid, for this purpose the impact of faults on the system does not need to be considered.

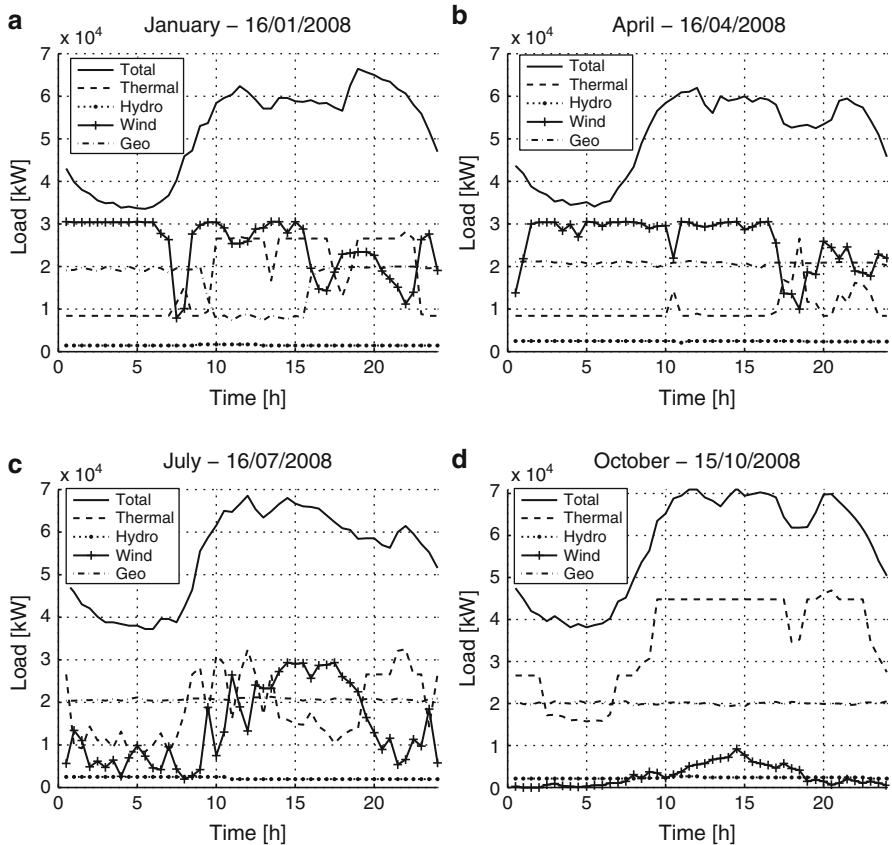


Fig. 5.8 Typical load diagram of São Miguel for each season of the year, assuming 10 wind turbines available on the grid. The wind power profile plotted refers to the wind power available, not necessarily the wind power injected into the grid. The lack of water flow in the summer has no impact on diesel production. There is a unit of geothermal production with low output power regulation—deviations from the balance between demand and generation are compensated for through diesel generation

5.2.3 Estimation of the Ideal Number of Turbines

Since both Flores and São Miguel have small power systems, the integration of wind power is limited. It is not always possible to inject all wind power available into the grid due to the inability to shut down all diesel generation and the existence of several noncontrollable hydro resources as well as geothermal units.

The reduction of wind power injected into the grid will raise the costs associated with the operation of these turbines. The levelized cost of energy (LCOE) expresses the cost of generation energy considering the investment, costs of operations and

Table 5.5 S.Miguel Oil costs—May to October

No. wind turbines	Total energy produced [MWh]	Cost [USD]
1	116,860.0	21,619,000.0
5	92,650.0	17,141,000.0
10	69,740.0	12,902,000.0
15	59,940.0	11,088,000.0
20	55,140.0	10,202,000.0
25	51,850.0	9,593,000.0
30	49,610.0	9,179,000.0

All groups are assumed to have 18.5c/kWh. There is a reduction in the cost and the power supplied by diesel units (columns 2 and 3) with an increase in the number of wind turbines, but that cost converges to a nonzero value

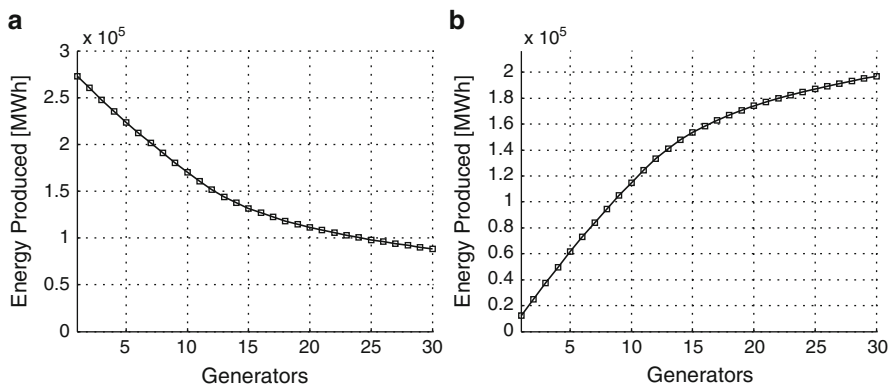


Fig. 5.9 São Miguel (a) Total energy produced by oil units for different numbers of wind turbines available on the grid on São Miguel. The diesel production does not converge to zero since it is impossible to shut down all thermal units. The X-axis starts from 1 turbine. (b) Total energy produced by wind generators for different numbers of wind generators available on the grid. Since there is no possibility of shutting down all diesel generation, and due to the small size of the power system, an increase in the number of wind turbines means an increase in wind spill. The X-axis starts from 1 turbine

costs of maintenance, (5.8). This value is got assuming that the turbine will produce and sell an expected amount of energy into the grid.

$$\text{LCOE}_t = \frac{I_t + M_t + F_t}{E_t} \quad (5.8)$$

With I_t as investment costs, M_t as operations and maintenance costs for time period t , F_t as fuel costs, and E_t the expected energy sell to the grid. The fuel costs for wind turbines are zero.

If the energy produced cannot be injected into the grid, the LCOE will rise. For the estimation of the ideal number of generators we assume that the grid is

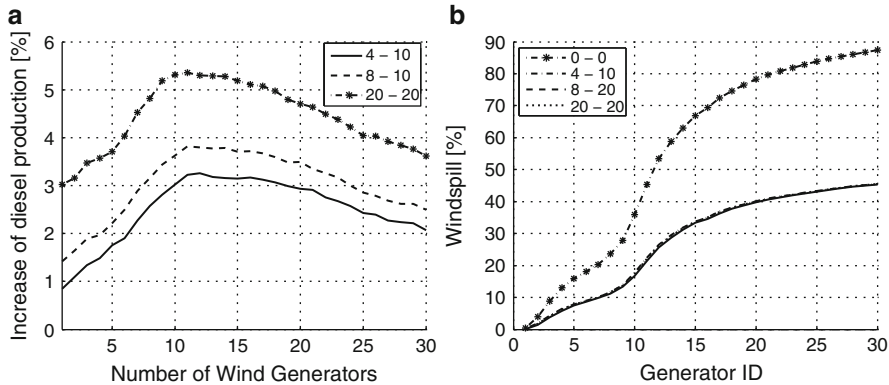


Fig. 5.10 São Miguel (a) Increase in energy output by diesel generators due to failure of wind or hydro resources. 4 or 8 faults/year dose not significantly impact diesel generation. (b) Wind spill considering several interruption scenarios. Since the fault regime is severe, the wind spill drops when wind power decreases

Table 5.6 Ideal number of wind turbines for Flores, considering different diesel and wind LCOE

	LCOE [c\$/kWh]	
Diesel cost [c\$/kWh]	5.0	8.8
26.1	7	5
30.0	8	6

Table 5.7 Ideal number of wind turbines for São Miguel, considering different oil and wind LCOE

	LCOE [c\$/kWh]	
Oil cost [c\$/kWh]	5.0	8.8
18.5	14	11
25.0	16	12

only interested in having a wind turbine if the LCOE is less than the cost of diesel operation. We assume that the LCOE for a turbine with any wind spill is 8.8 c/kWh.

Tables 5.6 and 5.7 present the ideal number of wind turbines, considering the LCOE and diesel/oil costs for each island. For instance, with a diesel cost of 26.1 c/kWh (Flores), 1 turbine has value if it has a maximum of 66.2 % wind spill, for LCOE = 8.8 c/kWh. If the LCOE is 5 c/kWh, this value rises to 80 % wind spill. For an oil cost of 18.5 c/kWh (São Miguel), 1 turbine has value if it has a maximum of 52.4 % wind spill. If the LCOE is 5 c/kWh, this value rises to 72.9 % wind spill.

Tables 5.8 and 5.9 present partial wind spill related to the total energy produced by each turbine. For wind spill purposes only, it is assumed that if all turbines are available to inject power into the grid, the wind turbines with smaller No. have priority.

Table 5.8 Wind spill by turbines—Flores, 2008

Wind turbine no.	Wind spill [%]	
	Reservoir	No reservoir
1	0	0.1
2	0	0.7
3	1.3	19.4
4	22.6	49.8
5	52.1	68.4
6	67.8	78.5
7	76.4	85.0
8	82.2	89.8
9	86.5	93.8
10	90.2	96.9

Comparison between hydro resources with and without reservoirs. An increase in wind spill will raise the LCOE—if the LCOE equals diesel costs then the wind turbine might not be attractive to the grid

5.2.3.1 Flores

From Table 5.8 considering a Diesel cost of 26,1c\$/kWh one can conclude that for an LCOE of 8.8c/kWh, the system can handle up to 5 turbines, and for an LCOE of 5c/kWh, the system can handle up to 7 turbines, if hydro resources have reservoirs available for peak-shaving. Otherwise, the system can handle only 4 turbines for an LCOE of 8.8c/kWh and 6 turbines for an LCOE of 5c/kWh.

5.2.3.2 São Miguel

From Table 5.9, considering a oil cost of 18,5c\$/kWh, one can conclude that for a LCOE of 8.8c/kWh, the system on São Miguel can handle up to 11 turbines. For a LCOE of 5c/kWh, the system can handle up to 14 turbines.

5.2.4 Other Scenarios

All the simulations presented are done assuming the thermal units have minimum output power. This restriction means that the grid is always being at least partially supplied from fossil-fuel sources even if there is enough power from other sources, since a thermal source is responsible for maintaining the balance between generation and demand. This limits the grid capacity to absorb wind and hydro power, so it is ideal to have thermal generation with low minimal power or fast storage systems.

To evaluate the impact of thermal dynamics, the results of the same grids in the same scenarios are presented in this section, but with the assumption that the thermal units do not have minimum output power.

Table 5.9 Wind spill by turbine—São Miguel 2008

Wind turbine no.	Wind spill [%]
5	17.6
6	20.0
7	22.5
8	26.2
9	30.9
10	39.9
11	50.4
12	59.3
13	65.4
14	69.9
15	74.2
16	77.0
17	80.4
18	82.9
19	84.9
20	86.9

An increase in wind spill will raise the LCOE—if the LCOE equals diesel costs then the wind turbine might not be attractive to the grid

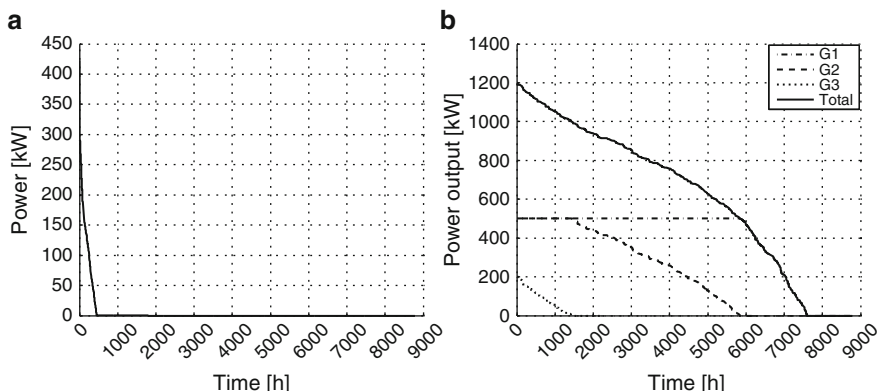


Fig. 5.11 Flores-Duration curves considering 4 wind turbines available on the grid, hydro resources with reservoirs, and no minimal output power for thermal units. (a) Total wind spill. The total energy spilled by all four turbines, in this scenario, is about 1.8% of all energy expected to be produced during the course of 1 year. (b) Duration curve associated with diesel production. The *solid line* represents the sum of all the generators. As expected, now total diesel power goes to zero, since there are no restraints concerning minimal output power

5.2.4.1 Flores

As expected, the elimination of minimal power constraints helps to reduce wind spill. Figure 5.11 shows a reduction down to about 1.8%, when originally it was about 6% (Fig. 5.3).

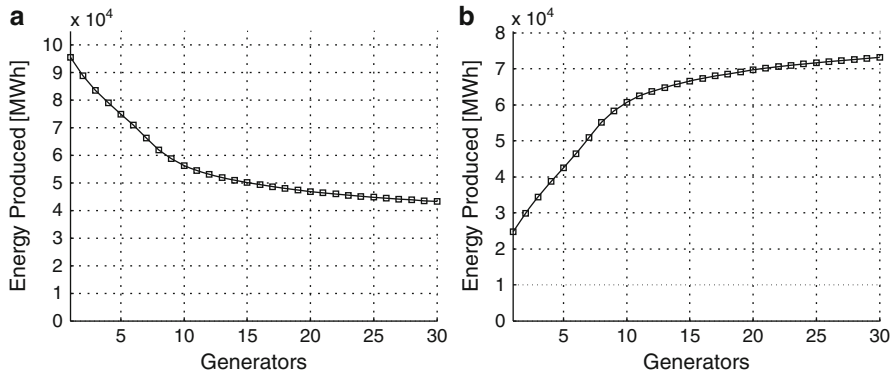


Fig. 5.12 São Miguel (a) Total energy produced by oil units—May to October. The diesel production does not converge to zero since it is impossible to shut down all thermal units. The X-axis starts from 1 turbine. (b) Energy produced by wind generators—May to October. Since there is no possibility of shutting down all diesel generation, and due to the small size of the power system, an increase in the number of wind turbines means an increase in wind spill. The X-axis starts from 1 turbine

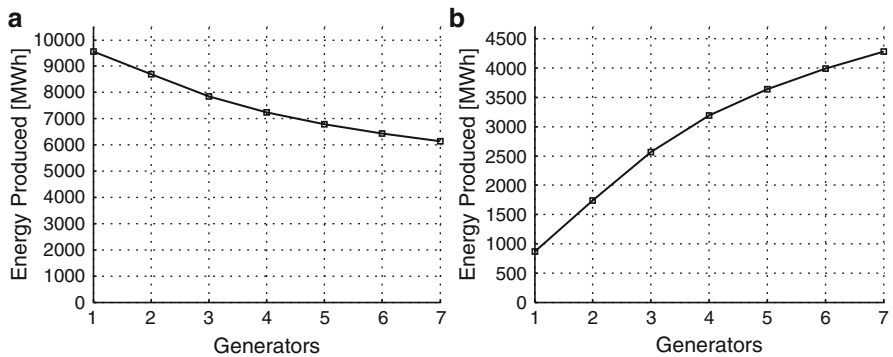


Fig. 5.13 Flores (a) Total energy produced by diesel units for different numbers of wind turbines available on the grid. (b) Total energy produced by wind generators for different numbers of wind generators available on the grid

From Fig. 5.13 and Table 5.10, and comparing them with Fig. 5.2 and Table 5.2, one can see that the elimination of minimal power constraints allows for savings of 3.3% in diesel production, for 1 turbine, and 9.2%, for 7 turbines in a non-reservoir scenario. When the possibility of managing the reservoir in some hydro resources is considered, the savings are 3.3% for 1 turbine and 12.9% for 7 turbines.

Table 5.11 shows the new wind spill values for the scenario in study. As is argued before, wind spill is used as a criterion for defining the ideal number of wind turbines for each grid. As the wind spill decreases, the ideal number of wind turbines increases. Considering a LCOE of 5c/kWh and Diesel cost of 8c/kWh, originally the maximum number was 8 (Table 5.6) and now it is 9 (Table 5.12).

Table 5.10 Flores—Total diesel costs—2008

No. wind turb.	Total energy produced [MWh]		Cost [USD]	
	Reservoir	No reservoir	Reservoir	No reservoir
1	7,799	9,557	2,035,700	2,494,500
2	6,929	8,689	1,808,500	2,268,000
3	6,094	7,859	1,590,700	2,051,400
4	5,463	7,232	1,425,900	1,887,700
5	5,014	6,784	1,308,700	1,770,700
6	4,668	6,435	1,218,300	1,679,500
7	4,386	6,142	1,144,800	1,603,100

Comparison between the scenarios where hydro resources have or do not have reservoirs with no minimal output power constraints on the thermal units. All groups are assumed to have 26.10 c/kWh. There is a reduction in the cost and the power supplied by diesel units (columns 2 and 4) with an increase in the number of wind turbines, but that cost converges to a nonzero value

Table 5.11 Wind spill by turbine—Flores, 2008

Wind turbine no.	Wind spill [%]	
	Reservoir	No reservoir
1	0.0	0.0
2	0.0	0.0
3	0.0	5.2
4	7.3	32.8
5	36.4	57.2
6	58.6	70.7
7	69.9	78.4
8	76.7	84.1
9	81.9	88.0
10	85.7	91.5

Comparison between hydro resources with and without reservoirs. An increase in wind spill will raise the LCOE—if the LCOE equals diesel costs then the wind turbine might not be attractive to the grid

5.2.4.2 São Miguel

Similarly to Flores, the elimination of minimal power constraints helps to reduce wind spill (Fig. 5.14). Figure 5.14 illustrates a reduction down to about 8% of the overall wind generation, whereas originally the wind spill was about 17% of the overall wind generation (Fig. 5.15).

Comparing Table 5.13, and Table 5.4, one can see that the elimination of minimal power constraints allows for savings of 5.9% in oil production, for 1 turbine, and 35%, for 30 turbines.

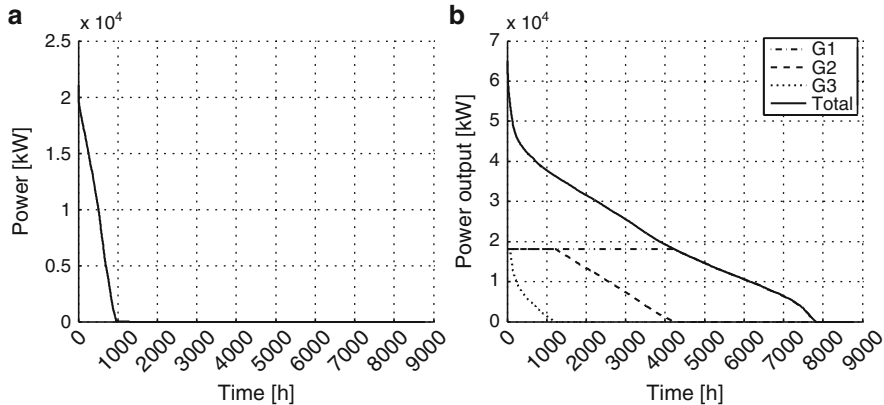


Fig. 5.14 São Miguel – Scenario where Diesel generation do not have minimal output power – Duration curves considering 10 wind turbines available on the grid. (a) Total wind spill. The total energy spilled by all four turbines, in this scenario, is about 8 % of all energy expected to be produced during the course of 1 year. (b) Duration curve associated with diesel production. The *solid line* represents the sum of all the generators. As expected, the total goes to zero, since the thermal generation now has no lower limit

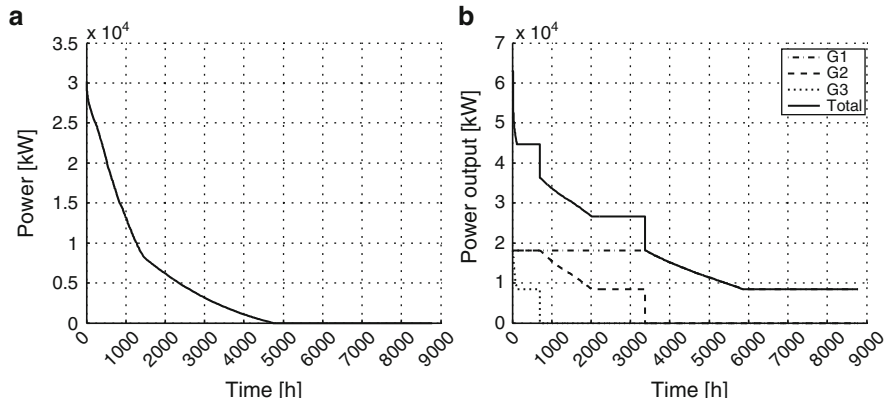


Fig. 5.15 São Miguel – Original Scenario where Diesel generation have minimal output power – Duration curves assuming 10 wind turbines available on the grid. (a) Total wind spill. The total energy spilled by all four turbines, in this scenario, is about 17 % of all the energy expected to be produced in the course of 1 year. (b) Duration curve associated with diesel production. The *solid line* represents the sum of all the generators. As expected, the total never goes to zero, as diesel generation is never shut down

Table 5.14 shows the new wind spill values. Again, the wind spill is used as a criterion for defining the ideal number of wind turbines for each grid. Similarly to Flores, the ideal number of wind turbines increased—originally the maximum ideal number of turbines was 16 (Tables 5.7 and 5.9) and now it is 21 (Table 5.15).

Table 5.12 Ideal number of wind turbines for Flores, considering different diesel and wind LCOE and no minimum output power on diesel generators

Diesel cost [c\$/kWh]	LCOE [c\$/kWh]	
	5.0	8.8
26.1	8	6
30.0	9	7

Table 5.13 São Miguel – Total oil cost—2008

No. wind turbines	Total energy produced [MWh]	Cost [USD]
1	272,970.0	50,499,000.0
5	223,770.0	41,398,000.0
10	170,053.0	31,548,000.0
15	131,890.0	24,400,000.0
20	114,640.0	20,043,000.0
25	98,210.0	18,170,000.0
30	88,580.0	16,388,000.0

All groups are assumed to have 18.5c/kWh. There is a reduction in the cost and the power supplied by diesel units (columns 2 and 3) with an increase in the number of wind turbines, but that cost converges to a nonzero value

5.3 Discussion

In this chapter, we study the impact of different-sized wind parks on Flores and São Miguel power systems and estimate the ideal number of wind turbines for both islands. A Unit Commitment (UC) with dispatch function is used to make the estimation. We assume that geothermal units and hydro generation without reservoir behave as negative loads. Hydro plants with reservoir are dispatched for peak-shaving, observing daily energy production constraints that give priority to wind power over the power produced by those plants. When there is no storage available, several diesel units are kept running at minimum power to be able to compensate for wind fluctuations.

We discuss the integration of a large number of wind turbines into a small power system such as those on Flores and São Miguel. The wind power injection is limited by (1) the small size of the power systems, (2) the impossibility of shutting down all diesel generation, and (3) the existence of geothermal generation and non-controllable hydro resources. However, the availability of reservoirs for some hydro resources allows for a wider integration of renewable resources, with a reduction of costs for diesel operation. We use the wind spill to estimate the optimal number of wind turbines for each island: between 11 and 16 turbines with 3,030kW for São Miguel and 5–8 turbines with 330kW for Flores. We also consider the effects of interruptions of hydro and wind units. For typical values of forced outage rates,

Table 5.14 Wind spill by turbine—São Miguel 2008

Wind turbine no.	Wind spill [%]
5	4.5
6	9.0
7	12.9
8	15.4
9	17.6
10	20.1
11	24.0
12	29.0
13	38.7
14	48.4
15	56.4
16	61.8
17	66.4
18	69.8
19	72.8
20	76.3
21	78.5
22	80.3
23	81.9
24	83.3
25	84.6

An increase in wind spill will raise the LCOE—if the LCOE equals diesel costs then the wind turbine might not be attractive to the grid

Table 5.15 Ideal number of wind turbines for São Miguel, considering different oil and wind LCOE and no minimum output power on thermal generators

Oil cost [c\$/kWh]	LCOE [c\$/kWh]	
	5.0	8.8
18.5	19	14
25.0	21	16

interruptions have no major impact. Finally, for comparison, a study was run where minimal output power regarding thermal dynamics was not considered. The results show that on Flores thermal dynamics does not have a significant impact on the optimal number of wind turbines but makes up for a 9.2% decrease in diesel consumption in a 7 turbine scenario. On São Miguel thermal dynamics has a significant impact on the number of turbines and on decreasing oil consumption.

Acknowledgements This work was partially supported by Fundação para a Ciência e Tecnologia via project CMU-PT/SIA/0043/2009. The authors are grateful for its financial support.

Chapter 6

Multi-scale Models for Decomposing Uncertainties in Load and Wind Power

Noha Abdel-Karim and Marija Ilić

6.1 Introduction

The operation and planning of electric power systems have become more challenging than in the past due to the presence of major new uncertainties and the risks related to them. These new uncertainties are created by a higher penetration of hard-to-predict intermittent power generation and by the responsive loads. Also, in parts of the world where electric power industry restructuring has taken place, power system operators and planners cannot predict nor control the availability of nonutility-owned generation. This ongoing and evolving situation is requiring a fundamental change in operating and planning methods, which can no longer be static nor deterministic. Instead, much can be gained by proactively learning the patterns of the dominant uncertainties and using these patterns to predict wind and load power and then conducting the operations and planning by taking these predictions into account. For example, instead of assuming an average constant capacity factor in a wind power plant, wind power prediction needs to be more dynamic as new information becomes available. Uncertainties in wind and load power patterns have a major impact on a system operator's ability to balance supply and demand by dispatching the least-cost and the cleanest power plants first. Therefore, new methods for economic dispatch and unit commitment are needed which use model-based predictions of wind power and demand. The longer-term the forecast is, the more reliable and efficient the balancing of supply and demand will be. This is because all the physical components—the power plants and the consumers—are constrained by their ramp rates as to how fast and by how much they can change their power produced or consumed. Often the ramp rates vary

N. Abdel-Karim (✉) • M. Ilić

Department of Engineering Public and Policy, Carnegie Mellon University,
5000 Forbes Ave, Pittsburgh, PA 15213, USA

e-mail: nohakarim81@gmail.com; milic@ece.cmu.edu

over broad ranges, with nuclear and coal power plants being the slowest, and gas power plants the fastest, to respond. It is this fundamental inability to respond instantaneously that makes it very critical, for operations purposes, to forecast demand and intermittent resources at least 24 h ahead. For operations it is necessary to have good weekly, monthly, and seasonal predictive models. For planning it is necessary to have very long-term annual predictive models. When longer-term predictions are available, it becomes possible to adjust the power outputs even of the slow-responding power plants so that one avoids the need to schedule fast-responding expensive units in near real time. In Chaps. 7 and 9 we pose the problem of least cost economic dispatch and unit commitment by using model-based predictions of wind power and demand. It is illustrated in these chapters how look-ahead generation dispatch, subject to ramp constraints which assume a knowledge of the wind power and demand forecasts, results in the dispatch of less expensive and less polluting generation. Longer-term predictive models are essential for avoiding the over- or under-building of new capacity. In Chap. 15 we illustrate how a combined use of long-term and short-term predictive models for demand and wind power can be used for dynamic investment decisions under uncertainties. As expected, the further one looks into the future, the harder it is to have accurate predictive models. Nevertheless, a careful derivation of model-based long-term predictions generally leads to less risk of over or under-building than the assumption of a worst-case scenario.

Because actual and real-time generation schedules are correlated with the accuracies of look-ahead forecasting models, and given power grid characteristics and system constraints, it becomes unclear (1) whether power system operation would be able to meet generation requirements and handle power balance within the look ahead horizon and (2) what scheduling costs would be incurred in order to achieve that balance. Therefore, providing uncertainty information in order to improve power system operation becomes an essential need.

The need for predicting wind and load is well recognized, and there exists a considerable literature on this subject. For example, Rui Bo and Fangxing Li [1] investigate the impact of load forecast on locational marginal prices (LMPs). Based on this, they propose a probabilistic model for LMPs. In [2], the author examines the effects of load forecast uncertainty on bulk power system reliability. In [3], C. Lindsay Anderson and Judith B. Cardell apply an auto-regressive moving average model to estimate the next 10-min ahead production level for a hypothetical wind farm, and they investigate the possibility of pairing wind output with responsive demand to reduce the variability in the net wind output. In [4], the authors develop an artificial neural network (ANN)-based model to forecast 10-min wind power changes. D. Hawkins and M. Rothleeder [5] describe the potential operational problems which might be caused by an increased penetration of wind energy in California. Of particular interest is the impact on the day-ahead-market (DAM) and hour-ahead-market (HAM). They stress the importance of forecasting accuracy for unit commitment and ancillary services and the need for additional load following or supplemental energy dispatch to compensate for the power imbalance caused by the deviations of actual wind power from the predicted wind power every 5 min.

The cost of this additional balancing is high as it requires the use of fast-responding expensive resources. In [6], the authors propose a probabilistic method of estimating forecasting errors in the Spanish electricity system. They provide an assessment of the cost of wind energy prediction errors. They propose that wind power generators should pay the additional cost of wind prediction errors. In [7], Dale Osborn discusses the impact of wind power on the LMP market in the US midwest area for different wind penetration levels. The conclusion is made that LMPs decrease with the increase of wind energy penetration. The authors of [8] introduce a short-term wind prediction model for both wind speed and wind direction. In our previous work [9] we present a short-term wind speed prediction model using a linearized time series model. Wind data is first collected from a weather station at a 10-min resolution for a period of 1 year. Based on this, a fitted two Weibull distribution parameter model is derived by performing regression analysis on the logarithms of the wind speed data. A transformation from Weibull into normal distribution is then made and linear predictive coefficients calculated by using a finite impulse response filter (FIR) and infinite impulse response filter (IIR) for the normalized wind speed random process. Predictive models for 10 min-ahead, 1 h-ahead, 12 h-ahead, and 24 h-ahead wind speed are derived, and the accuracy of each of these time-ahead prediction models is analyzed. Based on this analysis it is concluded that it is possible to represent wind speed signals as discrete time Markov processes since the accuracy is sufficient only when the most recent sample is used. In this chapter we introduce models, based on historical data, to be used for different purposes of operation, planning, and investment decision-making. The specific goal is to demonstrate how the use of the predictive models enables one to perform economic dispatch (ED), unit commitment (UC), and overall planning on the Azores island of Flores. Everything else being equal, it becomes possible to displace more expensive and polluting diesel power plants with wind power plants when relying on model-based predictions of wind power rather than only on an average capacity factor.

In this chapter, we derive three different characterizations of wind and load power uncertainties. We start with a statistical representation of wind and load power signals. This includes a characterization of load and wind power in terms of fitting distribution models and an evaluation of the distribution parameters, the mean, and the variance of the signals. We next derive auto-regression models for 10-min, 1-h and 24-h forecast models of wind and load power. Finally, we derive Markov models for the short-term and long-term characterization of the wind and load power, and obtain the short-and long-term decision trees for stochastic decision-making in operations and planning. These trees are more detailed than typical binomial trees, as they have the probabilities of several most likely states and their transitional probabilities. It is discussed in later chapters how these models can be used for short-term model-predictive dispatch and unit commitment on a daily basis, as well as how longer-term annual decision trees could be used for more dynamic and probabilistic decision-making regarding the best choice of technology to invest in under major uncertainties.

This chapter is organized as follows: We describe in Sect. 6.2 the multi-temporal aspects of wind and load power signals and propose a method for a systematic

decomposition of the actual signals into their high-, medium-, and low-frequency components. These signals are then transformed back from frequency to a time domain and used as a basis for deriving predictive models of interest. In Sect. 6.3 a statistical characterization of load and wind power signals is derived using data from Flores. In Sect. 6.4 auto-regressive multi-temporal models are derived for predicting wind and load power 10 min, 1 h, and 24 h into the future. Finally, in Sect. 6.5 we derive both short-term and long-term Markov models which can be used for probabilistic decision-making in operations and planning, respectively.

6.2 Multi-scale Decomposition-Based Modeling

Given actual 10-min data, we propose an approach to decomposing the Flores data given to us into signals, with the frequencies defined as follows:

1. *Low-frequency signals*: For economic development such as long-term policy adaptation and generation investment (time horizon: many years).
2. *Medium-frequency signals*: For detecting seasonal weather variations, and therefore helpful in assigning midterm generation capacities; these signals influence electricity market prices and power grid generation planning for a few weeks with no effect beyond a year.
3. *High-frequency signals*: For intra day and intra-week variations in regular generation dispatch, for forced generation outage, and for fast variations of a few hours, but not beyond a week.

In this section, we first apply the discrete Fourier transform (DFT) to decompose the available data into low-, medium-, and high-frequency components. We then perform inverse discrete Fourier transform (IDFT) to change these filtered signals from frequency to time domain representation. Later in this chapter, the time domain representation of the decomposed signals is used to derive predictive models of interest.

6.2.1 Multi-temporal Modeling of Low-, Medium-, and High-Frequency Signals

In general, a DFT is applied to decompose a signal (load/wind power) into its short-, medium-, and long-term components. We use this method to compute the frequencies of interest in wind and load power signals. A DFT $X[k]$, is computed for the wind/load signal sampled at time $[n]$, $x[n]$. The DFT is then decomposed into low-, medium-, and high-frequency components, each of a different frequency index range as

$$X[k] = X_L[k] + X_M[k] + X_H[k] \quad (6.1)$$

where $X_L[k]$, $X_M[k]$ and $X_H[k]$ are the low-, medium-, and high-frequency components, respectively. The DFT applies only to a finite discrete signal (i.e., a sequence of length “ N ”)

$$x[n] \text{ for } 0 \leq n \leq N - 1$$

where $[n]$ is a discrete time index. The DFT, $X[k]$, is also a discrete sequence of length “ N ” and k is a discrete frequency index. The main frequency coefficients for each component are given by

$$\begin{aligned} X_L[k] &= \begin{cases} X[k], & 0 \leq k \leq k_y \\ 0, & k_y \leq k \leq N/2 \end{cases} \\ X_M[k] &= \begin{cases} X[k], & k_y < k \leq k_d \\ 0, & \text{otherwise} \end{cases} \\ X_H[k] &= \begin{cases} X[k], & k_d < k \leq N/2 \\ 0, & 0 \leq k \leq k_d \end{cases} \end{aligned} \quad (6.2)$$

The DFT $X[k]$ representation exhibits a complex conjugate symmetry around $k = N/2$; hence, all decomposed components in (6.2) have conjugate symmetric coefficients within $N/2 < k \leq N - 1$. The thresholds k_y , k_w , and k_d are the yearly, weekly, and daily discrete frequency indices and are related to their analog frequency values by

$$\begin{aligned} f_y &= \frac{f_s}{8760} = \frac{k_y f_s}{N} \\ f_w &= \frac{f_s}{168} = \frac{k_w f_s}{N} \\ f_d &= \frac{f_s}{24} = \frac{k_d f_s}{N} \end{aligned} \quad (6.3)$$

where $f_s = 1$ sample/hr is the sampling frequency and N is the sample size in hourly resolution. Next we take the IDFT of each component in (6.2) and obtain the aggregated IDFT of (1) in the time domain:

$$x_t[n] = x_L[n] + x_M[n] + x_H[n] \quad (6.4)$$

Each pattern can be used to characterize the behavior of load/wind power for different purposes. Figure 6.1 shows the time domain decomposed components of the total load power. Figure 6.2 shows the time domain decomposition of the normalized wind power of 330kW. Each decomposed signal is important for different applications in power systems, e.g., predictions, scheduling, risk analysis, and investment decisions.

The high-frequency signals for both wind power and load on Flores are used as input data when we derive predictive models later in this chapter.

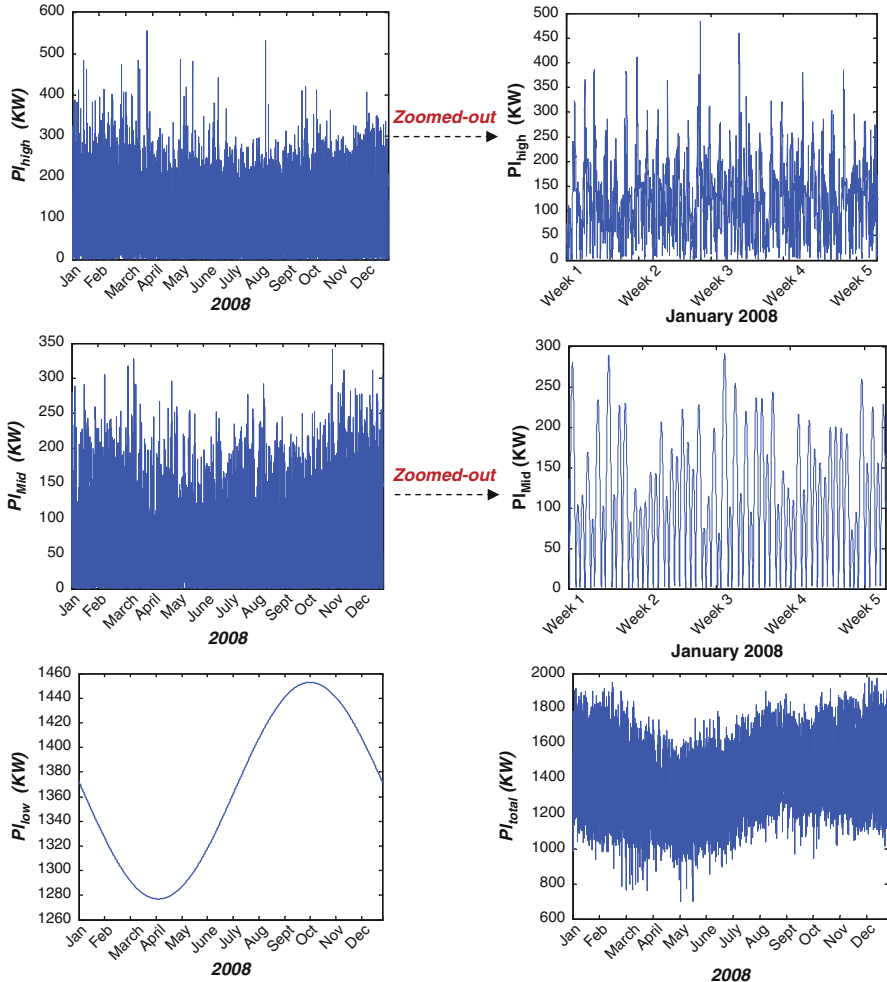


Fig. 6.1 Low-, medium-, and high-frequency components of load power

6.3 Statistical Characterization of Load and Wind Power Uncertainties

In this section, we obtain a statistical representation of uncertain data. Regression analysis is used to determine parameters such as mean value and variance.

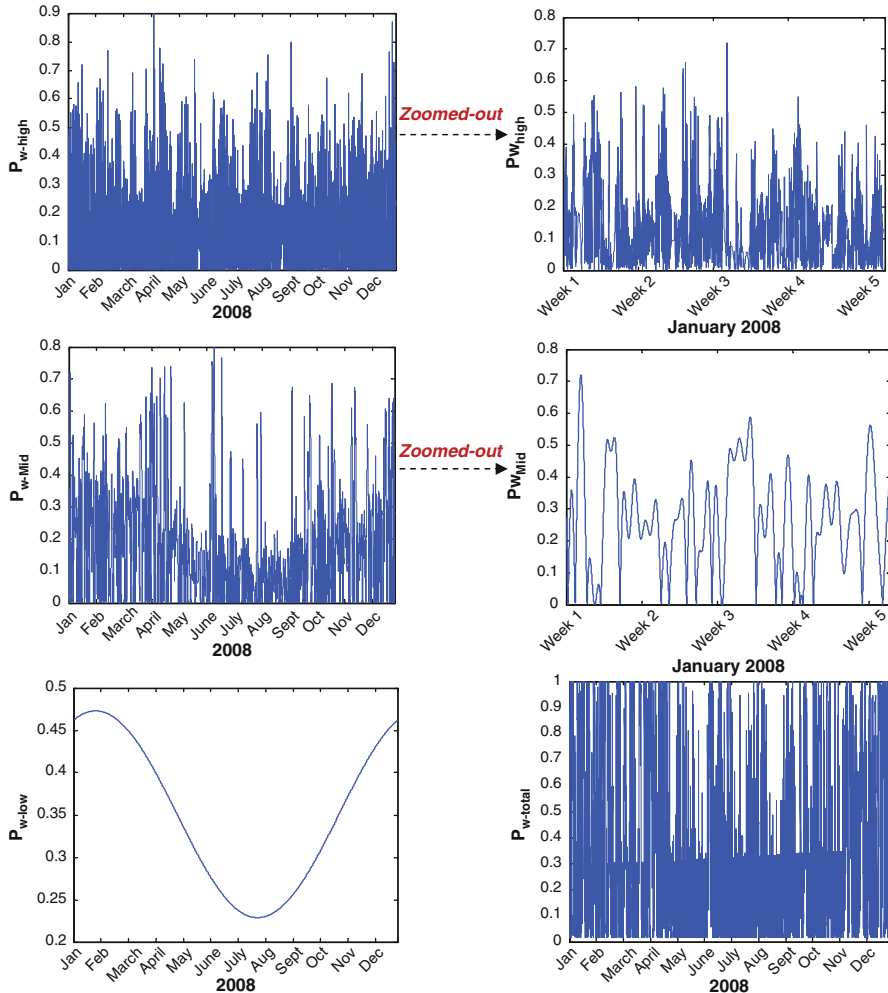


Fig. 6.2 Low-, medium-, and high-frequency components of normalized wind power (turbine capacity of 330 KW)

6.3.1 Statistical Representation of Load Power

The uncertainty associated with load power has always been one of the major sources of uncertainty in conventional power systems. Given its importance, much work has been done over the years to develop accurate predictive models of load power. Here we derive for completeness a statistical representation of load power and compare it later with a statistical representation of wind power. To start with, in Fig. 6.3, the load duration curves for Flores MW demand are presented for four seasons. The upper figure shows the hourly load duration curves for four different

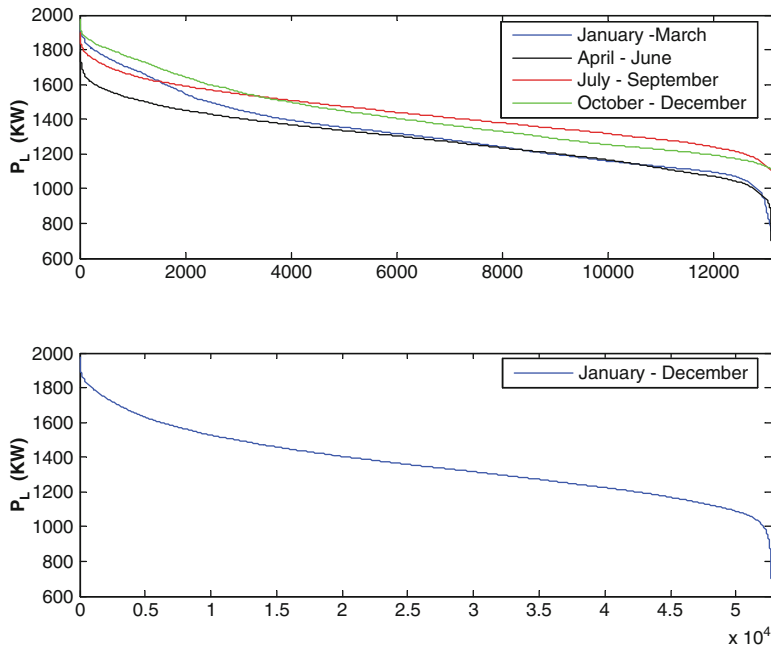


Fig. 6.3 Load duration curves for all four seasons of 2008

seasonal consumption levels, whereas the lower plot represents the annual 2008 demand. It appears that the greatest utilization of MW is from July to September, while the lowest capacity utilization rate appears in winter and spring (January–March, April–June).

Seasonal load variations affect planning decisions on different look-ahead time horizons. Therefore, seasonal load representation is important when modeling load uncertainty. Figure 6.4 shows both seasonal and total load histogram and plots. Near-normal distribution of load is obtained for all seasons at different means and variances.

6.3.1.1 Load Power Distribution Models

The empirical cumulative distribution function (CDF) for load power random variable (RV) X is evaluated using n samples as a reference distribution for the load data. Based on the above load statistical outcomes, the normal distribution of load power is computed and compared with the reference empirical distribution. Moreover, we add Weibull distribution in order to model the statistical characterization of load RV and compare it with wind power RV. In general, the Weibull formula is constructed using linear regression performed between $X = \ln(x)$ and, where x is the data (load power RV), plotted on the horizontal axis, and the resulting CDF metric is on the vertical axis, plotted on the vertical axis:

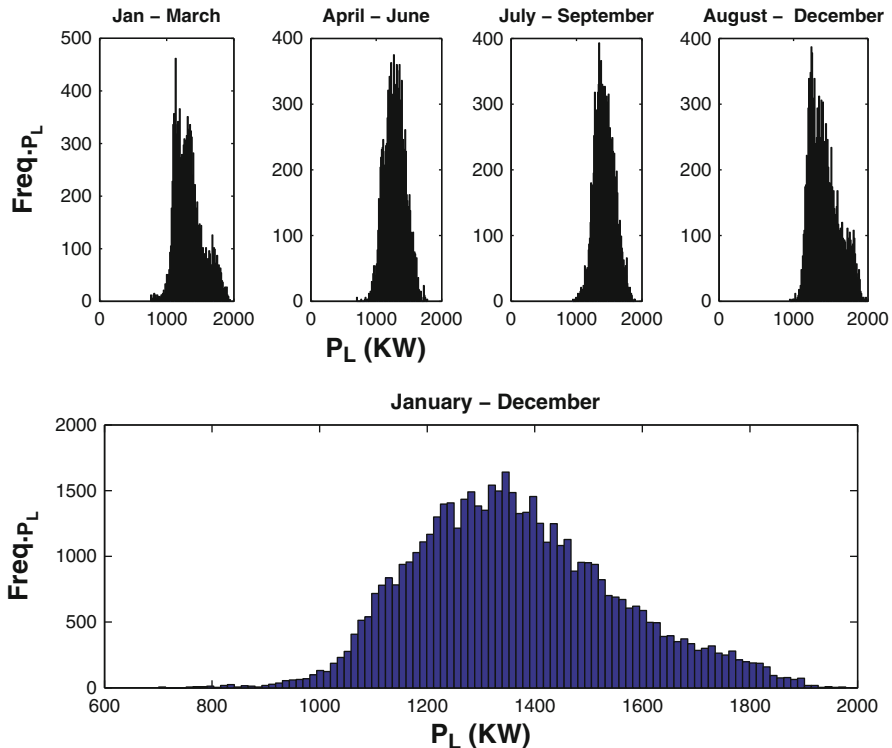


Fig. 6.4 Seasonal and total MW load curves for 2008

Table 6.1 Linear regression Weibull parameters

α	β	Standard error (intercept)	Standard error (slope)	R-square
4.3×10^{-29}	9.01	0.073	0.096	93.6 %

$$Y = \ln(-\ln(1 - \hat{F}_X(x))) \quad (6.5)$$

The PDF parameters are related to linear regression slope m and Y -intercept C , as follows:

$$\begin{aligned} \beta &= \text{slope} = m \\ \alpha &= \text{Exp}(Intercept = C) \end{aligned} \quad (6.6)$$

The regression results are shown in Table 6.1 and the empirical, normal, and Weibull CDFs are plotted in Fig. 6.5.

The multi-temporally decomposed load power signal distributions vary from the aggregated load distribution in that each decomposed distribution model is filtered

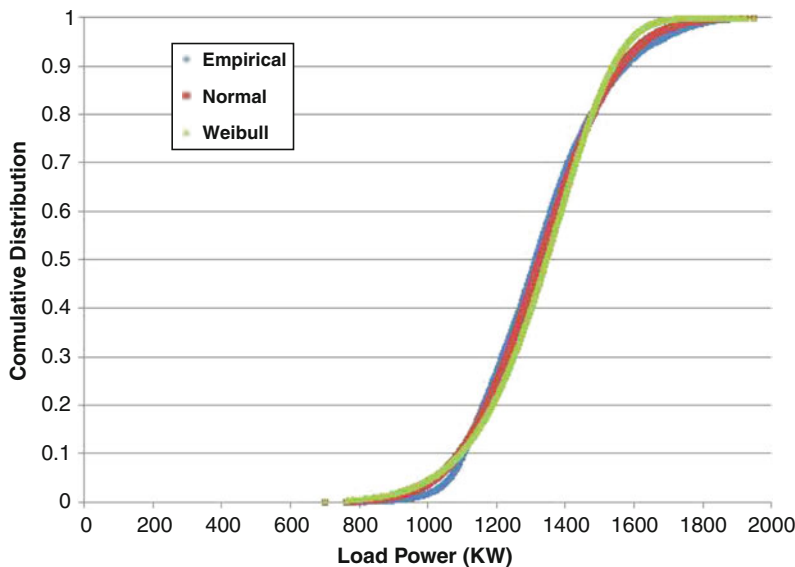


Fig. 6.5 Normal, empirical and Weibull cumulative distribution functions

Table 6.2 Statistical mean and standard deviation of decomposed load signals

	High	Medium	Low
μ (Kw)	102	105	1,365
σ (Kw)	73	67.3	62.2

to its corresponding frequency component and omits other frequency signals. For example, the low-frequency load power signal accounts only for low-frequency components and omits the medium and high frequencies altogether. Figure 6.6 shows decomposed signal distributions for low-, medium-, and high-frequency load power signals. Table 6.2 shows the statistical mean and standard deviation of all decomposed signal distributions.

6.3.2 Statistical Representation of Wind Power

The uncertainty of wind power is more volatile than that of load power; this is due to the intermittent nature of wind speed and other meteorological factors. Thus, it is likely to contribute most to the uncertainty of future energy systems. Figure 6.7 shows both seasonal and total wind power distributions. It can be stated that the Weibull distribution function models the intermittent characteristics of wind power fairly accurately and can account for long tails in the CDF.

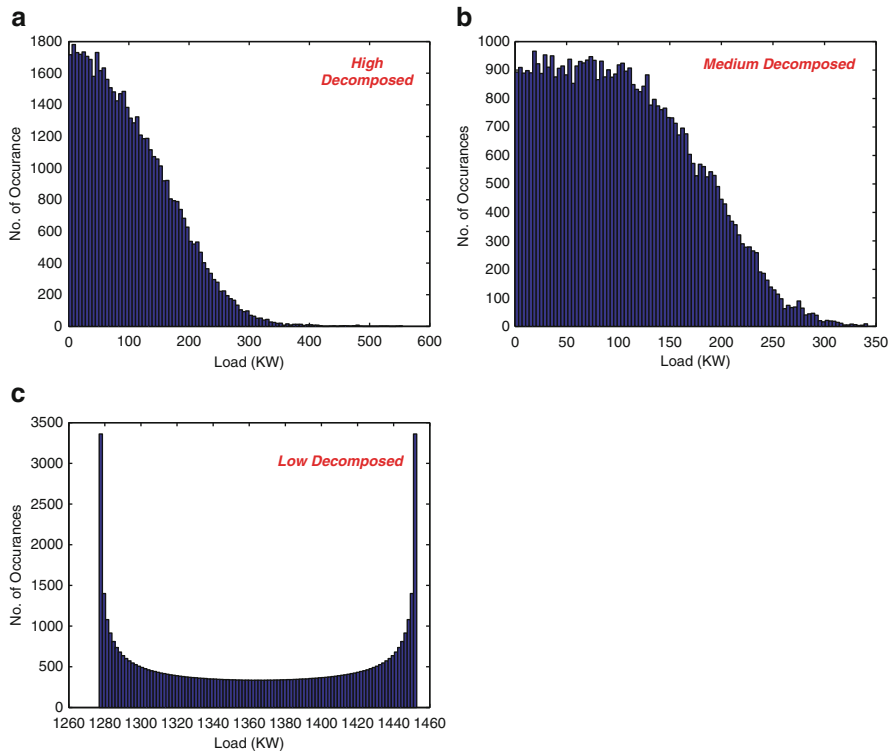


Fig. 6.6 Histogram distribution of (a) high-, (b) medium-, and (c) low-frequency decomposed load power signals

Table 6.3 Linear regression Weibull parameters

α	β	Standard error (intercept)	Standard error (slope)	R-square
0.0036	1.16	0.0134	0.003	82 %

6.3.2.1 Wind Power Distribution Models

The empirical, normal, and Weibull CDFs are constructed for wind power data the same way the functions were constructed in Sect. 6.3.1.1 above. The Weibull distribution parameters are obtained from linear regression using (6.5) and (6.6).

The regression results are shown in Table 6.3, and the empirical, normal, and Weibull CDFs are plotted in Fig. 6.8.

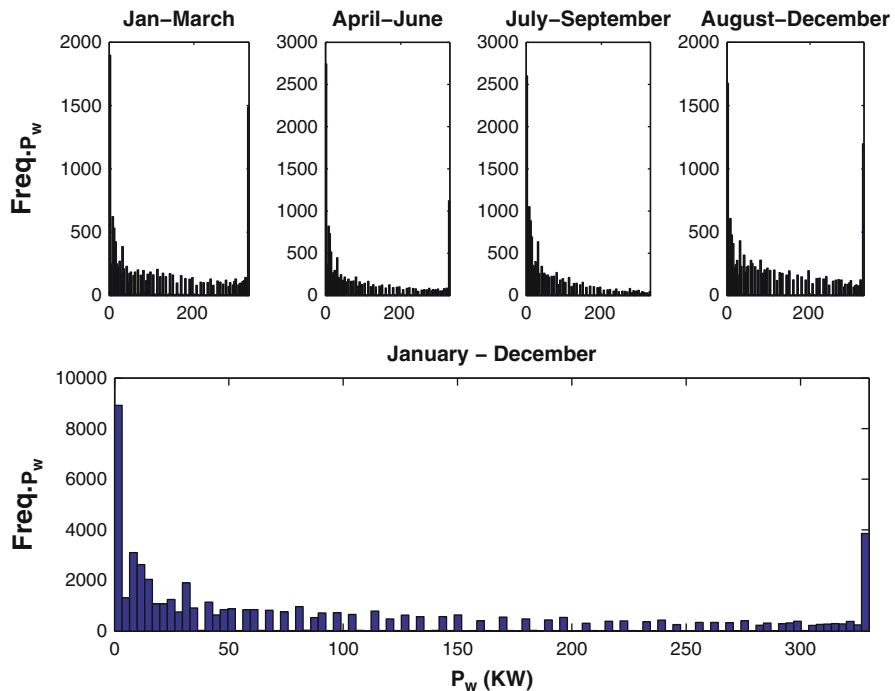


Fig. 6.7 Seasonal and total MW wind power distributions for 2008

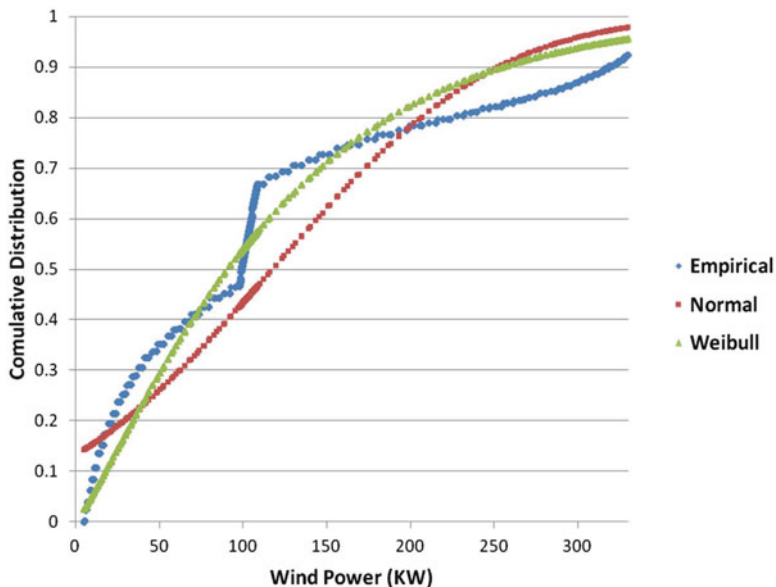


Fig. 6.8 Normal, empirical and Weibull cumulative distribution functions

6.4 Multi-temporal Prediction Models of Load and Wind Power

Section 6.4 takes the regression parameters for wind and load power and estimates a short-term pattern that captures the uncertainties of the stochastic nature of the data sources for different lookup time horizons 10 min, 1 h, and 24 h for both the load demand and the wind power of Flores Island [10]. The predictions are evaluated in the least square error sense, and deviations of the mean forecasting values from the measured ones show the greater accuracy of load demand prediction outcomes over wind power prediction outcomes.

In this section, the forecasts of wind and load power signals are used to derive linear prediction models for the short, medium, and long term. The predictive model uses distribution parameters, calculated in the above sections, with a linear predictive coding (LPC) method explained below. The forecast outcomes and the uncertainties associated with wind and load demand powers are also included.

We present a short-term linear prediction model that uses LPC, FIR, and IRR filters [9]. About 50,000 normalized wind power and load demand data points for 2008 have been used in 10-min resolutions to obtain prediction coefficients in the least square sense.

6.4.1 Linear Predictive Coding and Finite Impulse Response Filters

For short-term load demand and normalized wind power data prediction purposes, we use LPC, based on the autocorrelation method, to determine the coefficients of a forward linear predictor. Prediction coefficients are calculated by minimizing the prediction error in the least squares sense [11]. This method provides the LPC predictor and its prediction error as follows:

$$\begin{aligned}\hat{x}_{\text{LPC}}(n) &= - \sum_{i=1}^N b_i x(n-i) \\ e_N(n) &= x(n) - \hat{x}_{\text{LPC}}(n) = x(n) + \sum_{i=1}^N b_i x(n-i)\end{aligned}\quad (6.7)$$

where N is defined as the prediction order (using N past data samples) and the coefficients $\{b_1, \dots, b_N\}$ are the fitting coefficients which minimize the mean square (MS) prediction error signal. Yule-Walker (or normal) equations based on an autocorrelation matrix have been used to compute those prediction coefficients [11].

Figure 6.9 shows how to obtain the output error signal using two equivalent forms: (a) LPC prediction and subtraction, and (b) direct FIR filter design [9].

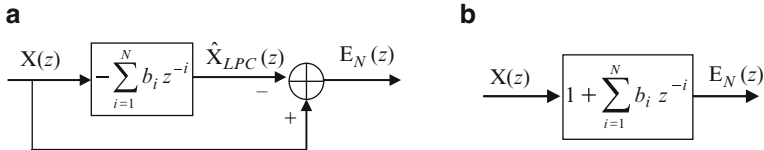
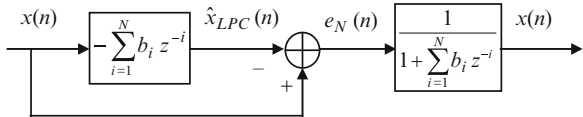


Fig. 6.9 Output prediction error signal using (a) LPC prediction and subtraction and (b) direct FIR filter design

Fig. 6.10 Auto-regression generation process using the LPC estimation method



6.4.2 Auto-regressive Model Prediction and Infinite Impulse Response Filtering

A true stochastic signal can be obtained by multiplying the error signal $E_N(z)$ —if it is known—by the inverse of the FIR filter $B_N^{-1}(z)$, which is now an all-pole IIR filter. If the error signal is equivalent to white noise for large prediction order N , then the z -multiplication (i.e., convolution or filtering in discrete time) now yields a signal that is modeled as a Gaussian auto-regressive (AR) process. Figure 6.10 shows the AR model block diagram, while the reproduced AR signal is obtained by rewriting (6.7) in terms of error as

$$x(n) = - \sum_{i=1}^N b_{i,N} x(n-i) + e_N(n) \quad (6.8)$$

6.4.3 Linear Prediction Phases

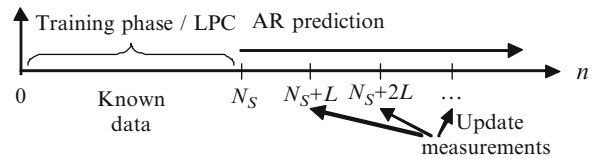
More than 50,000 data samples collected at 10-min intervals have been used in this short-term prediction. A time reference $n = N_S$ has been used which sets the end of the known data and the start of prediction, where $N_S \leq 50,000$ and the remaining samples can be used for tracking the algorithm.

A measurement reporting interval of L samples, and no error in the measurement or the reporting process, have been assumed. At time epochs $n = N_S + mL$, where m is an integer, the L measurements $x(n-L+1), x(n-L+2), \dots, x(n)$ are reported and will be available to use at the next epoch, $(N_S + mL + 1)$. Depending on L , we have the following extreme cases:

$L = 1 : \rightarrow$ point estimator case

$L = \infty : \rightarrow$ time series case, i.e., no estimation at all

Fig. 6.11 The two phases of the prediction process



Two prediction phases are defined in our prediction algorithm and can be summarized as follows:

1. *Training phase:* Within $0 \leq n \leq N_S$, we apply the LPC algorithm to the true samples $x(0), \dots, x(N_S)$ in order to obtain the prediction coefficients $\{1, b_1, \dots, b_N\}$. Then we filter the same samples using the FIR coefficients $\{-b_1, \dots, -b_N\}$ to compute the predictor \hat{x}_n and true prediction error $e_N(n) = x(n) - \hat{x}(n)$
2. *Prediction phase:* For $n \geq N_S + 1$, we apply the AR model of (6.8) after computing the error estimate $\hat{e}_N(n)$. We use the same prediction coefficients obtained in the training phase if we are interested in short-term prediction, which is so in our case. Otherwise, we have to update the coefficients for long-term prediction.

Figure 6.11 shows the two phases of the prediction process.

In (6.8), we use the true past data at time (N_s). $N_s - 1, \dots, 1$ to calculate a prediction for time $N_s + 1$. However, in the prediction phase, $n > N_s$, we do not, according to our algorithm, have all the past data available except at the measurement update time epochs given by $n = N_s + mL$, where m is an integer. At these time epochs, the previous L samples $(N_s + mL - 1, N_s + mL - 2, \dots, N_s + (m - 1)L)$ have been already measured and will become available for update. The value of L can vary from $L = 1$ (single-point estimator) to $L = 6$ (1-h estimation) to $L = 144$ (24 h estimation). If L goes to infinity, this means no estimation or update at all.

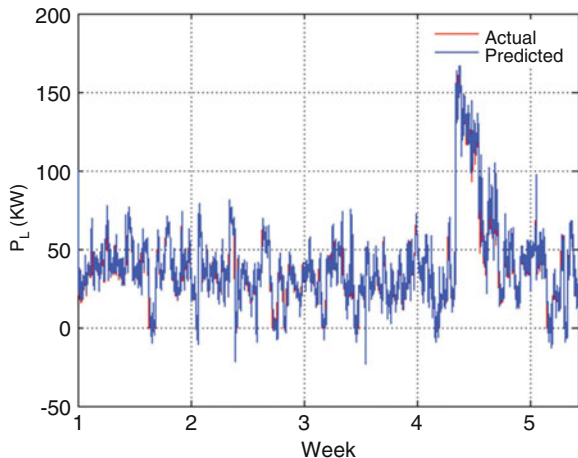
Now, at other time epochs, $n \neq N_s + mL$, there will be a number of missing measurements less than L and more than N_s . At those times we use predicted samples from the past instead of measurements.

$x(n)$ in (6.8) represents the true past data. Therefore, in this algorithm, we define another representative signal that contains both the true past data and its updates. This signal is named reference signal $x_{\text{REF}}(n)$, which takes into account the available measurements at update times ($n = N_s + mL$) as well as the past predicted samples at other times ($n \neq N_s + mL$), to calculate the overall predicted data; this is explained in the equation below.

In this equation, $x_{\text{REF}}(n)$ will be continuously updated in the prediction algorithm

$$\hat{x}(n) = - \sum_{i=1}^N b_{i,N} x_{\text{REF}}(n-i) + e_N(n) \quad (6.9)$$

Fig. 6.12 Seasonal and total MW load power for 2008



where $\hat{x}(n)$ is the predicted signal using either IIR filtering or AR recursion, and $e_N(n)$ is the true prediction error, known if and only if $x(n)$ and $\hat{x}(n)$ are known:

$$e(n) = \hat{x}(n) - x(n) \quad (6.10)$$

We formulate the predictor using reference signal $x_{\text{REF}}(n)$ and it can be updated according to the following equation:

$$\begin{aligned} \text{If } n \neq N_s + mL &\rightarrow x_{\text{REF}}(n) = \hat{x}_{\text{AR}} \\ \text{If } n = N_s + mL &\rightarrow [x_{\text{REF}}(n-L+1), x_{\text{REF}}(n-L+2), \dots, x_{\text{REF}}(n)] \\ &= [x(n-L+1), x(n-L+2), \dots, x(n)] \end{aligned}$$

The following flowchart explains the algorithm steps taken for prediction.

6.4.4 The Resulting Prediction Model for Flores

6.4.4.1 Load Power

An auto-regressive (AR) model prediction, (6.8), has been applied in order to derive a load prediction model (Fig. 6.12). The model uses the first 6 months of 2008 data in the training phase to generate the error signal to be used in the 2008 prediction phase. Figure 6.13 shows 10-min look-ahead load forecasting signals for the month of January.

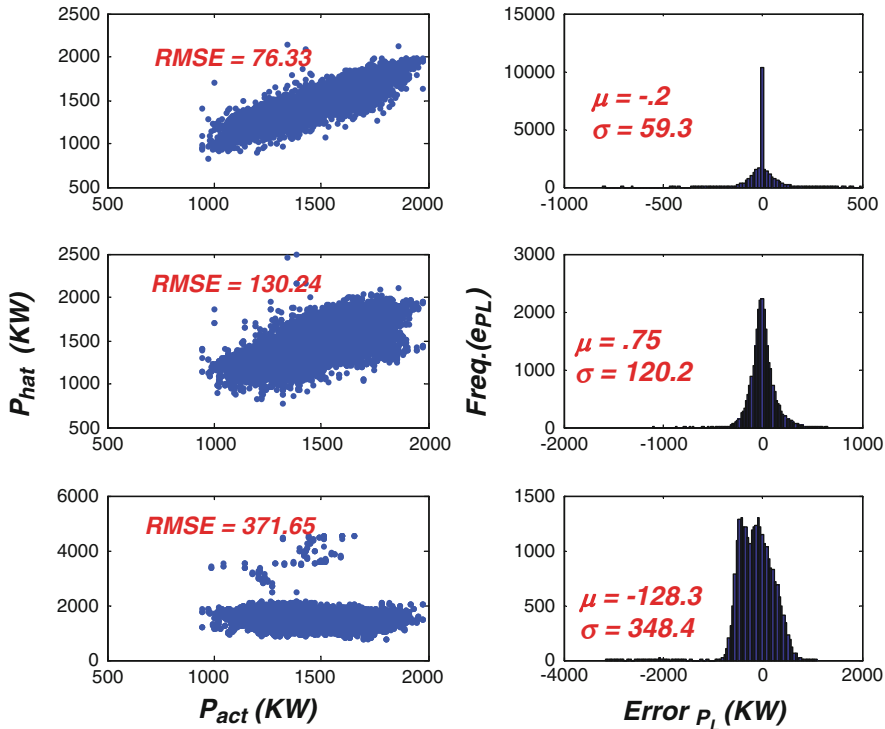


Fig. 6.13 Actual vs. predicted 2008 MW load power of on the *left side* and error distribution using histogram on the *right side* for (a) 10-min load ahead, (b) 1-h look ahead, and (c) 24 h

10-Min Load Prediction Model

By subtracting the actual 10-min signal for 1 year and the 10 min predicted signal based on the LPC formula in (6.8), we obtain the 10-min error for 1 year. Shown in Fig. 6.14a are the deviations of the actual signals from the predicted signals and the mean and variance of the true errors $e(n) = \hat{x}(n) - x(n)$ defined in (6.10).

In Fig. 6.14a, it can be seen that the 10 min error can be represented accurately as a normal distribution, $E(t) \sim N(\mu, \sigma)$.

The coefficients $b_{i,NX}(n-i)$ in the LPC-based formula given in (6.8) for 10 min predictions are shown in Fig. 6.15a. As shown in Fig. 6.11, N is 26,352, which is half the 10 min data points in 1 year. Half of the available data is used for training, namely, for deriving coefficients $b_{i,NX}(n-i)$ for $i = 1, \dots, N$; the other half of the data is used to predict and derive the error in order to check the accuracy of the model.

Following the method in Sect. 6.4.3 above, the coefficients for the LPC-based formula are obtained and shown in Table 6.4.

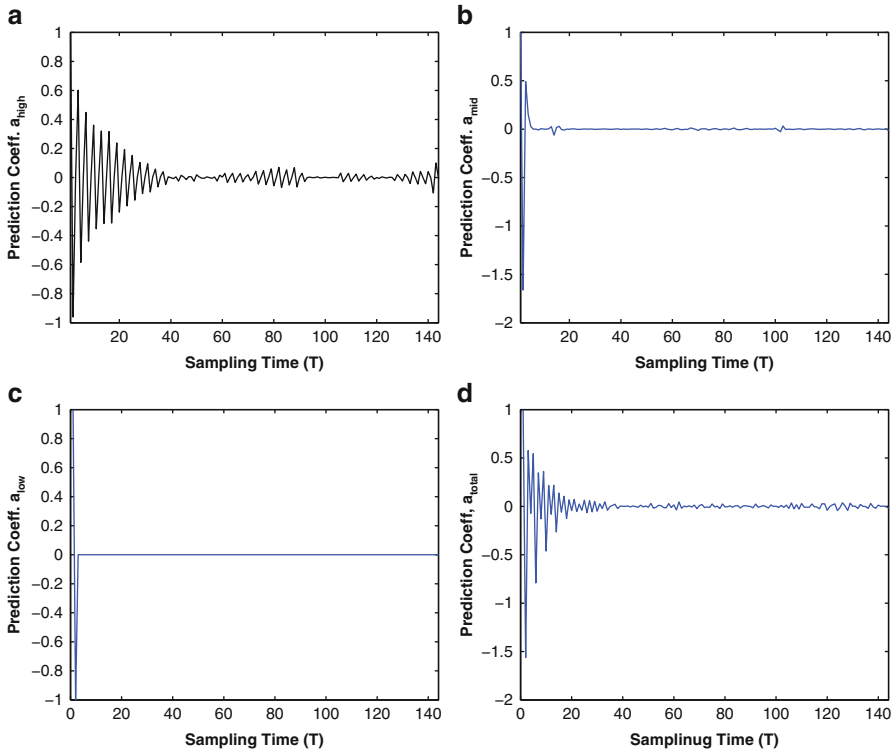


Fig. 6.14 Resulting prediction coefficients for (a) high-, (b) medium-, (c) low-, and (d) total-frequency component load power signal

Table 6.4 LPC-based 10 min prediction coefficients

Prediction coefficients	$b_{1,N}$	$b_{2,N}$	$b_{3,N}$	$b_{4,N}$	$b_{5,N}$	$b_{6,N}$
High freq.						
$b_{i,N}^H$	-0.96	0.004	0.6	-0.58	0.005	0.45
Medium freq.						
$b_{i,N}^M$	-1.66	0.5	0.15	0.026	0	0
Low freq.						
$b_{i,N}^L$	-1	0	0	0	0	0
Total signal						
$b_{i,N}^T$	-1	0	0.42	-0.42	0	0.2

Therefore, it can be seen that the short-term predicted signal can be approximated as

$$\begin{aligned}
 \hat{P}_L^H(N_s + 10 \text{ min}) &= 0.96P_L^H(N_s) - 0.004P_L^H(N_s - 10 \text{ min}) \\
 &\quad - 0.6P_L^H(N_s - 2 \times 10 \text{ min}) + 0.58P_L^H(N_s - 3 \times 10 \text{ min}) \\
 &\quad - 0.005P_L^H(N_s - 4 \times 10 \text{ min}) - 0.45P_L^H(N_s - 5 \times 10 \text{ min}) + \hat{\epsilon}^H(10 \text{ min}) \quad (6.11)
 \end{aligned}$$

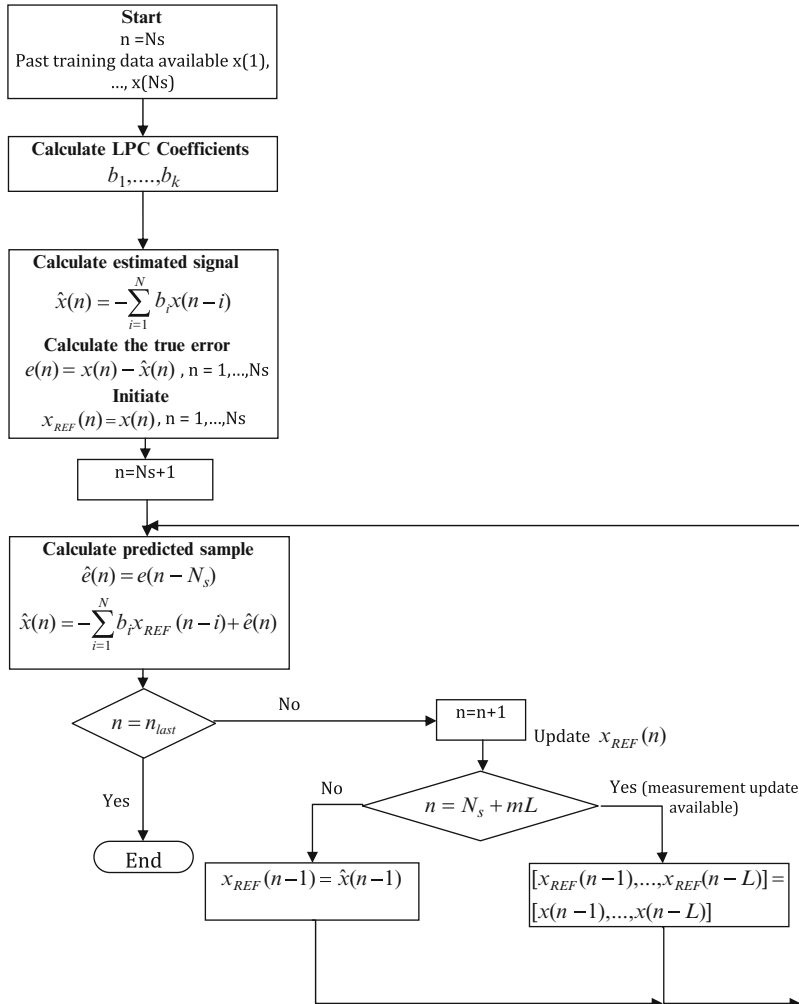


Fig. 6.15 Prediction algorithm flow chart

where \hat{P}_L^H is the estimated highly decomposed load power signal. Also, $\hat{e}(10 \text{ min}) = e(10 \text{ min} - N_s)$ is the estimated error and we assume that it is the same $e(10 \text{ min} - N_s)$ true error calculated in the training phase. Other methods of estimating the error can be used, including the Gaussian model and the error differential between the past two samples.

Note that the formula in (6.11) is obtained only using the fast component of the decomposed signal.

However, if the 10-min LPC-based prediction is done using only the medium-frequency decomposed model, the coefficients obtained in (6.8) become $b_{1,N}^M =$

-1.6 and $b_{2,N}^M = 0.5$. Only two sufficient coefficients are needed for fairly accurate prediction of a medium load signal. Therefore, the formula becomes

$$\hat{P}_L^M(N_s + 10 \text{ min}) = 1.6P_L^M(N_s) - 0.5P_L^M(N_s - 10 \text{ min}) + \hat{e}^M(10 \text{ min}) \quad (6.12)$$

Similarly, a fairly accurate prediction of low decomposed signal is presented as follows:

$$\hat{P}_L^L(N_s + 10 \text{ min}) = 1P_L^L(N_s) + \hat{e}^L(10 \text{ min}) \quad (6.13)$$

where \hat{P}_L^L is the estimated low frequency component load signal. Equation 6.13 shows the low component of a load decomposed load power model. Only one prediction coefficient is needed for accurate prediction of the slow load power trend. Shown in Fig. 6.15b, c are the medium- and low-frequency coefficients used in the above formula.

Shown in Fig. 6.15d are the coefficients obtained for predicting actual 10-min data signals for the aggregated load power.

Here again, to predict the actual signal accurately, it becomes necessary to have a higher number of coefficients which results in the following formula:

$$\begin{aligned} \hat{P}_L^T(N_s + 10 \text{ min}) &= 1P_L^T(N_s) - 0.42P_L^T(N_s - 2 \times 10 \text{ min}) \\ &\quad + 0.42P_L^T(N_s - 3 \times 10 \text{ min}) - 0.2P_L^M(N_s - 5 \times 10 \text{ min}) + \hat{e}^T(10 \text{ min}) \end{aligned} \quad (6.14)$$

where \hat{P}_L^T is the estimated aggregate load signal.

It can be concluded that if only medium- and/or low-frequency fluctuations in the actual signal are important for a particular operating function in system operations, then the 10 min predictive model can be represented using only two coefficients in the LPC formula.

Hourly and Day-Ahead Load Prediction Models

Using a similar approach to the one described above, hourly load prediction is evaluated at every hour time epoch where the data is available to predict. The hourly prediction model starts at time $n = N_s + L$, and it continues for $L = 6$ samples until another measurement update becomes available at $n = N_s + (m+1)L$. For short-term prediction, we use the same prediction coefficients, b_1, \dots, b_N throughout the whole prediction phase. Referring to (6.9), the hourly prediction model becomes a single-point predictor because measurements are available. Equation (6.15) defines the hourly prediction model for high-frequency decomposed signal:

$$\begin{aligned} \hat{P}_L^H(N_s + 60 \text{ min}) &= 0.96P_L^H(N_s + 50 \text{ min}) - 0.004P_L^H(N_s + 40 \text{ min}) \\ &\quad + 0.6P_L^H(N_s + 30 \text{ min}) - 0.58P_L^H(N_s + 20 \text{ min}) \\ &\quad - 0.005P_L^H(N_s + 10 \text{ min}) - 0.45P_L^H(N_s) + \hat{e}^H(60 \text{ min}) \end{aligned} \quad (6.15)$$

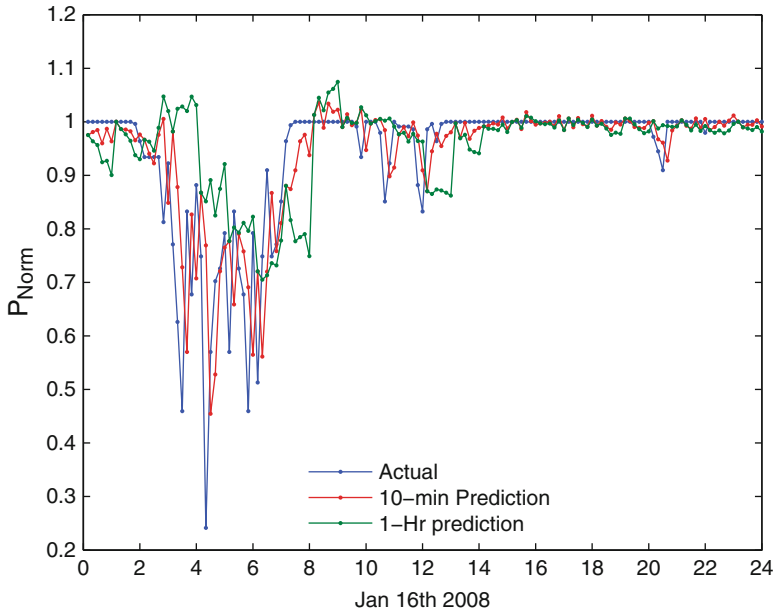


Fig. 6.16 Normalized values of actual wind power and 10-min and 1-h look-ahead forecasts for January 16, 2008

A similar example can be made for $L = 144$ (24 h) or a general form can be depicted in a flowchart as shown above.

Figure 6.14 shows three look ahead time horizon forecasting results, 10 min, 1 h, and 24 h. On the LHS of the plot, actual and predicted MW loads and their associated root mean square errors (RMSE) are presented. On the RHS of the plot, error distribution/histograms with means and standard deviations are presented.

Error distributions for longer look-ahead time forecast show more disturbance from normal distribution and longer tails. This is expected without updating forecasting signal to include new available measured values.

6.4.4.2 Multi-scale Decomposed Prediction Coefficients

The prediction parameters, b , used in the Auto-regressive prediction model of (6.8) and (6.9) are sometimes called autocorrelation parameters; in the auto-regressive equation (6.8) prediction parameters are obtained from solving Yule-Walker equations or autocorrelation matrix. Figure 6.16 shows predictive coefficients for low, medium, high, and total load frequency components signals. Volatility in prediction coefficients for high decomposed load power is due to the variation between actual and estimated load signals, and it goes less volatile and loses information when variances between actual and estimated signals narrowed.

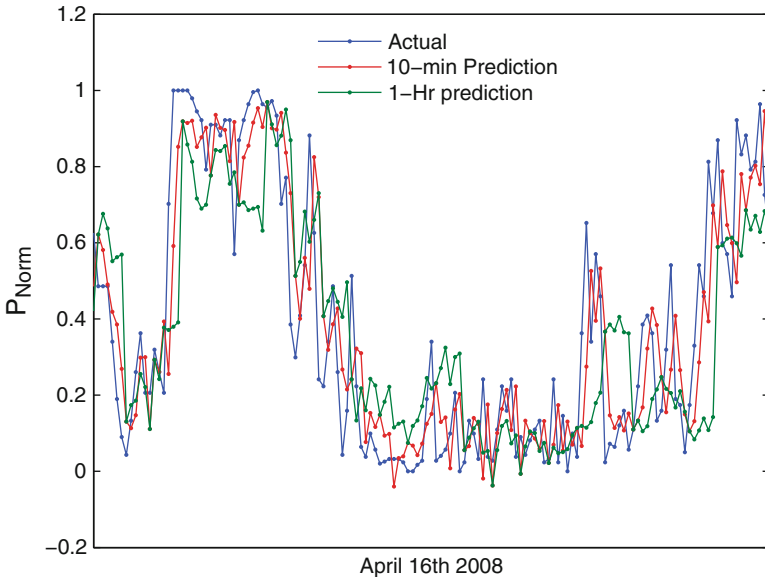


Fig. 6.17 Normalized values of actual wind power and 10-min and 1-h look-ahead forecast for April 16, 2008

6.4.4.3 Wind Power

We apply the AR prediction model to a normalized wind power signal on Flores. Figure 6.16 shows actual, 10-min, and 1-h look-ahead forecasting signals for January 16, 2008. An overestimation of normalized values dominates the underestimation.

However, in Fig. 6.17, normalized wind power forecasting for different look-ahead time horizons differs in the values assigned to each horizon. This is due to the seasonal trends of wind power.

The same observation made above for Figs. 6.16 and 6.17 concerning the utilization of wind power is shown in Fig. 6.18 for the July month and in Fig. 6.19 for October month.

10-Min Wind Prediction Model

Similarly to what we discussed above in Sect. 6.4.4.1 concerning the load prediction, 10-min actual and predicted wind power signals are obtained, see Fig. 6.20, and the error signal is calculated based on the LPC-based formula of (6.8). Shown in Fig. 6.21a is the deviation of the actual signals from the predicted signals and the mean and variance of the true errors $e(n) = \hat{x}(n) - x(n)$ defined in (6.10).

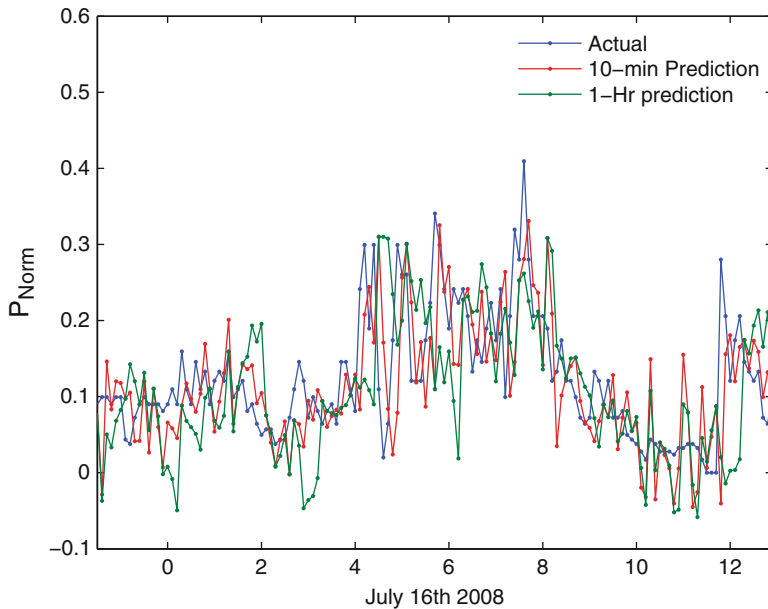


Fig. 6.18 Normalized values of actual wind power and 10-min and 1-h look-ahead forecast for July 16, 2008

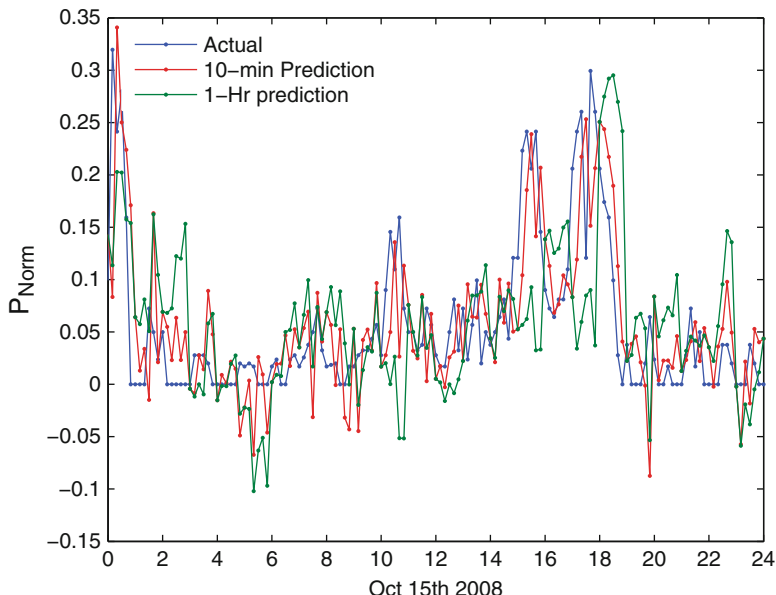
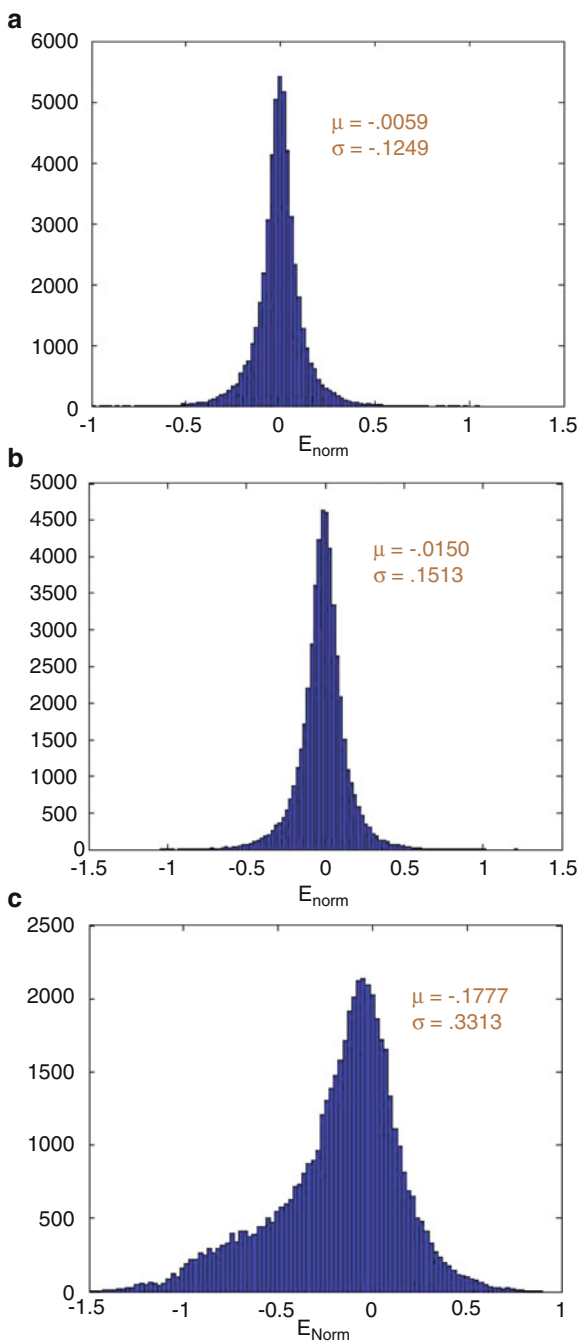


Fig. 6.19 Normalized values of actual wind power, 10 min and 1 h look ahead forecast for October 15th, 2008

Fig. 6.20 Forecast error distributions for (a) 10-min, (b) 1-h, and (c) 24-h look-ahead time horizons



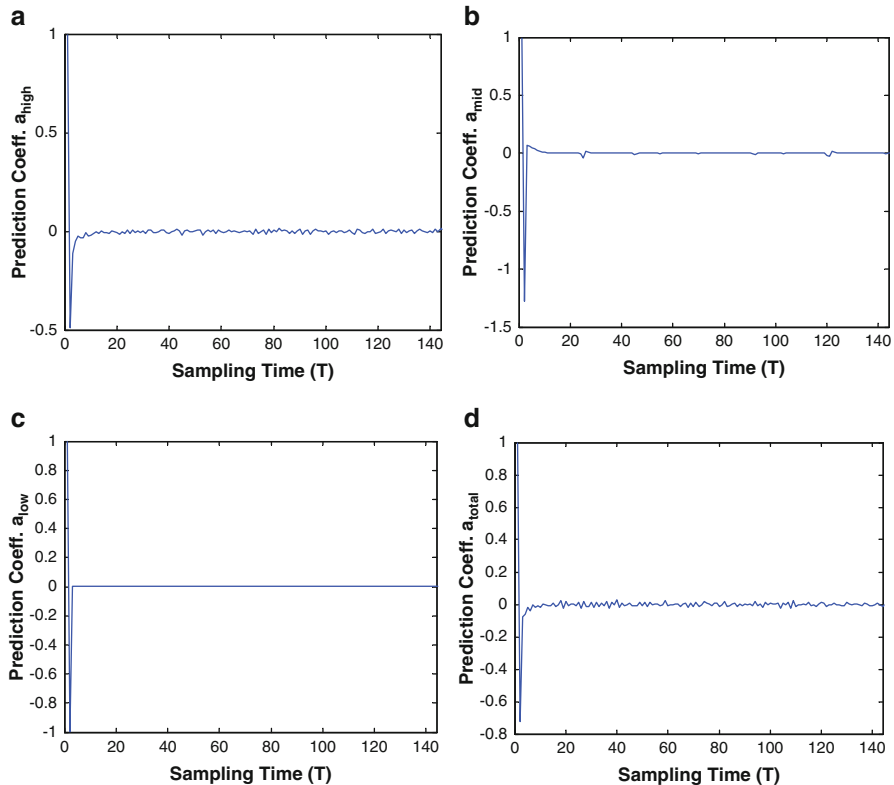


Fig. 6.21 Resulting prediction coefficients for (a) high-, (b) medium-, (c) low-, and (d) total-frequency component wind power signals

In Fig. 6.21a, likewise the normal distribution for 10-min load power model, the 10-min error distribution of wind power can be also represented accurately as a normal distribution $E(t) \sim N(\mu, \sigma)$.

The coefficients, $b_{i,N}(n-i)$ in the LPC-based formula given in (6.8) for 10-min predictions are shown in Fig. 6.22. Following the method we used in Sect. 6.4.3 above, the coefficients for the LPC-based formula are obtained and are shown in Table 6.5.

The short-term wind predicted signal obtained using only the fast component of the decomposed signal can be approximated as

$$\hat{P}_W^H(N_s + 10 \text{ min}) = 0.5P_W^H(N_s) + 0.11P_W^H(N_s - 10 \text{ min}) + \hat{e}^H(10 \text{ min}) \quad (6.16)$$

where \hat{P}_W^H is the estimated high decomposed wind power signal. Also, as in the previous sub-section, $\hat{e}(10 \text{ min}) = e(10 \text{ min} - N_s)$ is the estimated error and we assume it is the same true error calculated in the training phase while other methods of estimating the 10-min LPC-based prediction model for decomposed coefficients

Table 6.5 LPC-based 10-min prediction coefficients

Prediction coefficients	$b_{1,N}$	$b_{2,N}$	$b_{3,N}$	$b_{4,N}$	$b_{5,N}$	$b_{6,N}$
High freq. $b_{i,N}^H$	-0.5	0.11	-0.05	-0.02	-0.03	-0.03
Medium freq. $b_{i,N}^M$	-1.28	0.065	0.06	0.005	0.03	0.02
Low freq. $b_{i,N}^L$	-1	0	0	0	0	0
Total signal $b_{i,N}^T$	-0.72	-0.08	0.062	-0.02	-0.03	-0.004

at all frequencies are shown in Table 6.5. The dominant coefficients are shown to be the first 2 coefficients that can sufficiently represent the wind power short prediction model for all frequency component signals, whereas in the load prediction model, more coefficients are needed to represent the prediction. Therefore, the medium-frequency prediction formula becomes

$$\hat{P}_W^M(N_s + 10 \text{ min}) = 1.28P_W^M(N_s) - 0.065P_W^M(N_s - 10 \text{ min}) + \hat{e}^M(10 \text{ min}) \quad (6.17)$$

Similarly, a fairly accurate prediction of a low decomposed signal requires the following representation:

$$\hat{P}_W^L(N_s + 10 \text{ min}) = 1P_W^L(N_s) + \hat{e}^H(10 \text{ min}) \quad (6.18)$$

where \hat{P}_W^L is the estimated low-frequency component load signal. Only one prediction coefficient is needed for an accurate prediction of the slow wind power trend. Shown in Fig. 6.22b, c are the medium and low frequency coefficients used in the above formula.

Shown in Fig. 6.22d are the coefficients obtained for predicting the actual 10 min data signals for actual 2008 wind power.

The prediction model for the actual wind power signal is given as

$$\hat{P}_W^T(N_s + 10 \text{ min}) = 0.72P_W^T(N_s) + 0.08P_W^T(N_s - 2 \times 10 \text{ min}) + \hat{e}^T(10 \text{ min}) \quad (6.19)$$

where \hat{P}_W^T is the estimated aggregate wind signal. The second term of (6.19) can be neglected, and therefore, the short-term prediction model for aggregated wind power can be calculated using the first prediction term plus the error term. This special model of wind power is the basic introduction of the Markov model, where the next wind signal value is dependent on the value just before it.

It can be concluded that the 10-min predictive model can be represented using only two coefficients in the LPC formula.

Hourly and Day-Ahead Wind Prediction Models

Using similar prediction approach described for hourly load prediction is evaluated every hour time epoch for wind power prediction. Equation (6.20) defines the hourly prediction model for high-frequency decomposed signals:

$$\hat{P}_W^H(N_s + 60 \text{ min}) = 0.5P_W^H(N_s + 50 \text{ min}) + 0.11P_W^H(N_s + 40 \text{ min}) + \hat{e}^H(60 \text{ min}) \quad (6.20)$$

A similar example can be made for $L = 144$ (24 h).

In Fig. 6.21, error distributions for different look-ahead time forecasts are shown with more disturbances from normal distribution and longer tails for the longer day-ahead prediction model.

6.4.4.4 Multi-scale Decomposed Prediction Coefficients

The prediction parameters, b , have been calculated by applying in the same way the auto-regressive equation (6.8) to both wind power and load power. Figure 6.22 shows the predictive coefficients for low, medium and high load frequency component load power signals. The prediction coefficients for all decomposed wind power signals have their highest weights in their first values and drop to zero afterwards. The prediction coefficient values for the most recent decomposed signals ensure the Markovian properties that wind power exhibits [9].

6.4.5 Wind and Load Power Forecast Accuracies

The above forecast results for normalized wind and load power are discussed in units of MW for load power and per unit values for normalized wind power (range from 0 to 1). In order to compare the forecast outcomes between the two sources of uncertainties, one metric is to apply the percentage deviation of mean value to both signals, defined as:

$$\Delta\mu = 100 \times \frac{\mu_{px} - \hat{\mu}_{px}}{\mu_{px}} \quad (6.21)$$

where μ_{px} is the mean value of x power (load or normalized wind), Table 6.6.

The deviation of the actual measured values from the mean values of the forecasted load power is considered negligible compared to the deviation of the actual normalized values from the forecasted wind. This is understandable, as the stochastic nature of wind power, and wind power's volatility over time, is considered a challenging source of uncertainty while load power follows a homogeneous predictable pattern over time.

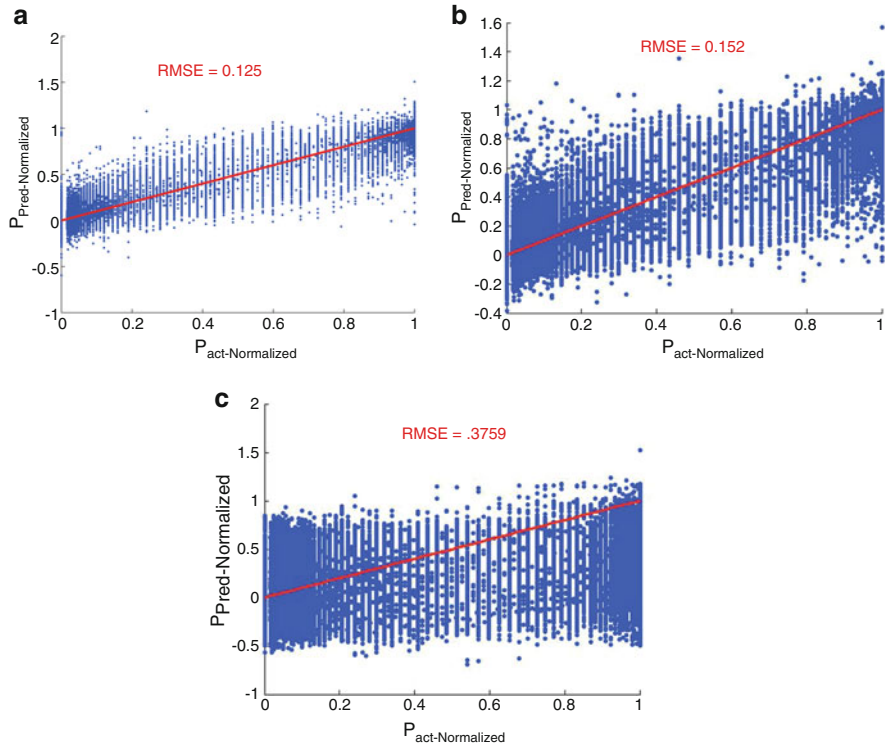


Fig. 6.22 Predicted vs. actual normalized wind power for (a) 10-min, (b) 1-h, and (c) 24-h look-ahead time forecasts

Table 6.6 Percentage mean deviation for different look-ahead time horizon forecasts

	10 min	1 h	24 h
$\Delta\mu_{Pl}(\%)$	-0.0139	0.0523	-9.0170
$\Delta\mu_{Pw}(\%)$	27.52	62.36	97.8

6.5 Discrete Markov Model

In this section, a Markov model for load and wind power signals is presented. Based on the results of the forecasting model discussed in the previous section, it has been shown that both the load demand and wind power, at time t , depend on the previous value, $t - 1$, for the Markovian model to take place. For that, a quantization process is carried out to optimize the time step between different state levels for both stochastic signals. Also, the state and transition probability matrices are evaluated using actual wind and load data. The transition probabilities show smooth transitions between the states that point to clustering around the diagonal matrices.

Our previous work in [9] proves that wind power follows a Markovian model. Here, we illustrate the model process and apply it to multi-scale wind and load

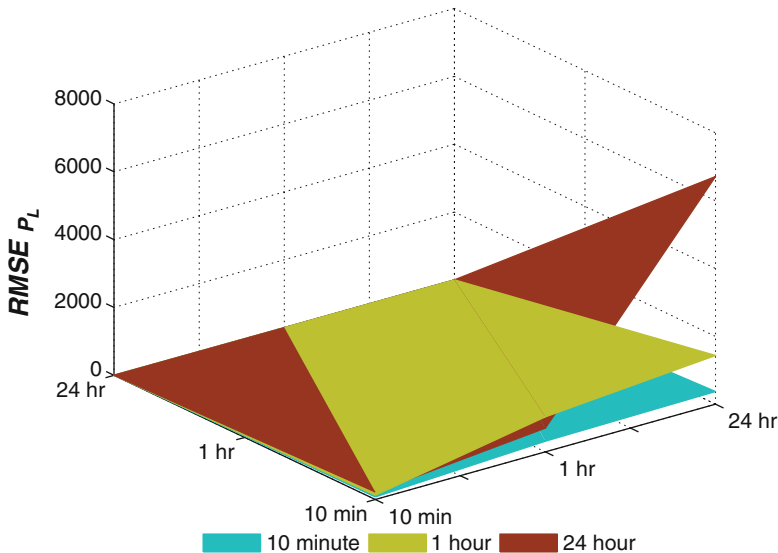


Fig. 6.23 Forecast root mean square errors for 10-min, 1-h, and 24-h look-ahead time horizons using 10 min, 1 h, and 24 h past load data

power data. The Markov model, which is defined as the likelihood of the next signal value in state k , is conditioned on the most recent wind speed value in state m . Equation (6.22) defines this likelihood—state relationship:

$$P(X_k = i | X_m = x_m, x_{m-1}, \dots, X_1 = j) = P(X_k = i | X_m = x_m) \quad (6.22)$$

The Markovian model is also applicable to load patterns. The value of $P_L(t+1)$ is conditioned on the value of $P_L(t)$. Figure 6.23 shows the RMSE of 10-min, 1-h, and 24-h look-ahead forecasts using 10 min, 1 h, and 24 h past load power signals.

The least RMSE for all look-ahead load forecast signals is obtained using the most recent load values. Both 10-min and 1-h look-ahead load forecast RMSEs increase when using 1 h of recent data and then decrease with higher values than when using only 10 min of recent data. For the 24-h look-ahead load forecast, the RMSE goes high with the use of more recent data. This observation opposes the concept of the accuracy of forecast outcomes increasing with an increase in the amount of data history used, which is what happens with wind power. The only explanation is that the distribution of load is less volatile than the distribution of wind signal, and therefore, adding more data to the forecasting model only adds noisy/unwanted signals and hence increases the chance of forecast error.

Given that both load and wind power signals follow the Markovian model, a uniform midrise quantization process is carried out to identify state levels and state values; this process discretizes the wind/load signals to state levels with

optimum threshold or cutoff values. Next, we drive the algorithm used to obtain the optimum value of quantization step (to both Weibull and normal distributions) which minimizes the mean square quantization error (MSQE) [9].

6.5.1 Design of the Optimum Uniform Quantizer

We implement a midrise uniform quantizer that minimizes the MSQE given a set of M states; we define $X = [X_1 X_2 \dots X_M]$ as a state value vector, and $X_t = [X_t(1) X_t(2) \dots X_t(M-1)]$ as a quantized threshold level or partition vector. X is the original analog wind speed signal and x_q is the quantized signal. The quantization step Δ is defined as

$$\Delta = X_{m+1} - X_m = X_t(m+1) - X_t(m) \quad (6.23)$$

The operation of the quantizer is as follows:

$$x_q = \begin{cases} X_1 & , x \leq X_t(1) \\ X_M & , x \leq X_t(1) \\ X_m & , X_t(m-1) < x \leq X_t(m) \end{cases} \quad (6.24)$$

6.5.2 State and Transition Probabilities in a Discrete State Space Markov Model

Given the initial and final boundaries of each state, state probabilities can now be defined as

$$\begin{aligned} P(m) &= Pr[x_i(m) < x \leq x_f(m)] \\ &= P[x(m)] = \int_{x_i(m)}^{x_f(m)} f_X(x) dx \\ &= F_X(x_f(m)) - F_X(x_i(m)) \end{aligned} \quad (6.25)$$

where $m = 1, 2, \dots, M$, is the state index.

Transition probabilities are calculated based on the counting method discussed in [12], in which we define:

$N_{\text{trans}}(k|m) \equiv$ the number of transitions from state m to state k in the time series, where m is the originating state and k is the next state

$N_{\text{state}}(m) \equiv$ the number of occurrences of state m in the time series signal where both state and transition counters are related by (6.25) and the total size of the time series is defined in (6.26).

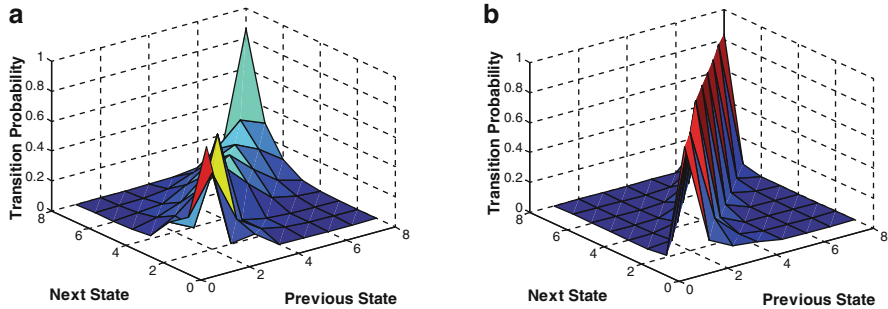


Fig. 6.24 Transition probabilities for (a) wind power, (b) load power

$$N_{\text{state}}(m) = \sum_{k=1}^M N_{\text{trans}}(k|m) \quad (6.26)$$

$$N = \sum_{m=1}^M N_{\text{state}}(m) = \sum_{m=1}^M \sum_{k=1}^M N_{\text{trans}}(k|m) \quad (6.27)$$

Using the statistical counter values of $N_{\text{state}}(m)$ and $N_{\text{trans}}(k|m)$, the transition and state probabilities can be statistically computed as

$$P_{\text{trans}}(k|m) = \frac{N_{\text{trans}}(k|m)}{N_{\text{state}}(m)} \quad (6.28)$$

where, $K = 1, \dots, M$

$$P_{\text{state}}(m) = \frac{N_{\text{state}}(m)}{N} \quad (6.29)$$

where, $m = 1, \dots, M$. Note that (6.29) represents the statistical (actual) state probabilities of wind speed signal while (6.24) represents the theoretical state probabilities defined as normal probability density functions.

We choose 8 states ($M = 8$) in the Markov model representation of wind and load power to represent state and transition probabilities within the time series of the real stochastic data. Figure 6.24 shows the transition probabilities of the 8 states for load power and wind power. The transitions from state m to state k in wind power is larger than that of load; this is due to the variable nature of wind power. Figure 6.24b also shows almost zero dominant transitions between the load power states, while in Fig. 6.24a, the transitions between states appear more frequently but are clustered around the diagonal. The probabilities of the 8 states are shown in Fig. 6.25. The dominant state of wind power appears to be state 1 (Fig. 6.25a) while the dominant state of load power appears to be state 4 (Fig. 6.25b).

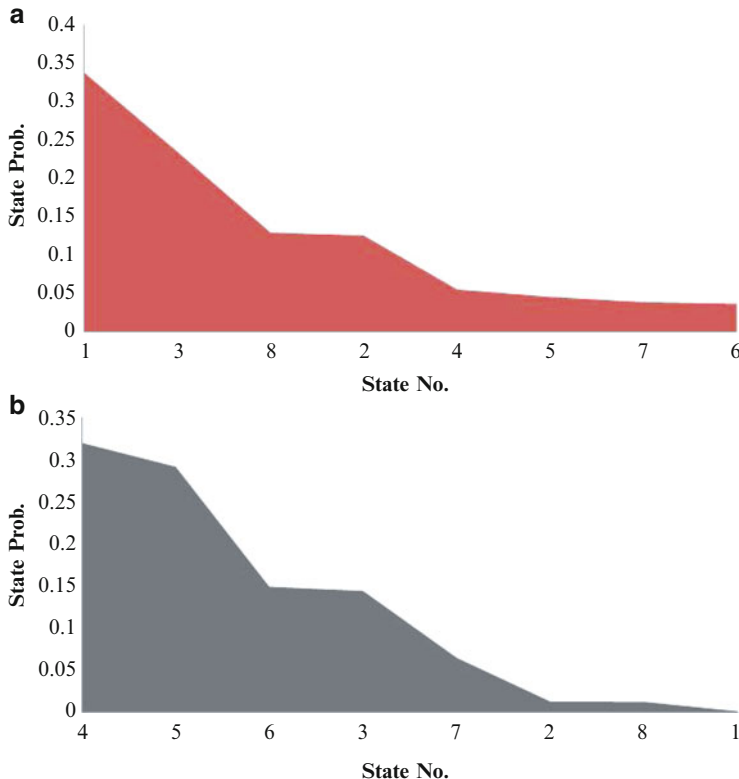


Fig. 6.25 State probabilities for (a) wind power and (b) load power

6.5.3 Decision Trees for Operation and Planning Models

The propose of this section is to help develop a multi-temporal risk approach by analyzing short-, medium-, and long-trend risk approaches and uncertainty variables associated with them. Here, we use the Markovian frequency decomposed model to construct a decision tree that can be used in many different power system applications, such as planning and expansion and ancillary services.

In tackling the planning problem, we are interested in the probability that a signal will be in k th state Y time periods after being in the m th state [13]:

$$P^Y(m \rightarrow k) = P[X(n+y) = k | X(n) = m] \quad (6.30)$$

Figure 6.26 shows a color map transition probability matrix for a decomposed low-frequency load power of Flores Island. The transition from the current state probability to its next state over time, (6.18), shows the differences in probability over time.

Fig. 6.26 Load power annual state transition probability plots for the years (a) 2008, (b) 2009, and (c) 2010

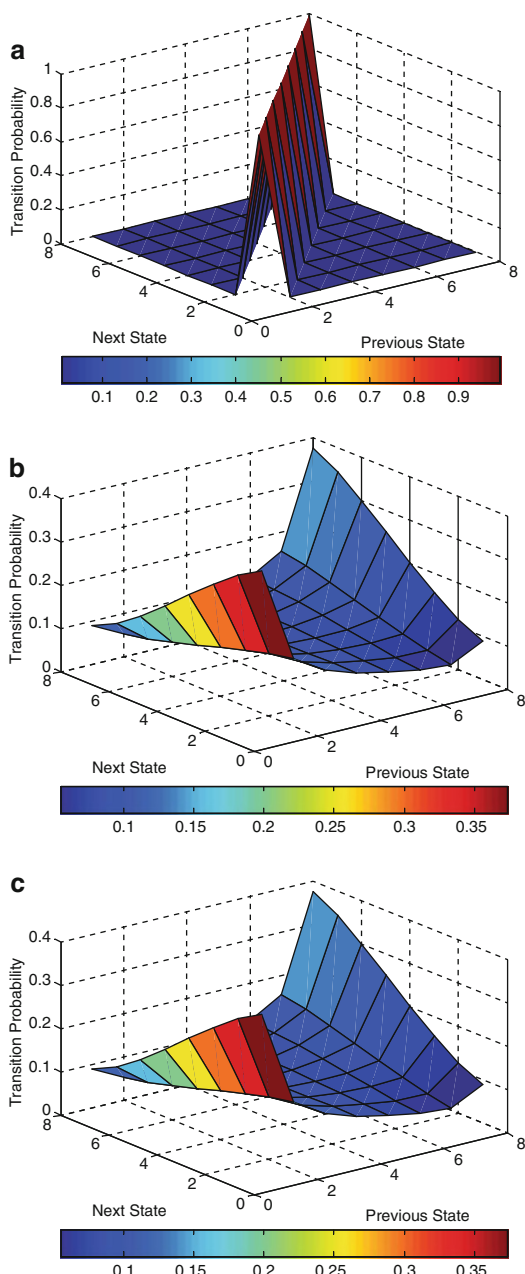
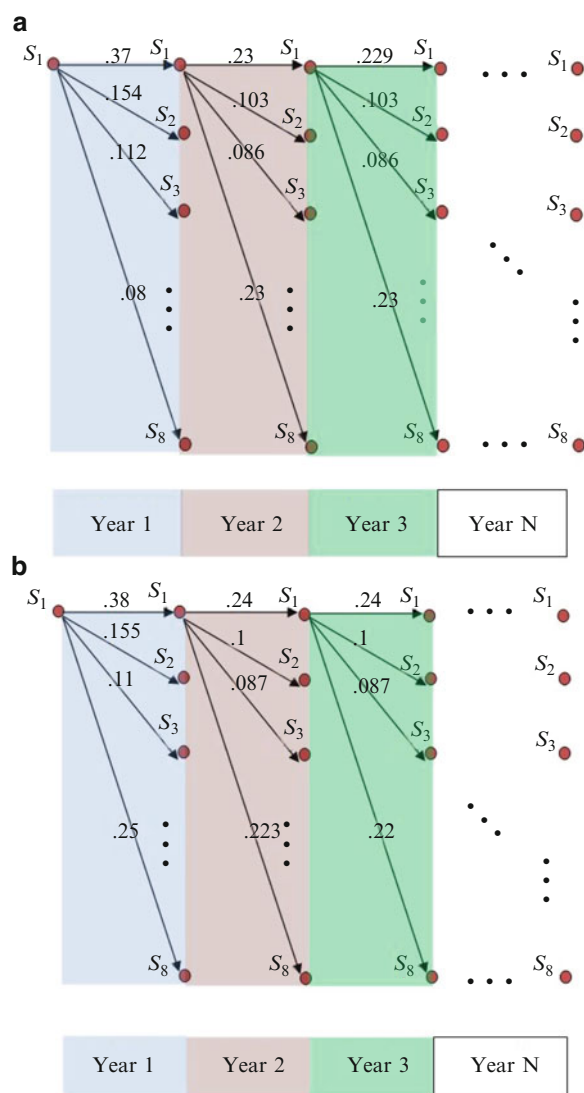


Figure 6.27 shows the long-term uncertainties presented by the low-frequency decomposed annual wind and load power transition probability/decision tree.

Fig. 6.27 Long-term uncertainty/decision tree for (a) wind power and (b) load power



Both wind and load power long-term transitional probabilities are calculated for the 8 states; each power state has its own probability. For simplicity, in Fig. 6.26, we only show the highest state probability (State 1) for the low decomposed wind power signal.

For short-term uncertainty modeling, transition probabilities and decision tree matrices are presented for Flores Island load and wind power as shown below.

Figure 6.28 shows 8 states of short-term Markovian state probability distribution for both Flores Island wind and load power on an hourly basis.

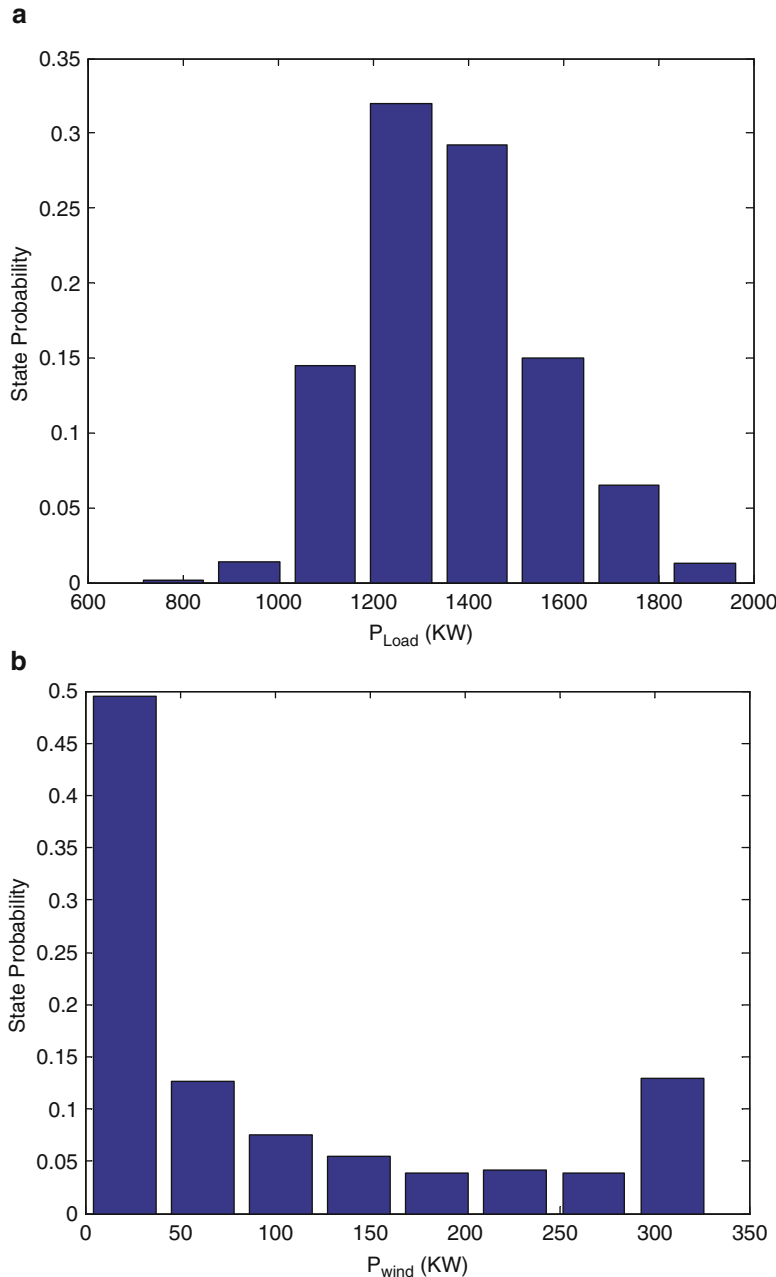


Fig. 6.28 Short-term state probability distributions for (a) load and (b) wind power

Fig. 6.29 Wind power short-term state uncertainty/decision tree

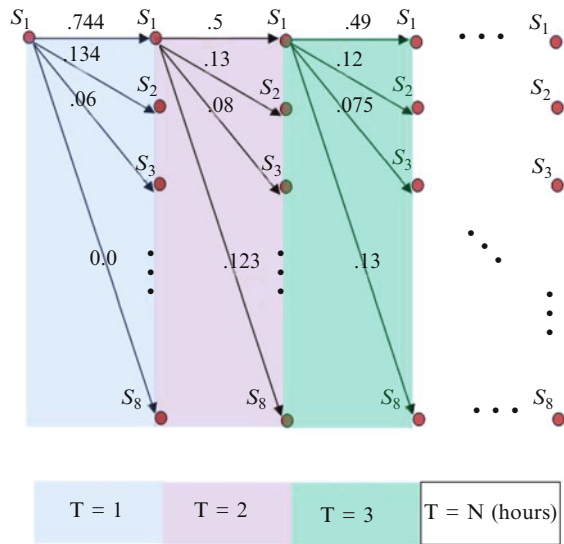
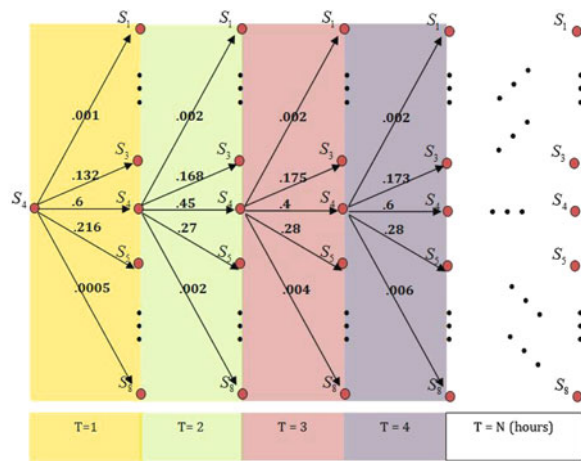


Fig. 6.30 Load power short-term state uncertainty/decision tree



Decision trees for short-term applications in an electric power system are shown in Figs. 6.29 and 6.30. For sketching simplicity, the Figures show the highest short-term Markovian state power. For load power, an uncertainty tree is graphed for the first power state; for wind power, the fourth power state decision tree is shown.

Probability theory law applies at each probability layer of the decision tree ($\sum_i P_i = 1$). Due to long-term limiting probability theory, multistep probabilities vary less and get saturated at values that depend on the time series and time steps used in the Markovian model. The short-term and long-term uncertainties of wind and load power are of importance to power planners and operators for short-term decisions.

such as spot market, economic dispatch, and unit commitment, and for long-term decisions such as generation maintenance, scheduling, generation expansion, and investments.

6.6 Concluding Remarks and Open Questions

It is very important to understand the sources of uncertainty in power systems. In this chapter, we presented load and wind power uncertainty models by posing short-term prediction models and Markov representations with associated state and transition probabilities for them. Linear prediction with FIR and IIR filtering has been used to predict load power and normalized wind power. The prediction results show that a small prediction order based on the most recent data is sufficient for good accuracy. The success of forecast outcomes between the two sources of uncertainties has been illustrated with the concept of percentage deviation of mean value: the difference between the forecasted load power and its actual measured values is considered negligible compared to the difference between forecasted wind and its actual normalized values. Next, Normal PDFs have been used to discretize the signal for representation as a discrete Markov process for both load and normalized wind powers. The state probabilities of the Markov process have been calculated both statistically (by counting the time series data) and theoretically (by integrating the modeled signal PDF). Load power transition probabilities show almost zero values due to the less volatile nature of load signals, while wind power transition probabilities show a higher rate of transition between states, reflecting the nature of wind as a power source. Also, the computed transition probability matrix of the Markov process is shown to be clustered around the diagonal, which indicates the absence of frequent wind gusts/large load transitions in the time series used. Decision trees for low decomposed wind power signals are plotted, and the multi-stage transition probabilities are calculated for use in multi-scale risk analysis for power system applications.

Acknowledgment This work is funded by the Semiconductor Research Corporation Smart Grid Research Center (SRC SGRC).

References

1. R. Bo, F. Li, Probabilistic LMP forecasting considering load uncertainty. *IEEE Trans.* **24**, 1279–1289 (2009)
2. D. Huang, R. Billinton, Load forecast uncertainty considerations in bulk electric system reliability assessment, in *Proceedings of 40th North American Power Symposium*, NAPS, Calgary, AB, Canada, 418–425 (2008)

3. C.L. Anderson, J.B. Cardell, Reducing the variability of wind power generation for participation in day ahead electricity markets, in *Proceedings of 41st Hawaii International Conference on System Sciences*, IEEE, Hawaii, 178–178 (2008)
4. M. Kittipong, Y. Shitra, W. Lee, R. James, An integration of ANN wind power estimation into unit commitment considering the forecasting uncertainty. *IEEE Trans. Ind. Appl.* **43**(6), 1441–1448 (2007)
5. D. Hawkins, M. Rothleider, Evolving role of wind forecasting in market operation at the CAISO, in IEEE PES, Atlanta (2006), pp. 234–238
6. F. Alberto, G. Tomas, A. Juan, Q. Victor, Assessment of the cost associated with wind generation prediction errors in a liberalized electricity market. *Power Syst. IEEE Trans.* **20**(3), 1440–1446 (2005)
7. D.L. Osborn, Impact of wind on LMP market, in IEEE PES, Atlanta (2006), pp. 216–218
8. C.W. Potter, M. Negnevistsky, Very short-term wind forecasting for tasmanian power generation, in *Proceedings of IEEE TPWRS Conference*, 2005
9. N. Abdel-Karim, M.J. Small, M.D. Ilić, Short term wind speed prediction by finite and infinite impulse response filters: a state space model representation using discrete Markov process, in *Proceedings of IEEE Power Tech Conference*, Bucharest, Romania, 2009
10. Data Folder Chap. 6 in M.D. Ilic, L. Xie, Q. Liu (eds.), *Engineering IT-Based Electricity Services of the Future: The Tale of Two Low-cost Green Azores Islands* (Springer, New York, 2013) (to appear)
11. P.P. Vaidyanathan, *The Theory of Linear Prediction*, California Institute of Technology, 1st edn. (Morgan & Claypool, Caltech University, California 2008)
12. F. Castellanos, Wind resource analysis and characterization with Markov's transition matrices, in *IEEE Transmission and Distribution Conference*, Latin America, August 2008
13. J.J. Higgins, S. Keller-Mcnulty, *Concepts in Probability and Stochastic Modeling* (Wadsworth Inc.) (1994)

Chapter 7

Look-Ahead Model-Predictive Generation Dispatch Methods

Le Xie, Yingzhong Gu, and Marija Ilić

7.1 Mathematical Formulation of Different Dispatch Methods

In this chapter, three different dispatch methods are tested and compared in Flores island. They are (1) physically implementable static dispatch, (2) centralized look-ahead dispatch, and (3) distributed look-ahead dispatch. The following notations are used throughout the chapter:

G : Set of all available generators

G_f, G_s : Set of fast and slow conventional generators

G_w : Set of wind energy generators

$\hat{L}(k)$: Expected demand at time step k

$C_i(P_{G_i})$: Cost function of generator i

$S_i(P_{G_i}(k))$: Supply bid function of unit i

$P_{G_i}^{\min}, P_{G_i}^{\max}$: Minimum and maximum generation output

$\hat{P}_{G_w}^{\min}, \hat{P}_{G_w}^{\max}$: Expected minimum and maximum wind generation output at time step k

R_i : Ramping rate of generator $i, i \in G$

K : Time steps in a look-ahead optimization period

$\lambda(k)$: Price of electricity at time step k

L. Xie (✉) • Y. Gu

Department of Electrical and Computer Engineering, Texas A&M University,
College Station, TX 77843, USA

e-mail: lxie@ece.tamu.edu; gzydmgqy@tamu.edu

M. Ilić

Department of Electrical and Computer Engineering, Carnegie Mellon University,
5000 Forbes Ave, Pittsburgh, PA 15213, USA
e-mail: milic@ece.cmu.edu

Method 1: Physically Implementable Static Dispatch with Inelastic Demand:

In this formulation a simple static dispatch problem which is physically implementable is formulated as multistage optimization problem. Slow dispatchable power plants such as hydro units are dispatched hour ahead for the predicted load and predicted wind generation. This way, no explicit ramping rate exists, and only security-constrained economic dispatch (SCED) is carried out. Consequently, intra-hour, it becomes necessary to re-dispatch only fast-responding conventional units (e.g., diesel generation) in order to balance supply and demand in response to temporal deviations in wind and load. The mathematical formulation of Problem 1 is as follows:

At each hour H , solve the static economic dispatch problem

$$\min_{P_G} \sum_{i \in G \setminus G_w} (C_i(P_{G_i}(k))), \quad (7.1)$$

$$s.t. \quad \sum_{i \in G \setminus G_w} P_{G_i}(k) = \hat{L}(k) - \hat{P}_{G_w}(k); \quad (7.2)$$

$$P_{G_i}^{\min} \leq P_{G_i}(k) \leq P_{G_i}^{\max}, i \in G \setminus G_w; \quad (7.3)$$

The load and wind forecast are obtained from the data specified in Chap. 4. In principle, the wind forecast function would be based on finite impulse response filter-based models such as the methods specified in Chap. 6. The result of this optimization is $P_G^*(H) = [P_{G_s}^*(H) \ P_{G_f}^*(H)]^T$.

Then at each 10-min-interval k , the system operator updates the wind power forecast and rerun optimization (7.1)–(7.3) assuming the slow generator units' output stays the same within that hour.

Method 2: Centralized Look-Ahead Dispatch with Inelastic Demand

$$\min_{P_G} \sum_{k=1}^K \sum_{i \in G} (C_i(P_{G_i}(k))), i \in G \quad (7.4)$$

$$s.t. \quad \sum_i P_{G_i}(k) = \hat{L}(k), i \in G; \quad (7.5)$$

$$\hat{P}_{G_w}^{\max}(k) = g_j(\hat{P}_{G_w}^{\max}(k-1)); \quad (7.6)$$

$$\hat{P}_{G_w}^{\min}(k) \leq P_{G_w}(k) \leq \hat{P}_{G_w}^{\max}(k); \quad (7.7)$$

$$P_{G_i}^{\min}(k) \leq P_{G_i}(k) \leq P_{G_i}^{\max}(k), i \in G \setminus G_w; \quad (7.8)$$

$$|P_{G_i}(k+1) - P_{G_i}(k)| \leq R_i, i \in G \quad (7.9)$$

Here instead of representing wind generation outputs as negative loads, the wind generation outputs $P_{G_r}(k)$ are considered as decision variables. A look-ahead moving horizon consisting of K samples is chosen over which all generation outputs are

optimized. Intertemporal constraints such as ramping rates are explicitly modeled in this formulation, therefore eliminating the need for a two-step optimization stated above in Problem 1.

Method 3: Distributed Look-Ahead Dispatch with Inelastic Demand

For a given vector of prices $\hat{\lambda}(k)$ defined as $[\hat{\lambda}(k) \dots \hat{\lambda}(k+K-1)]$, each power producer will solve a local look-ahead optimization problem with the objective of maximizing its own profits in the next K time steps:

$$\max_{P_{G_i}(k)} \sum_{k+1}^{k+K} \hat{\lambda}(k)(P_{G_i}(k)) - (C_i(P_{G_i}(k))) \quad (7.10)$$

$$\text{s.t. } \hat{P}_{G_i}^{\max}(k) = g_i(\hat{P}_{G_i}^{\max}(k-1)); \quad (7.11)$$

$$\hat{P}_{G_i}^{\min}(k) = h_i(\hat{P}_{G_i}^{\min}(k-1)); \quad (7.12)$$

$$|P_{G_i}(k+1) - P_{G_i}(k)| \leq R_i; \text{ and,} \quad (7.13)$$

$$\hat{P}_{G_i}^{\min} \leq P_{G_i}(k) \leq \hat{P}_{G_i}^{\max} \quad (7.14)$$

The outcome of the above optimization procedure is vector of quantities scheduled $P_{G_i}^*(k)$ defined as $[P_{G_i}^*(k+1) P_{G_i}^*(k+2) \dots P_{G_i}^*(k+K)]$. Then, by varying the price uniformly up and down by $x\%$ generator obtains a set of optimal points corresponding to these perturbed prices by resolving the above formulation. These solutions are used to create a price sensitivity-based supply vector function $S_i(P_{G_i}(k))$ around the assumed electricity price. All generators are required to submit their supply functions to the system operator, and the market clears bids which are the least generation cost bids needed to balance supply and demand at time k . The system operator will then solve a static economic dispatch.

7.2 Simulation

7.2.1 Characterizing Different Generators

Generation equipment can be classified by characteristics of cost, physical dynamics, and controllability. Cost of electrical generation can be broken into O&M costs and capital costs. For unit commitment and economic dispatch, O&M costs are of primary concern, while capital costs are more important during planning stages. Diesel and fuel oil generators have nearly constant heat rates, giving a constant marginal cost related to the price of fuel as estimated in Chap. 4 and shown below in Tables 7.1 and 7.2. Relative cost is more important for generators that have very low fuel costs such as wind power, hydropower, and geothermal. Due to the inertia of rotating masses, throttle characteristics, existence of reservoirs, or communication

Table 7.1 Aggregated generation parameters for Flores

	Pgmax (MW)	Pgmin (MW)	Ramp rate (%/min)	Marginal cost (\$/MWh)
Diesel	2.2	0.18	100	261
Hydro	1.8	0	5.10	88
Wind	0.66	0	67	87

Table 7.2 Aggregated generation parameters for St. Miguel

	Pgmax (MW)	Pgmin (MW)	Ramp rate (%/min)	Marginal cost (\$/MWh)
Oil	102.66	8.41	100	185
Hydro	5.03	0	5.10	87
Wind	30	0	67	88
Geothermal	27.8	0	50	28.1

systems utilized, generators can have different dynamic capabilities. This is of importance when solving economic dispatch problems which require generators to change output from one time step to the next. Hydropower and wind power generators are believed to be able to generate power up to the amount allowed by the wind or water resource. How fast generation output can change is discussed thoroughly in Chap. 4 and shown below as the limiting ramp rates in Tables 7.1 and 7.2.

Controllability is also a key characteristic of generation resources. In Flores Island, hydropower is controllable and may even have some storage capability. In Sao Miguel island, geothermal and run-of-the-river hydropower generators are not generally controllable, other than shutting down for maintenance. Wind power and fossil fuel generators however can be dispatched such that the electric grid can be balanced.

7.2.2 The Computation of Supply Bids

For the distributed look-ahead dispatch formulation as described in Problem Formulation 3, all the generators solve 1-hour look-ahead optimization by perturbing around the vector of expected price $\lambda(k)$. The expected price $\lambda(k)$ can be obtained in day-ahead dispatch process (which, in this chapter, is obtained from the physically implementable static dispatch). By varying the expected price uniformly up and down by $x\%$, all the generators calculate optimal points corresponding to these perturbed prices by resolving the formulation in Problem 3. The typical supply bid function for diesel, wind, and hydro units is represented in Figs. 7.1–7.6. These supply curves provided at market participants' level already internalize the inter-temporal constraints such as ramping rates. Therefore, at the system operator level, static economic dispatch results will be physically implementable results.

Fig. 7.1 Representative supply bids from diesel generation on Flores island

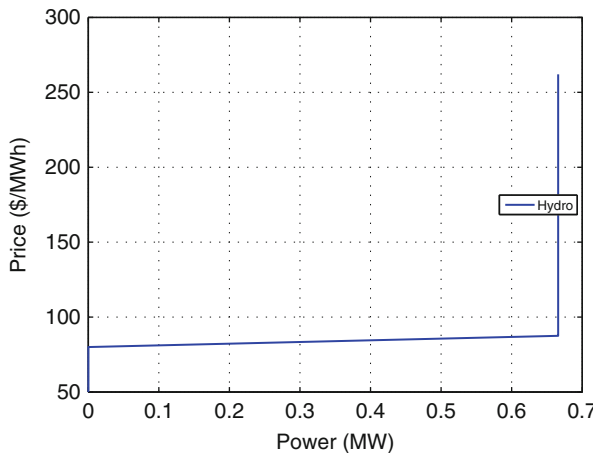
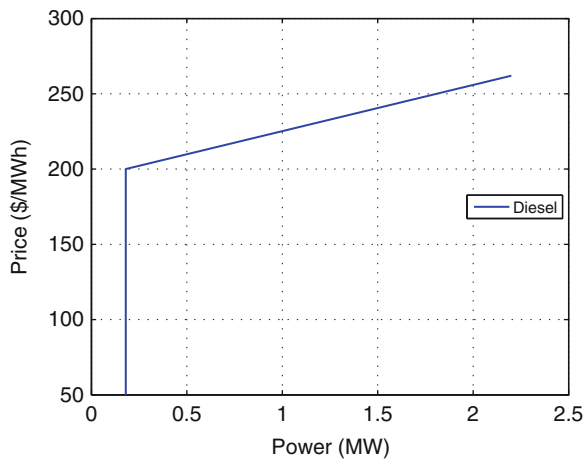


Fig. 7.2 Representative supply bids from hydro generation on Flores island

7.2.3 Flores Island Simulation

Figures 7.7–7.18 represent the unit dispatch results in Flores island under the aforementioned three dispatch methods. In particular, the physically implementable dispatch (Method 1) results are compared and benchmarked with the results presented in the previous chapter. Generation output from 4 representative days in each season are displayed.

In the physically implementable static dispatch, wind generation is treated as negative loads. Therefore, the wind generation is equal to whatever wind power that is available. In the MPC based look-ahead dispatch however, the wind generation becomes an active decision variable instead of an exogenous inputs in the dispatch.

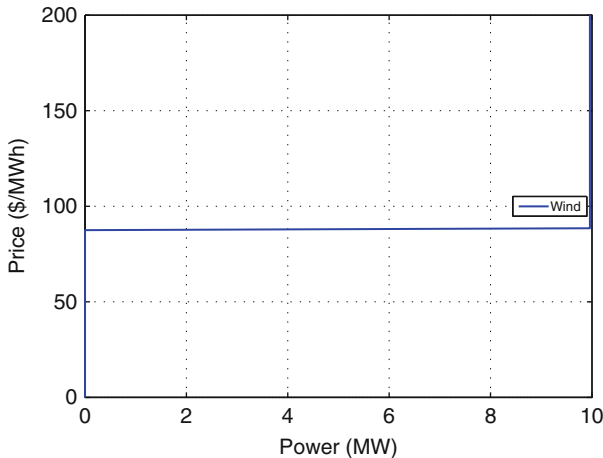
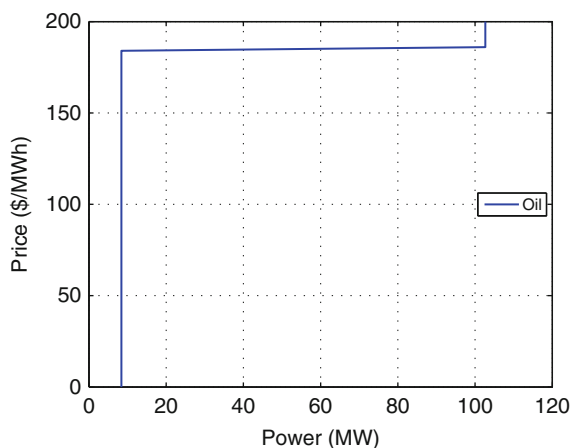


Fig. 7.3 Representative supply bids from wind generation on Flores island

Fig. 7.4 Representative supply bids from oil generation on St. Miguel island



At times when the cost of using expensive diesel to follow the wind ramping offsets the relative cost saving from wind generation, it is more economic to the system to curtail the wind. In the static dispatch, the more expensive diesel unit generation is dispatched at higher level compared with MPC dispatch. The slower hydro unit, on the other hand, increases its output in the look-ahead dispatch because the look-ahead window allows even slower units to follow the fluctuations from wind and load. Compared with static dispatch which takes wind as negative load, the MPC-based dispatch may reduce the cheapest wind generation. However, the MPC dispatch will lead to an overall more economic total generation cost. Table 7.3 shows the daily economic dispatch results from these three dispatch methods. In Flores island, compared with static economic dispatch methods, the cost savings

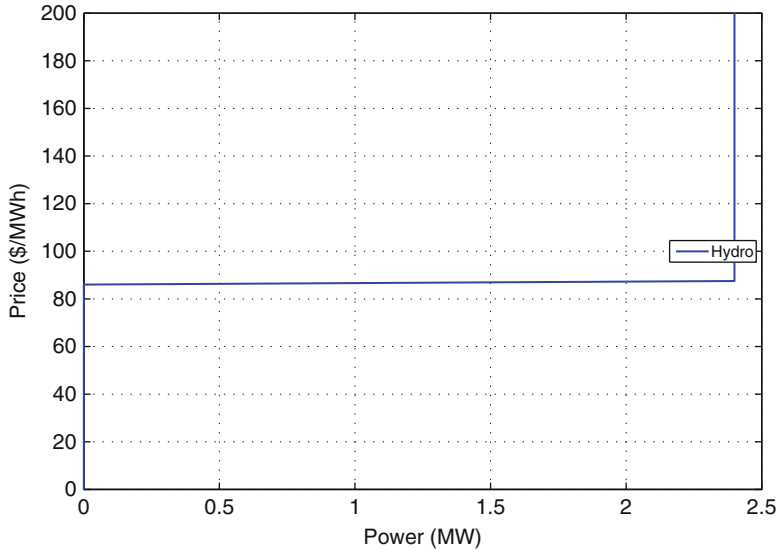
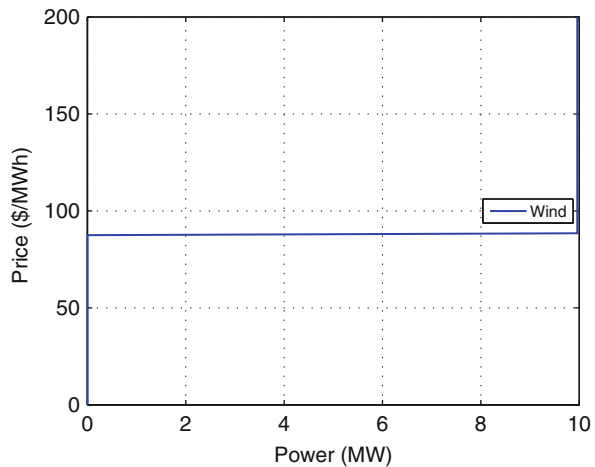


Fig. 7.5 Representative supply bids from hydro generation on St. Miguel island

Fig. 7.6 Representative supply bids from wind generation on St. Miguel island



of look-ahead dispatch is approximately 1%. The duality gap between centralized look-ahead dispatch and the distributed look-ahead dispatch is approximately 0.3% of the overall objective function. In other words, the look-ahead dispatch could be implemented in both centralized approach and distributed approach without too much performance degradation.

Sensitivity of Dispatch Cost Updating Rules of Distributed Look-Ahead Dispatch
 We study the impact of different updating rules of distributed look-ahead dispatch

Fig. 7.7 Generation outputs with dispatch Method 1 in Flores on Jan 16

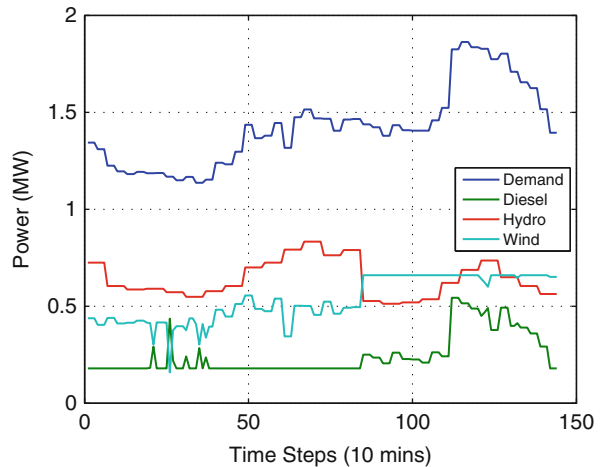
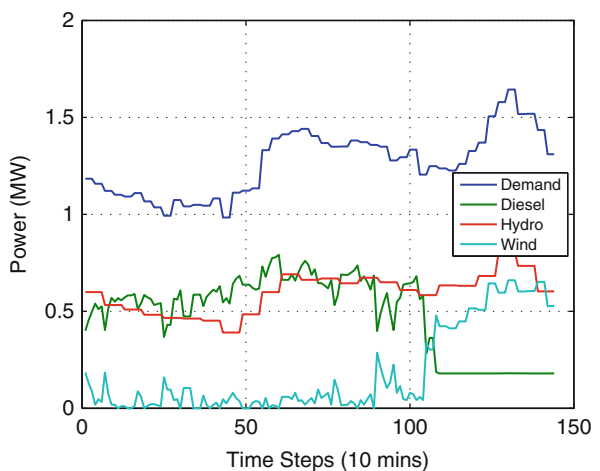


Fig. 7.8 Generation outputs with dispatch Method 1 in Flores on Apr 16



on the dispatch cost. Whereas in the formulation of Method 3, the initial price vector $\hat{\lambda}(k) = [\hat{\lambda}(k) \dots \hat{\lambda}(k+K-1)]$ is assumed to be obtained from day-ahead market clearing, and stay unchanged for the optimization within that day, there is possibility of updating the initial price vector $\hat{\lambda}(k+1)$ for the next time step based on the updated real-time market clearing price at k . Therefore, the initial price vector for the next time step $k+1$ becomes:

$$\underline{\hat{\lambda}(k+1)} = [\lambda(k+1) \dots \hat{\lambda}(k+K)] \quad (7.15)$$

where $\lambda(k+1)$ is the *actual* real-time market clearing price from the previous 10-min interval dispatch at the system operator level. The updated information brings about more accurate price forecast for the next time step. In this simulation,

Fig. 7.9 Generation outputs with dispatch Method 1 in Flores on Jul 16

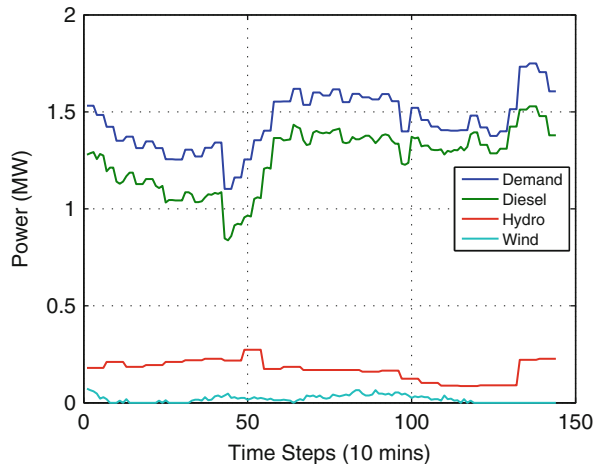
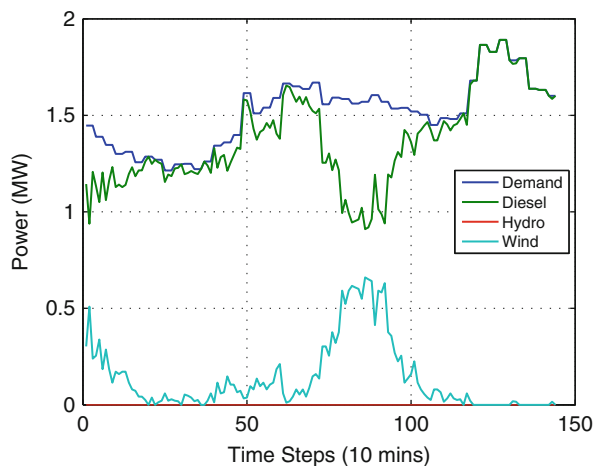


Fig. 7.10 Generation outputs with dispatch Method 1 in Flores on Oct 15



however, even if we update the price this way, the dispatch cost of Method 3 stays the same with the last column of Table 7.3. This is likely due to the fact that there are only three discretized price points possible in the island (the marginal costs of the three units). When the system becomes larger, the set of possible clearing prices will also increase. It would be likely that price updating rules may impact the economic performance of the distributed look-ahead dispatch .

Sensitivity of Dispatch Cost Savings with Respect to Cost Parameters

We also study the impact of different generation cost parameters on the performance of different dispatch methods. As specified in the Data Input chapter, we assume that the short-run marginal cost of wind, hydro, and diesel units in Flores are 87\$/MWh, 88\$/MWh, and 261\$/MWh, respectively. Given this set of marginal cost data, the

Fig. 7.11 Generation outputs with dispatch Method 2 in Flores on Jan 16

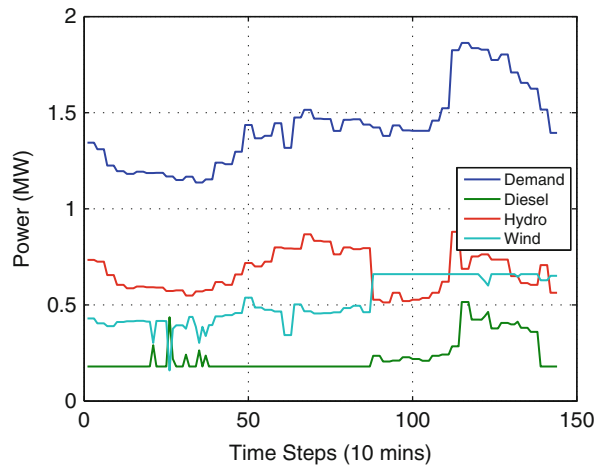
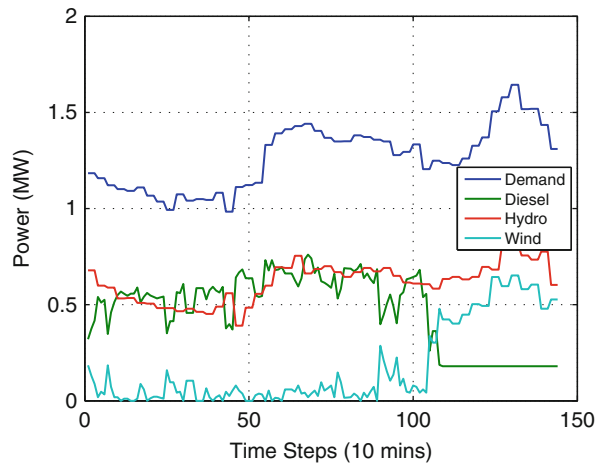


Fig. 7.12 Generation outputs with dispatch Method 2 in Flores on Apr 16



relative economic saving of look-ahead dispatch compared with static dispatch is approximately 1%. However, if the marginal cost of the wind, hydro, and diesel units are changed to 5\$/MWh, 9\$/MWh, and 50\$/MWh, respectively, then the relative economic saving of look-ahead dispatch compared to static dispatch for the same period of time becomes 20%. Namely, the *relative cost difference* of various generating units will have significant impact on the economic performance difference between static and look-ahead dispatches. This could be explained as follows: given the same level of loads (loads assumed to be inelastic), the relative cost saving from look-ahead dispatch is the result of shifting some of the generation from more expensive units to the less expensive units. It is anticipated that with more diverse groups of generating units which have broader range of marginal costs, the potential economic saving from look-ahead dispatch is likely to be higher.

Fig. 7.13 Generation outputs with dispatch Method 2 in Flores on Jul 16

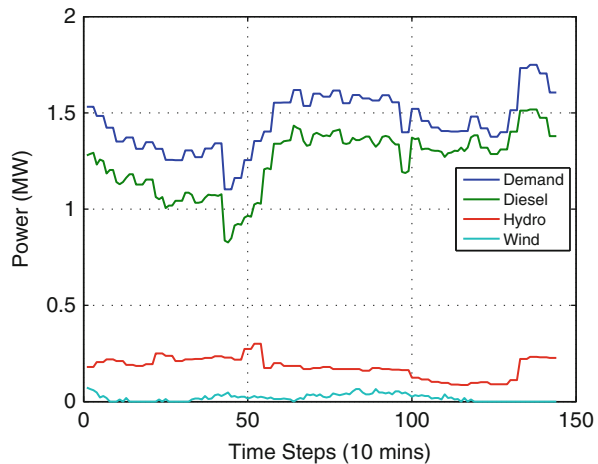
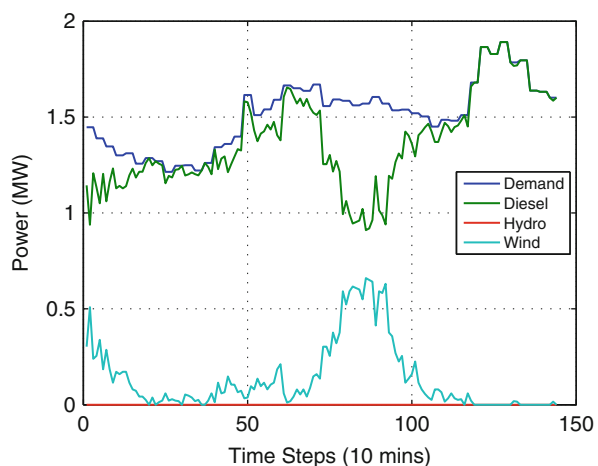


Fig. 7.14 Generation outputs with dispatch Method 2 in Flores on Oct 15



7.2.4 St. Miguel Simulation

Figures 7.19–7.22 represent the unit dispatch results in St. Miguel island under the aforementioned three dispatch methods. In contrast to the Flores island, the hydro units in St. Miguel are assumed to be run-of-the-river type. In other words, the hydro units also become non-dispatchable “negative loads.” Table 7.4 shows the daily cost of economic dispatch under these three methods. For each of the 4 days, the dispatch cost stays the same across all the three dispatch methods. This is due to the fact that hydro units are run-of-the-river type, which are not dispatchable as in the case of Flores. The only dispatchable units in the St. Miguel island are the diesel units. Since both hydro and wind generation units are less expensive than the diesel units,

Fig. 7.15 Generation outputs with dispatch Method 3 in Flores on Jan 16

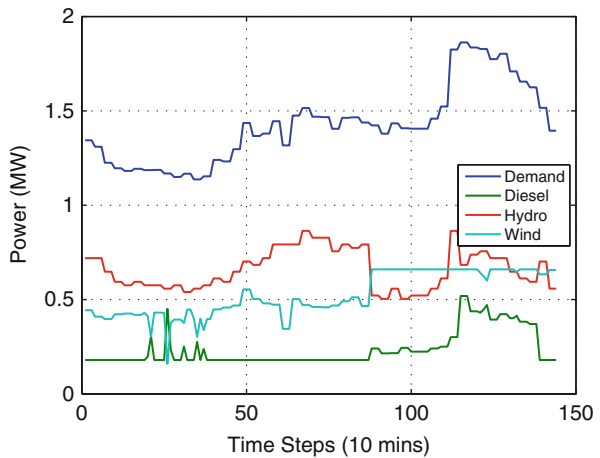
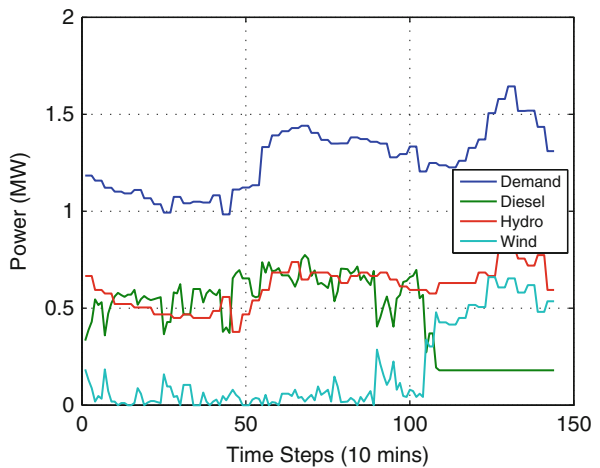


Fig. 7.16 Generation outputs with dispatch Method 3 in Flores on Apr 16



the diesel units always serve as the marginal units in that system. In other words, the dispatch results will stay unchanged due to the limited set of dispatchable units in St. Miguel island.

7.3 Discussions and Summary

In this chapter different dispatch methods are tested in Flores and St. Miguel islands assuming loads are inelastic. The value of incorporating near-term wind/load forecast information is manifested in more cost-effective dispatch results. The cost savings from advanced dispatch methods are heavily dependent on (1) the relative generation cost difference of the power plants in the system and (2) the ramp

Fig. 7.17 Generation outputs with dispatch Method 3 in Flores on Jul 16

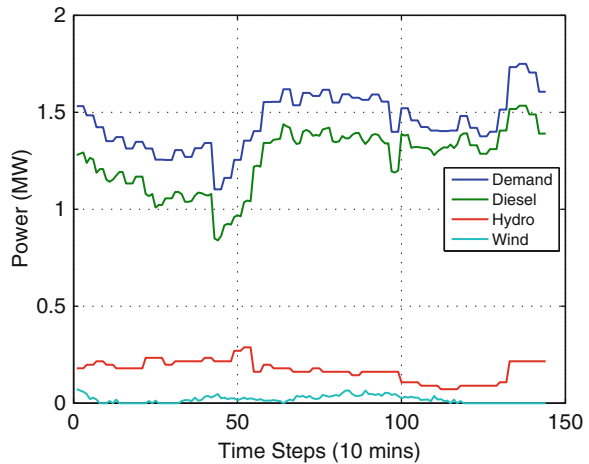


Fig. 7.18 Generation outputs with dispatch Method 3 in Flores on Oct 15

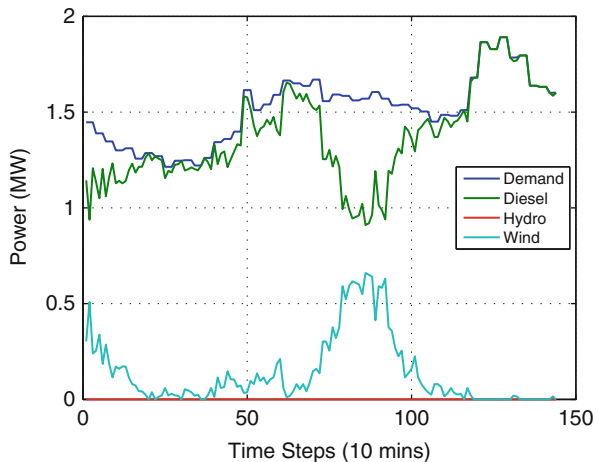


Table 7.3 Daily dispatch cost comparison (\$) for Flores

Date	Method 1	Method 2	Method 3
Jan 16	4,017.11	3,953.94	3,970.28
Apr 16	4,676.08	4,604.45	4,633.94
Jul 16	8,287.53	8,257.15	8,290.98
Oct 15	8,890.01	8,890.01	8,890.01

rate capabilities of different units. In Flores island, compared with static economic dispatch methods , the cost savings of look-ahead dispatch is approximately 1%. The duality gap between centralized look-ahead dispatch and the distributed look-ahead dispatch is approximately 0.3% of the overall objective function. In other words, the look-ahead dispatch could be implemented in both centralized approach and distributed approach without too much performance degradation.

Fig. 7.19 Generation outputs in St. Miguel on Jan 16

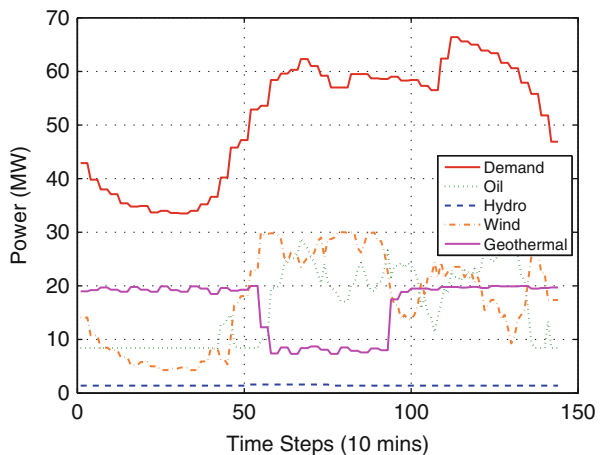
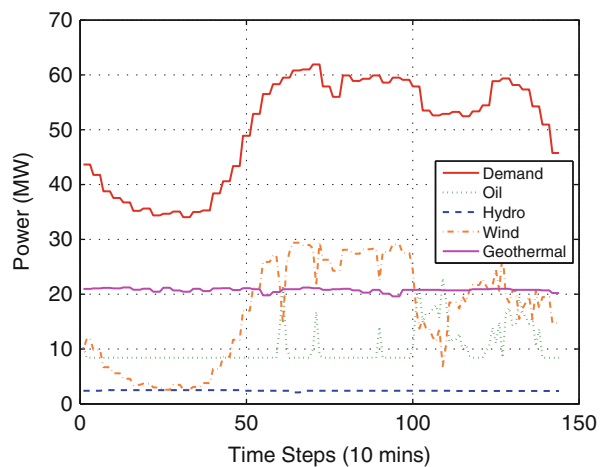


Fig. 7.20 Generation outputs in St. Miguel on Apr 16



In the case of St. Miguel island, on the other hand, there is limited cost savings from more advanced dispatch method. This is due to the fact that hydro units are run-of-the-river type, which are not dispatchable as in the case of Flores. The only dispatchable units in the St. Miguel island are the diesel units. Since both hydro and wind generation units are less expensive than the diesel units, the diesel units always serve as the marginal units in that system. In other words, the dispatch results will stay unchanged due to the limited set of dispatchable units in St. Miguel island.

One major assumption of simulation in this chapter is that the loads are assumed to be *inelastic*. When the loads are assumed to be flexible with respect to electricity price, the potential cost savings from more advanced dispatch methods are expected to be higher. In the next chapter we will discuss the economic cost savings when the advanced dispatch methods are coupled with adaptive load management (ALM).

Fig. 7.21 Generation outputs in St. Miguel on Jul 16

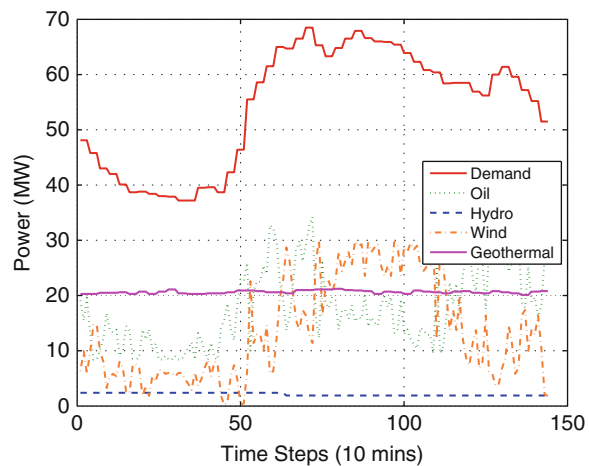


Fig. 7.22 Generation outputs in St. Miguel on Oct 15

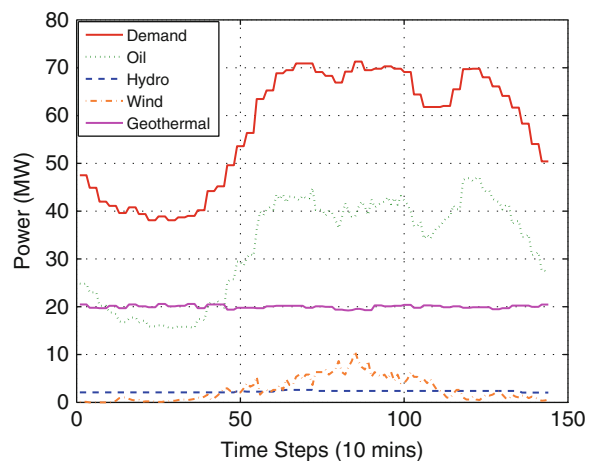


Table 7.4 Daily dispatch cost comparison (\$) for St. Miguel

Date	Method 1	Method 2	Method 3
Jan 16	122,149.27	122,149.27	122,149.27
Apr 16	99,451.98	99,451.98	99,451.98
Jul 16	114,124.32	114,124.32	114,124.32
Oct 15	168,017.17	168,017.17	168,017.17

Acknowledgments This work was supported in part by the US National Science Foundation ECCS Grant 1029873 and in part by the US Power System Engineering Research Center. The authors greatly appreciate the financial support.

Chapter 8

Assessing the Ability of Different Types of Loads to Participate in Adaptive Load Management

Jhi-Young Joo, Jonathan Donadee, and Marija Ilić

8.1 Introduction: Adaptive Load Management for the Islands

Adaptive load management (ALM) is a new way to balance power supply and demand that captures the economic value each market participant sees. It aims to find the system optimum by iterating the information between various market layers and adjusting their energy transactions accordingly [5]. The economic values that ALM takes come not only from supply entities that are usually expressed as bid functions but also from individual electric energy consumption demand. The optimum or suboptimum where these different values clear is recognized as the system price. Ideally, price is a signal of the system that tells where the system is balanced, given different values that every entity of the system (i.e., end-users, power-producing units, load aggregators) takes for energy transactions. In other words, each entity of the system contributes to the clearing price by informing the system what value it is willing to take for its own energy transaction. Once the price is settled by considering all these values, each entity responds to the settled price by adjusting its transaction quantity. For example, in the case of a generating unit, the unit gives its bid functions to the system to tell how much it is willing to produce at a certain price. The system/market operator takes all bid functions from every participating generator and clears the market price. When the generators receive this information about the market-clearing price, they adjust their production according to the price and their bids. The same procedure takes place on the demand side as well, with the demand functions telling the system how much each demand entity is willing to pay for a certain amount of energy.

J.-Y. Joo (✉) • J. Donadee • M. Ilić

Department of Electrical and Computer Engineering, Carnegie Mellon University,
5000 Forbes Ave, Pittsburgh, PA 15213, USA

e-mail: jjoo@andrew.cmu.edu; jdona@andrew.cmu.edu; milic@ece.cmu.edu

Even though the power systems in the Azores islands are not operated by a market mechanism and vertically integrated, the operational criteria come from the cost of operating the generators. Also, while there are not any load aggregators or mediators that represent the end-users' value of electricity on the market, the end-users do respond to the tariffs that their bills are based on. This implies that even when the market is not explicitly run in the Azores' systems, we can capture the long-run or short-run costs of producing energy and the value of consuming energy for the end-users, in order to optimize system operations and planning.

To design the right demand response program for the islands, we explore various ways of adjusting the demand to reduce the costs of installing or producing electric energy in the systems in both the long and short run. Some types of demand can be adjusted with respect to the cost or *price* of producing electricity, while others may not be very flexible. The design process to utilize demand most efficiently on the islands can be summarized in three steps.

The first step is to use more energy when electricity is abundant and available, and to suppress consumption when it is not, in both the long run and short run. For long-run optimization, we analyze the correlation between wind power and the loads and explore the benefit of shifting the load according to the availability of wind. For short-run operations, we give an hourly expected operational cost to responsive loads as a price signal to help them adapt to the availability of power.

The second is to relate the uncertainty of the supply with the rate of response of the demand. In order to operate volatile generation resources, such as wind power, more efficiently in the short run, it is important for the suitable loads to obtain the signal of supply availability (i.e., price) and respond to it within the right period of time. For the loads that are less uncertain and can be shifted, such as loads that operate particular machinery in a bakery or a factory, generation resources with less volatility can be scheduled to supply their needs. Intermittent resources may be more suitable for more flexible and uncertain loads that can respond quickly within a certain range.

This brings us to the third step: to relate the physical characteristics of the loads to the time interval of the system dynamics. The storage effect time constant, or the period of time that the load can withhold its consumption without violating its physical constraints, is crucial when designing the right demand response program framework for a particular type of load. This also leads us to categorize loads with respect to their own suitable time scales.

With all these ideas in mind, we try to find the right program and signal for various types of demand. It is also important to note that within the ALM framework, controlled demand should not compromise the end-users' utility of consuming energy. We also show this point in the demand response schemes that we suggest and in the numerical examples.

8.2 Characterizing Different Loads

8.2.1 Candidate Loads for Adaptive Load Management

In order to see a significant impact in terms of the magnitude of the demand reduction or shift, we first investigate if the largest consumers in the system are flexible at all and which of their loads can be controlled. Another way to have effective demand control is to aggregate small flexible loads. We explain in more detail later what types of loads should be used and scheduled at which points in time over the course of the whole dispatch in the long and short terms.

We look at the types of loads on Flores and São Miguel and generalize the idea of utilizing different types of loads on different dispatch time scales, or shifting the loads in the longer term.

8.2.1.1 Flores

Since the climate is very mild throughout the islands, and there are not many large business and commercial end-users on Flores, we explore the possibility of aggregating small residential loads. A 2004 analysis of energy consumption in the Azores attributes roughly 42 % of residential consumption to household refrigerators [3]. Residential loads are a large part of the total energy consumption on all the islands. We use ALM to model on Flores as price-responsive loads.

8.2.1.2 São Miguel

The largest end-users in São Miguel are mostly commercial or industrial: a large shopping mall and a cement company with an electricity bill of around 50,000 Euros a month are among them. Shopping malls generally consume most of their electricity on lighting and air-conditioning. While lighting is not so flexible in terms of load adjustment since lights need to be consistently on during business hours, air-conditioning is; the air-conditioning load can be adjusted as long as the people in the mall feel comfortable with the temperature. There are also a few other industrial end-users that have potential demand resources: a dairy farm that runs boilers and a pig farm that runs biofuel plants using animal waste and sells the surplus electricity to the EDA (Electricidade dos Açores; the utility company of the Azores).

Smaller end-users include small businesses and residential homes. Potential demand resources of these users are air-conditioning, lighting and laundry loads in hotels, and refrigeration loads in large grocery stores. An average three-star hotel with 200 rooms and a grocery store both pay about 4,000 Euros a month. Residential users have small appliances such as dehumidifiers and refrigerators. Since the climate in the Azores is very moderate, the air-conditioning load, especially from the residential sector, is not significant; only 2.4 % of residential houses have

air-conditioning. However, due to the humid winters, about 30 % of residential households use dehumidifiers at that time of year [6].

8.2.2 Which Loads to Use When

We note that there is no one fast solution that applies to every type of load to be utilized as a demand resource. First, the different physical and economic characteristics of the loads define the suitable time frame for the optimal demand control frame. The physical characteristics of the loads to consider include storage availability of any type (does the load have thermal/electric storage that can shift its consumption?) and the storage time constant (how long can the load withhold consumption?).

The economic characteristics of loads have more to do with the end-users' use of the loads, e.g., the temperature/humidity setpoints of the air-conditioners/dehumidifiers, or the maximum/minimum energy consumption limits that an end-user would allow or set for a certain appliance. This information can be included in a demand function as price elasticity/sensitivity of demand by calculating the optimal energy usage with respect to different prices. For example, air-conditioning loads with different temperature deviation bands show different price sensitivities of demand [5].

There are also various factors, such as regulations on emission or noise, business hours, and labor laws, that can affect the controllability of the loads. All these different factors determine which types of technology are suitable, and when and how to schedule them for ALM. Then the questions are, what is the right framework to include these various characteristics of demand, the individual objectives of better operating the system, and the global objectives of minimizing cost and emissions, and utilizing more renewable energy resources? Certainly there is no one-size-fits-all solution for this. In this chapter, however, we attempt to answer this question by examining the current tariff system in the Azores and proposing a new framework for operating the system with flexible demand. The reason we examine the tariff is because the price of electricity is what drives the end-users to adjust their consumption behavior.

The bottom line of our approach is to apply different frameworks for demand response according to the time intervals and time scales of different types of loads; in other words, more deterministic, pre-programmable or schedulable loads (e.g., factory operation schedules, A/C, dehumidifiers) can be scheduled ahead of time whenever the necessary information is available. This information includes not only the demand side and its characteristics but also system conditions such as wind power forecast. On the other hand, more unpredictable, volatile, and fast-changing loads (e.g., refrigerators, dehumidifiers) can be adjusted in real-time if there exists an adequate two-way communication infrastructure between the loads and the system. However, we also understand that the only current framework in the

islands to induce more demand response is the tariff that charges different prices by season for different time blocks within a day (shown in Chap. 4), which can be categorized as time-of-use (TOU) pricing.

8.2.3 End-Users' Response to Current Tariff and Energy Policies, and the Alternatives

End-users (especially large industrial users) are already responding to the current TOU by (1) shifting their loads to cheaper time blocks, (e.g., a dairy company running its boilers at night, even when it has to pay the labor force overtime) and (2) installing more energy-efficient equipment (e.g., a big grocery store replacing light bulbs in the refrigerators with LED lights). Also, in the Azores, intensive energy consumers are required by law to reduce their energy consumption by 6 % in 6 years. In response to this longer time scale energy savings plan, large industrial end-users are trying to curtail their energy bills. However, there are some end-users that are not able to shift their loads, due to problems such as regulatory issues and/or the characteristics of their loads. For example, a pig farm that also runs a cookie manufacturing business cannot run its fodder production machines at night because of noise regulations, even though electricity is cheaper at night. It can and does, however, run cookie mills at night.

The current TOU system is shown in Fig. 4.41 in Chap. 4 for MT (medium voltage level). It is not clear how the rate for each time block is calculated. The system operators for the Azores simply take the end-user rates that the regulatory body responsible for the whole Portuguese electric power system imposes. From observing the rates shown in Fig. 4.41, it seems that the tariff is designed to suppress demand during peak hours by imposing a higher rate. The time blocks also change by season, reflecting the general seasonal operation conditions. However, it is not clear whether this tariff is effective even in terms of the operational cost. The tariff is applied across all the islands, and the system conditions and/or the generation resource mix are quite different depending on the island. Therefore, it is not very cost-efficient to impose a one-size-fits-all tariff on the Azores as a whole.

We suggest that this tariff can improve by deciding on the rates for every season, month, the cost of the generation resources unique to each island, and the information available on the system condition and the changing demand. This information can include the availability of the generation resources, especially that of wind and hydro, and the change in demand conditions, e.g., anticipated changes in the manufacturing schedules of large industrial end-users. We call this tariff “better time-of-use (TOU)” pricing.

The accuracy or credibility of wind power forecasts can differ significantly in different time frames, especially if the system aims to operate on a large portion of wind power that is dispatchable. Therefore, modifications in system operations and planning are needed ahead of time with respect to the different predictions

of how much wind power is available. This can be done on a seasonal, monthly, weekly, and/or daily basis. The right signal that depends on available information about system conditions along each of these different time lines, should be sent to the flexible loads. The signals can be the expected value of the marginal cost of system generation, local marginal prices, or prices that incorporate the availability of renewable resources. The system operator should, in designing the signal, also consider the general price responsiveness of the loads so that the responsive loads can most efficiently respond to system conditions at different time scales.

The right signal for the responsive loads depends on the regulatory constraints (market existence and price tariffs to the end-users), system operation conditions and priorities (deploying more wind, reducing gas emissions, generation resource mix), and the technology of the loads to be deployed (the response/communication rate of the loads). In the case of the Azores where they do not have a real-time market, a communication system/infrastructure between the loads and the wind availability can be constructed to exploit more wind in real time and make the loads respond to it promptly.

In order for ALM to work, the system operation/scheduling and the tariff designs should consider the following: (1) the value of energy to the users, (2) the forecast accuracy at different times and the dependency of designing the time line of scheduling/operation on the forecast, and (3) the physical characteristics of the loads.

Demand functions capture the information on how the users value their energy usage [5]. A demand function characterizes the relationship between price and demand and tells what the marginal demand is for a given price, or how much the optimal willingness to pay is for an additional unit of a given level of demand. This is an important piece of information that can be incorporated into system operations in order to reflect the economic value of energy as seen from the demand side.

For forecast accuracy and the dependency of time lines on it, the current goals of the Azores to include more renewable generation resources should heavily integrate this information into system operations and optimization. For example, how much wind should be scheduled before a season, a day ahead or an hour ahead will determine how much of the generation and demand resources available can be scheduled and dispatched at what point over the time horizon.

Finally, the physical characteristics of the loads should be determined in accordance with the time scales and intervals of the scheduling of the resources. The questions to consider include the following: how long is the storage time constant of each load? How fast can it respond and communicate with the system or the price signal? Can it be scheduled a day ahead? Can it be adjusted flexibly in real time?

These three factors in combination determine the optimal framework to incorporate demand and renewable resources as much and as efficient as possible.

8.3 Types of Adaptive Load Management Frameworks for Different Loads

The scheduling of the adaptive loads for ALM should be done in a way such that the loads with higher uncertainty and the loads that cannot be well-predicted and prescheduled pay for the corresponding cost of the risk to the system operation. Loads that can be planned ahead with higher certainty should be scheduled in advance so as to be met with lower-cost base generation. On the other hand, the more volatile and uncertain loads are adjusted or simply met by generation resources that are more expensive and fast ramping.

In accordance with this idea, we categorize the loads into several different groups with respect to their physical characteristics and to the time lines. We give examples of loads that can be scheduled in each of long and short time scales.

8.3.1 Better Time-of-Use (Long-Term Scheduling)

This section analyzes the potential for reduction in fossil fuel-supplied electric energy by simply scheduling energy consumption over a long time horizon. In a hypothetical scenario where 33 MW of wind power have been installed on São Miguel, we quantify the possible benefits of some energy consumption being moved from weekdays to weekends. The benefits of such a shift are analyzed probabilistically because of the random nature of wind power. The factors that influence the size of these benefits are also analyzed. It is proposed that energy consumers and producers can negotiate an agreement on how to share the benefits and risks of such a shift.

8.3.1.1 Motivating Load Shifting

Other parts of this monograph suggest that it is economical to install large amounts of wind power in the Azores, even to the point where the sum of renewable energy generation often exceeds the system load. To reduce the amount of fossil fuels burned, energy consumption should be shifted to times when there is an excess of renewable energy from times when it does not meet the total load. As shown in Chap. 4, wind power shows steady daily and seasonal patterns on average, but is highly variable over the course of any particular day. Without the use of communication and control systems, it is difficult for energy consumers to react to real-time wind power conditions and shift consumption times. Because of this difficulty, we will investigate the use of long-term scheduling to reduce the amount of wind power that goes unused or is “spilled” on average.

Chapter 4 shows that electricity demand is generally higher on the weekdays than on the weekends, yet the day of the week does not affect wind power. This leads to

a situation where the load exceeds the output of clean energy sources more often on weekdays than on weekends. More importantly, essentially free wind power is more likely to go unused on the weekends. Our method for estimating the average wind power spilled on weekdays and weekends is described next.

Using historical generation dispatch data from São Miguel in 2008 and normalized wind data scaled to a proposed capacity, we can calculate the amount of wind power that would likely be spilled in each half hour of the year. The wind power is scaled to represent a power output with an installed capacity of 33 MW. If hydropower and geothermal power are assumed to be uncontrollable, then we only need to compare wind power with fossil fuel power. The formula below calculates the wind that would be spilled at each time step of the year:

$$\max\{\text{WindPower} - \text{OilPower}, 0\}. \quad (8.1)$$

Based on this method, we find that an average of 42.75 MWh of wind power is spilled per weekday, while an average of 53.82 MWh of wind power is spilled on each weekend day. This indicates an opportunity to reduce the amount of fuel burned and wind spilled by shifting consumption to the weekends. Next, we propose one way that energy consumption might be rescheduled, and estimate how much this would reduce the wind power spillage.

8.3.1.2 Investigation of Load Shifting

In this section we describe how load shifting can work in practice, propose a method for quantifying the benefits of such a shift, and describe the results of our method when applied to São Miguel.

When energy consumers shift their loads, they face an opportunity cost of not behaving as they would have otherwise preferred. For example, workers at energy-consuming companies may ask to be paid extra for working on Saturday while taking Friday off because it breaks up their weekend. However, if it reduces the amount of fuel that electricity suppliers must burn, there is savings that can be paid out to shifting consumers. Energy suppliers and consumers can negotiate long-term contracts outlining how much consumers are paid each month for their shifting.

Because future wind power and consumption both contain uncertainty, fuel savings from shifting will have a number of possible outcomes. The negotiated payment to consumers could be the actual fuel savings from shifting, or a smaller but certain payment, depending on how much risk each party is willing to accept. For these negotiations to succeed, the parties should be aware of the value of the load shifting. The parties would most likely want to know the mean, variance, and distribution of savings outcomes for each month. We now describe our method for determining this information.

To quantify the benefits of shifting energy consumption from weekdays to weekends, we need data sets of fossil fuel energy consumed under the baseline and shifted load conditions. The 2008 load data described in Chap. 4 is used as the

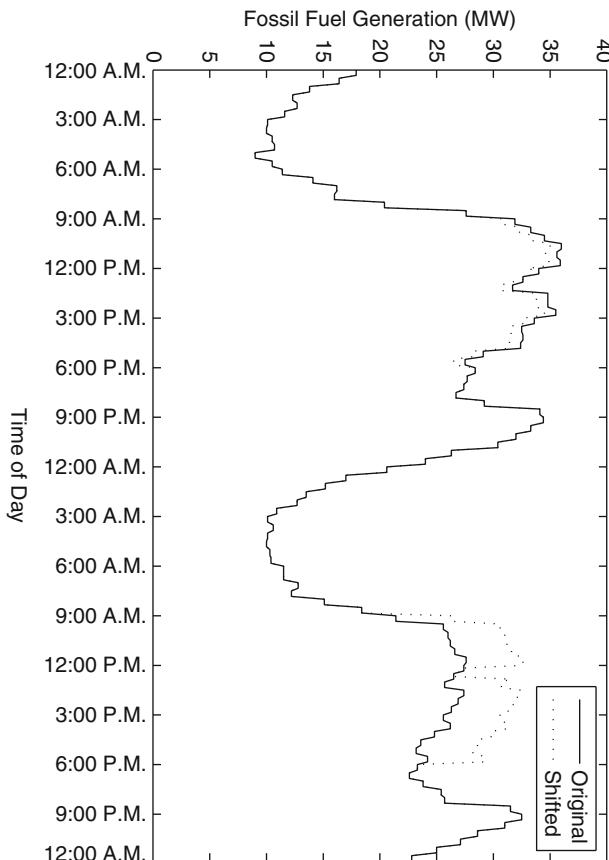


Fig. 8.1 Original and shifted fossil fuel generation for a Friday and Saturday

baseline load data. The baseline data is then altered to create a shifted consumption data set. It is assumed that 5 different electricity-consuming firms each agree to shift consumption from one weekday to Saturday every week. Each of the 5 firms shifts load from a different weekday. The firms are assumed to have a constant consumption of 1 MW between the hours of 9 a.m. and noon, and again from 1 p.m. until 6 p.m. The hours were chosen because they are typical working hours and because one can see a dip in the weekday system load profile during the lunch hour from noon to 1 p.m. For each weekday of the year, 1 MW is subtracted from the load data during these hours. For each Saturday of the year, 5 MW of load is added during these hours. The data sets are then modified to represent the energy consumption supplied by fossil fuel. This is done by subtracting the hydropower, geothermal, and biogas energy from the load data sets. The plots below show the final electricity consumption supplied by fossil fuels over the course of a Friday and Saturday. Figure 8.1 shows a plot of the baseline scenario and the shifted load scenario.

For our probabilistic analysis, we need an understanding of the dependences of the wind and load data. Load and wind speed are both determined in large part by weather patterns. This makes load or wind speed highly correlated with themselves in the preceding and following days. However, over the time scale of a week, which is the scale that weather systems can be thought to change on, the correlation dies off. This means that we can consider single weeks of wind or load data as contiguous observations, but that weeks of data are independent of each other. Also, it is hard to think of a mechanism by which wind speed would strongly affect the load at any single point in time more than other predictors such as temperature or time of day. Therefore, we can also consider load and wind speed as independent of each other. This allows us to use the wind data from multiple years and increase the number of observations used in the estimation procedure. One of the largest determinants of both load and wind is the season of the year, as shown in Chap. 4. Therefore, we need to quantify the savings separately for each month of the year.

The data we use for the estimation consists of the baseline and shifted load fossil fuel energy use, as well as the wind power data, from the years 2008, 2007, and 2004. The normalized wind power data described in Chap. 4 is multiplied by 33 to scale it to the proposed installed capacity of 33 MW. All of the data is split into weeklong observations, starting at 12:00 midnight each Sunday. A week of data is associated with the month in which its Sunday lies. This gives us between 3 and 5 weeks of fossil fuel energy and between 9 and 15 weeks of wind for each month.

For each month of the year, we estimate the fuel savings per week by shifting the load. For each weeklong observation of fossil fuel energy use, we loop through all the observations of wind power from the same month and subtract the wind power from the fossil fuel energy. At each time step, the maximum of this difference or zero is the amount of fossil fuel energy that would still be required if 33 MW of wind power generation had been installed on the island. This is done for both the baseline and shifted load scenarios. The residual fossil fuel energy in the shifted load scenario is subtracted from that of the baseline scenario. This value is summed over all the time steps in the week to obtain an observation of the weekly fossil fuel energy savings from shifting. Histograms of the resulting savings observations are shown below in Fig. 8.2. These histograms show the distribution of possible savings outcomes for each month.

All of the histograms, except for April, have dominant modes near zero. None of the histograms show instances where Oil Power increases by more than 10 MWh, but some months have multiple instances of reductions of greater than 35 MWh.

The mean and standard deviation of the weekly savings are calculated for each month and shown in Table 8.1. The far right column of Table 8.1 titled *Mean hourly benefit per firm* is calculated by multiplying the mean fossil fuel energy savings by the cost of oil generation on São Miguel as calculated in Chap. 4, 185\$/MWh, dividing it among the five firms, and then dividing it by the number of hours in the working day, 8. This is the average amount of money per hour that the electricity supplier would be able to pay to each of the load shifting firms. Even for the large positive values, this may or may not be an appealing offer, depending on the preferences of the firm's management and employees.

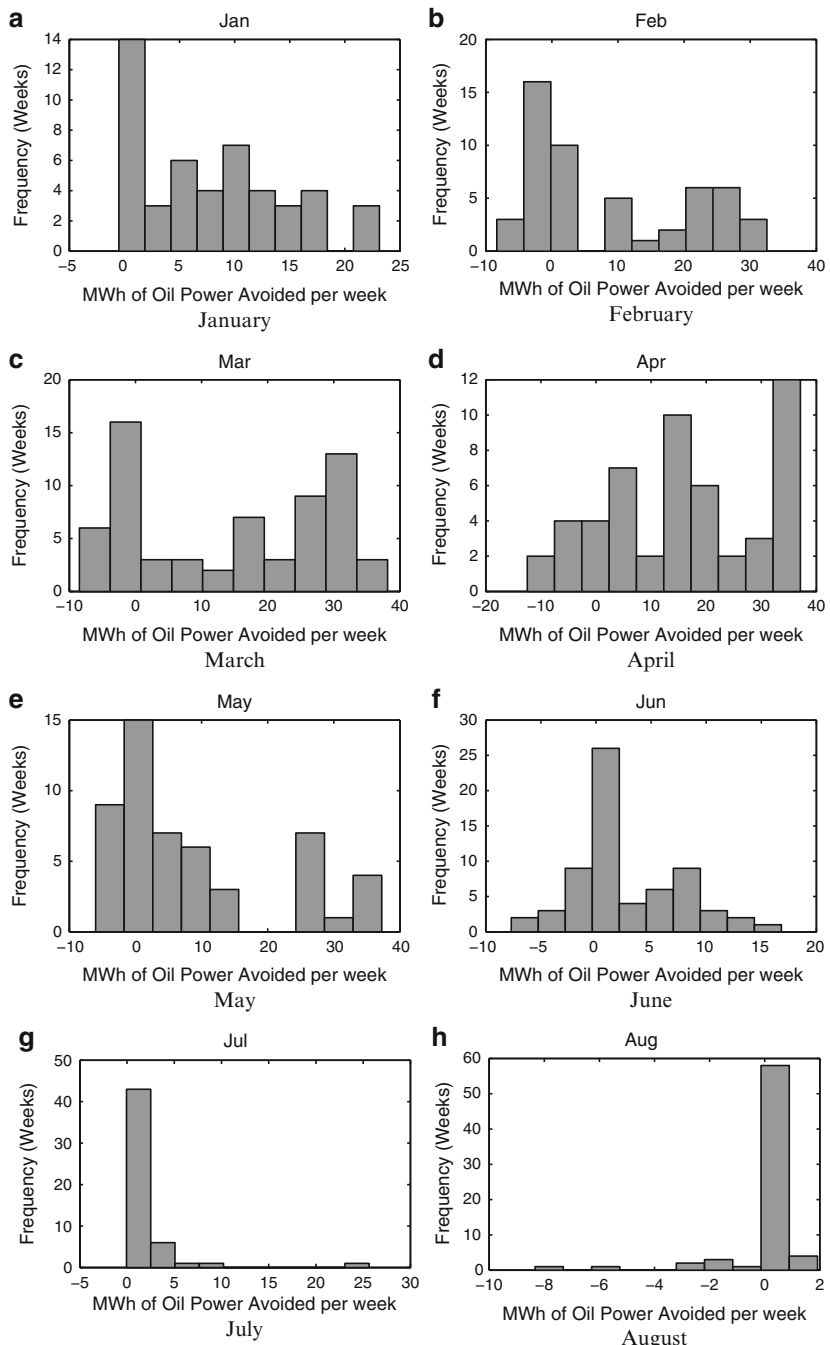


Fig. 8.2 MWh of oil-generated energy avoided each month

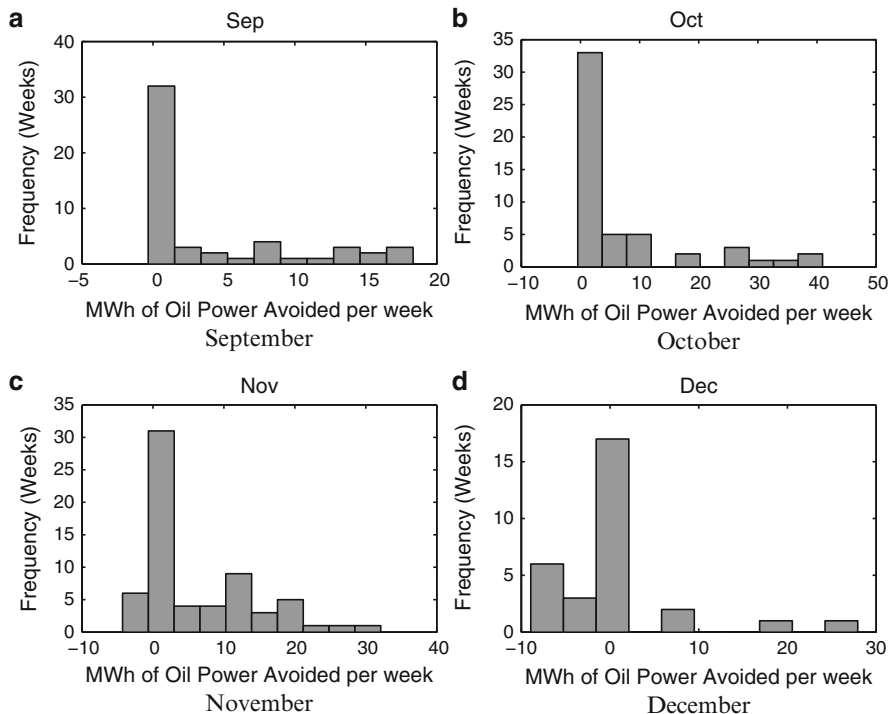


Fig. 8.2 (continued)

Table 8.1 The mean and standard deviation of the weekly savings for each month, 2008, on São Miguel

Month	Mean fossil fuel energy savings (MWh/week)	Standard deviation of fuel savings (MWh/week)	Mean hourly benefit per firm (\$/hour)
January	7.91	6.87	36.58
February	8.53	12.26	39.46
March	14.39	14.61	66.54
April	16.06	14.16	74.26
May	8.59	12.86	39.72
June	2.56	4.90	11.86
July	1.55	3.87	7.16
August	-0.25	1.37	-1.18
September	3.91	5.93	18.1
October	6.68	11.53	30.91
November	5.87	8.47	27.13
December	0.23	7.56	1.05

8.3.2 Day-Ahead Scheduling and Real-Time Adjustment

For day-ahead scheduling, the loads can submit one of two different types of information to the system. First, some loads can inform the system of their price-responsiveness. Deterministic or pre-programmable loads such as automated machinery operations in a factory, or loads that have storage with a longer time constant such as air-conditioning or water heating, can be grouped in this category. With respect to the anticipated price that is either given by the system operator or calculated by the end-user, the load aggregator, or the electricity distributor, a demand function can be calculated based on this price information [5]. The minimum and maximum energy consumption constraints should also be included in addition to the price sensitivity information of the load sent to the system.

Another form of information that the loads can exchange with the system operator for day-ahead scheduling is the energy minutes/hours. This is to notify the system how many kilo or megawatts of energy the end-user plans to use each hour on the following day. The loads that have a predetermined amount of energy usage within a time interval are more suitable to give this information to the system. The end-users with this type of load can notify the system operator the minimum amount of energy that they must consume, which is an inelastic demand for the hour. If the market mechanism develops, the end-users can also attach a price that they are willing to pay for this demand and bid into the market.

Now, with the day-ahead scheduling done with the more certain and predictable loads with the cheapest and schedulable generation resources, the demand should still be met with the next least expensive supply of reserve in real time. The day-ahead scheduled loads may or may not have contracts with hard constraints (e.g., a high penalty if the goal is not met). Regardless, there is always some degree of uncertainty surrounding the predicted or prescheduled demand. Also, the scheduled day-ahead demand may not be physically implementable by every scheduled load in every hour.

The real-time adjustment of flexible loads should therefore have real-time information exchange between the status of the loads and the system optimum. More unpredictable loads, or loads that have storage with a shorter time constant than a time interval of day-ahead scheduling (e.g., refrigerators), are suitable for this real-time adjustment scheme. Price sensitivity with respect to the real-time price/signal, such as wind availability, that reflects the status of the system should be sent to the system operator from the loads. The minimum and maximum energy constraints calculated from the current status of the load (e.g., the current temperature inside a refrigerator or the current motor speed of a dryer) should also be communicated to the system operator, so that the system dispatch of this adjustable load is within the physical limits and the end-users' preferences of the particular loads.

8.3.2.1 Data Preparation for Dispatch with Price-Responsive Demand

Flores: Calculating the Demand Functions of Refrigerators

For the year of 2008, the total electric energy produced on Flores was 11.6 GWh. The statistics of the system operator show that residential customers used roughly 4.5 GWh of energy. Knowing the percentage of residential consumption that is used for refrigeration, we can calculate the annual energy consumption of household refrigerators. Because refrigerators run constantly, we can divide the annual consumption by the number of time steps to get the energy per unit of time. On Flores, the estimated aggregate energy consumption of refrigerators is 35.7 kWh per 10 min, or a constant load of 214.2 kW. Because the duty cycle of refrigerators is 50 % [1], 35.7 kWh represents the consumption when half of all the refrigerator compressors on the island are running. Therefore, ALM assumes that the maximum amount of energy that can be consumed in a 10-min period by price-responsive refrigerators is double this number, or 71.4 kWh per 10 min. In terms of instantaneous power, assuming constant consumption over the period, this is equivalent to a load of 428.4 kW.

For ALM-enabled refrigerators to participate in energy markets, a physical model must be used to derive the demand functions for energy. First, we model the temperature dynamics of an individual refrigerator. We assume a linear temperature increase/decrease according to the on/off state of the compressor, within the maximum and minimum temperature bounds [7]. We assume both the cooling and warming time constants to be 20 min [1]. The minimum temperature bound is 3°C, and the maximum is 8°C:

$$T(t) = T_i + at \text{ with } \begin{cases} a = a_{\text{cooling}} = \frac{(T_{\min} - T_{\max})}{\tau_{\text{cooling}}} \\ a = a_{\text{warming}} = \frac{(T_{\max} - T_{\min})}{\tau_{\text{warming}}}. \end{cases} \quad (8.2)$$

Based on the uncontrolled dynamics of the refrigerator's temperature in 8.2 from [4], we derive the temperature dynamics of the refrigerator with control allowed. This yields

$$T(t_1) - T(t_0) = (t_1 - t_0) \left\{ \frac{60u}{(t_1 - t_0)P} * a_d + \left(1 - \frac{60u}{(t_1 - t_0)P} \right) * a_u \right\} \quad (8.3)$$

where t_1 and t_0 are the final and initial time points, $T(\cdot)$ is the temperature in the refrigerator at a given time step, P is the power rating [kW] of the refrigerator, and a_d and a_u are the heat transfer rates [°C/min] for the cooling and warming periods, respectively. u is the electric energy input [kWh] within the time period.

Second, giving this temperature dynamic equation as a constraint and u in the equation above as the control variable, we solve an optimization problem of minimizing the total energy cost. The 10-min interval electricity prices of a day are given as input, and the price is denoted as p in the following problem formulation:

$$\begin{aligned}
 & \min_u \sum_{k=1}^{144} p[k]u[k] \\
 \text{subject to } & T[k+1] = T[k] + 10 \left\{ \frac{6u}{P} * a_d + \left(1 - \frac{6u}{P}\right) * a_u \right\} \\
 & T_{\min} \leq T[k] \leq T_{\max} \quad \forall k \\
 & u_{\min} \leq u[k] \leq u_{\max} \quad \forall k.
 \end{aligned} \tag{8.4}$$

This optimization problem can be transformed into simple linear programming with an equality constraint and minimum and maximum bounds. By solving this optimization with respect to the given set of 144-by-1 vector p , we obtain an optimal energy usage for the whole time horizon of the day.

Third, in order to obtain the price sensitivity of this individual refrigerator load, we repeat the same optimization with respect to different price settings. We obtained the different values of optimal energy usage at each time step by perturbing the expected price given by $\pm 10\%$ and $\pm 20\%$. This way, we have five different pairs of price and demand at each time step. We interpolate, for each time step, these five points of price and demand quantity to obtain a demand function, which is the relation between the demand quantity and the price that the demand is willing to pay. We assume a linear (first-order polynomial) demand function. The details for calculating a demand function and the overall idea of ALM can be found in [5].

The price sensitivity of demand calculated this way corresponds to only a portion of the whole system demand. Therefore, in order to include this in the economic dispatch of the system, the demand sensitivities for an individual refrigerator were scaled to coincide with the value of the total refrigeration load size, which was 214.2 kW according to our calculation.

The price sensitivities of a refrigeration load for a day were calculated with the expected price at each time step of the day.

The resulting price sensitivities of demand on April 16, assuming two wind turbines installed (with a total wind capacity of 0.66 MW), are shown in Fig. 8.3. Demand function slopes indicate the level of the demand's sensitivity with respect to the price. Note that a higher value, or a value closer to zero, of the demand function slope indicates a higher price sensitivity of demand, i.e., a more elastic demand with respect to the price.

The overall tendency in this study is that a higher price induces the demand to be more inelastic to price. Also, an interesting point to note is that at the time points where there is an abrupt change in price level, such as at the first time step (0:00 a.m. in Fig. 8.3) and around hour 18 (5:50 p.m. in Fig. 8.3), the demand was inelastic with respect to the price. At Point 1, the optimal demand was fixed to be at its maximum level, while at Point 2 the inelastic optimal demand was the minimum bound. This shows that look-ahead optimization works with respect to the price and adjusts the demand based on the price forthcoming. Demand functions at some representative time points are plotted in Fig. 8.4.

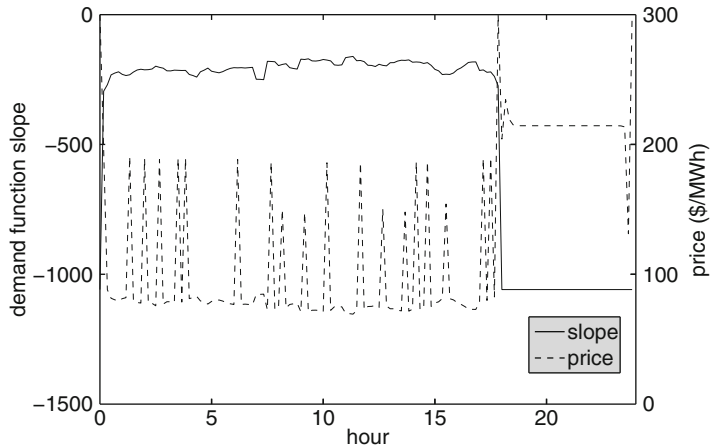


Fig. 8.3 Expected market price and the corresponding demand function slopes on April 16, 2008

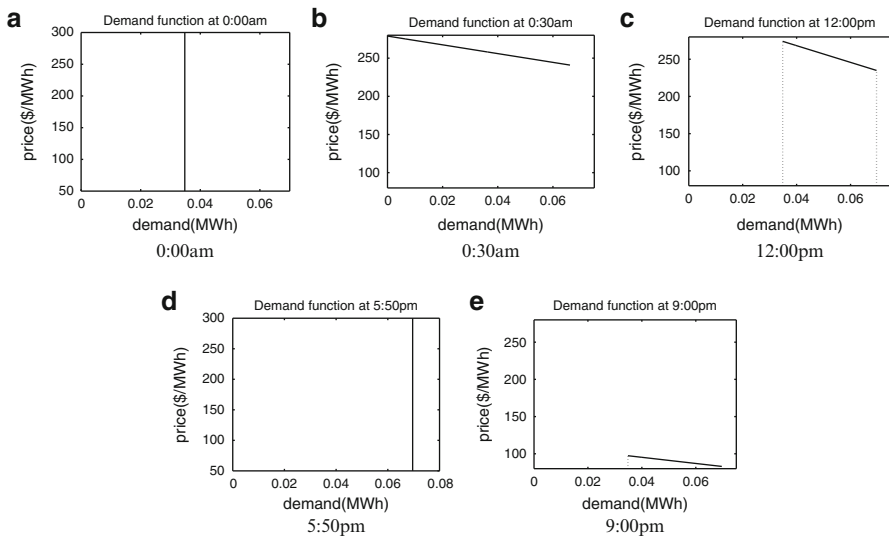


Fig. 8.4 Demand functions at 0 a.m., 0:30 a.m., 12 p.m., 5:50 p.m., and 9 p.m. on April 16, 2008

Flores: Calculating the Demand Functions of an Air-Conditioning Load in a Shopping Mall

A large shopping mall recently opened on São Miguel. Since the climate of the Azores is very moderate, as shown in Fig. 8.5, we find that there is little air-conditioning usage there, except for perhaps big commercial buildings and offices. Therefore, based on estimations of the physical parameters of the shopping mall building, we simulated the air-conditioning usage of the shopping mall and

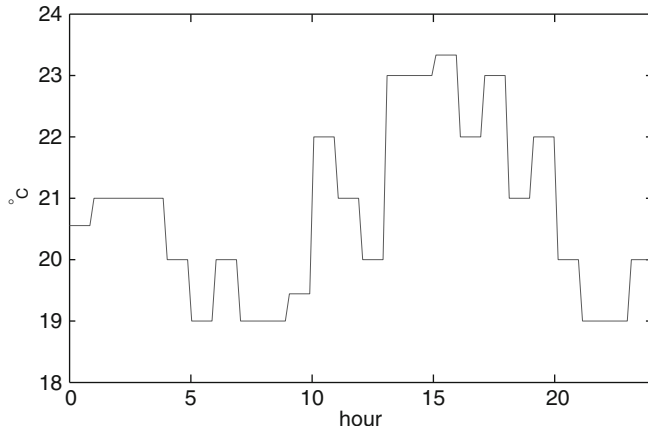


Fig. 8.5 Weather temperature in Ponta Delgada, São Miguel, on July 16, 2008

attempted to prove how ALM can help move forward the efficient and clean use of electric energy.

The detailed procedure is as follows: we first obtain the market price data from the economic dispatch for the given day. Then we calculate the optimal energy usage for 24 hour with respect to the price. Note that we optimize the energy usage based on the whole 24-hour horizon instead of one interval at a time; we call this look-ahead optimization. Besides calculating the optimal hourly energy usage, we also calculate the price sensitivity of demand by obtaining the optimal energy usage with respect to a slightly perturbed value from the expected price.

For the representative summer day of July 16, 2008, we first obtain the operational cost of energy in 10-min intervals from the system. We take this as the hourly price input of the optimization problem for controlling the air-conditioning system inside the mall. We assume that the mall is open from 11 a.m. to 10 p.m., so the thermostat is set to be 21°C during those hours. We also assume that for 1 h both before and after business hours, the mall shop owners and staff will prepare for opening or closing, so we set the temperature setpoints at 22°C for those hours. We assume that the initial temperature is 22°C, and we set the last temperature setpoint to go back to this initial state, too.

Since the weather temperature is close to the setpoints throughout the day, and the inertia factor of the indoor temperature is large because of the vast area of the mall, the largest heat sources are the lighting and people. Therefore, we attempt to estimate the values of the heat sources first. The recommended illumination for supermarkets is 750 lux or lumen/m², and this intensity of light will emit approximately 25 W of heat per meter squared, according to the following equation.¹

¹All the equations and parameters regarding the heat sources and the temperature from them were taken from The Engineering Toolbox (<http://www.engineeringtoolbox.com>).

$$P = b / (\eta_e \eta_r l_s) \quad (8.5)$$

where

P : installed electric power (W/m^2 floor area)

b : recommended light level (lux, lumen/m^2)

η_e : light equipment efficiency

η_r : room lighting efficiency

l_s : emitted light from the source (lumen/W).

The total land area of the shopping mall is estimated to be about $25,000 \text{ m}^2$. Since the mall has two stories, the total floor area is $50,000 \text{ m}^2$, and the total emitted heat is 1.25 MW .

The heat emitted from the people in the stores is estimated at $220 \text{ btu}/\text{hr}$ per person, which is equivalent to $4.795 \text{ joules}/\text{hr}$ per person. Assuming there are about 300 persons in the mall at all business hours, the total heat that people emit will be $4.795 \times 300 \text{ J}/3,600 \text{ s} = 0.4 \text{ W}$. This is negligible compared to the heat emitted from the lighting; therefore, we only consider the heat from the lighting.

Since we have a dynamic equation of the temperature inside a building with a heating/cooling system, we are interested in how much this heat will raise the indoor temperature. The amount of heat needed to heat a subject from one temperature level to another can be expressed as follows:

$$Q = c_p m dT \quad (8.6)$$

where

Q : amount of heat (kJ)

c_p : specific heat ($\text{kJ}/\text{kg}\cdot\text{K}$)

m : mass (kg)

dT : temperature difference between hot and cold sides (K).

In one hour, the heat from the lighting will emit $4,500 \text{ MJ}$. The volume of the air in the shopping mall, assuming the height of the whole building (two-story) is 30 m , is $25,000 \text{ m}^2 \times 30 \text{ m} = 750,000 \text{ m}^3$. The air density at 20°C is $1.204 \text{ kg}/\text{m}^3$, so the mass of the air in the mall is $903,000 \text{ kg}$. Applying these values to the equation above, we have $4,500,000 \text{ kJ} = 1 \text{ kJ}/\text{kg}\cdot\text{K} \times 903,000 \text{ kg} \times dT$, and $dT = (4,500/903) \text{ K} = 4.98 \text{ K} = 4.98^\circ\text{C}$. Therefore, when the lights are on in the shopping mall, the indoor temperature will rise by 4.98°C in an hour, or 0.83°C in 10 min, without any temperature control.

Based on all these estimations and the temperature dynamics of the air-conditioning system [2], the resulting indoor temperature dynamic equation becomes

$$T[k+1] = \varepsilon T[k] + (1 - \varepsilon)(T_{\text{out}}[k] + \gamma u[k]) \quad (8.7)$$

$T[k]$: the indoor temperature at hour k

$T_{\text{out}}[k]$: the outdoor temperature at hour k

$u[k]$: the electric energy usage of the air-conditioning system at hour k

ε : air inertia factor calculated to be $e^{-\tau/TC}$ where τ is the time interval and TC is the time constant (equal to the total thermal mass divided by the thermal conductivity)

γ : steady-state temperature gain (− for cooling, + for heating)

during the closed hours, and +4.98 is added to the right-hand side for business hours due to the heat emitted. The specific values of the parameters are calculated based on [2]. The optimization of the whole time horizon of 24 h can be formulated as

$$\min_u \sum_{k \in \text{open}} \{\alpha p[k]u[k] + (1 - \alpha)(T[k] - T_{\text{set}}[k])^2\} + \sum_{k \in \text{closed}} \alpha p[k]u[k] \quad (8.8)$$

subject to $T[k+1] = \varepsilon T[k] + (1 - \varepsilon)(T_{\text{out}}[k] + \gamma u[k]) + 4.98$ for $k \in \text{open}$ hours

$T[k+1] = \varepsilon T[k] + (1 - \varepsilon)(T_{\text{out}}[k] + \gamma u[k])$ for $k \in \text{closed}$ hours

$$u_{\min} \leq u[k] \leq u_{\max} \forall k.$$

Note that the objective functions are different depending on the hours when the desired temperature is set (open hours) or not (closed hours). Figure 8.6 shows the difference in the calculated optimal energy usage between the look-ahead approach and static optimization. Static optimization is defined here as adjusting the electric energy usage according to the expected temperature only at the very next time step. Static optimization is a more myopic temperature control than look-ahead optimization, and does not include price information in its optimization. In this Fig. 8.6, one can see that look-ahead optimization has a lower peak than the static approach, and the energy usage during peak hours is shifted to the off-peak hours. This is more obvious in Fig. 8.7. With look-ahead optimization, we can observe that they pre-cool the air before business hours when the electricity price is cheaper (Fig. 8.8). For this simulated day alone, the look-ahead approach cost 127 Euros less than the static approach.

8.3.3 Direct Load Control

Direct load control is also an option to utilize flexible demand most efficiently. Loads that can be interrupted on short notice and for a short period of time are good

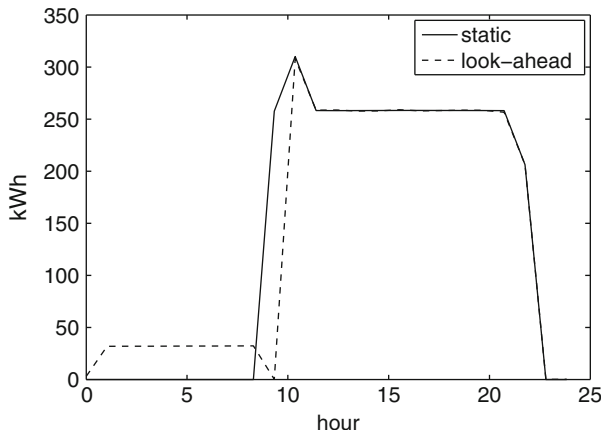


Fig. 8.6 Optimal energy usage with different optimization methods

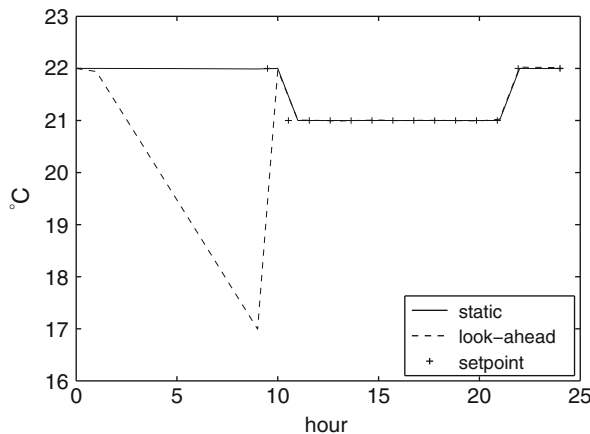


Fig. 8.7 Controlled indoor temperature with different optimization methods

candidates for this. On São Miguel, dehumidifiers fit this description. End-users should notify the system operator about how much of their loads can be curtailed and the maximum disconnection time allowed for the loads. Depending on the contract, they may also want to specify how long in advance they would like to be notified before any upcoming curtailment.

According to a report on the energy use of the residential users on São Miguel, 14.2 % of residential households on São Miguel have their dehumidifiers on most of the time during the winter [6]. This means that the number of dehumidifiers running in residential homes would be about 7,570. Since an average dehumidifier consumes about 0.5 kW, the amount of power consumed by the dehumidifiers at a random moment would be 3,785 kW. This is a substantial amount of power considering

Fig. 8.8 Hourly price input for look-ahead optimization

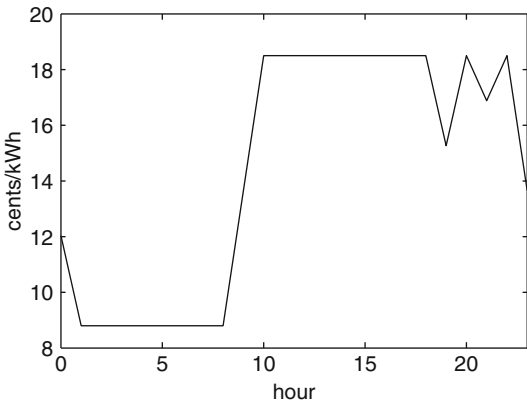


Table 8.2 Comparison of different tariffs

Tariff	Description
Time-of-use	Rates fixed within a season
Better time-of-use	Better representation of seasonal or monthly changes of generation and demand resources
	Transitional tariff between the current one and the more advanced and detailed day-ahead scheduling and real-time adjustment
	Induce large loads to schedule to shift to lower-cost periods
Day-ahead scheduling	Loads that can be scheduled a day ahead by quantity (physical commitment) or that can give information about price sensitivity (financial contract)
Day-ahead scheduling	Real-time two-way communication with the appliance and the system operation
Real-time adjustment	Loads that can respond promptly within a time step of the real-time operation

that the peak capacity in winter is about 60–70 MW. Assuming that turning off the dehumidifiers for about 10 minutes will not discomfort end-users much, the system operator can consider shaving small spikes of oil dispatch (shown in Fig. 7.19 in Chap. 7), such as around 7:20 a.m., 10:30 a.m., 12:20 p.m., 2:00 p.m., 3:10 p.m., and 11:50 p.m. Turning off oil generators for 10 minutes five times each day can save about 700 Euros a season.

8.4 Discussions and Summary

In this section, we attempted to select the right types of loads for demand response on the islands of Flores and São Miguel. We recognize that there are many different types of loads that are suitable for a certain framework of demand response with the system dispatch or longer-term scheduling. Table 8.2 summarizes the overall view

of the possible tariffs or dispatch frameworks and the corresponding loads that are suitable for each of them.

Each of the demand response technologies has different costs and savings associated with it. Real-time adjustment demand dispatch requires near real-time communication and control devices on both the end-users' and the system operator's premises, while the longer-term demand scheduling by better time-of-use may not require any investment in sophisticated infrastructure. Therefore, in order to evaluate fully the potentials of the demand response programs suggested, further research on the trade-off between the investment costs and the benefit of each scheme should follow this work.

Acknowledgments Most of the data on the specific end-users on São Miguel were obtained from a survey conducted by Canay Ozden, doctoral student in History, Anthropology, Science, Technology, and Society at MIT. The authors are grateful for her work.

This work was supported partly by Semiconductor Research Corporation (SRC) Energy Research Initiative (ERI) for Smart Grid Research Center (SGRC) Task 2111.001 Adaptive Load Management, and partly by the Fundação para a Ciência e a Tecnologia (Portuguese Foundation for Science and Technology) through the Carnegie Mellon Portugal Program. The authors are grateful to each sponsor for their financial support.

References

1. J. Cavallo, J. Mapp, Targeting Refrigerators for Repair or Replacement, Argonne National Laboratory, March 2000
2. P. Constantopoulos, F.C. Scheppele, R.C. Larson, ESTIA: a real-time consumer control scheme for space conditioning usage under spot electricity pricing. *Comp. Oper. Res.* **18**(8), 751–756 (1991)
3. Edifícios, Saudáveis, Consultores, Plano para a Utilização Racional de Energia nos Edifícios: Região Autónoma dos Açores Programa INTERREG IIIB Projecto ERAMAC (Maximização da Penetração das Energias Renováveis e Utilização Racional de Energia nas Ilhas da Macaronésia), September, 2004
4. I. Troch, F. Breitenecker (eds.), in Proceedings of Mathmod 2009 - 6th Vienna International Conference on Mathematical Modelling. Argesim Report No. I.35 (on CD-ROM). ISBN 978-3-901608-35-3 (2009)
5. J.-Y. Joo, M.D. Ilić, A multi-layered adaptive load management (ALM) system: information exchange between market participants for efficient and reliable energy use. *Transmission and Distribution Conference and Exposition 2010 IEEE Power and Energy Society*, pp. 1–7, 19–22 April 2010
6. MIT Portugal, Universidade dos Açores, Characterization of the Azorean Residential Building Stock, Report, 2010. Available at http://www.green-islands-azores.uac.pt/admin/ficheiros/uploads/Final_Report_04.02.2011_2.pdf
7. M. Stadler, W. Krause, M. Sonnenschein, U. Vogel, Modelling and evaluation of control schemes for enhancing load shift of electricity demand for cooling devices. *Environ. Model. Software* **24**, 285–295 (2009)

Chapter 9

Look-Ahead Model-Predictive Generation and Demand Dispatch for Managing Uncertainties

Jhi-Young Joo, Yingzhong Gu, Le Xie, Jonathan Donadee,
and Marija Ilić

9.1 Formulation of Dispatch with Price-Responsive Demand

In this chapter, we take the formulation of Problem 3—the distributed look-ahead dispatch of Chap. 7—and modify it to fit elastic or price-responsive demand. Price-responsive demand takes the anticipated price of electricity as the input for its optimization over a time horizon. As we discussed in Chap. 8, the time horizon that a certain load or end user oversees varies according to the physical characteristics of the load and the needs and preferences for the use of electric energy. This section discusses economic dispatch with price-responsive demand over the course of a day.

The sensitivity of demand to price is formulated as a demand function. The demand functions of different loads are calculated with respect to their unique physical dynamics and attributes as discussed in Chap. 8. Given these demand functions, we can construct quadratic benefit functions that are analogous to the quadratic cost functions of supply by integrating the demand functions [1]. The following notations are used for the formulation:

G : set of all available generators

G_r : set of intermittent energy generators

Z : set of load zones

$\hat{L}_z(k)$: expected demand at load zone z time step k

J.-Y. Joo (✉) • J. Donadee • M. Ilić

Department of Electrical and Computer Engineering, Carnegie Mellon University,
5000 Forbes Ave, Pittsburgh, PA 15213, USA

e-mail: jjoo@andrew.cmu.edu; jdona@andrew.cmu.edu; milic@ece.cmu.edu

Y. Gu • L. Xie

Department of Electrical and Computer Engineering, Texas A&M University,
College Station, TX 77843, USA

e-mail: gzydmgqy@gmail.com; lxie@ece.tamu.edu

$C_i(P_{G_i})$: cost function of generator i

$B_z(L_z(k))$: benefit function of load z consuming $L_z(k)$

$P_{G_i}^{\min}, P_{G_i}^{\max}$: minimum and maximum output of generator i

$\hat{P}_{G_j}^{\min}, \hat{P}_{G_j}^{\max}$: expected minimum and maximum wind generation output at time step k , $j \in G_r$

$g_j(\hat{P}_{G_j})$: forecast of available output for generator j

R_i : ramping rate of generator i , $i \in G$

K : number of time steps in the optimization period

F, F^{\max} : vector of line flows and their limits

$$\min_{P_G, L} \sum_{k=1}^K \left(\sum_{i \in G} (C_i(P_{G_i}(k))) - \sum_{z \in Z} (B_z(L_z(k))) \right) \quad (9.1)$$

$$\text{s.t. } \sum_{i \in G} P_{G_i}(k) = \sum_{z \in Z} L_z(k);$$

$$\hat{P}_{G_j}^{\max}(k) = g_j(\hat{P}_{G_j}^{\max}(k-1)), j \in G_r;$$

$$\hat{P}_{G_j}^{\min}(k) = h_j(\hat{P}_{G_j}^{\min}(k-1)), j \in G_r;$$

$$\hat{P}_{G_j}^{\min}(k) \leq P_{G_j}(k) \leq \hat{P}_{G_j}^{\max}(k), j \in G_r;$$

$$0 \leq L_z(k), z \in Z;$$

$$P_{G_i}^{\min}(k) \leq P_{G_i}(k) \leq P_{G_i}^{\max}(k), i \in G \setminus G_r;$$

$$|P_{G_i}(k+1) - P_{G_i}(k)| \leq R_i, i \in G; \text{ and,}$$

$$|F(k, P, L)| \leq F^{\max} \quad \forall k$$

We apply this economic dispatch with elastic demand to the *price-responsive* loads that we calculated in Chap. 8 and compare the results. We apply this dispatch to two different schemes, as explained in Chap. 8. *Day-ahead scheduling* resembles the market clearance from markets in many operational regions in the USA. End-users or load-serving entities (or power producers) submit their demand (or supply) bid before the day of clearance. They optimize their bid with respect to an anticipated price signal since the price is only determined after the market is cleared with all the supply and demand bids. They calculate the demand/supply bids for the next day at every time step; the interval of each time step is set by the system/market operator.

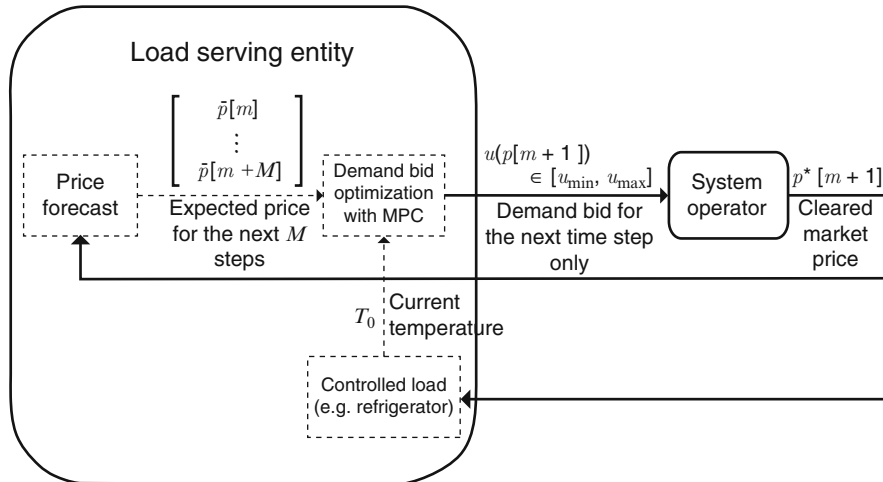


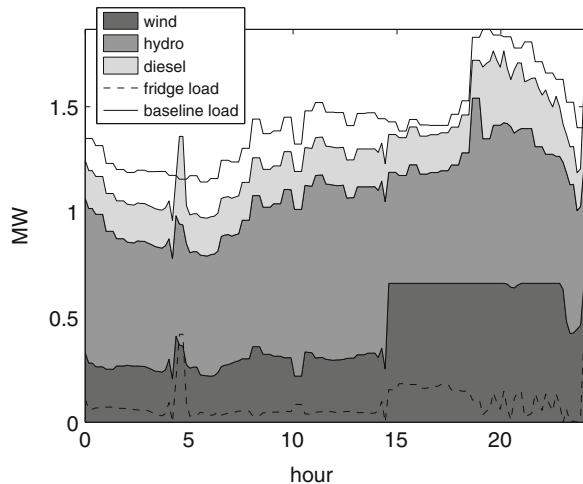
Fig. 9.1 The procedure of real-time adjustment with ALM[2]

Real-time adjustment is a more advanced demand response framework that we propose be used in real-time energy operation. Assuming an adequate communication infrastructure, and the control of small devices such as refrigerators on the end-users' premises, the end-users' appliances and the system operator communicate every time step in the real-time market (e.g., 5 or 10 min) to exchange real-time price signals and the price sensitivity of the demand based on the current physical status of the appliance. The procedure of real-time adjustment is shown in Fig. 9.1.

9.2 Simulation

We discuss the simulation results of the dispatch with elastic loads for both Flores and São Miguel. Both the day-ahead scheduling and real-time adjustment methods are simulated and presented in this section. The simulations were conducted for each island, with different candidate loads for ALM that were determined in Chap. 8. The time interval for all the simulations is 10 min, and optimization is done for a day or 24 hours.

Fig. 9.2 Day-ahead scheduling with control on the refrigerators load on January 16, 2008, for Flores



9.2.1 Dispatch with Refrigerators on Flores

Calculating the demand functions as shown in Chap. 8, we calculate the optimal dispatch for four seasonally representative days in 2008. As in the generation dispatch of the Flores system, described in Chap. 7, the power supply sources on Flores consist of diesel, hydro, and wind power generators. The same marginal costs were used for these simulations, too.

9.2.1.1 Day-Ahead Scheduling

The algorithm of day-ahead scheduling is identical to what is shown in Chap. 7, except that now we have an additional unit “elastic demand” also bidding into the system. The procedure of getting the demand bids was explained in Chap. 8, and the system dispatch formulation is shown in Sect. 9.1. In the simulations for the Flores system with the refrigerator loads, we assume that the aggregate refrigeration load acts as one large refrigerator. In other words, we do not include an algorithm that aggregates multiple refrigerators with different temperature statuses. The results of the system dispatch with this algorithm are shown for the four seasonally representative days in Figs. 9.2–9.5.

Issues with day-ahead scheduling

The dispatch results for day-ahead scheduling do not keep track of the physical state of the elastic load at each time step, and thus the cleared dispatch can be physically infeasible. The bids that are submitted by market participants are based

Fig. 9.3 Day-ahead scheduling with control on the refrigerators load on April 16, 2008, for Flores

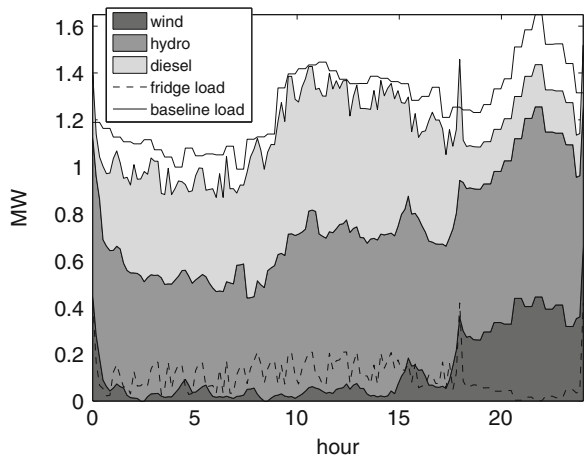
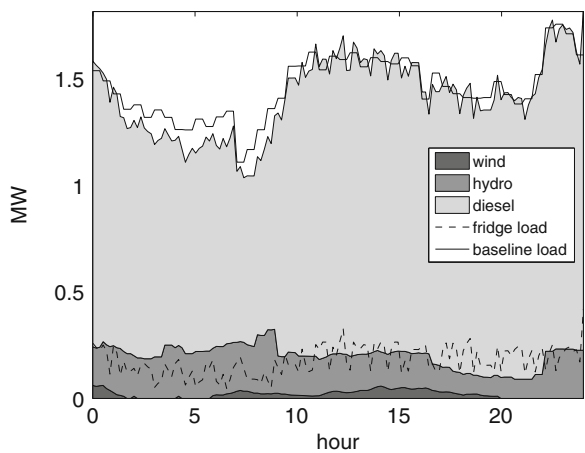


Fig. 9.4 Day-ahead scheduling with control on the refrigerators load on July 16, 2008, for Flores



on expected price, but cannot be forecast by the amount of energy to be consumed. The bid curves are highly dependent on the current state of a market participant. If the state of a participant deviates from the state calculated ahead of the actual consumption, then the current and future bid functions are not guaranteed to be feasible or representative of the current price sensitivity. The first instance where the market clears at something other than the expected price will cause this deviation.

Using the day-ahead scheduling described above and the model of ALM-enabled refrigerators described in Chap. 8 results in the violation of temperature bounds for the price-responsive refrigerator. Figures 9.2–9.5 show the generation dispatch resulting from using this day-ahead scheduling algorithm. The price-responsive load consumes less than in the inelastic case at nearly all the time steps, as shown by the gap between the stacked generation output and the baseline load. Figure 9.6 shows how the modeled temperature state of ALM-enabled refrigerators would evolve

Fig. 9.5 Day-ahead scheduling with control on the refrigerators load on October 15, 2008, for Flores

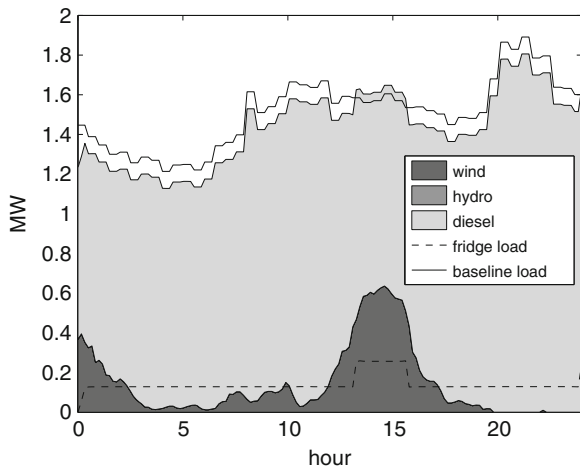
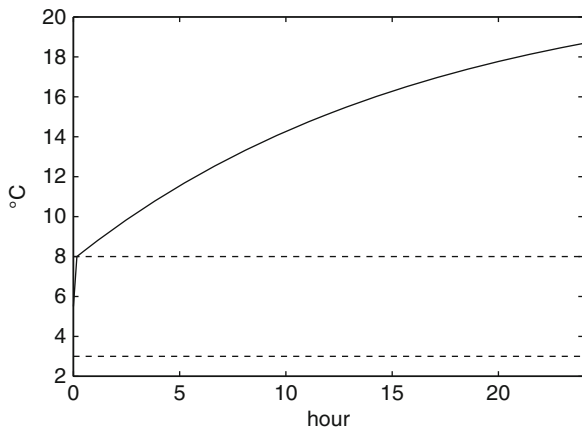


Fig. 9.6 Temperature inside the refrigerator assuming the load dispatch under day-ahead scheduling on October 15, 2008, for Flores

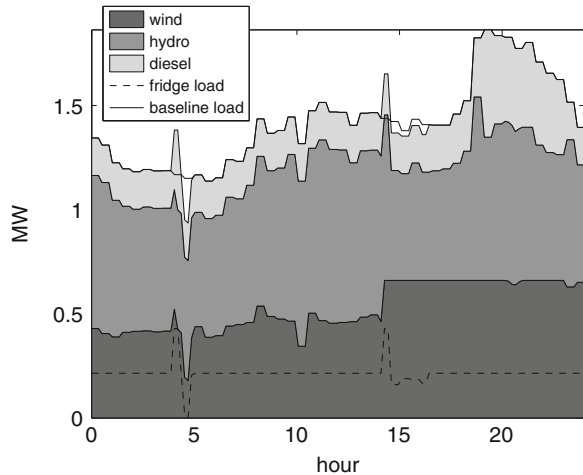


if operated according to the dispatch results. The refrigerator temperature model should only be considered valid within a reasonable proximity to the minimum and maximum temperature bounds, so one should disregard the resulting temperature evolution after the maximum temperature constraint has been violated. Still the results clearly show that day-ahead scheduling dispatch results in an inadequate amount of energy consumption to satisfy the temperature constraints. This pushes one toward the use of the real-time adjustment algorithm where a new bid curve is formulated at each time step using the current state of a market participant.

9.2.1.2 Real-Time Adjustment

In real-time adjustment dispatch, we overcome the problems of day-ahead scheduling by making a loop between the elastic load dispatch and the physical dynamics of the elastic load, i.e., the temperature of the refrigerator. At each time step, once

Fig. 9.7 Real-time adjustment with control on the refrigerators load on January 16, 2008, for Flores



the system operator clears the market, ALM uses the energy dispatched from the system to calculate the temperature of the refrigerator at the next time step. Now the demand bid function of the next time step will be calculated in the same way as the system dispatch with day-ahead scheduling, but with a specific initial temperature calculated from the systems dispatch to the price-responsive load. This process is iterated at every time step so that the dispatched energy amount follows the temperature dynamics of the refrigerator across the time horizon. Figures 9.7–9.10 show that the total amount of energy consumed over a day is close to the daily consumption of the baseline load. Figure 9.11 shows the evolution of the refrigerator temperature when using this real-time adjustment algorithm. We note that the temperature is kept within the bounds of 3–8 °C in this real-time adjustment case.

9.2.2 Dispatch with an Air-Conditioning Load on São Miguel

We calculated the air-conditioning load in the shopping mall described in Chap. 8, optimizing the load with the anticipated operational cost for July 16, 2008. Compared to the total load, the air-conditioning load was insignificant in terms of the magnitude. However, as shown in Chap. 8, if the price signal given to the end user reflected the true cost of the system operations, then the savings from shifting the load during peak hours to off-peak were considerable at least from the end user's perspective.

São Miguel has four different sources of generation: oil, hydro, wind, and geothermal, as described in Chap. 7.

Fig. 9.8 Real-time adjustment with control on the refrigerators load on April 16, 2008, for Flores

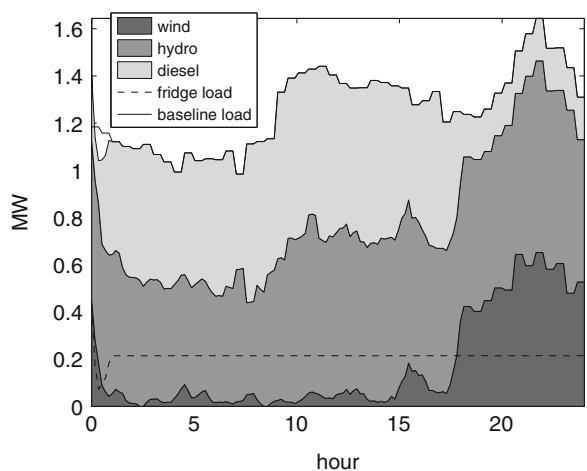


Fig. 9.9 Real-time adjustment with control on the refrigerators load on July 16, 2008, for Flores

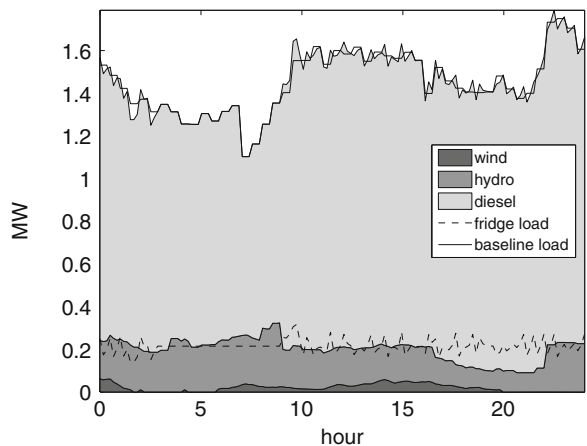


Fig. 9.10 Real-time adjustment with control on the refrigerators load on October 15, 2008, for Flores

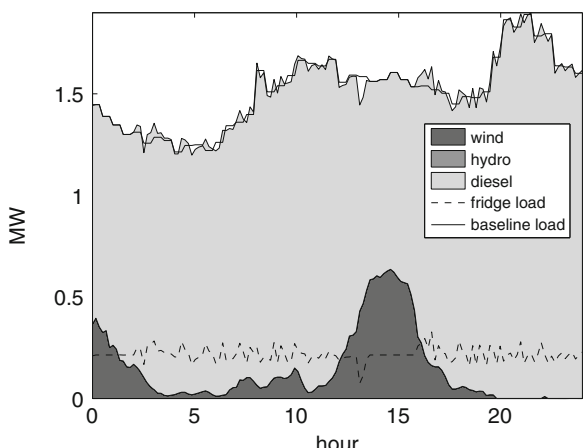


Fig. 9.11 Temperature inside the refrigerator with load dispatch under real-time adjustment on October 15, 2008, for Flores

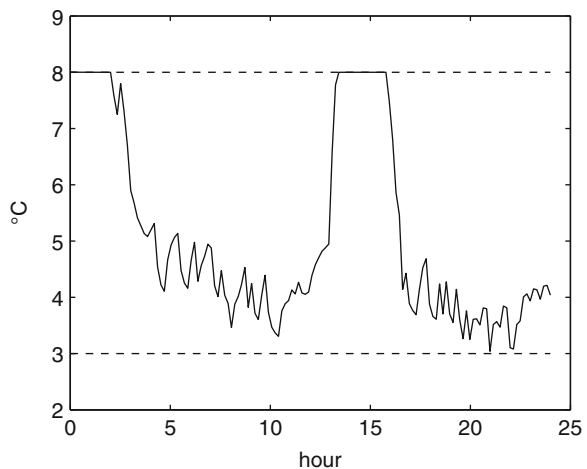
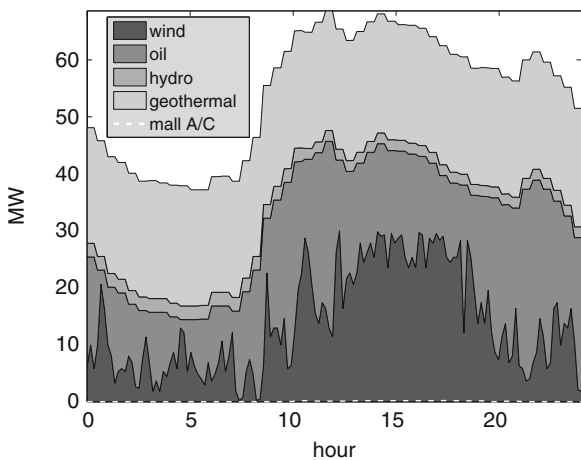


Fig. 9.12 Day-ahead scheduling with control on the air-conditioning load on July 16, 2008, for São Miguel



9.2.2.1 Day-Ahead Scheduling

The generation and demand dispatch results of day-ahead scheduling are shown in Fig. 9.12. As can be noted, the elastic demand is very small. The air-conditioning load is separately plotted in Fig. 9.13.

As pointed out in the previous simulations for Flores, day-ahead scheduling dispatch results can be infeasible for the load. Therefore, the resulting temperature change in the mall is plotted in Fig. 9.14 assuming that the air-conditioning system follows the day-ahead scheduling dispatch. As with the results from the day-ahead scheduling on Flores, the results on São Miguel also turn out to be infeasible. This is more obvious in a much warmer weather temperature setting, as shown in Fig. 9.15.

Fig. 9.13 Air-conditioning load dispatch under day-ahead scheduling on July 16, 2008, for São Miguel

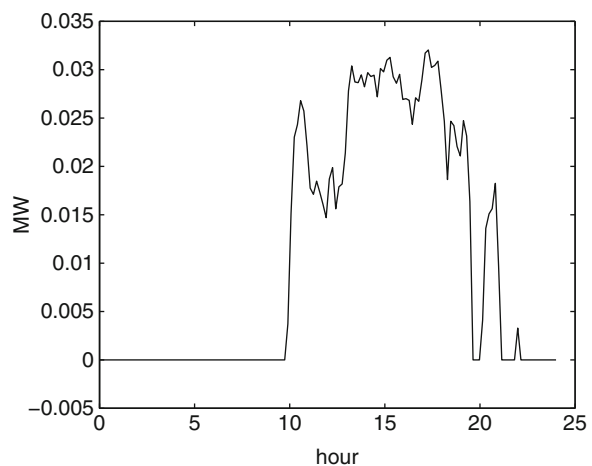


Fig. 9.14 Temperature inside the mall assuming air-conditioning load dispatch under day-ahead scheduling on July 16, 2008, for São Miguel

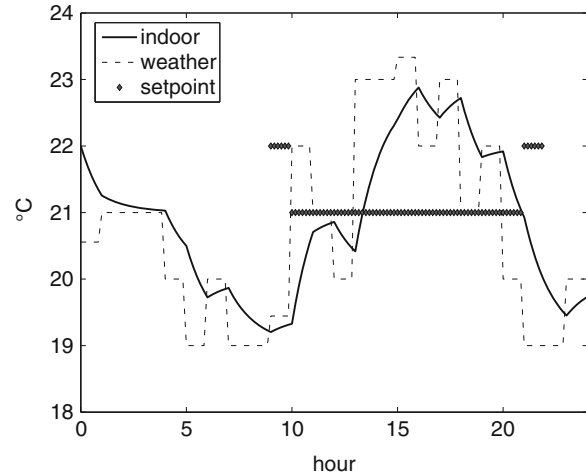


Fig. 9.15 Air-conditioning load dispatch under day-ahead scheduling assuming a warmer weather condition

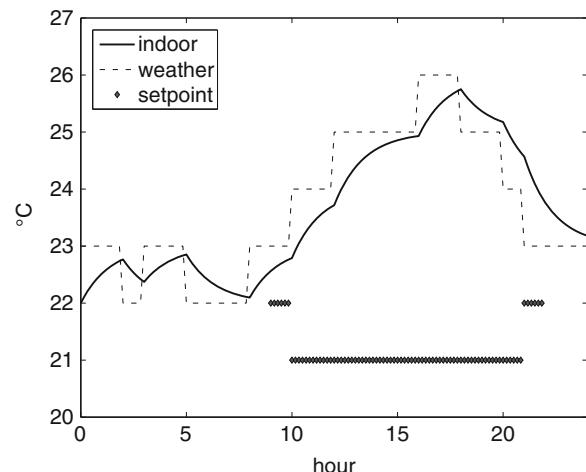


Fig. 9.16 Real-time adjustment with control on the air-conditioning load on July 16, 2008, for São Miguel

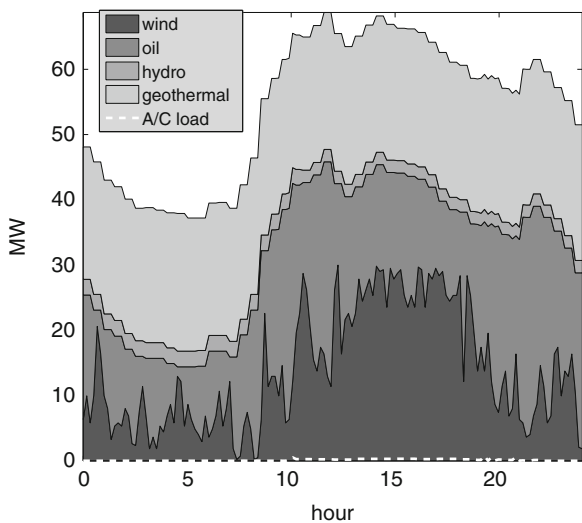
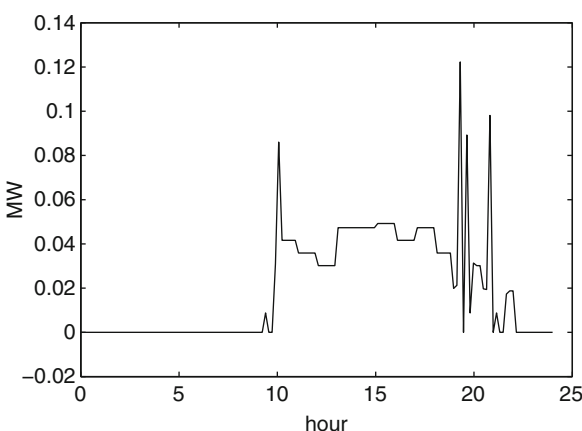


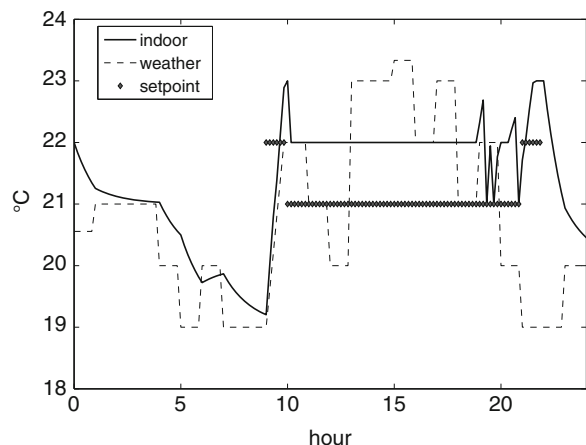
Fig. 9.17 Air-conditioning load dispatch under real-time adjustment on July 16, 2008, for São Miguel



9.2.2.2 Real-Time Adjustment

The algorithm for real-time adjustment on Flores was applied to the system on São Miguel as well for the air-conditioning load in the mall. The resulting generation and demand dispatch, the air-conditioning load, and the temperature change inside the mall are shown in Figs. 9.16, 9.17, and 9.18, respectively. We note that with this algorithm, the temperature inside the mall is kept close to the desired temperature set points.

Fig. 9.18 Temperature inside the mall with the air-conditioning load dispatch under real-time adjustment on July 16, 2008, for São Miguel



9.3 Discussions and Summary

In this chapter, *demand and generation* dispatch on the islands of Flores and São Miguel were presented. Two distinct algorithms for this dispatch day-ahead scheduling and real-time adjustment were analyzed. By comparing the results of these two methods, we conclude that timely information exchange between the demand unit and the system operator is crucial for two reasons. First, the demand can be adjusted within tolerable bounds due to accurate energy consumption limits based on the current physical status of the load. Second, the system can guarantee the commitment of the participating load by obtaining accurate energy consumption limits and load flexibility.

This implies that a successful demand response program for greening a system requires far more than simply getting more end users or loads enrolled. An adequate communication and control infrastructure is crucial for both the end-users' and the system operator's objectives. The time interval and the duration of the communication between the loads and the system must be well designed depending on the types of loads.

Acknowledgments This work was supported partly by the Semiconductor Research Corporation (SRC) Energy Research Initiative (ERI) for Smart Grid Research Center (SGRC) Task 2111.001 Adaptive Load Management, partly by the Fundação para a Ciência e a Tecnologia (Portuguese Foundation for Science and Technology) through the Carnegie Mellon Portugal Program, partly by U.S. National Science Foundation ECCS Grant 1029873, and partly by the Power Systems Engineering Research Center (PSERC). The authors are grateful for each sponsor for their financial support. The authors also like to thank Remco Verzijlbergh at Delft University for his valuable feedback on this work.

References

1. M.D. Ilić, L. Xie, J.-Y. Joo, Efficient coordination of wind power and price-responsive demand—Part II: case studies. *IEEE Trans. Power Syst.* **26**(4), 1885–1893, (November 2011)
2. J.-Y. Joo, M. Ilić, Multi-temporal risk minimization of adaptive load management in electricity spot markets, *Innovative Smart Grid Technologies (ISGT Europe), 2nd IEEE PES International Conference and Exhibition*, December 2011, pp. 1–7, 5–7

Chapter 10

Counterexamples to Commonly Held Assumptions on Unit Commitment and Market Power Assessment

Wolfgang Gatterbauer and Marija Ilić

10.1 Centralized Versus Decentralized Unit Commitment (UC)

This first subsection disproves the commonly held assumption that, in theory and under the condition of perfect information, decentralized and centralized UC would lead to the same power quantities traded and, hence, to the same optimal social welfare [1]. We see that, even in the absence of any uncertainties, independent optimization of the individual performance objectives by the decentralized market participants can lead to lower efficiency than centralized minimization of total operating cost.¹

10.1.1 *The Standard Argument: Centralized UC is identical to Decentralized UC*

Mathematically, a *centralized economic dispatch* is the problem of minimizing the total generation cost, using the quantities produced by each of the possible generators as decision variables such that total generation equals total demand Q_D [1]. Using the variables Q_i and C_i for the quantities produced and the cost incurred

¹This result concerns short-term supply optimization for a given demand and does not consider long-term investment issues.

W. Gatterbauer (✉)

Tepper School of Business, Carnegie Mellon University 5000 Forbes Avenue

e-mail: gatt@cmu.edu

M. Ilić

Department of Electrical and Computer Engineering, Carnegie Mellon University,
5000 Forbes Ave, Pittsburgh, PA 15213, USA

e-mail: milic@ece.cmu.edu

by generator i , respectively, and the variable n for the total number of available generators, we can write the problem as

$$\min_{\mathbf{Q}} \sum_{i=1}^n C_i(Q_i) \quad \text{s.t.} \quad \sum_{i=1}^n Q_i = Q_D.$$

This basic version of an unconstrained economic dispatch remains indeterminate. An economically motivated condition for solving this problem is the equal incremental condition

$$\frac{\delta C_1}{\delta Q_1} = \dots = \frac{\delta C_n}{\delta Q_n} = \lambda.$$

The term λ is known as the short-run marginal cost (SRMC) and, at the optimum, all unit marginal costs are equal to it. Using u_i as a binary variable that determines whether the generation unit i is turned on or off at a given moment, the basic *centralized unit commitment problem* without start-up costs or minimum up/down time constraints is

$$\min_{\mathbf{u}, \mathbf{Q}} \sum_{i=1}^n u_i C_i(Q_i) \quad \text{s.t.} \quad \sum_{i=1}^n Q_i = Q_D.$$

Following the Lagrangian relaxation method, we first form the Lagrangian function

$$L(\mathbf{u}, \mathbf{Q}, \lambda) = \sum_{i=1}^n u_i (C_i(Q_i) - \lambda Q_i) + \lambda Q_D.$$

By minimizing this last equation over \mathbf{Q} , we obtain the conventional economic dispatch equal incremental condition from above which permits us to solve for Q in terms of λ , the system incremental cost. Rewriting the Lagrangian as

$$L(\mathbf{u}, \lambda) = \sum_{i=1}^n u_i (C_i(Q_i(\lambda)) - \lambda Q_i(\lambda)) + \lambda Q_D$$

and using the Lagrangian method to minimize $L(\mathbf{u}, \lambda)$ with respect to \mathbf{u} gives us the switching curve law or the average cost rule

$$u_i = \begin{cases} 1 & \text{if } C_i - \lambda Q_i < 0 \\ 0 & \text{if } C_i - \lambda Q_i > 0, \end{cases}$$

that is, the unit i is turned on if the average cost $\frac{C_i}{Q_i} < \lambda$ and off otherwise. Once on, a conventional economic dispatch is used to adjust to demand changes if these are monitored more frequently [1].

With competitive bilateral transactions taking place in a *decentralized economic dispatch* and each party's objective being the maximization of its individual profit, the decentralized problem is

$$\max_{Q_i} \pi_i(Q_i).$$

Here $\pi_i(Q_i) = PQ_i - C_i(Q_i)$ stands for the profit made by the market participant i through some sort of trading process, given price P . Thus, under perfect conditions, when the market converges to a single electricity price, one can maximize π_i by setting marginal cost equal to price:

$$\frac{\delta C_1}{\delta Q_1} = \dots = \frac{\delta C_n}{\delta Q_n} = P.$$

The process of bilateral decisions will stabilize P at the system-wide economic equilibrium under a perfect information exchange among all market participants. This result is simply obtained by each market participant optimizing its own profit for the assumed exogenous market price P [1]. In the *decentralized unit commitment* setting, all generator owners are assumed to be price takers in a competitive market place. Each participant makes a unit commitment decision typically for each hour one day ahead, before knowing the actual spot price. After the spot price of a respective hour is known, the generator decides how much power to sell in order to maximize profit. The only control for generator i is u_i , whether to turn on or off at a given hour. The expected generation level \hat{Q}_i may be regarded as a function of the control u_i and the expected price \hat{P} . In the case of deterministic prices and ignored start-up costs and must-run time constraints, a generator's profit while on is $\hat{\pi}_{i,\text{on}} = \hat{P}\hat{Q}_i - C_i(\hat{Q}_i)$. The generator will turn on only if $\hat{\pi}_{i,\text{on}} > 0$, which is equivalent to $\frac{C_i(\hat{Q}_i)}{\hat{Q}_i} < \hat{P}$, which is exactly the average cost rule used for coordinated unit commitment [1].

Based on this derivation, current teaching is that, under perfect market assumptions and when neglecting start-up costs and intertemporal time constraints, individual power producers would schedule the same power units in a decentralized market as would a central system operator in a coordinated market. *Thus, both centralized and decentralized UC should lead to the same power quantities traded, the same minimum operating cost, and, with given inelastic demand, to the same total social welfare optimum.* The performance objectives of the individual market participants (to maximize profits) and the objective of a centralized entity (to maximize social welfare by minimizing operating cost) would then be equivalent [1].

10.1.2 The Counterexample: The “Tragedy” of Decentralized UC

We next prove that centralized and decentralized UC are, in general, not economically equivalent. Under certain conditions, some generators would not self-schedule to prevent loss; those units, however, would be scheduled by a PoolCo-type market (or a “social planner”) to minimize overall operating cost and, in turn, would receive fixed operating costs to prevent them from loss. These situations are missed by the previous argument, as *the average cost rule does not always lead to the total social welfare optimum that a centralized operator strives for*.

To prove this claim by example, we derive the strict conditions under which this situation takes place in the case of two generators with quadratic operating cost $C_i(Q_i) = a_i Q_i^2 + b_i Q_i + c_i$. We consider only one particular hour for which demand Q_D is given. In the case of inelastic demand, the total social welfare optimum is attained by minimizing total operating cost. Without loss of generality, we consider generator 2 to be the one that would not self-schedule in order to avoid loss when bidding marginal costs. Three conditions must hold simultaneously in order to produce the specific situation:

1. Generator 1 makes profit, independent of generator 2 participating during the hour or not: $\frac{C_1(Q_1)}{Q_1} < P$.
2. Generator 2 incurs loss if it is scheduled and receives no extra payment: $\frac{C_2(Q_2)}{Q_2} > P$.
3. The total cost for satisfying the given load is smaller if both generators operate instead of only generator 1: $C_1(Q_1) + C_2(Q_2) < C_1(Q_D)$.

Performing some mathematical operations that are described in more detail in [2] and [3], we obtain the following *three conditions on the demand which, if fulfilled, lead to different units scheduled and, hence, different economic outcomes from either centralized or decentralized UC*:

$$Q_D > Q_{\min \pi_1} := \max \left[\frac{(a_1 + a_2) \sqrt{\frac{c_1}{a_1}} + \frac{b_1 - b_2}{2}}{a_2}, \sqrt{\frac{c_1}{a_1}} \right],$$

$$Q_D < Q_{\max \pi_2} := \frac{(a_1 + a_2) \sqrt{\frac{c_2}{a_2}} + \frac{b_2 - b_1}{2}}{a_1},$$

$$Q_D > Q_{\min C} := \frac{\sqrt{(a_1 + a_2)c_2} + \frac{b_2 - b_1}{2}}{a_1}.$$

Table 10.1 and Fig. 10.1 provide an illustrative example with numbers and graphs. Parameters for generator 2 stem from a best quadratic fit to heat rate data

Table 10.1 Example generator parameters (a), resulting demand conditions (b), and higher prices and total operating cost with decentralized instead of centralized UC for example demand of 800 MW (c)

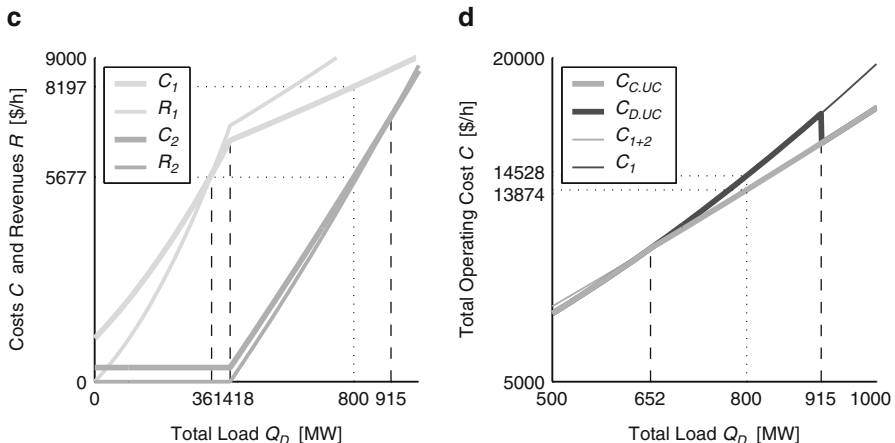
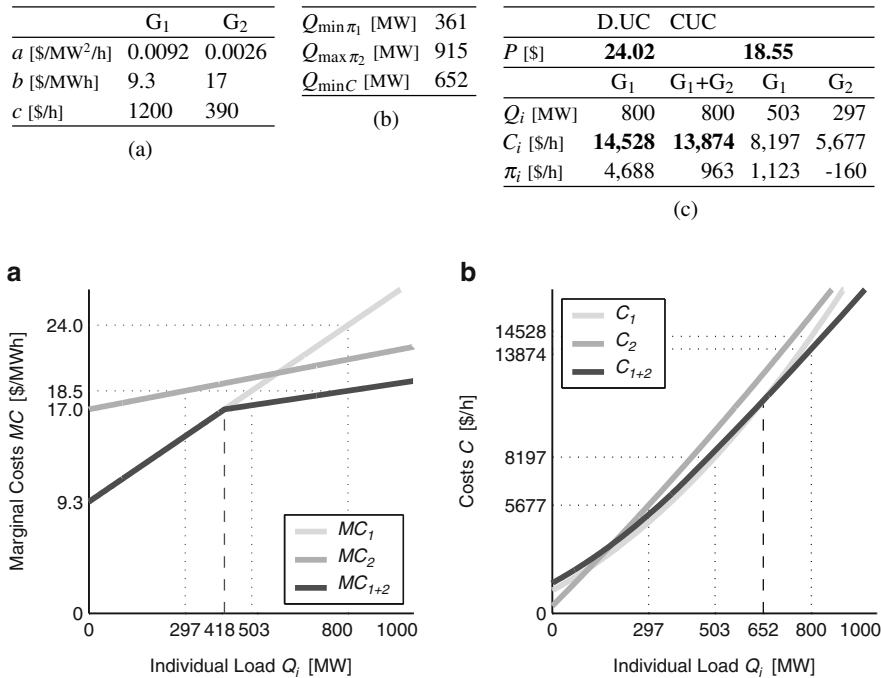


Fig. 10.1 Situation with centralized UC leading to lower operating cost than decentralized UC: Market supply functions (a), generator operating cost function (b), individual operating costs and revenues following marginal cost bids (c), and total operating cost (d)

of the thermal plant ‘‘Morro Bay 4’’ published in [4] and an assumed fuel price of 2 \$/MBtu. The parameters were slightly changed for generator 1 in order to create a sample situation.

10.1.3 Discussion

The literature gives several examples of cases in which individual objective functions are not aligned with those of the overall social welfare. The most often cited example was given by Hardin in *The Tragedy of the Commons* [5]. Another one is Braess’ article on traffic networks [6] in which he gives an example in which drivers’ attempt to minimize their transit times leads to increased congestion and increased traffic times for all participants. Braess’ paradox has become an important issue in the context of queuing networks [7]. In power systems, however, the commonly held assumption is still that, at least in theory, a centralized and a decentralized UC should lead to the same power quantities traded and to the same optimal social welfare. The performance objectives of the individual market participants are considered equal to the one of minimizing total operating cost [1, 8, 9].

The important implication of the example given before is that, even in the absence of load uncertainties and intertemporal constraints, *decentralized UC does not necessarily lead to the same maximized welfare as centralized decision making*. The reason is that, under certain circumstances, several generators can supply the load at a lower overall cost than the subset of generators that would make positive profits in a market setting if switched on during the hour.

In the Pennsylvania–New Jersey–Maryland and the New York electricity markets, the ISO (Independent System Operator) offers a voluntary unit commitment service, based on three-part bids, allowing generators to bid actual operating costs more precisely and permitting a more efficient unit commitment. Generators may also self-schedule their own units, but they may also allow the ISO to determine the most economic unit commitment for their plants. Participating generators are guaranteed recovery of their start-up and minimum generation costs in the event they fail to recover these costs from the prices received in the ISO-coordinated markets [10, 11]. This mechanism eliminates the uncertainty of whether a generator will be committed only to lose money, and it allows for a more efficient dispatch. The quadratic cost curve example shows how a PoolCo-type market would work more efficiently than a power exchange (for which the one-part bids result in some inefficiency).

It is important to note that the conclusions here focus on the short run, in that they do not take into account the long-term motivational effects of a decentralized commitment on investment decisions and the possible entry of new firms or generating plants. The literature gives several qualitative arguments why a decentralized commitment process might be preferable despite the better overall efficiency of the centralized process [11, 12].

10.2 Marginal Cost Bidding and Market Power

This second subsection illustrates that a generator owner's optimum bid sequence for a centralized wholesale market under a decentralized UC regime is generally above marginal cost even in the complete absence of market power. This result challenges economic literature stating that market prices above marginal cost would unambiguously indicate gaming and the abuse of market power.

10.2.1 An Illustrative Model

We will use a simple model to show how prices above marginal cost arise in a decentralized UC scheme as a natural consequence of the decentralized decision process and intertemporal constraints. We deploy the dynamic programming formulation from [13] for calculating a generator's optimal bidding strategy in the presence of a price forecast with given standard variation. For simplification, we consider a generator whose marginal operating cost is constant over the output range: $MC = b$. The owner can offer electricity by submitting a bid to a centralized market for each hour and is scheduled if the bid price turns out to be lower than or equal to the market price. We neglect the case of the generator being the marginal unit and scheduled for less than full output. Because of the constant marginal cost, the most efficient way to operate the generator is to either produce full output Q_G or nothing and to use a flat bid curve. In addition to variable costs, the generator incurs fixed operating cost c for every hour of operation regardless of whether it is producing electricity or not and also start-up cost c_u and shutdown cost c_d . As intertemporal constraint, once the generator is switched on, it has to remain in that state for at least 2 hours, during which it incurs the fixed operating cost. If the generator gets scheduled for 1 hour but not for the other, it still incurs the fixed operating cost c for the second hour as well. Hence, the generator has to internalize these intricacies when it is bidding into an hourly market. The generator does not know the market prices when bidding but has some knowledge about the probability distribution of the prices, which are considered to be exogenous variables, not influenced by the behavior of the generator.

We now consider the specific situation in which only 2 successive hours have price distributions above MC (Fig. 10.2a). The problem of finding the optimal bids is drastically simplified and can be solved in a closed form. In this special example, the sum of the fixed costs can be united into one term total incurred fixed cost $c_{\text{tot}} = c_u + c_d + 2c$ which will be incurred once the generator starts up. This aggregation does not change the optimal strategy but simplifies the formulation. Fixed nonoperating costs, such as sunk capital costs, which are incurred regardless of the generator producing output or not during 1 h, do not affect the optimal decision and can be disregarded. For the numerical calculation, we assume that prices can have only a

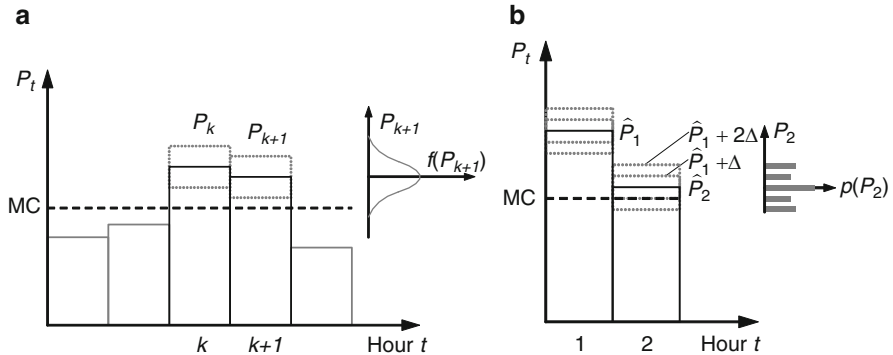


Fig. 10.2 Marginal cost and hourly predicted prices for the next day (a) and assumed discrete price distribution of two relevant hours (b)

limited number of discrete values during the two hours and are uncorrelated: $P_k \in \{\hat{P}_k - 2\Delta, \hat{P}_k - \Delta, \hat{P}_k, \hat{P}_k + \Delta, \hat{P}_k + 2\Delta\}$ (Fig. 10.2b).

10.2.2 Profit Optimization in a Competitive Market

In order to find the optimal bidding sequence, the profits for all possible combinations of bid heights have to be compared:

$$J = \max_{x_1, x_2} [J(x_1, x_2)]$$

with $\{(x_1, x_2) | (x_1, x_2) = (P_i, P_j)\}$ and (P_i, P_j) being possible prices for the 2 hours. In order to calculate the expected profit for the bid combinations, all possible price outcomes have to be compared:

$$\begin{aligned} J(x_1, x_2) &= \sum_{P_i | P_i \geq x_1} \sum_{P_j | P_j \geq x_2} p(P_1 = P_i) p(P_2 = P_j) ((P_i + P_j - 2b) Q_G - c) \\ &+ \sum_{P_i | P_i \geq x_1} \sum_{P_j | P_j < x_2} p(P_1 = P_i) p(P_2 = P_j) ((P_i - b) Q_G - c) \\ &+ \sum_{P_i | P_i < x_1} \sum_{P_j | P_j \geq x_2} p(P_1 = P_i) p(P_2 = P_j) ((P_j - b) Q_G - c). \end{aligned}$$

Whereas finding the optimal bid sequence in our example is still possible, this task becomes increasingly intractable when optimizing for more periods. The time for calculation increases exponentially with the number of periods.

Table 10.2 shows an illustrative example. The optimum bids are not only higher than the marginal cost but also higher than the average operating cost. In addition,

Table 10.2 Example of optimal bids being above MC: Prices (a), generator cost (b), expected profits for different bid sequences (c).

Price distributions	Generator	Bid Sequence	Exp. Profit
\hat{P}_1	MC 50	(58,52) or (60,54)	1.172
\hat{P}_2	Q_G 1	(58,54)	1.154
Δ	c 4	(56,50) or (56,52)	1.080
$p(P_k = \hat{P}_k \pm 2\Delta)$	c_u 1	(60,56) or (62,56)	
$p(P_k = \hat{P}_k \pm \Delta)$	c_d 1	(60,52)	0.927
$p(P_k = \hat{P}_k)$	c_{tot} 10		(c)

we see that the optimum bids vary between different hours and are dependent on the assumed forecast prices and related price dynamics.

10.2.3 Discussion

Many of the recent papers on assumed market power abuse in deregulated electricity markets assume that market participants bid their true marginal costs in a competitive market if no market power is exerted. However, in the context of bidding decisions of power plants, which not only incur MC but also start-up and shutdown costs and minimum commitment constraints, these assumptions are not valid. Generators bid higher than MC, not because they can exercise market power, but because of intertemporal constraints and uncertainties about prices of consecutive hours.

The literature disagrees as to what exactly constitutes market power but generally agrees that it has to do with actively raising the prices at which one is willing to sell output (one's price offer) above MC in order to change the market price [14] ("If suppliers exercise market power, prices could be higher than marginal costs."). MC include both the variable costs due to fuel and the other variable operating and maintenance costs. For example, [15] states that "The fundamental measure of market power is the margin between price and the marginal cost of the highest cost unit necessary to meet demand. (...) if no firm were exercising market power, then all units with marginal cost below the market price would be operating."

In the formulation of this chapter, the *power producer is modeled as a price taker*. He has assumptions about the probability distributions of prices for certain hours. His bidding decision does not affect the prices and, hence he has no market power. Nevertheless, his optimum bids deviate from MC. *It is, therefore, not market power that creates prices above MC but the necessity to incorporate start-up and shut-down constraints in the presence of uncertain prices.* The generator in the example responds to the simple economic incentive of maximizing profits given uncertain prices. As a result, the competitive price does not equal marginal cost at peak periods under competition, and therefore simple price-cost margin studies cannot confirm the exercise of market power. We thus conclude that above MC bids of generators

do not necessarily indicate the exercise of market power. Especially in times when prices are very volatile, generators have to bid above marginal costs in order to take account of the possibility of being scheduled for one hour and not the following one.

10.3 Summary and Take-Aways

By adopting the perspective of an individual market participant in a decentralized UC regime and simulating economically optimal behavior, we could draw the following two conclusions:

1. *Coordination Value*: Decentralized UC does not lead to the same short-time efficient economic outcome as centralized UC, even in the theoretical case of perfect information. The non-obvious reason is that, under certain load and cost conditions, the overall minimum operating cost to supply a given demand could be achieved with some generators switched on which would not operate in a completely decentralized market. The consequence of this observation does not limit itself to electricity markets only, but can be considered a more general situation where the performance objectives of the individual market participants are not equal to the one of minimizing total production cost, quite analogous to the *Tragedy of the Commons*.
2. *Market Power*: Above marginal costs in electricity markets are a necessary consequence of the decentralized decision making under uncertainty and do not necessarily indicate gaming in the presence of market power. The reason is that generators face intertemporal time constraints not common in other industries. As a consequence, and in contrast to economic teaching, price taking generators have to bid above marginal cost in order to internalize the uncertainties of being on but not selling any power into the market into their bids.

The results of this chapter were published in [2]. More details and an extended optimization algorithm that also considers intertemporal correlation between price forecast errors can be found in [3].

Acknowledgments This work was partially supported by a Rotary Ambassadorial Scholarship, a fellowship from the MIT graduate student office, a DOC scholarship from the Austrian Academy of Sciences, and by NSF IIS-0915054.

References

1. M.D. Ilić, F. Galiana, L. Fink (eds.), *Electric Power Systems Restructuring: Engineering and Economics* (Kluwer, Dordrecht, 1998)
2. W. Gatterbauer, M.D. Ilić, Counterexamples to commonly held assumptions on unit commitment and market power assessment, in *Proceedings of the 34th Annual North American Power Symposium (NAPS 2002)* (IEEE, New York, 2002), pp. 219–225

3. W. Gatterbauer, Interdependencies of electricity market characteristics and bidding strategies of power producers, Master's thesis, Massachusetts Institute of Technology, May 2002
4. J.B. Klein, The use of heat rates in production cost modeling and market modeling, Electricity Analysis Office, California Energy Commission, April 1998
5. G. Hardin, The tragedy of the commons. *Science* **162**(3859), 1243–1248 (1968)
6. D. Braess, Über ein Paradoxon aus der Verkehrsplanung. *Unternehmensforschung* **12**, 258–268 (1969)
7. J.E. Cohen, F.P. Kelly, A paradox of congestion in a queueing network. *J. Appl. Probab.* **27**, 730–734 (1990)
8. F. Wu, P. Varaiya, P. Spiller, S. Oren, Folk theorems on transmission access: Proofs and counterexamples. *J. Regul. Econ.* **10**(1), 5–23 (1996)
9. C.J. Day, B.F. Hobbs, J.-S. Pang, Oligopolistic competition in power networks: A conjectured supply function approach. *IEEE Trans. Power Syst.* **17**, 597–607 (2002)
10. J. Chandley, A standard market design for regional transmission organizations. *Electricity J.* **14**(10), 27–53 (2001)
11. R.P. O'Neill, U. Helman, P.M. Sotkiewicz, M.H. Rothkopf, W.R. Stewart, Regulatory evolution, market design, and unit commitment, in *The Next Generation of Unit Commitment Models*. International Series in Operations Research and Management Science (Kluwer, Dordrecht, 2001)
12. R.D. Tabors, Unbundling of transmission: The operation and economics of a for-profit transmission company, *33rd Hawaii International Conference on System Sciences (HICSS)*. IEEE Computer Society, Maui, Hawaii, vol. 4 (2000), p. 4034
13. E. Allen, M.D. Ilić, *Price-Based Commitment Decisions in the Electricity Market*. Advances in Industrial Control (Springer, Berlin, 1999)
14. D.O.E. Energy Information Administration, Electricity prices in a competitive environment: Marginal cost pricing of generation services and financial status of electric utilities, August 1997, DOE/EIA-0614. <ftp://ftp.eia.doe.gov/electricity/0614.pdf>
15. S. Borenstein, J.B. Bushnell, F.A. Wolak, Measuring market inefficiencies in California's restructured wholesale electricity market. *Am. Econ. Rev.* **92**(5), 1376–1405 (2002)

Chapter 11

The Role of Electric Vehicles in Making Azores Islands Green

R.A. Verzijlbergh, M.D. Ilić, and Z. Lukszo

11.1 Introduction

Environmental, as well as economical and geopolitical concerns, continue to drive the transition to energy systems that are less dependent on fossil fuels. In the case of islands or isolated communities, there are additional logistic challenges related to importing all necessary fuels. The Portuguese islands the Azores are therefore an interesting case to investigate an all green energy system. Next to this, the notion of a green island is almost a metaphor for sustainable energy systems in general because it touches upon the very essence of sustainable development: to be able to meet one's needs with the resources that nature provides. This idea will be the guiding perspective of the research that is described in this chapter, which partially builds on the work described in [1].

The focus of this chapter will be on Flores: with approximately 4,000 inhabitants one of the smallest of the Azores island. The island does not have a large industrial sector; so most of its fossil fuel use and related emissions are caused by electricity generation and transport. The main fuel for both is diesel, since the island's thermal power plant is diesel powered and so is the majority of the cars. Hence, when renewable energy sources are used for electricity generation and diesel powered cars are replaced by electric vehicles (EVs), a significant reduction in emissions could

R.A. Verzijlbergh (✉) • Z. Lukszo

Faculty of Technology, Policy and Management, Energy and Industry Group, Delft University of Technology, P.O. Box 5015, 2600 GA Delft, The Netherlands
e-mail: R.A.Verzijlbergh@tudelft.nl; Z.Lukszo@tudelft.nl

M.D. Ilić

Faculty of Technology, Policy and Management, Energy and Industry Group, Delft University of Technology, P.O. Box 5015, 2600 GA Delft, The Netherlands

Department of Electrical and Computer Engineering, Carnegie Mellon University,
5000 Forbes Ave, Pittsburgh, PA 15213, USA
e-mail: milic@ece.cmu.edu

be realized. In this chapter we will explore how intermittent renewable generation and EVs have the potential to be a successful combination. The main idea is that the EVs can adjust their energy needs to the availability of wind and solar power, thereby reducing both the need for back-up diesel generation and the amount of curtailed renewable energy.

This chapter is structured as follows: first the model of the system and description of various relevant data are given. The results will focus on three different generation scenarios and the comparison between the situation with and without controlled charging of the EVs will be made. Our main objective criterion is the amount of emitted CO₂ in the various scenarios, but we invoke economic feasibility by assessing the amounts of spilled energy too.

An important requirement for intelligent EV charging is the existence of an IT infrastructure that makes active control of EVs possible. We will assume in the remainder of this text that such an infrastructure is in place. Furthermore, we emphasize that this chapter has a slightly different perspective than most other chapters in this book. While most simulations described in previous and later chapters are based on current system parameters, our focus is on future situations with very high penetrations of renewables and EVs. Although we base our simulations as much as possible on current system parameters and meteorological data, we are inevitably making strong modeling assumptions about future wind and solar generation as well as the penetration of EVs. Hence, this chapter should be understood to investigate the *potential* of EVs in combination with high wind and solar.

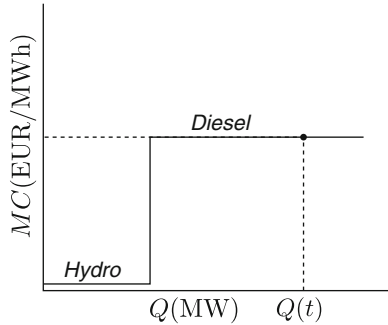
11.2 Simulation

11.2.1 Electricity Demand and Conventional Generation

The island of Flores is one of the smallest islands in the Azores, measuring 143 km². Its 4,000 inhabitants are responsible for a peak load of about 2 MW (see [2] for details of the electricity system of Flores). Electricity generation is done by a thermal diesel plant (2.3 MW installed capacity), hydro (1.5 MW), and wind power (0.6 MW). Typical demand and generation profiles are given in [2]. These profiles show that the availability of hydro power depends strongly on the season: in winter and spring there is much more hydro power available, due to the typical seasonal precipitation trend that is present on the Azores.

In this study we are interested in large penetrations of renewable energy sources and the effect of EVs as responsive demand to smoothen out fluctuations in renewable generation. We will therefore model the “normal” demand (not from EVs) as exogenous and we will subtract renewable generation from demand, to obtain the residual demand which has to be met by diesel generation. We simplify further to ignore ramping rates and start-up costs, so that the diesel generators

Fig. 11.1 Dispatch according to merit order. As the residual demand changes in time, the point moves along the merit order



respond immediately when there is a shortage of renewable generation. Finally, we ignore all constraints resulting from the network. The least cost centralized economic dispatch then takes the following form:

$$\begin{aligned} & \underset{P_{G_i}}{\text{minimize}} \quad \sum_{i \in G \setminus G_r} C_i(P_{G_i}(k)) \\ & \text{subject to} \quad \sum_{i \in G \setminus G_r} P_{G_i}(k) = \sum_{z \in Z} L_z(k) - \sum_{j \in G_r} P_{G_j}(k) \end{aligned} \quad (11.1)$$

where $P_{G_i}(k)$ denotes the output of generator i at discrete time step k , C_i the marginal costs associated with the output level P_{G_i} , G the set of all generators, G_r the set of all renewable generators, and Z the set of all loads z .

In the remainder of this chapter we will often consider the residual demand, defined as

$$Q = \sum_{z \in Z} L_z(k) - \sum_{j \in G_r} P_{G_j}(k) \quad (11.2)$$

According to (11.1) the plants are dispatched simply according to the merit order, as Fig. 11.1 shows schematically. Figure 11.2 shows how this dispatch model works out for the typical days in each season. The fact that we model the diesel generators with infinite ramping rates and no start-up costs leads to the dispatch of very small amounts of diesel generation. Most notably in the typical winter day, the difference between the actual dispatch [2] and the modeled dispatch (Fig. 11.2) becomes clear. Nevertheless, our simplified dispatch model resembles the actual dispatch quite well. As can be seen in Fig. 11.2, we also assume that hydro power is adjustable with an infinite ramping rate up to a maximum capacity that depends on the season.

11.2.2 Wind and Solar Generation

The availability of wind and solar power shows a similar strong seasonal dependence, depicted in Fig. 11.3. This figure suggests that it could be beneficial to supplement wind generation by solar, to overcome periods in summer with low wind output. Some preliminary simulations have indeed confirmed that this is the

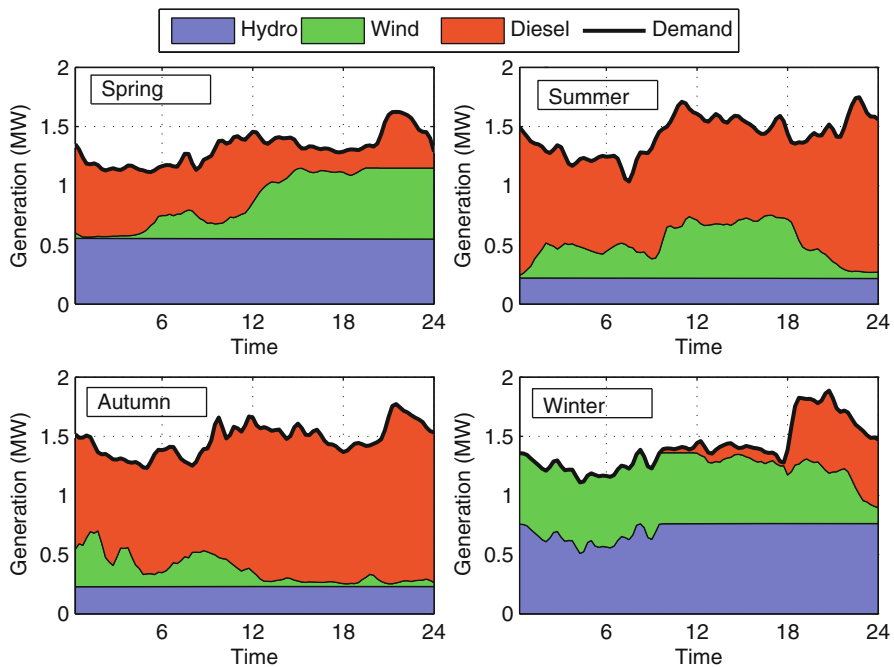


Fig. 11.2 Electricity demand and modeled dispatch of different generation types on 4 typical days in each season

Table 11.1 Sizes of installed generation capacities in different scenarios in MW

Generation scenario	Wind	Solar	Hydro	Diesel
Current generation mix	0.6	0	1.4	2.3
Moderate wind and solar	2.7	1.4	1.4	2.3
Maximum wind and solar	4.1	4.0	1.4	2.3

These numbers are for the case with 50% EVs. For the cases with no EVs and 100%, the amount of installed wind and solar are roughly 20% smaller and larger, respectively

case; so we will consider in the remainder of the text three generation scenarios, listed in Table 11.1. As described in previous chapters, wind power has been modeled based on meteorological time series of wind speed and where a model of the Enercon E33 wind turbine combined with a logarithmic wind profile have been used to convert wind speed measurements to wind power output (see also [3–5]). The solar power output has been modeled in a simplified manner using measurements of solar radiation on the island of Terceira [6, 7], since data for Flores were not readily available. All details regarding placement and orientation of PV panels have been ignored, and the solar radiation time series have been converted to solar power by normalizing the radiation series and multiplying by the installed capacity. Hence, if e.g. the installed solar capacity is 2 MW, the maximum value of the modeled solar power time series is also 2 MW. Furthermore, since no solar

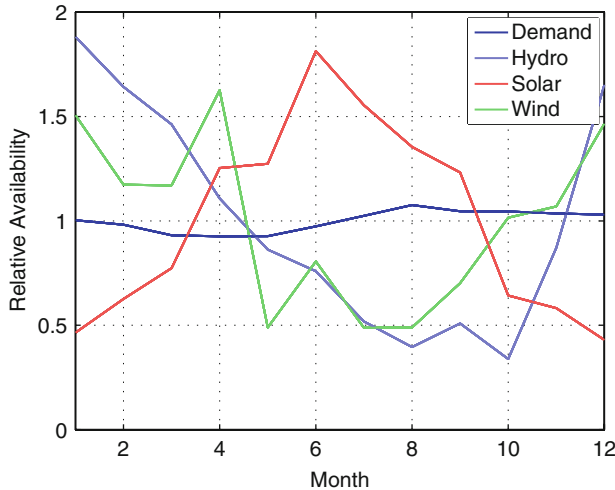


Fig. 11.3 Seasonal dependence of availability of renewable energy sources and demand

data from the year 2008 was readily available, we use the 2009 time series. By doing so, we effectively ignore the correlation on the short time scales (hours to days) between wind and solar. One could speculate that these would normally be inversely correlated: in periods of high winds (often associated with low pressure systems) there will be lower insolation than in periods with low winds (associated with high pressure systems). This inverse correlation is also suggested by Fig. 11.3, which shows this effect on the seasonal timescale. So although our model is clearly a crude approximation of solar power production, one could argue that we even underestimate the complementarity of solar and wind because in our simulations the inverse correlation between wind and solar is not present. Summarizing, we emphasize that it is not our intention to model solar generation in detail. Rather, we are interested in finding out whether solar generation can play some role to complement wind and hydro energy because of the seasonal trends in the availability of these resources.

11.2.3 Transportation Data

Modeling the effect of EVs on the power system requires detailed knowledge about driving patterns of the EVs. Since specific EV data are, given the still low penetration of EVs, only very scarcely available, we will model the EV usage based on current driving statistics of normal passenger cars. Driving behavior statistics of the Azores were described in [8], but the specific data that are needed for the EV charging model were, however, not readily available. We will therefore use a dataset of Dutch driving behavior that is described in [9] based on [10]

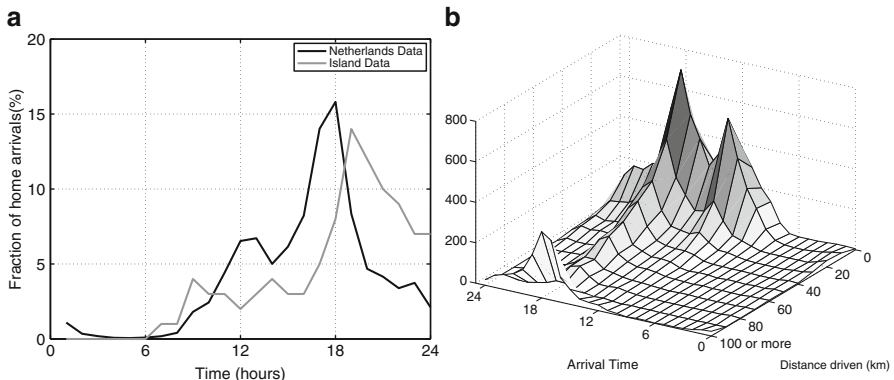


Fig. 11.4 Comparison of car arrival times at home between the Dutch data and the Azores (a) and distribution of arrival times and daily driving distances in the Netherlands (b)

instead. A comparison between the arrival times of the Azores data set and the data representing the Netherlands shows that the patterns are more or less similar, see Fig. 11.4a. Moreover, the average daily driving distance of 34 km was equal between the Netherlands and the Azores.

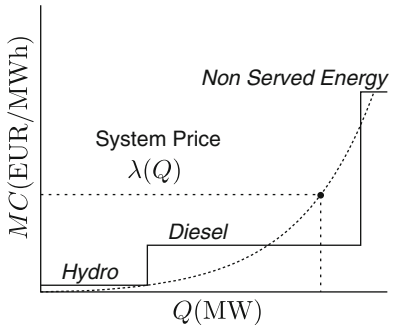
The distribution of home arrival times and daily driving distance of the dataset that has been used is shown in Fig. 11.4b. Based on these data we have also constructed the uncontrolled charging profiles that we use for comparison with the controlled charging case. More details about the driving data and the uncontrolled charging profiles can be found in [9].

11.2.4 Price Signal

The approach we take to model the behavior of the EVs assumes that there exists a real-time price signal, since the EVs will base their charging schedule on the expected price for electricity. This price should somehow reflect the marginal costs of the marginal production unit. In a system with high penetrations of renewables, this poses a problem due to the fact that many renewable energy technologies have practically zero marginal cost. Furthermore, in a liberalized market environment, generators recover their capital costs in a number of hours when the electricity price is higher than their marginal generation costs. Important for capital cost recovery of peak generators are thus the periods with high prices due to a (threatening) shortage of generation with market prices approaching the price of non-served energy. Alternatively, a system operator could pay a capacity payment when hours with non-served energy are unacceptable.

While we recognize the complexity of how electricity prices emerge in various electricity systems, in this study we are mostly interested in the role of EVs and

Fig. 11.5 Approximation of long run marginal cost (LRMC) curve based on marginal cost of diesel generators, the expected amount of produced energy, and the value of loss of load



therefore take a simplified and pragmatic approach to model the electricity price based on a number of simple economic arguments. First we note that the price should be related to the shortage of renewable generation (i.e., the residual demand: demand minus baseload and renewable generation), since that has to be met by the diesel generators. Furthermore, yearly average prices should be such that the capital costs of the production units can be recovered. Also, somehow the cost of diesel generators and the value of non-served energy should be reflected in the price.

Based on these arguments, we take a rather heuristic approach and model the electricity price as exponentially depending on the residual demand, which in a way mimics the merit order of power plants. Note that the shortage can be negative when there is a surplus of generation. The price is then given by the following formula:

$$\lambda(t) = A e^{bQ(t)} \quad (11.3)$$

with λ denoting the real-time electricity price and $Q(t)$ the residual demand (or shortage) as defined in (11.2).

The values of the constants A and b are thus related to capital costs of the renewable energy technologies, the marginal costs of the diesel generators, and also to the value of non-served energy. Another way of interpreting (11.3) is by seeing it as a long run marginal cost (LRMC) curve. The LRMC of a certain technology consists of both the marginal cost of generation and the capital costs which have to be recovered in the expected number of hours that this generation technology will be dispatched in its lifetime. A back-up diesel generator that is expected to operate only a few hours per year therefore has much larger LRMC, although its short run marginal costs may be similar to other diesel generators. According to micro-economic theory, either in a centrally planned system or a perfect market, so much generation capacity will be built that the LRMC of the next plant would be higher than the value of non-served energy. It therefore makes sense to model the real-time price based on the LRMC curve. Figure 11.5 shows this schematically, with the value of non-served energy added to the merit order.

By curve fitting and some trial and error, it was found that values of $A = 1$ and $b = 5$ produce electricity price profiles that fulfill the criteria outlined above. With these values, the yearly average price equals the capital costs of a modern wind

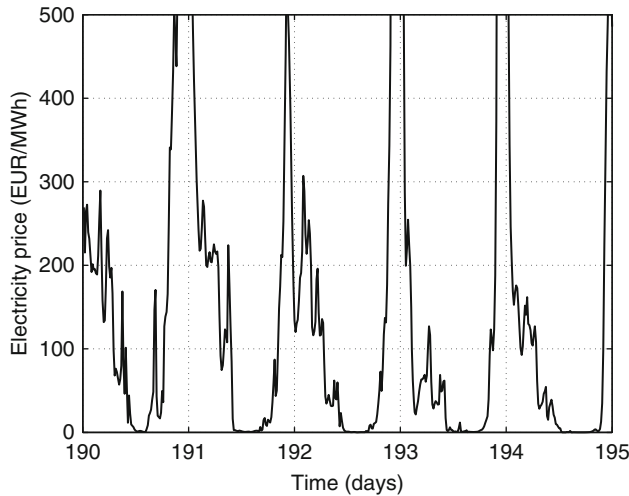


Fig. 11.6 Modeled electricity price in a typical summer period of 5 days

turbine. The latter depends again on many factors such as size, location, and capacity factor, but here a rather conservative value of 100\$/MWh is chosen [11]. As an example the modeled electricity price for a period in summer is shown in Fig. 11.6. Compared to typical wholesale electricity prices, these prices might appear quite high, but it should be noted that this period has the highest prices of the whole year, due to relatively high demand and low wind and hydro power output. The average price in this year is around 100\$/MWh. To place these prices into perspective it is also good to recall that with diesel prices over \$ 3 per Gallon (as of May 2011 [11]), marginal costs of a typical diesel generator are in the range of 250–300\$/MWh.

11.2.5 Charging Model

This section will briefly describe the model used for the controlled charging of the EVs. The description of the model is similar as presented in [1], but for better readability we repeat most of the description here. An illustrative result for a single EV is given to facilitate understanding of the functioning of the model. It is emphasized that EVs base their optimal charging schedule based on anticipated price, so we implicitly assume that accurate predictions of load, wind, and solar are available. We do not take into account uncertainty in these predictions.

The optimal charging of an EV can conveniently be described using a discrete time state-space model of the following form:

$$x_{k+1} = f_k(x_k, u_k, w_k), \quad k = 0, 1, \dots, N-1. \quad (11.4)$$

That is: the next state of state variable x_k depends on the control u_k and a disturbance w_k where the discrete-time horizon lies at $k = N$. For the problem at hand, x denotes the battery state of charge (SOC), u denotes the charging power when the car is plugged in and we model the discharge of the battery while driving as a disturbance w without paying further attention to the details of the electro motor. Furthermore, the charge efficiency is assumed to be one, so we are ignoring the losses associated with charging. In [12] a round trip efficiency of over 95% is reported, which makes the error we are making small.

With this assumption, (11.5) simply becomes:

$$x_{k+1} = x_k + u_k \Delta t - w_k, \quad k = 0, 1, \dots, N-1. \quad (11.5)$$

The task is to find the sequence of u_k that minimizes the charge costs within the constraints that are prescribed by the battery limits as well as the transportation needs. In other words, this means that a driver can always make his planned trip.

The optimal charge schedule can be found by a deterministic dynamic programming algorithm, see e.g. [13]. The algorithm can be described as a recursive algorithm that starts with the cost of the final step and then proceeds backwards until the optimal policy is found that minimizes the costs of the total trajectory. Following [13], the algorithm is given by the following equations. Starting with the cost of the final step:

$$J_N(x_N) = g_N(x_N) \quad (11.6)$$

where g denotes the cost function. The cost of the intermediate steps (also known as cost-to-go) is given by:

$$J_k(x_k) = \min_{u_k \in U_k(x_k)} \{g_k(x_k, u_k, w_k) + J_{k+1}(f_k(x_k, u_k, w_k))\}, \quad k = 0, 1, \dots, N-1 \quad (11.7)$$

Then the cost of the last step $J_0(x_0)$ denotes the optimal cost $J^*(x_0)$ and the policy $\pi^* = \{u_0^*, \dots, u_{N-1}^*\}$ where $u_k^*(x_k)$ minimizes for each k and x_k the cost of (11.7) is optimal.

In our case, since we have a deterministic setup and we are optimizing over the horizon of a whole year, this cost of the final step does not really affect the solution, because an empty battery is not a permitted intermediate state anyway. A linear function that assigns a cost to the final state of the battery according to:

$$g_N = C(1 - x_N) \quad (11.8)$$

with C any large enough number works well and ensures the battery is charged at the final step.

The cost of the intermediate steps is given by:

$$g_k(u_k) = \begin{cases} \lambda(k)u_k \Delta t & \text{if } u_k \geq 0 \\ (\lambda(k) - C_{\text{degr}})u_k \Delta t & \text{if } u_k < 0 \end{cases}$$

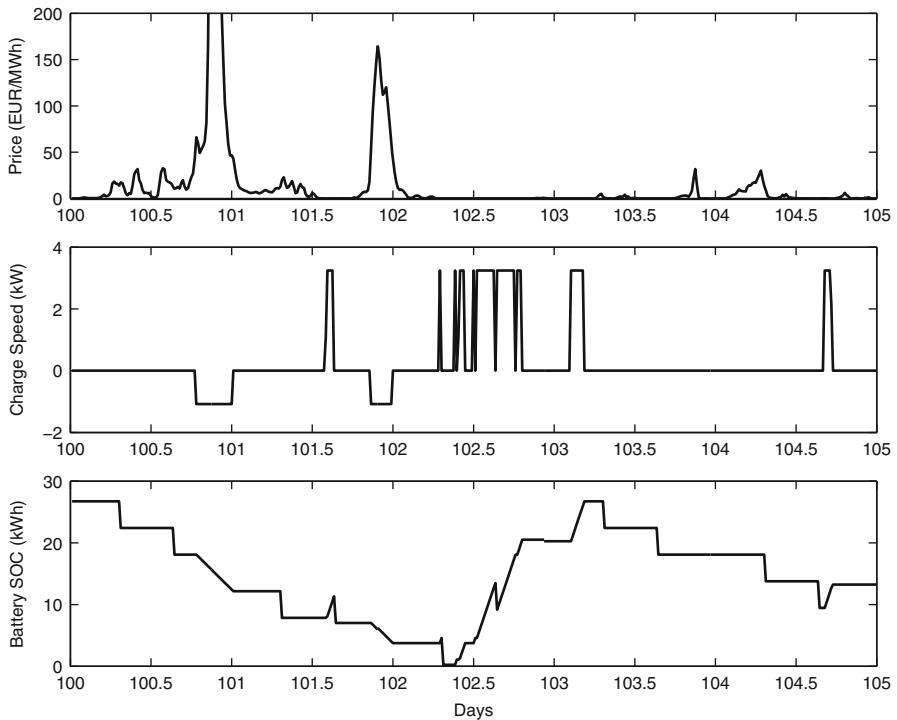


Fig. 11.7 Electricity price, battery state evolution, and optimal policy for a single EV during a period of 4 days with both low and high prices. Note that discharges due to driving are only visible in the battery state and not in the control

These cost functions express that a car charges against the real-time electricity price and gets paid the same price if it delivers back to the grid, but it does so at the cost of degrading its battery. The battery degradation costs are assumed to be constant here (not a function of discharge power or depth) and have a value of \$4.2ct/kWh served. This value was found experimentally as described in [12]. This formulation also allows to easily incorporate other tariff structures where there is a difference between consuming and supplying electricity to or from the grid.

Figure 11.7 shows for a single car the electricity price, the optimal control, and the battery state as determined by the model. It can be seen that the model acts as a sort of bang–bang controller, where the battery is charged/discharged at the power limits when the prices are right. This is in line with the results described in [14], where a more advanced battery model has been used.

Since our goal is to simulate the simultaneous effect of all EVs on the island, the model is run for a large number of EVs where each car has its own technical characteristics. Furthermore, each EV has its own driving characteristics (departure time, arrival time, and daily driving distance), and we assume that each day of the year it repeats the same driving cycle. The battery and charging characteristics also

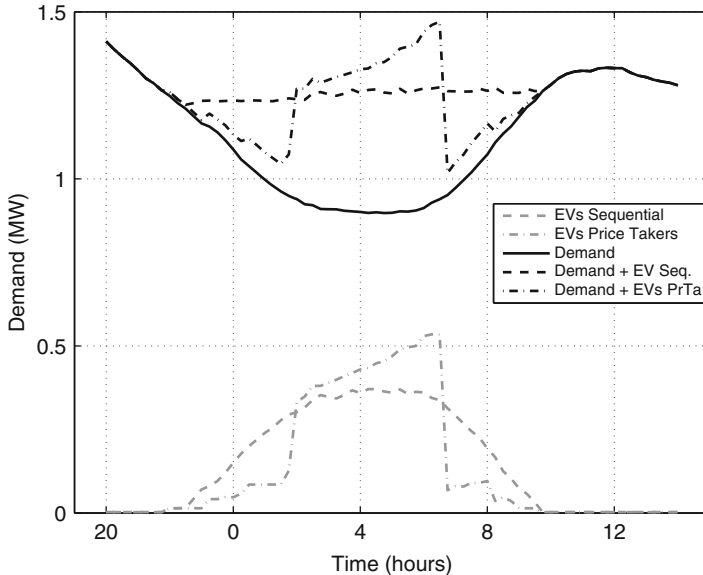


Fig. 11.8 Difference between the aggregate EV demand of many EVs as modeled by (11.9) and modeled as price takers

vary per EV and are sampled from a Gaussian distribution around the following average values: $E_{\text{battery}} = 24 \text{ kWh}$, $P_{\max} = 3 \text{ kW}$, and $P_{\min} = -1 \text{ kW}$ with a standard deviation of 10% of the average values. The EV efficiency is taken to be 5 km/kWh .

Since the combined effect of a large number of EVs alters the electricity demand substantially (in fact this is precisely what we are interested in: the effect on the demand) and hence on the real-time price, we run the charging model sequentially where for each car the new expected electricity price is recalculated based on the change in demand of the previous car:

$$\mathbf{u}^*(i+1) = f(\lambda(\mathbf{Q} + \mathbf{u}^*(i))), \quad i = 1, \dots, N_{\text{cars}} - 1 \quad (11.9)$$

where the boldface notation is now used to indicate that a vector with values for all time steps is used. In other words, this means that we do not model the EVs as price takers. Figure 11.8 shows the aggregate demand of a number of EVs as modeled by (11.9) and modeled as price takers. It is clear that the effect of the EVs on demand and hence price cannot be ignored.

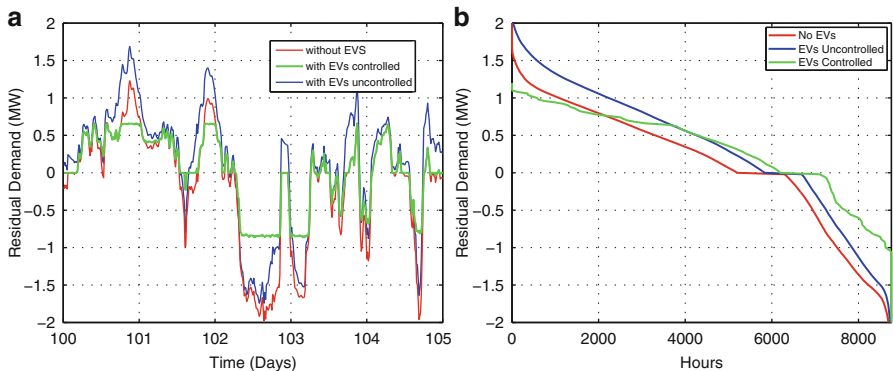


Fig. 11.9 Residual demand in three scenarios for the moderate wind and solar scenario and 1,000 EVs in a 5-day spring period (a) and the load duration curves (b)

11.3 Results

11.3.1 Demand and Generation

As stated in the previous sections, the EVs will charge based on electricity price, which in turn is depending on the residual demand. It is therefore instructive to first show the effects of controlled EV charging on the residual demand which is to be met by diesel generation. Figure 11.9a shows the residual demand in a typical spring period for the controlled EV case, the uncontrolled EV case, and the case without EVs. It can be seen that the EVs reduce the peak of residual demand and, more markedly, they fill the periods with negative residual demand by absorbing much more renewable energy generation. The effect for the whole year can be seen in Fig. 11.9b where the load duration curves of residual demand are shown. Recalling that positive residual demand has to be met by diesel, whereas negative residual demand means spilled energy, these load duration curve clearly demonstrate the positive effect of the EVs.

The dispatch of the different generation technologies is shown in Fig. 11.10 for the typical spring period. Again, here it can clearly be seen that the EVs significantly reduce the use of the diesel generators and profit more from renewable energy generation if it is present. Another observation is that even in the situation with controlled EVs, there is still spilled wind or solar energy at some hours, which is not surprising considering the relatively large installed capacities of wind and solar in comparison with the demand.

Next we consider the scenario with maximum wind and solar penetration and a high number of EVs: 2,000. The residual demand profile for the typical spring period is shown in Fig. 11.11a and the residual demand duration curve in Fig. 11.11b.

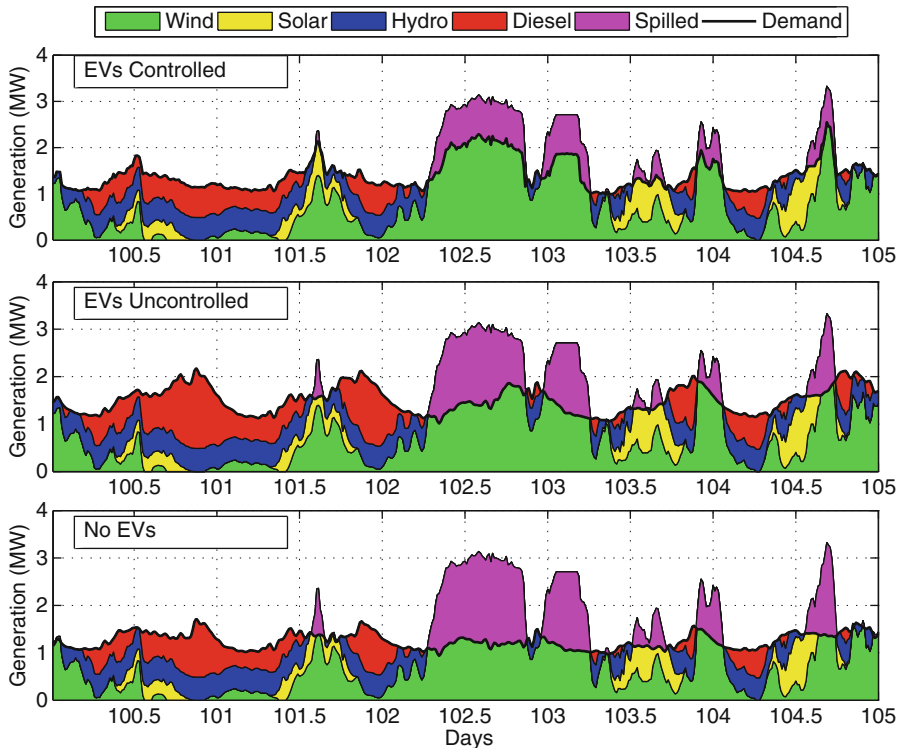


Fig. 11.10 Use of different generation types for a period in spring with 1,000 EVs in different scenarios for the case with moderate wind and solar

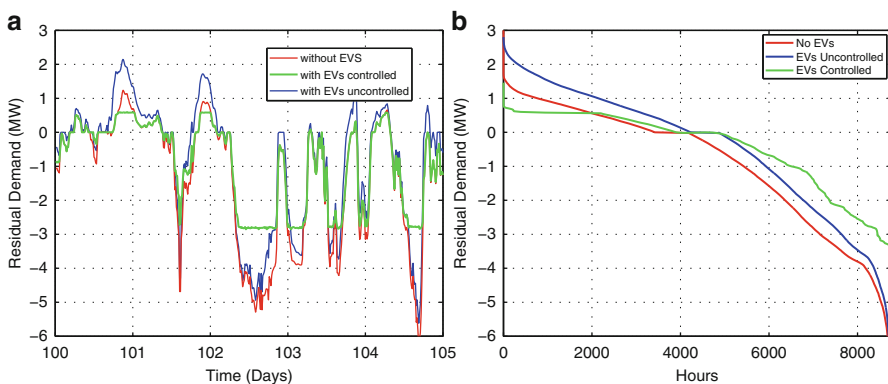


Fig. 11.11 Residual demand for the maximum wind and solar scenario and 2,000 EVs in a 5-day spring period (a) and the load duration curves (b)

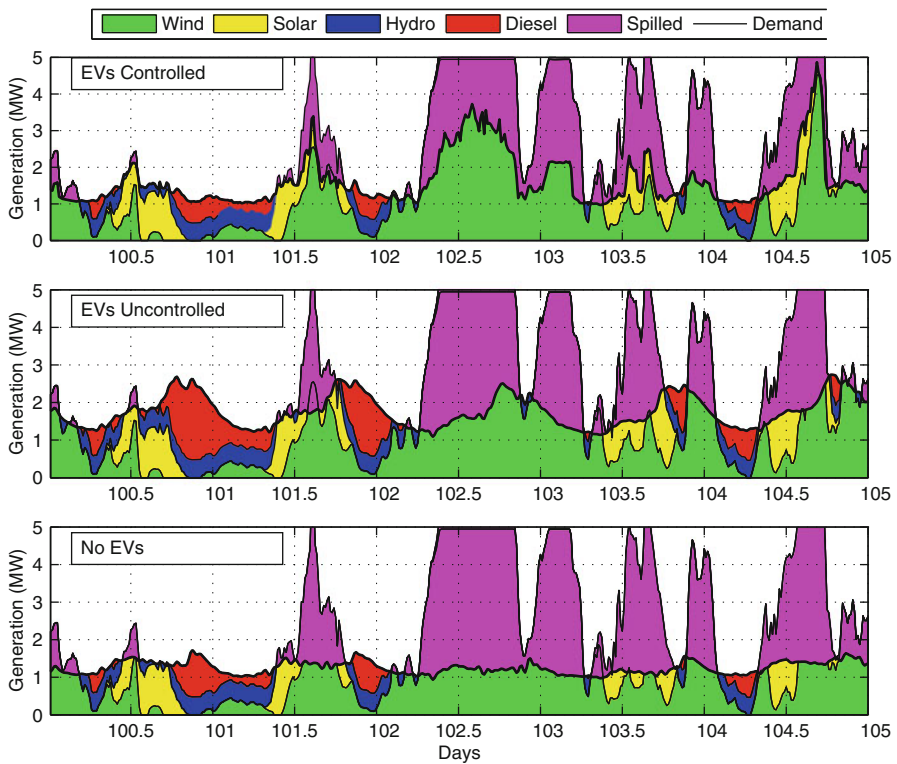


Fig. 11.12 Use of different generation types for a period in spring with 2,000 EVs in different scenarios for the case with maximum wind and solar distribution

The residual demand curves show that there are now far more situations with a surplus of renewable generation. Again, the EVs manage to absorb a significant portion of this surplus. Nonetheless, an even larger share of renewable generation has to be spilled. It is interesting to note that the *maximum* amount of diesel power needed in the controlled EV scenario is even smaller than in the case with only 1,000 EVs. This is an important observation in regard to the amount of back-up generation required in systems with high penetrations of renewable energy sources. The *total* amount of diesel dispatched is significantly smaller too, which is as expected since there is much more renewable generation. Figure 11.12 shows the different generation technologies for the typical spring period. The amount of spilled wind and solar is now significant, indicating that it becomes less efficient when more capacity is already in place.

Table 11.2 Total (electricity generation + vehicle emissions) yearly CO₂ emissions in kton for different scenarios

Electricity scenario	Vehicle scenario				
	All diesel	50%EVs	50%EVs	100%EVs	100%EVs
	ICE	Uncont.	Cont.	Uncont.	Cont.
Current generation mix	8.38	8.08	8.06	7.80	7.76
Moderate wind and solar	6.18	5.37	4.65	4.26	3.05
Aggressive wind and solar	5.52	4.42	3.29	3.13	1.29

11.3.2 Effects on Emissions

From the obtained time series of dispatched diesel generation, the CO₂ emissions can be calculated in a straightforward manner, assuming that the diesel generator emits 0.7 ton/MWh [15]. We will compare the total emissions of the island under different electricity generation and vehicle scenarios. Currently the fleet of roughly 2,000 passenger cars is mostly powered by an internal combustion engine (ICE) fueled with diesel with a typical emission of 150 g/km [16]. Table 11.2 gives an overview of the total emissions in the various scenarios.

The most important conclusion from this table is the large emission reduction potential that EVs offer in combination with renewable generation. In the most aggressive scenario, the total reduction of CO₂ emission is more than 85% compared to the current situation. In this scenario, the *value* of controlled charging is also the most prominent: a reduction of more than 60% (from 3.13 to 1.29 kton), only due to shifting the energy needs of the vehicles.

The table shows also that with the current generation mix (dominated by diesel), replacing ICE diesel cars with EVs leads to only modest emission reductions. This number is, however, quite sensitive for the typical values of the emissions of the diesel generators and diesel cars that have been used here. If one would consider the change in efficiency of diesel generators with respect to their optimal operating point, there could possibly be more reductions with the current generation mix.

11.3.3 Optimal Wind and Solar Mix

It is instructive to compare the cost-effectiveness of investments in wind and solar generation with respect to the emissions of CO₂. By varying the amount of installed wind and solar and running the model for the whole year for each combination, the emissions as a function of installed wind and solar have been determined. To take into account that wind has lower total levelized costs than solar [11], the extra capacity of solar has been scaled according to the ratio of levelized costs, so that one unit of capacity of wind has the same costs as one unit of capacity in solar. In terms of MW, the maximum capacity value of 3 corresponds to roughly 4 MW

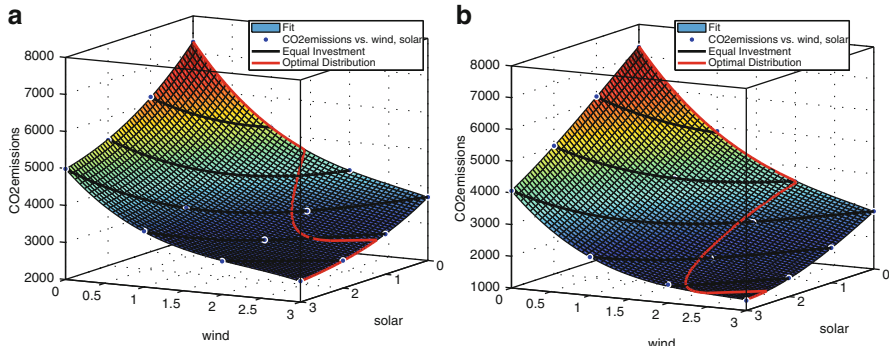


Fig. 11.13 CO₂ emissions as a function of installed wind and solar capacity in both the controlled (a) and uncontrolled scenario (b). Also shown are the line of the optimal mix and lines of equal investment. The units of wind and solar capacity are dimensionless and are such that the maximum of 3 correspond to the maximum values listed in Table 11.1

(see Table 11.1) for both technologies. Figure 11.13a, b shows the resulting CO₂ emission as a function of installed wind and solar capacity for the case with 1,000 EVs (controlled and uncontrolled).

Since one unit of wind has the same costs as one unit of solar, the lines given by wind + solar = Const. denote the lines of a certain investment. The values of wind and solar where these lines are minimal then correspond to the optimal distribution of a given amount of investment in new capacity.

So in both the uncontrolled and the controlled EV charging scenario, it is better to invest in more wind capacity first. At some point, however, building more wind leads to much more spilled generation and it is better to diversify the generation mix by adding some solar, despite the fact that this is roughly two times more expensive. An interesting observation is that the optimal mix depends on whether or not there is controlled charging of EVs in place. In the controlled EV scenario, the EVs are able to avoid spilling energy much longer, so here it is beneficial to build more of the cheaper wind capacity. But even in this case, at some point it becomes more beneficial to invest in extra solar instead of building more wind.

To understand the results on the cost-effectiveness of new wind and solar generation, it is useful to invoke the amount of spilled renewable energy (hydro has not been counted as such). Table 11.3 lists the amount of spilled renewables in the different considered scenarios. It is important to notice that in the current generation mix there is never any spilling of wind or solar, but this is partly a result of the fact that we did not include start-up or ramping costs of diesel generators. In practice, some diesel generators will probably be kept running while wind is spilled, for reliability reasons and because the start-up costs will be higher than the saved fuel costs. The table also shows that in the moderate wind and solar scenario, the EVs are very effective to avoid spilling wind or solar. At some point though, there is simply too much extra energy to absorb and the amount of spilled energy starts to increase dramatically. Considering cost-effectiveness, it is good to compare Table 11.3 with the levelized cost of wind, solar, and diesel. As stated before, with

Table 11.3 Percentage of spilled renewable generation (wind + solar) for different scenarios

Electricity scenario	Vehicle scenario				
	No EVs	50% EVs	50% EVs	100% EVs	100% EVs
Current generation mix	0	0	0	0	0
Moderate wind and solar	28%	21%	10%	23%	8%
Aggressive wind and solar	49%	42%	30%	45%	29%

Recall that the amounts of installed renewables are larger in the case with 100% EVs by approximately 20%

current diesel prices, the marginal costs of diesel generators are in the order of 250–300\$/MWh. In [11], levelized cost of wind and solar are roughly 100 and 200\$/MWh, respectively. This means that if 60% of all wind is spilled, it is still cheaper than diesel generation. For solar this is the case if 20% is spilled. These numbers strongly suggest that it does not only make sense to invest in wind and solar from an environmental point of view, but also from an economical.

11.4 Conclusions and Discussion

The work described in this chapter has explored the potential of EVs in reducing CO₂ emissions on the island of Flores. The key to this potential is the fact that a large fleet of EVs can adjust its demand based on the predicted availability of wind and solar generation. This study has shown that the value of controlled EV charging increases dramatically with the amount of intermittent generation installed. Although not able to avoid the dispatch of diesel generation completely, the capacity of the back-up units can be reduced significantly and, moreover, the use of them is very limited. The emission reduction potential of EVs has been found to possibly be up to 85% compared to the case with the current generation mix and diesel fueled vehicles. However, this reduction and especially the effect of the optimal scheduling of EV charging is strongly dependent on the accuracy of the forecasts; so we emphasize that this value should be regarded as an upper bound. Furthermore, we have neglected issues related to reliability and dynamic stability, which could lead to spinning reserve requirements of back-up diesel generation.

Related to the economic feasibility of renewable generation, controlled charging of EVs lowers the amount of spilled renewable energy considerably, especially in a moderate extra wind and solar generation scenario. At the highest levels of wind and solar capacities, there is roughly 30% of spilled renewable energy, but a comparison of the costs of wind, solar, and diesel suggests that it is still beneficial to build these levels of wind and solar. The optimal (in the sense of cost-effectiveness with respect to CO₂ reduction) mix of wind and solar was found to be dependent of whether

or not there is controlled charging of EVs. The general picture was that it is most optimal to build more wind capacity initially, but after some point it becomes more beneficial to add solar power.

An important aspect of an electricity system where EVs are to fulfill the role as grid storage and responsive demand is the right price signal to do so. In systems with high penetrations of renewables, this implies that a real-time price which reflects the shortage or surplus of renewable generation is critical. Using a real-time price based on long-term marginal cost curve was found to give the right incentives. In the system under consideration in this study, the marginal cost of the back-up diesel generators is high enough so that the degradation costs of EV batteries delivering energy back into the grid are no real obstacle for EVs to temporarily provide energy when needed.

Although this study has not specifically considered automated generation control for frequency regulation or other ancillary services to be provided by EVs, one could argue that, with the right price incentives, these sort of services can also be provided by EVs. In our study we have not considered possible effects of EV charging on the networks. Future research should provide more insight in these topics.

Other interesting venues for future research would be to include uncertainties in the forecasts of electricity price and driving behavior in the model and have a more advanced representation of the battery physics. Analyses of long time series of wind and solar generation in combination with vehicle fleet developments could provide more insights on issues related to the planning of new generation capacity.

Acknowledgements This work was supported by the Next Generation Infrastructures Foundation (<http://www.nginfra.nl/>) and the Delft Research Centre for Next Generation Infrastructures. The authors are also grateful to the University of Azores that is responsible, in cooperation with the Portuguese Meteorological Institute, for operating the solar irradiation instrumentation. The funding for this operation has been supported by several projects and programs namely the Azores Regional Secretariat for Science and Technology (Project M1.2.1/I/006/2005, Project M1.2.1/I/001/2008, Project M1.2.1/I/002/2008) and the Program INTERREG IIIB, Azores, Madeira, and Canarias (Project CLIMAAT FEDER - INTERREG IIIB - MAC 2.3/A.3, Project CLIMAAT II FEDER - INTERREG IIIB - 03/MAC/2.3/A.5, Project CLIMARCOST FEDER - INTERREG IIIB - 05/MAC/2.3/A1).

References

1. R.A. Verzijlbergh, M.D. Ilic, Z. Lukszo, The role of electric vehicles on a green island, in *North American Power Symposium (NAPS)*, 2011, August 2011, pp. 1–7
2. Electricidade dos Açores, Caracterização das Redes de Transporte e Distribuição da Região Autónoma dos Açores, (Azores Electric Utility), Electricidade dos Açores, Tech. Rep., 2010
3. J.F. Manwell, J.G. McGowan, A.L. Rogers, *Wind Energy Explained: Theory, Design and Application* (Wiley, Birmingham, 2002)
4. V. Thapar, G. Agnihotri, V. Sethi, Critical analysis of methods for mathematical modelling of wind turbines. *Renew. Energy* **36**(11), 3166–3177 (2011)
5. Enercon, Enercon wind energy converters product overview, Tech. Rep., 2010

6. Instituto de Meteorologia I.P. (Portugal Meteorological Institute), www.meteo.pt. Accessed July 2012
7. R. Aguiar, A.R. Silva, R. Coelho, Solar climate of Azores: results of monitoring at Faial and Terceira islands, in *Eurosun 2008—1st International Conference on Solar Heating, Cooling and Buildings*, 2008
8. Instituto de Seguros de Portugal (ISP), www.isp.pt, 2005. Accessed July 2012
9. R. Verzijlbergh, Z. Lukszo, J. Slootweg, M. Ilic, Ev charging profiles derived from driving statistics, 2011, in *Proceedings of the IEEE Power & Energy Society General Meeting*, 2011
10. Ministry of Transport, Public Works and Water Management, Mobiliteitsonderzoek Nederland (in Dutch), April 2009. www.mobilitsonderzoeknederland.nl. Accessed October 2010
11. EIA, Energy information administration, www.eia.doe.gov. Accessed July 2012
12. S.B. Peterson, J. Apt, J. Whitacre, Lithium-ion battery cell degradation resulting from realistic vehicle and vehicle-to-grid utilization. *J. Power Sources* **195**(8), 2385–2392 (2010)
13. D.P. Bertsekas, *Dynamic Programming and Optimal Control*, 2nd edn. (Athena Scientific, Belmont, 2000)
14. N. Rotering, M. Ilic, Optimal charge control of plug-in hybrid electric vehicles in deregulated electricity markets. *IEEE Trans. Power Syst.* **26**(3), 1021–1029 (2011)
15. L. Gagnon, C. Belanger, Y. Uchiyama, Life-cycle assessment of electricity generation options: the status of research in year 2001. *Energy Policy* **30**(14), 1267–1278 (2002)
16. J.L. Sullivan, R.E. Baker, B.A. Boyer, R.H. Hammerle, T.E. Kenney, L. Muniz, T.J. Wallington, CO₂ emission benefit of diesel (versus gasoline) powered vehicles. *Environ. Sci. Technol.* **38**(12), 3217–3223 (2004)

Part IV

Efficient and Viable Power Delivery

During Normal System Conditions

Chapter 12

Optimal Placement of Wind Power Plants for Delivery Loss Minimization

Masoud Honarvar Nazari

12.1 Introduction

The dissipation of power delivery in distribution and transmission networks imposes large social and environmental costs. These costs are closely related to the average price of electricity, the characteristics of electric power systems, and the technology of the power plants. In isolated electric power systems, like those of the Azores Archipelago, these costs can be much higher than in continental power systems, such as that of the US. As an illustration, the average price of electricity on Flores is around \$174 per MWh, while the average price of electricity in the USA is about \$94 per MWh. Therefore, a 1 MWh loss in the distribution system of Flores costs 1.85 times more than a 1 MWh loss in the distribution system of the US. This implies that minimizing power delivery losses is an indispensable step toward economic and environmental sustainability for the Azores Archipelago.

In general, there are several conventional approaches to minimizing power delivery losses. The most well-known and commercialized method is implementing shunt and/or series capacitors in order to cancel out reactive currents through the lines. In this chapter, we show that using capacitor banks eliminates only a small portion of the power delivery losses, since reactive currents through the lines only contribute to about 20% of the losses. On the other hand, small-scale power plants, such as wind plants, can significantly reduce losses by producing both real and reactive power.

In Sect. 12.2, we investigate loss minimization on Flores. Our technical findings illustrate that by optimizing voltage settings and output powers of the available power plants, about 35% of the power delivery losses can be eliminated. Further-

M. Honarvar Nazari (✉)

Department of Engineering and Public Policy, Carnegie Mellon University, 5000 Forbes Ave,
Pittsburgh, PA 15213, USA

e-mail: mhonarva@andrew.cmu.edu

more, we investigate a scenario in which 20 % of the available diesel generation is replaced by generation from new wind power plants that are optimally located in the distribution system of the island. The results indicate that up to 57 % of the distribution losses can be eliminated by strategically locating the new wind power plants and optimally utilizing them in coordination with other generators. In the next step, the voltage profile of the distribution system of Flores is investigated using three different scenarios. The results show that when all the power plants are controlling their terminal voltage, a very flat voltage profile is obtained.

In Sect. 12.3, we close the chapter with a brief discussion of needs for developing a systematic framework that can assess the optimum locations and the methods of utilizing the new wind power plants that will achieve the results discussed throughout the chapter.

12.2 Power Delivery Losses on Flores

The electric network on Flores consists of a 15-kV radial distribution network with 45 nodes and 44 branches. Total demand on the island is around 2 MW. Four diesel power plants provide more than 50 % of the electric energy. Around 35 % of the demand is supplied by four hydro plants, and two synchronous wind plants provide the rest (approximately 15 %). Figure 12.1 illustrates the schematic of the distribution network on Flores. In this model, the diesel generator is located at the reference node. The hydro plant is located next to the diesel generator, and the wind plant is located in the middle of the island.

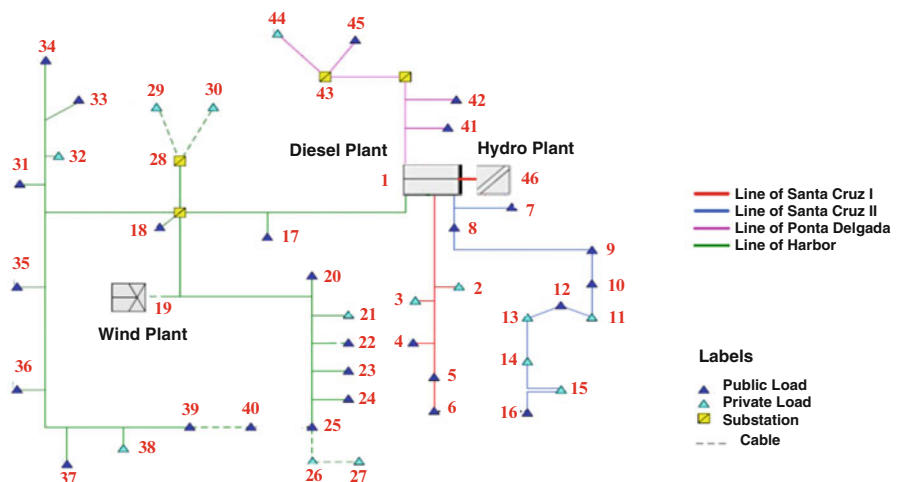


Fig. 12.1 Schematics of the distribution network on Flores Island [1]

Table 12.1 Average cost of producing electricity for different power plants on Flores [1]

	Costs (\$/MWh)
Diesel plant	261
Hydro plant	88
Wind plant	87

The difference between the system shown in Chap. 3 and the one shown in Fig. 12.1 is that here a switch with the reactance and resistance of 0.04 pu connects the hydro plant to the diesel generator. Power flow analysis for Flores demonstrates that more than 2 % of the power delivery is dissipated in the distribution network. This accounts for approximately a 1 MWh loss of energy per day and a 365 MWh waste of electric energy per year.

Given the average price of electricity on the island (\$174/MWh), 2 % power delivery losses cost the island more than \$61,000 per year. Table 12.1 demonstrates the average cost of producing electricity for the different power plants. The 2% losses also cause more than 117 tons of CO₂ emissions per year; the average CO₂ emissions on Flores are 0.32 tons/MWh. In the next section, we explore possible approaches to minimizing these power delivery losses.

12.2.1 Possible Approaches to Minimizing Losses on Flores

In this sub-section, two main approaches to minimizing the power delivery losses are studied: (1) optimizing voltage settings and output powers of the available generators and (2) optimizing the location and utilization of new small-scale power plants such as wind and/or solar plants. The second approach is motivated by the fact that the general policy of Electricidade Dos Acores (EDA) is to make the Azores Islands green. Therefore, it is expected that in the future diesel plants will be replaced by renewable sources of energy such as wind power plants. Consequently, optimal placement of the new plants will be a key factor in loss minimization.

The first step in minimizing power delivery losses is to carry out an AC optimum power flow (AC OPF) for the original system (shown in Fig. 12.1). The objective function of the optimization algorithm is to minimize total distribution losses by optimally scheduling voltage settings and output powers of the available power plants. The control variables of the optimization algorithm are the voltage and phase angles of the generators (V_G and δ_G). The mathematical representation of the optimization algorithm is presented in (12.1)–(12.7) [2, 3, 5].

$$\underset{V_G, \delta_G}{\text{Minimize}} P_{\text{Loss}} = \sum_{i=1}^{N_G} P_G^{(i)}(\delta_G, \delta_L, V_G, V_L) - \sum_{j=1}^{N_L} P_L^{(j)}(\delta_G, \delta_L, V_G, V_L) \quad (12.1)$$

Subject to:

$$P_i - V_i^2 G_{ii} - \sum_{\substack{j=1 \\ j \neq i}}^{N_G+N_L} |V_i| |V_j| (G_{ij} \cos(\delta_i - \delta_j) + B_{ij} \sin(\delta_i - \delta_j)) = 0 \quad (12.2)$$

$$Q_i + V_i^2 B_{ii} - \sum_{\substack{j=1 \\ j \neq i}}^{N_G+N_L} |V_i| |V_j| (G_{ij} \sin(\delta_i - \delta_j) - B_{ij} \cos(\delta_i - \delta_j)) = 0 \quad (12.3)$$

$$P_{\min}^{(i)} \leq P_G^{(i)} \leq P_{\max}^{(i)} \quad \forall i \in N_G \quad (12.4)$$

$$Q_{\min}^{(i)} \leq Q_G^{(i)} \leq Q_{\max}^{(i)} \quad \forall i \in N_G \quad (12.5)$$

$$P_i^2 + Q_i^2 \leq S_i^2 \quad \forall i \in N_G \quad (12.6)$$

$$V_{\min}^{(j)} \leq |V_j| \leq V_{\max}^{(j)} \quad \forall j \in N_G + N_L \quad (12.7)$$

Here N_G is the number of generator nodes and N_L is the number of load nodes in the system. In addition, V_L and δ_L are the voltages and phase angles of the system loads.

The results of AC OPF illustrate that more than 35 % of the distribution losses could be eliminated by optimizing the voltage settings and output powers of the available power plants on the island. This would mean more than 146 MWh energy savings per year, which would save the island more than \$24,500 per year. Moreover, it would reduce CO₂ emissions by 46.8 tons per year.

The second approach to minimizing losses is based on strategically locating the new wind power plants. Here, we investigate a scenario in which 20 % of the diesel generation is replaced by new wind power plant generation. The wind plants are synchronous generators with the ability to produce both real and reactive power. Given the average production of the diesel generators (1 MW), the average generation of the new wind power plants should be around 200 kW or about 10 % of the overall demand.

In order to find the optimum locations for the new wind plants, an optimization algorithm, fully elaborated in [4, 7] is carried out. Figure 12.2 shows the optimal locations for the new wind plants, highlighted by the green rectangle. Note that optimizing these locations would reduce losses by 57 %, saving the island about \$36,800 per year and reducing CO₂ emissions by 70 tons per year.

Placing the new wind plants at optimal locations would also increase reliability of the system. For example, if the line connecting the diesel plant to the center of the island is disconnected (Line 1–17 or 17–18), the wind power plants can supply loads in the center and south parts of the island.

Since the average cost of producing electricity with diesel generators is about 3 times larger than that with wind power plants, offsetting 20 % of the diesel

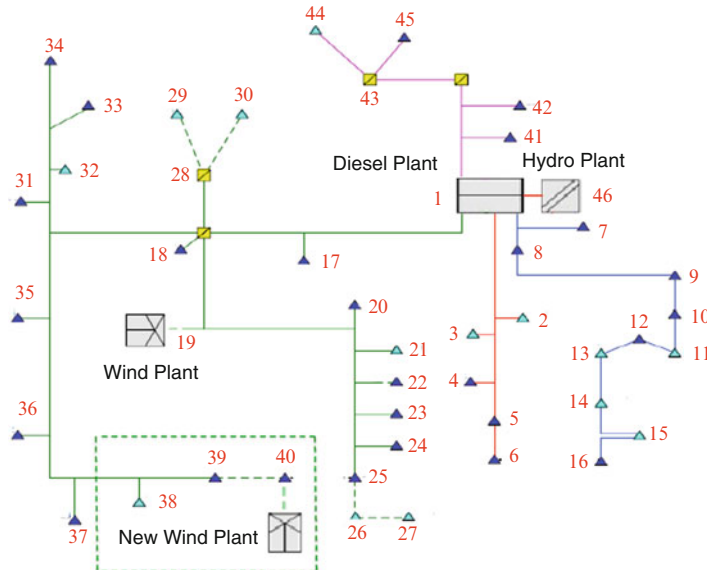


Fig. 12.2 Schematics of the optimal area of locating new wind plants

generation with wind generation, furthermore, would result in a 10 % reduction in the total cost of electricity. Therefore, the total dollar savings to the island would be more than \$250,000 per year. About 15 % of the overall savings is due to reducing losses and more than 85 % is due to the offsetting of diesel generation with wind generation.

Moreover, overall CO₂ emissions would be reduced by about 1300 tons per year. Around 5 % of the reduction would be due to reducing the delivery losses and more than 95 % would be due to the offsetting of diesel generation with wind generation.

12.2.2 Comparison Between Small-Scale Power Plants and Capacitor Banks

In this sub-section, we show that shunt and/or series capacitors cannot notably reduce power delivery losses, whereas small-scale power plants, such as synchronous wind plants, can significantly eliminate losses by offsetting real and reactive currents. To this end, we explore first the effects of active and reactive currents on power delivery losses. We see in Fig. 12.3 that active currents through the lines are about two times larger than reactive currents. Since power delivery losses are related to the square of the current, the losses due to active currents (\mathbf{Pr}) are four times larger than the losses due to reactive currents (\mathbf{Px}).

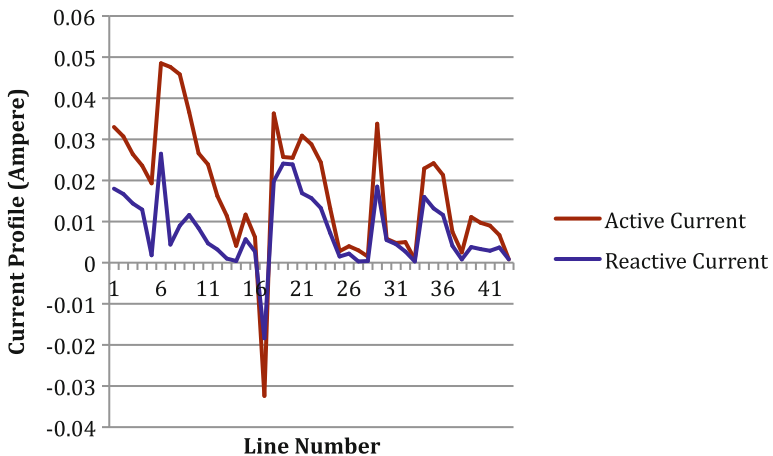


Fig. 12.3 Active and reactive current profile through the lines

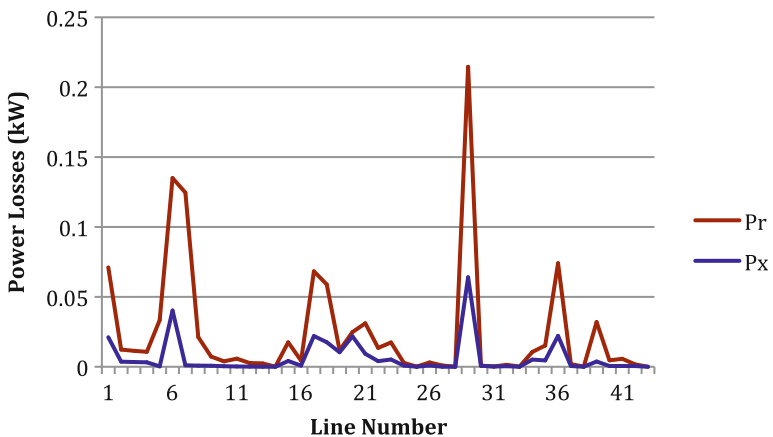


Fig. 12.4 Distribution losses due to active and reactive currents

In other words, reactive currents contribute to only 20 % of the losses; active currents cause the rest (80 %). This implies that installing shunt and/or series capacitors, which compensate for reactive currents only, can eliminate only a small portion of power delivery losses.

On the other hand, small-scale power plants can offset both real and reactive currents through the lines and therefore reduce a large portion of the power delivery losses. We have shown in the previous section that by producing 10 % of the demand with strategically placed and utilized wind power plants about 57 % of the power delivery losses can be eliminated.

In general, minimizing power delivery losses has profound social and environmental advantages. Therefore, using AC OPF-based dispatch to gain such

advantages, which would otherwise not be possible, is an indispensable step toward sustainability of Flores. To this end, EDA needs to implement both SCADA and computer tools such as AC OPF for computing the on-line voltage adjustments and the output power of the generators. Given that today the distribution power system on Flores does not rely on on-line monitoring and dispatch, it is essential to understand the necessity of doing this in order to allow the transformation of Flores into a green and sustainable island.

12.2.3 Improvement of the Voltage Profile on Flores

In this sub-section, we investigate the effect of automatic voltage control of the wind power plants on the improvement of the overall voltage profile of the island. To this end, three main scenarios are assessed: (1) operating the available wind plants without voltage control, (2) operating the available wind generators with voltage control, and (3) strategically locating and utilizing the new wind power plants. In the third scenario, all the wind plants have automatic voltage control.

In general, there exists an acceptable voltage range for electric distribution systems. Violating this limit can damage electrical equipment or diminish its life expectancy. In the worst case, this can lead to overall voltage collapse. Hence, from the perspective of consumers, an ideal voltage profile is a flat voltage profile with a voltage level of 1 pu throughout the distribution system [6]. In this condition, all the electrical equipment operates at the nominal voltage (1 pu), and therefore, the risk of damage is minimized.

Investigating the voltage profile of the island in the three scenarios shows that in Case 1 the wind power plant absorbs the reactive power. Therefore, voltage drops in the vicinity of the plant. In Case 2 the wind plant controls its terminal voltage at 1 pu. As shown in Fig. 12.5, in this scenario the overall voltage profile of the system is much closer to the idea scenario.

In Case 3 all the power plants adjust their terminal voltage to 1 pu. Figure 12.6 illustrates the voltage profile of the system for all the scenarios. The technical results show that a voltage profile closest to the ideal is obtained when all the plants adjust their terminal voltage.

12.3 Conclusions and Future Outlook

In this chapter, we highlight that by strategically placing new wind power plants and optimally operating them in coordination with other generators about 57 % of the power delivery losses can be eliminated from the distribution system of Flores. This would result in energy saving per year of more than 220MWh. In addition, it would save the island more than \$250,000 per year and reduce CO₂ emissions by 1,300 tons per year.

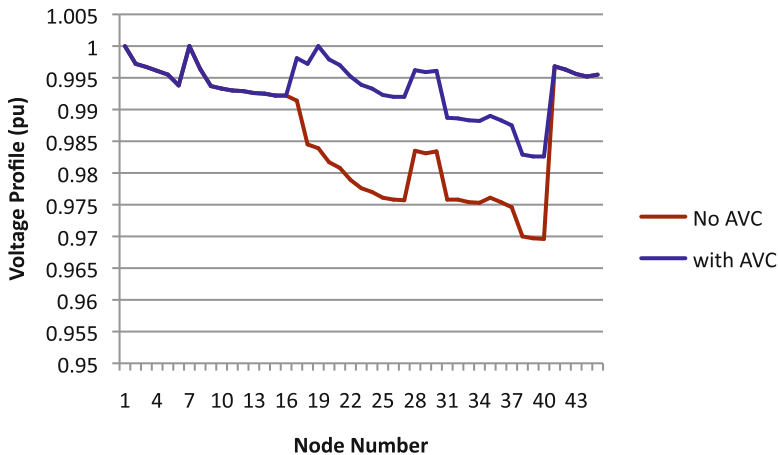


Fig. 12.5 Voltage profile of the island with and without voltage control for the wind power plant

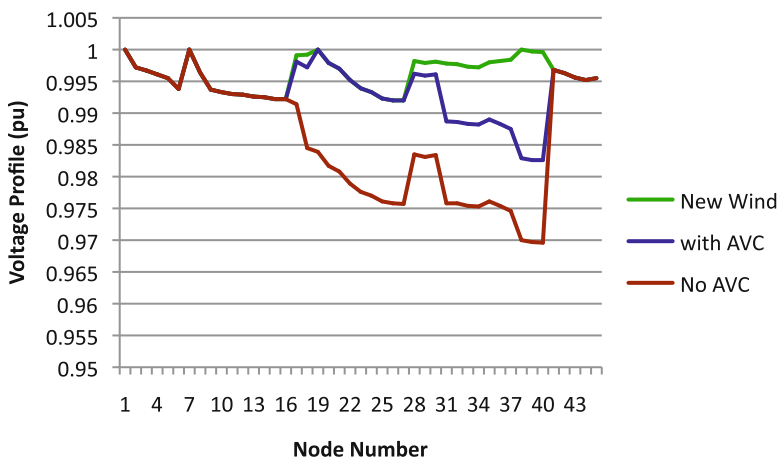


Fig. 12.6 Voltage profile of the island in three different scenarios

Our technical findings furthermore illustrate that loss reduction highly depends on the location and voltage settings of the power plants. We show that capacitor banks can eliminate only a small portion of the power delivery losses, while wind power plants with automatic voltage regulators can significantly reduce power delivery losses by offsetting both real and reactive currents through the lines.

In order to improve voltage profile and minimize the risk of voltage collapse, all wind plants need to be equipped with automatic voltage regulators whose set points should be optimized as conditions vary. This helps the system to maintain a flat voltage profile throughout the distribution system.

While the utility studies are being carried, and new candidate power plants are being considered, it is essential to develop a systematic framework that assess the optimal locations and utilization methods for the new power plants in order to minimize power delivery losses and maximize environmental sustainability.

Acknowledgments The author greatly acknowledges Professor Marija Ilić and Professor Jeffrey Lang for fruitful discussions on this topic. Support for this work was provided by the Fundao para a Ciéncia e a Tecnologia (Portuguese Foundation for Science and Technology) through the Carnegie Mellon Portugal Program under Grant 18396.6.5004458.

References

1. EDA Report, *Characterization of Transmission and Distribution Network of Azores Islands*, March 2009. Available on website: http://www.google.com/url?sa=t&rct=j&q=&esrc=s&source=web&cd=3&cad=rja&ved=0CEAQFjAC&url=http%3A%2F%2Fpaginas.fe.up.pt%2F~ee02072%2Fdocs%2Fcare_eda_2009_2010_03_31.pdf&ei=cEAMuDCbKIhs8wTDpoHoDw&usg=AFQjCNFLLQgM_37AokB5t9oo3VGPiXeeSw&sig2=r-6tom2CXHRd07B2Dvn88Q&bvm=bv.42661473,d.eWU
2. M. Ilić, J. Zaborszky, *Dynamics and Control of Large Electric Power Systems* (Wiley, New York, 2000)
3. J. Machowski, J.W. Bialek, J.R. Bumby, *Power System Dynamics and Stability* (Wiley, New York, 1997)
4. M.H. Nazari, M. Ilić, Potential for efficiency improvement of future electric energy systems with distributed generation units, in *Proceedings of the IEEE General Meeting*, Minneapolis, MN, July 2010
5. M.A. Pai et al., *Power System Analysis: Operation and Control* (Prentice Hall of India, New Delhi, 2006)
6. K. Purchala, L. Meeus, D.V. Dommelen, R. Belmans, Usefulness of dc power flow for active power flow analysis, in *Proceedings of IEEE Power Engineering Society Annual Meeting*, (San Francisco, 2005), p. 454, 2005
7. M.H. Nazari, Making the most out of distributed generation without endangering normal operation: model-based policy-technical approach, Doctoral of Philosophy Dissertation, Carnegie Mellon University, September 2012

Chapter 13

Toward an Extended AC OPF-Based Approach to Wind Power Integration and Pricing

Marija Ilić and Jeffrey H. Lang

13.1 Introduction

The challenges and opportunities presented to operators and planners of today's electric power systems are multifold. Supplying demand with continuously varying resources such as wind and solar power requires tools for predicting and dispatching available resources in a look-ahead manner; this is needed to best manage ramp rates at which power outputs can change. Methods for this are discussed in Part III of this book. It is observed that the simplest way of managing rates is to internalize these as part of generation marginal cost [1,2]. If this is done, then the remaining challenge is power delivery from intermittent resources to the consumers. In this chapter we consider the problem of power and voltage dispatch in systems with intermittent resources assuming that the ramp rate of the power plants is internalized when generation-cost functions are created, as described in Part III of this book. As new intermittent resources begin to replace conventional power plants, it is necessary to carry out an on-line resource management of all the available dispatchable equipment. Voltage optimization is critical during operations to enable delivery of most economic real power generation. In particular, it is necessary to make the following decisions:

M. Ilić (✉)

Department of Electrical and Computer Engineering, Carnegie Mellon University,
5000 Forbes Ave, Pittsburgh, PA 15213, USA

e-mail: milic@ece.cmu.edu

J.H. Lang

Electrical Engineering and Computer Science Department, Massachusetts Institute of
Technology, 77 Mass Avenue, Cambridge, MA 02139, USA

e-mail: lang@mit.edu

- Given an existing system, how to operate new power plants without experiencing power delivery problems.
- Given an existing system, how much new, renewable, generation to build and at which locations.
- Assess the effect of different pricing rules for integrating renewable resources on long- and short-term economic efficiency and the ability to recover capital investment cost.

We start in Sect. 13.2 by showing that resource management can be implemented using an AC OPF as the key software as conditions vary. The use of an AC OPF instead of DC OPF helps optimize voltage-controllable T&D and generation equipment.¹ This is important since the wind power plants often consume significant reactive power even when they do not produce real power. Similarly, solar power plants could distort the voltage profile without system-wide voltage dispatch [7]. In particular we stress that it is no longer possible to dispatch well real power without optimizing the schedules for voltage settings of automatic voltage regulators (AVRs) on power generators and the schedules for voltage-controllable T&D equipment, such as on-load tap changing transformers (OLTCs) and/or controllable shunt capacitors.

Today's rules for voltage dispatch are based on the system operator's knowledge of the system and on extensive off-line power flow analyses for ensuring that the system remains reliable during the “worst-case” conditions. Both the operator's insights about power grid's ability to deliver power reliably with the newly added wind and/or solar power plants and the notion of the “worst-case” scenario are challenging at present. The combinatorial aspect of many possible conditions as the intermittent resources vary makes it impossible to define the worst-case scenario. Similarly, the system operator has very little experience in operating the grid with these new resources. Therefore, it becomes necessary to rely on more flexible technologies such as on-line dispatch of available resources, generation, and T&D equipment when managing the ever-changing system conditions. At least in principle, any technology which is capable of ensuring uninterrupted service as conditions vary should be considered to be a plausible means of supplying demand in future electric energy systems as suggested in Section 13.3.

In Sect. 13.4 we consider the electric power system in Flores island for several seasonal peak load conditions and for seasonal availability of intermittent power generation, such as geothermal, hydro-, and wind power. We first illustrate the use

¹Over time the notions of AC OPF have evolved. The early theoretical formulations [4] are not always practiced by the industry [5]. Moreover, the choice of decision variables is often selected for the specific performance objectives. For example, real power transfer across large electrical distances and the least-cost generation dispatch are as a rule optimized by dispatching real power only. On the other hand, voltage dispatch is used to minimize delivery losses only. It is possible to create simple counterexamples that show how optimizing real power for least-cost generation and optimizing voltage for loss minimization is sub-optimal to optimizing both real power and voltage for the purposes of both maximizing real power transfer and minimizing generation cost. The outcomes are generally system specific.

of an AC XOPF for computing optimal voltage and optimal real power generation dispatch for those different generation and demand profiles. We then illustrate the use of AC XOPF for assessing the effects of replacing the existing diesel power plants by wind and/or solar power plants. Notably, we illustrate the trade-off between (1) dispatching wind power plants as must-run power plants and paying their O&M marginal cost, (2) dispatching wind power plants according to their leveled marginal cost and paying them accordingly, and (3) comparing (1) and (2) when payments are based on locational marginal pricing (LMPs). Depending on which of these pricing mechanisms is used, the value of candidate technologies will be very different. This is an important issue, and AC XOPF can be used to study the implications of these regulatory rules on long- and short-term social welfare, on generators' revenues and profits, and on customers' payments for electricity services. Most generally, none of these can be directly interpreted to support feed-in tariff rules. We observe that it is indeed possible to deploy and utilize new technologies at well-defined value as long as marginal cost internalizes the costs associated with each technology.

In Sect. 13.5 we use the electric power system of São Miguel island to illustrate the use of AC XOPF for optimizing the voltage set points for generators and on-load tap-changing transformers (OLTCs). We show how these optimal schedules vary with different seasons. We close by summarizing our main findings, recommendations, and open future issues. System data used in this chapter is made publicly available together with the other data in this book and can be used for further research and comparisons with other software presently used by the industry and/or under development. The numerical results are intended for illustration purposes only since further discussion with Electricite de Azores (EDA) engineers is needed to make sure that the data used is consistent with the data known to them. The objective is, again, to illustrate how one can proceed to explore different options and their effects on managing network congestion and not on specific numerical findings.

13.2 Basic Needs for Corrective Resource Management by Means of an AC XOPF

As electric power systems are required to support line power flow patterns which vary significantly over time, and/or are qualitatively different from the power flows anticipated when the system was built, the complexity of ensuring delivery within predefined voltage and thermal line limits becomes increasingly challenging. The highly combinatorial nature of what must be done by the system operator to avoid grid "congestion" makes it almost impossible to pre-program set points of the controllable equipment. Instead, as conditions vary, different combinations of controlled equipment require adjustments necessary to support reliable delivery of the least expensive and the cleanest power to the customers.

This chapter is concerned with methods for power and voltage dispatch which optimize a given system objective without violating hardware limits, such as minimum and maximum bus voltages and thermal line flow limits. This must be done so that both real and reactive power flows are balanced at each bus in the system. Given generation and demand dispatch obtained using ramp-rate-limited unit commitment/economic dispatch (UC/ED), industry practice has been to perform AC power flow analysis and check whether the steady-state solution is within pre-specified limits. A major problem arises when the solution is outside the acceptable limits and/or the AC power flow fails to converge; the latter is most often the case.² Resolving this problem requires decision-making software tools to find the best combination of what must be adjusted within the complex system to ensure that an AC power flow solution exists within the physical network limits.

Therefore, there exists a clear need for using AC OPF-based scheduling instead of AC power flow-based analyses. This distinction between the role of AC OPF and AC power flow, as decision and analysis tools, respectively, for managing network congestion is often blurry. We stress that having decision-making tools which find the best solution measured in terms of total generation cost, for example, is key to utilizing efficiently the available resources without creating steady-state power delivery problems. It is with this observation in mind that this chapter is written to illustrate how resources on today's Azores islands of Flores and São Miguel can be utilized efficiently based on carefully computed adaptations of set points on controlled generation and T&D equipment. These adaptations must be done during both "normal" operations when the equipment status is as expected and during "abnormal" conditions when unexpected forced equipment failures take place and/or during large wind power variations. In this chapter we illustrate the use of AC OPF for ensuring reliable and efficient asset utilization as seasonal generation and loads vary. The AC OPF-based mitigation methods for non-time-critical forced outages are in principle very similar to the scheduling methods during normal conditions, as long as the AC OPF can be performed to compute the most critical adjustments on line. In this chapter we assume that sufficient automation is in place to ensure that the system remains stable over the operating ranges of interest. This assumption implies that as generation and demand change, system dynamics transition from one steady-state to the next without experiencing stability problems.³

²See Part III for UC/ED review and its use for dispatch in the Azores islands.

³See Chap. 19 concerning automation for stabilizing dynamic transitions following large time-critical outages.

13.2.1 An Extended AC OPF Problem (AC XOPF)

An extended AC XOPF is fundamentally based on optimizing a cost function of interest subject to all network and equipment constraints. In particular, an AC XOPF can be characterized as follows:

- Having the ability to find a solution within specified network and hardware constraints
- Having the ability to optimize with respect to all available decision variables, such as real power generation, demand, and T&D voltage-controllable equipment
- Providing support of effective resource management according to several optimization objectives, such as economic dispatch, loss minimization, management of extreme voltages, maximum loadability into large load areas, and maximum power transfer [6]
- Providing as part of its output optimization sensitivities for assessing the effects of voltage constraints on performance objective of interest (optimization sensitivities with respect to voltage constraints (OSVs); optimization sensitivities with respect to real power generation constraints (OSPs); optimization sensitivities with respect to reactive power constraints (OSQs); and optimization sensitivities with respect to line flow constraints (OSFs))
- Providing as part of its output LMPs, which are sensitivities of the performance objective with respect to power injection change at each node in the network

Appendix A contrasts the use of such AC XOPF to today's use of DC OPF. We show that the DC OPF solution cannot be implemented without further adjustments because it does not observe real power generation limits, bus voltage limits, nor reactive power flow balance. Because of this, either it typically requires iterative reductions of optimal real power generation until the AC power flow solves or it requires actions by the system operator. In both cases the performance obtained is suboptimal by the time these adjustments are made. The second major cause of suboptimality comes from not optimizing voltage-dispatchable equipment while optimizing real power generation. We illustrate in this chapter the use of an AC OPF for on-line resource management in the electric systems of Flores and São Miguel. Results for both optimal real power and voltage dispatch are shown.

13.3 From Analysis to Optimization

are being presented with a variety of diverse energy resources, such as wind and solar power, adjustable load, and controllable T&D equipment. These new energy resources and controllable equipment offer opportunities to operate power grids in a different way as “smart grids”; the near real-time sensed data can be used for adjusting controllable equipment as system conditions vary. The measurements/data necessary to control a smart grid are becoming more readily available as syn-

chrophasors are being deployed in large numbers. Also, remote control of T&D equipment in new substations is becoming possible. At the same time, system integration and operations of these unconventional components represent multifold challenges, such as (1) lack of necessary data, (2) lack of robust software for timely decision-making given on-line SCADA data, (3) lack of remote monitoring and control of dispatchable equipment, such as controllable capacitors and OLTCs, and (4) lack of incentives to utilize these resources efficiently. Conditions vary with the status of the equipment and with constantly changing load and renewable power generation, decisions must be made on-line. Notably, making the most out of these new technologies requires system-level resource management, and this is generally very complex. It is generally difficult for the system operators to decide in an on line setting what should be the key adjustments. To make this possible it is necessary to provide engineers and other decision makers with software tools which can facilitate use of near real-time measurements, process them, and advise the operators regarding the most effective actions to take.

We stress the fact that an iterative process between running DC OPF to optimize real power dispatch and checking whether this dispatch ensures an AC power flow solution within the voltage limits is too combinatorial and often fails to converge. An AC XOPF provides answers to what else must be adjusted simultaneously and in an optimized way to enable the feasible and the least-cost generation dispatch.

Finally, an important use of AC XOPF is to provide insights about how the LMPs within a spatially vast complex power network with diverse resources connected to different nodes vary as a function of grid-related limitations. At present we have very little understanding and insights about this dependency. We show later in this chapter the trade-off between doing adjustable resource management, using central cheap generation and/or distributed generation in the island of Flores. As we move forward with relying on distributed resources, computer software for assessing these options will become essential. Notably, an AC XOPF capable of adaptively switching between using different performance metrics is essential for reconciling reliability and efficiency on-line when system conditions and topology change significantly over time [6].

13.4 AC XOPF-Based Dispatch in Flores

In this section we illustrate the use of an extended AC OPF in Flores island to show the results of network-constrained dispatch during normal conditions assuming different O&M costs of wind power. A 45-bus radial distribution system model is used to illustrate how AC power flow-constrained dispatch of existing power plants could be optimized as more wind power plants are built. We also examine the best locations to replace existing diesel power plants so that the LMPs on the island are the lowest.

Shown in Fig. 13.1 is a partial one-line diagram of a Flores electric power system. It can be seen that the existing hydro and diesel power plants are connected to two

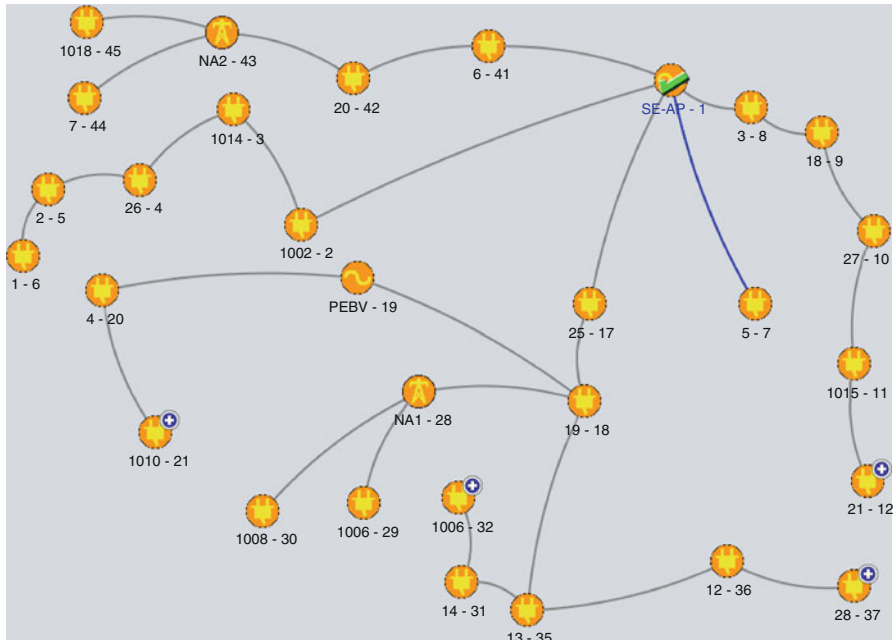


Fig. 13.1 One-line diagram of Flores electric power grid

major electrically close nodes numbered 1 and 46. While in the real system the two power plants are next to each other, the simulations performed here model the breaker connection between the diesel plant at node 1 and the hydro plant at node 46 as a very small impedance. A blue symbol + in this diagram indicates that the node is connected to more nodes on the same feeder beyond the scope of the figure. The spatial load distribution in Flores is shown in Fig. 13.2. The power unit base for this system is 10 MVA.

The AC input data for this system are made publicly available as part of this book. It can be seen in this input data file that the system begins with 12 islanded nodes. These nodes are disconnected for further discussion here. To illustrate the potential use of AC XOPF during normal operations, we consider the problem of minimizing generation dispatch cost assuming different costs of wind power.

Before starting to analyze different cases, we point out that at present there are major issues concerning the integration of wind and solar power relative to using central generation. The concerns are (1) possible technical problems leading to being unable to physically operate the system with the new resources because of not having feasible solutions within the hardware limits defined in (13.1)–(13.7)

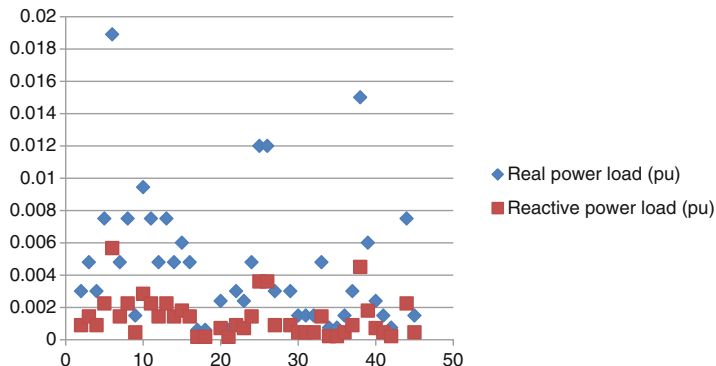


Fig. 13.2 Geographical distribution of load in Flores; the *x*-axis is the bus number 1–46; the *y*-axis is load in per unit (pu)

and/or maximum power transfer limitations to balancing real and reactive power at all nodes, as defined in (13.8)–(13.9) and (2) to reward new technologies for their contribution to reliability and efficiency.⁴ At present, the LMPs are only used at the EHV/HV wholesale level, and there are no retail prices which differentiate among distributed energy resources (DERs) located below the substation level. Three qualitatively different approaches for pricing wind power in operations are as follows (1) wind power bids are based on incremental wind power cost; (2) wind power bids are only O&M cost-based, like for conventional power, and it is expected that wind power plants would recover their capital cost in operations; and (3) wind power bids are only O&M cost-based, but there are feed-in tariffs which help offset capital cost. It is becoming necessary, however, to quantify the value of DERs to reliability and efficiency. This need is particularly pronounced in small confined systems like microgrids and islands.

To illustrate these issues three qualitatively different cases are considered:

- *Case 1:* Existing power plants, incremental cost of wind power similar to the cost of hydro
- *Case 2:* Existing power plants, incremental cost of wind power significantly lower than the cost of hydro
- *Case 3:* Diesel power plant replaced by inexpensive wind power plant of the same capacity

⁴The equations referred to are in the Appendix A.

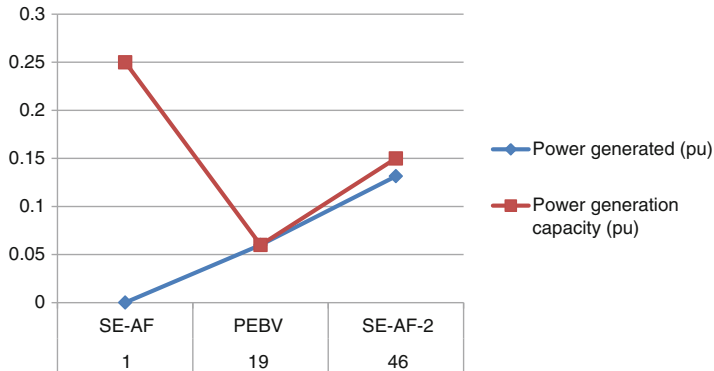


Fig. 13.3 Geographical distribution of optimal generation in Flores, wind power O&M cost 88 \$/MWh

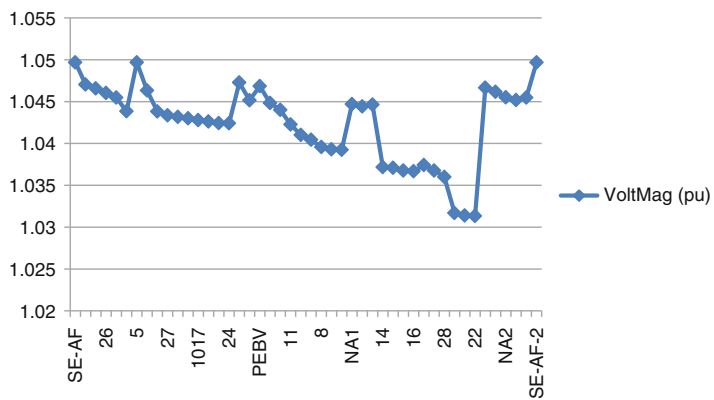


Fig. 13.4 Geographical distribution of optimized voltages in Flores, wind power O&M cost 88 \$/MWh

13.4.1 Optimal Dispatch of Existing Generation in Flores: Expensive O&M Wind Power (Case 1)

The O&M cost assumed for diesel, hydro, and wind power is 261 \$/MWh, 88 \$/MWh and 87 \$/MWh, respectively. These costs are used in all other chapters in this book, and the rationale for choosing them is described in Chaps. 4 and 11. Wind power plant is located at bus 19, hydro power plant at bus 46, and diesel power plant at bus 1. Total system load is 0.1697 pu, total generation is 0.1706 pu. Shown in Figs. 13.3 and 13.4 are the results of using AC OPF in this case. It can be seen in Fig. 13.5 that there is no need to dispatch diesel power generation in this case;

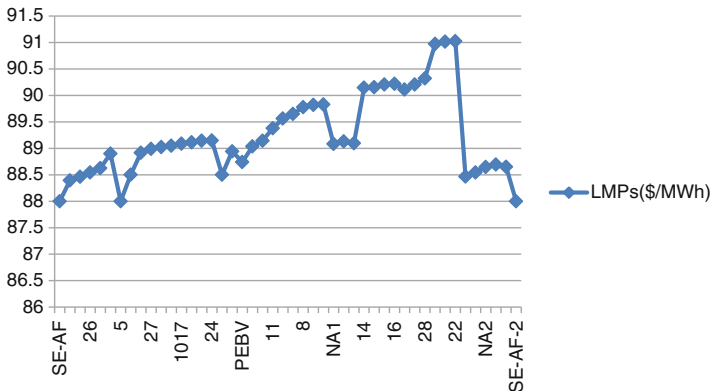


Fig. 13.5 Geographical distribution of LMPs in Flores; wind power O&M cost 88 \$/MWh

wind power plant is fully dispatched to its capacity of 0.05 pu, and the remaining generation is produced by the wind hydro power plant at bus 46. The corresponding generation dispatch cost is \$ 168.50 per given hour.

Consequently, all LMPs shown in Fig. 13.5 are near the highest marginal cost of the unit scheduled, in this case, hydro power plant. Notably, when voltages are allowed to vary between 0.95 and 1.05 pu, the effect of these constraints and of the nodal reactive power balance constraints is negligible. The optimal voltage profile obtained within these limits are shown in Fig. 13.4. Buses 1, 19, and 46 are generators supporting system voltage. There are no capacitors modeled in this system.

As introduced above, several key optimization sensitivities are available from the output of the AC XOPF used here. In this case, the optimization sensitivities with respect to the power limit at each node i (OSP_i) show that an increase of wind power at node 19 would further reduce the total generation cost. The generation OSP_{19} is -1.74 \$/pu and indicates that an increase of 10 MW capacity would further reduce total generation cost by \$1.74, namely, by roughly 1%. Moreover, the only non-negligible optimization sensitivity with respect to voltage (OSV) is at node 1 and it is OSV_1 is -0.22 \$/pu, and it implies that to reduce total generation cost by \$0.22 one would need to increase the voltage by 1 pu. This is insignificant and not feasible since voltages must remain within relatively tight limits. This is confirmed by re-running the AC OPF with slightly relaxed voltage limits on bus 1 from 1.05 to 1.1 pu. No significant cost difference is seen.

It is also interesting and important to understand how optimization sensitivities with respect to real power (OSP_i) at non-generation nodes could affect cost reduction. It can be seen from Fig. 13.5 that the highest LMPs are at load buses 39 and 40. These are the same nodes found in Chap. 12 to be the locations where new DERs should be placed to reduce delivery losses in Flores. The relatively small differences in LMPs between those at the generation locations and those at the far away load nodes are attributable in this case primarily to the delivery losses. The

delivery losses are less than 1 % of total load (0.1319 MW delivery loss) when voltage is optimized. It is important to note that total generation cost is almost the same (\$168.04 per hour) as the fixed load charges (\$169.98 per hour) and the difference is largely attributed to delivery losses. The difference between the total generation cost and load charges in later cases will be more pronounced.

It can be concluded based on our simulations of this case that Flores power grid is not limited in its ability to deliver the least-cost generation during normal conditions when all equipment is functioning. The determining cost factor is simply the availability of less expensive generation. The most significant optimization sensitivity is with respect to power generation (OSP_i) limit at bus number 19 to which the wind power plant is connected; this means that placing more wind at the same location would decrease the cost. It is $-1.74 \text{ \$/MW}$, meaning that in order to decrease the total generation cost of $168.95 \text{ \$/MWh}$ by \$1.74 one would need to connect 10 MW more generation wind power at bus 19. On the other hand, the highest OSPs are at loads connected to buses 39 and 40 and they are around $-90 \text{ \$/pu}$. This means that in order to decrease total generation cost by \$90 one would need to adjust the load at this bus by 10 MW, or place a large inexpensive DER at that location.

13.4.2 Optimal Dispatch of Existing Generation in Flores; Low-Cost O&M Wind Power (Case 2)

Case 2 has exactly the same optimization objectives, and the allowed voltage limits are the same as in Case 1. The only difference is that the O&M wind generation cost is $50 \text{ \$/MWh}$ instead of $88 \text{ \$/MWh}$. The resulting total generation cost is significantly reduced to $\$145.87$ per hour. However, the fixed load charges, if based on LMPs, in this case are much higher than the total generation cost, namely, they are about the same as in Case 1 (\$169.98 per hour). The merchandise surplus (MS) is caused by the LMPs at load buses remaining almost the same as in Case 1, and it amounts to \$1.735 per hour; the MS is attributable to the LMP differences caused by the delivery losses. The generation revenue is \$168.90 per hour, and the generation profit is high, around \$23.03 per hour. The system generation profit is much higher than in Case 1. All LMPs are the same as in Case 1, but the O&M costs are different. This results in higher generation revenue of the cheapest power plant connected to bus 19. Here, again, the power grid is not limiting, and the same generation is dispatched. Therefore, as expected, the only difference is seen in the settlement costs.

Finally, a comparison of optimization sensitivities with respect to reactive power (OSQs) for Cases 1 and 2 shown in Figs. 13.6 and 13.7, respectively, indicates that they are slightly different.

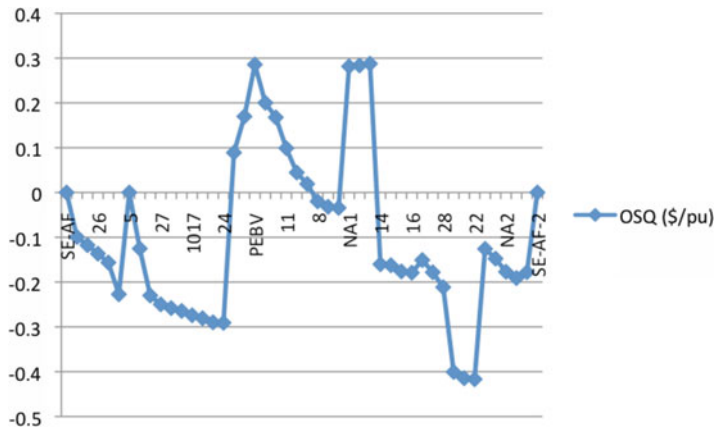


Fig. 13.6 Geographical distribution of OSQs in Flores, wind power O&M cost 50 \$/MWh

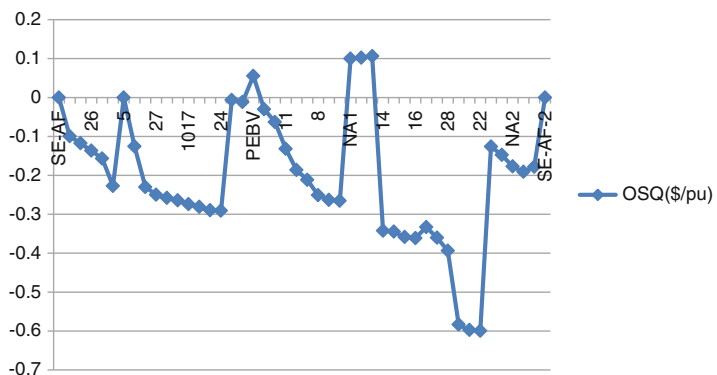


Fig. 13.7 Geographical distribution of OSQs in Flores; wind power O&M cost 88 \$/MWh

13.4.3 Diesel Power Plant Replaced by Inexpensive Wind Power Plant of the Same Capacity (Case 3)

This case considers a scenario in which a large amount of expensive diesel power currently connected to 1 is replaced by inexpensive wind power (50 \$/MWh) and the same inexpensive wind power plant is connected to node 19 as in Case 1. In this case the optimal economic dispatch results in a much lower total generation cost of \$95.58 per hour than in Cases 1 and 2; however, the generation revenue is almost the same and the system load charges are only slightly higher because of slightly increased delivery loss. The generator connected to bus 19 will produce at full capacity of 0.06 pu, and the generator connected to bus 1 would produce the

remaining 0.13 pu. All generator LMPs would be 50 \$/MWh, and all load LMPs would be very close to 50 \$/MWh (ranging from 51.73 \$/MWh at buses 40, 39, and 38 to 50 \$/MWh at the three generator locations).

The assessment in the entire section is done assuming fully predictable wind power generation. Since this is not realistic, further analysis of cost of uncertainties created by wind power deviations from its predictable patterns is needed.

13.4.4 The Effects of Electricity Pricing on Economic Outcomes

Based on the observations in Cases 1–3 above, it can be concluded that the effects of location choice for inexpensive wind power integration in Flores on O&M generation cost are not significant. However, the selection of pricing mechanism are shown to be significant. In particular, in Cases 2 and 3, while the total generation cost is not very different, the generation profits and revenues collected, as well as the payments by the electricity users, could be qualitatively different depending on whether wind power is paid using levelized cost or only O&M cost. Therefore, the ultimate ability of wind power plants to recover their capital cost depends on their location and the overall amount of inexpensive generation available. If all power is provided by the inexpensive resources, the generation revenue and profit will be insignificant. In this case, either LMPs created by higher costs of other power plants or incremental marginal cost (which includes capital cost) should be allowed to recover the cost. The LMP-based pricing mechanism charges load the LMPs at their locations, and generators are paid the LMPs at their own locations. Assuming such pricing mechanisms, for a given system, and a typical annual load profile, one could compute the breakeven wind power capacity which can be built so that its cost is recovered. This breakeven point depends on other LMPs in the system and cannot be estimated by the wind power plant itself without an estimate of what LMPs will be.

Everything else equal, load charges depend on the locations and the electrical characteristics of the system to which renewable resources are connected. For the island of Flores, typical load charges vary in the range of \$160–\$170 per hour, for any combination of resources. This includes having a large capacity of inexpensive wind power close to the users. The total generation cost is the lowest, but the load charges cannot be reduced significantly because the marginal hydro unit sets the LMPs. In Cases 1–3 there is no sufficient generation to supply the entire demand with inexpensive wind power generation. For the case of Flores, total generation cost can be reduced depending on how much inexpensive generation is available. On the other hand, the rate at which generators can recover their capital cost based on their profits (difference of revenue and cost) is definitely dependent on other available generation, system demand, and the electrical characteristics of the grid.

Similarly, the actual load charges paid by the customers will depend on the combination of available generation and the electrical grid characteristics. As policy decisions are made regarding wind power tariffs these factors should be taken into consideration. It is possible to estimate the “optimal” investment and location of new power plants by considering them as replacements of the existing more expensive power plants, which would guarantee that the expected total cost of new power plants would be recovered over certain prespecified time. While the locational aspects of LMPs make it more complicated to compute such investments, it is worthwhile performing such planning studies to ensure the lowest possible long-term social welfare maximization.

13.5 AC XOPF-Based Dispatch for São Miguel Island

In this section a large 2000-bus meshed-radial power system model of the São Miguel island grid is used to illustrate how grid constraints change with seasonal variations in geothermal power and system demand. We describe the use of an AC XOPF-based approach for optimizing resources in two different seasons, winter and summer, using the data of São Miguel island. We compute optimal resource management for both seasons and illustrate the need for different dispatch strategies in each season. For completeness, we include the power flow data used in this chapter for São Miguel Island in the publicly available data accompanying this book. In this system data only several transmission and distribution lines are assumed to be thermally limited. Several transformers are modeled as the OLTCs having voltage-controlling capabilities. They are considered to be a potential means of helping support the voltage profile on the island by changing their tap ratios. Also, generator voltages are assumed to be voltage-controlled by adjusting the set points of their AVR. The AVR of generators and OLTCs are the main voltage-controlled equipment on the island. It is assumed that all power plants can control their real power generated within the minimum and maximum limits. The hydro- and geothermal power plants have different maximum power generation limits in different seasons, as documented in Chap. 4 of this book. Similarly, the peak and minimum forecast system demand vary with seasons.

The cost and locations of the generations within the 2,000 bus network power system representation of São Miguel electric system are shown in Fig. 13.8. Physical variables are in per unit (pu) with a power base of 100 MVA. The O&M cost is given in 100 \$/MWh. For the island of São Miguel, the O&M cost of diesel-, hydro-, and geothermal power is 185 \$/MWh, 88 \$/MWh, and 28.10 \$/MWh. Clearly, given these O&M costs, it is beneficial for this island to build more geothermal power; most recently two new 900 kW wind power plants were built and are already in operations; they are not part of the analysis in this book. They are located in the Graminhais facility, the Northeast part of the island. Voltage-controlled transformers and their ratio ranges are shown in Fig. 13.9.

Gen #		Pmin	Pmax	Qmin	Qmax	MCost
1	932	1	0	0.32688	-0.29453	0.29453
2	933	1	0	0.32688	-0.29453	0.29453
3	934	1	0	0.32688	-0.29453	0.29453
4	963	1	0	0.1	0	0
5	1049	1	0	0.1	-0.10954	0.10954
6	1666	1	0	0.0067	-0.00742	0.00742
7	1669	1	0	0.008	-0.006	0.006
8	1672	1	0	0.00608	-0.005	0.005
9	1675	1	0	0.00553	-0.00373	0.00373
10	1676	1	0	0.00553	-0.00373	0.00373
11	1677	1	0	0.00553	-0.00373	0.00373
12	1680	1	0	0.00094	-0.00129	0.00129
13	1683	1	0	0.004	-0.003	0.003
14	1686	1	0	0.004	-0.003	0.003
15	1687	1	0	0.004	-0.003	0.003

Fig. 13.8 Characteristics of generators on the island of São Miguel

13.5.1 Results of Using AC XOPF to Optimize Economic Efficiency

In this section we use the AC XOPF to compute optimal real power generation and optimal set points of voltage-controlled equipment to ensure that the forecast demand is met in the least-cost manner. The total generation cost of supplying demand by scheduling the least expensive units is generally considered to be the basic measure of short-term economic efficiency. Extensions of this objective to include environmental constraints can also be done [8]. We show that the optimal voltage profile and real power generation are different for winter and summer load and generation, in particular. Moreover, we show that the total generation cost depends on the type of scheduling performed and on the line flow limits observed.

From Bus	To Bus				Min Ratio	Max Ration
939	942	0	1	1	0.911247	1.071247
940	941	0	1	1	0.911247	1.071247
958	957	0	1	1	0.93059	1.09059
974	84	0	1	1	0.902988	1.062988
982	983	0	1	1	0.904659	1.064659
999	1000	0	1	1	0.94693	1.04693
1012	1010	0	1	1	0.914655	1.074655
1013	1011	0	1	1	0.914655	1.074655
1021	1024	0	1	1	0.970245	1.130245
1615	956	0	1	1	0.882775	1.002775
1616	959	0	1	1	0.882775	1.002775
1639	1023	0	1	1	0.94519	1.10519

Fig. 13.9 Characteristics of voltage-controlled transformers on the Island of São Miguel

13.5.2 *Dependence of Generation Dispatch and Its Cost on Control Equipment Used*

To illustrate the potential use of an AC XOPF for adjusting voltage-controlled T&D and generation equipment in support of efficient economic dispatch, we consider the following cases:

- *Case 1*: Maximum load winter case
- *Case 2*: Maximum load summer case

We next describe the resulting voltage profile, optimal real power generated, total generation cost, and LMPs for these two cases. We illustrate their dependence on the observed network constraints and on the type of voltage-controllable T&D and generation equipment optimized. The two cases are qualitatively different in terms of load served and maximum geothermal and hydropower generation available. The load is somewhat higher in summers, primarily because of tourism. Also, maximum available real power generation capacity from geothermal plants is higher in the summer than in the winter. In what follows we summarize the results of using an AC OPF for dispatching optimally generation available in each season.

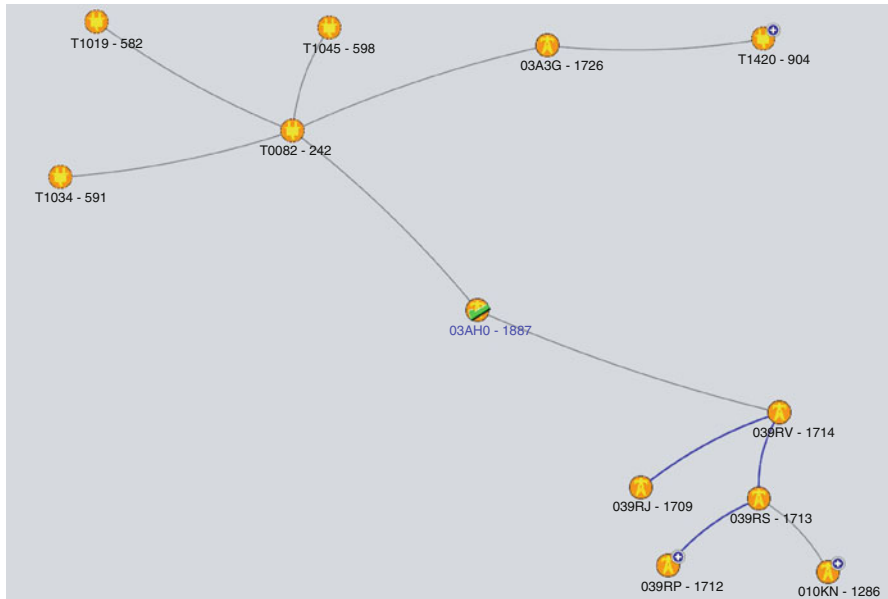


Fig. 13.10 One-line diagram of the São Miguel electric power grid in the vicinity of the congested line 1887-1714

13.5.3 Economic Dispatch and Its Cost for Maximum Load Winter Case (WC)

The binding thermal line constraint for this case is found to be the 10-kV line connecting buses 1,887 and 1,714. A portion of São Miguel electric network in the vicinity of this line is shown in Fig. 13.10. To begin, it is not possible to fully supply load when this thermal limit is observed. It becomes necessary to partially shed load or relax some of the network constraints. Longer term, it is necessary to deploy smaller-scale distributed generation at some key locations in order to serve loads in that area without overloading the distribution equipment. For purposes of further analysis, we demonstrate the effects of thermal limits on power dispatched and its cost while observing thermal line flow limits given in (13.5) for all lines except for this low-voltage line. Minimum and maximum voltage limits at all buses in the system as defined in (13.4) and (13.3) are set to 0.95 and 1.05 pu, respectively. Settings of voltage-controlled transformers shown in Fig. 13.9 have nominal transformer ratio of 1. For this case the total hourly generation cost shown in (13.10) is \$10,394. Total AC line losses are 0.0106 pu and total real power generated is 0.63056 pu and total load served is 0.620146 pu. Total reactive power generated is 0.12288 pu. Total AC line reactive power losses are -0.03208 pu, and total transformer reactive power losses are 0.017559 pu. Optimized voltage load profile of 60 kV generators, optimized voltage profile of all buses, loads and

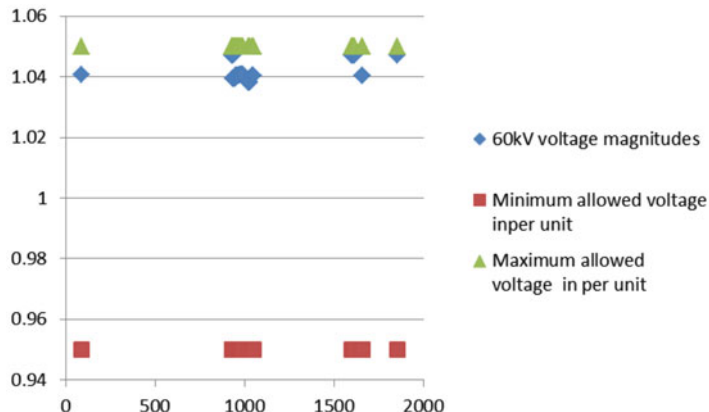


Fig. 13.11 Optimized voltage profile of generators; 1887-1714 thermal line flow limit ignored (WC)

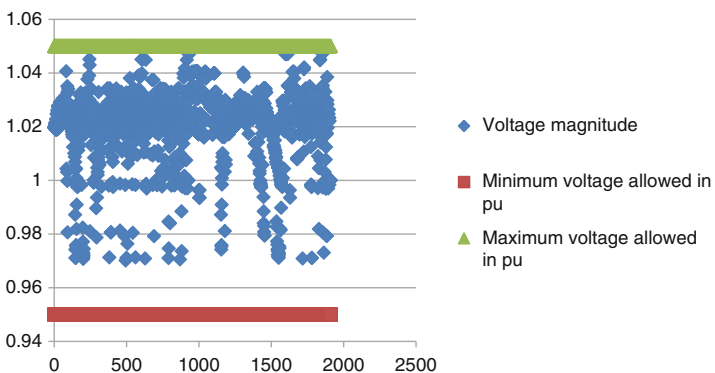


Fig. 13.12 Optimized voltage profile of all buses; 1887-1714 thermal line flow limit ignored (WC)

generators, real power generated, and electricity prices are shown in Figs. 13.11–13.14, respectively. Generators are ordered as shown in Fig. 13.8. It can be seen that by using AC XOPF, it is possible to maintain all voltages within the prespecified operating limits. Two most expensive oil generators are scheduled to full capacity of 0.32 and 0.22 pu, respectively. The resulting LMPs of these generators are shown in Fig. 13.14. The generation output and LMPs of other generators are also shown in this figure.

Notably, LMPs of many generators are higher than the O&M cost of the marginal diesel power plant which is 185 \$/MWh as shown in Fig. 13.14. This means that the effect of various network constraints jointly contribute in a non-negligible way to the locational price increase. The AC XOPF used for analysis in this chapter

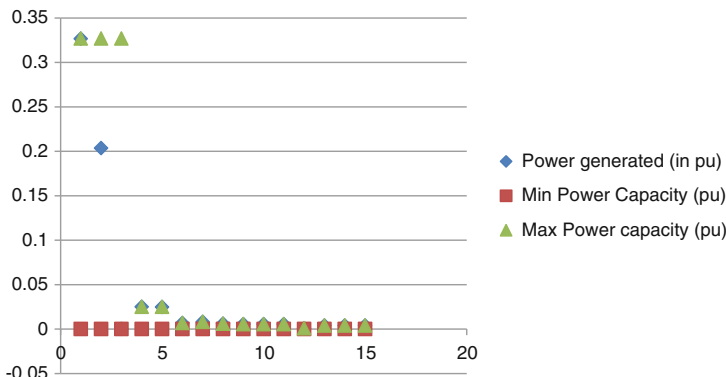


Fig. 13.13 Real power generated (WC)

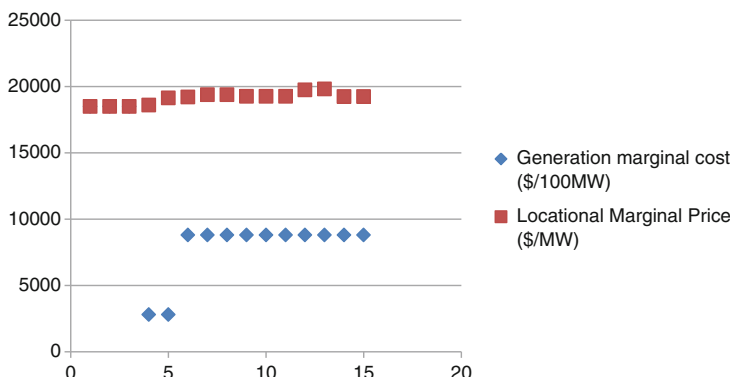


Fig. 13.14 Locational marginal prices of generators (WC)

[9] indicates that the solution has several binding voltage constraints. In particular, optimization sensitivities with respect to both real and reactive power injections (OSPs and OSQs, respectively) at different low-voltage buses are quite high.

13.5.4 Use of AC XOPF for Managing the Effects of Critically Congested Lines

The optimization sensitivities with respect to flows (OSFs) indicate that a small line connecting nodes 1887-1714 is thermally limited; moreover, it becomes necessary to adjust settings of OLTCs to obtain a solution within the given voltage limits. Most of the runs in this section for the maximum load winter case are made with the thermal limit disabled. The effects of optimizing set points of OLTCs are illustrated in the next section for the maximum load summer case. Interestingly, when the

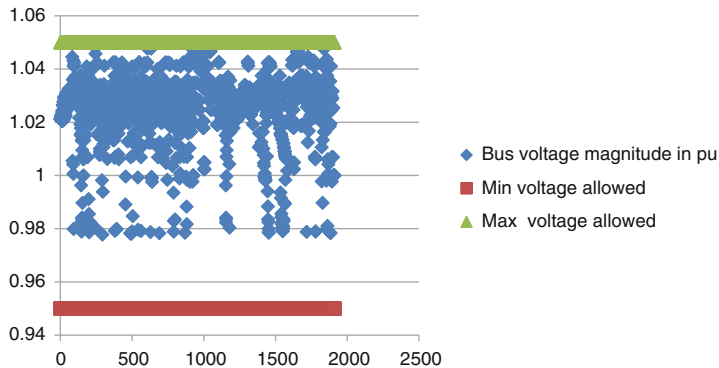


Fig. 13.15 Optimized voltage profile of all buses, 1887-1714 thermal line flow limit ignored (SC)



Fig. 13.16 Real power generated, 1887-1714 thermal line flow limit ignored (SC)

limiting line 1887-1714 is taken out of operations, the AC power flow is easily obtained and the resulting total economic dispatch cost is \$10,400 per hour at peak load. In Sects. 13.5.6 and 13.6 below we illustrate the use of other performance objectives available in an AC XOPF to find the alternative relaxation of line flow or voltage limits which help solve the power flow. Finding such actions gives system operator other options since some of the hardware limits are not necessarily hard limits.

13.5.5 Economic Dispatch and Its Cost for Maximum Load Summer Case (SC)

Shown in Figs. 13.15–13.17 are the optimized voltages at all buses, optimal power dispatched, and LMPs for the case when the thermal line flow limit is not observed

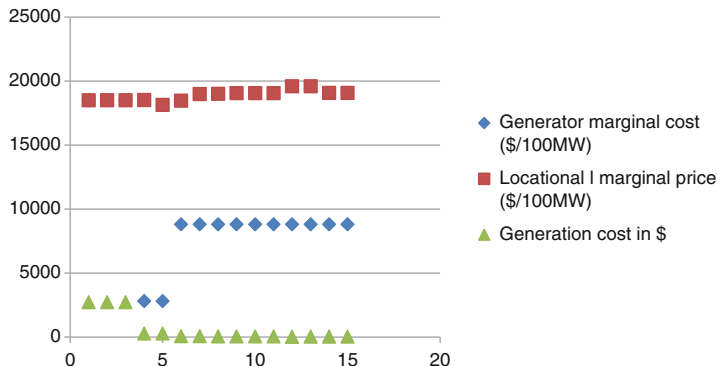


Fig. 13.17 Locational marginal prices of generators with 1887-1714 line limit observed (SC)

on line 1887-1714, and transformer ratio of controllable generators is set to 1. The total generation cost in this case is \$ 9,147 per hour. The total power generated is 0.69045 pu and power consumed is 0.6773 pu. Three expensive generators are dispatched at about 0.147 pu output each, and the rest of the power is produced by the geothermal power plants at buses 1,049 and 963 producing about 0.1 pu power. The highest LMPs are, similar to the winter load case, at the low-voltage 10 kV buses. The highest LMPs are \$208./MWh at buses number 494 and 294. The highest optimization sensitivity with respect to voltage constraint is $OSV_{1049} = -1.610$, and with respect to real power is OSP_i is $-15710 \$/pu$ at one of the 60-kV generators. The highest LMPs are at 6.3 kV low-voltage load buses numbered 1600-1615 in the input data.

13.5.6 Use of AC XOPF for Relaxing Voltage Limits for Reliability

Another option for minimizing economic dispatch cost when the critical thermal line limit prevents power flow solution within the prespecified limits is to first find the key limits which should be relaxed. Once this is found, an economic dispatch minimization can be attempted within the relaxed limits [6]. This use of different performance objectives is made possible by an AC XOPF, such as the one used in this chapter [9]. In this case the first performance objective is to minimize the voltage limit which must be relaxed in order to ensure that power flow converges within these relaxed limits. The use of an AC XOPF for this purpose is referred to as the manage extreme voltage (MXV) function in the AC XOPF used. Alternatively another performance objective would determine the amount by which the critical line flow limit itself should be relaxed can be used to find by how much in this case the thermal limit of line 1887-1714 should be relaxed to find a power flow

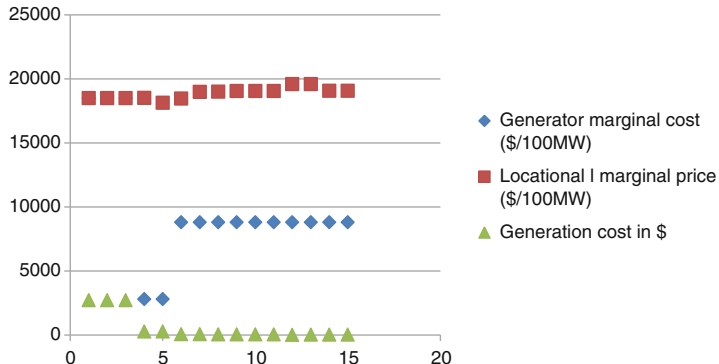


Fig. 13.18 Locational marginal prices of generators, 1887-1714 thermal line flow limit ignored (SC)

solution. The desired objective function is referred to in the AC XOPF used for simulations in this chapter as the optimal branch flows (OBF). We point out that having these new functions for relaxing prespecified limits first is an important feature as more sensing and management of T&D equipment becomes available. In particular, having so-called dynamic line rating sensors (DLRs) will enable more adaptive use of equipment. Trade-offs between reliability and efficiency benefits obtained from relaxing equipment limits, on one side, and the reduced lifetime of the equipment need to be assessed to make the most out of available resources at value. These alternative actions are particularly suited during short-term emergencies.

13.5.7 Effects of Optimizing Tap Transformer Voltage Settings

In order to assess the potential of optimizing set points of voltage-controlling transformer ratios, a network-constrained economic dispatch is run when observing all thermal line limits, including line limit for 1887-1714 congested line. Simulations have shown that when ratios are kept fixed, it is not possible to supply the entire load without relaxing some other constraints. It is possible to build more distributed generation, but in the actual operations only partial load shedding is possible by either allowing for load voltage limits to exceed prespecified limits and/or by selectively reducing load served.

Notably, when the ratios of voltage-controlled transformers are optimized, it becomes possible to serve the entire load without having to relax any prespecified thermal or voltage limits. The results of this optimization are shown in Figs. 13.19 and 13.20. Also, shown in Fig. 13.21 are the optimized settings for controllable transformers when thermal line limit of line 1887-1714 is taken into consideration.

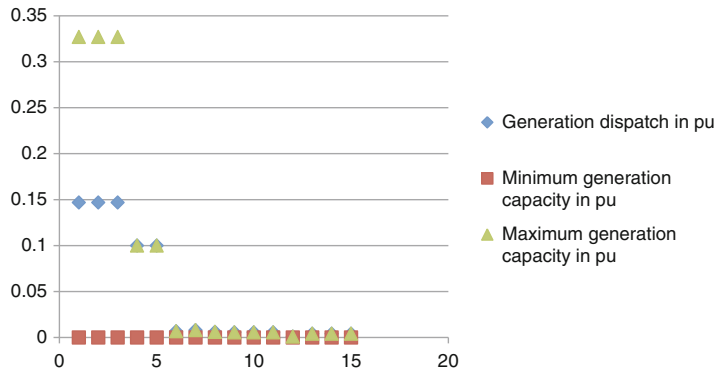


Fig. 13.19 Real power generated with 1887-1714 line limit observed (SC)

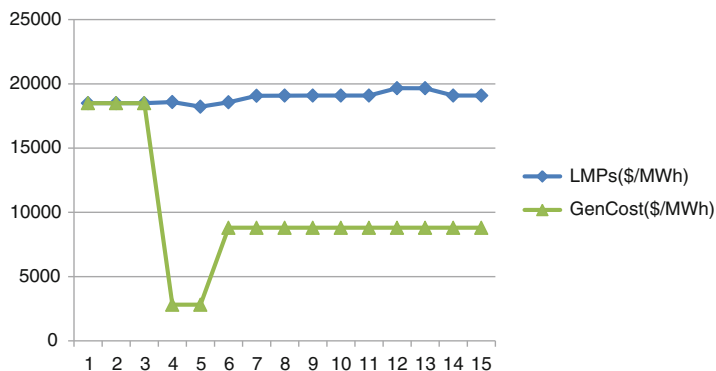


Fig. 13.20 Locational marginal prices of generators with 1887-1714 line limit observed (SC)

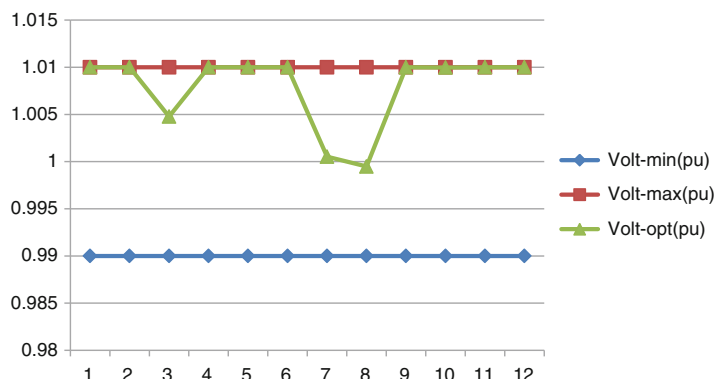


Fig. 13.21 Optimal ratios with 1887-1714 line limit observed (SC)

The total generation cost is increased only very slightly to \$9,157/hour when compared to the case when the line limit is not observed. These simulations show that it is indeed possible to have both reliable and very efficient dispatch when selectively adjusting the settings of controllable T&D equipment. When running AC power flow analyses without adjusting settings of OLTCs, the scenario is simply labeled as being “improperly posed” because power flow fails to converge. On the other hand, an AC XOPF seeks the most effective adjustments over all controllable equipment and manages to find a feasible power flow solution. The value of voltage-controlled T&D equipment is, therefore, not only for reducing delivery losses, as it is commonly thought to be. As illustrated here, this equipment plays a key role in enabling reliable solutions.

13.6 Use of an AC XOPF to Maximize Physical Efficiency of Power Delivery: Loss Minimization

An AC XOPF is used next to minimize delivery losses. The results should be compared to the results obtained above when optimizing for economic efficiency. While the equipment limits within which the power delivery can be made are the same in these two optimizations, the optimized real power and voltage are very different because the cost functions are not the same. The minimum power delivery generally requires higher generator voltage settings. This is not the case when optimizing for economic efficiency which requires dispatch from the least-cost and cleanest resources first, independent from the resulting delivery losses created.

13.6.1 Dependence of Delivery Losses on T&D Equipment Adjustments

An AC XOPF was run to illustrate the effects of optimizing voltage-controllable T&D equipment on loss optimization. Shown in Figs. 13.22 and 13.23 are optimized real power generation and voltage in support of loss minimization. It can be seen by comparing Figs. 13.18 and 13.22 that minimizing T&D losses in São Miguel results in higher generation by all three expensive diesel power plants and in the reduced use of one of the inexpensive and clean geothermal power units when compared to the economic dispatch results. As expected, this leads to lower economic efficiency measured in terms of total generation cost than when scheduling is done for optimizing economic efficiency. Also, it can be seen in Fig. 13.23 that the generator voltages needed to minimize delivery losses are very close to the high voltage limits allowed. This comparison highlights an important distinction between physical delivery efficiency and economic efficiency in future electric energy systems.

In summary, when voltage settings on both generators and OLTCs are optimized for loss minimization, the minimum loss achieved is 1.253 MW (AC line losses)

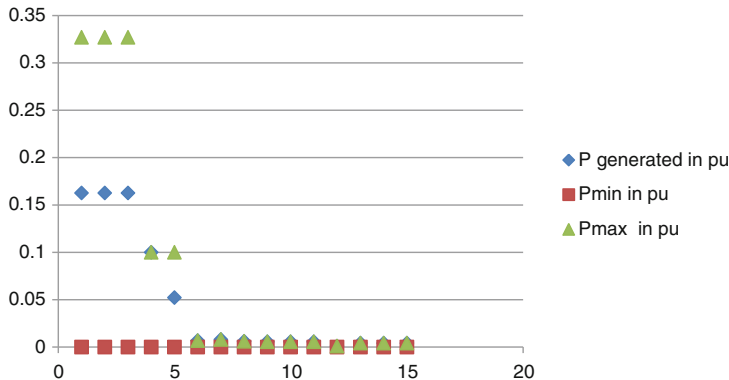


Fig. 13.22 Optimal power generation, loss minimization

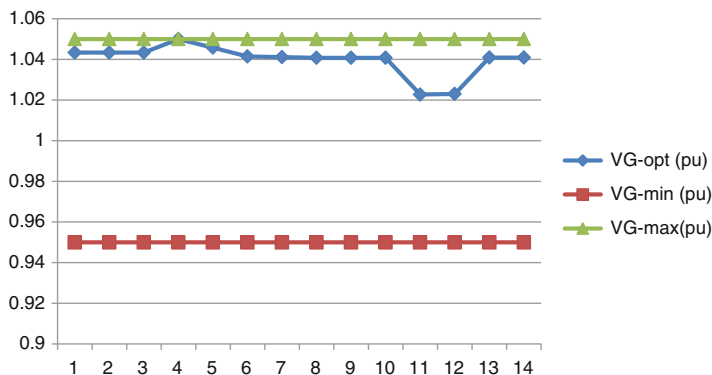


Fig. 13.23 Optimal generation voltage profile; loss minimization

and the transformer losses are negligible. All voltages are kept between 0.95 and 1.05 pu. Total generation needed to meet load of 67.73 MW is 69.04 MW. Even with all voltage-controllable equipment optimized the OSF of the 10 kV line 1887-1714 is significant, namely, $-8.25 \text{ \$/pu}$. This clearly indicates that the line thermal limit prevents a fully solved power flow. Attempting either economic efficiency or physical efficiency requires that this thermal limit be increased by building a stronger line. The most sensitive voltages are at buses 1049, 1048, and 1659, and they are around $-1.98 \text{ \$/pu}$; this means that increasing the upper voltage limit at these buses would help further reduction of delivery losses. It is important to observe that several low voltage buses (01NMD, 01NM7, and 039K5) have voltage limits set too high; this is reflected in their OSVs being positive. The OSPs are most significant at buses 1680 and 1683, and they are around $-5.68 \text{ \$/pu}$. They indicate that placing small power sources, PVs, for example, at these locations may help reduce system losses as well. There are also several other buses enumerated 1670-1680 at which placing small PVs may also reduce system losses. Finally, placing more reactive

power support at several power plants (geothermal at bus 963; and hydro at 1666, 1672, 1680, and 1683) could help reduce system losses. This effect is not very major as the OSQs at these buses are only around -0.5 \$/pu; therefore, building more capacitors would not solve the problem.

13.7 Concluding Remarks

Based on the simulations above, it can be concluded that the use of AC XOPF-based dispatch of real power generation and T&D and generation voltage-controlled equipment offers an important approach to utilizing the assets efficiently while ensuring that all equipment and network constraints are met. It is shown that optimization of mechanically switched transformer ratios could improve reliability by helping maintain thermal line flows within the prespecified limits. This ensures that the least-cost and the cleanest possible generation is utilized. The use of AC XOPF-based optimization of all controllable equipment is shown to lead to lower cost of generation dispatch during summer when demand is higher than during winter. This is a result of combined optimization of voltage and larger maximum hydro power capacity. For complex systems it is effectively impossible to find the best combination of controllable equipment and optimal setting without relying on a powerful nonlinear optimization tool such as AC XOPF. This point is greatly confirmed by comparing the optimized ratios of voltage-controlled transformers when a thermal limit of a critically congested line is observed and when it is relaxed.

While the corrective on-line approach to adjusting settings of controllable T&D and generation equipment is shown to be potentially very useful for efficient and reliable delivery of clean and inexpensive power, the actual implementation of AC OPF power flow should be pursued with care. In particular, only the most effective control actions should be implemented to ensure that most of the benefit is achieved in timely manner and without adjusting equipment with small effects on performance. The AC OPF used for optimizing adjustments in this chapter has useful features of showing the highest optimization sensitivities with respect to different candidate controllers. The same optimization sensitivities can be used to decide on the best locations for placing many small distributed generation resources and controllers as the system evolves. A particularly interesting question concerns locating the best places for low voltage photovoltaics and the calculation of cost-effective investments in solar power to help further reduce the economic dispatch cost.

Finally, the use of on-line corrective adjustments of the existing controllable equipment generally requires more frequent resetting of mechanically switched T&D equipment and leads to some wear-and-tear and shortened lifetime of this equipment. While this is generally not optimal when viewed from the long-term investment point of view, it is necessary to compare the cost of wear-and-tear with the lost opportunity cost from not utilizing system resources efficiently. In principle, there exists a break-even point at which the two become equal. Deviations from this

optimal use of controllable equipment invariably lead to worsened long-term system performance. It is important to use AC OPF-based simulations to understand the trade-offs between different software and hardware solutions.

Appendix A: An Extended AC OPF (AC XOPF)-Based Dispatch for Future Electric Energy Systems

As the electric power systems are required to support power flow patterns which vary significantly over time, and/or are qualitatively different from the power flows anticipated when the system was built, the complexity of ensuring delivery within predefined voltage and thermal limits becomes increasingly challenging. The highly combinatorial nature of what must be done by the system operator to avoid grid congestion makes it almost impossible to find a single set of adjustments needed by the controlled equipment. Instead, as conditions vary, a combination of controlled equipment needs adjustments to support delivery of the least expensive and cleanest power to the customers.

In operations the main problem is how to adjust the set points of controllable generators (power generated and voltage) and of controllable T&D equipment (transformers, capacitor banks) so that the least-cost and cleanest generation is used to the greatest extent possible. Even more complex are decisions concerning how to adjust loads and at which locations in the grid to differentiate among their unique needs and preferences. On-line decisions should also be made about which soft limits, such as thermal line limits dependent on weather, to temporarily relax, and by how much, given technologies such as DLRs.

The problem of optimal network-constrained dispatch is well known, and its formulation can be found throughout the literature. While all formulations draw on the early AC OPF formulations [4], the many software implementations are diverse and formulated with different objectives and under different assumptions. To avoid confusion, we briefly summarize the problem formulation of what we refer to as an AC XOPF next.

As discussed earlier in this chapter, an AC XOPF should have several new characteristics, when compared to today's optimization tools in order to advise system operators seamlessly about the state of system and the actions to take and reasons for such actions. These characteristics are restated and described in some detail next.

- An AC XOPF should be capable of computing a solution within all hardware and network constraints.
- An AC XOPF should have the ability to optimize with respect to all available decision variables, such as real power generation, demand, and T&D voltage-controllable equipment.
- An AC XOPF should be able to provide support of effective resource management according to several optimization objectives, such as economic

dispatch, loss minimization, management of extreme voltages, maximum loadability into large load areas, and maximum power transfer [6].

- An AC XOPF should provide as part of its output optimization sensitivities for assessing the effects of voltage constraints on performance objective of interest such as Optimization Sensitivities with respect to voltage constraints (OSVs); Optimization Sensitivities with respect to Real Power Generation constraints (OSPs); Optimization Sensitivities with respect to Reactive Power constraints (OSQs); and Optimization Sensitivities with respect to Line Flow constraints (OSFs)).
- An AC XOPF should provide as part of its output LMPs, which are Optimization Sensitivities of Performance Objective with respect to Power Injections at each node in the network.

AC XOPF Must Optimize with Respect to All Available Decision Variables

Optimizing with respect to all available variables is numerically challenging. The AC XOPF used for simulations in this chapter is numerically robust; this feature is essential when one needs on-line decisions. In early implementations of AC OPF programs, it was typical to optimize with respect to the subset of the decision variables of interest. In particular, when optimizing the decision variables are real power injections. Similarly, when optimizing delivery losses, voltage controllable T&D equipment is optimized. An AC XOPF generally out-performs such AC OPFs because it generally finds a combination of adjustments which is an optimal mix of both real power injections and the voltage-controllable equipment.

AC XOPF Must Satisfy all Hardware and Network Constraints

A typical electric power system is characterized by defining⁵:

- The capacity and rate of response of power plants
- The loads
- The transmission lines and their thermal limits
- Switching equipment, such as controllable capacitor shunts and phase-angle regulators

⁵The transient response is not considered here; therefore, no dynamic equations are offered to define this. The assumption is that the transitions from one state to the next are stable. For more detailed treatment of secure operating regions which account for system dynamics see Chaps. 2 and 2 of this book.

- Power-electronically switched devices, such as DC lines and Flexible AC Transmission Systems (FACTS)
- Network connections, topology, and parameters of the above listed individual hardware

More specifically, the characterization of individual components and the network constraints, respectively, is as follows:

- The constituent relations of all grid components must be satisfied.
 - (a) Each generator i is characterized as a component whose real power output can be set to any value P_{Gi} within the physical capacity of the generator, namely, the minimal permissible power P_{Gi}^{\min} and the maximum possible power P_{Gi}^{\max} , for all generators i . Simultaneously, each generator can maintain constant voltage (magnitude) V_{Gi} at its terminals as long as there is enough reactive power generation within the minimum and maximum limits Q_{Gi}^{\min} and Q_{Gi}^{\max} . These constraints are expressed as

$$P_{Gi}^{\min} \leq P_{Gi} \leq P_{Gi}^{\max} \quad (13.1)$$

$$Q_{Gi}^{\min} \leq Q_{Gi} \leq Q_{Gi}^{\max} \quad (13.2)$$

$$V_{Gi}^{\min} \leq V_{Gi} \leq V_{Gi}^{\max} \quad (13.3)$$

If these limits are violated, the under- and/or overvoltage protection of a power plant will disconnect the power plant from the rest of the system for safety.

- (b) Each load j is characterized as a sink of constant real and reactive power P_{Lj} and Q_{Lj} , respectively. The voltage magnitude V_{Lj} at the bus where the load is connected is allowed to vary within the prespecified minimum and maximum limits V_{Lj}^{\min} and V_{Lj}^{\max} , namely,⁶

$$V_{Lj}^{\min} \leq V_{Lj} \leq V_{Lj}^{\max} \quad (13.4)$$

- (c) Each transmission line connected between buses i and j is characterized by its lumped parameters, resistance R_{ij} , reactance X_{ij} and shunt capacitance B_{ij} , and by its thermal line flow limit F_{ij}^{\max} .⁷

$$F_{ij}^{\min} \leq F_{ij} \leq F_{ij}^{\max} \quad (13.5)$$

⁶These limits are specified strictly for the purpose of ensuring that the customer power quality specifications are met. Depending on the type of load and the degree of aggregation, more complicated load characterization can be used, such as voltage- and frequency-dependent real and reactive power consumption of the load. Also, an important open question concerns representation of the load participating for the purposes of demand-side management.

⁷The power flow is limited in both directions. The F_{ij}^{\min} defines the thermal limit in the opposite direction.

Similar flow limits must be observed for transformers. Flow limits can be real, reactive, or apparent power.

Depending on the time over which the line constraint would be active, the line flow limit can be lower or higher. Typical ratings for thermal line limits are known as the normal (A), long-term emergency (B), and short-term emergency (C) line ratings and are more relaxed for shorter durations.⁸ In particular, ratings B and C are used during equipment outage, and rating A during normal prolonged operations. For purposes of discussion in this chapter, it is important to differentiate these limits, which are defined by the properties of the line, from the line flow transfer limits introduced for purposes of avoiding system problems.

- (d) Each controllable shunt capacitor is characterized by its electrical parameters and its control logic. Today's practice has been to pre-program the settings based on off-line worst-case studies and, less frequently, for normal, peak, and low load conditions. For the purposes of this chapter it is important to observe that the susceptance of the shunt capacitors has control limits

$$C_i^{\min} \leq C_i \leq C_i^{\max} \quad (13.6)$$

- (e) Each controllable transformer is characterized by its electrical variables and its control logic; today's practice has been to pre-program the settings based on off-line worst-case studies and, less frequently, for normal, peak, and low load conditions. Each transformer has limits to its range of controllable transformer ratios

$$R_{ij}^{\min} \leq R_{ij} \leq R_{ij}^{\max} \quad (13.7)$$

- Network power flow constraints must be satisfied at all nodes. These state that real power P_i injected into any bus i which is the sum of power generated P_{Gi} , consumed by the load P_{Li} and by the shunt P_{Shi} must equal to the sum of real power line flows F_{ij} flowing away from the bus into the network according to

$$P_i = P_{Gi} - P_{Li} - P_{Shi} = \sum_j C_i F_{ij} \quad (13.8)$$

Similarly, the reactive power balance at each bus must be met. The net reactive power injected into the node i , which is the algebraic sum of reactive power generated at the node Q_{Gi} , reactive power consumed by the load Q_{Li} and by the shunt Q_{Shi} , must equal the sum of reactive power line flows Q_{ij} flowing away from the bus into the network:

$$Q_i = Q_{Gi} - Q_{Li} - Q_{Shi} = \sum_j C_i Q_{ij} \quad (13.9)$$

⁸Rating A is a normal conditions rating; ratings B is a long-term emergency rating; rating C is a short-term emergency rating. All ratings are weather dependent. More recently DLR sensors are beginning to be used to estimate actual ratings as whether conditions vary.

Implied by current industry, rules and regulations is the requirement that all equality and inequality constraints (13.1)–(13.9) above must be simultaneously met for network protection not to disconnect pieces of equipment whose inequality constraints are violated and for the network as a whole to balance and stay interconnected. This must hold for any network topology for protection not to activate.⁹

Conditions-Dependent Selection of Performance Objectives

It is fairly straightforward to observe that there are potentially many combinations of power injections and voltage settings that meet the above system constraints for a given power network, such as the Flores or São Miguel electric power grids. Typically, the larger the network, the larger is the number of such combinations. We recommend the use of an AC XOPF for on-line adjustments of set points of controllable equipment in order to find the best combinations of adjustments as system conditions vary. We recommend that more flexible software is needed to select what is “the best” as system conditions vary. This raises the question of how to select appropriate performance objectives as discussed next.

The selection of performance objective (cost function) for doing optimization in electric power systems has long been an open problem [10, 11]. The key reason underlying this issue comes from often conflicting objectives in operations and in between operations and planning. It was illustrated in this chapter, for example, that maximizing physical efficiency of delivery does not give the same real power generation and voltage dispatch as when maximizing economic efficiency, such as total generation cost. Most common approach has been to consider the role of T&D voltage controllable equipment when optimizing delivery loss and to consider real power generation when optimizing economic efficiency. Most recently, the economic efficiency has been attempted by utilizing the cleanest resources first. It is straightforward to show that using the cleanest resources as must-run generation (negative load) does not necessarily lead to the lowest O&M generation cost [2].

Given these often conflicting performance objectives, as the complexity of operating future electric energy systems increases, it is becoming necessary to adaptively change decision-making objectives and make the most out of the available resources. In particular, this means that the most effective performance objective should be selected to manage the most dominant problem at the time [6].

⁹Current industry practice is to ensure that the constraints are met, that is, there exists a feasible steady-state network solution even when any single (or double) equipment becomes disconnected from the power network. Moreover, the reliability standards typically require that actions be taken so that within 30 min the system is brought back to normal, even without the equipment which has failed. Part IV of this book only concerns corrective methods for efficient and feasible operations during normal conditions, namely in the absence of equipment outages. Meeting reliability objectives is the subject of Part V of this book.

Since reliability always comes first, it is essential to first perform corrective actions to ensure reliable operations as conditions change. However, instead of scheduling preventively according to the $(N - 1)$ criteria, it is becoming necessary to compute adjustments on-line in real time as conditions vary and to implement the key adjustments. It is described in Sect. 13.5.6 why is this necessary. For example, when a line gets disconnected this typically leads to thermal overloads in neighboring lines. By simply recognizing that the line rating can be increased for a short time when needed, it becomes possible to perform an AC XOPF and find the feasible power flow solution. In this case neither economic dispatch nor loss minimization is effective cost functions. Instead, one can minimize the locations where the line flow limit needs adjustment; the appropriate AC XOPF objective function is basically the total sum of deviations from the given line flow limits; in the AC XOPF used in this chapter this function is known as the OBF (optimize branch flow) function [9]. Similarly, when there is a reliability problem caused by not having a power flow solution within the given voltage limits, a performance objective should be used to enable finding a solution within the minimally relaxed voltage limits. In the AC XOPF used in this chapter, this function is referred to as the maximize extreme voltage (MXV) [9].

Ultimately, as IT enhancements reach the stage that fast automation is placed to ensure stable transitions over a broad ranges of conditions, one can envision corrective resource management adaptation of set points for controllable equipment during both normal and abnormal conditions. The automation will be working at the much faster rate to ensure stable transitions between the quasi-stationary changes caused by variations in input and non-time critical equipment status changes. Notably, the equipment status itself could be used as a means of best managing what is available at the time.¹⁰

By way of a mathematical illustration, this chapter uses economic dispatch as the primary performance metric. Minimizing the generation-cost performance objective J can be expressed mathematically as the objective of minimizing

$$J = \sum_j c_j(P_{G,j}) \quad (13.10)$$

Here, $c_j(P_{G,j})$ stands for the operations and maintenance (O&M) generation cost of power plant G_j . An AC OPF problem is basically the problem of finding this minimum of (13.10) subject to all of the constraints given above in (13.1)–(13.9) by optimizing within the allowable ranges real power generation $P_{G,j}$, set points of AVR on generators $V_{G,j}$, and voltage set points $V_{L,k}$ at load buses k which are directly controlled by the on-load-tap-changing transformers (OLTCs) and capacitor banks (CBs).

As new technologies are deployed, it is important to keep in mind that DERs generally can be used for producing additional generation, to compensate for

¹⁰See Parts V and VI for detailed description of possible automation for managing most likely faults and large wind gusts without losing synchronism and/or experiencing voltage collapse.

reactive power, and to support voltage at their locations. This multiple functionality of solar and wind power, for example, is hard to coordinate in actual operations. To overcome this problem, it is necessary to have IT tools for deciding what must be done when and by how much. Perhaps the most challenging problem when selecting the complexity of control for these new resources is that relative incremental benefits from smarter technologies are system-dependent. Because of this, a systematic AC XOPF is needed to identify the most critical constraints, to select performance objective as conditions vary and to compare benefits of candidate solutions. The software used in today's industry generally does not lend itself to such functionalities.

An AC XOPF Must Provide Optimization Sensitivities for Finding the Most Effective Adjustments

The optimization sensitivities with respect to equality and inequality constraints characterizing a complex power grid are a powerful means of identifying the most critical causes of reliability and/or efficiency problems. The use of these optimization sensitivities is illustrated in the earlier part of this chapter. For example, the deficiencies in real power, reactive power, voltage, and thermal capacity of the lines are measured in terms of optimization sensitivities with respect to real power (OSPs), optimization sensitivities with respect to reactive power (OSQs), optimization sensitivities with respect to voltage (OSVs), and optimization sensitivities with respect to flows (OSFs), respectively. While using the AC XOPF, we have found these to be invaluable in explaining the optimization results and for making recommendations for enhancements, both in operations and/or in planning [12].

13.7.1 An AC XOPF Must Provide LMPs for Electricity Pricing

In several parts of the world, today's electricity is provided competitively. Instead of using generation cost, bids are offered by the generators, and these are cleared on daily, hourly, or even a 10-min basis. On-line pricing is based on so-called LMPs. A LMP at bus i is the optimization sensitivity with respect to the change in injection P_i at this node computed at the optimum total cost given in (13.10), namely,

$$\text{LMP}_i = \frac{\delta J}{\delta P_i} \quad (13.11)$$

Generators are paid for their power generated based on the LMPs at the grid location where they are connected. System generation revenue is the sum of these payments to all scheduled generators. System generation profit is the difference between the

generation revenue and the total O&M generation cost. Similarly, loads pay for their power consumed based on the LMPs at the grid locations to which they are connected. System load charges represent the sum of payments made by all loads.

The difference between system load charge and system generation revenue is known as the merchandise surplus (MS). It is known that the MS obtained using DC OPF is always nonnegative. However, there is very little understanding of how actual locations of power plants affect the financial settlements (merchandise surplus, generation profit, load charges) when an AC XOPF is computed and why. Furthermore, there are no electricity pricing mechanisms at present that would rely on AC XOPF-based clearing of power bids. We have recently proposed that computing incentives for voltage support, for adding real power sources, for adding reactive power sources, and for enhancing line flow limits can be computed in an on-line setting using LMPs to identify the economic cost of certain constraint, and then using OSVs, OSPs, OSQs, and OSFs to allocate the right incentives to the right enhancements [12, 13]. Finally, a combination of new performance objectives, such as MXV and OBF with their optimization sensitivities, provides incentives for relaxing voltage and line flow limits in operations to ensure reliability.

Today's Industry Approach to Implementing Network-Constrained Dispatch

The network-constrained AC OPF dispatch is a non-convex optimization problem subject to nonlinear constraints. It has been difficult to numerically solve because of convergence problems and problems with not being able to find a feasible solution. Moreover, a typical result of an AC OPF solution indicates that all available controls must be adjusted, which makes it impractical to implement on-line. As such, AC OPF is presently not used on-line by the utilities. Instead, a security-constrained DC OPF is used which has the same performance objectives (13.10), but voltage constraints (13.4), (13.3), and reactive power constraints (13.2), as well as reactive power balance equations (13.9) are not observed. The only observed constraints are the real power balance equations (13.8) linearized around a given equilibrium and the real power generation constraints given in (13.1).

Importantly, the line power flow thermal limits (13.5) needed to ensure that the transmission equipment does not overheat and become damaged are modified by so-called proxy line flow limits. These are obtained by carrying out extensive off-line simulations annually when planning new equipment and at the operations planning stage, when scheduling routine equipment maintenance, in order to account for the constraints which do not appear explicitly in the DC OPF problem formulation. Most of the simulations used are analysis based. No systematic optimization of resources is executed at the planning and/or operations planning stages. Instead, for the forecast demand, a sequence of AC power flows is carried out to identify the line flow proxy limit so that the omitted constraints are met. In particular, the

thermal line flow limit (13.5) is replaced by a proxy line flow limit which is intended to ensure that no voltage-reactive power problems occur for the scenarios of interest. Thus, less conservative thermal line flow constraints shown in (13.5) are routinely replaced by generally more conservative line flow limits as follows:

$$F_{ij}^{\min,\text{proxy}} \leq F_{ij} \leq F_{ij}^{\max,\text{proxy}} \quad (13.12)$$

Similarly, procedures are put in place to limit the load voltages to

$$V_{Lj}^{\min,\text{proxy}} \leq V_{Lj} \leq V_{Lj}^{\max,\text{proxy}} \quad (13.13)$$

for a subset of loads which are considered to be critical for ensuring no voltage-reactive power delivery problems. The modified limits (13.12) and (13.13) are then observed when the real power generation is dispatched during operations.

We stress that the use of these proxy limits can be problematic because when conditions occur that were not previously simulated, AC power flow analysis will indicate that there is either no solution due to reactive power-voltage problems and/or the reactive power and voltage-related constraints are not met. In either case it becomes infeasible to implement the result of DC OPF-based economic dispatch. As a result, it becomes necessary to iterate in a suboptimal and often heuristic way between solving the DC OPF and obtaining AC power flow solution with updated real power generation to check whether an acceptable voltage-reactive power profile can be found. Iterative modifications are carried out based on the system operator's knowledge of the specifics of the simulated electric power network. This iterative process often fails to converge and/or results in a suboptimal solution when compared to the one which can be obtained by solving a full AC OPF problem. Recently, progress has been made toward having a robust AC OPF software for meshed transmission networks and potential benefits from using it are reported in [14]. Notably, the use of DC OPF does not allow for explicitly optimizing the settings of voltage-controlling equipment. This represents one of the major missed opportunities for supporting efficient economic dispatch.

Summary

Today's practice is to perform extensive power-flow-based scenario analyses and determine technical limits regarding the locations and the amount of wind power plants that can be installed without creating operating problems. A typical result of these studies is a recommendation to build new T&D lines and modernize existing substations. This approach is suboptimal and it requires significant computational effort to try all possible scenarios and solutions that would prove to be suboptimal. In this chapter we propose, instead, that prior to deciding to build new lines, optimization methods should be used to consider non-transmission alternatives to supporting wind and solar power plant integration. In particular, software should

be used for on-line scheduling of the existing and new resources so that real power can be delivered to the greatest number of users, at the lowest possible cost without creating technical delivery problems. It is suggested that an extended AC Optimal Power Flow (AC XOPF) can be used as a basic means for (1) computing the most effective schedules as conditions change during operations, (2) for assessing potential value of candidate new plants, and (3) for reinforcing the T&D system to enable efficient and reliable use of newly added resources. We illustrate the potential use of AC XOPF for seasonal dispatch of resources in the electric power systems of Flores and São Miguel in the Azores Islands.

Acknowledgment The authors appreciate use of the New Electricity Transmission Software Solutions (NETSS), Inc AC XOPF program for demonstrating potential of corrective actions for enabling efficient and technically feasible delivery of the cleanest and the least expensive power for the Azores Islands.

References

1. M. Ilić, Dynamic Monitoring and Decision Systems for Enabling Sustainable Energy Services, Proc. of the IEEE, Special Issue on Network Systems Engineering for Meeting Energy and Environment Future, **99**(1), 58–79 January 2011
2. M. Ilić, L. Xie, J.-Y. Joo, Efficient Coordination of Wind Power and Price-Responsive Demand Part I: Theoretical Foundations, IEEE Transactions on Power Systems, **26**(4), 1875–1884 November 2011
3. M. Ilić, L. Xie, J.-Y. Joo, Efficient Coordination of Wind Power and Price-Responsive Demand Part II: Case Studies, IEEE Transactions on Power Systems, **26**(4), 1885–1893 November 2011
4. R. Lugtu, Security constrained dispatch. IEEE Trans. Power Apparatus **PAS-98**, 270–274 (1979)
5. B. Stott, O. Alsac, J. Bright, M. Prais, Some key requirements for practical OPF calculations, in *Opportunities for Increasing Real-Time & Day-Ahead Market Efficiency Through Improved Software, FERC Conference*, Washington, DC, 25–27 June 2012
6. M. Ilić, J. Lang, E. Litvinov, X. Luo, J. Tong, B. Fardanesh, G. Stefanopoulos, Toward coordinated-voltage-control-enabled HV smart grids, in *ISGT Europe 2011*, Manchester, December 2011
7. D. Jenicek, W. Imman, M. Ilić, Locational Dependence of Maximum Installable PV Capacity in LV Networks while Maintaining Voltage Limits, in *43rd North American Power Symposium*, Boston, MA (2011)
8. L. Xie, M. Ilić, Emission-concerned economic dispatch: possible formulations and implementations, in *IEEE PES Transmission and Distribution Conference and Exposition*, New Orleans, 2010
9. M. Ilić, J. Lang, Experience with AC extended power flow (AC XOPF) on the New York system, in *FERC Conference on Increasing Real-Time and Day-Ahead Market Efficiency Through Improved Software (Docket No. AD10-12-001)*, Washington, DC, 28–30 June 2011
10. A. Carpasso, E. Mariani, C. Sabelli, On the objective functions for reactive power optimization, in *IEEE Winter Power Meeting No. 80WM 090-1*, 1980
11. M. Ilić, X. Liu, C. Vialas, Some optimality notions of voltage profile for the steady-state operation of electric power systems, in *Proceedings Symposium Bulk Power Systems, Voltage Phenomena III: Voltage Stability and Security*, Davos, 1994
12. M. Ilić, Making the Most out of Technology at Value, White Paper, 2012

13. M. Ilić, J. Lang, Voltage dispatch and pricing in support of efficient real power dispatch. NYSERDA NETSS Project # 10476, 2012
14. M. Ilić, J.H. Lang, E.H. Allen, The role of numerical tools in maintaining reliability during economic transfers: an illustration using the NPCC equivalent system model, in *Bulk Power System Dynamics and Control VII*, Charleston, 19–24 August 2007

Part V

Enhanced Methods for Intra-dispatch Automated Balancing of Hard-to-Predict Wind Power Fluctuations

Chapter 14

Modeling and Control Framework to Ensure Intra-dispatch Regulation Reserves

Nipun Popli and Marija Ilić

14.1 Introduction

In this chapter we propose a model-based control framework for generating the real-power needed to follow the sustained wind power deviations within each dispatch interval. A quasi-stationary model is derived that explicitly states the dependence of real power output of conventional generators as *states* on nonzero mean wind power variations as *disturbances*. This model is obtained by subjecting the steady-state droop characteristics of generators to real-power flow constraints. No thermal line flow congestion is modeled.

Next, the model is utilized to design the control of set points on conventional governors. The readjusting of governor set points is in response to sustained wind ramps, and it could be viewed as the slowest tertiary-level automated load-following function. The wind power output is modeled as a negative load and varies around its long-term average 10-min forecast.

Our proposed approach is qualitatively different than the faster secondary-level balancing function known as Automatic Generation Control (AGC). The task of AGC is to ensure prespecified short-term frequency standards. Treating frequency deviations as a system output, AGC responds on a much shorter second-by-second timescale to frequency offsets resulting from faster wind power fluctuations. However, the control we propose is intended to balance the wind power deviations on a longer time horizon, specifically on a minute-by-minute basis, resulting in acceptable mid- and long-term frequency. Intra-dispatch wind variations are hard to predict accurately. The objective is to ensure sufficient fast regulation reserves so that AGC can balance fast fringe fluctuations in wind power output. Therefore,

N. Popli (✉) • M. Ilić

Department of Electrical and Computer Engineering, Carnegie Mellon University,
5000 Forbes Avenue, Pittsburgh, PA 15213, USA
e-mail: nipun@cmu.edu; milic@ece.cmu.edu

any effect of sustained surplus or shortage in scheduled wind power output, forecasted 10-min ahead of time, can be offset without requiring extremely fast generation resources. It is suggested that the proposed wind-following function can be automated to respond to varying wind power profiles with a feedback control. Nevertheless, if generation resources are scheduled on an hourly basis, the intra-dispatch real-power balancing control scheme can be implemented every 10 min in a feed-forward predictive way. In this chapter we illustrate only the automated non-predictive version of intra-10-min real-power balancing, on the islands of Flores and São Miguel. For the given conventional generation control on these islands, the efficacy of combined intra-dispatch and AGC in reducing frequency deviations within a dispatch interval is notably better than when conventional AGC is implemented. If intra-dispatch real-power balancing is to result in prespecified frequency response, we illustrate that compared to conventional AGC, combined intra-dispatch and AGC requires less expensive fast reserves.

14.2 Problem Overview

The balancing of electricity supply and demand requires a two-pronged approach. First, generation resources are scheduled based on predictions, primarily of load and wind. As the decision variables from scheduling are obtained, the set points of the conventional generators are readjusted to ramp up/down their power outputs to the scheduled values in a feed-forward way. As reviewed in Chaps. 7 and 9, the dispatch of generation resources involves a maximization of social welfare on a longer time horizon, without taking into account intra-dispatch wind ramps. Therefore, scheduling alone will not ensure that acceptable quality of power is delivered to the end users. Subsequent to dispatch, a real-time balancing of the mismatch between the actual demand and the scheduled supply must be achieved through feedback control actions. In the previous chapters, balancing functions involved the optimum utilization of conventional resources on a 10-min timescale, with the 10-min average wind power output assumed to be known ahead of time. To balance intra-10-min temporal variations in wind speed, which are not known ahead of time, we now propose a control model to follow hard-to-predict sustained variations in the wind power output. Only the conventional generation technologies are considered for intra-dispatch balancing, i.e., hydro- and diesel power plants.

14.2.1 The Challenges of Intra-dispatch Power Balancing

While balancing intra-dispatch supply-and-demand error in real time, the system operator faces two critical challenges. These are summarized below:

- 1 *Lack of Intra-dispatch Wind Speed Information:* The control functions for real-power balancing include frequency stabilization, frequency regulation, and

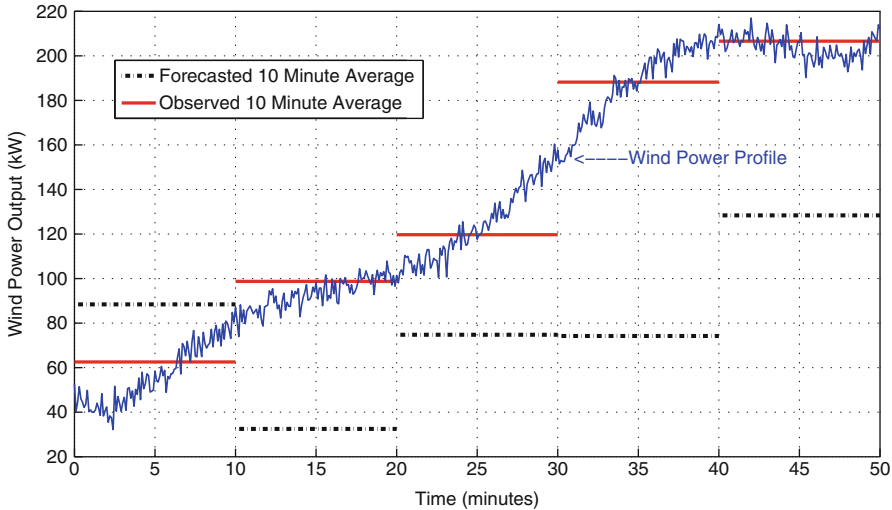


Fig. 14.1 10-Min ahead wind power forecast and actual wind power output

wind/load power following. These closed-loop control schemes balance the hard-to-predict real-power supply-and-demand mismatch over multiple time horizons. Also, closed-loop control can be either feed-forward or feedback. Feed-forward control is a proactive approach to ramp up/down the balancing resources in anticipation of power imbalances, such as varying load patterns, based on historical data and very short-term predictions. For example, if intra-10-min wind speed data is available, one can predict, using the forecast models described in Chap. 6, minute-by-minute variations in wind speed. Therefore, with the availability of wind speed information on a much shorter timescale, it becomes possible to extend the feed-forward approach in order to balance anticipated intra-10-min variations in wind power. Alternatively, the feed-back control loop is a reactive approach to balance stochastic/white noise or fringe fluctuations with a tolerable nonzero mean around the load. In general, the higher the accuracy of the forecast and shorter the timescale of the predictions, the lower the reliance on feedback closed-loop AGC. Subsequently, less regulation reserves will be required for non-predictive balancing approach or feedback control. However, due to the fact that there is typically a lack of accurate intra-10-min wind speed information, it is critical to ensure sufficient balancing reserves for short-term fluctuations as well as for long-term sustained variations in wind. The difference between the actual and predicted wind power outputs for Flores is shown in Fig. 14.1.

2. *Island-Type System with High Wind Penetration:* In large continental power networks, for the purpose of frequency stabilization and regulation, spinning reserves are shared among multiple balancing authorities through

interconnecting tie-lines. The reserves are relieved once the affected control area corrects its power shortage or surplus through AGC. Presently, wind power penetration in large-scale electric power networks is low. Wind supplies only a small fraction of the total demand. Wind fluctuations are, therefore, typically modeled as stochastic disturbance, even though their deviations are not white noise [1]. However, a full spectrum of problems arises if significantly high percentage of wind generation penetrates an island network, such as the Azores. Today, wind generation accounts for 14 % of the total installed capacity on Flores. At times, the scheduled wind is as high as 21 % of the system load. To plan sustainably for future demand, it is expected that additional wind generators will be installed. For stand-alone island networks with limited conventional resources, which have high wind penetration and lack external support through tie-lines, it is imperative that real-power balancing control be redesigned systematically. Since intra-dispatch wind variations will be much more pronounced in this kind of setting, the conventional hypothesis of modeling wind fluctuations as zero mean deviations may not be valid for Flores. As more wind connects to island networks, it will be hard to meet mid- and long-range frequency standards through AGC alone.

Based on the discussion so far it is apparent that the operational challenges to maintain a close to nominal frequency in the Azores networks, i.e., 50Hz, are qualitatively different from conventional frequency control problem. Generation resources are limited for intra-dispatch supply-demand error balancing. Since the Azores Islands are not electrically connected to each other, a lack of stabilization support from adjoining networks is also a fundamental limitation. Therefore, fast-responsive generators are needed in these networks, particularly those with combustion turbine technology such as diesel power generation. Although unsustainable, they are essential for the reliable operation of the Azores. A novel approach is thus required to ensure the effective implementation of all control actions, i.e., stabilization, regulation, and wind/load following, with a minimal use of combustion generators, i.e., diesel plants.

14.3 Granularity of Scheduling and Balancing Wind

The preceding section provides a qualitative description of the challenges to real-time balancing of the supply-demand error. To interpret the effect of scheduling on error balancing explicitly, we now illustrate the consequences of inaccurate wind forecasts and scheduling errors on the amount of reserves required for intra-dispatch power balancing. Figure 14.1 depicts three curves. Plotted over five dispatch intervals, i.e., 50 min, they represent 10-min-ahead wind power forecasts based on wind speed predictions, the observed 10-min average wind power output, and the actual wind power output profile. The step plots are based on the available 10-min average wind speed measurements and 10-min wind speed

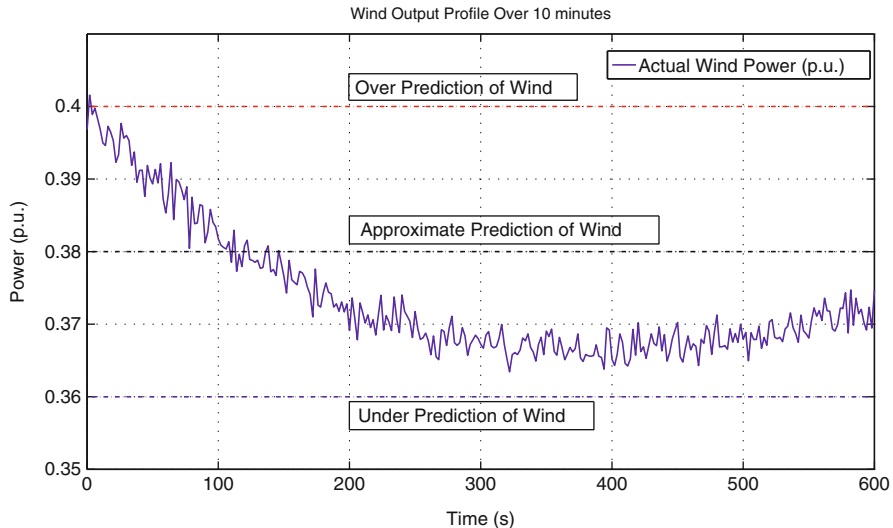


Fig. 14.2 Flores: scheduling error due to lack of intra-10 min wind speed information

predictions obtained from the forecast models (Chap. 6). Based on these plots, we re-summarize the challenges to intra-dispatch real-power balancing:

1. An inaccurate prediction of wind power output will lead to an error in dispatch. This will result in the under- or over-scheduling of conventional generators (Fig. 14.2).
2. Intra-10-min variations in wind power output are not only large but sustained as well. These can no longer be treated as white noise deviations. Also, unlike load ramps, it is hard to define intra-dispatch wind ramps.

These two factors will have profound effects on the balancing of the intra-dispatch supply-demand mismatch. A detailed interpretation of these challenges is covered in the following subsections.

14.3.1 Feed-Forward Generation Schedule

Before we begin to describe the effect of scheduling error on intra-dispatch power balancing, let us summarize the scheduling approach proposed in the preceding chapters. Under the assumption that wind speed has memory, or that it behaves like a state, 10-min-ahead wind speed forecast is made and an average wind power output for the dispatch interval is predicted. Out of the two generation dispatch algorithms, static dispatch and look-ahead dispatch (Chap. 7), the latter results in least-cost scheduling since it takes into account the predicted average wind generation

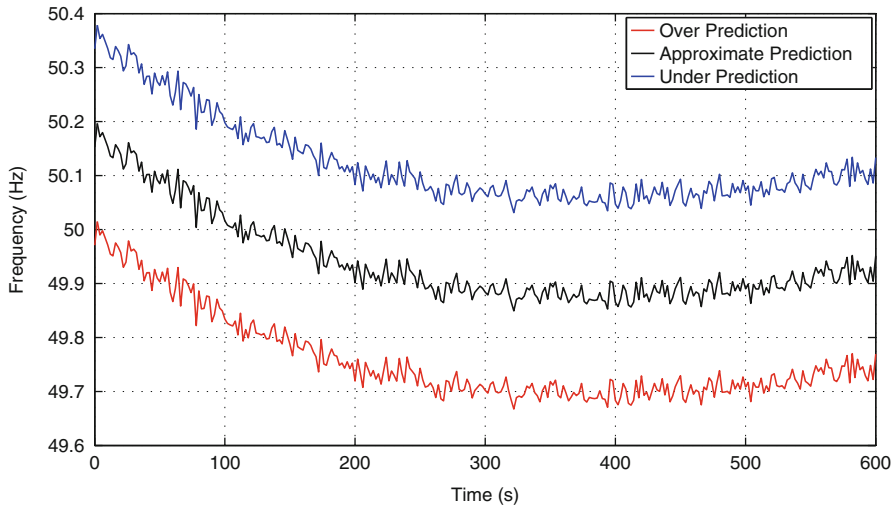


Fig. 14.3 Flores: persistent frequency deviations in the system

over 10 min. Analogously, while scheduling the load, adaptive load management (Chap. 8) accounts for price-responsive demand in the system. When implemented in tandem, model predictive control and adaptive load management effectively balance the long-term temporal variations in system demand and wind power output. This is on a timescale ranging from 10 min to 1 h (Chap. 9). With least-cost dispatch as the primary objective, the maximum utilization of renewable resources without spillage, particularly of the forecasted wind generation, determines the schedule of conventional generators and price-responsive demand. This is to ensure a full utilization of the predicted wind power output. However, an error in wind speed predictions, short term as well as long term, will result in intra-dispatch real-power imbalances:

$$e_W^{10} = \hat{P}_W^{10} - P_W^{10} \quad (14.1)$$

Equation (14.1) is a mathematical representation of wind forecast error. Here, e_W^{10} represents prediction error in average wind power output over 10 min. \hat{P}_W^{10} and P_W^{10} denote the predicted average wind generation and the observed or measured average wind generation, respectively. Figure 14.1 summarizes the prediction error in wind generation for Flores. For some dispatch intervals, the forecast error e_W^{10} is larger than 70 kW. In addition, the system operator may experience error in the load forecast as well. Nevertheless, given the rich load data history available to the system operator, daily demand curves can be predicted with a high degree of accuracy. However, if wind generation is to be scheduled as a negative load, a very accurate wind speed forecast is necessary to support its increasing penetration reliably. Figure 14.2 illustrates possible cases of scheduling error based on the anticipated wind power output on Flores. For each case, corresponding offsets in the system frequency are shown in Fig. 14.3 if the set points of the governors are not readjusted

between 0 and 10 min. An underprediction of wind power generation leads to over-frequency operation of the system within the 10-min interval. Similarly, in the case of an overprediction of wind power output, under-frequency operation of the system results.

14.3.2 Conventional AGC (AGC)

In order to ensure quality of service (QoS) to customers, the forecast error (e_W^{10}) and sustained minute-by-minute temporal variations in wind generation must be balanced. One possible way to offset these nonzero mean real-power imbalances is to implement the conventional generation control scheme by utilizing fast secondary regulation reserves [2]. Most utilities regulate the system frequency by using the tried-and-tested concept of area control error (ACE). ACE represents load-generation mismatch in a control area. The offsets in frequency and tie-line flows are bundled into ACE signals, simplifying the task of regulating frequency and inter-area exchange through a single control input. The fast regulation reserves respond to signals communicated from the control center. Equation (14.2) is a mathematical representation of area control error. ΔT_i represents the error in net tie-line flow into i th control area, with the error being the actual minus the scheduled tie-line flow exchange. Similarly, Δf represents the actual frequency minus scheduled frequency of the control area. β_i is the control area's frequency bias setting in MW/0.1 Hz, represented with a negative sign:

$$\text{ACE}_i = \Delta T_i - 10\beta_i \Delta f \quad (14.2)$$

In the case of an island-type network, there are no tie-line interconnections. Therefore, the term ΔT_i does not exist. The above mathematical formulation for ACE will change for the Azores. There will only be one control area with $i = 1$:

$$\text{ACE}_{\text{Island}} = -10\beta \Delta f \quad (14.3)$$

Large continental utilities estimate the value of ACE every few seconds. The rate of sensing varies for different ISOs. For example, in American utilities it is mandatory to sample ACE at least every 6 s. The updated control is implemented over a 1-min period, communicating the weighted ACE signal. This may be seen as a low-pass filter for intra-dispatch balancing, capturing only the sustained supply-and-demand mismatch. Real-power imbalances are expected to be highly volatile in the Azores. Therefore, a higher rate of sampling and updating of the ACE signals will be needed. Also, the regulation capacity for feedback control is limited on the Azores Islands, and only a small error in supply and demand can be balanced. In the case of a surplus wind power, diesel units can be ramped down quickly. However, it may not be possible to ramp them up beyond their rated capacity in response to a large scheduling error (e_W^{10}) and sustained intra-dispatch variations in wind. For example, on Flores, even though the installed capacity of the diesel generation

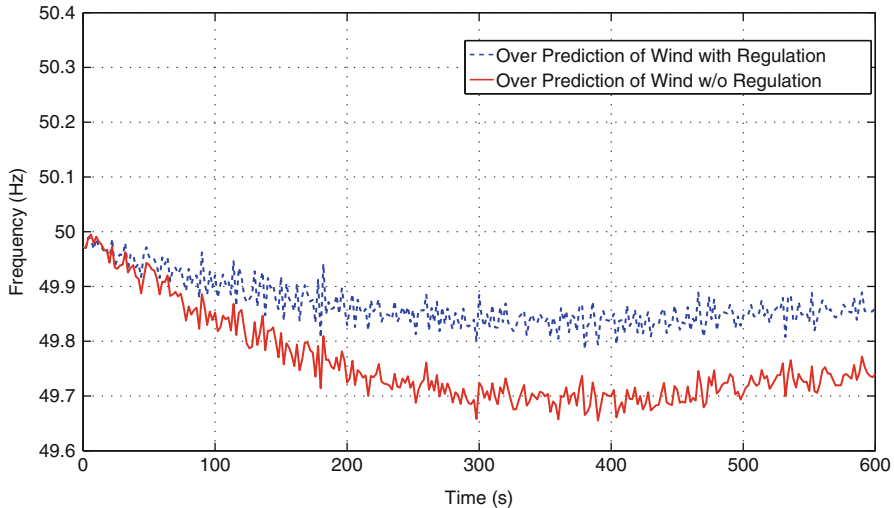


Fig. 14.4 Island-1: sustained frequency deviations even with AGC

exceeds total demand, it is not plausible to have all four diesel units online 24 h a day. This is particularly the case when there is a shortage of combustion fuel, such as when the sea is too rough to allow oil imports to arrive. In the worst-case scenario, the islands have to withstand the problem of an oil shortage for a week or two. In Fig. 14.2, let us take the case where the system operator under-schedules conventional generation resources by overpredicting the wind power output. Over the next 10 min, we aim to compensate for the wind power shortage with a limited capacity of fast regulation reserves. Figure 14.4 shows that when the regulation reserves have been utilized completely, frequency deviations are still as large as 0.15 Hz. The North American Electric Reliability Councils, control performance standards state that ACE or power imbalance within a control area must cross zero every 10 min. Such standards are hard to achieve in the Azores by means of conventional generation control, as reflected in the sustained frequency deviations in Fig. 14.4.

From the discussion so far, it is now clear that the deviations in wind power can be filtered into two components. These are fast second-by-second fluctuations and slow but sustained minute-by-minute variations (Fig. 14.5). The high cost of operation and limited balancing capacity of diesel units make them unviable for tracking of slow variations. On Flores, a possible approach is to ramp controllable hydro on a minute-by-minute basis within each dispatch interval. Compared to the secondary-level function of AGC, the generation output of the hydro unit can be increased on a much slower timescale to balance the wind as well as the load ramps. Diesel units or AGC reserves respond on a second-by-second basis to ensure short-term frequency quality. Moreover, they are much needed for contingency conditions such as wind

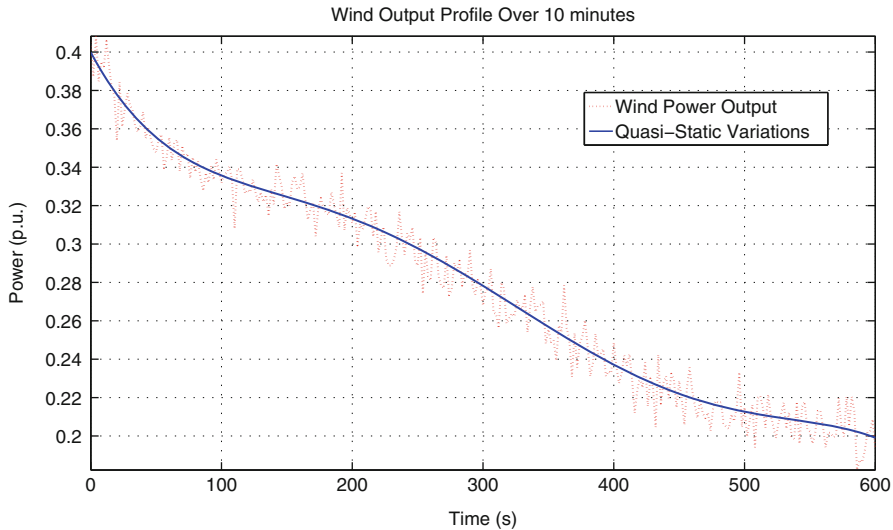


Fig. 14.5 Typical intra-10-min wind power profile

gusts or a sudden loss of wind turbines due to a voltage drop. Therefore, it is not prudent to balance wind and load ramps through fast regulation reserves. These fast reserves are required for worst-case scenarios to ensure the reliable operation of an island-type network and must be preserved to the greatest extent possible.

14.4 Managing Wind Variations: A Qualitative Outline

For systems with high wind penetration, spatial and temporal variability in wind should be taken into account while balancing intra-dispatch variations and scheduling error in wind power:

- (a) *Spatial Variability:* The planning of balancing reserves must be based upon the electrical distances between the balancing units and the sources of disturbances, i.e., wind farms. One may observe potentially larger imbalances at locations where the installed wind capacity is high. The mapping of spatially nonuniform penetration of wind may not be of much significance for the small Flores network, where the impedances of the wires between different nodes are of the same order. However, it is critical for large island networks. For example, São Miguel's power network spreads over a large geographical area with 1,900 buses. Some of the generator nodes in the São Miguel's network are weakly interconnected as the admittance of electrical wires connecting them is low. As a result they can be modeled as a set of weakly coupled subsystems.

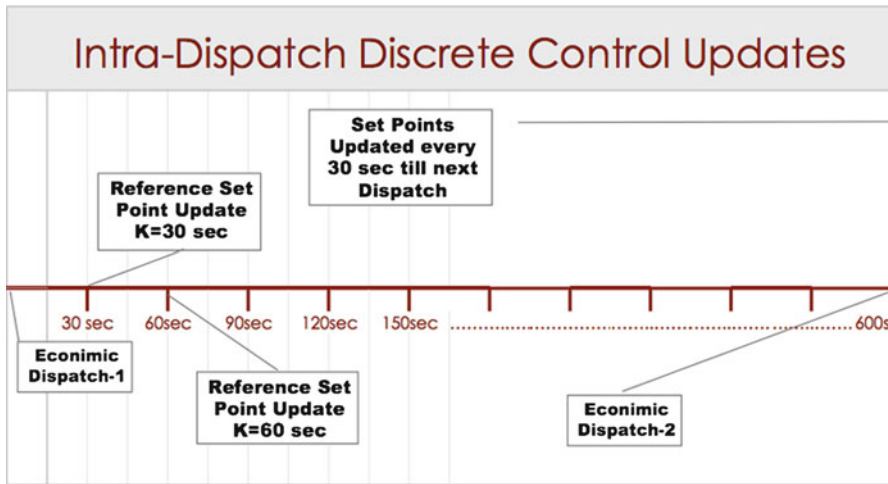


Fig. 14.6 Quasi-static control updates between consecutive schedules

A decentralized intra-dispatch power balancing approach is needed in such a case. In order to map location-based variations in wind power output, it is imperative that network constraints be taken into account. Thereafter, spatially differentiated or even decentralized intra-dispatch real-power balancing can be implemented. It can be supported by means of PMUs and dedicated communication between the balancing unit and the source of disturbance.

- (b) *Temporal Variability:* Intra-dispatch wind variations will span over multiple timescales. A balancing over all time horizons is essential for reliable operation. For intra-dispatch balancing, wind variations are filtered into two components, shown in Fig. 14.5. Firstly, there are large but slow sustained variations sampled every $[K]$ seconds, where K equals 30 s. A quasi-stationary control approach can be applied to balance this slow component. As shown in Fig. 14.6, the reference setpoints of the slow generators on Flores, particularly controllable hydro, can be updated every 30 s in response to intra-dispatch quasi-stationary wind variations. The rationale behind the choice of $K = 30$ is explained in next section. Secondly, there are fast fringe fluctuations around the slow wind variations. Fast regulation reserves, or AGC units such as a diesel plant, flywheels, dVars, electric vehicles, and batteries, respond to fringe fluctuations in wind power output; this is covered in subsequent chapters (Chaps. 15 and 16). These fluctuations are assumed to stabilize before the slow quasi-static control scheme responds, the model for which is described in the next section.

14.5 Proposed Intra-dispatch Balancing Approach

Next we propose a quasi-static control approach for following sustained intra-dispatch wind variations on Flores. Before the control framework is derived, it is necessary to revisit the concept of steady-state droop characteristics.

14.5.1 Steady-State Droop and Gain of a Generator

For synchronous generation technologies, the standard state-space model of their governor-turbine-generator (GTG) is a dynamical controller represented by a set of ordinary linear differential equations. To derive the steady-state droop characteristics, and hence the quasi-stationary control framework, the primary dynamics are assumed to be stabilizable. In other words, the derivatives of the states are set to zero and the steady-state droop of the generator obtained. Numerically, a generator's droop is the rate of change of its rotational speed with respect to the change in its power output. The generator's power output is represented by a three-way relation [3]:

$$\omega_G [K] = a\omega_G^{\text{ref}} [K] - \sigma_{ss} P_G [K] \quad (14.4)$$

Variables P_G , ω_G^{ref} , and ω_G refer to the power output, governor frequency set points, and the rotational frequency of the prime mover, respectively. Equation (14.4) is obtained from the linearized GTG model. Therefore, the states represent deviations from their nominal values. σ_{ss} is the steady-state droop characteristics of the generator; the coefficient a also depends on the generation technology. The droop σ_{ss} determines the governing action of a generator. It represents the sensitivity of generator frequency ω_G with respect to any change in its power generation P_G , at a constant set point value ω_G^{ref} . σ_{ss} in turn determines the frequency bias of the island-type network, i.e., β parameter in Eq. (14.3). However, before β is calculated, the steady-state gain G_{ss} of all controllable generators must be estimated. Parameter β can thereafter be obtained by adding the gains of all N controllable generators in the network:

$$G_{ss} = \frac{1}{\sigma_{ss}} \quad (14.5a)$$

$$-10\beta = (G_{ss1} + G_{ss2} + G_{ss3} + \dots + G_{ssN}) \quad (14.5b)$$

Equation (14.6) represents the closed-loop primary dynamical model of GTG for a hydropower plant:

$$\begin{bmatrix} \dot{\omega}_{G_h} \\ \dot{q} \\ \dot{v} \\ \dot{a} \end{bmatrix} = \begin{bmatrix} -\frac{(e_h + D_h)}{M_h} & k_q & 0 & -k_w \\ \frac{1}{T_f} & -\frac{1}{T_q} & 0 & \frac{1}{T_w} \\ 0 & 0 & -\frac{1}{T_e} & \frac{r'}{T_e} \\ -\frac{1}{T_s} & 0 & \frac{1}{T_s} & -\frac{(r_h + r')}{T_s} \end{bmatrix} \begin{bmatrix} \omega_{G_h} \\ q \\ v \\ a \end{bmatrix} + \begin{bmatrix} 0 \\ 0 \\ 0 \\ \frac{1}{T_s} \end{bmatrix} \omega_G^{\text{ref}}[K] + \begin{bmatrix} -\frac{1}{M_h} \\ 0 \\ 0 \\ 0 \end{bmatrix} P_G \quad (14.6)$$

The state variables for the hydro governor are ω_{G_h} for the generator frequency, q for the penstock flow, and v and a for the governor droop and the gate position, respectively. M_h and D_h are the inertia and damping constants. T_e and T_s represent the time constant of the valve-turbine gate system and the servomotor gates, respectively. r_h and r' are the permanent speed droop and the transient speed droop of the hydro generator, respectively. e_h , k_q , k_w , T_f , T_q , and T_w are all ratios of constants of the standard hydro turbine [4]. Now the rate of update of the set point ω_G^{ref} , i.e., 30 s, is relatively slow with respect to the closed-loop primary dynamics. This is much slower than the rate at which the gate position a can be changed. The gate position controller is the slowest component of the dynamical controller [Eq. (14.6)] with a time constant of approximately 4 s. Therefore, the transients of the hydropower plant settle to steady-state before the reference set point of the governor is updated. Following is the steady-state droop characteristic of hydro, arrived at by assuming the primary dynamics to be stabilizable:

$$\left(e_h + D_h - \frac{k_q T_q}{T_f} + \frac{k_q T_q}{r_h T_w} - \frac{k_w}{r_h} \right) \omega_G[K] = \left(\frac{k_q T_q}{r_h T_w} - \frac{k_w}{r_h} \right) \omega_G^{\text{ref}}[K] - P_G[K] \quad (14.7)$$

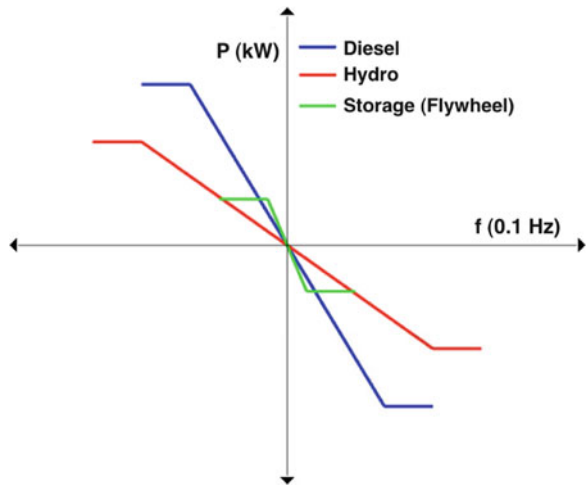
The primary dynamical equation for diesel or a combustion turbine can be represented as:

$$\begin{bmatrix} \dot{\omega}_{G_d} \\ \dot{V}_{CE} \\ \dot{W}_F \\ \dot{W}_{Fdot} \end{bmatrix} = \begin{bmatrix} -\frac{D_d}{M_d} & 0 & \frac{c}{M_d} & 0 \\ -\frac{K_D}{b} & -\frac{1}{b} & 0 & 0 \\ 0 & 0 & 0 & 1 \\ 0 & \frac{a}{\alpha} & -\frac{\gamma}{\alpha} & -\frac{\beta}{\alpha} \end{bmatrix} \begin{bmatrix} \omega_G \\ V_{CE} \\ W_F \\ W_{Fdot} \end{bmatrix} + \begin{bmatrix} 0 \\ \frac{K_D}{b} \\ 0 \\ 0 \end{bmatrix} \omega_G^{\text{ref}}[K] + \begin{bmatrix} -\frac{1}{M_d} \\ 0 \\ 0 \\ 0 \end{bmatrix} P_G \quad (14.8)$$

State variables ω_{G_d} and V_{CE} represent the generator's frequency and fuel controller. Variables W_F and W_{Fdot} represent the fuel flow, while M_d and D_d are the inertia and damping constants. More details about the model can be found in [5, 6]. By assuming the primary dynamics to be stabilizable, a three-way relation between can be derived for a diesel generator as well:

$$\left(D_d + \frac{c K_D a}{\gamma} \right) \omega_G[K] = \left(\frac{c K_D a}{\gamma} \right) \omega_G^{\text{ref}}[K] - P_G[K] \quad (14.9)$$

Fig. 14.7 Qualitative representation of steady-state droops



14.5.2 Droop Characteristics of Generators on Flores

The steady-state droop of controllable generators can be figuratively represented as a straight line, with a slope as a negative of its steady-state gain G_{ss} . Figure 14.7 is a qualitative representation of the droops for diverse balancing technologies on Flores. While flywheels can be much more responsive compared to conventional units, they have limited reserves. Therefore, to balance sustained intra-dispatch wind variations, we consider only the droops of conventional technologies. The steady-state gains or droops of controllable hydro and diesel generators on Flores can be summarized as:

$$G_{ss}^{\text{Hydro}} = \frac{1}{\sigma_{ss}^{\text{Hydro}}} = \left(e_h + D_h - \frac{k_q T_q}{T_f} + \frac{k_q T_q}{r_h T_w} - \frac{k_w}{r_h} \right) \quad (14.10a)$$

$$G_{ss}^{\text{Diesel}} = \frac{1}{\sigma_{ss}^{\text{Diesel}}} = \left(D_d + \frac{c K_{DA}}{\gamma} \right) \quad (14.10b)$$

Based on the generator's parameters, we now evaluate and compare these gains for hydro and diesel plants on Flores:

$$G_{ss}^{\text{Hydro}} = \frac{1}{\sigma_{ss}^{\text{Hydro}}} = 0.4485 \quad (14.11a)$$

$$G_{ss}^{\text{Diesel}} = \frac{1}{\sigma_{ss}^{\text{Diesel}}} = 10.005 \quad (14.11b)$$

Or, alternatively it can be concluded that:

$$G_{ss}^{\text{Diesel}} = (22.305) G_{ss}^{\text{Hydro}} \quad (14.12)$$

If the set points of diesel and hydro plants are not adjusted in response to intra-dispatch imbalances, the diesel generator can produce about 22 times more power than the hydro plant for a given frequency offset.

14.6 Proposed Quasi-Stationary Balancing Model

As described in Sect. 14.4, the spatial variability in wind generation must be mapped for the purpose of differentiating real-power imbalances at multiple locations. We propose a control model that utilizes local power output as measurements [7].

14.6.1 Seamless Integration of Heterogeneous Balancing Resources

A control scheme with generation power outputs as state variables is critical for incorporating novel regulation technologies like batteries and electric vehicles. Unlike conventional synchronous generators, these technologies lack a prime mover and do not have frequency as state variable. For the purpose of intra-dispatch power balancing, these generation resources can only be modeled through their power output. Hence, for this reason, our model is based on the power output of the balancing resources as state variables. Assuming a decoupling between real and reactive power, the following sensitivity matrix can be obtained for real-power balancing:

$$\begin{bmatrix} P_G[K] \\ P_L[K] \end{bmatrix} = \begin{bmatrix} J_{GG} & J_{GL} \\ J_{LG} & J_{LL} \end{bmatrix} \begin{bmatrix} \delta_G[K] \\ \delta_L[K] \end{bmatrix} \quad (14.13a)$$

Here, δ represents the phase angles of the buses and subscript L signifies the load buses [3]. Equation (14.13a) can be rewritten in terms of only the generator bus phase angles δ_L^1 :

$$P_G[K] = (J_{GG} - J_{GL}J_{LL}^{-1}J_{LG}) \delta_G[K] + J_{GL}J_{LL}^{-1}P_L[K] \quad (14.13b)$$

It is critical to note that P_G is a column vector and consists of conventional generation technology as well as wind farms. Denoting the term $(J_{GG} - J_{GL}J_{LL}^{-1}J_{LG})$ as K_P , Eq. (14.13b) can be reformulated as:

¹All variables represent deviations from their nominal values for a given equilibrium point.

$$\begin{bmatrix} P_{GC}[K] \\ P_W[K] \end{bmatrix} = \begin{bmatrix} K_{P_{GC}G_C} & K_{P_{GC}W} \\ K_{P_{WG}C} & K_{P_{WW}} \end{bmatrix} \begin{bmatrix} \delta_{GC}[K] \\ \delta_W[K] \end{bmatrix} \quad (14.14a)$$

Subscripts G_C and W refer to conventional generators and wind farms, respectively. Now eliminating δ_W since P_W or intra-dispatch sustained wind variations are to be modeled as disturbances:

$$P_{GC}[K] = \left(K_{P_{GC}G_C} - K_{P_{GC}W} K_{P_{WW}}^{-1} K_{P_{WG}C} \right) \delta_{GC}[K] + K_{P_{GC}W} K_{P_{WW}}^{-1} P_W[K] \quad (14.14b)$$

A relation between the bus angle and the frequency of the conventional generator can be derived in a causal way:

$$\delta_{GC}[K+1] = \delta_{GC}[K] + T_t \omega_{GC}[K] \quad (14.15)$$

The three-way droop equation and the network constraints over two time steps K and K + 1 lead us to following state-space model:

$$P_{GC}[K+1] = AP_{GC}[K] + B\omega_{GC}^{\text{ref}}[K] + W(P_W[K+1] - P_W[K]) \quad (14.16)$$

The matrices A and B are (n – 1)-dimensional square matrices, where n is the number of controllable balancing resources within the network. Their numerical values depend on GTG's parameters and the sensitivity matrix of real power with respect to the bus angles.

14.6.2 Mid- and Long-Term Stability

The system matrix A in Eq. (14.16) is represented as:

$$A = I_{n-1} - \alpha T_t \sigma \quad (14.17)$$

I represents an identity matrix. The parameter α equals (K_{P_{GG}} – K_{P_{GW}}K_{P_{WW}}⁻¹ K_{P_{WG}}) in Eq. (14.14b). T_t, a scalar, is the sampling rate of 30 s. The diagonal matrix σ represents the steady-state droops of (n – 1) controllable generators. Since Eq. (14.16) is a discrete-time state-space model, the eigenvalues of matrix A must be less than unity. This is to ensure mid- and long-term system stability.

14.6.3 Intra-dispatch Balancing: Control Gain

Based on the structure of system matrix A, as well as the control objective, there can be multiple ways of designing the gain for intra-dispatch real-power balancing:

14.6.3.1 Tracking Wind Variations

One possible approach of designing the control gain is to track quasi-static variation in wind power output. This can be achieved by having the following control input:

$$\omega_{\text{GC}}^{\text{ref}}[K] = -B^{-1}W(P_{\text{W}}[K] - P_{\text{W}}[K-1]) \quad (14.18)$$

In Eq.(14.18), the set points of the governors ($\omega_{\text{G}}^{\text{ref}}$) are updated in response to $(P_{\text{W}}[K] - P_{\text{W}}[K-1])$. The wind variations are balanced with a delay. Since Eq. (14.18) represents a delayed response of the generation resources to the sustained wind variations, error will always exist. The residual real-power error will be balanced by the slack generator or by AGC units in a distributed way. Therefore, for the purpose of tracking, communication between balancing resources and source of disturbances is needed.

14.6.3.2 Ensuring Long-Term Stability

As described in the preceding subsection, long-term system stability can be ensured only if eigenvalues of system matrix A are less than unity magnitude. The matrix A is dependent on the parameters α , T_i , and σ . The network constraints, i.e., how much power can be delivered by the balancing resources to the sources of disturbance, are represented by matrix α . Similarly, the sampling time T_i is chosen so that the transients of the dynamical controller stabilize before reference points are updated. The steady-state droop matrix σ of controllable generators is technology dependent. As per Eq. (14.17), long-term system stability is determined by these three factors.

For the case when the matrix A has eigenvalues greater than unity magnitude, it is not possible to track wind variations with an unstable system. Therefore, the tracking input described in Eq. (14.18) cannot ensure long-term system stability. A similar observation of long-term instability was noticed in Flores. With two controllable generators, i.e., $n = 2$, there can be two possible system matrices of unity dimension $(n-1)$, one each for the case when either the controllable hydro plant or the diesel generator is used for intra-dispatch power balancing. The eigenvalues of matrix A , when the hydro plant and the diesel generator serve as intra-dispatch balancing resource, are -8.35×10^2 and -36.48 , respectively.

In such a case, an alternative is to design a feedback gain for a stable system. For example, a discrete linear-quadratic regulator to design control input $\omega_{\text{GC}}^{\text{ref}}[K]$ minimizes the quadratic cost function:

$$J = \sum_{K=1}^{\alpha} \left(\omega_{\text{GC}}[K]^T Q \omega_{\text{GC}}[K] + \omega_{\text{GC}}^{\text{ref}}[K]^T R \omega_{\text{GC}}^{\text{ref}}[K] \right) \quad (14.19)$$

The objective is to minimize locational frequency offsets as well as the cost of control. Matrices Q and R are the state and control weighting matrices, respectively. The matrices must be so chosen as to reflect the relative quality of service and the

cost of balancing at different nodes. For example, at the locations where frequency offsets are expected to be larger or where a better quality of service is needed, the corresponding diagonal element in the matrix Q should be relatively high. Similarly, for expensive balancing resources such as diesel, the corresponding elements in the R matrix must reflect the high cost of control. The gain k obtained by solving discrete-time Riccati equation is used to design the input as:

$$\omega_{G_C}^{\text{ref}}[K] = -(k)(\omega_{G_C}[K]) \quad (14.20)$$

Therefore, the generators respond to the deviations in their frequency. The deviations in the frequencies are a result of wind variations ($P_W[K+1] - P_W[K]$). This may be seen as output-based closed-loop stable power balancing. The communication among balancing resources will be determined by the structure of closed-loop matrix ($A - B \times k$).

14.6.3.3 Tracking Wind Variations with a Stable System

On Flores there is just one balancing resource (i.e., $n - 1 = 1$). Therefore, the only option of designing a gain is to provide full-state feedback using discrete linear regulator gain and stabilize the system. However, for large networks there can be multiple balancing resources with $(n - 1) > 1$. If the system is unstable to begin with, some of the balancing resources can be deployed to just ensure long-term system stability. Subsequently, other balancing technologies can be used for tracking of wind variations based on their electrical proximity to sources of disturbances:

$$P_G[K+1] = AP_G[K] + B_{\text{Stab}}\omega_{G_{C1}}^{\text{ref}}[K] + B_{\text{Track}}\omega_{G_{C2}}^{\text{ref}}[K] + W(P_W[K+1] - P_W[K]) \quad (14.21)$$

Here, the input $\omega_{G_{C1}}^{\text{ref}}$ stabilizes the system. Similarly, the sustained wind power variations are tracked through the input $\omega_{G_{C2}}^{\text{ref}}$. This can be one possible approach to design control gain for a large island like São Miguel which has three diesel generators ($n = 3$).

14.7 Enabling Sustainable Integration of Wind on Flores

Through simulations we now illustrate the efficacy of the quasi-stationary control framework to track sustained wind variations on Flores. To ensure long-term stability for Flores with ($n - 1 = 1$), discrete-time Riccati equation gain (k) was designed for intra-dispatch power balancing. While equal weights were chosen for frequency offsets (ω_{G_C}) for the case of hydro and diesel as balancing resources, the cost of control through diesel was chosen to be ten times as much as that of a hydropower plant. The control gain was estimated through an infinite horizon solution of the Riccati equation to ensure provable performance over a time horizon

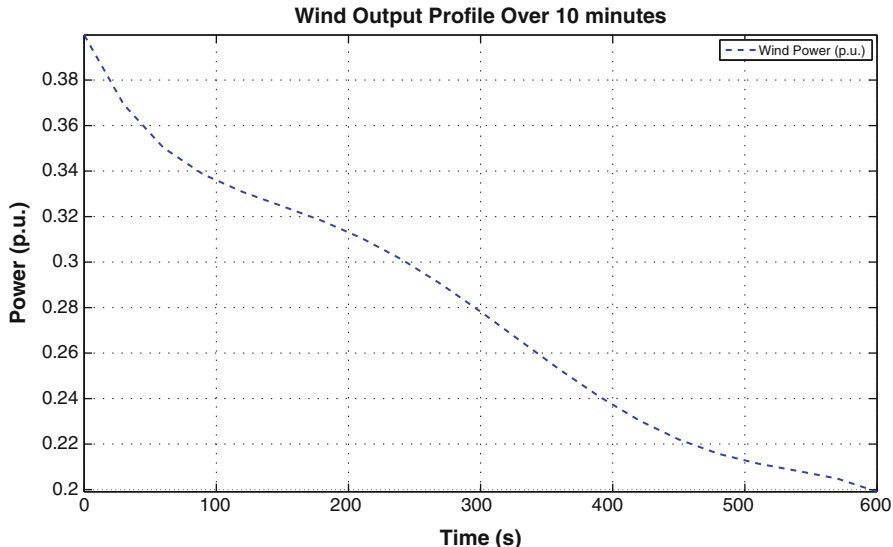


Fig. 14.8 Intra-dispatch wind power output profile on Flores

as long as 10 min. The discrete-time Riccati equation gain (k) was (7.84) when hydro was used for intra-dispatch power balancing. Similarly it was (-0.09) when diesel unit balanced intra-dispatch wind variations. Figure 14.8 shows a possible profile of wind power output between two consecutive dispatches that the Flores network was subjected to.

Figures 14.9 and 14.10 depict the frequency deviations and power outputs when hydro and diesel generators are alternately used for balancing sustained wind variations. The simulations reflect long-term frequency deviations at the generator buses over 10 min. Since a balancing resource cannot follow wind variations accurately, a residual error will always exist. Therefore, a fraction of the real-power mismatch will be balanced by AGC or the slack bus. In Fig. 14.9, while the hydro follows the wind variations, the residual power imbalance is corrected by diesel since it serves as a reference bus. Similarly, when diesel is following wind (Fig. 14.10), hydro responds as a slack bus. For the slack bus or the reference bus, the power output is a result of generator droop, and there is no change in the frequency set point. With the steady-state gain of hydro unit G_{ss}^{Hydro} being smaller than that of diesel unit G_{ss}^{Diesel} by a factor of 22, the frequency offset in Fig. 14.10 is larger as compared to that in Fig. 14.9. Hence, the technology with low gain, i.e., hydro, must be used for tracking slow variations in wind, and the technology with high gain must be used as the AGC unit. Wind can be balanced in a much cheaper and more environmentally cleaner way if the hydro is slowly ramped up to follow wind and diesel unit balances residual error.

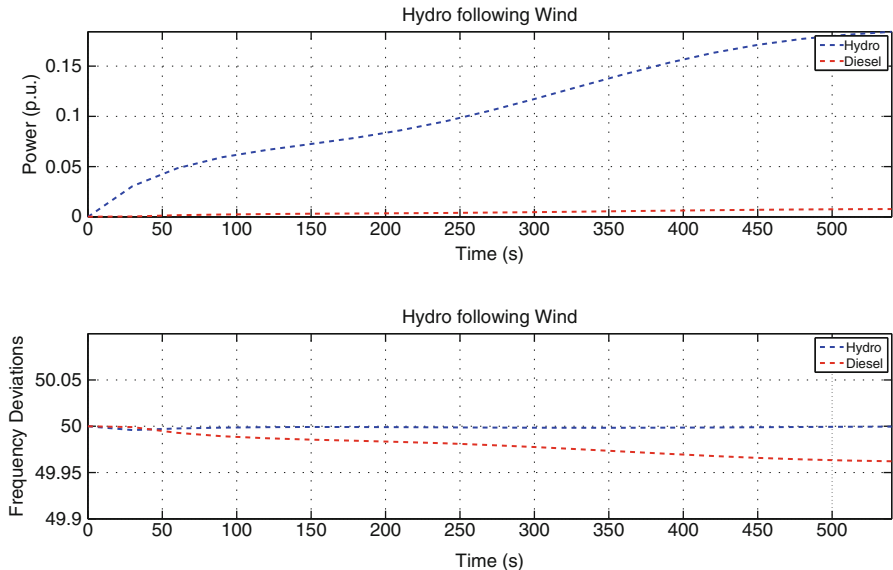


Fig. 14.9 Hydro unit balancing intra-dispatch wind variations

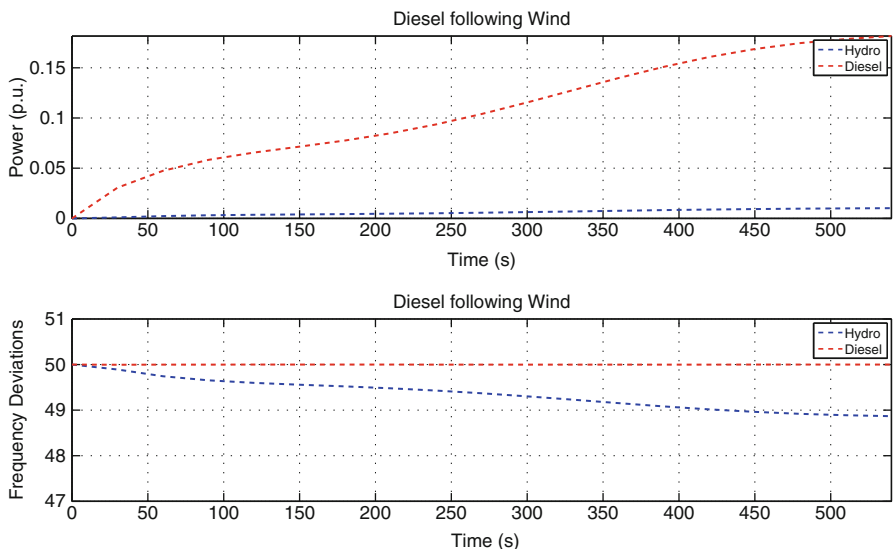


Fig. 14.10 Diesel unit balancing intra-dispatch wind variations

14.8 Electrical Distances: Effects on Intra-dispatch Power Balancing

Electrical wires act as transporter of energy between different nodes. The electrical distance between two nodes is numerically equal to the transmission time in microseconds, i.e., the duration of travel of an electromagnetic wave through them. The transmission time depends on the impedances of the electrical wires. Therefore, power transferred from one end to another is based on system conditions such as bus angles, voltages, and wire impedances. Ensuring enough generation capacity does not guarantee power delivery to the load. On Flores, the impedances of electrical wires between different nodes are of the same order. The generator nodes are strongly coupled to the wind farm. If the impedance of the electrical connections between the source of disturbance and the balancing resources on Flores was weak, different generator power outputs would result for the purpose of intra-dispatch real power balancing. Figure 14.11 illustrates the change in power output of the hydro and diesel generators, subject to wind variations in Fig. 14.8, if the impedances of connection between the wind farm and the conventional generators were reduced by a factor of 5.

In contrast, on São Miguel, the electrical impedances between the nodes differ significantly. While planning wind farms on São Miguel, the electrical distance between the wind farms and the conventional balancing resources must be taken into account. The island has only three controllable diesel generators on bus 1, 2, and 3. If São Miguel operators plan to integrate wind, they must carefully select its location in the network, in order to ensure efficient balancing of intra-10-min wind

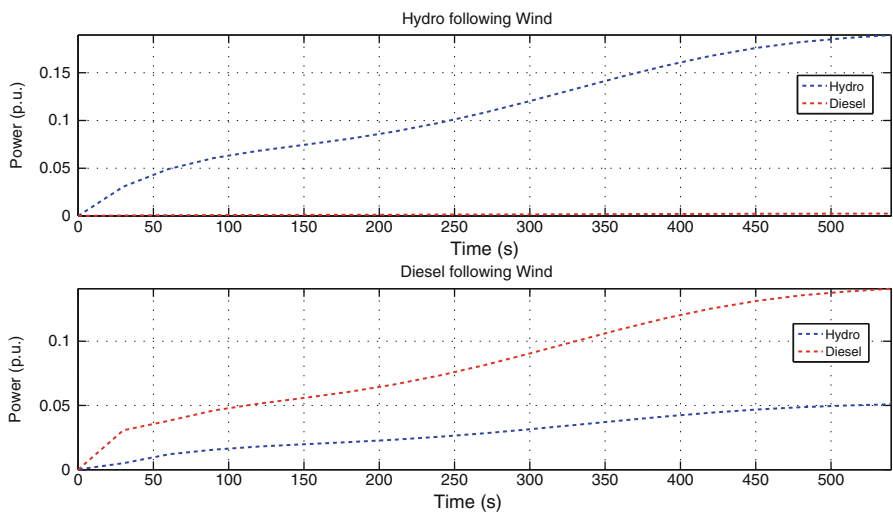


Fig. 14.11 Generator outputs for weakly connected wind farm on Flores

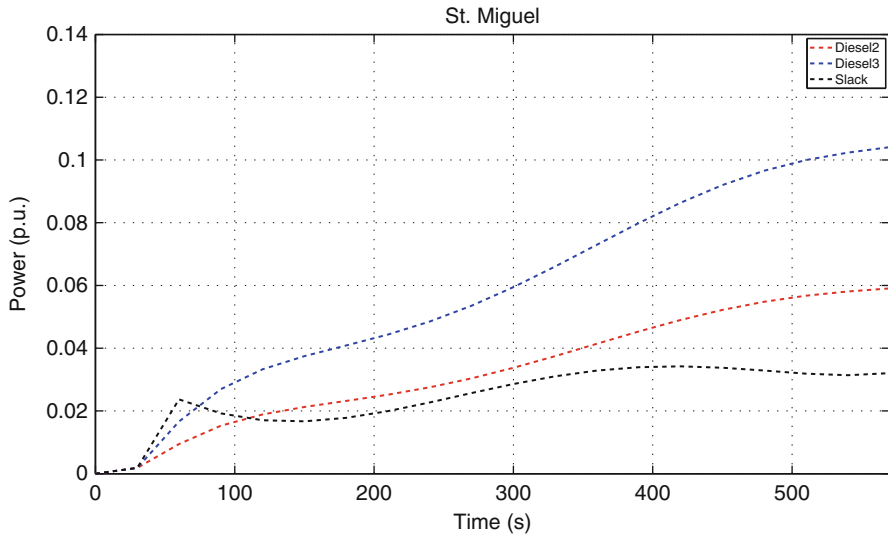


Fig. 14.12 Wind farm built at bus 4 on São Miguel

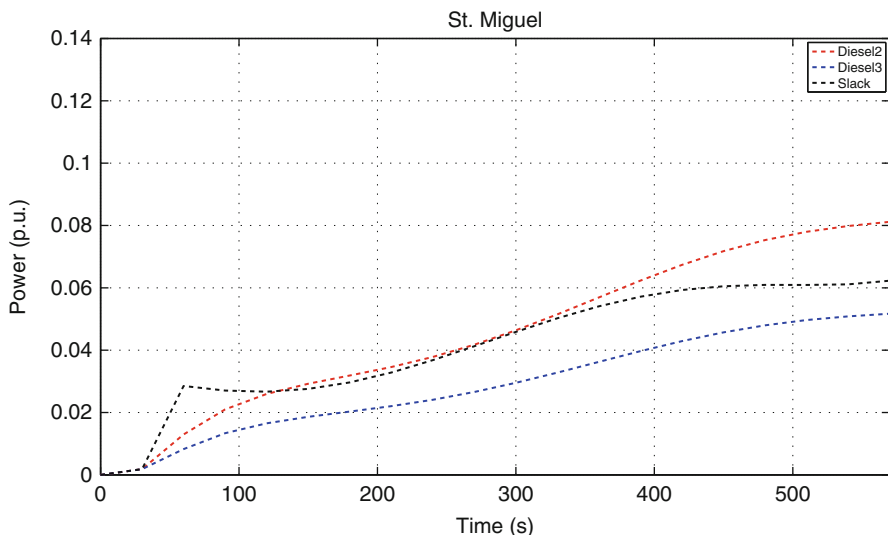


Fig. 14.13 Wind farm built at bus 15 on São Miguel

variations. Different power output profiles for the diesel generators on São Miguel will result if the wind turbines are built at different locations. The wind power output profile shown in Figs. 14.8, 14.12, and 14.13 depicts the power generated by diesel generators for two possible scenarios, i.e., when the wind farm is built at bus 4 or at bus 15.

14.9 Intra-dispatch Demand Response

Motors or inductive loads form a large component of utility demand: typically 40–60 %. Similarly, in the Azores, various kinds of induction motor loads can be found. With their aggregate inertia being high, they can contribute significantly to intra-dispatch balancing through real-time demand response as well as direct load control. It is imperative to identify and classify inductive loads based on their type (residential/commercial/industrial), size (large/small based on power consumption), time-scale or rate of response to system imbalances, and willingness to participate. For the purpose of scheduling demand based on the customer's willingness to pay, such physical attributes of the loads in the Azores have been described in Chap. 8. Once scheduled, these load characteristics can be further utilized to balance intra-dispatch supply-demand error.

To implement the concept of real-time demand response, it is critical to relate the timescales of the load response to those of the system imbalances. For example, to balance sustained variations (Fig. 14.8), the system operator can possibly utilize large commercial and industrial loads as well as a large aggregate of small residential loads. There are two ways to implement intra-dispatch demand response. First, it is possible for loads, utilizing frequency sensors embedded in variable speed drives, to act as balancing resources through homeostatic control. The induction motor loads can be converted into variable speed drives like constant power and constant torque based on the utility of the end user. The second way to implement intra-dispatch demand response is direct control of the load by the system operator. While the first approach can be applied to all kinds of inductive loads, small or large, the second approach is more useful for noninductive or resistive loads such as lighting in shopping malls. Also, direct load control is practical for large induction motors (industrial loads) if the system operator wishes to refrain from initial investment expenditure on load automation or the embedding of sensors. Likewise, the automation of small induction motors to variable speed drives, through sensors and power electronics, is the only way of implementing intra-dispatch demand response at the household level. On Flores, household refrigerators account for 42 % of residential consumption. Always online, these loads can serve as a large aggregate for short-run intra-dispatch balancing reserve. Experiments prove that freezer temperatures rise by one and a half degrees Celsius following 30 min of power deficit. Refrigerators are designed to handle the fast on/off switching of cycles. By controlling their switching cycles, significant levels of short-term power balancing capacity can be achieved. However, it is critical to note that only short-term variations in wind power can be balanced by refrigeration load (Fig. 14.5), not long-term sustained variations (Fig. 14.8). Nevertheless, long-term sustained intra-dispatch wind power variations can be balanced by direct or automated control of commercial and/or industrial loads. For example, on São Miguel island, a shopping mall with large air-conditioners, cement factory with a substantial motor load for the cutting/grinding/sieving/mixing of raw material, a dairy farm that runs boilers, refrigeration loads in grocery stores, and laundry (washer, dryer) loads in hotels

are potential candidates for the balancing of sustained intra-dispatch wind power variations. Particularly, air-conditioners can be employed for power balancing in ten of seconds or less. Their input power can be quickly adjusted through power electronics, and switching its operating state within a short period of time will not significantly affect the end user's comfort level [8,9].

Intra-dispatch demand response can cut down on reserve requirements. Besides, the response of small distributed inertia in the network can be much faster as compared to controlling the prime mover of the slow hydro unit or the fast but expensive diesel unit. Recently, modeling and control principles were introduced to support the implementation of demand response in frequency regulation in [10]. The authors refer to their model as Automatic Generation and Demand Control (AGDC). To plan balancing reserves for the future, the frequency response characteristics of smart loads in the Azores can be taken into account [11]. Also, there must be incentives for the consumer to buy frequency responsive Smart Appliances. This is due to the fact that there is much interest in beginning to rely on demand side response to compensate for hard-to-predict wind variations in the system.

14.10 Summary

A possible control design for cost-effective intra-dispatch real-power balancing is illustrated for two islands in the Azores. Wind speed variations span over multiple timescales. Our objective is to balance intra-10-min sustained deviations in wind power between two consecutive dispatch actions. Of particular interest is the balancing of nonzero mean energy offset in wind power from its forecast or scheduled value. A high degree of efficiency can be achieved if sustainable natural cycles of conventional generators align with those of wind fluctuations. Consequently, the system cost can be minimized and the quality of service enhanced. To increase system efficiency in the Azores, within a non-congested network, the natural timescales of diesel and hydro generator response must align with those of wind power deviations. Hence, for balancing purposes, conventional power plants available on the islands must be utilized judiciously. Economic and environmental sustainability can be increased seamlessly if this is done.

Based on the results for Flores, it is evident that a prudent approach is to balance error on a 10-min horizon through slow technology, i.e., a hydropower plant. By utilizing wind forecasts, the potential of slower technologies can be harnessed to correct real-power imbalances on longer time horizons. Then fast fringe fluctuations around the prediction error can be balanced by diesel power plants. The advantages are twofold. First, hydro is economically and environmentally sustainable. In addition, the wear and tear on an expensive diesel plant can be minimized. Figure 14.14 illustrates how much can be saved if the timescale of balancing resources aligns with the timescales of the wind variations. It represents cumulative cost over intra-dispatch time period of 10 min to follow wind variations on Flores

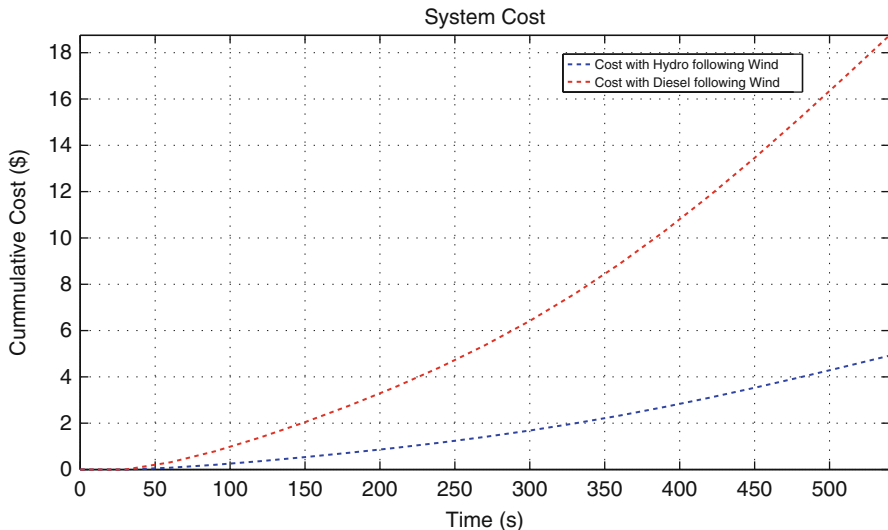


Fig. 14.14 Comparing cumulative cost over 10 min

(Fig. 14.8). As shown, it is much cheaper to balance sustained intra-dispatch wind variations with the sustainable and cheap hydropower plant (blue curve) than with the diesel generator (red curve). Cumulatively, the savings would be much more over the longer time horizons of months or years. Furthermore, additional savings can be achieved through intra-dispatch demand response. Other potential balancing resources include storage devices which are capable of responding much faster than conventional generators. New balancing resources, such as EVs, flywheels, and batteries, where the response rate is on a much shorter timescale, require decentralized approach proposed in this chapter and higher order models. More has been written about the storage devices in subsequent chapters.

References

1. J. Apt, The spectrum of power from wind turbines. *J. Power Sources* **169**(2), 369–374 (2007)
2. N. Cohn, *Control of Generation and Power Flow on Interconnected Power Systems* (John Wiley and Sons Inc., New York, 1961)
3. M. Ilić, J. Zaborszky, *Dynamics and Control of Large Electric Power Systems*, Sons Inc., (John Wiley and Sons Inc., New York, 2000)
4. M. Calovic, Dynamic state-space models of electric power systems. Technical Report, University of Illinois, Urbana (1971)
5. J. Cardell, Integrating small scale distributed generation into a deregulated market: control strategies and price feedback. Doctoral Thesis, MIT (September 1997)
6. W.I. Rowen, Simplified mathematical representations of heavy duty gas turbines. *J. Eng. Power Transactions of ASME* **105**, 865–869 (1983)

7. M. Ilić, S.X. Liu, *Hierarchical Power Systems Control; Its Value in a Changing Industry* (Springer, London, 1996)
8. Lawrence Berkeley National Laboratory, Demand Response Spinning Reserve Demonstration. (2007) certs.lbl.gov/pdf/62761.pdf
9. D. Bargiolas, J.D. Birdwell, Residential air conditioner dynamic model for direct load control. *IEEE Trans. Power Deliv.* **3**, 2119–2126 (1988)
10. M. Ilić, N. Popli, Automatic generation and demand control (AGDC) for system with high wind penetration. Working Paper, Electric Energy System Group R-WP15, Carnegie Mellon University (July 2011)
11. M. Ilić , N. Popli, J.Y. Joo, Y. Hou, A possible engineering and economic framework for implementing demand side participation in frequency regulation at value, in *IEEE Power Engineering Society General Meeting*, 2011

Chapter 15

Stabilization and Regulation of Small Frequency Fluctuations by Means of Governor and Flywheel Control

Qixing Liu, Milos Cvetković, and Marija Ilić

15.1 Potential Frequency Problems in Systems with High Wind Penetration

As the interest to deploy more wind power in future electric energy systems increases, there is a growing concern that the ever-changing electric energy systems will encounter new operating problems not common in electric power systems with conventional power plants. These problems may show up either as unacceptable deviations of nominal frequency and therefore poor power quality, or even as more frequent interruptions of electricity services. Wind fluctuations and the resulting frequency deviations can vary over time in amplitude, rate of change, and duration. An illustration of such fluctuations is shown in Fig. 15.1. Moreover, as more conventional fossil-fuel type power plants are replaced by wind power plants, there are growing concerns about the decrease of inertia and damping in such systems; this may, in turn, lead to a much more sensitive system response to disturbances and even to instability of the system. Possible unstable system response to persistent, low-amplitude wind disturbances has become a concern to the large continental electric power utilities as more wind power is being deployed. These instability problems may become even more pronounced in the small-scale island-type electric power systems studied in this chapter. Figures 15.2 and 15.3 show one-line diagram representation of the electric grid interconnecting generators on Flores and São Miguel [1], respectively.¹ These systems are potentially unstable when highly

¹These one-line diagrams include the effects of loads after a topological model reduction is performed to eliminate the load buses; see appendices in this chapter.

Q. Liu (✉) • M. Cvetković • Marija Ilić

Department of Electrical and Computer Engineering, Carnegie Mellon University,
5000 Forbes Avenue, Pittsburgh, PA 15213, USA

e-mail: lqx@cmu.edu; mcvetkov@andrew.cmu.edu; milic@ece.cmu.edu

Fig. 15.1 A typical 30-min wind disturbance with three types [type A: small amplitude disturbance with zero, negative, and positive means, type B: short-term (3 s) large wind gust, and type C: long-term (180 s) large wind failure]

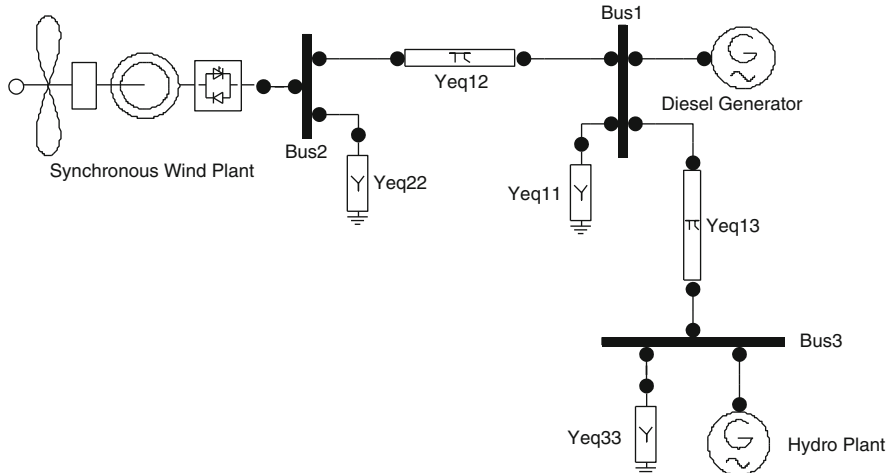
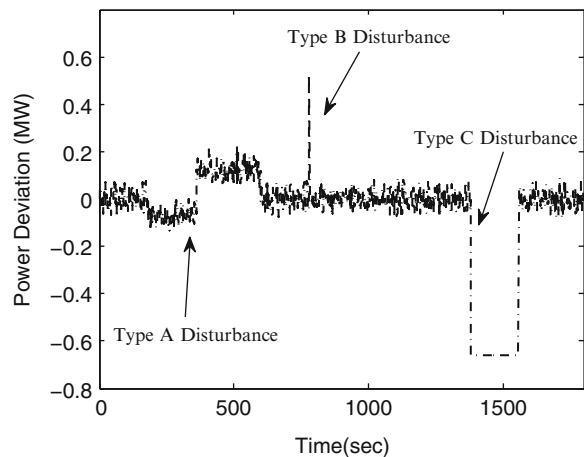


Fig. 15.2 One-line diagram of Flores Island power system

fluctuating renewable power resources are connected to the existing grids; both small system inertia and lack of spinning reserve units may contribute to the stability problems. Because of these potential problems, it is necessary to assess the stability of these systems and enhance the control of the existing power plants as well as the control of newly added storage, such as flywheels. In this chapter we recognize this need and proceed by first briefly summarizing the state of the art of today's frequency stabilization and regulation and describing why the existing control may be inadequate for ensuring stable and high-quality service in systems with a high penetration of wind power.

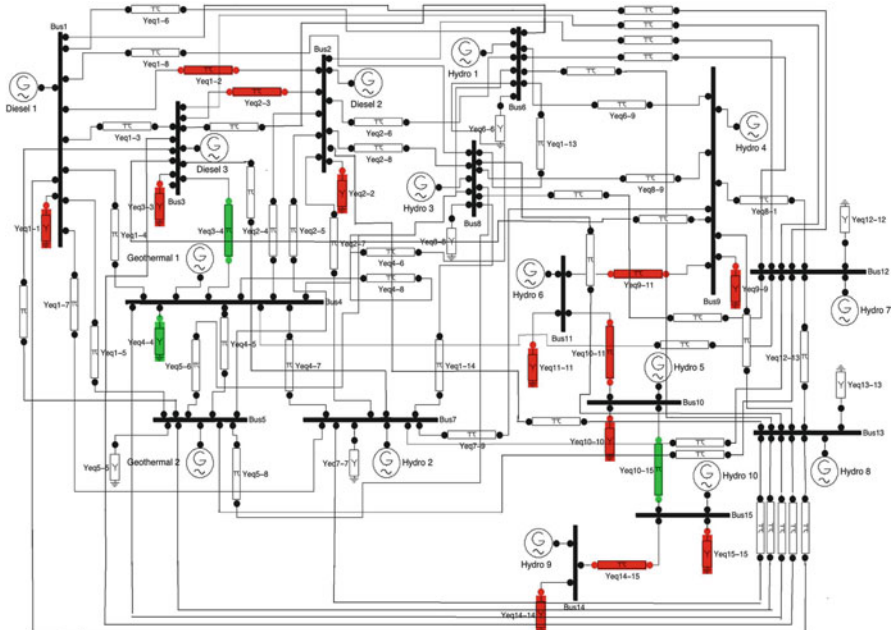


Fig. 15.3 One-line diagram of São Miguel Island power system

15.2 Typical Methods for Frequency Stabilization and Regulation in Today's Electric Energy Systems

The frequency stabilization and regulation approaches used in today's electric energy systems are hierarchical; the primary control is local and intended to stabilize fast frequency fluctuations, and the secondary control, also known as automatic generation control (AGC), is intended to ensure that there are no cumulative net power imbalances at the utility level. Each conventional generator has a speed governor which responds to deviations in local frequency from its set point either as a proportional (P) or as a proportional-integral (PI) controller [2–6].

To identify why today's primary and secondary controls may be inadequate for managing persistent wind power fluctuations, we first recall that the dynamics of the states in each generator i can be represented in terms of its state variables $\mathbf{x}_{Gi} \in \mathbf{R}^{G_i}$ and the coupling variables \mathbf{x}_{ij} of generator i with directly connected generators j . The primary controller reacts continuously to local frequency deviations from the reference frequency. This dependence can be written as a set of linearized ordinary differential equations (ODEs) of the form given in Eq. (15.1) as follows:

$$\dot{\mathbf{x}}_{Gi} = \mathbf{A}_{Gi}\mathbf{x}_{Gi} + \mathbf{B}_{Gi}u_{Gi} + \sum_{j \in N, j \neq i} \mathbf{A}_{ij}\mathbf{x}_{ij}, \quad (15.1a)$$

$$u_{Gi} = -\mathbf{K}_{Gi}\mathbf{C}_{Gi}(\mathbf{x}_{Gi} - \mathbf{x}_{Gi}^{\text{ref}}). \quad (15.1b)$$

The control u_{Gi} is defined as the primary control input which locally stabilizes the generator component by placing the eigenvalues of the closed-loop matrix

$$\tilde{\mathbf{A}}_{Gi} = \mathbf{A}_{Gi} - \mathbf{K}_{Gi}\mathbf{C}_{Gi}$$

to the left side of the complex plane.

However, today's primary control is designed as a localized control in which the dynamic interactions of component i with the rest of the system are not considered. It is shown later in this chapter that the state-space dynamic model of the interconnected system comprising all generators has a system matrix \mathbf{A}_{sys} given in the form of Eq. (15.2). At least in principle, it is possible that when the off-diagonal entries A_{ijs} are large, reflecting strong interactions between the various system components, the system matrix may become unstable even when the diagonal blocks are stabilized individually by using decentralized primary controls Eq. (15.1b).

$$\mathbf{A}_{sys} = \begin{bmatrix} \tilde{\mathbf{A}}_{G1} & \mathbf{A}_{12} & \cdots & \mathbf{A}_{1n} \\ \mathbf{A}_{21} & \tilde{\mathbf{A}}_{G2} & \cdots & \mathbf{A}_{2n} \\ \vdots & \vdots & \ddots & \vdots \\ \mathbf{A}_{n1} & \mathbf{A}_{n2} & \cdots & \tilde{\mathbf{A}}_{Gn} \end{bmatrix}. \quad (15.2)$$

It is possible, therefore, that fully decentralized primary control which does not account for dynamic interactions with the rest of the system is unable to ensure the overall stability of the interconnected system. Therefore, it will become necessary to assess the stability of the interconnected system in future electric energy systems and not only tune individual controllers for meeting stand-alone stability requirements. Moreover, since the stabilizing control is typically proportional (P) and not proportional integral (PI), each time disturbance occurs, the system remains stable but settles to another frequency equilibrium away from the desired nominal frequency. In order to eliminate this steady-state error and return the frequency back to the nominal value needed to ensure service at the desired frequency quality, the secondary control (AGC) is used. The objective of AGC is to maintain system frequency and interarea power exchange as they are prescheduled by adjusting the steady-state reference value x_{Gi}^{ref} of all participating generators in a manner of integral control.

However, in future electric energy systems with an increasingly high penetration of variable renewable resources, the steady-state equilibrium-based assumption becomes hard to justify because the persistent disturbances created by the renewable resources will cause fluctuations in the system states and the steady state will never be reached. Therefore, the secondary control may not be adequate for frequency regulation in these systems. Moreover, as more and more conventional fossil-fuel synchronous generator units are being replaced by smaller distributed energy resources, the remaining synchronous generator units will have smaller inertia and damping. The off-diagonal terms in matrix \mathbf{A}_{sys} will become relatively larger

than the diagonal terms, and this is likely to affect the stability of the entire interconnected system. In short, today's frequency control and regulation logic may not be sufficient to meet the frequency stability and frequency quality specifications of the evolving electric energy systems. It is therefore crucial to rethink the dynamic standards for both component- and system-level responses in order to integrate renewable sources without sacrificing the quality of electricity service.

In this chapter we first derive a state-space model of the future electric energy systems in Sect. 15.3. This model is used to propose a systematic stabilization and regulation approach capable of managing low-amplitude persistent wind power fluctuations (type A), in Fig. 15.1 in Sect. 15.4.1. This approach is illustrated in the electric energy systems of Flores and São Miguel in Sect. 15.5. It is shown that the complexity of sensing and communications varies according to the design criteria and with qualitatively different operating conditions. In this framework, newly developed technologies, such as phasor measurement units (PMUs) and fast energy storage devices, such as flywheels, are shown to be critical to the implementation of systematic control that doesn't entail excessive wear and tear .

15.3 Dynamic Model of Linearized Frequency Dynamics in State-Space Form

Our module-based approach to modeling the frequency dynamics of systems with wind power plants builds upon the modeling approach in [7]. Each linearized model of a conventional generator takes on the general form given in Eq. (15.1). We review here that a synchronous machine-type wind power plant model takes on a similar form.² When represented as a negative load, the wind power plant is simply modeled as a disturbance, much the same way as load disturbances are modeled in [7]. All the modules are then interconnected by using linearized real power flow equations as network constraints. In what follows only models of synchronous generator-type modules presently installed on Flores and São Miguel Islands are presented. The approach can be extended to include the dynamics of many other resources and to model the electric energy systems of any given topology.

15.3.1 State-Space Form of Stand-Alone Generator Modules

The modeling of generator modules is briefly introduced below. Each model is written in the form of ODEs, Eq. (15.1), and can be derived for any generation type.

²In this chapter the induction machine-type wind power plant is not considered. For this, see Chaps. 16 and 19.

15.3.1.1 State-Space Model of a Stand-Alone Diesel Generator

The model of a diesel generator [8] written in standard state-space form is as follows:

$$\dot{\mathbf{x}}_{Gd} = \tilde{\mathbf{A}}_{Gd}\mathbf{x}_{Gd} + \mathbf{B}_{Gd}u_{Gd} + \mathbf{C}_{pd}\Delta P_{Gd}, \quad (15.3)$$

where the states, control, and component matrices are defined as

$$\begin{aligned} \mathbf{x}_{Gd} &= [\Delta\delta_{Gd} \ \Delta\omega_{Gd} \ \Delta m_{Bd}]^T, \\ u_{Gd} &= \Delta\omega_{Gd}^{\text{ref}}, \\ \tilde{\mathbf{A}}_{Gd} &= \begin{bmatrix} 0 & \omega_0 & 0 \\ 0 & -\frac{D_d}{M_d} & \frac{1}{M_d} \\ \frac{K_I C_d K_d}{\omega_0 T_d} - \frac{C_d K_d}{T_d R_c} & -\frac{1}{T_d} & \end{bmatrix}, \\ \mathbf{B}_{Gd} &= \begin{bmatrix} 0 \\ 0 \\ \frac{C_d K_d}{T_d R_c} \end{bmatrix}, \\ \mathbf{C}_{pd} &= \begin{bmatrix} 0 \\ -\frac{1}{M_d} \\ 0 \end{bmatrix}. \end{aligned}$$

The state variables $\Delta\delta_{Gd}$, $\Delta\omega_{Gd}$, and Δm_{Bd} correspond to the voltage phase angle deviation, speed deviation, and change in diesel engine consumption. $\Delta\omega_{Gd}^{\text{ref}}$ is the adjustment of the reference value of the diesel's speed-governor system, which is usually utilized for secondary frequency control. ω_0 is the rated angular velocity (120π rad/s in the US power systems). M_d and D_d stand for the inertia and damping coefficient, respectively. C_d and K_d are the transfer function coefficients for the fuel system. T_d is the time constant of the fuel system. ΔP_{Gd} refers to the electrical power output of the generator, which is defined as the coupling of the generator with the rest of the system. Matrix \mathbf{C}_{pd} is the coupling matrix for the coupling variable.

15.3.1.2 State-Space Model of a Stand-Alone Hydro Generator

The standard state-space model of hydro generator is [9]

$$\dot{\mathbf{x}}_{Gh} = \tilde{\mathbf{A}}_{Gh}\mathbf{x}_{Gh} + \mathbf{B}_{Gh}u_{Gh} + \mathbf{C}_{ph}\Delta P_{Gh}, \quad (15.4)$$

where the states, control, and matrices are defined as

$$\begin{aligned} \mathbf{x}_{Gh} &= [\Delta\delta_{Gh} \ \Delta\omega_{Gh} \ \Delta q_h \ \Delta v_h \ \Delta a_h]^T, \\ u_{Gh} &= \Delta\omega_{Gh}^{\text{ref}}, \end{aligned}$$

$$\tilde{\mathbf{A}}_{Gh} = \begin{bmatrix} 0 & \omega_0 & 0 & 0 & 0 \\ 0 & -\frac{e_H + D_h}{M_h} & \frac{k_q}{M_h} & 0 & -\frac{k_w}{M_h} \\ 0 & \frac{1}{T_f} & -\frac{1}{T_q} & 0 & \frac{1}{T_w} \\ 0 & 0 & 0 & -\frac{1}{T_e} & \frac{a}{T_e} \\ 0 & -\frac{G_p}{T_s} & 0 & \frac{1}{T_s} & -\frac{r_h + r'}{T_s} \end{bmatrix},$$

$$\mathbf{B}_{Gh} = \begin{bmatrix} 0 \\ 0 \\ 0 \\ \frac{G_p}{T_s} \\ 0 \end{bmatrix},$$

$$\mathbf{C}_{ph} = \begin{bmatrix} 0 \\ -\frac{1}{M_h} \\ 0 \\ 0 \\ 0 \end{bmatrix}.$$

The state variables Δq_h , Δv_h , and Δa_h denote the penstock flow, the governor droop, and the gate position of the hydro generator, respectively. e_H , k_q , k_w , T_f , T_q , and T_w are constants reflecting state interdependence within the hydro turbine. T_e stands for the time constant of the valve-turbine gate system. T_s is the time constant of the servomotor gates. r_h and r' are the permanent speed droop and transient speed droop of the hydro generator. G_p represents the feedback gain of the speed governor.

15.3.1.3 State-Space Model of a Stand-Alone Wind Generator

The module of a wind generator varies with respect to the generation technology that is deployed in the system. It can be an induction generator, a synchronous generator, or a directly connected negative load. In this chapter, the wind generator is assumed to be either a synchronous generator or a negative load. The model of a synchronous wind power generator with no pitch control is introduced as the following Eq. (15.5). Wind power considered as a negative load will be discussed in the next subsection.

$$\dot{\mathbf{x}}_{Gws} = \tilde{\mathbf{A}}_{Gws} \mathbf{x}_{Gws} + \mathbf{C}_{pws} \Delta P_{Gws}, \quad (15.5)$$

where the states and matrices are defined as

$$\mathbf{x}_{Gws} = [\Delta \delta_{Gws} \Delta \omega_{Gws}],$$

$$\tilde{\mathbf{A}}_{Gws} = \begin{bmatrix} 0 & \omega_0 \\ 0 & -\frac{D_{ws}}{M_{ws}} \end{bmatrix},$$

$$\mathbf{C}_{pws} = \begin{bmatrix} 0 \\ -\frac{1}{M_{ws}} \end{bmatrix}.$$

15.3.1.4 State-Space Model of Uncontrolled Stand-Alone Generators in the Azores Islands

São Miguel Island, in particular, has several geothermal power and run-of-the-river hydro power plants. These plants have no primary governor control. The dynamic model of geothermal generators is

$$\dot{\mathbf{x}}_{Gge} = \tilde{\mathbf{A}}_{Gge}\mathbf{x}_{Gge} + \mathbf{B}_{Gge}u_{Gge} + \mathbf{C}_{pge}\Delta P_{Gge}, \quad (15.6)$$

where the states and matrices are defined as

$$\mathbf{x}_{Gge} = [\Delta\delta_{Gge} \ \Delta\omega_{Gge}],$$

$$\tilde{\mathbf{A}}_{Gge} = \begin{bmatrix} 0 & \omega_0 \\ 0 & -\frac{D_{ge}}{M_{ge}} \end{bmatrix},$$

$$\mathbf{C}_{pge} = \begin{bmatrix} 0 \\ -\frac{1}{M_{ge}} \end{bmatrix}.$$

The run-of-the-river hydro generators are modeled as

$$\dot{\mathbf{x}}_{Grh} = \tilde{\mathbf{A}}_{Grh}\mathbf{x}_{Grh} + \mathbf{B}_{Grh}u_{Grh} + \mathbf{C}_{prh}\Delta P_{Grh}, \quad (15.7)$$

where the states and matrices are defined as

$$\mathbf{x}_{Grh} = [\Delta\delta_{Grh} \ \Delta\omega_{Grh}],$$

$$\tilde{\mathbf{A}}_{Grh} = \begin{bmatrix} 0 & \omega_0 \\ 0 & -\frac{D_{rh}}{M_{rh}} \end{bmatrix},$$

$$\mathbf{C}_{prh} = \begin{bmatrix} 0 \\ -\frac{1}{M_{rh}} \end{bmatrix}.$$

15.3.2 Load Modules

Load deviations $\Delta P_L(t)$ around the forecast load $P_L(0)$ create disturbances in the dynamics of the interconnected power system. One can consider $\Delta P_L(t)$ to be a hard-to-predict deviation in demand and/or a hard-to-predict deviations in the renewable source located at the load bus. When a renewable power source is thought of as a negative variable load, it injects random power disturbances into the grid. Therefore, the actual load $P_L(t)$ can be represented as

$$P_L(t) = P_L(0) + \Delta P_L(t). \quad (15.8)$$

15.3.3 Flywheel Module

A detailed dynamical model of a flywheel is introduced in Chap. 19. The flywheel participates in frequency control and regulates the system as a control device that absorbs power from or provides power to the system in order to compensate for disturbances. Theoretically speaking, this device is not able to absorb or provide power instantaneously because it has its own dynamics. However, in practice, since the time constant of a flywheel is much smaller than the mechanical time constants of the conventional generating units, it is justifiable to neglect the dynamics of the flywheel and assume that it can instantaneously adjust its power output. A flywheel can be then assumed to be a controllable negative load. We define ΔP_f as the flywheel power output that will enter the system model as a control input variable. The control matrix of the flywheel installed on the i th generator is defined as

$$\mathbf{B}_{fi} = -\mathbf{C}_{pi}.$$

15.3.4 Network Constraints

Both the dynamics of generators and load deviations are related via electric power network constraints. When modeling systems with low-amplitude disturbances, which is the main focus of this section, the linearized real power flow equations are sufficient accurate models of the power grid constraints. The real power injections are grouped into those from the generator buses \mathbf{P}_G and the load buses \mathbf{P}_L that include both wind and flywheel injections. The linearized real power flow equations around the operating point can then be written as [10]

$$\Delta \mathbf{P}_G = \mathbf{J}_{GG}\Delta\delta_G + \mathbf{J}_{GL}\Delta\delta_L \quad (15.9a)$$

$$-\Delta \mathbf{P}_L = \mathbf{J}_{GL}\Delta\delta_G + \mathbf{J}_{LL}\Delta\delta_L, \quad (15.9b)$$

where

$$\mathbf{J}_{ij} = \left. \frac{\partial \mathbf{P}_i}{\partial \delta_j} \right|_{\delta_j=\delta_j^*}, \quad i, j \in \{G, L\}$$

are the Jacobian matrices evaluated at the given operating point. $\Delta\delta_L$ stands for the phase angle deviations on the load buses. Assuming that \mathbf{J}_{LL} is invertible under normal operating conditions, we can substitute $\Delta\delta_L$ from (15.9b) to (15.9a) and obtain the system-level algebraic network coupling equation:

$$\Delta \mathbf{P}_G = \mathbf{K}_p \Delta\delta_G + \mathbf{D}_p \Delta \mathbf{P}_L, \quad (15.10)$$

where

$$\mathbf{K}_p = \mathbf{J}_{GG} - \mathbf{J}_{GL}\mathbf{J}_{LL}^{-1}\mathbf{J}_{LG} \quad (15.11a)$$

$$\mathbf{D}_p = -\mathbf{J}_{GL}\mathbf{J}_{LL}^{-1}. \quad (15.11b)$$

15.3.5 Modeling of the Interconnected System

The dynamic model of the interconnected system with n generators is composed of the individual generator modules and the network constraints (15.10). The full-state-space model with the n generator modules and m flywheels explicitly connected has the following form:

$$\dot{\mathbf{x}} = \tilde{\mathbf{A}}\mathbf{x} + \mathbf{B}\mathbf{u}_G + \mathbf{B}_f\mathbf{u}_f + \mathbf{F}\mathbf{w}, \quad (15.12)$$

where vector \mathbf{u}_G stands for the reference value adjustments ω_G^{ref} on the primary controllers and vector \mathbf{u}_f is the control variable of the flywheel. \mathbf{w} are the disturbances to the interconnected system. They are explicitly expressed as

$$\begin{aligned} \mathbf{x} &= [x_{G1}^T \ x_{G2}^T \ \dots \ x_{Gn}^T]^T, \\ \mathbf{u}_G &= [u_{G1}^T \ u_{G2}^T \ \dots \ u_{Gn}^T]^T, \\ \mathbf{u}_f &= [u_{f1}^T \ u_{f2}^T \ \dots \ u_{fm}^T]^T, \\ \mathbf{w} &= \Delta\mathbf{P}_L. \end{aligned}$$

The following equations show the derivation of the matrices:

$$\begin{aligned} \tilde{\mathbf{A}} &= \begin{bmatrix} \tilde{\mathbf{A}}_{G1} & 0 & \dots & 0 \\ 0 & \tilde{\mathbf{A}}_{G2} & \dots & 0 \\ \vdots & \vdots & \ddots & \vdots \\ 0 & 0 & \dots & \tilde{\mathbf{A}}_{Gn} \end{bmatrix} + \begin{bmatrix} \mathbf{C}_{p1} & 0 & \dots & 0 \\ 0 & \mathbf{C}_{p2} & \dots & 0 \\ \vdots & \vdots & \ddots & \vdots \\ 0 & 0 & \dots & \mathbf{C}_{pn} \end{bmatrix} \mathbf{K}_p \mathbf{S}_\delta, \\ \mathbf{B} &= \begin{bmatrix} \mathbf{B}_{G1} & 0 & \dots & 0 \\ 0 & \mathbf{B}_{G2} & \dots & 0 \\ \vdots & \vdots & \ddots & \vdots \\ 0 & 0 & \dots & \mathbf{B}_{Gn} \end{bmatrix}, \end{aligned}$$

$$\mathbf{B}_f = \begin{bmatrix} \mathbf{B}_{f1} & 0 & \cdots & 0 \\ 0 & \mathbf{B}_{f2} & \cdots & 0 \\ \vdots & \vdots & \ddots & \vdots \\ 0 & 0 & \cdots & \mathbf{B}_{fm} \end{bmatrix},$$

$$\mathbf{F} = \begin{bmatrix} \mathbf{C}_{p1} & 0 & \cdots & 0 \\ 0 & \mathbf{C}_{p2} & \cdots & 0 \\ \vdots & \vdots & \ddots & \vdots \\ 0 & 0 & \cdots & \mathbf{C}_{pn} \end{bmatrix} \mathbf{D}_p.$$

The matrix \mathbf{S}_δ comprises 0's and 1's, and it is used to extract the state variables $\boldsymbol{\delta}_G$ from the system states \mathbf{x} :

$$\boldsymbol{\delta}_G = \mathbf{S}_\delta \mathbf{x}. \quad (15.13)$$

15.4 Enhanced Frequency Stabilization and Regulation Framework

In this section we propose a framework to enhance the frequency stabilization and regulation of future electric energy systems. This framework can be used to support the stable operation of future systems with renewable energy sources. The newly developed sensing and energy storage technologies are shown to be key to implementing the proposed control framework.

15.4.1 Our Proposed Control Framework

A general flowchart (Fig. 15.4) is used to illustrate the framework which is hierarchical. The stabilization of stand-alone components first, and the interconnected systems second, is considered. The stabilization process is described below:

Check to see if the stand-alone components are stable. If they are, design the stabilization using flywheels. This will reduce the wear and tear caused by extensive tuning of the governor-turbine systems of the conventional generators. If the components are not stable, the stabilization design can either use the component's local control or rely on the control of the other components via coordination. If coordinated control is preferred for designing the control at the interconnected system level to stabilize the unstable modes; if local control is preferred, do so at the component level (and then design the stabilization using flywheels as described above).

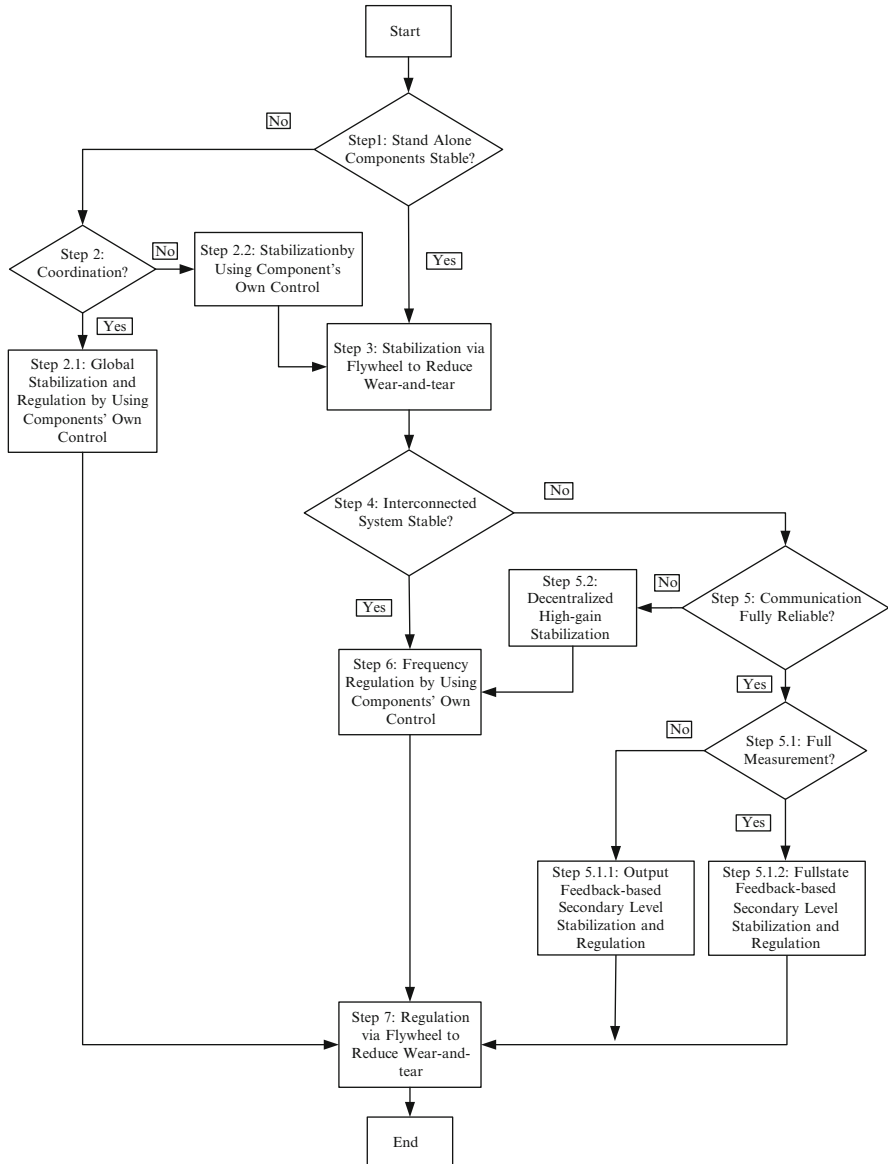


Fig. 15.4 An enhanced frequency stabilization and regulation framework for systems with renewable energy sources and new control technologies

Check to see if the entire interconnected system is stable. If it is, design the frequency regulation by using the components' own control. If it is not, design a coordinated control at the system level when the communication is fully reliable. If the entire system is equipped with full measurement, design a linear optimal control-

based full-state feedback control for both stabilization and regulation; if the entire system is not equipped with full measurement, design a linear optimal control-based output feedback control.

If communication fails, however, design a high-gain control, at the component level, to stabilize the interconnected system, and then design the frequency regulation by using the components' own control.

The final step in all these, no matter what route it has taken so far, is to design the frequency regulation using flywheels in order to reduce the wear and tear caused by governor-turbine systems in fast frequency regulation service.

Step 1: Check to see if each of the stand-alone components is stable. If yes, go to Step 3; otherwise, go to Step 2.

Step 2: To stabilize the unstable components, the design can either use the component's local control or rely on the control of other components via coordination.

If the coordinated control is preferred, go to Step 2.1; otherwise, Step 2.2.

Step 2.1: At the interconnected system level, design the control to stabilize the unstable modes. Go to Step 7.

Step 2.2: At the component level, design the control to stabilize the unstable modes. Go to Step 3.

Step 3: In order to reduce the wear and tear caused by extensive tuning on the governor-turbine systems of conventional generators, design the stabilization using flywheel devices.

Step 4: Check to see if the entire interconnected system is stable. If yes, go to Step 6; otherwise, go to Step 5.

Step 5: A coordinated control at the system level is designed when the communication is fully reliable (Step 5.1). If communication fails, a decentralized high-gain control is designed at the component level for backup purposes (Step 5.2).

Step 5.1: If the entire system is equipped with full measurement, design a full-state feedback control (Step 5.1.1); otherwise, design an output feedback control (Step 5.1.2).

Step 5.1.1: Design a linear optimal control-based full-state feedback control for both stabilization and regulation. Go to Step 7.

Step 5.1.2: Design a linear optimal control-based output feedback control for both stabilization and regulation. Go to Step 7.

Step 5.2: At the component level, design a high-gain control to stabilize the interconnected system. Go to Step 6.

Step 6: Design the frequency regulation by using the components' own control. Go to Step 7.

Step 7: In order to reduce the wear and tear caused by utilizing governor-turbine systems in fast frequency regulation service, design the frequency regulation using flywheel devices.

15.4.2 Stabilization Control Approaches

In this subsection we introduce three qualitatively different control logics that could be utilized in the general framework for different objectives.

15.4.2.1 Eigenvalue Placement

In Step 2.2, the eigenvalue placement technique can be applied to design localized stabilization for unstable components by using their own primary controls. This design can be based on the component dynamic model in Eq. (15.1), which adjusts the feedback control gain \mathbf{K}_{Gi} such that the eigenvalues of the closed-loop system matrix are all located on the left side of the complex plane.

In Step 3, an extra control input u_{fi} is added to the component model, and the control can be designed by using the same eigenvalue placement technique as described above.

15.4.2.2 High-Gain Decentralized Control

In Step 5.2, High-gain decentralized control is designed on the component level to stabilize the entire interconnected system. The component dynamic model (15.1) can still be used to design the control in this case except that a high-gain factor $g_{Gi} (\gg 1)$ is added ahead of \mathbf{K}_{Gi} , which is illustrated as

$$u_{Gi} = -g_{Gi} \mathbf{K}_{Gi} \mathbf{C}_{Gi} (\mathbf{x}_{Gi} - \mathbf{x}_{Gi}^{\text{ref}}). \quad (15.14)$$

To choose g_{Gi} and obtain guaranteed interconnected system stability, one can refer to literatures that develop sufficient conditions for stabilizing the interconnected system by using decentralized control [11, 12].

15.4.2.3 Coordinated Stabilization and Regulation

In Steps 2.1, 5.1.1, 5.1.2, 6, and 7, coordinated stabilization and regulation can be implemented by using either the set-point adjustments on the primary control of the components or flywheel energy storage devices via linear optimal control techniques such as linear quadratic regulator (LQR)-based full-state feedback control and/or output feedback control. These controls are introduced below.

15.4.2.3.1 LQR-Based Full-State Feedback Control

First, LQR-based full-state feedback control is designed on the interconnected system model (15.12).

$$\begin{aligned} \underset{\mathbf{u}_G, \mathbf{u}_f}{\text{minimize}} \quad J &= \frac{1}{2} \int_0^\infty \{ \mathbf{x}^T \mathbf{Q} \mathbf{x} + [\mathbf{u}_G, \mathbf{u}_f]^T \mathbf{R} [\mathbf{u}_G, \mathbf{u}_f] \} dt \\ \text{subject to} \quad \dot{\mathbf{x}} &= \mathbf{A} \mathbf{x} + \mathbf{B} \mathbf{u}_G + \mathbf{B}_f \mathbf{u}_f, \end{aligned} \quad (15.15)$$

where matrix \mathbf{Q} is positive semi-definite, which assigns the weights for the quadratic error of the state variables, and matrix \mathbf{R} is positive definite which defines the cost of the generator control input \mathbf{u}_G and the flywheel control input \mathbf{u}_f . By solving this optimization problem we can attain the feedback control gains as

$$\begin{aligned} \mathbf{u}_G &= -\mathbf{K}_G^{\text{LQR}} \mathbf{x}, \\ \mathbf{u}_f &= -\mathbf{K}_f^{\text{LQR}} \mathbf{x}. \end{aligned}$$

15.4.2.4 LQR-Based Interaction Variable Output Control

Second, LQR-based output feedback control is implemented by using an interactions variable (IntV)-based enhanced-AGC approach which we proposed in earlier work [7]. The IntV of an interconnected system z_a is defined as the linear combination of the full states of the system:

$$z_a = \mathbf{T}_a \mathbf{x}, \quad (15.16)$$

where row vector \mathbf{T}_a is characterized with the singularity property that

$$\mathbf{T}_a \mathbf{A} = 0.$$

The singularity is due to the linear dependence of the network coupling constraints. Then the dynamic equation of the IntV (no control applied yet) can be written as

$$\dot{z}_a = \mathbf{T}_a \mathbf{F}_W, \quad (15.17)$$

which is only driven by the disturbances.

In [7], IntV z_a is shown to represent the interconnected system's dynamics in response to disturbances w . More deeply, by integrating the two sides of Eq. (15.17), we show that IntV z_a stands for the energy mismatch which will cause deviations in stored kinetic energy as well as frequency. An LQR-based output feedback control is designed to minimize the IntV of the system over a long time horizon and consequently keep the IntV and frequency around the nominal value.

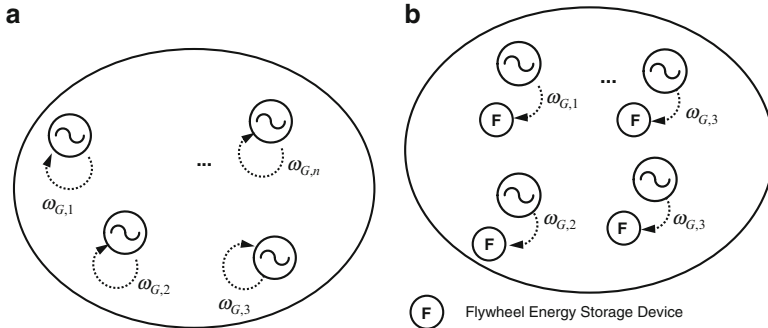


Fig. 15.5 Communication infrastructure of the decentralized control logics. **(a)** Control with conventional generators. **(b)** Control with flywheels

$$\begin{aligned}
 & \text{minimize}_{\mathbf{u}_G, \mathbf{u}_f} \quad J = \frac{1}{2} \int_0^{\infty} (\mathbf{z}_a^T \mathbf{Q}_a \mathbf{z}_a + [\mathbf{u}_G^T, \mathbf{u}_f^T] \mathbf{R} [\mathbf{u}_G^T, \mathbf{u}_f^T]^T) dt \\
 & \text{subject to} \quad \dot{\mathbf{x}} = \mathbf{A}\mathbf{x} + \mathbf{B}\mathbf{u}_G + \mathbf{B}_f\mathbf{u}_f \\
 & \quad \mathbf{u}_G = -\mathbf{K}_G^{\text{IntV}} \mathbf{z}_a \\
 & \quad \mathbf{u}_f = -\mathbf{K}_f^{\text{IntV}} \mathbf{z}_a. \tag{15.18}
 \end{aligned}$$

In this output feedback control, IntV is used as a feedback signal to drive the controller. In practice, \mathbf{z}_a can either be obtained by measuring all the state variables and using Eq. (15.16) or by measuring the dominant disturbances w and integrating Eq. (15.17). These two methods give the same \mathbf{z}_a but require a qualitatively different amount of sensing and communications.

15.4.3 Communication Complexity and Control Cost Analysis

The underlying communication infrastructures of the control logics introduced in Sect. 15.4.2 are illustrated in Figs. 15.5 and 15.6. It can be shown through comparison between these figures that the decentralized control logics require much less complicated communications than the coordinated control logics. Decentralized control locally measures the rotational frequency of the generator and communicates to either the speed governor or the flywheel devices for stabilization. Coordinated control requires all generators to upload their state variables information to a centralized control center where the control signals are generated and then distributed back to the conventional generators and/or the flywheel devices (Fig. 15.6).

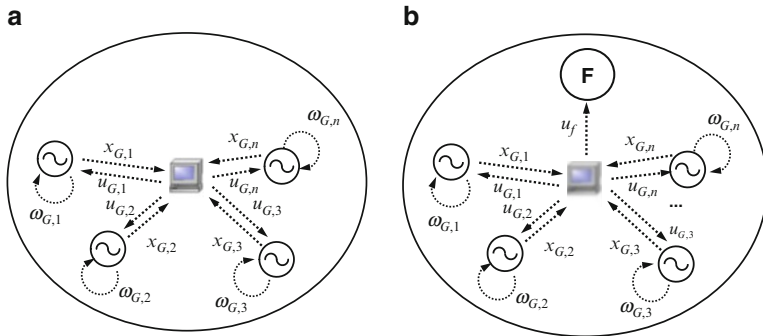


Fig. 15.6 Communication infrastructure of the coordinated control logics with full-state or output feedback. **(a)** Control with conventional generators. **(b)** Control with flywheels

Regarding the cost of these control logics, using flywheel devices is much more expensive than using the speed governors of conventional generators due to the high cost of the energy storage devices. Nevertheless, there still exists the trade-off between the cost of purchasing the expensive storage devices and the cost of the wear and tear of conventional generators. When large amounts of renewable energy sources are integrated, wear and tear can occur due to the overuse of speed governors in order to compensate for the output power variation of the renewable generators and the high-gain control that stabilizes the entire system. Another alternative is to use excitation control to manage the fast disturbances. This will be discussed in Chap. 16.

15.4.4 The Role of Phasor Measurement Units

In the proposed framework for frequency stabilization and regulation, the role of PMUs is pronounced. To implement the coordinated control approach, the states of rotor angle deviations $\Delta\delta_G$ need to be measured as part of the feedback signals. However, obtaining this measurement is not possible unless PMUs are installed. The rotor deviations angle $\Delta\delta_G$ is characterized as an integral of rotational speed $\Delta\omega_G$:

$$\Delta\delta_G(t) = \Delta\delta_G(t_0) + \int_{t_0}^t \Delta\omega_G d\tau.$$

Consequently, in order to obtain an accurate and synchronized measurement of the $\Delta\delta_G(t)$ of the entire system at any given time t , it is critical to have a unified time reference with which only PMUs are equipped.

15.5 Stabilization and Regulation of Flores and São Miguel Islands

In this section, two electric power systems are studied to illustrate the proposed frequency stabilization and regulation framework. In the first case, the small electric power system of Flores (Fig. 15.2) is studied. The relatively larger electric power system of São Miguel (Fig. 15.3) is considered as the second case.

15.5.1 Flores Island Case

The sensitivity matrices \mathbf{K}_p and \mathbf{D}_p and parameters of the dynamic components are included in Appendices B and D. They are obtained by using the linearized model in Eqs. (15.9)–(15.11). The equilibrium of the linearization is given in the data file for Chap. 15 online. The current wind power capacity of the island is 0.66 MW, which is approximately 13% of the entire electric power capacity. A high-gain PI control is installed on the diesel generator to manage both frequency stability and the steady-state error of the frequency after disturbances; therefore, no AGC is installed for this system. The persistent disturbances due to the uncertainty of the wind are plotted in Fig. 15.7 for a 1-min duration. The wind generator modeled as synchronous generator and as negative load are studied separately and compared in the following.

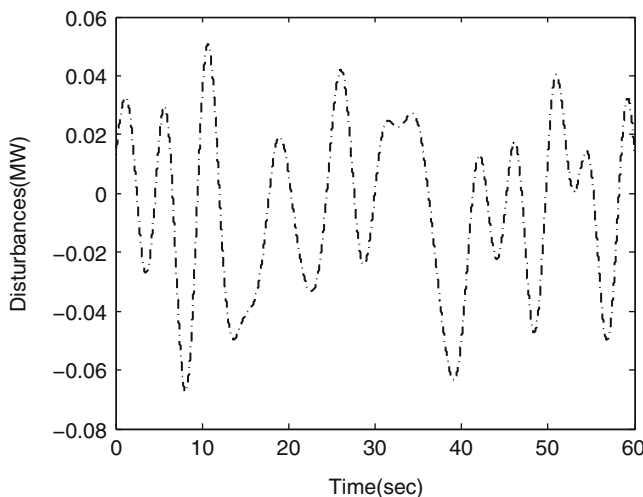


Fig. 15.7 Wind power disturbances under current penetration level

Table 15.1 Eigenvalues of the dynamic components

Generator components	Eigenvalues of the components
Diesel	$-0.03, -0.8238 \pm 9.867i$
Hydro	$0, -126.71, -1.3742, -0.0330, -0.4606$
Wind	$0, -0.0215$

Table 15.2 Eigenvalues of the dynamic components with a flywheel as local control

Generator components	Eigenvalues of the components
Diesel	$-0.03, -0.8349 \pm 9.867i$
Hydro	$0, -126.7109, -1.3741, -0.0447, -0.4606$
Wind	$0, -0.1288$

Table 15.3 Eigenvalues of the interconnected system

	Eigenvalues
Interconnected Flores system without local flywheel	$0.03 \pm 32.73i, -126.71, -0.65 \pm 9.83,$ $-0.17 \pm 2.86i, -0.03, -1.39, -0.46$
Interconnected Flores system with local flywheel	$0.07 \pm 32.73i, -126.71, -0.67 \pm 9.83,$ $-0.18 \pm 2.87i, -0.03, -1.39, -0.46$

15.5.1.1 Case 1: Flores System with the Wind Generator Modeled as a Synchronous Machine

To enhance the frequency stabilization and regulation of the test system by following the proposed framework, we first check the stability of the dynamic components, which are the diesel, hydro, and wind generators. Table 15.1 shows the eigenvalues of the components.

We then add local flywheel devices in Step 3 as extra damping to improve the frequency stability and reduce the wear and tear on the conventional generators. The resulting eigenvalues are shown in Table 15.2.

In Step 4, we check the stability of the interconnected system. From the eigenvalues of the interconnected system (listed in Table 15.3), it can be concluded that the system is stable in both cases with or without the local flywheel control added in Step 3; however, adding the local flywheels can increase the stability margin of the system.

Step 6 is skipped since a high-gain PI control has already been implemented on the diesel so no AGC is needed, which can also be seen from Fig. 15.8. The black dash dotted plots in this figure indicates a satisfactory performance of the PI control on maintaining the stability and quality of frequency.

In Step 7 we use flywheel devices to support the frequency regulation and reduce the wear and tear caused by overuse of the diesel generator. In Fig. 15.9, we can see by comparing the plots for system with and without flywheel for regulation that part of the disturbances is picked up by the flywheel after it is installed and the use of the

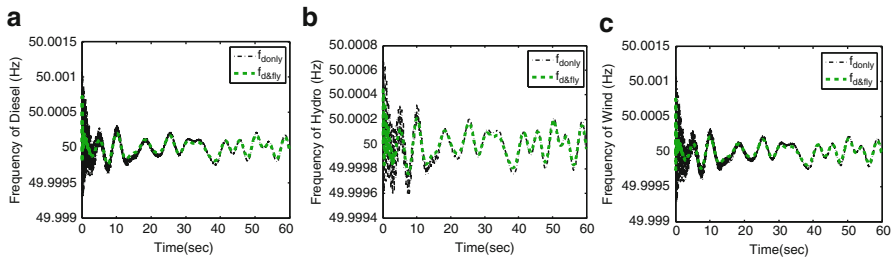


Fig. 15.8 Time response of frequency on Flores Island, Case 1: system with synchronous wind generator. (a) Diesel generator. (b) Hydro generator. (c) Wind generator

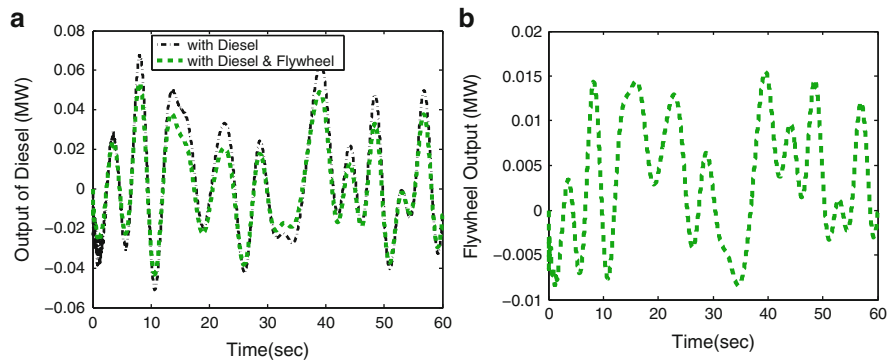


Fig. 15.9 Output of diesel and flywheel in response to frequency deviations, Case 1: system with synchronous wind generator. (a) Output of diesel generator. (b) Output of flywheel

Table 15.4 Eigenvalues of the dynamic components

Generator components	Eigenvalues of the components
Diesel	$-0.03, -0.8238 \pm 9.8670i$
Hydro	$0, -126.7109, -1.3742, -0.0330, -0.4606$

conventional diesel generator for this fast adjustment is reduced. The green dashed lines in Fig. 15.8 show that the frequency deviations can be further reduced by the flywheel devices.

15.5.1.2 Case 2: Flores System with the Wind Generator Modeled as a Negative Load

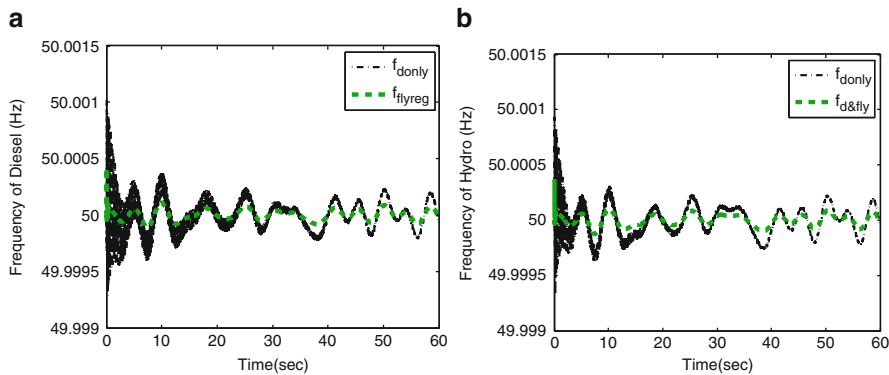
In this section, the wind power is modeled as negative load. We repeat the steps in the previous subsection for enhancing the frequency stability and quality of the Flores Island system. Table 15.4 shows the eigenvalues of the stand-alone components which are still stable in this case.

Table 15.5 Eigenvalues of the dynamic components with flywheel as local control

Generator components	Eigenvalues of the components
Diesel	$-0.03, -0.8349 \pm 9.8679i$
Hydro	$0, -126.7109, -1.3741, -0.0447, -0.4606$

Table 15.6 Eigenvalues of the interconnected system

	Eigenvalues
Interconnected Flores system without flywheel	$-0.64 \pm 5.14i, -126.71, -0.19 \pm 18.54i, -1.39, -0.03, -0.46$
Interconnected Flores system with flywheel	$-0.65 \pm 5.14i, -126.71, -0.2 \pm 18.54i, -1.39, -0.03, -0.46$

**Fig. 15.10** Time response of frequency on Flores Island, Case 2: system with negative load wind generator. (a) Diesel generator. (b) Hydro generator

We then add flywheel devices as in Step 3 as an extra damping to improve frequency stability and reduce the wear and tear on the conventional generators. The resulting eigenvalues are shown in Table 15.5.

The eigenvalues of the interconnected system are listed in Table 15.6, and it can be concluded that the system is stable both with or without the flywheel as local control.

Step 6 is skipped since a high-gain PI control has already been implemented on the diesel so no AGC is needed, which can also be seen from Fig. 15.10. The black dash dotted plots in this figure demonstrate the satisfactory performance of the PI control in maintaining the stability and quality of frequency.

In Step 7 we use flywheel devices to support frequency regulation and reduce the wear and tear caused by overuse of the diesel generator. In Fig. 15.11, we can see by comparing the plots for system with and without flywheel for regulation that part of the disturbances is picked up by flywheel after it is installed and the use of the conventional diesel generator for this fast adjustment is reduced. The green dashed

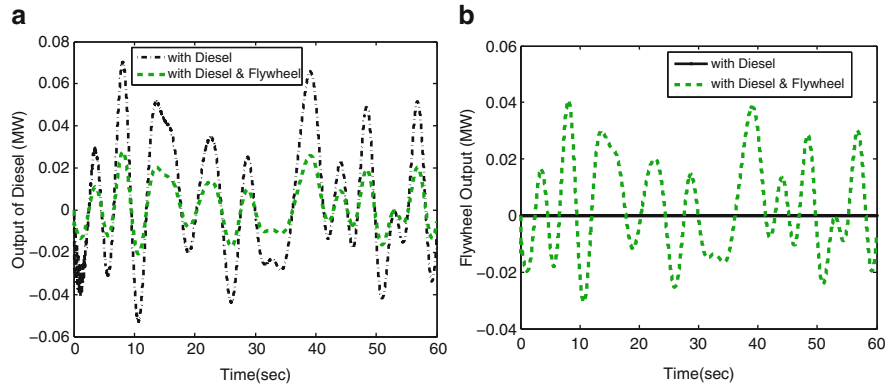


Fig. 15.11 Output of diesel and flywheel in response to frequency deviations, Case 2: system with negative load wind generator. **(a)** Output of diesel generator. **(b)** Output of flywheel

lines in Fig. 15.10 show that the frequency deviations can be further reduced by the flywheel devices. It can also be seen from comparing Figs. 15.8 and 15.10 that when the wind generator is modeled as a synchronous generator with its dynamics included in the system dynamics, less frequency oscillation is observed. This is because the response of frequency to the disturbances slows down when additional inertia of wind synchronous generator is added to the system.

15.5.2 São Miguel System

In this subsection, the frequency stabilization and regulation of the São Miguel electric power system are studied. This system has an average demand around 65 MW, with 3 large diesel power plants, 2 medium geothermal plants, 3 large hydro plants, 1 medium hydro plant, and 6 small hydro plants providing the electricity. The hydro plants are run-of-the-river hydroelectric generators and providing electricity based on the availability of the stream. The geothermal power plants provide electricity based on the availability of heat. There are no advanced governor controls in these hydro/geothermal power plants for frequency stabilization and regulation. Therefore, it is crucial to investigate their frequency stability and quality in order to ensure the QoS of the island's power supply. Moreover, since no wind power is currently penetrated to this system, it is worthwhile to research the frequency quality that results when the potential wind power plants are placed at different locations of the system. By comparing these different results, we can recommend the best location for future wind integration.

Table 15.7 Eigenvalues of the dynamic components with a flywheel as local control

Generator components	Eigenvalues of the components
Diesel 1	$-0.3000, -0.3988 \pm 25.6047i$
Diesel 2	$-0.3001, -0.3191 \pm 20.8188i$
Diesel 3	$-0.3001, -0.3191 \pm 20.8188i$
Geothermal 1	$0, -0.0461$
Geothermal 2	$0, -0.0461$
Large hydro	$0, -0.0461$
Medium hydro	$0, -0.0462$
Small hydro	$0, -0.0462$

Table 15.8 Eigenvalues of the interconnected system

	Eigenvalues
São Miguel system	$-0.023 \pm 2793.553i, -0.0231 \pm 2388.333i, -0.023 \pm 1615.891i,$ $-0.072 \pm 636.276i, -0.076 \pm 382.897i, -0.023 \pm 129.450i,$ $-0.023 \pm 104.737i, -0.023 \pm 99.096i, -0.023 \pm 51.791i,$ $-0.123 \pm 37.930i, -0.023 \pm 41.004i, -0.028 \pm 20.908i,$ $-0.079 \pm 19.790i, -0.042 \pm 14.381i, -0.166 \pm 10.822i,$ $-0.3, -0.883, -0.799$

First of all, we examine the stability of both the generator components and the interconnected system by following the general framework we propose in Sect. 15.4. The sensitivity matrices K_p of the system are shown in Appendix D. The eigenvalues of the stand-alone dynamic components and the interconnected system are shown in Tables 15.7 and 15.8. Since all the eigenvalues are placed either at zero or the left-hand side of the complex plane, the stand-alone components and the interconnected system are stable.

15.5.2.1 Relevance of Electrical Distances

We then introduce wind integration into our study on the future energy system of São Miguel. By using the simulation results, we show that the frequency quality and the infrastructure of the frequency regulation system will qualitatively differ depending on the different locations that wind power connects to. The persistent disturbances depicted in Fig. 15.7 for 1-min duration are assumed to be the disturbances caused by wind power to the future São Miguel system.

We compare the cases in Figs. 15.12–15.14, which are as follows: wind connects to diesel, wind connects to geothermal, and wind connects to hydro. It is seen that when wind is connected to the diesel generator or geothermal generator bus connecting to the diesel generator with small electrical distances, the frequency fluctuations caused by wind disturbances fall within the acceptable range. This is because the PI controllers on diesel generators are able to pick up the close-by power

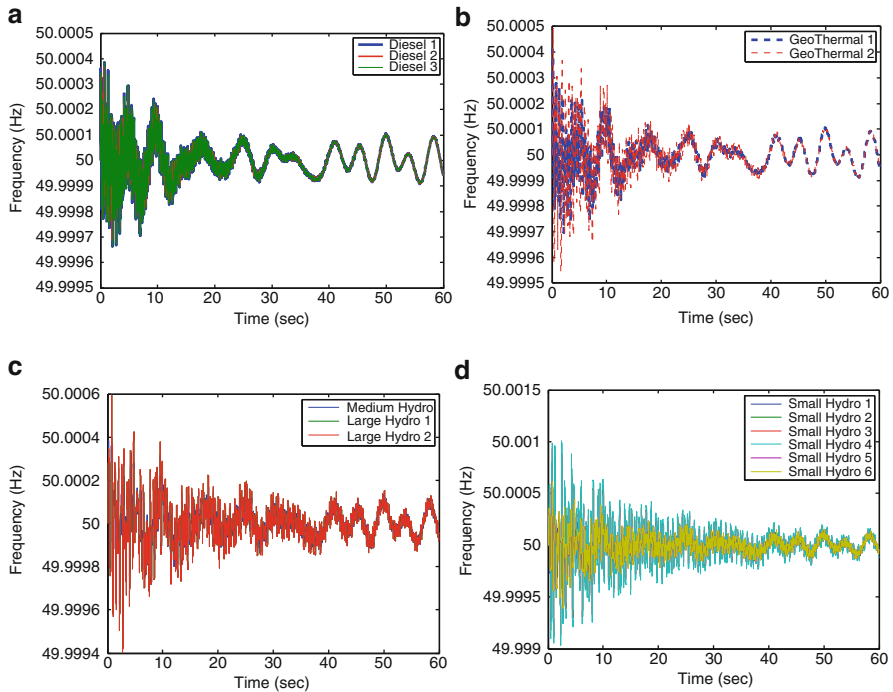


Fig. 15.12 Time response of frequency on São Miguel Island with wind connected to diesel. **(a)** Diesel frequency. **(b)** Geothermal frequency. **(c)** Large and medium hydro frequency. **(d)** Small hydro frequency

deviations. On the other hand, when the wind is connected to the hydro generator buses, high-magnitude frequency oscillations occur in the hydro generators. This is due to the fact that hydro generators are not equipped with any governor-turbine control and the disturbances are connected electrically far from the diesel generators.

Following the frequency stabilization and regulation framework proposed in this chapter, the sensing, communications, and control infrastructure needs to be designed differently with respect to the choice of wind integration locations. When wind power is connected to diesel or thermal generator buses, deploying a flywheel with coordinated control will reduce the wear and tear caused by overuse of the diesel generators. When wind is connected to hydro generator buses, implementing a flywheel with coordinated control will reduce the frequency oscillations on hydro generators. We designed the controls corresponding for each scenario and show the simulation results below:

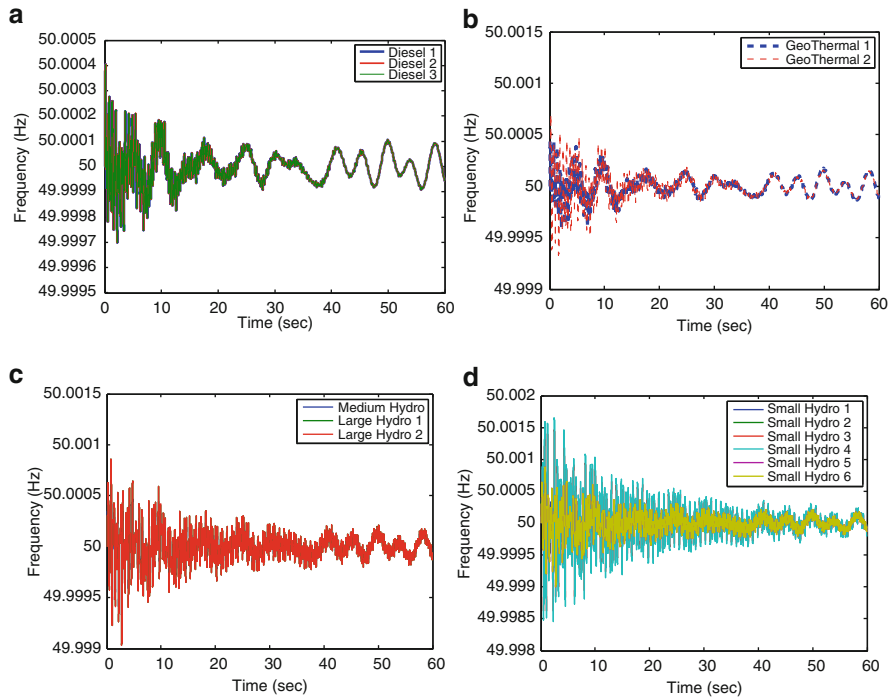


Fig. 15.13 Time response of frequency on São Miguel Island with wind connected to geothermal. (a) Diesel frequency. (b) Geothermal frequency. (c) Large and medium hydro frequency. (d) Small hydro frequency

In Fig. 15.15, it is seen that when a flywheel is implemented to support frequency regulation, diesel power output and therefore the wear and tear on diesel generators are reduced. In Fig. 15.16, by comparing the two frequency regulation cases of with flywheel and without flywheel, we can see that the high oscillations in the hydro generators are significantly smoothed when a flywheel is utilized.

15.5.3 Conclusions

In this chapter, a general framework is proposed to enhance frequency stabilization and regulation performances when there is a large amount of wind power penetration. The next step of this work is to implement the framework with large-scale

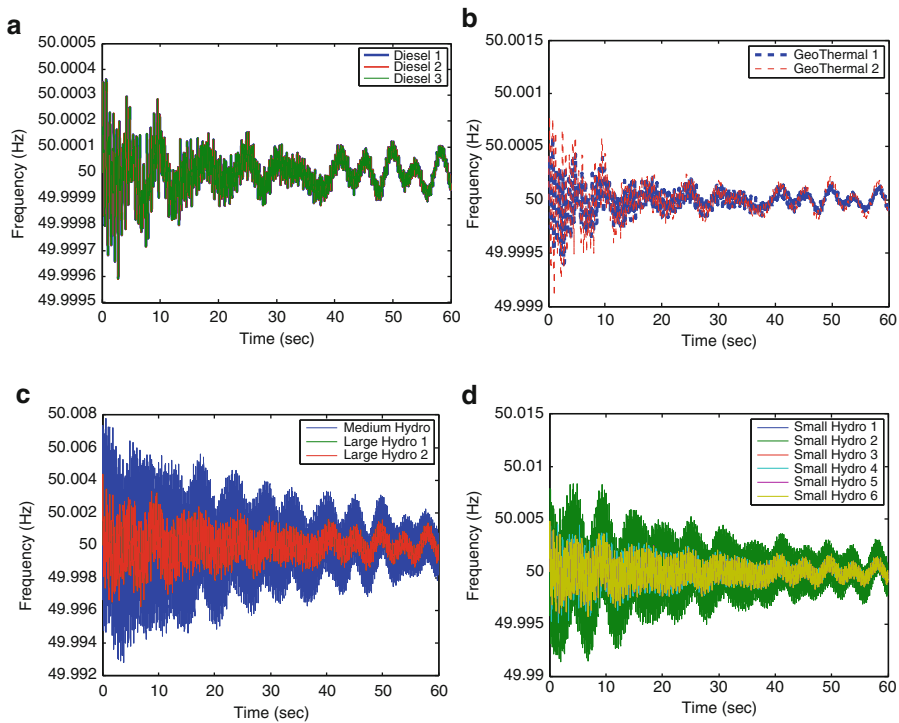


Fig. 15.14 Time response of frequency on São Miguel Island with wind connected to hydro. (a) Diesel frequency. (b) Geothermal frequency. (c) Large and medium hydro frequency. (d) Small hydro frequency

electric power systems. Many more problems will appear in that scenario. As was discussed, the LQR-based control approach needs a large sensing and communication effort to bring about satisfactory performance. As the system increases in size, the communication system may reach its capacity, causing communication delay in the feedback control loop that consequently degrades the control performance. The approach relying on more distributed control infrastructure becomes necessary to overcome the problem caused by communications with high complexity. The high cost of flywheels also needs to be taken into consideration. If the system does not have enough flywheels installed, coordinating the control areas with large amounts of wind and the areas with large amounts of cheap, fast conventional generating units could serve as a possible substitution.

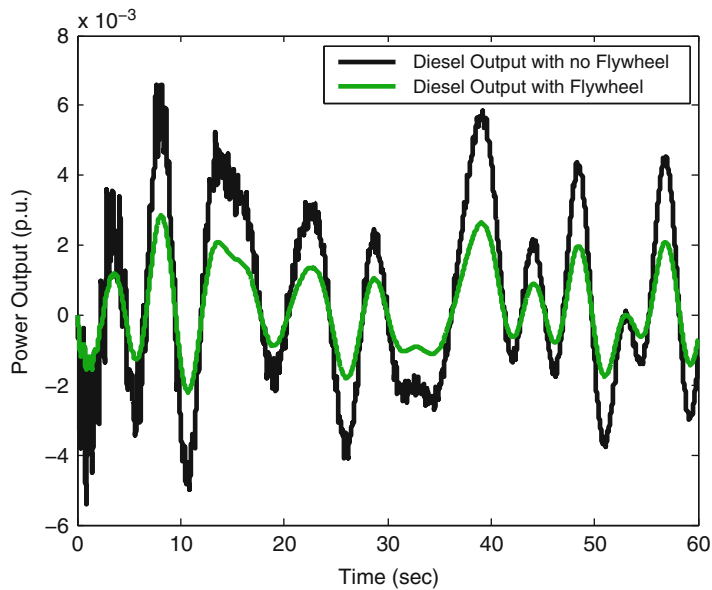


Fig. 15.15 Diesel output in São Miguel system with wind connected to diesel

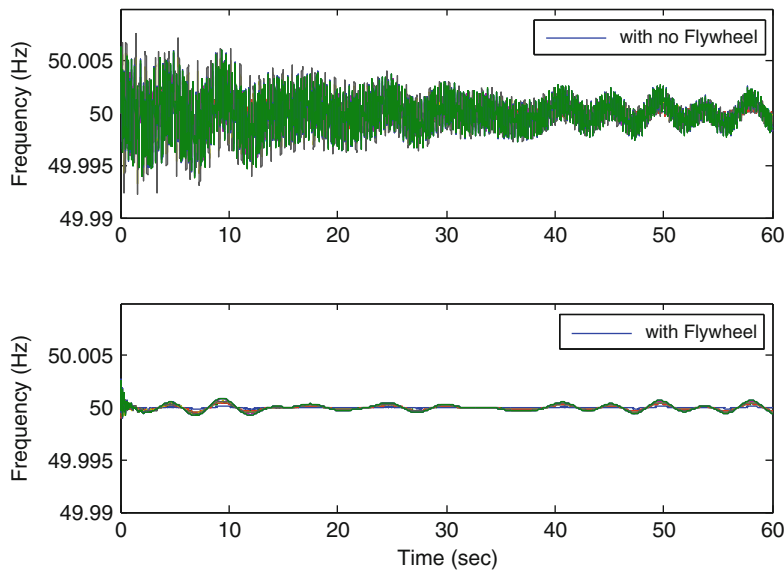


Fig. 15.16 Frequency of hydro generators in São Miguel system with wind connected to hydro

Acknowledgments This work was supported by US National Science Foundation Award No. 0931978, the Semiconductor Research Corporation (SRC) Smart Grid Research Center (SGRC) at Carnegie Mellon University Research Tasks 2111.002 and 2111.003, and Carnegie Mellon University ECE Fellowship. The authors greatly appreciate their permission to use input data provided in Chap. 3 by Masoud Nazari.

15.6 Appendix A

15.6.1 Network Topology Reduction

A systematic approach to network topology reduction is presented in this appendix. The parameters of the reduced topology networks of Flores and São Miguel are given.

The network topology reduction procedure starts by converting constant power loads to constant impedance loads on all the buses one is trying to remove from the network. The loads are converted using

$$\hat{Z}_{l_i} = \frac{V_i^2}{\hat{S}_{l_i}^*} \quad i = 1 \dots n_b, \quad (15.19)$$

where V is the value of the bus voltage calculated as the solution of the power flow and n_b the number of buses we would like to reduce.

Kirchhoff's First Law can be written for all the nodes to be removed from the system topology. Subscript i is used to indicate those buses.

$$0 = \sum_j (\hat{V}_i - \hat{V}_j) \hat{Y}_{ij} \quad j = 1 \dots n_{tl_i} \quad (15.20)$$

The number of branches going in/out from node i is n_{tl_i} .

Kirchhoff's First Law can be written for all the boundary nodes as well. The boundary nodes are the ones which will exist in the new reduced topology, but the impedances of the branches going in/out of them might change. Subscript k is used to indicate all such nodes.

$$\hat{I}_k = \sum_j (\hat{V}_k - \hat{V}_j) \hat{Y}_{kj} \quad j = 1 \dots n_{tl_k}^{\text{red}} \quad (15.21)$$

Current I_k is the current injected into boundary node k from the side of the network which will not be reduced, while $n_{tl_k}^{\text{red}}$ is the number of branches going in/out of the boundary node toward the buses which will be reduced.

These two equations can be rewritten in the matrix form.

Table 15.9 Flores reduced topology admittance matrix

Bus	46 – Hydro	1 – Diesel	19 – Wind
46 – Hydro	$12.5 - j12.5$	$-12.5 + j12.5$	0
1 – Diesel	$-12.5 + j12.5$	$15.116 - j13.908$	$-2.4959 + j1.3779$
19 – Wind	0	$-2.4959 + j1.3779$	$2.5726 - j1.3957$

The base values are $S_b = 10 \text{ MVA}$ and $V_b = 15 \text{ kV}$

Table 15.10 Mapping of the generator buses of the Flores Island system from the original system to the reduced system

Bus 46	Becomes	Bus 3
Bus 1	Stays	Bus 1
Bus 19	Becomes	Bus 2

$$\begin{aligned} 0 &= A\hat{V}_i + B\hat{V}_k \\ \hat{I}_k &= C\hat{V}_i + D\hat{V}_k \end{aligned} \quad (15.22)$$

where V_i is the vector of the voltages of the buses to be reduced while V_k is the vector of the voltages of the boundary buses. The first equation can be solved for V_i , and the solution can be inserted into the second equation.

$$\hat{I}_k = (D - CA^{-1}B)\hat{V}_k \quad (15.23)$$

Therefore, the admittance matrix of the reduced network is $Y = D - CA^{-1}B$. By inspecting the elements of this matrix, one can reconstruct the values of branches connecting the boundary buses as well as the new shunt impedances on boundary buses.

15.6.2 Flores Island Power System Equivalent Model

Flores Island power system is shown in Fig. 15.2.

Flores Island power system reduced topology admittance matrix is given in Table 15.9.

Starting from Table 15.9, the equivalent network topology of the Flores Island power system, Fig. 15.2, can be determined. The following bus mapping is used (Table 15.10).

The equivalent impedances are

Table 15.11 Equilibrium of the transmission system of Flores power system

Voltage	Magnitude (p.u.)	Phase angle (°)
V_3	0.997	0.18
V_1	0.995	0
V_2	0.98	1.03
Power inj	Active (MW)	Reactive (MVAr)
\hat{S}_3	0.7	-0.08
\hat{S}_1	0.58	1.058
\hat{V}_2	0.6	-0.29

Table 15.12 Mapping of generator buses of São Miguel Island system from the original system to the reduced system

Bus 932	Becomes	Bus 1
Bus 933	Becomes	Bus 2
Bus 934	Becomes	Bus 3
Bus 963	Becomes	Bus 4
Bus 1049	Becomes	Bus 5
Bus 1666	Becomes	Bus 6
Bus 1669	Becomes	Bus 7
Bus 1672	Becomes	Bus 8
Bus 1675	Becomes	Bus 9
Bus 1676	Becomes	Bus 10
Bus 1677	Becomes	Bus 11
Bus 1680	Becomes	Bus 12
Bus 1683	Becomes	Bus 13
Bus 1686	Becomes	Bus 14
Bus 1887	Becomes	Bus 15

$$Y_{eq22} = 0.0767 - j0.0178,$$

$$Y_{eq12} = 2.4959 - j1.3779,$$

$$Y_{eq11} = 0.1201 - j0.0301,$$

$$Y_{eq13} = 12.5 - j12.5,$$

$$Y_{eq33} = 0 + j0.$$

The equilibrium of this system is given in Table 15.11.

15.6.3 São Miguel Power System Equivalent Model

Generator buses of São Miguel power system are mapped as follows (Table 15.12).

São Miguel power system reduced topology admittance matrix is given in Tables 15.13 and 15.14. This reduced topology admittance matrix corresponds to the one-line diagram from Fig. 15.3.

Table 15.13 Real part of São Miguel reduced topology admittance matrix

Bus 15	14	13	12	11	10	9	8	7	6	5	4	3	2	1
15 1.09E+1	0	0	0	0	-1.09E+1	0	0	0	0	0	0	0	0	0
14 0	3.43E-3	0	0	0	0	0	0	0	0	0	0	0	0	0
13 0	0	7.99E-1	-7.10E-1	0	0	-5.29E-2	-7.52E-3	-5.59E-3	-1.10E-2	-5.92E-3	-5.65E-4	-1.93E-4	-2.27E-4	-3.50E-4
12 0	0	-7.10E-1	9.01E-1	0	0	-1.47E-1	-1.34E-2	-1.01E-2	-9.37E-3	-5.13E-3	-3.25E-4	-2.43E-4	-1.33E-4	-2.86E-4
11 0	0	0	0	5.31E-4	0	0	0	0	0	0	0	0	0	0
10 -1.09E+1	0	0	0	0	1.09E+1	0	0	0	0	0	0	0	0	0
9 0	0	-5.29E-2	-1.47E-1	0	0	1.14E+0	-4.41E-1	-3.34E-1	-8.81E-2	-5.12E-2	-2.69E-3	-5.44E-3	-1.01E-3	-4.01E-3
8 0	0	-7.52E-3	-1.34E-2	0	0	-4.41E-1	4.41E+0	-3.41E+0	-1.11E-1	-9.42E-2	-7.89E-2	-3.47E-2	-1.10E-1	-8.99E-2
7 0	0	-5.59E-3	-1.01E-2	0	0	-3.34E-1	-3.41E+0	4.11E+0	-7.76E-2	-6.37E-2	-5.06E-2	-2.23E-2	-7.00E-2	-5.73E-2
6 0	0	-1.10E-2	-9.37E-3	0	0	-8.81E-2	-1.11E-1	-7.76E-2	3.41E+0	-2.63E+0	-1.88E-1	-5.92E-2	-7.54E-2	-1.23E-1
5 0	0	-5.99E-3	-5.13E-3	0	0	-5.12E-2	-9.42E-2	-6.37E-2	-2.63E+0	3.47E+0	-2.35E-1	-8.14E-2	-1.02E-1	-1.66E-1
4 0	0	-5.65E-4	-3.25E-4	0	0	-2.69E-3	-7.89E-2	-5.06E-2	-1.88E-1	-2.35E-1	6.27E+0	-3.43E+0	-1.79E+0	-4.21E-1
3 0	0	-1.93E-4	-2.43E-4	0	0	-5.44E-3	-3.47E-2	-2.23E-2	-5.92E-2	-8.14E-2	-3.43E+0	4.91E+0	-3.05E-1	-8.92E-1
2 0	0	-2.27E-4	-1.33E-4	0	0	-1.01E-3	-1.10E-1	-7.00E-2	-7.54E-2	-1.02E-1	-1.79E+0	-3.05E-1	3.24E+0	-7.33E-1
1 0	0	-3.50E-4	-2.86E-4	0	0	-4.01E-3	-8.99E-2	-5.73E-2	-1.23E-1	-1.66E-1	-4.21E-1	-8.92E-1	-7.33E-1	2.59E+0

The base values are $S_b = 100 \text{ MVA}$ and $V_b = 60 \text{ kV}$

Table 15.14 Imaginary part of São Miguel reduced topology admittance matrix

Bus 15	14	13	12	11	10	9	8	7	6	5	4	3	2	1
15 -1.01E+3	1.00E+3	0	0	0	9.11E+0	0	0	0	0	0	0	0	0	0
14 1.00E+3	-1.00E+3	0	0	0	0	0	0	0	0	0	0	0	0	0
13 0	0	-3.36E-1	2.56E-1	0	0	4.64E-2	9.42E-3	6.48E-3	7.48E-3	3.85E-3	2.30E-3	8.41E-5	6.48E-4	6.82E-4
12 0	0	2.56E-1	-4.30E-1	0	0	1.17E-1	2.24E-2	1.55E-2	7.48E-3	3.95E-3	2.53E-3	1.53E-4	1.21E-3	1.07E-3
11 0	0	0	0	-2.00E+3	1.00E+3	1.00E+3	0	0	0	0	0	0	0	0
10 9.11E+0	0	0	0	1.00E+3	-1.01E+3	0	0	0	0	0	0	0	0	0
9 0	0	4.64E-2	1.17E-1	1.00E+3	0	-1.00E+3	7.43E-1	5.15E-1	6.94E-2	3.98E-2	4.06E-2	3.93E-3	3.64E-2	2.76E-2
8 0	0	9.42E-3	2.24E-2	0	0	7.43E-1	-3.01E+0	1.69E+0	5.48E-2	3.69E-2	1.40E-1	4.14E-3	1.81E-1	1.22E-1
7 0	0	6.48E-3	1.55E-2	0	0	5.15E-1	1.69E+0	-2.58E+0	3.66E-2	2.46E-2	9.16E-2	2.86E-3	1.17E-1	7.93E-2
6 0	0	7.48E-3	7.48E-3	0	0	6.94E-2	5.48E-2	3.66E-2	-3.44E+0	2.01E+0	9.61E-1	2.54E-2	8.79E-2	1.77E-1
5 0	0	3.85E-3	3.95E-3	0	0	3.98E-2	3.69E-2	2.46E-2	2.01E+0	-3.88E+0	1.34E+0	3.70E-2	1.22E-1	2.49E-1
4 0	0	2.30E-3	2.53E-3	0	0	4.06E-2	1.40E-1	9.16E-2	9.61E-1	1.34E+0	-1.46E+1	6.92E+0	3.68E+0	1.40E+0
3 0	0	8.41E-5	1.53E-4	0	0	3.93E-3	4.14E-3	2.86E-3	2.54E-2	3.70E-2	6.92E+0	-1.01E+3	1.00E+3	9.42E-1
2 0	0	6.48E-4	1.21E-3	0	0	3.64E-2	1.81E-1	1.17E-1	8.79E-2	1.22E-1	3.68E+0	1.00E+3	-2.01E+3	1.00E+3
1 0	0	6.82E-4	1.07E-3	0	0	2.76E-2	1.22E-1	7.93E-2	1.77E-1	2.49E-1	1.40E+0	9.42E-1	1.00E+3	-1.01E+3

The base values are $S_b = 100 \text{ MVA}$ and $V_b = 60 \text{ kV}$

15.7 Appendix B

15.7.1 Sensitivity Matrices of Flores Island Power System

The sensitivity matrices K_p and D_p of Flores Island when wind power generator is modeled as a negative load are given respectively in Table 15.19 and

$$K_p = \begin{bmatrix} 12.9062 & -12.9062 \\ -12.9068 & 12.9068 \end{bmatrix}$$

$$D_p = \begin{bmatrix} 1.0368 \\ 0 \end{bmatrix}.$$

The sensitivity matrices K_p and D_p of Flores Island when wind is modeled as a synchronous generator are given as

$$K_p = \begin{bmatrix} 14.3346 & -1.4284 & -12.9062 \\ -1.3777 & 1.3777 & 0 \\ -12.9068 & 0 & 12.9068 \end{bmatrix}$$

$$D_p = 0.$$

15.8 Appendix C

15.8.1 Parameters of the Flores Island Power System

The characteristics of the electric power plants in Flores Island are listed in Table 15.15.

Electromechanical parameters of the plants in Flores Island are presented in Tables 15.16–15.18. In addition, dynamic parameters of the electromagnetic parts of the plants are presented in Tables 16.14–16.16 in Chap. 16. The bases are $S_{\text{base}} = 1 \text{ MVA}$, $V_{\text{base}} = 0.4 \text{ kV}$, and $f_{\text{base}} = 50 \text{ Hz}$ (Table 15.19).

Table 15.15 Characteristics of the plants in Flores Island power system

# Node in the reduced system	# Node in the original system	Capacity (MW)	Type of plant
1	1	2.5	Diesel (slack)
2	19	0.6	Wind
3	46	1.5	Hydro

Table 15.16 Electromechanical parameters of the diesel power plant

H_d (s)	D_d (p.u.)	T_2 (s)	K_2 (p.u.)	R_d	C_d (p.u.)	K_I (p.u.)	C_c (p.u.)
11.53	0.25	0.6	40	0.03	1	10	1

Table 15.17 Electromechanical parameters of the wind power plant

H_w (s)	D_w (p.u.)
9.33	0

Table 15.18 Electromechanical parameters of the hydro power plant

H_h (s)	D_h (p.u.)	e_h (p.u.)	K_q (p.u.)	K_w (p.u.)	T_f (p.u.)	T_q (s)	T_w (s)	T_e (s)	T_s (s)	r_p	r_h
21.59	11.85	-10.85	2.78	1.52	-3.6	0.72	4	2	0.06	0.6	7

15.9 Appendix D

15.9.1 Sensitivity Matrices of São Miguel Island Power System

The sensitivity matrices K_p and D_p of the decoupled active power flow of São Miguel Island are shown respectively in Table 15.19 and

$$D_p = 0$$

15.10 Appendix E

15.10.1 Parameters of the São Miguel Island Power System

The characteristics of the electric power plants in São Miguel Island are listed in Table 15.20.

Electromechanical parameters of the plants in São Miguel Island are presented in Tables 15.21–15.27. For medium and small hydro plants, the total inertia and damping of the plants are presented. In order to calculate the inertia and damping of each plant, one can scale down the parameters base on the capacity of the plant. Sbase = 100 MVA, Vbase = 1 kV, and fbase = 50 Hz.

Table 15.19 K_p sensitivity matrix of São Miguel Island power system

Bus	B1Diesel	B2Diesel	B3Diesel	B4Geo1	B5Geo2	B6Hydr1	B7Hydr1	B8Hydr2	B9Hydr3	B10Hydr4	B11Hydr5	B12Hydr6	B13Hydr7	B14Hydr8	B15Hydr9	B15Hydr10
B1Diesel	1004.64	-1002.09	-0.5577	-1.4585	-0.1973	-0.1408	-0.0641	-0.0971	-0.0267	0	0	-0.00096	-0.00035	0	0	0
B2Diesel	-1002.10	20006.45	-1000.12	-3.7936	-0.0937	-0.0681	-0.0945	-0.1433	-0.0379	0	0	-0.00122	-0.0006	0	0	0
B2Diesel2	-0.6034	-1000.13	10007.87	-7.0805	-0.0207	-0.01477	-0.0058	-0.0088	-0.0024	0	0	-0.00091	-0.00053	0	0	0
B4Geo1	-1.4806	-3.8307	-7.139	14.8401	-1.2603	-0.8933	-0.0768	-0.1157	-0.0398	0	0	-0.0022	-0.0017	0	0	0
B5Geo2	-0.2152	-0.1013	-0.0209	-1.2947	3.7593	-2.003	-0.0336	-0.0494	-0.0348	0	0	-0.00333	-0.0031	0	0	0
B6Hydr1	-0.1501	-0.07198	-0.0146	-0.8968	-1.9572	3.2649	-0.043	-0.0622	-0.0573	0	0	-0.00598	-0.0057	0	0	0
B7Hydr2	-0.0664	-0.0972	-0.0056	-0.0776	-0.0321	-0.0421	2.3196	-1.5798	-0.4011	0	0	-0.01217	-0.0056	0	0	0
B8Hydr3	-0.1006	-0.1472	-0.0085	-0.1169	-0.0471	-0.0607	-1.5782	2.6533	-0.5688	0	0	-0.0172	-0.0079	0	0	0
B9Hydr4	-0.02789	-0.0392	-0.0024	-0.0402	-0.0335	-0.0563	-0.4037	-0.5731	9576.57	0	-9575.30	-0.0729	-0.0305	0	0	0
B10Hydr5	0	0	0	0	0	0	0	0	0	9582.12	-9575.29	0	0	0	-6.836	0
B11Hydr6	0	0	0	0	0	0	0	0	-0.575.29	-9575.29	19150.58	0	0	0	0	0
B12Hydr7	-0.001	-0.0013	-0.0009	-0.0023	-0.0033	-0.0061	-0.01241	-0.0176	-0.07382	0	0	0.3550	-0.2371	0	0	0
B13Hydr8	-0.0006	-0.00065	-5.3107	-0.0017	-0.0031	-0.0058	-0.0057	-0.0082	-0.0311	0	0	-0.2385	0.29551	0	0	0
B14Hydr9	0	0	0	0	0	0	0	0	0	0	0	0	9578.078	-9578.077	0	0
B15Hydr10	0	0	0	0	0	0	0	-6.8421	0	0	0	0	9578.08	9584.92	0	0

Table 15.20 Characteristics of the plants in São Miguel Island power system

# Node in the reduced system	# Node in the original system	Capacity (MW)	Type of plant
1	932	32.688	Diesel 1 (slack)
2	933	32.688	Diesel 2
3	934	32.688	Diesel 3
4	963	14.8	Geothermal 1
5	1049	13	Geothermal 2
6	1666	0.67	Hydro 1
7	1669	0.8	Hydro 2
8	1672	0.608	Hydro 3
9	1675	0.553	Hydro 4
10	1676	0.553	Hydro 5
11	1677	0.553	Hydro 6
12	1680	0.094	Hydro 7
13	1683	0.4	Hydro 8
14	1686	0.4	Hydro 9
15	1687	0.4	Hydro 10

Table 15.21 Electromechanical parameters of the first diesel power plant

H_d (s)	D_d (p.u.)	T_2 (s)	K_2 (p.u.)	R_d	C_d (p.u.)	K_I (p.u.)	C_c (p.u.)
9.9662	0.186	1.07	40	0.03	1	10	1

Table 15.22 Electromechanical parameters of the second diesel power plant

H_d (s)	D_d (p.u.)	T_2 (s)	K_2 (p.u.)	R_d	C_d (p.u.)	K_I (p.u.)	C_c (p.u.)
12.9036	0.204	1.25	40	0.03	1	10	1

Table 15.23 Electromechanical parameters of the first geothermal power plant

H_{geo} (s)	D_{geo} (p.u.)
37.7667	0.1992

Table 15.24 Electromechanical parameters of the second geothermal power plant

H_{geo} (s)	D_{geo} (p.u.)
14.7919	0.078

Table 15.25 Electromechanical parameters of the large hydro power plant (hydro 4–6)

H_{hL} (s)	D_{hL} (p.u.)
1.8201	0.0096

Table 15.26 Electromechanical parameters of the medium hydro power plant (hydro 2)

H_{hM} (s)	D_{hM} (p.u.)
0.6924	0.0037

Table 15.27 Electromechanical parameters of the small hydro power plant (hydro 1, 3 and 7–10)

H_{hS} (s)	D_{hS} (p.u.)
3.3256	0.0176

References

1. M. Nazari, Electrical networks of the Azores Archipelago, in Chapter 3 of *Engineering IT-Enabled Sustainable Electricity Services: The Case of Low-Cost-Green Azores Islands*, Springer, 2013.
2. M. Ilić, Dynamic monitoring and decision systems for enabling sustainable energy services, in *Proceedings of the IEEE*, January 2011, pp. 58–79
3. M. Ilić, J.-Y. Joo, L. Xie, M. Prica, N. Rotering, A decision-making framework and simulator for sustainable energy services, *IEEE Trans. Sustain. Energy* **2**(1), 37–49 (2011)
4. M. Elizondo, M. Ilić, P. Marcado, Determining the cost of dynamic control capacity for improving system efficiency, in *Proceedings of the IEEE General Power Meeting*, Montreal, CA, June 2006
5. M. Ilić , Large-scale dynamic systems. Lecture Notes, Course number 18-618 (Spring 2012)
6. K.D. Young, On near-optimal decentralized control. IFAC Automatica, pp. 607–610 (September 1985)
7. M. Ilić, Q. Liu, Toward sensing, communications and control architectures for frequency regulation in systems with highly variable resources, in Chapter 1 of *Control and Optimization Theory for Electric Smart Grids* (Springer, New York 2012)
8. G.S. Stavrakakis, G.N. Kariniotakis, A general simulation algorithm for the accurate assessment of isolated diesel-wind turbines systems interaction—Part I: A general multimachine power system model. *IEEE Trans. Energy Convers.* **10**(3), 577–583 (September 1995)
9. M. Calovic, Dynamic state-space models of electric power systems. Technical report, University of Illinois, Urbana, 1971
10. M. Ilić, J. Zaborszky, *Dynamics and Control of Large Electric Power Systems* (Wiley, New York, 2000)
11. M. Hanmandlu, N.V. Suryanarayana, High gain decentralised control. *IEE Proc. Control Theory Appl.* **140**(4), 255–260 (1993)
12. M. Abrishamchian, M.H. Kazemi, Sufficient condition for stability of decentralized control feedback structures, in *Proceedings of the 36th IEEE Conference on Decision and Control*, vol. 3, December 1997, pp. 2621–2622

Chapter 16

The Role of Enhanced Voltage Control in Stabilizing Dynamics of Electric Energy Systems

Qixing Liu, Milos Cvetković, and Marija Ilić

16.1 Introduction

For assessing possible stability problems in systems with high wind power penetration, it is insufficient to model only the real power-frequency dynamics when attempting to select the most effective stabilizing controllers. The candidate controllers are the governors of conventional power plants, the blades control of wind power plants, fast energy storage (flywheels, batteries of various types), Flexible Alternating Current Transmission System (FACTS) devices, the excitation systems of conventional power plants, and the Doubly Fed Induction Generator (DFIG) voltage control of wind turbines. The list of controllers is likely to become even more diverse in the future and very different from the governor and excitation control of conventional power plants. Given these choices, it is critical to develop a more systematic framework than in the past for designing primary control in order to manage specific types of disturbances and have quantifiable performance metrics for assessing the potential of different types of controllers and their logic. In this chapter we consider only small fast wind power fluctuations of the same type as in Chap. 15. We next recall the main conclusion in Chap. 15 that managing such disturbances by means of governor control or energy storage, such as flywheels, leads to wear-and-tear with the former and high cost on storage devices with the latter. This leads us to consider more systematically in this chapter the potential of fast voltage control by means of rotor excitation in conventional power plants, DFIG in wind power plants, and/or FACTS-based voltage control on wind power plants. Dynamic VAR (D-VAR) is one such representative FACTS voltage controller typically used for squirrel cage induction machines in wind power plants. The objective is to explore

Q. Liu (✉) • M. Cvetković • M. Ilić
Department of Electrical and Computer Engineering, Carnegie Mellon University, 5000 Forbes Avenue, Pittsburgh, PA 15213, USA
e-mail: lqx@cmu.edu; mcvetkov@andrew.cmu.edu; milic@ece.cmu.edu

whether voltage control will be sufficient to stabilize the effects of very fast wind power fluctuations and have governors control slower disturbances only. Moreover, the stabilization of all relevant states in the coupled frequency–voltage dynamics is of interest. Recently, there have been operating problems in systems with wind power plants caused by the plants disconnecting themselves from the grid or by unacceptable voltage fluctuations in parts of the system. These problems cannot be modeled, analyzed, or controlled using the decoupled real power-frequency dynamical model of the interconnected grid.

In order to explore the potential of controlling persistent wind fluctuations by means of voltage control, the coupled frequency–voltage dynamic model is derived first in Sect. 16.4. This model is used next in Sects. 16.5 and 16.6 for analyzing the stability of the interconnected grid and for posing the control design problem of stabilizing potentially unstable dynamics. This, in turn, protects governors from excessive wear-and-tear, and eliminates the need for expensive storage.¹

16.2 State of the Art of Coupled Frequency–Voltage Stabilization Approaches

Each conventional power plant generally has two primary controllers: the governor and the Automatic Voltage Regulator (AVR). The governor controls how much mechanical power is applied to the rotor shaft of a generator. The governor control logic generally requires major components, such as valves, to change their positions. This in turn, creates wear-and-tear problems. The high-gain bang-bang fast on-off adjustments of the prime mover output are normally prevented in order to protect the mechanical parts of the generator from the wear-and-tear problems. The AVR, on the other hand, stabilizes the terminal voltage of the generator using fast power-electronically controlled excitation control applied to the rotor windings of a generator. More recently many power plants have become equipped with Power Systems Stabilizers (PSSs) responding to voltage deviations as supplementary signals to the AVR [1]. The PSS, jointly with the AVR, is used to ensure small-signal stabilization of the fast frequency–voltage dynamics.

In contrast to the conventional power plants, the intermittent resources do not have a standardized primary control yet. It is common for many intermittent power plants to directly apply the mechanical torque created by the wind to the generator shaft. Only recently it has become clear that the dispatch of wind power involving decisions of how much wind power to store or provide leads to lower generation costs than when wind is sent to the power grid as it becomes available. This is illustrated in earlier chapters of this book [3]. Similarly, we show in this chapter that a carefully designed control of wind power plants in between the dispatch intervals

¹Storage is needed, as shown in Chap. 19, when managing a wind power disturbance of significant energy deviations.

is especially critical in order to ensure that no stability problems arise in future electric energy systems [4]. However, blade control of wind power plants is prone to major wear-and-tear problems; this results in shortened lifetime of the plants. For this reason, it is better to rely on a less damaging stabilization of system dynamics in response to persistent wind power fluctuations. Two basic alternatives are (1) PSS-type control of the wind power plant and (2) coordinated compensation for wind disturbances by other fast resources—flywheels and batteries in particular—which do not have as many wear-and-tear problems. PSS-type control of an induction machine wind power plant could be either a D-VAR- or DFIG-type design (shown in the Appendix). It is fundamentally impossible to implement the latter without fast synchronized communications. Synchrophasors, Wide Area Measurement System (WAMS)-based special protection system (SPS) have recently become possible means of implementing such coordination. Prior to the recent availability of synchronized fast measurements, standards for power system dynamics have required that each conventional power plant have primary controllers and also be able to ensure stand-alone stability.

However, one serious issue remains even when the stand-alone power plants are stable. The robustness of stabilizing control with respect to the operating equilibrium conditions is not always guaranteed. We show in this chapter that the given model around different operating conditions may exhibit instability of the interconnected system even though the system was tuned to have stand-alone stable modules for a typical equilibrium. At present all primary controllers are decentralized and do not account for the explicit dynamic interactions between the various controllers. So the non-robustness with respect to the equilibrium conditions and/or parameter uncertainties remains a major issue, which is likely to become more serious as different nonstandard components get deployed into the grid. This problem was recognized long ago. Several controllers, ranging across High-Voltage Direct Current (HVDC) transmission, the On-Load Tap Changer (OLTC) transformer, and the Static VAR Compensator (SVC) could not be tuned simultaneously without destabilizing the interconnected system dynamics. As many new controllers get deployed within relatively small electrical distances in smart grids this once rare potential problem is likely to become very prevalent. A brute force solution to this issue is to equip each (group of) power plants with a controller which nearly decouples the interactions from the rest of the system. Assuming such protocol is in place, and each (group of) components implements sufficient control to decouple itself and cancel out the effects of the other (groups of) components, the interconnected system will remain stable. However, some of these solutions are extremely cost-ineffective. The decentralized decoupling control of large-scale network systems of this type has had a very long history of theoretical developments, but it has never been deployed in a systematic way. In addition to the infrastructure cost which is sometimes hard to quantify and, therefore, hard to justify, a serious technical problem concerns the specifications of the ranges of disturbances which any given (group of) controllers would be capable of decoupling from the rest of the system. Moreover, if some fail to control, the system as a whole becomes less controllable and it is no longer possible to guarantee stable performance using

decentralized control. Some striking examples of this problem have been the voltage collapse-related blackout occurrences caused by some key power plants reaching saturation in their voltage control, and generators behaving not as PV plants in steady state (with well controlled voltage), but rather as PQ loads whose voltage is no longer controllable. This loss of control by some primary controllers leads to qualitatively different interaction variables which are caused by instabilities in the voltage dynamics.

In order to compare the performances of different control alternatives for a given system, it is essential to start with a model of the interconnected system in the standard state-space form. This is an open problem, since a coupled frequency–voltage linearized model in the standard state-space form is not readily available for a general electric power system topology. So in this chapter we derive this kind of model, using the Flores Island system as the illustration. Further generalizations are possible. Based on the standard state-space model, we explore the impact on system small-signal stability caused by different wind generator technologies and qualitatively different electrical distances between the wind generator and the main power grid. Proper control strategies are suggested for the scenarios in which small-signal instability exists.

16.3 Flores Island Power System

The Flores Island power system has 46 buses, and its current electricity demand is provided by a diesel power plant (capacity: 2.5 MW), a hydro-power plant (capacity: 1.5 MW) and a wind power plant (capacity: 0.66 MW) [2]. Figure 16.1 shows

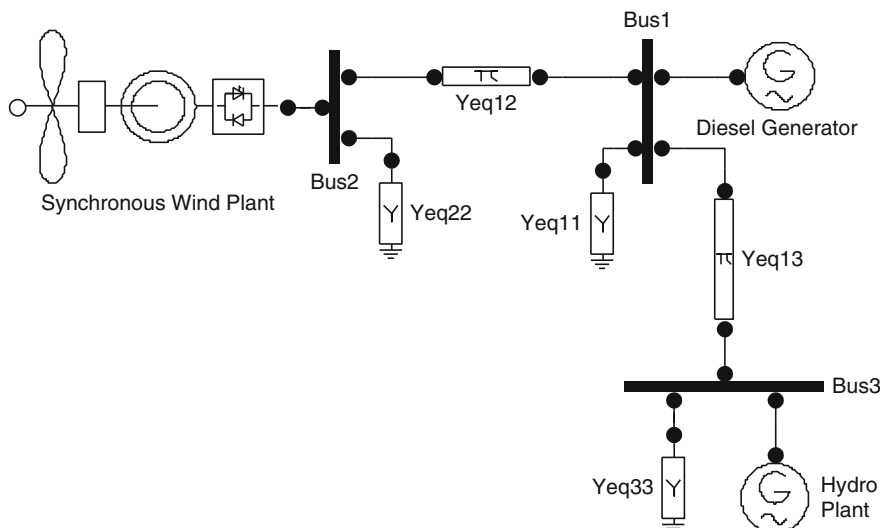


Fig. 16.1 One-line diagram of Flores Island power system

the reduced one-line diagram of this system. In order for the system to deploy more environmentally friendly wind generation as a substitute for the conventional diesel generation, the impacts of the wind generator on system performance needs to be assessed and managed. In this chapter, we focus mainly on the potential stability problems of the coupled electromechanics and electromagnetics which are caused by integration of wind power plants. In light of the existing wind generation technologies, two scenarios will be discussed:

- The system with an induction machine wind power generator
- The system with a synchronous wind power generator

16.4 PV Linearized Coupled Power System Model With Wind Power Generator Dynamic Model

In this section, the dynamic models of generator components of the Flores power system and a model of the interconnected system are introduced in the standard state-space form. These models are in the form of linear Ordinary Differential Equations (ODEs) derived by linearizing a previously introduced power system model [5]. This model uses a form of nonlinear ODEs since it was primarily introduced for modeling the response of the system to very large disturbances (models and parameters given in Appendix) around a particular equilibrium.

16.4.1 Wind Generator Modeled as an Induction Machine

In the dynamic model of the wind induction generator, we represent the generator as a DFIG which has excitation control inputs on the rotor of the induction machine. We assume that there is no pitch control on the mechanical part of the wind generator. In standard state-space form, the linearized model is written as

$$\dot{x}_w = A_w x_w + B_w u_w + C_{PE}^w x_{EW} + C_{PI}^w I_w + C_{PCOI}^w \omega_{COI}, \quad (16.1)$$

where x_w represents the system states. u_w refers to the rotor winding excitation control inputs of the DFIG. x_{EW} , I_w , and ω_{COI} are defined as the variables contributing to the coupling of the induction machine and to the rest of the system. These couplings are contributed by voltages behind the transient reactance (x_{EW}) which are state variables of the system, the stator current (I_w), and the center of inertia frequency (ω_{COI}). The specifications of the dynamic model are shown below:

$$x_w = \begin{bmatrix} \Delta\delta_w & \Delta\omega_w & \Delta E'_{Dw} & \Delta E'_{Qw} \end{bmatrix}^T$$

$$u_w = \begin{bmatrix} \Delta e_{fd} & \Delta e_{fq} \end{bmatrix}^T$$

Table 16.1 Variables of the wind induction generator

Variable(s)	Description
$\Delta\delta_w$ and $\Delta\omega_w$	Rotor angle and speed of the wind induction machine
$\Delta E'_{Dw}$ and $\Delta E'_{Qw}$	Voltages behind the transient reactance in the network reference frame
ΔI_{Dw} and ΔI_{Qw}	Stator currents in the network reference frame
Δe_{fd} and Δe_{fq}	Rotor winding excitation control inputs of the DFIG
ω_{COI}	Center of inertia frequency, defined as $\omega_{COI} = \sum_{i \in G} M_i \omega_i$, G stands for synchronous generators
M_w and D_w	Inertia and damping coefficient of the wind induction machine

$$x_{Ew} = \begin{bmatrix} \Delta E'_{Dw} & \Delta E'_{Qw} \end{bmatrix}^T$$

$$I_w = \begin{bmatrix} \Delta I_{Dw} & \Delta I_{Qw} \end{bmatrix}^T$$

$$A_w = \begin{bmatrix} 0 & \omega_0 & 0 & 0 \\ 0 & -\frac{D_w}{M_w} & 0 & 0 \\ L_{11}^w & L_{12}^w & L_{13}^w & L_{14}^w \\ L_{21}^w & L_{22}^w & L_{23}^w & L_{24}^w \end{bmatrix}, B_w = \begin{bmatrix} 0 & 0 \\ 0 & 0 \\ L_{18}^w & L_{19}^w \\ L_{28}^w & L_{29}^w \end{bmatrix}$$

$$C_{PE}^w = \begin{bmatrix} 0 & 0 \\ L_{31}^w & L_{32}^w \\ 0 & 0 \\ 0 & 0 \end{bmatrix}, C_{PI}^w = \begin{bmatrix} 0 & 0 \\ L_{33}^w & L_{34}^w \\ L_{15}^w & L_{16}^w \\ L_{25}^w & L_{26}^w \end{bmatrix}, C_{PCOI}^w = \begin{bmatrix} -\omega_0 \\ -\frac{D_w}{M_w} \\ L_{17}^w \\ L_{27}^w \end{bmatrix}.$$

The physical meanings of the variables can be seen in Table 16.1. The Δ stands for the deviations around an equilibrium. The elements L^w 's of the system matrices are shown in Appendix.

16.4.2 Wind Generator Modeled as a Synchronous Machine

In this subsection, a linearized model of the synchronous wind generator is derived. It is assumed that there is no pitch control on the mechanical part of the wind generator: this is consistent with the modeling in the previous subsection. To control the frequency–voltage dynamics, the IEEE Type I exciter [6] as well as a linear feedback PSS are deployed for control of the terminal voltage and rotor rotating speed. In the standard state-space form, the linearized model is written as

$$\dot{x}_{ws} = A_{ws}x_{ws} + B_{ws}u_{ws} + C_{PE}^{ws}x_{Ews} + C_{PI}^{ws}I_{ws} + C_{PCOI}^{ws}\omega_{COI}, \quad (16.2)$$

where x_{ws} represents the system states, u_{ws} stands for the PSS control input $V_{ws,pss}$. x_{Ews} , I_{ws} , and ω_{COI} are defined as the variables contributing to the coupling of the

Table 16.2 Variables of the wind power synchronous generator

Variable(s)	Description
$\Delta\delta_{ws}$ and $\Delta\omega_{ws}$	Rotor angle and speed of the wind synchronous machine
$\Delta E'_{Dws}$ and $\Delta E'_{Qws}$	Voltages behind the transient reactance in the network reference frame
ΔI_{Dws} and ΔI_{Qws}	Stator currents in the network reference frame
Δe_{fdws}	Rotor excitation control inputs of the exciter
ω_{COI}	Center of inertia frequency of the system contributed by the synchronous generators
M_{ws} and D_{ws}	Inertia and damping coefficient of the wind power synchronous machine

synchronous machine to the rest of the system. These coupling variables are voltages behind the transient reactance (x_{Ews}), the stator current (I_{ws}), and the center of inertia frequency (ω_{COI}). The details of the dynamic model are shown below:

$$x_{ws} = \begin{bmatrix} \Delta\delta_{ws} & \Delta\omega_{ws} & \Delta E'_{Dws} & \Delta E'_{Qws} & \Delta V_{Rws} & \Delta e_{fdws} & \Delta V_{Fws} \end{bmatrix}^T$$

$$u_{ws} = V_{ws,pss}$$

$$x_{Ews} = \begin{bmatrix} \Delta E'_{Dws} & \Delta E'_{Qws} \end{bmatrix}^T$$

$$I_{ws} = \begin{bmatrix} \Delta I_{Dws} & \Delta I_{Qws} \end{bmatrix}^T$$

$$A_{ws} = \begin{bmatrix} 0 & \omega_0 & 0 & 0 & 0 & 0 & 0 \\ 0 & -\frac{D_{ws}}{M_{ws}} & 0 & 0 & 0 & 0 & 0 \\ L_{11}^{ws} & L_{12}^{ws} & L_{13}^{ws} & L_{14}^{ws} & 0 & L_{17}^{ws} & 0 \\ L_{21}^{ws} & L_{22}^{ws} & L_{23}^{ws} & L_{24}^{ws} & 0 & L_{27}^{ws} & 0 \\ 0 & 0 & L_{41}^{ws} & L_{42}^{ws} & -\frac{1}{T_{Aws}} & 0 & -\frac{K_{Aws}}{T_{Aws}} \\ 0 & 0 & 0 & 0 & \frac{1}{T_{Ews}} & -\frac{K_{Ews} + S_{Ews}}{T_{Ews}} & 0 \\ 0 & 0 & 0 & 0 & \frac{K_{Fws}}{T_{Fws} * T_{Ews}} & -\frac{K_{Fws}(K_{Ews} + S_{Ews})}{T_{Fws} T_{Ews}} & -\frac{1}{T_{Fws}} \end{bmatrix}, B_{ws} = \begin{bmatrix} 0 \\ 0 \\ 0 \\ 0 \\ -\frac{K_{Aws}}{T_{Aws}} \\ 0 \\ 0 \end{bmatrix}$$

$$C_{PE}^{ws} = \begin{bmatrix} 0 & 0 \\ L_{31}^{ws} & L_{32}^{ws} \\ 0 & 0 \\ 0 & 0 \\ 0 & 0 \\ 0 & 0 \\ 0 & 0 \end{bmatrix}, C_{PI}^{ws} = \begin{bmatrix} 0 & 0 \\ L_{33}^{ws} & L_{34}^{ws} \\ L_{15}^{ws} & L_{16}^{ws} \\ L_{25}^{ws} & L_{26}^{ws} \\ -L_{42}^{ws} X_d' & L_{41}^{ws} X_d' \\ 0 & 0 \\ 0 & 0 \end{bmatrix}, C_{PCOI}^{ws} = \begin{bmatrix} -\omega_0 \\ -\frac{D_{ws}}{M_{ws}} \\ L_{18}^{ws} \\ L_{28}^{ws} \\ 0 \\ 0 \\ 0 \end{bmatrix}.$$

The physical meanings of the state variables can be seen in Table 16.2. The elements L^{ws} 's of the system matrices appear in the Appendix.

16.4.3 Hydro Generator

The hydro generator is a synchronous generator with an excitation control on the rotor as well as speed-governor equipped with a proportional controller. A third-order model is employed to represent the dynamics of governor-turbine. The IEEE Type I exciter and linear feedback PSS, which were used for modeling wind synchronous generator, are adopted to model the hydro synchronous generator as well.

$$\dot{x}_h = A_h x_h + B_h u_h + C_{\text{PE}}^h x_{Eh} + C_{\text{PI}}^h I_h + C_{\text{PCOI}}^h \omega_{\text{COI}}, \quad (16.3)$$

where x_h represents the states of the generator. u_h stands for the PSS control input $V_{h,\text{pss}}$. x_{Eh} , I_h , and ω_{COI} are defined as the variables contributing to the coupling of the synchronous machine to the rest of the system. These couplings are carried on voltages behind the transient reactance (x_{Eh}), the stator current (I_h), and the center of inertia frequency (ω_{COI}). The specifications of the dynamic model are shown in the following:

$$x_h = \left[\Delta q_h \ \Delta v_h \ \Delta a_h \ \Delta \delta_h \ \Delta \omega_h \ \Delta E'_{Dh} \ \Delta E'_{Qh} \ \Delta V_{Rh} \ \Delta e_{fdh} \ \Delta V_{Fh} \right]^T$$

$$u_h = V_{h,\text{pss}}$$

$$x_{Eh} = \left[\Delta E'_{Dh} \ \Delta E'_{Qh} \right]^T$$

$$I_h = \left[\Delta I_{Dh} \ \Delta I_{Qh} \right]^T$$

$$A_h = \begin{bmatrix} -\frac{1}{T_q} & 0 & \frac{1}{T_w} & 0 & \frac{1}{T_f} & 0 & 0 & 0 & 0 & 0 \\ 0 & -\frac{1}{T_e} & \frac{r'_h}{T_e} & 0 & 0 & 0 & 0 & 0 & 0 & 0 \\ 0 & \frac{1}{T_s} & \frac{r_h + r'_h}{T_s} & 0 & -\frac{G_p}{T_s} & 0 & 0 & 0 & 0 & 0 \\ 0 & 0 & 0 & 0 & \omega_0 & 0 & 0 & 0 & 0 & 0 \\ \frac{k_q}{M_h} & 0 & -\frac{k_w}{M_h} & -\frac{D_h}{M_h} & 0 & 0 & 0 & 0 & 0 & 0 \\ 0 & 0 & 0 & L_{11}^h & L_{12}^h & L_{13}^h & L_{14}^h & 0 & L_{17}^h & 0 \\ 0 & 0 & 0 & L_{21}^h & L_{22}^h & L_{23}^h & L_{24}^h & 0 & L_{27}^h & 0 \\ 0 & 0 & 0 & 0 & 0 & L_{41}^h & L_{42}^h & -\frac{1}{T_{Ah}} & 0 & -\frac{K_{Ah}}{T_{Ah}} \\ 0 & 0 & 0 & 0 & 0 & 0 & 0 & \frac{1}{T_{Eh}} & -\frac{K_{Eh} + S_{Eh}}{T_{Eh}} & 0 \\ 0 & 0 & 0 & 0 & 0 & 0 & 0 & \frac{K_{Fh}}{T_{Fh} * T_{Eh}} & -\frac{K_{Fh}(K_{Eh} + S_{Eh})}{T_{Fh} T_{Eh}} & -\frac{1}{T_{Fh}} \end{bmatrix}$$

Table 16.3 Variables of the hydro synchronous generator

Variable(s)	Description
$\Delta q_h, \Delta v_h$ and Δa_h	Penstock flow, governor droop, and gate position of the hydro governor-turbine
$\Delta \delta_h$ and $\Delta \omega_h$	Rotor angle and speed of the hydro synchronous machine
$\Delta E'_{Dh}$ and $\Delta E'_{Qh}$	Voltages behind the transient reactance in the network reference frame
ΔI_{Dh} and ΔI_{Qh}	Stator currents in the network reference frame
Δe_{fdh}	Rotor winding excitation control inputs of the exciter
ω_{COI}	Center of inertia frequency of the system contributed by the synchronous generators
M_h and D_h	Inertia and damping coefficient of the hydro synchronous machine

$$B_h = \begin{bmatrix} 0 \\ 0 \\ 0 \\ 0 \\ 0 \\ 0 \\ -\frac{K_{Ah}}{T_{Ah}} \\ 0 \\ 0 \end{bmatrix}, C_{PE}^h = \begin{bmatrix} 0 & 0 \\ 0 & 0 \\ 0 & 0 \\ 0 & 0 \\ 0 & 0 \\ 0 & 0 \\ 0 & 0 \\ 0 & 0 \end{bmatrix}, C_{PI}^h = \begin{bmatrix} 0 & 0 \\ L_{33}^h & L_{34}^h \\ L_{15}^h & L_{16}^h \\ L_{25}^h & L_{26}^h \\ -L_{42}^h X_d' & L_{41}^h X_d' \end{bmatrix}, C_{PCOI}^h = \begin{bmatrix} 0 \\ 0 \\ 0 \\ -\omega_0 \\ -\frac{D_h}{M_h} \\ L_{18}^h b \\ L_{28}^h \\ 0 \\ 0 \\ 0 \end{bmatrix}.$$

The physical meanings of the state variables can be seen in Table 16.3. The elements L^h 's of the system matrices are shown in the Appendix.

16.4.4 Diesel Generator

The diesel generator is a synchronous generator with an excitation control on the rotor as well as speed governor equipped with a proportional-integral (PI) controller. A second-order model is employed to represent the dynamics of the governor-turbine. The IEEE Type I exciter and the linear feedback PSS models, which were used with the wind and hydro synchronous generators in the previous sections, are adopted to the mode of the diesel synchronous generator as well.

$$\dot{x}_d = A_d x_d + B_d u_d + C_{PE}^d x_{Ed} + C_{PI}^d I_d + C_{PCOI}^d \omega_{COI}, \quad (16.4)$$

where x_d represents the states of the generator. u_d stands for the PSS control input $V_{d,pss}$. x_{Ed} , I_d , and ω_{COI} are defined as the variables contributing to the coupling of the synchronous machine to the rest of the system. These coupling variables are voltages behind the transient reactance (x_{Ed}), the stator current (I_d), and the center of inertia frequency (ω_{COI}). The specifications of the dynamic model are shown as follows:

Table 16.4 Variables of the wind synchronous generator

Variable(s)	Description
Δm_{Bd} and ΔP_{cd}	Fuel rate and fuel control of the diesel generator
$\Delta\delta_d$ and $\Delta\omega_d$	Rotor angle and speed of the diesel synchronous machine
$\Delta E'_{Dd}$ and $\Delta E'_{Qd}$	Voltages behind the transient reactance in the network reference frame
ΔI_{Dd} and ΔI_{Qd}	Stator currents in the network reference frame
Δe_{fdd}	Rotor winding excitation control inputs of the exciter
ω_{COI}	Center of inertia frequency of the system contributed by the synchronous generators
M_d and D_d	Inertia and damping coefficient of the diesel synchronous machine

$$x_h = \left[\Delta m_{Bd} \ \Delta P_{cd} \ \Delta\delta_d \ \Delta\omega_d \ \Delta E'_{Dd} \ \Delta E'_{Qd} \ \Delta V_{Rd} \ \Delta e_{fdd} \ \Delta V_{Fd} \right]^T$$

$$u_d = V_{d,pss}$$

$$x_{Ed} = \left[\Delta E'_{Dd} \ \Delta E'_{Qd} \right]^T$$

$$I_d = \left[\Delta I_{Dd} \ \Delta I_{Qd} \right]^T$$

$$A_d = \begin{bmatrix} -\frac{1}{T_{dd}} & -\frac{C_d K_d}{T_{dd}} & 0 & -\frac{C_d K_d}{T_{dd} R_d} & 0 & 0 & 0 & 0 & 0 \\ 0 & 0 & 0 & K_{Id} & 0 & 0 & 0 & 0 & 0 \\ 0 & 0 & 0 & \omega_0 & 0 & 0 & 0 & 0 & 0 \\ \frac{1}{M_d} & 0 & -\frac{D_d}{M_d} & 0 & 0 & 0 & 0 & 0 & 0 \\ 0 & 0 & L_{11}^d & L_{12}^d & L_{13}^d & L_{14}^d & 0 & L_{17}^d & 0 \\ 0 & 0 & L_{21}^d & L_{22}^d & L_{23}^d & L_{24}^d & 0 & L_{27}^d & 0 \\ 0 & 0 & 0 & 0 & L_{41}^d & L_{42}^d & -\frac{1}{T_{Ad}} & 0 & -\frac{K_{Ad}}{T_{Ad}} \\ 0 & 0 & 0 & 0 & 0 & 0 & \frac{1}{T_{Ed}} & -\frac{K_{Ed} + S_{Ed}}{T_{Ed}} & 0 \\ 0 & 0 & 0 & 0 & 0 & 0 & \frac{K_{Fd}}{T_{Fd} * T_{Ed}} & -\frac{K_{Fd}(K_{Ed} + S_{Ed})}{T_{Fd} T_{Ed}} & -\frac{1}{T_{Fd}} \end{bmatrix}$$

$$B_d = \begin{bmatrix} 0 \\ 0 \\ 0 \\ 0 \\ 0 \\ 0 \\ -\frac{K_{Ad}}{T_{Ad}} \\ 0 \\ 0 \end{bmatrix}, C_{PE}^d = \begin{bmatrix} 0 & 0 \\ 0 & 0 \\ 0 & 0 \\ L_{31}^d & L_{32}^d \\ 0 & 0 \\ 0 & 0 \\ 0 & 0 \\ 0 & 0 \\ 0 & 0 \end{bmatrix}, C_{PI}^d = \begin{bmatrix} 0 & 0 \\ 0 & 0 \\ 0 & 0 \\ L_{33}^d & L_{34}^d \\ L_{15}^d & L_{16}^d \\ L_{25}^d & L_{26}^d \\ -L_{42}^d X'_d & L_{41}^d X'_d \\ 0 & 0 \\ 0 & 0 \end{bmatrix}, C_{PCOI}^d = \begin{bmatrix} 0 \\ 0 \\ -\omega_0 \\ -\frac{D_d}{M_d} \\ L_{18}^d \\ L_{28}^d \\ 0 \\ 0 \\ 0 \end{bmatrix}.$$

The physical interpretation of the state variables can be seen in Table 16.4. The elements L^d 's of the system matrices are shown in the Appendix.

16.4.5 Network Coupling Constraints

The dynamic components in the interconnected system have to satisfy the network coupling constraints. In this subsection, we apply the network constraints equations proposed in [7] to model the interactions among the generator components introduced in the previous subsections.

In general, Kirchoff's current law (KCL) has to hold for any electrical power grid, which yields the following equation:

$$\hat{\mathbf{I}} = \hat{\mathbf{Y}}\hat{\mathbf{V}}, \quad (16.5)$$

where the complex voltage vector $\hat{\mathbf{V}}$ and the complex current vector $\hat{\mathbf{I}}$ refer to the bus voltages and net current injection on each bus. $\hat{\mathbf{Y}}$ is the admittance matrix of the interconnected system.

The proposed network coupling model [7] assumes that all constant real power and reactive power loads (PQ loads) in the interconnected system can be equivalently represented as constant admittances in the study of short-term stability problems. This assumption allows PQ loads to be represented as constant admittance loads and to include the load admittances into the grid's admittance matrix.

With an admittance matrix that incorporates load admittances, the KCL requires that the net current injection be zero at any bus not connected to a voltage source. As a result, Eq. (16.5) can be rewritten as

$$\begin{bmatrix} \hat{\mathbf{I}}_G \\ 0 \end{bmatrix} = \begin{bmatrix} \hat{\mathbf{Y}}_{GG} & \hat{\mathbf{Y}}_{GL} \\ \hat{\mathbf{Y}}_{LG} & \hat{\mathbf{Y}}_{LL} \end{bmatrix} \begin{bmatrix} \hat{\mathbf{V}}_G \\ \hat{\mathbf{V}}_L \end{bmatrix}. \quad (16.6)$$

We then solve $\hat{\mathbf{I}}_G$ out of the equations and obtain

$$\hat{\mathbf{I}}_G = \left(\hat{\mathbf{Y}}_{GG} - \hat{\mathbf{Y}}_{GL}\hat{\mathbf{Y}}_{LL}^{-1}\hat{\mathbf{Y}}_{LG} \right) \hat{\mathbf{V}}_G \quad (16.7)$$

by defining

$$\mathbf{Y}_r = \hat{\mathbf{Y}}_{GG} - \hat{\mathbf{Y}}_{GL}\hat{\mathbf{Y}}_{LL}^{-1}\hat{\mathbf{Y}}_{LG},$$

and $\bar{\mathbf{Y}}_r$ for \mathbf{Y}_r incorporating the transient reactance of all generators. To obtain $\bar{\mathbf{Y}}_r$, we first define a diagonal matrix \mathbf{Z}_{tr} with the transient reactance of all the generators as the diagonal elements. Then $\bar{\mathbf{Y}}_r$ can be given as

$$\begin{aligned} \mathbf{Z}_r &= \bar{\mathbf{Y}}_r^{-1} \\ \bar{\mathbf{Y}}_r &= (\mathbf{Z}_r + \mathbf{Z}_{tr})^{-1}. \end{aligned}$$

We can write the network constraints in the network reference frame as

$$\begin{bmatrix} \mathbf{I}_D \\ \mathbf{I}_Q \end{bmatrix} = \begin{bmatrix} \bar{\mathbf{G}}_r & -\bar{\mathbf{B}}_r \\ \bar{\mathbf{B}}_r & \bar{\mathbf{G}}_r \end{bmatrix} \begin{bmatrix} \mathbf{E}'_D \\ \mathbf{E}'_Q \end{bmatrix}, \quad (16.8)$$

where $\bar{\mathbf{G}}_r$ and $\bar{\mathbf{B}}_r$ are the real part and imaginary part of $\bar{\mathbf{Y}}_r$, respectively.

16.4.5.1 Center of Inertia (COI) Frequency

Dynamic equations of the three generators are coupled in one more way and that is through the electrical frequency of the grid. In this chapter, we choose to define electrical frequency in one of the following two ways: either as a weighted sum of the frequencies of all three generators if the wind generator is represented as a synchronous machine, Eq. (16.9); or as a weighted sum of frequencies of the diesel and hydro if the wind generator is represented as an induction machine, Eq. (16.10).

$$\omega_{COI} = \frac{M_h \omega_h + M_d \omega_d + M_w \omega_w}{M_h + M_d + M_w} \quad (16.9)$$

$$\omega_{COI} = \frac{M_h \omega_h + M_d \omega_d}{M_h + M_d} \quad (16.10)$$

16.4.6 Model of the Interconnected System

The standard state-space model of interconnected system is obtained by combining the generator modules [Eq. (16.1) or (16.2), (16.3), and (16.4)] and the network coupling constraints [Eq. (16.8)] to obtain

$$\dot{x} = Ax + Bu, \quad (16.11)$$

in which x contains the state variables of all generator components and u is comprised of the control input variables of all generators. A and B are the system matrix and control input matrix, respectively. For the Flores power system with its induction wind generator, the variables and matrices are defined as

$$x = [x_h^T \ x_d^T \ x_w^T]^T,$$

$$u = [u_h^T \ u_d^T \ u_w^T]^T,$$

$$\begin{aligned}
A &= \begin{bmatrix} A_h & 0 & 0 \\ 0 & A_d & 0 \\ 0 & 0 & A_w \end{bmatrix} + \left(\begin{bmatrix} C_{\text{PE}}^h & 0 & 0 \\ 0 & C_{\text{PE}}^d & 0 \\ 0 & 0 & C_{\text{PE}}^w \end{bmatrix} + \begin{bmatrix} C_{\text{PI}}^h & 0 & 0 \\ 0 & C_{\text{PI}}^d & 0 \\ 0 & 0 & C_{\text{PI}}^w \end{bmatrix} \begin{bmatrix} \bar{\mathbf{G}}_r & -\bar{\mathbf{B}}_r \\ \bar{\mathbf{B}}_r & \bar{\mathbf{G}}_r \end{bmatrix} \right) S_E \\
&\quad + \begin{bmatrix} C_{\text{PCOI}}^h & 0 & 0 \\ 0 & C_{\text{PCOI}}^d & 0 \\ 0 & 0 & C_{\text{PCOI}}^w \end{bmatrix} S_\omega, \\
B &= \begin{bmatrix} B_h & 0 & 0 \\ 0 & B_d & 0 \\ 0 & 0 & B_w \end{bmatrix}.
\end{aligned} \tag{16.12}$$

S_E and S_ω are the selection matrices containing 0s and 1s that select the state variables corresponding to voltages $\Delta E'_{D\{\cdot\}}$ and $\Delta E'_{Q\{\cdot\}}$ and the speed $\Delta \omega_{\{\cdot\}}$.

$$\begin{bmatrix} E'_{Dh} \\ E'_{Qh} \\ E'_{Dd} \\ E'_{Qd} \\ E'_{Dw} \\ E'_{Qw} \end{bmatrix} = S_E x, \quad \begin{bmatrix} \omega_h \\ \omega_d \\ \omega_w \end{bmatrix} = S_\omega x.$$

When the Flores system is equipped with a synchronous wind generator, the variables and matrices can be similarly written to those of the Flores power system equipped with an induction wind generator. The variables and matrices in this case are then defined as

$$\begin{aligned}
x &= [x_h^T \ x_d^T \ x_{ws}^T]^T, \\
u &= [u_h^T \ u_d^T \ u_{ws}^T]^T, \\
A &= \begin{bmatrix} A_h & 0 & 0 \\ 0 & A_d & 0 \\ 0 & 0 & A_{ws} \end{bmatrix} + \left(\begin{bmatrix} C_{\text{PE}}^h & 0 & 0 \\ 0 & C_{\text{PE}}^d & 0 \\ 0 & 0 & C_{\text{PE}}^{ws} \end{bmatrix} + \begin{bmatrix} C_{\text{PI}}^h & 0 & 0 \\ 0 & C_{\text{PI}}^d & 0 \\ 0 & 0 & C_{\text{PI}}^{ws} \end{bmatrix} \begin{bmatrix} \bar{\mathbf{G}}_r & -\bar{\mathbf{B}}_r \\ \bar{\mathbf{B}}_r & \bar{\mathbf{G}}_r \end{bmatrix} \right) S_E \\
&\quad + \begin{bmatrix} C_{\text{PCOI}}^h & 0 & 0 \\ 0 & C_{\text{PCOI}}^d & 0 \\ 0 & 0 & C_{\text{PCOI}}^{ws} \end{bmatrix} S_\omega, \\
B &= \begin{bmatrix} B_h & 0 & 0 \\ 0 & B_d & 0 \\ 0 & 0 & B_{ws} \end{bmatrix}.
\end{aligned} \tag{16.13}$$

16.5 Stability Analysis in Flores Systems Characterized by Small Electrical Distances Between Wind and Diesel

In this section, the small-signal stability of the Flores power system is investigated through simulation studies. The electrical distances used in this section are representative of the actual Flores system, in which the electrical distance between the wind power plant and the diesel power plant is small. It is shown how the deployments of different wind generation technologies and voltage excitation controls affect the overall system dynamic behaviors. The specific control devices and techniques are introduced in the Appendix.

16.5.1 Wind as an Induction Machine

We first examine the small-signal stability of the stand-alone generators. In Table 16.5, the eigenvalues of the induction wind, synchronous hydro, and diesel generators are listed. Table 16.6 shows the eigenvalues of the interconnected system. The results indicate that the stand-alone components and interconnected system are small-signal stable regardless of the availability of exciter control on the synchronous generators. If no exciter control is applied to any of the generators, the overall stability is mainly maintained by the speed governor control.

Table 16.5 Eigenvalues of stand-alone components when induction wind generator is deployed

	Generator components	Eigenvalues of the components
Without exciter	Wind	$-1.5129 \pm 5.1966i, -0.0054, 0$
	Diesel	$-0.8 \pm 9.865i, -0.077, -0.425, -0.425, 0$
	Hydro	$-126.71, -1.3742, -0.46, -0.033, -0.286, -0.286, 0$
With exciter	Wind	$-1.5129 \pm 5.1966i, -0.0054, 0$
	Diesel	$-42.2242, -4.5256 \pm 11.0913i, -0.8005 \pm 9.8652i, -1.0475, -0.4255, -0.0767, 0$
	Hydro	$-126.71, -40.85, -5.12 \pm 8.48i, -1.37, -1.09, -0.03, -0.46, -0.29, 0$

Table 16.6 Eigenvalues of the interconnected system when induction wind generator is deployed

Type of system	Eigenvalues of the components
System with no exciter control	$-126.711, -1.554 \pm 16.934i, -7.978 \pm 7.900i, -8.249, -1.607 \pm 4.417i, -4.119, -1.39, -0.46, -0.531, -0.367, -0.274, -0.077, 0, 0$
System with exciter control	$-126.711, -41.134, -1.508 \pm 16.958i, -14.08, -5.239 \pm 9.459i, -7.576 \pm 7.508i, -9.014, -1.588 \pm 4.373i, -4.169, -1.391, -1.096, -0.754, -0.46, -0.282, -0.177, -0.077, 0, 0$

Table 16.7 Eigenvalues of stand-alone components when synchronous wind generator is deployed

	Generator components	Eigenvalues of the components
Without exciter	Wind	$-1.5129, -1.5129, -0.0054, 0$
	Diesel	$-0.8 \pm 9.865i, -0.077, -0.425, -0.425, 0$
	Hydro	$-126.71, -1.3742, -0.46, -0.033, -0.286, -0.286, 0$
With exciter	Wind	$-43.2703, -4.5855 \pm 12.9286i, -0.9689, -1.5129, -0.0054, 0$
	Diesel	$-41.576, -4.8448 \pm 9.9426i, -0.8005 \pm 9.8652i,$ $-1.0575, -0.4255, -0.0767, 0$
	Hydro	$-126.71, -40.87, -5.11 \pm 8.52i,$ $-1.37, -1.06, -0.033, -0.46, -0.29, 0$

Table 16.8 Eigenvalues of interconnected system when synchronous wind generator is deployed

Type of system	Eigenvalues of the components
System with no exciter control	$-126.711, -1.554 \pm 16.834i, -1.773 \pm 4.875i, -5.37 \pm 2.416i,$ $-4.255, -1.39, -0.736, -0.5, -0.46, -0.205, -0.278,$ $-0.077, 0$
System with exciter control	$-126.711, -43.61, -40.93, -37.14, -1.533 \pm 16.838i,$ $-8.747 \pm 14.476i, -14.036, -13.914, -5.061 \pm 8.905i,$ $-1.182 \pm 5.602i, -4.338, -0.669 \pm 3.127i, -1.391, -1.097,$ $-1.021, -0.585, -0.46, -0.294, -0.077, -0.198, 0$

In order to investigate the system response to small disturbances, we apply a 0.01 pu step-change disturbance to the wind mechanical power input and simulate the system response. The response of the speed governor outputs of the diesel and hydro generators is shown in Fig. 16.2. By comparing the two cases, we can draw the conclusion that when the Flores system is equipped with exciter control, the voltage deviations from the same disturbance can be reduced and the system becomes more stable in response to small disturbances. Frequency stability is ensured in both cases but the wear-and-tear on the speed governor is reduced when exciter control is implemented.

16.5.2 Wind as a Synchronous Machine

The small-signal stability of the Flores system with synchronous wind generator integrated is studied in this subsection. Following the logic of the previous subsection, we first show in Tables 16.7 and 16.8 the eigenvalues of the stand-alone generators and the interconnected system, respectively.

The same conclusion is drawn as in the previous subsection for the small-signal stability of the stand-alone components and the interconnected system. Speed

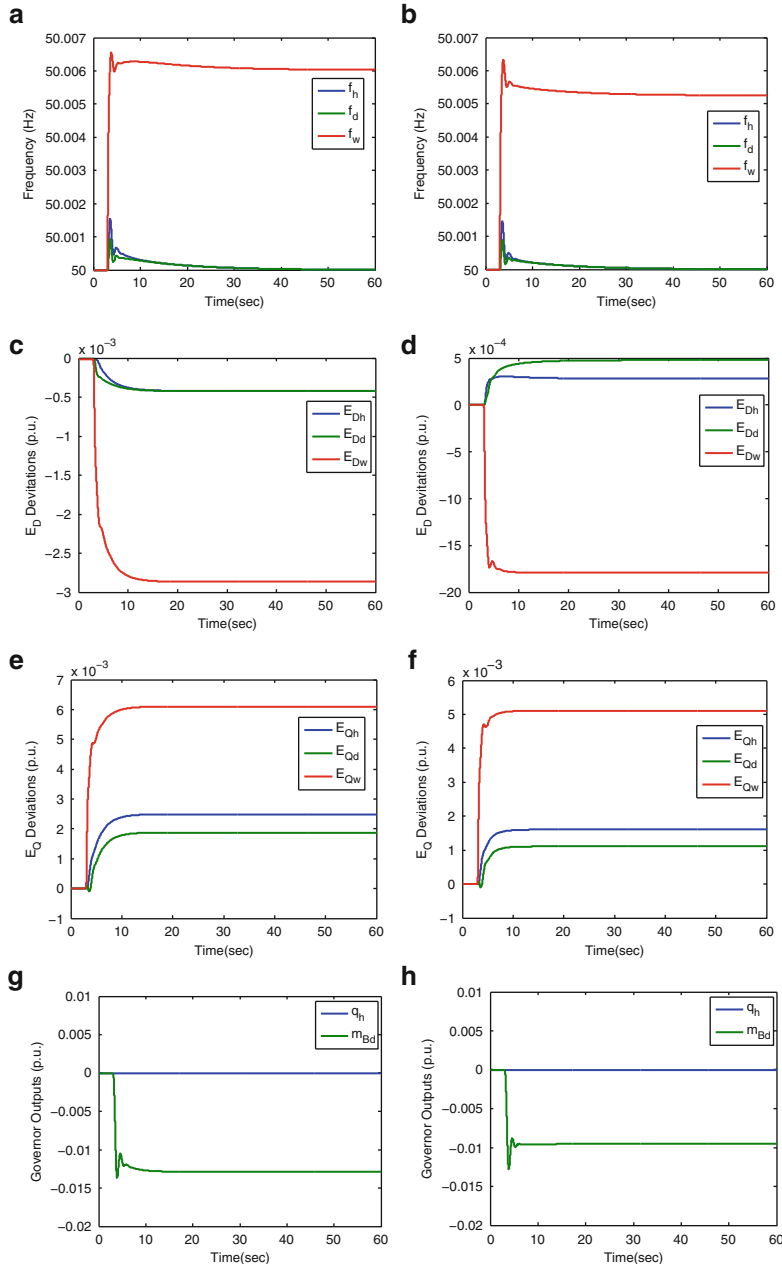


Fig. 16.2 Time response of the system with wind induction generator, small electrical distance. (a) Frequency: without exciter. (b) Frequency: with exciter. (c) Deviations of E_D : without exciter. (d) Deviations of E_D : with exciter. (e) Deviations of E_Q : without exciter. (f) Deviations of E_Q : with exciter. (g) Governor outputs: without exciter. (h) Governor outputs: with exciter

governor control contribute the most significantly to the system stability when no exciter control is implemented.

In order to investigate the system response to small disturbances, we apply a 0.01 pu step-change disturbance to the wind mechanical power input and simulate the system response, which is shown in Fig. 16.3. A comparison of the two cases reveals that the voltage deviations as well as the speed governor wear-and-tear of the system are significantly reduced when exciter control is implemented. Hence the small-signal stability is enhanced with exciter control.

16.6 Stability Analysis in Systems with Large Electrical Distances Between Wind and Diesel

In this section, we analyze the small-signal stability of the Flores power system with large electrical distances between the wind generator and the diesel generator. The electrical distance used in this section is ten times larger than the actual electrical distance between the wind generator and diesel generator in the Flores system. The impact of electrical distance on the stability of the interconnected system is assessed. Different technologies for controlling the wind generator are also illustrated with their enhancement of system stability compared via simulation studies.

16.6.1 Wind as an Induction Machine

We assume that all the synchronous generators studied in this subsection are equipped with exciter control, and we focus on comparing the alternatives for controlling the wind induction machine. Specifically, the technologies of DFIG and SVC will be investigated. For the Flores system with these alternative controls, the corresponding eigenvalues of stand-alone generator components and the interconnected system are listed in Tables 16.9 and 16.10, respectively.

As can be seen from the eigenvalues in the tables, the interconnected system is unstable, with one positive eigenvalue, 1.195, when there is no control on the wind induction generator, even though exciter controllers are installed on diesel and hydro generators and the stand-alone components are stable. The selective modal analysis method [8] is applied to compute the contribution of each state variable to this unstable eigenvalue. Table 16.11 gives the participation factor corresponding to the unstable eigenvalue $\lambda = 1.195$. The states of the mechanical rotating speed ($\Delta\omega_w$) and voltages ($\Delta E'_{Dw}$ and $\Delta E'_{Hw}$) contribute most to the unstable mode. This is because no voltage control is applied to the wind generator to produce sufficient reactive power and the reactive power, generated by diesel and hydro barely affects the voltage of the wind generator due to the large electrical distance.

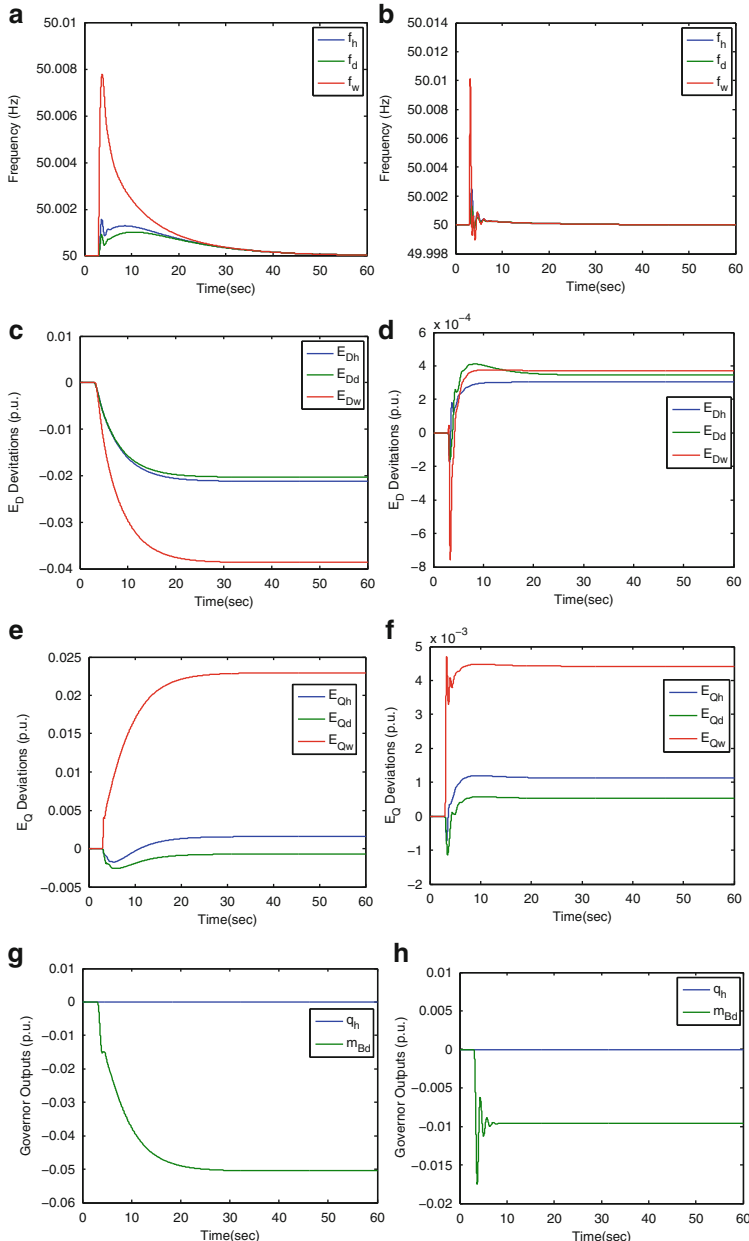


Fig. 16.3 Time response of the system with wind synchronous generator, small electrical distance. **(a)** Frequency: without exciter. **(b)** Frequency: with exciter. **(c)** Deviations of E_D : without exciter. **(d)** Deviations of E_D : with exciter. **(e)** Deviations of E_Q : without exciter. **(f)** Deviations of E_Q : with exciter. **(g)** Governor outputs: without exciter. **(h)** Governor outputs: with exciter

Table 16.9 Eigenvalues of stand-alone components when induction wind generator is deployed

	Generator components	Eigenvalues of the components
No control on wind	Wind induction	$-1.5129 \pm 12.7549i, -0.0054, 0$
	Diesel	$-42.2019, -4.5367 \pm 11.0532i,$ $-0.8005 \pm 9.8652i, -1.0478, -0.4255,$ $-0.0767, 0$
	Hydro	$-126.71, 40.85, -5.12 \pm 8.48, -1.37,$ $-1.09, -0.46, -0.29 - 0.03, 0$
	Wind induction	$-1.5129, -1.5129, -0.0054, 0, 0$
	Diesel	$-42.0567, -4.6082 \pm 10.8036i,$ $-0.8005 \pm 9.8652i, -1.0498, -0.4255, -0.0767, 0$
	Hydro	$-126.71, -40.85, -5.12 \pm 8.47i,$ $-1.37, -1.09, -0.033, -0.46, -0.29, 0$
	Wind induction	$-1.5129 \pm 6i, -0.0054, 0$
	Diesel	$-42.0567, -4.6082 \pm 10.698i, -0.8005 \pm 9.8652i,$ $-1.0507, -0.4255, -0.0767, 0$
	Hydro	$-126.71, -40.85, -5.12 \pm 8.47i,$ $-1.37, -1.09, -0.033, -0.46, -0.29, 0$

Table 16.10 Eigenvalues of interconnected system when wind induction generator is deployed

Type of system	Eigenvalues of the components
System with no control on wind	$-126.711, -41.372, -37.124, -1.448 \pm 16.955i, -14.07,$ $-6.421 \pm 10.436, -5.392 \pm 9.6i, -0.945 \pm 4.7i, -4.128,$ $-1.391, -1.093, -0.754, -0.46, -0.289,$ $-0.179, -0.077, 0, 0, 1.195$
System with DFIG on wind	$-126.711, -41.31, -37.13, -1.516 \pm 16.838i, -5.149 \pm 9.446i,$ $-14.06, -3.428 \pm 7.647i, -1.867 \pm 4.391i, -4.153,$ $-3 \pm 0.741i, -1.391, -1.092, -0.551 \pm 0.058,$ $-0.46, -0.27, -0.18, -0.076, 0$
System with SVC on wind	$-126.711, -41.29, -37.14, -1.517 \pm 16.822i, -5.15 \pm 9.45i,$ $-17.96, -14.06, -5.15 \pm 9.46i, -1.844 \pm 6.626i, -4.153,$ $-1.522 \pm 3.75i, -4.193, -1.39, -1.09,$ $-0.46, -0.526, -0.272, -0.076, -0.185, 0, 0$

In comparison, when DFIG or SVC controls are implemented on the wind generator, the interconnected system can be stabilized. Linear proportional feedback control, which responds to the terminal voltage of the wind generator, is applied to both devices. The performances of these two control approaches are shown and compared in Fig. 16.4. The stability of the interconnected system is ensured by means of both DFIG control and SVC control. The use of a governor on the synchronous generators is also limited.

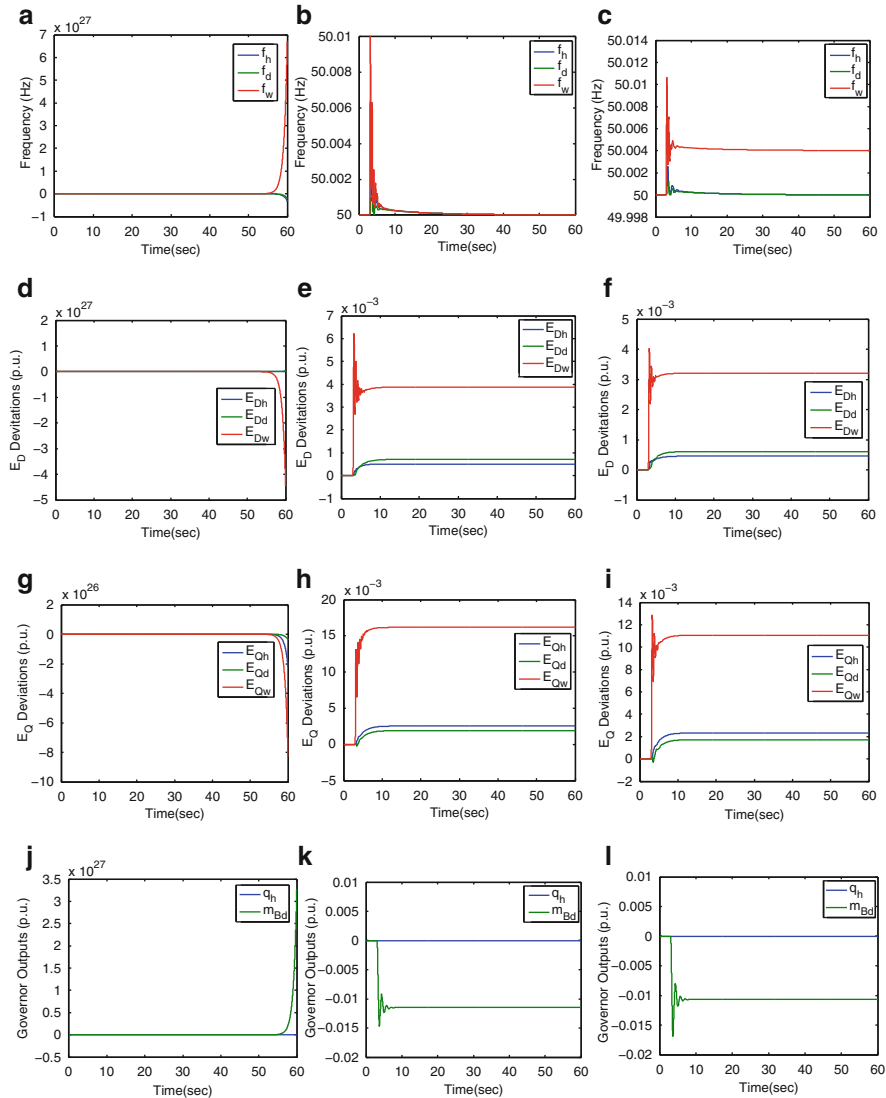


Fig. 16.4 Time response of the system with wind induction generator, large electrical distance. (a) Frequency: no control on wind. (b) Frequency: DFIG on wind. (c) Frequency: SVC on wind. (d) ΔE_D : no control on wind. (e) ΔE_D : DFIG on wind. (f) ΔE_D : SVC on wind. (g) ΔE_Q : no control on wind. (h) ΔE_Q : DFIG on wind. (i) ΔE_Q : SVC on wind. (j) Governor outputs: no control on wind. (k) Governor outputs: DFIG on wind. (l) Governor outputs: SVC on wind

Table 16.11 Participation factors of the unstable eigenvalue $\lambda = 1.195$

State variable	Participation factor
Δq_h	$-0.0000 + 0.0000i$
Δv_h	$0.0000 - 0.0000i$
Δa_h	$0.0000 - 0.0000i$
$\Delta \delta_h$	$-0.0046 + 0.0000i$
$\Delta \omega_h$	$0.0020 - 0.0000i$
$\Delta E'_{Dh}$	$-0.0002 - 0.0000i$
$\Delta E'_{Qh}$	$-0.0194 + 0.0000i$
ΔV_{Rh}	$-0.0000 - 0.0000i$
Δe_{fdh}	$-0.0019 + 0.0000i$
ΔV_{Fh}	$0.0008 - 0.0000i$
Δm_{Bd}	$-0.0091 - 0.0000i$
ΔP_{cd}	$-0.0013 + 0.0000i$
$\Delta \delta_d$	$0.0060 + 0.0000i$
$\Delta \omega_d$	$0.0007 + 0.0000i$
$\Delta E'_{Dd}$	$-0.0001 + 0.0000i$
$\Delta E'_{Qd}$	$-0.0007 + 0.0000i$
ΔV_{Rd}	$-0.0000 + 0.0000i$
Δe_{fdd}	$-0.0010 - 0.0000i$
ΔV_{Fd}	$0.0005 + 0.0000i$
$\Delta \delta_w$	0
$\Delta \omega_w$	$0.8021 - 0.0000i$
$\Delta E'_{Dw}$	$0.2065 + 0.0000i$
$\Delta E'_{Qw}$	$0.0197 + 0.0000i$

16.6.2 Wind as an Synchronous Machine

We assume that all the generators in this subsection are equipped with exciter control. Recall that the main objective of this chapter is to evaluate the effect of control on voltage dynamics to enhance the stability of the interconnected system and reduce the wear-and-tear on the speed governor. We focus on simulating the scenarios in which the PSS control is deployed on the wind synchronous generator to enhance system stability and reduce the oscillations on both the diesel and hydro generators. Here, all the PSS controllers on these synchronous generators are designed in a linear proportional feedback fashion in response to the generator's rotating speed deviation. The eigenvalues of concern corresponding to the scenarios are presented in Tables 16.12 and 16.13.

Since no eigenvalue has positive real part. The stand-alone components and interconnected system are small-signal stable regardless of the deployment of PSS control on the wind generator. We then compare the time response of the system in the two scenarios and evaluate the performance of PSS control. In Fig. 16.5, we show that with PSS control on the wind generator, the oscillations on the state variables, including the responses of the diesel and hydro speed governors, are significantly reduced. The results show that, by using our proposed approach, the

Table 16.12 Eigenvalues of stand-alone components when synchronous wind generator is deployed

	Generator components	Eigenvalues of the components
No control on wind	Wind	$-48.8165, -1.8030 \pm 20.1186i,$ $-0.9878, -1.5128, -0.0054, 0$
	Diesel	$-41.1109, -5.0725 \pm 9.0497i,$ $-0.8005 \pm 9.8652i, -1.0671, -0.4256, -0.0767, 0$
	Hydro	$-126.71, 40.87, -5.11 \pm 8.52, -1.37,$ $-1.09, -0.46, -0.29 - 0.033, 0$
PSS on wind	Wind	$-48.8165, -1.8030 \pm 20.1186i, -0.9878, -1.5128,$ $-0.0054, 0$
	Diesel	$-41.1109, -5.0725 \pm 9.0497i, -0.8005 \pm 9.8652i,$ $-1.0671, -0.4256, -0.0767, 0$
	Hydro	$-126.71, 40.87, -5.11 \pm 8.52, -1.37,$ $-1.09, -0.46, -0.29 - 0.033, 0$

Table 16.13 Eigenvalues of the interconnected system when wind induction generator is deployed

Type of system	Eigenvalues of the components
System with no control on wind	$-126.711, -48.88, -40.964, -37.149, -2.752 \pm 20.677i,$ $-1.556 \pm 16.742, -14.07, -5.159 \pm 8.805,$ $-7.248, -1.085 \pm 5.309i, -4.515, -0.627 \pm 2.542,,$ $-1.39, -1.097, -0.879, -0.426, -0.46, -0.289 - 0.232,$ $-0.077, 0$
System with PSS on wind	$-126.711, -48.67, -40.964, -37.149, -2.21 \pm 20.44i,$ $-1.556 \pm 16.742, -14.08, -5.159 \pm 8.805, -7.48,,$ $-1.07 \pm 5.309i, -4.515, -1.27 \pm 2.43, -1.39, -1.097, -0.868,$ $-0.411, -0.46, -0.289, -0.232, -0.075, 0$

wear-and-tear on the mechanical part of the generator can be lessened by using control on the electromagnetic part.

16.7 Comparison and Discussion

The simulation results show that in three out of the four scenarios, the interconnected system is small-signal stable. The stability across the different scenarios indicates that in normal operation conditions, there is a certain stability margin in the Flores power system. However, small-signal instability can still occur when an induction wind generator is installed with a large electrical distance to the main power grid; in this case, the system can be stabilized when controls are applied to the wind generator. This result sheds light on future consideration of renewable energy integration. A standard for interconnected system dynamics is crucial. It is critical to take the dynamics of the renewable energy components, as well as the electrical

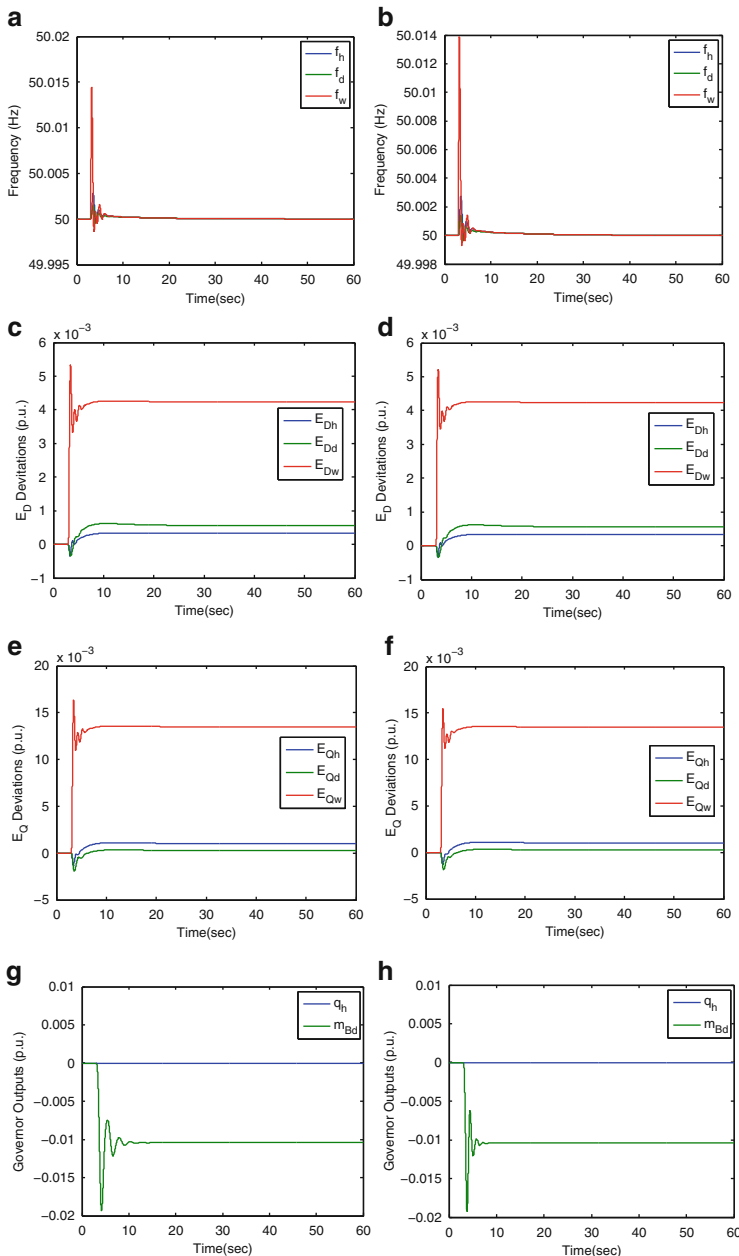


Fig. 16.5 Time response of the system with wind synchronous generator, large electrical distance. **(a)** Frequency: no control on wind. **(b)** Frequency: PSS on wind. **(c)** ΔE_D : no control on wind. **(d)** ΔE_D : PSS on wind. **(e)** ΔE_Q : no control on wind. **(f)** ΔE_Q : PSS on wind. **(g)** Governor: no control on wind. **(h)** Governor: PSS on wind

distance between the renewable source and the main power grid, into consideration. If the overall system with renewable energy components is unstable, alternative renewable generator technologies, a relocation of renewable components, or an application of control should be considered in order to have a stable interconnected system.

16.8 Conclusions

This chapter studies small-signal stability problem in electric power grids with variable wind penetration. The main focus of the chapter assesses power system small-signal stability by using a coupled (electromechanics and electromagnetics) linearized dynamic model. In the previous chapter we have shown how the wear-and-tear of governor equipment is inevitable if frequency stabilization is to be achieved by using only these devices. On the other hand, flywheels are the expensive alternative. This chapter, however, shows alternatives deployed as voltage controllers. It is shown that the use of excitation control on generators, enhanced by power system stabilizers (PSS), improves the frequency response to small-signal wind disturbances. However, the problem of voltage instability can appear in the coupled model when not enough controllers are installed on the wind generator. The static VAR compensator (SVC) and Doubly Fed Induction Generator (DFIG) are used to control the system dynamics and ensure small-signal stability. A comparison is made between systems with small and large electrical distances between the wind generators and the conventional generators.

Acknowledgment This work is supported by US National Science Foundation Award 0931978, the Semiconductor Research Corporation (SRC) Smart Grid Research Center (SGRC) at Carnegie Mellon University Research Task 2111.002 and 2111.003, and the Carnegie Mellon University ECE Fellowship. The authors also want to express much appreciation to Kevin Bachovchin for his technical proof reading of the entire chapter.

Appendix

Equilibrium of the Flores Island Power System

The equilibrium of the Flores Island power system in which wind generator is represented using a synchronous machine is shown in Fig. 16.6. A linearized model for one of the simulations in this chapter is derived around this equilibrium.

Hydro Generator Dynamic Model

The hydro generator is represented with a two-axis synchronous generator model. The two-axis synchronous generator model is described using four states: d -axis E'_D and q -axis E'_Q component of voltage behind the transient reactance, the rotor angle position δ , and the angular frequency of the rotor ω .

In order to be connected with other machines, the two-axis synchronous generator model has to be transformed from a rotating reference frame into a network reference frame. This is done by using the Park/Blondel transform. The two-axis synchronous machine model in the network reference frame is given with the following set of equations:

$$\begin{aligned}\dot{E}'_D &= -T_1 E'_D - T_2(E'_D \cos(2\delta) + E'_Q \sin(2\delta)) \\ &\quad + X_1 I_Q - X_2(I_D \sin(2\delta) - I_Q \cos(2\delta)) \\ &\quad - \omega_b(\omega - \omega_0) E'_Q \\ &\quad + \frac{1}{T'_{d0}} \cos(\delta) e_{fd}\end{aligned}$$

$$\begin{aligned}\dot{E}'_Q &= -T_1 E'_Q - T_2(E'_Q \sin(2\delta) - E'_D \cos(2\delta)) \\ &\quad - X_1 I_D + X_2(I_D \cos(2\delta) + I_Q \sin(2\delta)) \\ &\quad + \omega_b(\omega - \omega_0) E'_D\end{aligned}$$

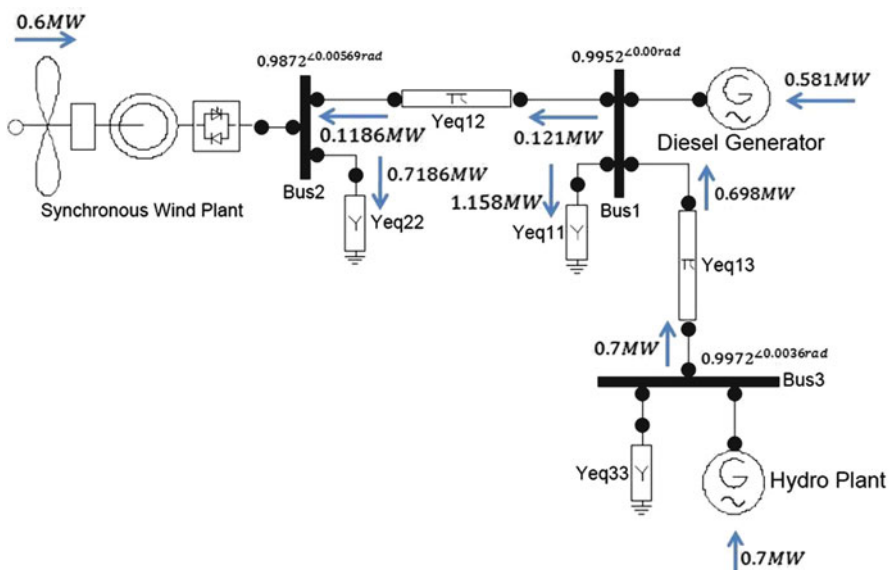


Fig. 16.6 Equilibrium of the FLores Island power system

$$\begin{aligned}
& + \frac{1}{T'_{d0}} \sin(\delta) e_{fd} \\
\dot{\delta} &= \omega_b (\omega - \omega_0) \\
\dot{\omega} &= \frac{1}{M} (T_m - (E'_D I_D + E'_Q I_Q) - D(\omega - \omega_{COI})) \\
\dot{V}_R &= -\frac{1}{T_A} V_R + \frac{K_A}{T_A} (V^{\text{ref}} - V - V_F) \\
\dot{E}_{fd} &= \frac{1}{T_E} (V_R - (K_E + S_E) E_{fd}) \\
\dot{V}_F &= -\frac{1}{T_F} V_F + \frac{K_F}{T_F} \dot{E}_{fd}
\end{aligned} \tag{16.14}$$

The voltage behind the transient reactance and the current of the generator are given in the network reference frame. The parameters of interest in these equations are

$$\begin{aligned}
T_1 &= \frac{1}{2} \left(\frac{1}{T'_{d0}} + \frac{1}{T'_{q0}} \right) \\
T_2 &= \frac{1}{2} \left(\frac{1}{T'_{d0}} - \frac{1}{T'_{q0}} \right) \\
X_1 &= \frac{1}{2} \left(\frac{x_d - x'_d}{T'_{d0}} + \frac{x_q - x'_q}{T'_{q0}} \right) \\
X_2 &= \frac{1}{2} \left(\frac{x_d - x'_d}{T'_{d0}} - \frac{x_q - x'_q}{T'_{q0}} \right)
\end{aligned} \tag{16.15}$$

The linearized model of the hydro generator is

$$\begin{aligned}
\Delta \dot{q}_h &= -\frac{1}{T_q} \Delta q_h + \frac{1}{T_w} \Delta \alpha_h + \frac{1}{T_f} \Delta \omega \\
\Delta \dot{v}_h &= -\frac{1}{T_e} \Delta v_h + \frac{r'_h}{T_e} \Delta \alpha_h \\
\Delta \dot{\alpha}_h &= \frac{1}{T_s} \Delta v_h + \frac{r_h + r'_h}{T_s} \Delta \alpha_h - \frac{G_p}{T_s} \Delta \omega \\
\Delta \dot{E}'_D &= L_{13}^h \Delta E'_D + L_{14}^h \Delta E'_Q + L_{11}^h \Delta \delta + L_{12}^h \Delta \omega + L_{17}^h \Delta e_{fd} \\
&\quad + L_{15}^h \Delta I_D + L_{16}^h \Delta I_Q + L_{18}^h \Delta \omega_{COI} \\
\Delta \dot{E}'_Q &= L_{23}^h \Delta E'_D + L_{24}^h \Delta E'_Q + L_{21}^h \Delta \delta + L_{22}^h \Delta \omega + L_{27}^h \Delta e_{fd} \\
&\quad + L_{25}^h \Delta I_D + L_{26}^h \Delta I_Q + L_{28}^h \Delta \omega_{COI}
\end{aligned}$$

$$\begin{aligned}
\Delta \dot{\delta} &= \omega_b \Delta \omega - \omega_b \Delta \omega_{COI} \\
\Delta \dot{\omega} &= \frac{k_q}{M_h} \Delta q_h - \frac{k_w}{M_h} \Delta \alpha_h - \frac{D_h}{M_h} \Delta \omega + L_{31}^h \Delta E'_D \\
&\quad + L_{32}^h \Delta E'_Q + L_{33}^h \Delta I_D + L_{34}^h \Delta I_Q + \frac{D_h}{M_h} \Delta \omega_{COI} \\
\Delta \dot{V}_{Rh} &= L_{41}^h \Delta E'_D + L_{42}^h \Delta E'_Q - \frac{1}{T_{Ah}} \Delta V_{Rh} - \frac{K_{Ah}}{T_{Ah}} \Delta V_{Fh} \\
&\quad - \frac{T_{Ah}}{K_{Ah}} \Delta V_{h,pss} - L_{42}^h X_d' \Delta I_D + L_{41}^h X_d' \Delta I_Q \\
\Delta \dot{e}_{fdh} &= \frac{1}{T_{Eh}} \Delta V_{Rh} - \frac{K_{Eh} + S_{Eh}}{T_{Eh}} \Delta e_{fdh} \\
\Delta \dot{V}_{Fh} &= \frac{K_{Fh}}{T_{Eh} T_{Fh}} \Delta V_{Rh} - \frac{K_{Fh}(K_{Eh} + S_{Eh})}{T_{Fh} T_{Eh}} \Delta e_{fdh} - \frac{1}{T_{Fh}} \Delta V_{Fh} \quad (16.16)
\end{aligned}$$

Diesel Generator Dynamic Model

The diesel generator is represented with a two-axis synchronous generator model. The two-axis synchronous generator model is described using four states: d -axis E'_D and q -axis E'_Q component of voltage behind the transient reactance, the rotor angle position δ , and the angular frequency of the rotor ω .

In order to be connected with other machines, the two-axis synchronous generator model has to be transformed from a rotating into a network reference frame. This is done by using the Park/Blondel transform. The two-axis synchronous machine model in the network reference frame is given with the following set of equations

$$\begin{aligned}
\dot{E}'_D &= -T_1 E'_D - T_2 (E'_D \cos(2\delta) + E'_Q \sin(2\delta)) \\
&\quad + X_1 I_Q - X_2 (I_D \sin(2\delta) - I_Q \cos(2\delta)) \\
&\quad - \omega_b (\omega - \omega_0) E'_Q \\
&\quad + \frac{1}{T'_{d0}} \cos(\delta) e_{fd} \\
\dot{E}'_Q &= -T_1 E'_Q - T_2 (E'_D \sin(2\delta) - E'_Q \cos(2\delta)) \\
&\quad - X_1 I_D + X_2 (I_D \cos(2\delta) + I_Q \sin(2\delta)) \\
&\quad + \omega_b (\omega - \omega_0) E'_D \\
&\quad + \frac{1}{T'_{d0}} \sin(\delta) e_{fd} \\
\dot{\delta} &= \omega_b (\omega - \omega_0)
\end{aligned}$$

$$\begin{aligned}
\dot{\omega} &= \frac{1}{M}(T_m - (E'_D I_D + E'_Q I_Q) - D(\omega - \omega_{COI})) \\
\dot{V}_R &= -\frac{1}{T_A} V_R + \frac{K_A}{T_A} (V^{\text{ref}} - V - V_F) \\
\dot{E}_{fd} &= \frac{1}{T_E} (V_R - (K_E + S_E) E_{fd}) \\
\dot{V}_F &= -\frac{1}{T_F} V_F + \frac{K_F}{T_F} \dot{E}_{fd}
\end{aligned} \tag{16.17}$$

The voltage behind the transient reactance and the current of the generator are given in the network reference frame. The parameters of interest in these equations are

$$\begin{aligned}
T_1 &= \frac{1}{2} \left(\frac{1}{T'_{d0}} + \frac{1}{T'_{q0}} \right) \\
T_2 &= \frac{1}{2} \left(\frac{1}{T'_{d0}} - \frac{1}{T'_{q0}} \right) \\
X_1 &= \frac{1}{2} \left(\frac{x_d - x'_d}{T'_{d0}} + \frac{x_q - x'_q}{T'_{q0}} \right) \\
X_2 &= \frac{1}{2} \left(\frac{x_d - x'_d}{T'_{d0}} - \frac{x_q - x'_q}{T'_{q0}} \right)
\end{aligned} \tag{16.18}$$

The linearized model of the diesel generator is

$$\begin{aligned}
\Delta \dot{m}_{Bd} &= -\frac{1}{T_{dd}} \Delta m_{Bd} - \frac{C_d K_d}{T_{dd}} \Delta P_{cd} + \frac{C_d K_d}{T_{dd} R_d} \Delta \omega \\
\Delta \dot{P}_{cd} &= K_{Id} \Delta \omega \\
\Delta \dot{E}'_D &= L_{13}^d \Delta E'_D + L_{14}^d \Delta E'_Q + L_{11}^d \Delta \delta + L_{12}^d \Delta \omega + L_{17}^d \Delta e_{fd} \\
&\quad + L_{15}^d \Delta I_D + L_{16}^d \Delta I_Q + L_{18}^d \Delta \omega_{COI} \\
\Delta \dot{E}'_Q &= L_{23}^d \Delta E'_D + L_{24}^d \Delta E'_Q + L_{21}^d \Delta \delta + L_{22}^d \Delta \omega + L_{27}^d \Delta e_{fd} \\
&\quad + L_{25}^d \Delta I_D + L_{26}^d \Delta I_Q + L_{28}^d \Delta \omega_{COI} \\
\Delta \dot{\delta} &= \omega_b \Delta \omega - \omega_b \Delta \omega_{COI} \\
\Delta \dot{\omega} &= \frac{k_q}{M_d} \Delta q_d - \frac{k_w}{M_d} \Delta \alpha_d - \frac{D_d}{M_d} \Delta \omega + L_{31}^d \Delta E'_D \\
&\quad + L_{32}^d \Delta E'_Q + L_{33}^d \Delta I_D + L_{34}^d \Delta I_Q + \frac{D_d}{M_d} \Delta \omega_{COI}
\end{aligned}$$

$$\begin{aligned}
\Delta \dot{V}_{Rd} &= L_{41}^d \Delta E'_D + L_{42}^d \Delta E'_Q - \frac{1}{T_{Ad}} \Delta V_{Rd} - \frac{K_{Ad}}{T_{Ad}} \Delta V_{Fd} \\
&\quad - \frac{T_{Ad}}{K_{Ad}} \Delta V_{d,\text{pss}} - L_{42}^d X_d' \Delta I_D + L_{41}^d X_d' \Delta I_Q \\
\Delta \dot{e}_{fd} &= \frac{1}{T_{Ed}} \Delta V_{Rd} - \frac{K_{Ed} + S_{Ed}}{T_{Ed}} \Delta e_{fd} \\
\Delta \dot{V}_{Fd} &= \frac{K_{Fd}}{T_{Ed} T_{Fd}} \Delta V_{Rd} - \frac{K_{Fd}(K_{Ed} + S_{Ed})}{T_{Fd} T_{Ed}} \Delta e_{fd} - \frac{1}{T_{Fd}} \Delta V_{Fd} \quad (16.19)
\end{aligned}$$

Wind Generator Dynamic Model

The wind generator is represented with either a two-axis synchronous generator model or a two-axis induction generator model. Both models are described using four states: d -axis E'_D and q -axis E'_Q component of voltage behind transient reactance, the rotor angle position δ and the angular frequency of the rotor ω .

Wind as an Induction Machine

In order to be connected with other machines, the two-axis induction generator model has to be transformed from a rotating into a network reference frame. This is done by using the Park/Blondel transform. The two-axis induction machine model in the network reference frame is given with the following set of equations:

$$\begin{aligned}
\dot{E}'_D &= -T_1 E'_D - T_2 (E'_D \cos(2\delta) + E'_Q \sin(2\delta)) \\
&\quad + X_1 I_Q - X_2 (I_D \sin(2\delta) - I_Q \cos(2\delta)) \\
&\quad - \omega_b (\omega - \omega_0) E'_Q \\
&\quad - 2\omega_b (\omega - \omega_0) E'_Q \\
&\quad + e_{fd} \cos(\delta) - e_{fq} \sin(\delta) \\
\dot{E}'_Q &= -T_1 E'_Q - T_2 (E'_D \sin(2\delta) - E'_Q \cos(2\delta)) \\
&\quad - X_1 I_D + X_2 (I_D \cos(2\delta) + I_Q \sin(2\delta)) \\
&\quad + \omega_b (\omega - \omega_0) E'_D \\
&\quad + 2\omega_b (\omega - \omega_0) E'_D \\
&\quad + e_{fd} \sin(\delta) + e_{fq} \cos(\delta) \\
\dot{\delta} &= \omega_b (\omega - \omega_0)
\end{aligned}$$

$$\dot{\omega} = \frac{1}{M} (T_m - (E'_D I_D + E'_Q I_Q) - D(\omega - \omega_{COI})) \quad (16.20)$$

The voltage behind the transient reactance and the current of the generator are given in the network reference frame. The parameters of interest in these equations are

$$\begin{aligned} T_1 &= \frac{1}{2} \left(\frac{1}{T'_{d0}} + \frac{1}{T'_{q0}} \right) \\ T_2 &= \frac{1}{2} \left(\frac{1}{T'_{d0}} - \frac{1}{T'_{q0}} \right) \\ X_1 &= \frac{1}{2} \left(\frac{x_d - x'_d}{T'_{d0}} + \frac{x_q - x'_q}{T'_{q0}} \right) \\ X_2 &= \frac{1}{2} \left(\frac{x_d - x'_d}{T'_{d0}} - \frac{x_q - x'_q}{T'_{q0}} \right) \end{aligned} \quad (16.21)$$

The linearized model of the wind generator is

$$\begin{aligned} \Delta \dot{E}'_D &= L_{13}^w \Delta E'_D + L_{14}^w \Delta E'_Q + L_{11}^w \Delta \delta + L_{12}^w \Delta \omega + L_{18}^w \Delta e_{fd} \\ &\quad + L_{19}^w \Delta e_{fq} + L_{15}^w \Delta I_D + L_{16}^w \Delta I_Q + L_{17}^w \Delta \omega_{COI} \\ \Delta \dot{E}'_Q &= L_{23}^w \Delta E'_D + L_{24}^w \Delta E'_Q + L_{21}^w \Delta \delta + L_{22}^w \Delta \omega + L_{28}^w \Delta e_{fd} \\ &\quad + L_{29}^w \Delta e_{fq} + L_{25}^w \Delta I_D + L_{26}^w \Delta I_Q + L_{27}^w \Delta \omega_{COI} \\ \Delta \dot{\delta} &= \omega_b \Delta \omega - \omega_b \Delta \omega_{COI} \\ \Delta \dot{\omega} &= -\frac{D_w}{M_w} \Delta \omega + \frac{D_w}{M_w} \Delta \omega_{COI} + L_{31}^w \Delta E'_D + L_{32}^w \Delta E'_Q \\ &\quad + L_{33}^w \Delta I_D + L_{34}^w \Delta I_Q \end{aligned} \quad (16.22)$$

Wind as a Synchronous Machine

In order to be connected with other machines the two-axis synchronous generator model has to be transformed from a rotating into a network reference frame. This is done by using the Park/Blondel transform. The two-axis synchronous machine model in the network reference frame is given with the following set of equations:

$$\dot{E}'_D = -T_1 E'_D - T_2 (E'_D \cos(2\delta) + E'_Q \sin(2\delta))$$

$$\begin{aligned}
& + X_1 I_Q - X_2 (I_D \sin(2\delta) - I_Q \cos(2\delta)) \\
& - \omega_b (\omega - \omega_0) E'_Q \\
& + \frac{1}{T'_{d0}} \cos(\delta) e_{fd} \\
E'_Q & = -T_1 E'_Q - T_2 (E'_D \sin(2\delta) - E'_Q \cos(2\delta)) \\
& - X_1 I_D + X_2 (I_D \cos(2\delta) + I_Q \sin(2\delta)) \\
& + \omega_b (\omega - \omega_0) E'_D \\
& + \frac{1}{T'_{d0}} \sin(\delta) e_{fd}
\end{aligned}$$

(16.23)

$$\begin{aligned}
\dot{\delta} &= \omega_b (\omega - \omega_0) \\
\dot{\omega} &= \frac{1}{M} (T_m - (E'_D I_D + E'_Q I_Q) - D(\omega - \omega_{COI})) \\
\dot{V}_R &= -\frac{1}{T_A} V_R + \frac{K_A}{T_A} (V^{\text{ref}} - V - V_F) \\
\dot{E}_{fd} &= \frac{1}{T_E} (V_R - (K_E + S_E) E_{fd}) \\
\dot{V}_F &= -\frac{1}{T_F} V_F + \frac{K_F}{T_F} \dot{E}_{fd}
\end{aligned}$$

The voltage behind the transient reactance and the current of the generator are given in the network reference frame. The parameters of interest in these equations are

$$\begin{aligned}
T_1 &= \frac{1}{2} \left(\frac{1}{T'_{d0}} + \frac{1}{T'_{q0}} \right) \\
T_2 &= \frac{1}{2} \left(\frac{1}{T'_{d0}} - \frac{1}{T'_{q0}} \right) \\
X_1 &= \frac{1}{2} \left(\frac{x_d - x'_d}{T'_{d0}} + \frac{x_q - x'_q}{T'_{q0}} \right) \\
X_2 &= \frac{1}{2} \left(\frac{x_d - x'_d}{T'_{d0}} - \frac{x_q - x'_q}{T'_{q0}} \right)
\end{aligned}$$

The linearized model of the wind generator is

$$\begin{aligned}
 \Delta\dot{E}'_D &= L_{13}^{ws}\Delta E'_D + L_{14}^{ws}\Delta E'_Q + L_{11}^{ws}\Delta\delta + L_{12}^{ws}\Delta\omega \\
 &\quad + L_{18}^{ws}\Delta e_{fd} + L_{19}^{ws}\Delta e_{fq} + L_{15}^{ws}\Delta I_D + L_{16}^{ws}\Delta I_Q + L_{17}^{ws}\Delta\omega_{COI} \\
 \Delta\dot{E}'_Q &= L_{23}^{ws}\Delta E'_D + L_{24}^{ws}\Delta E'_Q + L_{21}^{ws}\Delta\delta + L_{22}^{ws}\Delta\omega \\
 &\quad + L_{28}^{ws}\Delta e_{fd} + L_{29}^{ws}\Delta e_{fq} + L_{25}^{ws}\Delta I_D + L_{26}^{ws}\Delta I_Q + L_{27}^{ws}\Delta\omega_{COI} \\
 \Delta\dot{\delta} &= \omega_b\Delta\omega - \omega_b\Delta\omega_{COI} \\
 \Delta\dot{\omega} &= -\frac{D_{ws}}{M_{ws}}\Delta\omega + \frac{D_{ws}}{M_{ws}}\Delta\omega_{COI} + L_{31}^{ws}\Delta E'_D \\
 &\quad + L_{32}^{ws}\Delta E'_Q + L_{33}^{ws}\Delta I_D + L_{34}^{ws}\Delta I_Q \\
 \Delta\dot{V}_{Rh} &= L_{41}^h\Delta E'_D + L_{42}^h\Delta E'_Q - \frac{1}{T_{Ah}}\Delta V_{Rh} - \frac{K_{Ah}}{T_{Ah}}\Delta V_{Fh} \\
 &\quad - \frac{T_{Ah}}{K_{Ah}}\Delta V_{h,pss} - L_{42}^hX_d'\Delta I_D + L_{41}^hX_d'\Delta I_Q \\
 \Delta\dot{e}_{fdh} &= \frac{1}{T_{Eh}}\Delta V_{Rh} - \frac{K_{Eh} + S_{Eh}}{T_{Eh}}\Delta e_{fdh} \\
 \Delta\dot{V}_{Fh} &= \frac{K_{Fh}}{T_{Eh}T_{Fh}}\Delta V_{Rh} - \frac{K_{Fh}(K_{Eh} + S_{Eh})}{T_{Fh}T_{Eh}}\Delta e_{fdh} - \frac{1}{T_{Fh}}\Delta V_{Fh} \quad (16.25)
 \end{aligned}$$

Network Parameters

The network topology parameters are given in Table 16.14. The base values are $S_b = 10$ MVA and $V_b = 15$ kV. The loads are represented as constant impedance loads.

Table 16.14 Three bus system parameters

t. line.	From hydro to diesel	From diesel to wind
R (pu)	0.04	0.3071
L (pu)	0.04	0.1695
C_{ch} (pu)	0.0080	0.00446
Load	Bus diesel	Bus wind
R (pu)	7.8749	12.4954
L (pu)	2.3049	3.6506

Dynamic Parameters of Generators

The generator data is given in Table 16.15 with respect to base power $S_b = 10 \text{ MVA}$ and base voltage $V_b = 0.4 \text{ kV}$.

Type 1 IEEE Exciter

The parameters of all the excitors are the same and are given in Table 16.16. The block diagram of the exciter is shown in Fig. 16.7.

Table 16.15 Generator data

Generator	Hydro	Diesel	Wind
x_d (pu)	2.399	8.15	28.161
x_q (pu)	1.4375	8.15	28.161
x'_d (pu)	0.3609	0.5917	3.052
x'_q (pu)	0.1875	0.5917	3.052
T_{q0}' (s)	3.5	2.35	0.661
T_{d0}' (s)	3.5	2.35	0.661
H (s)	2.159	1.133	0.233
D (pu)	0.02	0.005	0

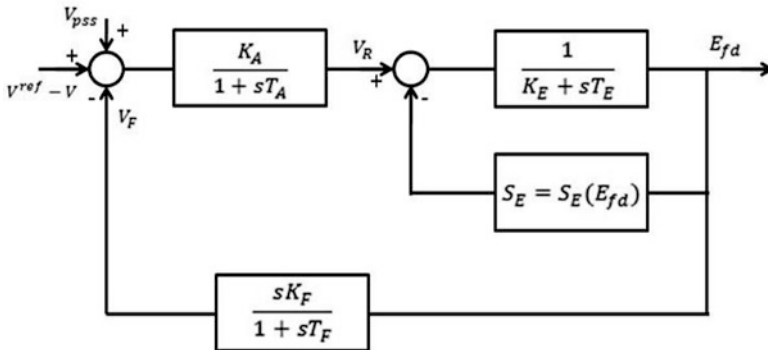
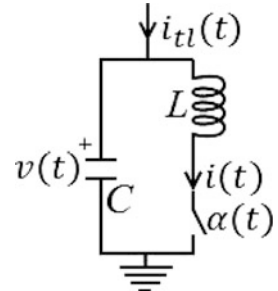


Fig. 16.7 Type 1 IEEE exciter

Table 16.16 Parameters of excitors

Parameter	Value
K_A (pu)	400
T_A (s)	0.02
K_E (pu)	1.3
T_E (s)	1
S_E (pu)	0.1667
K_F (pu)	0.03
T_F (s)	1

Fig. 16.8 Static VAR compensator (SVC)



Controller Design

The controllers used in Sect. 16.5 are the following. The excitation controller is a standard IEEE type 1 exciter [9] whose parameters are given in Table 16.16. The parameters of excitation control are the same in all the simulations in this chapter. T hydro and diesel generators are equipped with this kind of exciter, but the wind generator does not have an excitation voltage controller.

The excitation system is upgraded with a proportional gain power system stabilizer in Sect. 16.4.2. The equation of the stabilizer is

$$\Delta v_{\text{pss}}^i = -K_{\text{pss}}^i (\omega^i - \omega^{\text{ref}}) \quad (16.26)$$

where the gain of the hydro and diesel stabilizers are $K_{\text{pss}}^h = 150$ and $K_{\text{pss}}^d = 10$, respectively. Superscript i can be either h , which stands for hydro, or d , which stands for diesel. The reference frequency is the desired electrical frequency of the network.

The controllers used in Sect. 16.6 are the following. The same excitors are kept as in the previous section (without power system stabilizers) and on the same generators: hydro and diesel.

In Sect. 16.4.1, SVC, Fig. 16.8, and DFIG, Fig. 16.9, are used to control the disturbances in two independent simulations. The SVC controller is a linear PI controller which reacts to the deviation in the wind generator bus voltage V_W . Therefore, the firing angle of SVC is

$$\Delta\alpha = K_{P_{\text{svc}}} (V_W - V_W^{\text{ref}}) + K_{I_{\text{svc}}} \int (V_W - V_W^{\text{ref}}) dt \quad (16.27)$$

where the gains of the controller are $K_{P_{\text{svc}}} = 1$ and $K_{I_{\text{svc}}} = 1$.

DFIG control is designed in a similar fashion. A linear PI controller that reacts to the deviation in wind bus voltage magnitude is implemented. Excitation voltage $e_{f_q}^W$ changes according to a PI control law, while $e_{f_d}^W$ stays constant.

$$\Delta e_{f_q}^W = K_{P_{\text{dfig}}} (V_W - V_W^{\text{ref}}) + K_{I_{\text{dfig}}} \int (V_W - V_W^{\text{ref}}) dt \quad (16.28)$$

where the gains of the controller are $K_{P_{\text{dfig}}} = -10$ and $K_{I_{\text{dfig}}} = -10$.

In Sect. 16.4.2, an excitation control system is added to the synchronous wind generator. The exciter parameters are the same as for the other generators. A power system stabilizer is added on top of the exciter. A power system stabilizer controller

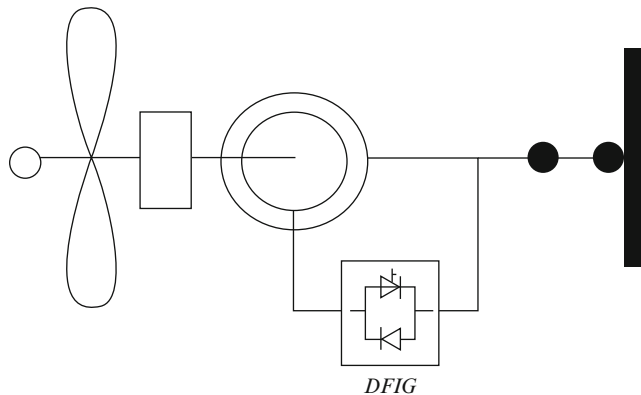


Fig. 16.9 Doubly fed induction generator (DFIG)

is given in Eq. (16.26) where superscript i can take one of the following three values: h hydro, d diesel, or w wind. The parameters of these stabilizers are $K_{\text{pss}}^h = 50$, $K_{\text{pss}}^d = 10$, and $K_{\text{pss}}^w = 50$ (Table 16.17).

Equilibrium of the Flores Power System in Different Simulations

References

1. M. Nazari, Electrical networks of the Azores Archipelago, in Chapter 3 of *Engineering IT-Enabled Sustainable Electricity Services: The Case of Low-Cost-Green Azores Islands* (Springer 2013)
2. M. Nazari, Optimal placement of wind power plants for delivery loss minimization, in Chapter 12 of *Engineering IT-Enabled Sustainable Electricity Services: The Tale of Two Low-Cost Green Azores Islands* (Springer 2013)
3. L. Xie, Y. Gu, M. Ilić, Look-ahead model-predictive generation dispatch methods, in Chapter 12 of *Engineering IT-Enabled Sustainable Electricity Services: The Tale of Two Low-Cost Green Azores Islands* (Springer 2013)
4. M. Nazari, Small signal stability of electric power systems on the Azores Archipelago, in Chapter 17 of *Engineering IT-Enabled Sustainable Electricity Services: The Tale of Two Low-Cost Green Azores Islands* (Springer 2013)
5. M. Cvetković, K. Bachovchin, M. Ilić, Transient stabilization in systems with wind power, in Chapter 19 of *Engineering IT-Enabled Sustainable Electricity Services: The Case of Low-Cost-Green Azores Islands* (2013, to be published in the monograph)
6. IEEE Committee Report, Excitation system models for power system stability studies. IEEE Trans. Power Apparatus Syst. **PAS-100**(2), 494–509 (1981)
7. J.W. Chapman, Power system control for large-disturbance stability: security, robustness and transient energy. Ph.D. Thesis, Massachusetts Institute of Technology, Cambridge, May 1996

Table 16.17 Equilibrium of the Flores power system for the following simulations: (*sim.1*) small electrical distance between diesel and wind with an induction wind generator, (*sim.2*) small electrical distance between diesel and wind with a synchronous wind generator, (*sim.3*) large electrical distance between diesel and wind with an induction wind generator and an SVC attached to the wind generator bus, and (*sim.4*) large electrical distance between diesel and wind with an induction DFIG wind generator

	<i>Sim.1</i>	<i>Sim.2</i>	<i>Sim.3</i>	<i>Sim.4</i>
E'_{Dh} (pu)	0.9955	0.9223	0.964	0.9675
E'_{Dd} (pu)	1.0410	0.9697	0.998	1.004
E'_{Dw} (pu)	0.8506	0.9571	0.8327	1.1
E'_{Qh} (pu)	-0.1413	-0.3577	-0.1931	-0.1783
E'_{Qd} (pu)	-0.1383	-0.3716	-0.1886	-0.177
E'_{Qw} (pu)	0.0601	-0.1965	-0.2582	-0.2992
δ_h (rad)	-0.046849	-0.27836	-0.1029	-0.08772
δ_d (rad)	0.093868	-0.10709	0.2006	0.1718
δ_w (rad)	N/A	0.77415	N/A	-0.56
ω_h (pu)	1	1	1	1
ω_d (pu)	1	1	1	1
ω_w (pu)	1.0083	1	1.0083	1
V_{Rh} (pu)	1.1494	1.1143	1.068	1.072
V_{Rd} (pu)	2.1695	1.9294	1.61	1.642
E_{fdh} (pu)	0.98528	0.95508	0.9148	0.9191
E_{fdd} (pu)	1.8597	1.6538	1.38	1.407
V_{Fh} (pu)	0	0	0	0
V_{Fd} (pu)	0	0	0	0
q_h (pu)	0	0	0	0
v_h (pu)	0	0	0	0
a_h (pu)	0	0	0	0
m_{Rd} (pu)	-0.093493	-0.092378	0.02636	-0.03047
P_{cd} (pu)	0.0023373	0.0023094	-0.0006571	0.0007575

All values are given with respect to base $S_b = 10$ MVA, $\omega_b = 2\pi 50$ rad/s, $V_b = 15$ kV on the network side, and $V_b = 0.4$ kV on the generator side

8. I.J. Perez-Arriaga, G. C. Verghese, F.C. Schweppe, Selective modal analysis with applications to electric power systems, Part I: Heuristic introduction. IEEE Trans. Power Apparatus Syst. **PAS-101**(9), 3117–3125 (1982)
9. L.M. Hajagos, M.J. Basler, Changes to IEEE 421.5 recommended practice for excitation system models for power system stability studies, in *Panel Session Paper for the IEEE/PES 2005 Meeting*, San Francisco, CA

Chapter 17

Small-Signal Stability Analysis of Electric Power Systems on the Azores Archipelago

Masoud Honarvar Nazari

In this chapter, a structure-based coupled real-power voltage dynamic is introduced for assessing small-signal stability when the Azores Archipelago has a high penetration of renewable energy resources. The small-signal stability of the Azores is investigated with and without considering the coupling of real-power and voltage dynamics. The decoupled scenario results illustrate that the system is stable in response to small perturbations. On the other hand, in the coupled scenario, due to strong interactions between the electromagnetic and mechanical parts of the power plants, frequency oscillations, which lead to small-signal instability, are exaggerated. The main conclusion is that tuning the governor control of the plants without considering the coupling of real-power and voltage dynamics can lead to system stability problems.

17.1 Introduction

A system is small-signal stable if it can regain an operating equilibrium after a small perturbation. In electric systems, perturbations occur due to changes in the loads, fluctuations in intermittent resources, or variations in the output power of the conventional power plants. If an electric system cannot maintain its stability, an overall blackout can occur.

Small-signal stability is an essential issue for the robustness and resilience of modern electric energy systems. It is more critical for systems with a high

M. Honarvar Nazari (✉)

Department of Engineering and Public Policy, Carnegie Mellon University,
5000 Forbes Avenue, Pittsburgh, PA 15213, USA

e-mail: mhonarva@andrew.cmu.edu

penetration of renewable energy resources, since the intermittency of these resources can intensify frequency oscillations . The electric energy systems in the Azores Archipelago are real-world examples of modern electric energy systems with a large penetration of renewable energy resources such as wind, hydro, and geothermal. In fact, small-signal stability is a major concern when renewable energy resources provide a large portion of the electricity. There have been several reports of outage in the islands brought on by stability issues [1,2].

In order to ensure the dynamic stability of the islands, it is essential to (a) introduce a sufficiently detailed dynamic model to assess the small-signal stability of the islands with their large penetration of distributed generators (DGs), (b) determine potential instability problems and identify the main causes of the instabilities, and (c) design an automatic control to enable the large penetration of DGs while at the same time ensuring the electrical stability of the islands. This chapter intends to model and analyze the small-signal stability of the two islands of Flores and São Miguel.

In Sect. 17.2, four scenarios concerning the dynamic stability of Flores are studied: (1) assuming the decoupling of real-power and voltage dynamics and treating fluctuations of wind as a bounded real-power disturbance to the system, (2) assuming the decoupling of real-power and voltage dynamics and modeling the dynamics of the wind plant as a synchronous generator, (3) assuming the coupling of real-power and voltage dynamics and treating fluctuations of wind as a bounded real-power disturbance, and; (4) assuming the coupling of real-power and voltage dynamics and including the dynamic model of the wind plant.

The technical findings illustrate that small-signal instability can occur when the governor control (GC) of the DGs is tuned without accounting for interactions between the mechanical and electromagnetic dynamics.

In Sect. 17.3, the small-signal stability of São Miguel is investigated assuming the decoupling of real-power and voltage dynamics. The results illustrate that slow modes of oscillation exist in the system. This is attributed to the weak interconnection between the thermal plants (diesel/geothermal) and hydro plants.

In Sect. 17.4, three main solutions to enhance the stability of the electrical systems in the Azores Archipelago are discussed: (1) implementing high-gain control in the hydro plants, (2) installing power system stabilizers (PSSs) in the controllable plants to stabilize frequency oscillations , and (3) using fast flywheel energy storage to increase damping. In Sect. 17.5, we close the chapter with a brief discussion of the overall findings.

17.2 The Small-Signal Stability of Flores

The main focus of this section is the problem of small-signal stability on Flores on a typical winter day with a sufficient availability of wind and hydro power. As shown in Fig. 17.1, wind and hydro are the two main sources of energy during the winter on Flores, and more than 50 % of the electricity is produced by these resources. Due to

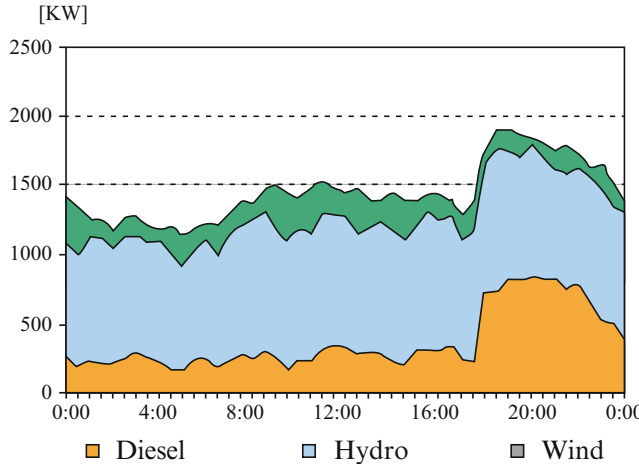


Fig. 17.1 Illustration of the availability of wind and hydro power on a typical winter day [1]

the intermittent nature of these resources, however, the distribution system is more vulnerable to frequency and/or voltage instability.

In order to assess the frequency and voltage dynamics in response to small disturbances, it is essential to model the electric power grid dynamics of the island first. The electric energy system of the island has three distributed generators and many loads which are interconnected by the distribution network.

17.2.1 Generator Models Used

The dynamics of the generators are represented with state-space models. In general, a generator includes a mechanical and an electromagnetic part. For conventional plants such as a diesel generator, the mechanical part consists of a prime mover, rotating mass, and a governor control (GC) system. Equation (17.1) illustrates the state-space model of the mechanical part of a diesel plant:

$$\frac{d}{dt} \begin{bmatrix} \omega_G \\ m_B \\ P_C \end{bmatrix} = \begin{bmatrix} \frac{-D_d}{2H_d} & \frac{C_c}{2H_d} & 0 \\ \frac{-C_d K_d}{T_d R_c} & \frac{-1}{T_d} & \frac{-C_d K_d}{T_d} \\ -K_I & 0 & 0 \end{bmatrix} \begin{bmatrix} \omega_G \\ m_B \\ P_C \end{bmatrix} + \begin{bmatrix} \frac{-1}{2H_d} \\ 0 \\ 0 \end{bmatrix} P_G + \begin{bmatrix} 0 \\ 0 \\ K_I \end{bmatrix} \omega_G^{\text{ref}} \quad (17.1)$$

In this model, ω_G is the frequency, m_B is the fuel rate, and P_C is the governor control. In addition, H_d and D_d are the inertia and damping coefficients, respectively. C_d and K_d are the transfer function coefficients for the fuel system, T_d is the time constant of the fuel system, and K_I is the integral gain of the GC system [3].

The electromagnetic part of the diesel plant is coupled to the mechanical subsystem by the magnetic field of the machine air gap [4,5]. For a diesel generator, the electromagnetic part consists of a synchronous machine and an excitation control. Equation (17.2) represents the state-space model of the electromagnetic subsystem:

$$\frac{d}{dt} \begin{bmatrix} V_R \\ e_{fd} \\ e'_q \\ V_F \end{bmatrix} = \begin{bmatrix} -\frac{1}{T_a} & -\frac{K_a K_f}{T_a T_f} & -\frac{K_a}{T_a} & \frac{K_a}{T_a} \\ \frac{1}{T_e} & -\frac{(K_e + S_e)}{T_e} & 0 & 0 \\ 0 & \frac{1}{T_d} & -\frac{1}{T_d} & 0 \\ 0 & \frac{k_f}{T_f^2} & 0 & -\frac{1}{T_f} \end{bmatrix} \begin{bmatrix} V_R \\ e_{fd} \\ e'_q \\ V_F \end{bmatrix} + \begin{bmatrix} 0 \\ 0 \\ -\frac{(x_d - x'_d)}{T_d} \\ 0 \end{bmatrix} i_d + \begin{bmatrix} \frac{K_a}{T_a} \\ 0 \\ 0 \\ 0 \end{bmatrix} V_G^{\text{ref}} \quad (17.2)$$

In this model, V_R is the regulator voltage, e_{fd} is the field excitation, e'_q is the machine voltage behind the direct transient impedance, and V_F is the feedback voltage (the voltage of the compensator) [6]. In addition, i_d is the reactive current out of the generator, and V_G^{ref} is the reference value for the generator terminal voltage [6,7]. Note that if the effects of damper winding are neglected, then $e'_q = V_G$ since $V_G = \sqrt{e'_q^2 + e_d'^2}$ and $e_d' = 0$ [6].

Likewise, the dynamics of the mechanical parts of a hydro plant are presented in Eq. (17.3). The electromagnetic aspects of the hydro plant have a similar state-space model to those of the diesel generator [Eq. (17.2)]:

$$\frac{d}{dt} \begin{bmatrix} \omega_G \\ q \\ v \\ a \end{bmatrix} = \begin{bmatrix} -\frac{D_h}{2H_h} & \frac{K_q}{2H_h} & 0 & -\frac{K_w}{2H_h} \\ \frac{1}{T_f} & -\frac{1}{T_d} & 0 & \frac{1}{T_w} \\ 0 & 0 & -\frac{1}{T_e} & \frac{r'}{T_e} \\ -\frac{1}{T_s} & 0 & \frac{1}{T_s} & -\frac{(r_h + r')}{T_s} \end{bmatrix} \begin{bmatrix} \omega_G \\ q \\ v \\ a \end{bmatrix} + \begin{bmatrix} \frac{-1}{2H_h} \\ 0 \\ 0 \\ 0 \end{bmatrix} P_G + \begin{bmatrix} 0 \\ 0 \\ 0 \\ \frac{1}{T_s} \end{bmatrix} \omega_G^{\text{ref}} \quad (17.3)$$

Here, q is the penstock flow, v is the governor droop, and a is the gate position. Moreover, T_a , T_f , and T_d are the time constants of the hydro plant. T_s is the time constant of the servomotor, and r_h and r' are the permanent and transient speed droop, respectively [8].

A wind plant is a synchronous machine connected to the grid through a power electronic interface. The mechanical part of the plant consists of a rotating mass and a wind turbine with a pitch control system. Equations (17.4) and (17.5) illustrate the dynamics of the rotating mass and the wind turbine, respectively. As shown in Eq. (17.6) the electromagnetic part includes a synchronous machine without excitation control:

$$\frac{d\omega_G}{dt} = \frac{1}{2H_w} P_m - \frac{D_w}{2H_w} \omega_G - \frac{1}{2H_w} P_G \quad (17.4)$$

where

$$P_m = -K_m \omega_G \quad (17.5)$$

and

$$\frac{de'_q}{dt} = \frac{-1}{T_d} e'_q + \frac{-(x_d - x'_d)}{T_d} i_d \quad (17.6)$$

Here, P_m is the mechanical power, D_W is the damping coefficient, and K_m is the proportional gain of the pitch control system [9]. The data for the state-space models shown in Eqs. (17.1)–(17.6) are available in Appendix B.

Considering Eqs. (17.1)–(17.6), the general state-space model of the mechanical and electromagnetic subsystems of each generator take on the form

$$\frac{dx_{LC}^P}{dt} = A_{LC}^P x_{LC}^P + C^P P_G \quad (17.7)$$

$$\frac{dx_{LC}^Q}{dt} = A_{LC}^Q x_{LC}^Q + C^Q i_d \quad (17.8)$$

Here x_{LC}^P and x_{LC}^Q are the state variables of the mechanical and electromechanical subsystems, respectively.

17.2.2 Network Dynamics

In this chapter, it is assumed that loads are static. Changes in loads are modeled as disturbances to the grid. Furthermore, the distribution system is modeled by a set of power flow equations [8]. Its dynamics are modeled by a Jacobian matrix [5]:

$$\frac{d}{dt} \begin{bmatrix} P_G \\ i_d^G \\ P_L \\ i_d^L \end{bmatrix} = \begin{bmatrix} J_1 & J_2 \\ J_3 & J_4 \end{bmatrix} \begin{bmatrix} \omega_G \\ \frac{dV_G}{dt} \\ \omega_L \\ \frac{dV_L}{dt} \end{bmatrix} \quad (17.9)$$

where

$$J_1 = \begin{bmatrix} \frac{\partial P_G}{\partial \delta_G} \frac{\partial P_G}{\partial V_G} \\ \frac{\partial Q_G}{\partial \delta_G} \frac{\partial Q_G}{\partial V_G} \end{bmatrix} \quad (17.10)$$

$$J_2 = \begin{bmatrix} \frac{\partial P_G}{\partial \delta_L} \frac{\partial P_G}{\partial V_L} \\ \frac{\partial Q_G}{\partial \delta_L} \frac{\partial Q_G}{\partial V_L} \end{bmatrix} \quad (17.11)$$

$$J_3 = \begin{bmatrix} \frac{\partial P_L}{\partial \delta_G} \frac{\partial P_L}{\partial V_G} \\ \frac{\partial Q_L}{\partial \delta_G} \frac{\partial Q_L}{\partial V_G} \end{bmatrix} \quad (17.12)$$

$$J_4 = \begin{bmatrix} \frac{\partial P_L}{\partial \delta_L} \frac{\partial P_L}{\partial V_L} \\ \frac{\partial Q_L}{\partial \delta_L} \frac{\partial Q_L}{\partial V_L} \end{bmatrix} \quad (17.13)$$

17.2.3 Dynamic Model of the Interconnected System

Neglecting the dynamics of the loads, the state-space equation of the coupling variables (P_G and i_d^G) takes on the form

$$\begin{aligned} \frac{dP_G}{dt} &= Kp_{11}S_{\omega_G}x_{LC}^P + Kp_{12}\left(\frac{1}{T_d}S_{e_{fd}} - \frac{1}{T_d}S_{e'_q}\right)x_{LC}^Q \\ &\quad + Kp_{12}\frac{-(x_d - x'_d)}{T_d}i_d + Dp_{11}\frac{dP_L}{dt} + Dp_{12}\frac{di_d^L}{dt} \end{aligned} \quad (17.14)$$

$$\begin{aligned} \frac{di_d^G}{dt} &= Kp_{21}S_{\omega_G}x_{LC}^P + Kp_{22}\left(\frac{1}{T_d}S_{e_{fd}} - \frac{1}{T_d}S_{e'_q}\right)x_{LC}^Q \\ &\quad + Kp_{22}\frac{-(x_d - x'_d)}{T_d}i_d + Dp_{21}\frac{dP_L}{dt} + Dp_{22}\frac{di_d^L}{dt} \end{aligned} \quad (17.15)$$

with S_{ω_G} , $S_{e_{fd}}$, and $S_{e'_q}$ relating $\omega_G = S_{\omega_G}x_{LC}^P$, $e_{fd} = S_{e_{fd}}x_{LC}^Q$, and $e'_q = S_{e'_q}x_{LC}^Q$, respectively

Matrices Kp and Dp are defined as follows:

$$[J_1 - J_2 J_4^{-1} J_3] = \begin{bmatrix} Kp_{11} & Kp_{12} \\ Kp_{21} & Kp_{22} \end{bmatrix} \quad (17.16)$$

$$[J_2 J_4^{-1}] = \begin{bmatrix} Dp_{11} & Dp_{12} \\ Dp_{21} & Dp_{22} \end{bmatrix} \quad (17.17)$$

The desired dynamic model for Flores is obtained by adding Eqs. (17.14) and (17.15) to (17.17) and (17.18) and by ordering the state variables as internal state variables of the DGs and their coupling variables. This model lends itself to an intuitive understanding of the decentralized nature of distribution systems with a high penetration of distributed generators:

$$\frac{d}{dt} \begin{bmatrix} X_1 \\ X_2 \\ X_3 \end{bmatrix} = \begin{bmatrix} A_{11} & A_{12} & A_{13} \\ A_{21} & A_{22} & A_{23} \\ A_{31} & A_{32} & A_{33} \end{bmatrix} \begin{bmatrix} X_1 \\ X_2 \\ X_3 \end{bmatrix} + \begin{bmatrix} \gamma_1 \\ \gamma_2 \\ \gamma_3 \end{bmatrix} \quad (17.18)$$

where X_i , A_{ii} , A_{ij} , and γ_i are defined as

$$X_i = \begin{bmatrix} x_{LC}^{P(i)} \\ x_{LC}^{Q(i)} \\ P_G^{(i)} \\ i_d^{G(i)} \end{bmatrix} \quad (17.19)$$

$$A_{ii} = \begin{bmatrix} A_{LC}^{P(i)} & 0 & C^{P(i)} & 0 \\ 0 & A_{LC}^{Q(i)} & 0 & C^{Q(i)} \\ Kp_{11}^{(ii)} S_{\omega_G} Kp_{12}^{(ii)} \left(\frac{1}{T_d} S_{efd} - \frac{1}{T_d} S_{e'_q} \right) & 0 & Kp_{12}^{(ii)} \frac{-(x_d - x'_d)}{T_d} \\ Kp_{21}^{(ii)} S_{\omega_G} Kp_{22}^{(ii)} \left(\frac{1}{T_d} S_{efd} - \frac{1}{T_d} S_{e'_q} \right) & 0 & Kp_{22}^{(ii)} \frac{-(x_d - x'_d)}{T_d} \end{bmatrix} \quad (17.20)$$

$$A_{ij} = \begin{bmatrix} 0 & 0 & 0 & 0 \\ 0 & 0 & 0 & 0 \\ Kp_{11}^{(ij)} S_{\omega_G} Kp_{12}^{(ij)} \left(\frac{1}{T_d} S_{efd} - \frac{1}{T_d} S_{e'_q} \right) & 0 & Kp_{12}^{(ij)} \frac{-(x_d - x'_d)}{T_d} \\ Kp_{21}^{(ij)} S_{\omega_G} Kp_{22}^{(ij)} \left(\frac{1}{T_d} S_{efd} - \frac{1}{T_d} S_{e'_q} \right) & 0 & Kp_{22}^{(ij)} \frac{-(x_d - x'_d)}{T_d} \end{bmatrix} \quad (17.21)$$

$$\gamma_i = \begin{bmatrix} 0 \\ 0 \\ Dp_{11}^{(i)} \frac{dP_L}{dt} + Dp_{12}^{(i)} \frac{di_d^L}{dt} \\ Dp_{21}^{(i)} \frac{dP_L}{dt} + Dp_{22}^{(i)} \frac{di_d^L}{dt} \end{bmatrix} \quad (17.22)$$

Neglecting load dynamics leads to a new topology for the island. The equivalenced power system is obtained by adding a switch with a reactance and resistance of 0.04 pu between the diesel and hydro plants and calculating the equivalenced admittance between the plants or between a plant and ground. Note that the equivalenced admittance is obtained by the coupling matrix ($Y_{eqij} = Kp_{ij}$). Figure 17.2 illustrates the one-line diagram of the equivalenced power system for Flores. In the next sections, the system stability of Flores is explored in four main scenarios.

17.2.4 Decoupled Real-Power Voltage Dynamic Model: Treating Wind as a Disturbance

Considering a decoupling of real-power and voltage dynamics and neglecting the dynamics of the wind plant, result in a simpler dynamic model for the island, shown in Eq. (17.19):

$$\frac{d}{dt} \begin{bmatrix} X'_1 \\ X'_2 \end{bmatrix} = \begin{bmatrix} A'_{11} & A'_{12} \\ A'_{21} & A'_{22} \end{bmatrix} \begin{bmatrix} X'_1 \\ X'_2 \end{bmatrix} + \begin{bmatrix} \gamma'_1 \\ \gamma'_2 \end{bmatrix} \quad (17.23)$$

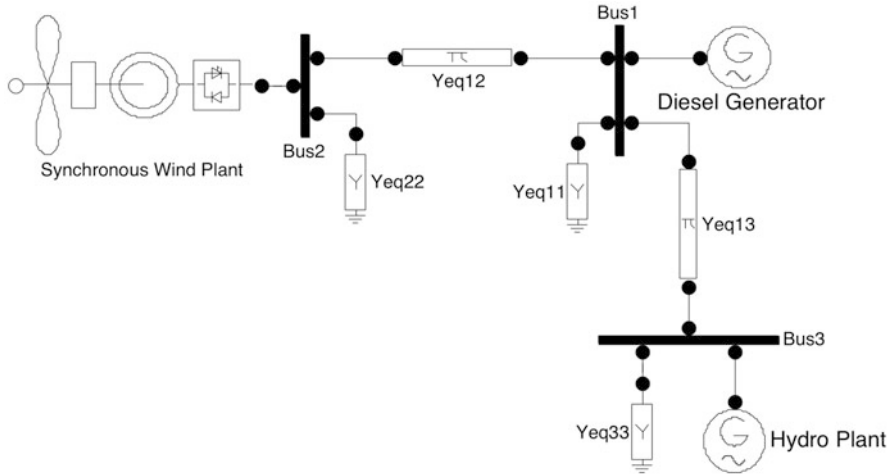


Fig. 17.2 One-line diagram of the equivalenced power system for Flores

where X'_i , A'_{ii} , A'_{ij} , and γ'_i are defined as

$$X'_i = \begin{bmatrix} x_{LC}^{P(i)} \\ P_G^{(i)} \end{bmatrix} \quad (17.24)$$

$$A'_{ii} = \begin{bmatrix} A_{LC}^{P(i)} & C^{P(i)} \\ Kp_G^{(ii)} S_{\omega_G} & 0 \end{bmatrix} \quad (17.25)$$

$$A'_{ij} = \begin{bmatrix} 0 & 0 \\ Kp_G^{(ij)} S_{\omega_G} & 0 \end{bmatrix} \quad (17.26)$$

$$\gamma'_i = \begin{bmatrix} 0 \\ Dp_L^{(i)} \frac{dP_L}{dt} \end{bmatrix} \quad (17.27)$$

Matrices Kp_G and Dp_L are described as [6]

$$Kp_G = J_{GG} - J_{GL} J_{LL}^{-1} J_{LG} \quad (17.28)$$

$$Dp_L = -J_{GL} J_{LL}^{-1} \quad (17.29)$$

where

$$J_{GG} = \frac{\partial P_G}{\partial \delta_G} \quad J_{GL} = \frac{\partial P_G}{\partial \delta_L} \quad J_{LG} = \frac{\partial P_L}{\partial \delta_G} \quad J_{LL} = \frac{\partial P_L}{\partial \delta_L}$$

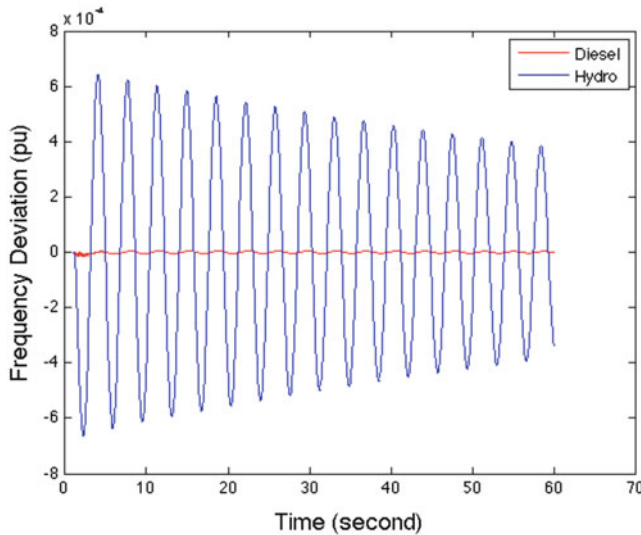


Fig. 17.3 Frequency deviation in the diesel and hydro plants after a small perturbation (0.01 pu)

The numerical data of the dynamic models are available in Appendix B. Note that the governor control of each plant is designed so that the system matrix of the stand-alone plant (A_{ii}^*) is stable in response to small perturbations.

An eigenvalue analysis of the system in this scenario shows that all the eigenvalues lie in the left-hand side of the complex plane. Figure 17.3 illustrates the oscillations in frequency of the diesel and hydro plants after a small disturbance on the island. The disturbance is a 0.01 pu decrease in wind power.

As shown in Fig. 17.3, the frequency of the hydro generator oscillates around its operating point, but it settles gradually. The oscillations result in smaller fluctuations in the frequency of the diesel plant. After the disturbance, the diesel generator increases its output power to balance the real-power mismatch. On the other hand, the hydro plant cannot ramp up rapidly, but it oscillates around the equilibrium point due to its non-minimal phase margin property. Figure 17.4 illustrates the deviations in the output power of the plants. The results illustrate that the system is oscillatory stable.

In order to measure the strength of the electrical interaction between the plants, the coupling matrix (K_p) is calculated. Figure 17.5 demonstrates the 3-D plot of the coupling matrix. The depth and horizontal axes of the figure represent the x - and y -axis of the coupling matrix, respectively. The z axis illustrates the strength of the coupling (K_{pij}). As shown in Fig. 17.5, the diesel and hydro plants are strongly coupled. This explains why oscillations in the hydro plant make the diesel generator oscillatory as well [10, 11].

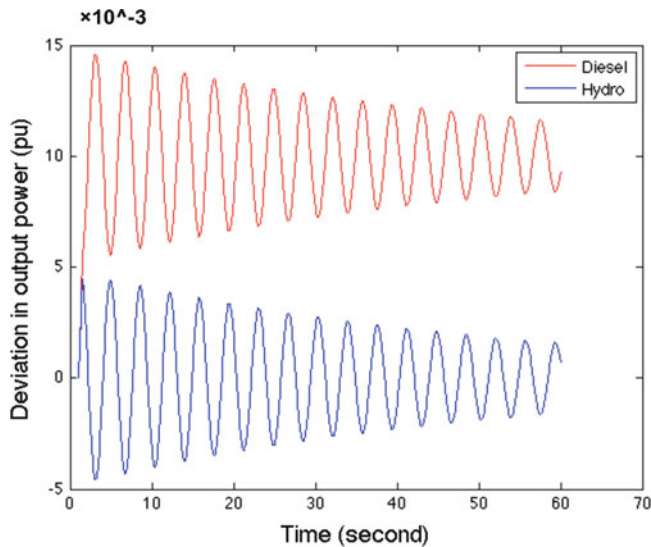


Fig. 17.4 Deviations in the output power of the power plants after the perturbation

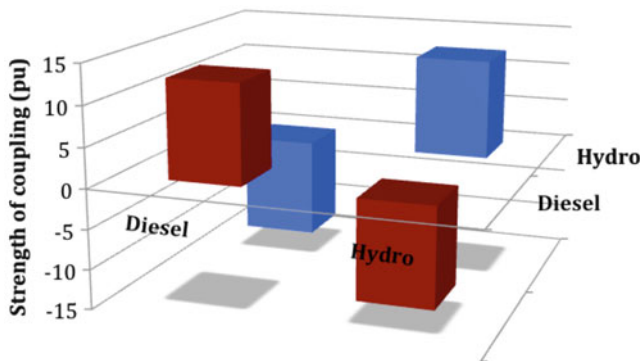


Fig. 17.5 3-D plot of the coupling matrix for the decoupled real-power voltage dynamic model

17.2.5 The Decoupled Real-Power Frequency Model

In this subsection, the small-signal stability of the island is studied by modeling the dynamics of the synchronous wind plant shown in Eqs. (17.4) and (17.5). The results illustrate that when the wind plant is poorly tuned or has no pitch control system, the overall fluctuations of frequency are exaggerated (shown in Fig. 17.6). In general, implementing a pitch control system increases the damping of the wind plant and

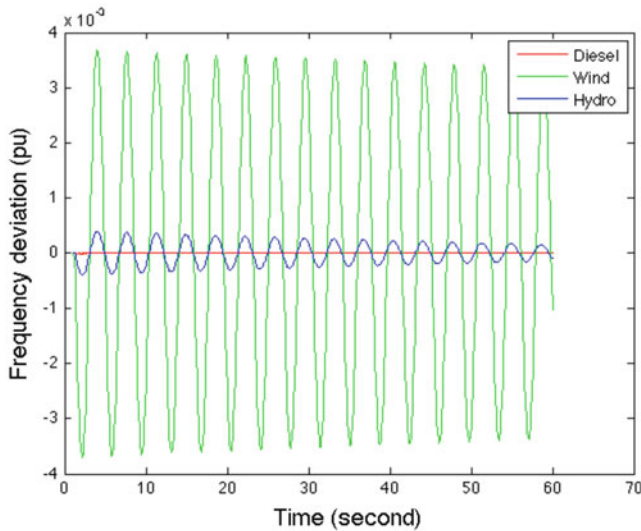


Fig. 17.6 Frequency deviation of the generators when the wind plant has no pitch control system

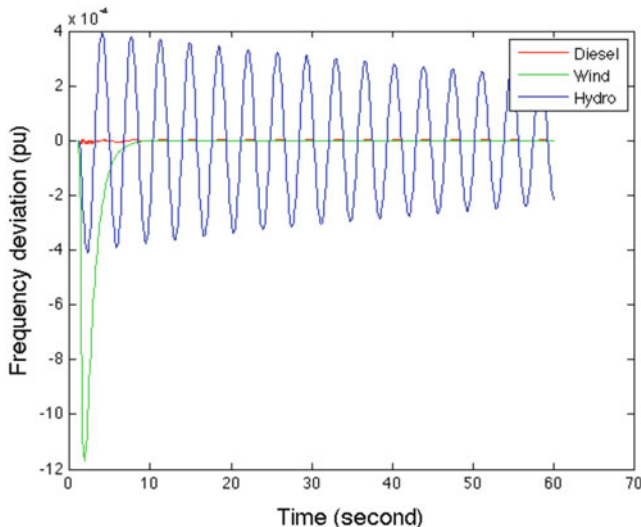


Fig. 17.7 Frequency deviation of the generators when the wind plant is equipped with a proportional pitch control system

lessens frequency oscillations. Figures 17.7 and 17.8 demonstrate the deviations of output power and the frequency of the power plants when the wind plant has a proportional pitch control system (gain = 2 pu). The results illustrate that the system has stable oscillatory response.

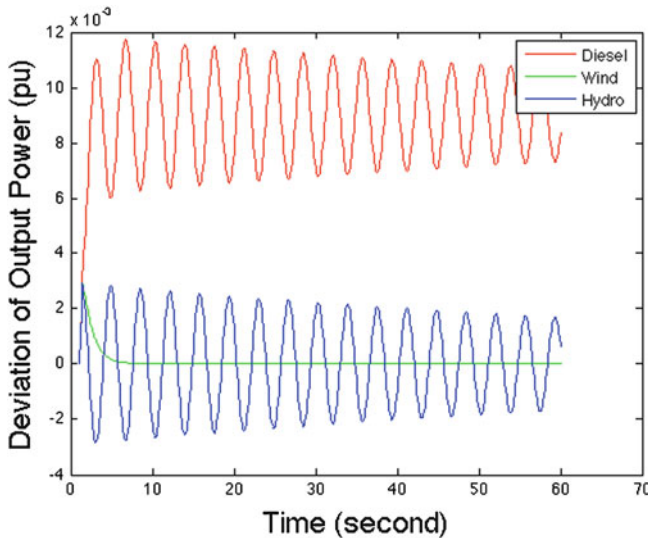


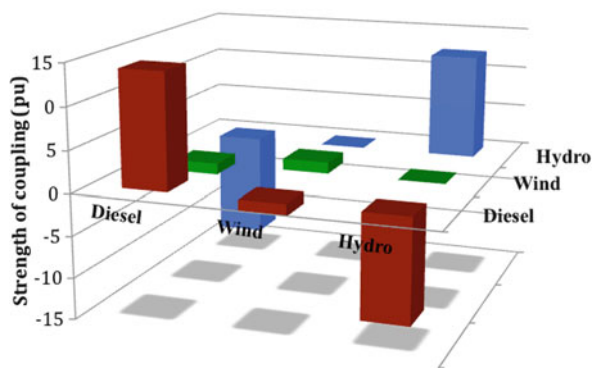
Fig. 17.8 Deviations in the output power of the generators when the wind plant is equipped with a proportional pitch control system

As shown in Fig. 17.7, after a small disturbance (a 0.01 pu increase in load), the frequency of the wind plant deviates, but it returns to the equilibrium point gradually. The hydro plant shows a different dynamic behavior. Due to its non-minimal phase margin characteristics, it has fast oscillations around the equilibrium point, and damps very sluggishly. On the other hand, the diesel plant has robust dynamic behavior because of its fast integral control system. The diesel plant is compensating real-time oscillations in real power.

In general, using the diesel generator for frequency regulation and to compensate for fast fluctuations of real power can cause wear and tear in the governor control of the plant. It can also increase the operating and maintenance costs of the plant and increase emissions. In [12] it is shown that if gas turbines are operated to compensate for fast fluctuations of intermittent energy resources such as wind, their CO₂ emissions may increase up to 20 % and their NO_x pollutions rise by 50–70 % compared to full power steady-state operation levels. Similarly, it is expected that in a fast ramping of the diesel plant, its CO₂ and NO_x emissions increase significantly.

In order to investigate the effect of the electrical interaction between the plants on system stability, the coupling matrix is calculated. The numerical results are available in Table 17.3. Figure 17.9 illustrates the 3-D plot of the coupling matrix and shows that the electrical interaction between the wind and diesel plants is weak but that the diesel and hydro plants are strongly coupled.

Fig. 17.9 3-D plot of the coupling matrix for the decoupled real-power voltage dynamic model



17.2.6 The Coupled Real-Power Voltage Dynamic Model: Treating Wind as a Disturbance

Neglecting the coupling between real-power and voltage dynamics may lead to an optimistic assessment of system stability. This section examines the small-signal stability of Flores considering a coupling of real-power and voltage dynamics. The wind plant is treated as a negative load, and its dynamics are neglected. Note that governors of the plants are designed based on the decoupled model.

The result of stability analysis demonstrates that with a small disturbance (a 0.01 pu increase in load), the frequency of the hydro plant deviates from the nominal point (50 Hz). These oscillations are exacerbated due to the strong interaction between the mechanical and electromagnetic parts of the plant. This leads to a frequency instability of the hydro plant. As shown in Figs. 17.10 and 17.11, the instabilities of the hydro plant make the diesel generator unstable. Therefore, the full system is unstable in response to small perturbations.

In order to determine the main cause of instabilities, a participation factor-based analysis, fully elaborated in [13], is carried out. The results show that the coupling variables (P_G and i_d^G) play the main role in instabilities. Comparing the coupling matrix with that of the decoupled scenario illustrates that the coupling between the plants is stronger in the coupled case.

17.2.7 The Coupled Real-Power Voltage Dynamic Model with Wind Power Dynamics Included

In this sub-section, the coupled real-power voltage dynamic model on Flores containing the dynamics of all the power plants is explored. Here, the wind plant is modeled as a synchronous generator with a proportional pitch control system. Governors of the diesel and hydro power plants are designed based on the decoupled model. The state-space model of the entire system is presented in Eq. (17.18).

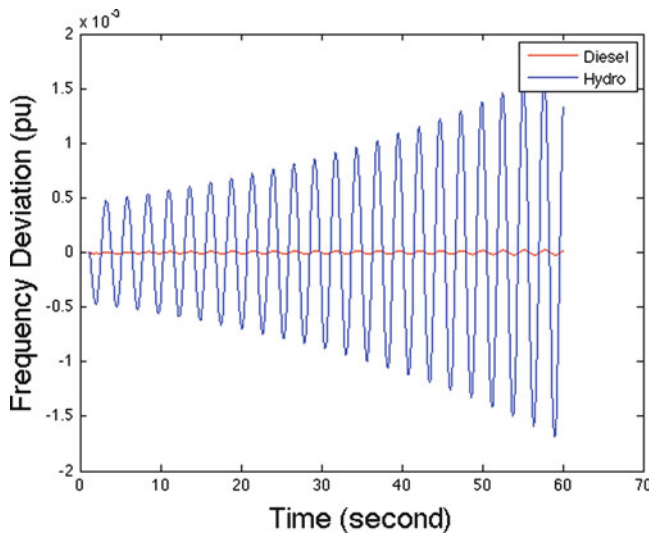


Fig. 17.10 Frequency deviation of the power plants after a small disturbance in the system

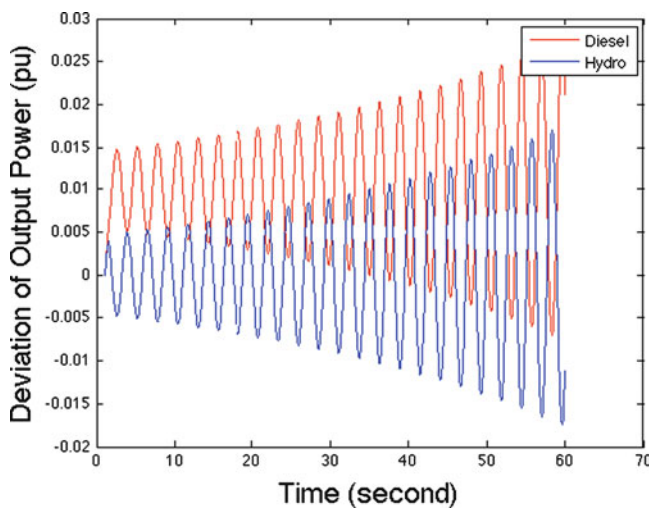


Fig. 17.11 Deviations in the output power of the power plants after the disturbance

The result of eigenvalue analysis illustrates that the stand-alone hydro plant has two eigenvalues in the right-hand side of the complex plane. These eigenvalues appear in the eigenvalues of the full system and lead to unstable response for the entire island. Table 17.2 shows the eigenvalues of the full system and the subsystems. Note that due to modeling the reference generator, a zero eigenvalue exists in the full system.

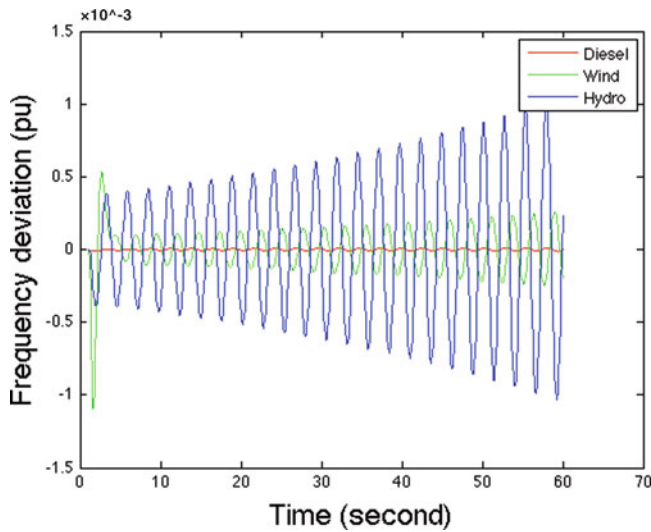


Fig. 17.12 Dynamic response of the diesel, hydro, and wind generators after the disturbance

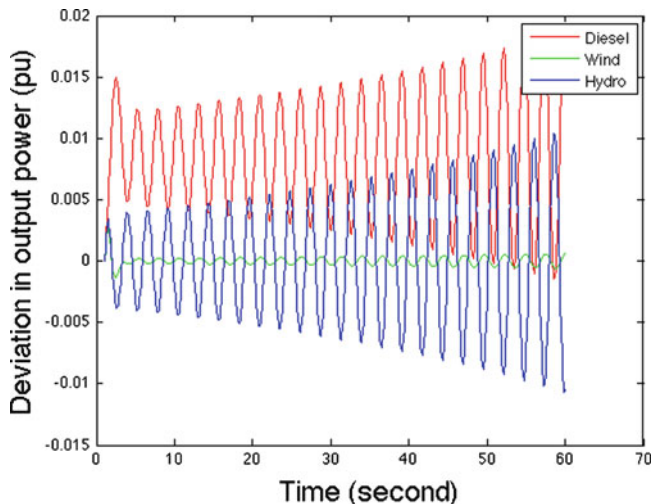


Fig. 17.13 Deviations in the output power of the generators after the disturbance

The interaction between the electromagnetic and mechanical parts of the hydro plant exaggerates the oscillations and makes the plant unstable. This instability penetrates across the island and leads to system-wide instability. Figures 17.12 and 17.13 demonstrate variations in the frequency and output power of the power plants after a disturbance. Similar dynamic behavior is reported in [2]. The instabilities found in these scenarios can be avoided by carefully designing the

governor control and excitation control of the plants based on the coupled real-power voltage dynamic model.

Comparing the coupling matrix of the full system with those of the previous scenarios illustrates that the coupling between the power plants (Kp_{ij}) and the self-coupling Kp_{ii} are larger if the interaction between real-power and voltage dynamics is considered. The numerical values of the coupling matrix are available in Table 17.4. In summary, our findings demonstrate that if the governor control and excitation control of the power plants are designed without considering the coupling between real-power and voltage dynamics, small-signal instability may occur in the system.

17.3 Small-Signal Stability on São Miguel

São Miguel is the largest island in the Azores Archipelago with an average demand of around 65 MW. Three large diesel generators, two medium-size geothermal plants, and ten small hydro plants supply the demand. The hydro plants are run-of-river hydroelectric generators and provide electricity based on the availability of the stream. These plants do not have advanced governor control and cannot participate in frequency regulation. The geothermal plants produce electricity based on the availability of steam. Both the hydro and geothermal plants supply base-load power. Figure 17.14 illustrates the role of each technology in providing the daily electricity of the island during the spring. As shown in Fig. 17.14, around 40 % of the electricity is provided by renewable sources of energy, and the rest is provided by conventional power plants (the diesel generators).

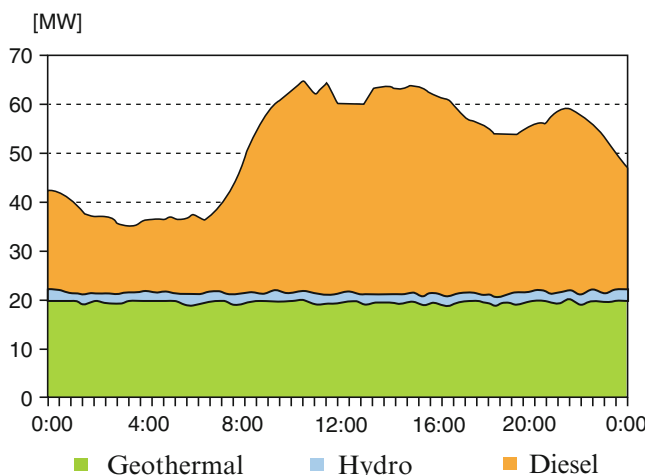


Fig. 17.14 Illustration of the availability of geothermal and hydro power on a typical spring day [1]

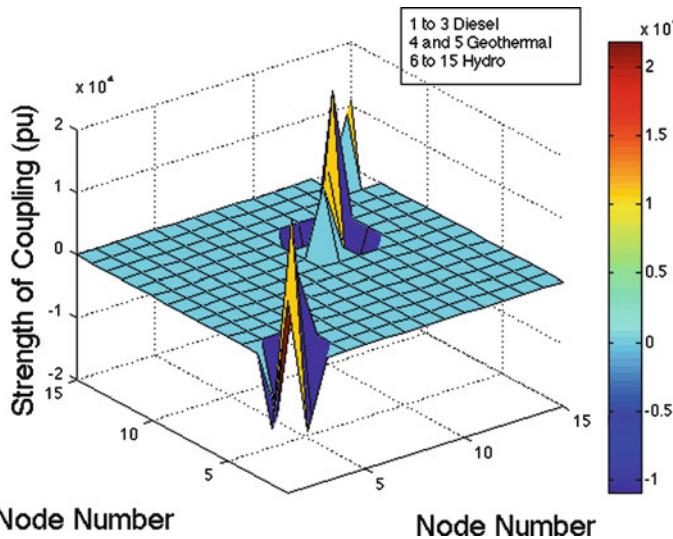


Fig. 17.15 3-D plot of the coupling matrix of São Miguel for the decoupled real-power voltage dynamic model

The diesel plants are the only fully controllable generators on the island. They balance the supply and demand and regulate frequency. In order to model the dynamics of the island, it is essential to pose the dynamics of each power plant first by modeling its prime mover, governor control, excitation control, and synchronous machine. The diesel plants have similar state-space models to the ones shown in Eqs. (17.1) and (17.2). On the other hand, the geothermal and hydro plants have no governor control and excitation control systems. Therefore, their mechanical part contains of a rotating mass, and their electromagnetic subsystem includes a synchronous machine. Equations (17.30) and (17.31) represent the general structure of the state-space model of these plants:

$$\frac{d\omega_G}{dt} = \frac{1}{M} P_m - \frac{D}{M} \omega_G - \frac{1}{M} P_G \quad (17.30)$$

$$\frac{de'_q}{dt} = \frac{-1}{T_d} e'_q + \frac{-(x_d - x'_d)}{T_d} i_d \quad (17.31)$$

On São Miguel, loads are modeled as noncontrollable elements, and their dynamics are modeled as a disturbance to the system. The dynamics of the generators are coupled via the distribution network. The strength of the coupling between generators is calculated by the sensitivity of active and reactive power with respect to rotor angle and voltage. This is similar to calculating, as shown in the previous section, the Jacobian matrix of the island. Since the dynamics of loads are neglected, a reduced Jacobian matrix needs to be calculated in order to obtain the coupling between generators. Figure 17.15 illustrates the 3-D plot of the reduced coupling matrix. The numerical values of the reduced coupling matrix are presented in Table 17.6.

As shown in Fig. 17.15, there is strong coupling between the diesel generators and the geothermal plants. However, the hydro plants have very weak coupling to either of these plants. Some hydro plants are strongly coupled to each other, but some are weakly connected to the rest of the system. In general, the coupling between generators is identified by the location of the generators and the electrical distance between the plants. Those plants electrically close to each other are strongly coupled, and those electrically far from each other are weakly coupled.

Figure 17.16 illustrates the schematic of the one-line diagram of São Miguel. This model presents the reduced dynamic model of the island. The equivalent admittance between the plants is equal to the coupling between them ($Y_{eqij} = K_{p_{ij}}$). In Fig. 17.16, the equivalent admittance is colored in red for strong coupling ($K_{p_{ij}} > 100$), green for moderate coupling ($7 < K_{p_{ij}} < 100$), and white for weak coupling ($K_{p_{ij}} < 7$). In addition, the equivalent admittance is neglected for very weak coupling ($K_{p_{ij}} < 0.05$).

Simulating the small-signal stability of the island demonstrates that due to weak coupling between the hydro plants and the thermal plants (diesel/geothermal), a slow mode of oscillation exists between the two clusters. Figures 17.17 and 17.18 demonstrate the variations in frequency and output power of the plants after a small perturbation on the island.

17.4 Possible Solutions to Enhance the Stability of Electrical Energy Systems in the Azores Archipelago

There are at least three major approaches to enhancing small-signal stability in the Azores Archipelago. The first method implements high-gain control for the hydro plant. Using high-gain control makes the plant faster and enables it to cancel out the effects of strong coupling. This solution is only applicable to Flores since the hydro plant on Flores is controllable. The main drawback of high-gain control is fast valving, which results in wear-and-tear problems as well as higher operating and maintenance costs for the plant [12].

Another approach to improving stability in the Azores Archipelago is to install a power system stabilizer (PSS) on the controllable plants. A PSS applies enhanced damping to the system by incorporating itself with the excitation system of the plant. A PSS can cancel out the oscillations between the mechanical and electromagnetic parts of the plant. In general, using a PSS to stabilize frequency oscillations can eliminate the wear-and-tear problem and reduce the overall pollution caused by the fast ramping of the diesel plants.

The third possible way to increase robustness is to implement fast flywheel storage next to critical plants such as the hydro and wind plants. A flywheel increases the damping of the plant and minimizes the effects of disturbances. In [2] it is shown how installing a 350 kW/5 kWh flywheel can improve the dynamic stability on Flores. As mentioned earlier, the oscillations between the mechanical

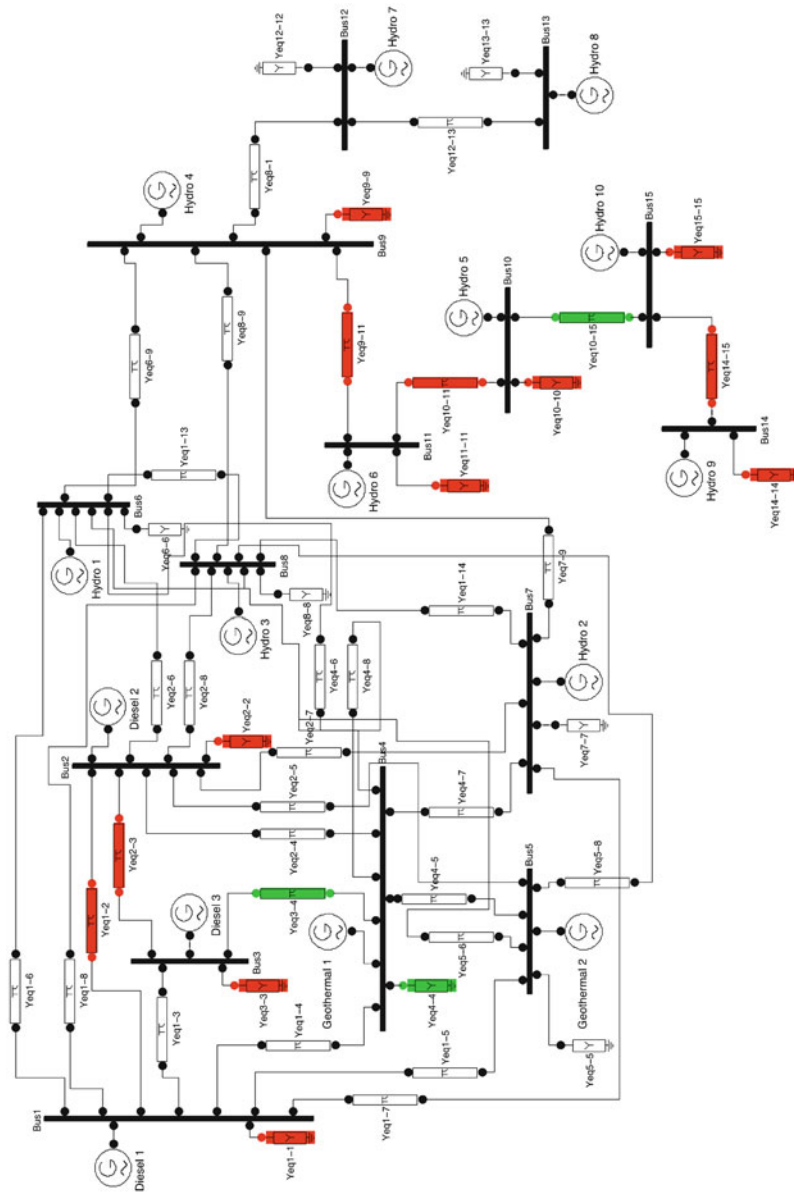


Fig. 17.16 One-line diagram of São Miguel

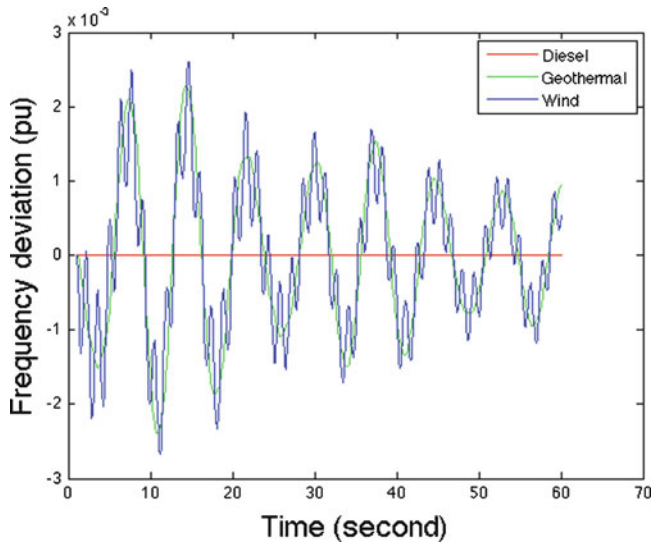


Fig. 17.17 Deviations in the output power of the generators after the disturbance

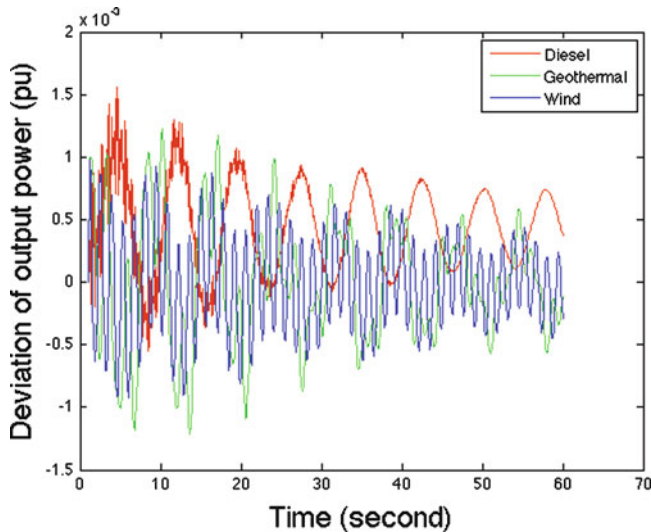


Fig. 17.18 Deviations in the output power of the generators

and electromagnetic parts of the plants exaggerate frequency oscillations. Therefore, the optimal control strategy for the control system of the flywheel is to compensate for disturbances in both active and reactive power. Specific control designs are introduced in Chaps. 15 and 16.

17.5 Conclusions and Future Outlook

This chapter shows that the large penetration of renewable energy resources in the Azores Archipelago may increase frequency oscillations and lead to small-signal instability unless advanced control strategies such as high-gain control or PSS are implemented. In addition, the findings illustrate that neglecting the strong interactions between the electromagnetic and mechanical parts of the plants can lead to an overly optimistic assessment of system stability. These interactions exaggerate overall frequency oscillations. Therefore, if the governor control of the plants is designed based on the decoupled model, the system may become very sensitive to even small perturbations.

Our findings, furthermore, demonstrate that the result of small-signal stability analysis is sensitive to the parameters of the system such as the inertia and the damping of the plants. Thus, for accurate stability analysis it is essential to precisely estimate the parameters of the system.

In general, it is not appropriate to use diesel generators to compensate for fast frequency oscillations because this can increase CO₂ and NO_x emissions, wear and tear on the governor control system, and operating and maintenance costs.

In order to ensure small-signal stability in the Azores Archipelago, three main solutions are suggested for consideration. The first approach is based on designing high-gain control for the hydro plants. The second approach implements a PSS on controllable plants in order to increase the overall damping of the system. The last solution is to install fast flywheel storage next to intermittent resources such as wind plants to enhance the damping of the plants.

Acknowledgments The author greatly acknowledges Professor Jeffrey Lang and Professor Marija Ilić for helping to prepare the input data of São Miguel Island in PTI 23 format. The author also appreciates the help of the EDA in providing technical data for the Azores Islands. Financial support for this work was provided by the Portugal-Carnegie Mellon joint program under Grant 18396.6.5004458.

17.6 Appendix A

Appendix A presents equilibrium point, coupling matrix (K_p), and eigenvalues of Flores Island. In addition, the coupling matrix of São Miguel Island is presented in Table 17.9.

Table 17.1 Eigenvalues of the decoupled real-power voltage dynamic model

The whole system	Diesel generator	Wind plant	Hydro generator
1.0e+02×	$-0.6845 + 31.3998i$	-3.4586	1.0e+02×
(-1.1772	$-0.6845 - 31.3998i$	-0.8353	(-1.1772
-0.0068 + 0.3140 <i>i</i>	-0.3086		-0.0002 + 0.0174 <i>i</i>
-0.0068 - 0.3140 <i>i</i>	-0.0000		-0.0002 - 0.0174 <i>i</i>
-0.0346			-0.0133
-0.0002 + 0.0173 <i>i</i>			-0.0050)
-0.0002 - 0.0173 <i>i</i>			
-0.0133			
-0.0084			
-0.0030			
-0.0050			
0.0000)			

Table 17.2 Eigenvalues of the coupled real-power voltage dynamic model

The whole system	Diesel generator	Wind plant	Hydro generator
1.0e+02×	-45.0995	-55.1861	1.0e+02×
(-0.1100 + 0.9898 <i>i</i>	$-0.6271 + 31.4737i$	$-1.4642 + 2.5122i$	(-1.1772
-0.1100 - 0.9898 <i>i</i>	$-0.6271 - 31.4737i$	$-1.4642 - 2.5122i$	-0.1100 + 0.9898 <i>i</i>
-1.1772	$-4.0688 + 17.2365i$	-1.1878	-0.1100 - 0.9898 <i>i</i>
-0.6805	$-4.0688 - 17.2365i$		-0.0809
-0.0063 + 0.3149 <i>i</i>	-0.3187		0.0014 + 0.0235 <i>i</i>
-0.0063 - 0.3149 <i>i</i>	-0.0499		0.0014 - 0.0235 <i>i</i>
-0.3955	0.0000		-0.0136
-0.0406 + 0.1722 <i>i</i>			-0.0050
-0.0406 - 0.1722 <i>i</i>			-0.0002
-0.0148 + 0.0251 <i>i</i>			
-0.0148 - 0.0251 <i>i</i>			
0.0002 + 0.0241 <i>i</i>			
0.0002 - 0.0241 <i>i</i>			
-0.0135			
-0.0118			
-0.0029 + 0.0047 <i>i</i>			
-0.0029 - 0.0047 <i>i</i>			
-0.0030			
-0.0050			
-0.0004			
-0.0000			

Table 17.3 Coupling matrix of Flores Island in the decoupled scenario

	Bus 1	Bus 2	Bus 3
Bus 1	13.9058	-1.4076	-12.4982
Bus 2	-1.3464	1.3464	0
Bus 3	-12.5017	0	12.5017

Table 17.4 J_1 matrix of Flores Island in the coupled scenario

	$J_1^{\text{Bus}1}$	$J_1^{\text{Bus}2}$	$J_1^{\text{Bus}3}$
$J_1^{\text{Bus}1}$	13.9058	-1.4076	-12.4982
$J_1^{\text{Bus}2}$	-1.3464	1.3464	0
$J_1^{\text{Bus}3}$	-12.5017	0	12.5017

Table 17.5 J_2 matrix of Flores Island in the coupled scenario

	$J_2^{\text{Bus}1}$	$J_2^{\text{Bus}2}$	$J_2^{\text{Bus}3}$
$J_2^{\text{Bus}1}$	15.0207	-2.4883	-12.5017
$J_2^{\text{Bus}2}$	-2.5220	2.4887	0
$J_2^{\text{Bus}3}$	-12.4982	0	12.5018

Table 17.6 J_3 matrix of Flores Island in the coupled scenario

	$J_3^{\text{Bus}1}$	$J_3^{\text{Bus}2}$	$J_3^{\text{Bus}3}$
$J_3^{\text{Bus}1}$	-14.9806	2.4788	12.5017
$J_3^{\text{Bus}2}$	2.5126	-2.5126	0
$J_3^{\text{Bus}3}$	12.4982	0	-12.4982

Table 17.7 J_4 matrix of Flores Island in the coupled scenario

	$J_4^{\text{Bus}1}$	$J_4^{\text{Bus}2}$	$J_4^{\text{Bus}3}$
$J_4^{\text{Bus}1}$	13.9056	-1.4073	-12.4982
$J_4^{\text{Bus}2}$	-1.3461	1.3461	0
$J_4^{\text{Bus}3}$	-12.5017	0	12.5017

Table 17.8 Power flow solution (equilibrium point) of Flores Island

Bus number in the original system	Bus number in the equivalent system	Names	V [pu]	phase [rad]	P gen [pu]	Q gen [pu]
Bus 1	Bus 1	Diesel	1	0	0.06739	0.0747
Bus 19	Bus 2	Wind	1	-0.01225	0.06	0.05391
Bus 46	Bus 3	Hydro	1	0.00014	0.07	-0.06999

17.7 Appendix B

Electromechanical and electromagnetic parameters of the power plants in Flores are presented in Tables 17.10–17.16. These parameters are estimated based on the data-set provided by Professor Pecas Lopes from INESC Porto [14, 15] and based on the models used in [16]. The bases are $S_{\text{base}} = 10 \text{ MVA}$, $V_{\text{base}} = 0.4 \text{ kV}$, and $f_{\text{base}} = 50 \text{ Hz}$.

Table 17.9 Coupling matrix of São Miguel Island

	Bus 1	Bus 2	Bus 3	Bus 4	Bus 5	Bus 6	Bus 7	Bus 8	Bus 9	Bus 10	Bus 11	Bus 12	Bus 13	Bus 14	Bus 15
Bus 1	10.935	-10.932	-0.61	-1.60	-0.22	-0.16	-0.08	-0.03	-0.00	-0.00	-0.00	-0.00	-0.00	-0.00	-0.00
Bus 2	-10.932	21.867	-10.930	-4.15	-0.10	-0.07	-0.12	-0.04	-0.00	-0.00	-0.00	-0.00	-0.00	-0.00	-0.00
Bus 3	-0.66	-10.930	10.938	-7.75	-0.02	-0.01	-0.00	-0.00	-0.00	-0.00	-0.00	-0.00	-0.00	-0.00	-0.00
Bus 4	-1.60	-4.16	-7.75	16.15	-1.38	-0.98	-0.10	-0.10	-0.04	-0.00	-0.00	-0.00	-0.00	-0.00	-0.00
Bus 5	-0.22	-0.10	-0.02	-1.38	4.03	-2.16	-0.04	-0.04	-0.04	-0.00	-0.00	-0.00	-0.00	-0.00	-0.00
Bus 6	-0.16	-0.07	-0.01	-0.97	-2.16	3.58	-0.05	-0.05	-0.06	-0.00	-0.00	-0.00	-0.00	-0.00	-0.00
Bus 7	-0.08	-0.12	-0.00	-0.10	-0.04	-0.05	2.38	-1.41	-0.52	-0.00	-0.00	-0.01	-0.00	-0.00	-0.00
Bus 8	-0.08	-0.12	-0.00	-0.10	-0.04	-0.05	-1.41	2.37	-0.51	-0.00	-0.00	-0.01	-0.00	-0.00	-0.00
Bus 9	-0.03	-0.04	-0.00	-0.04	-0.04	-0.06	-0.52	-0.51	10.791	-0.00	-10.789	-0.08	-0.03	-0.00	-0.00
Bus 10	-0.00	-0.00	-0.00	-0.00	-0.00	-0.00	-0.00	-0.00	-0.00	10.797	-10.789	-0.00	-0.00	-0.00	-7.70
Bus 11	-0.00	-0.00	-0.00	-0.00	-0.00	-0.00	-0.00	-0.00	-10.789	-10.789	-21.579	-0.00	-0.00	-0.00	-0.00
Bus 12	-0.00	-0.00	-0.00	-0.00	-0.00	-0.00	-0.01	-0.01	-0.08	-0.00	-0.00	0.40	-0.27	-0.00	-0.00
Bus 13	-0.00	-0.00	-0.00	-0.00	-0.00	-0.00	-0.00	-0.00	-0.03	-0.00	-0.00	-0.27	0.33	-0.00	-0.00
Bus 14	-0.00	-0.00	-0.00	-0.00	-0.00	-0.00	-0.00	-0.00	-0.00	-0.00	-0.00	-0.00	-0.00	-0.00	10.789
Bus 15	-0.00	-0.00	-0.00	-0.00	-0.00	-0.00	-0.00	-0.00	-0.00	-0.00	-7.70	-0.00	-0.00	-0.00	-10.789

Table 17.10 Electromechanical parameters of the diesel plant

M_d (MJ/Hz)	D_d (MW/Hz)	T_2 (s)	K_2 (pu)	R_d (pu)	C_d (pu)
0.216	0.005	0.6	40	0.03	1
KI (pu)	Cc (pu)				
10	1				

Table 17.11

Electromechanical
parameters of the wind plant

M_w (MJ/Hz)	D_w (MW/Hz)	Kp_w (pu)
0.089	0.002	2

Table 17.12 Electromechanical parameters of the hydro plant

M_h (MJ/Hz)	D_h (MW/Hz)	K_q (pu)	K_w (pu)	T_f (s)	r_h (pu)
0.2749	0.02	2.78	1.52	-3.6	7
T_q (s)	T_w (s)	T_e (s)	T_s (s)	r_p (pu)	
0.72	4	2	0.06	0.06	

Table 17.13 Electromagnetic parameters of the diesel plant

Ta_d (s)	Tfd (s)	Tdd (s)	Kad (pu)	Xdd (pu)	$X'dd$ (pu)
0.2	0.65	2.35	25	8.1479	0.5917
R_d (pu)	Te_d (s)	Ke_d (pu)	Se_d (pu)		
0.001	0.6544	1	0.105		

Table 17.14

Electromagnetic parameters
of the wind plant

Tdw (s)	Xdw (pu)	$X'dw$ (pu)	Rw (pu)
0.661	28.161	3.052	0.002

Table 17.15 Electromagnetic parameters of the hydro plant

Tah (s)	Tfh (s)	Tdh (s)	Kah (pu)	Xdh (pu)	$X'dh$ (pu)
0.05	0.9	3.5	400	2.399	0.3609
R_h (pu)	Te_h (s)	Ke_h (pu)	Se_h (pu)		
0.001	0.9	1	0.035		

Table 17.16 Characteristics of the plants in Flores Island

Node number in the 46-node system	Node number in the reduced system	Capacity (MW)	Type of plant
1	1	2.5	Diesel
19	2	0.6	Wind
46	3	1.5	Hydro

17.8 Appendix C

Electromechanical parameters of the power plants in São Miguel are presented in Appendix C (Tables 17.17–17.31). These parameters are estimated based on the dataset provided by Professor Pedro Carvalho from IST Lisbon and based on the models used in [14]. The bases are $S_{base} = 100$ MVA and $f_{base} = 50$ Hz.

Table 17.17 Electromechanical parameters of the first diesel plant

M_{d1} (MJ/Hz)	D_{d1} (MW/Hz)	T_{d1} (s)	K_{d1} (pu)	R_{d1} (pu)	C_{d1} (pu)
5.853	0.704	1.07	40	0.03	1
KI_1 (pu)	Cc_1 (pu)				
10	1				

Table 17.18 Electromechanical parameters of the second and third diesel plants

M_{d2} (MJ/Hz)	D_{d2} (MW/Hz)	T_{d2} (s)	K_{d2} (pu)	R_{d2} (pu)	C_{d2} (pu)
6.473	0.352	1.25	40	0.03	1
KI_2 (pu)	Cc_2 (pu)				
10	1				

Table 17.19 Electromechanical parameters of the first geothermal plant

M_{geo1} (MJ/Hz)	D_{geo1} (MW/Hz)
2.653	0.298

Table 17.20 Electromechanical parameters of the second geothermal plant

M_{geo2} (MJ/Hz)	D_{geo2} (MW/Hz)
2.331	0.262

Table 17.21
Electromechanical
parameters of Hydro 1

M_{h1} (MJ/Hz)	D_{h1} (MW/Hz)
0.2038	0.0036

Table 17.22
Electromechanical
parameters of Hydro 2

M_{h2} (MJ/Hz)	D_{h2} (MW/Hz)
0.162	0.0122

Table 17.23
Electromechanical
parameters of Hydro 3

M_{h3} (MJ/Hz)	D_{h3} (MW/Hz)
0.1849	0.0033

Table 17.24
Electromechanical
parameters of Hydro 4

M_{h4} (MJ/Hz)	D_{h4} (MW/Hz)
0.1424	0.0106

Table 17.25
Electromechanical
parameters of Hydro 5

M_{h5} (MJ/Hz)	D_{h5} (MW/Hz)
0.1424	0.0106

Table 17.26

Electromechanical parameters of Hydro 6

M_{h6} (MJ/Hz)	D_{h6} (MW/Hz)
0.1424	0.0106

Table 17.27

Electromechanical parameters of Hydro 7

M_{h7} (MJ/Hz)	D_{h7} (MW/Hz)
0.0285	0.00051

Table 17.28

Electromechanical parameters of Hydro 8

M_{h8} (MJ/Hz)	D_{h8} (MW/Hz)
0.1216	0.0022

Table 17.29

Electromechanical parameters of Hydro 9

M_{h9} (MJ/Hz)	D_{h9} (MW/Hz)
0.1217	0.0022

Table 17.30

Electromechanical parameters of Hydro 10

M_{h10} (MJ/Hz)	D_{h10} (MW/Hz)
0.1217	0.0022

Table 17.31 Characteristics of the plants in the electric power system of São Miguel

Node number in the original system	Node number in the reduced system	Capacity (MW)	Type of plant
932	1	32.688	Diesel 1 (slack)
933	2	32.688	Diesel 2
934	3	32.688	Diesel 3
963	4	14.8	Geothermal 1
1049	5	13	Geothermal 2
1666	6	0.67	Hydro 1
1669	7	0.8	Hydro 2
1672	8	0.608	Hydro 3
1675	9	0.553	Hydro 4
1676	10	0.553	Hydro 5
1677	11	0.553	Hydro 6
1680	12	0.094	Hydro 7
1683	13	0.4	Hydro 8
1686	14	0.4	Hydro 9
1687	15	0.4	Hydro 10

References

1. EDA Report, Characterization of transmission and distribution network of Azores Islands, March 2009. Available on website: http://www.google.com/url?sa=t&rct=j&q=&esrc=s&source=web&cd=3&cad=rja&ved=0CEAQFjAC&url=http%3A%2F%2Fpaginas.fe.up.pt%2F~ee02072%2Fdocs%2Fcare_eda_2009_2010_03_31.pdf&ei=cEAmUdCbKIHs8wTDpoHoDw&usg=AFQjCNFLQgM_37AokB5t9oo3VGPiXeeSw&sig2=r-6tom2CXHRd07B2Dvn88Q&bvm=bv.42661473,d.eWU

2. N. Hamsic et al., Increasing renewable energy penetration in isolated grids using a flywheel energy storage system, in *POWERENG 2007*, Setubal, 2007
3. H. Sharma, S. Islam, T. Pryor, Dynamic modeling and simulation of a hybrid wind diesel remote area power system. *Int. J. Renew. Energy Eng.* **2**(1), 123–128 (2000)
4. M. Ilić, J. Zaborszky, *Dynamics and Control of Large Electric Power Systems* (Wiley, New York, 2000)
5. M. Ilić et al., Preventing future blackouts by means of enhanced electric power systems control: from complexity to order. *Proc. IEEE* **93**(11), 1920–1941 (2005)
6. X. Liu, M. Ilić, *Structural Modeling and Hierarchical Control of Large-Scale Electric Power Systems*. Doctor of Philosophy, Massachusetts Institute of Technology, April 1994
7. M.A. Pai, D.P.S. Gupta, K.R. Padhy, *Small-signal Analysis of Power Systems* (Alpha Science International, Harrow, 2004)
8. J. Cardell, M. Ilić, Maintaining stability with distributed generation in the restructured electric power industry, in *Proceedings of the IEEE PES GM*, Boulder, June 2004
9. J. Pierik, J. Morren, E.J. Wiggelinkhuizen, S.W.H. de Haan, T.G. van Engelen, J. Bozelie, *Electrical and Control Aspects of Offshore Wind Farms II (Erao II)*, vol. 2: *Offshore Wind Farm Case Studies*. Technical report of ECN&TUD, ECN_C_04_051, Netherlands, 2004
10. M. Honarvar Nazari, M. Ilić, P. Lopes, Dynamic stability and control design of future electric energy systems with large penetration of distributed generators, in *IREP Symposium*, Rio de Janeiro, August 2010
11. M. Honarvar Nazari, M. Ilić, J. Peças Lopes, Small-signal stability and decentralized control design for electric energy systems with large penetration of distributed generators, *Control Eng. Pract.*, **20**(9), 823–831 (2012)
12. W. Katzenstein, J. Apt, Incorporating wind into a natural-gas turbine baseload power system increases NO_x and CO₂ emissions from the gas turbines, in *Future Energy Systems Conference*, Carnegie Mellon University, March 2008
13. D.L. Hau Aik, G. Andersson, Use of participation factors in model voltage stability analysis of multi-infeed HVDC systems. *IEEE Trans. Power Deliv.* **13**(1), 203–211 (1998)
14. A.M. Oliveira Mendonça et al., *Robust Stabilization of Power System Networks with Large integration of Wind* (Department of Electrical Engineering, University of Porto, 2008)
15. J.A. Peças Lopes et al., A Monte Carlo method to evaluate electric vehicles impacts in distribution networks, in *IEEE Conference on Innovative Technologies for an Efficient and Reliable Electricity Supply*, 2010
16. J. Cardell, M. Ilić, R.D. Tabors, *Integrating Small Scale Distributed Generation into a Deregulated Market: Control Strategies and Price Feedback* (Laboratory for Electromagnetic and Electronic Systems, Massachusetts Institute of Technology, 1998)

Part VI

**Corrective Adjustments and Transient
Stabilization for Ensuring Reliable
Operations During Large Wind
Disturbances and Equipment Outages**

Chapter 18

Toward Reconfigurable Smart Distribution Systems for Differentiated Reliability of Service

Siripha Junlakarn and Marija Ilić

18.1 Introduction

Distribution systems are usually designed to be radial. In other words, a substation usually has only one path by which it can deliver power to end users. Thus, when a fault occurs around an upstream feeder, downstream end users behind the fault location are left unsupplied. Reconfiguration of the system is one possible method that could create a new route to supply power to the downstream customers. However, a distribution system may need to be upgraded by adding more Normally-Closed Switches (NCSs) and Normally-Open Switches (NOs) to reconfigure the system and to deliver power to the right users during faults. When NCSs and NOs are installed in the distribution system, they can improve system reliability by supplying customers selectively from the Distributed Generations (DGs) located closer to the end users. The process of reconfiguring the distribution system to connect DGs to the selected customers is often referred to as islanding. While promising, islanding operation has not been deployed widely since there are still many operational issues which must be solved to ensure safety while performing system maintenance and/or restoration in systems with DG. In [1], the authors suggest that the utility must redesign its protection system, control of DGs, and post-islanding reconnection schemes before implementing any islanding. Moreover, coordination of switching in islanded mode requires suitable communication systems since state detection, including both islanding and grid reconnection detections, requires transferring information based on state of the distribution system. Many techniques of islanding detection have been developed, and they are reviewed in [2]. Notably, protection systems in distribution systems should change to adaptive protection and become

S. Junlakarn (✉) • M. Ilić

Department of Engineering and Public Policy, Carnegie Mellon University, 5000 Forbes Ave, Pittsburgh, PA 15213, USA

e-mail: sjunlaka@andrew.cmu.edu; milic@ece.cmu.edu

capable of responding to a change in system conditions or requirement in real time [3]. In this chapter we consider the decision tools for enhancing today's distribution systems with new NOSs and NCSs to enable implementation of differentiated reliability of service. As an illustration, we show the results of simulating this method using the distribution system on the island of Flores.

18.2 Illustration of the Need for Reconfiguration in the Island of Flores

The distribution system on the island of Flores is connected to diesel, hydro, and wind power plants. The capacities of the diesel, hydro, and wind power plants are 2.5 MW, 1.5 MW, and 0.6 MW, respectively. The generation costs of diesel, hydro, and wind are 180 \$/MWh, 88 \$/MWh, and 87 \$/MWh, respectively. Here, we consider the diesel and hydro power plants as central generation and the wind power plant as DG.

The system loads are classified into two types: public and private. We assume that public loads do not have critical reliability requirements and that they can be interruptible. On the other hand, private loads are defined as priority loads since they need high reliability and are willing to pay for it. These private loads may have an agreement with the utility to be served when the faults occur in the system; if the utility cannot live up to the agreement, it has to pay compensation. This compensation is defined as an interruption cost. For illustration purposes, the interruption cost for public and private loads is assumed to be \$0 and \$2,100 per kWh, respectively. The maximum system load is taken to be 1,978 kW, and the minimum system load is 701 kW.

In the Flores distribution system, two NOSs already exist in the system. One is located between buses 6 and 16 and the other between buses 25 and 40. We assume that circuit breakers are already installed in the system as shown in Fig. 18.1. When considering the topology of the system, we find that the critical fault area is the feeder between the diesel power plant and bus 18. This feeder is the main path that delivers power to most of the customers in the system.

When a fault occurs in this critical area, circuit breakers no. 4, 5, 7 and 8 will open to isolate the area, and DG will supply customers in the area as shown in Fig. 18.2. However, wind energy (DG) is unreliable, and its capacity is probably not enough to supply all the loads in the entire feeder. To utilize wind energy, the system needs to install NCSs to disconnect some of the loads and provide power to only some selected customers, not all customers. This is done to keep generation and load balanced in the feeder. Thus, installing more NCSs and NOSs would become a means to make the reconfiguration effective and improve the reliability of the system. In the next section, we show a possible method for selecting the optimal locations of new NCS and NOS.

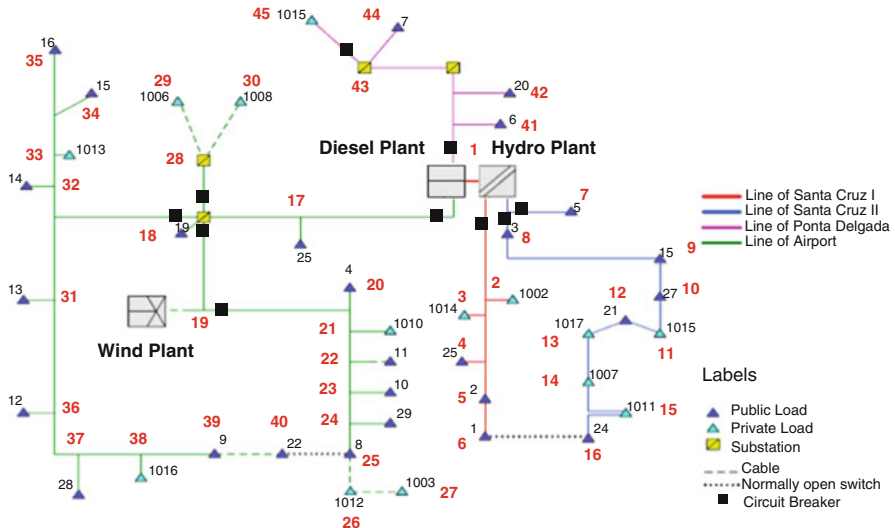


Fig. 18.1 The distribution system on the island of Flores

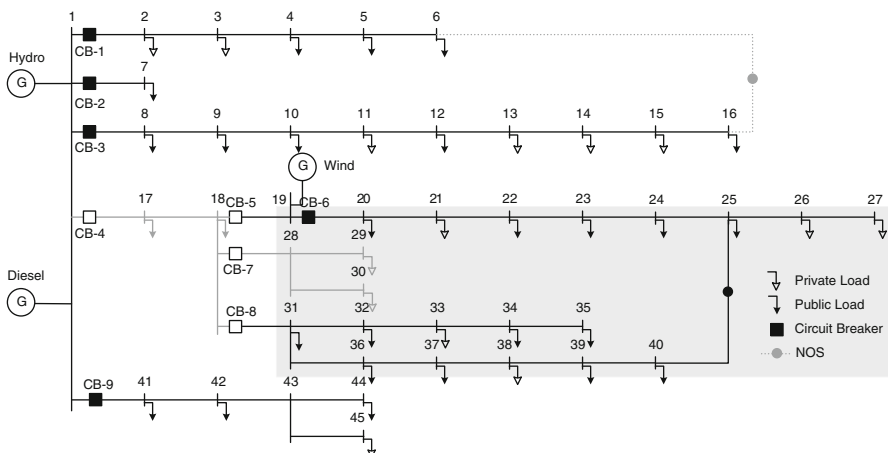


Fig. 18.2 The configuration of the Flores distribution system when a fault occurs in a critical fault area

18.3 A Possible Method for Selecting Best Locations of NCSs and NOSs to Minimize the Interruption Cost to Customers

In a distribution system, installing NOSs and NCSs can reduce the duration of outages and the number of unsupplied loads during power outages. This can be done by opening NCSs to isolate the fault area and by closing NOSs to create other

routes that supply the healthy part of the system. In addition, if there is DG in the distribution system, the islanding operation scheme can form when an outage occurs at the main substations. Given the DG limited capacity, the distribution utility can use these switches to reconfigure the system to supply priority customers. In other words, these switches can be used to implement the differentiated reliability service to different customers. These switches can be opened and closed to reconfigure the system in order to supply customers who need critical service or who are willing to pay more for high reliability during power outages. Thus, the optimal switch placement can improve and differentiate the reliability services of a distribution system.

The optimal switch placement is a nonlinear and discrete combinatorial problem. Heuristic algorithms and deterministic methods such as mixed-integer linear programming can be used to solve this problem. Algorithms may consider both technical and economic factors by minimizing the cost of investment and the cost of customer service outages. Most of the proposed algorithms are currently designed to improve the reliability of the system.

For example, C.H. Lin et al. propose the immune algorithm to find the optimal locations of line switches that can provide cost-effectiveness to a distribution automation system [4]. The algorithm attempts to minimize the total cost of customer service outages and investments. The customer interruption cost is estimated by statistically analyzing service outages, comprising the number of customers unsupplied and the outage duration time for each fault contingency. Moreover, the interruption costs are differentiated among the different types of customers.

A. Esteban and A. Alberto use fuzzy dynamic programming to solve a multicriteria optimization. The formulation takes technical, regulatory, and economic aspects into account to determine the optimal number and placement of sectionalizing switches [5]. The algorithm tries to minimize the total cost of investment, maintenance, and power interruption by including the requirement of reliability indexes as constraints. The power interruption costs are classified by the different types of customers.

A. Abiri-Jahromi et al. apply mixed-integer linear programming to determine the location of sectionalizing by minimizing the costs of investment, installation, annual operation and maintenance, and customer outage [6]. The cost of customer outage is calculated from the system expected outage cost to customers (ECOST), which is the reliability index typically used by distribution utilities. This index considers all possible contingencies, the different customer types, and also their damage functions.

Here, we propose an algorithm to find the optimal location to install NCSs and NOSs. The algorithm attempts to minimize the investment cost of the switches and the annual interruption cost when a power outage occurs. A greater number of NCSs and NOSs installed in the system will increase the number of new configurations for supplying power to customers. However, this also increases the infrastructure investment cost. Thus, the decision is based on a trade-off between the cost of investment and the number of new configurations for supplying power. In the proposed method, we differentiate between the reliability choices to different

customers. Private loads are customers who are willing to pay for being supplied during power outages. If the utility cannot supply power to these customers, the utility has to pay them compensation. This compensation is defined as the interruption cost. The proposed algorithm is to minimize the infrastructure and interruption cost as shown in (18.1). In other words, the algorithm finds the switch locations that increase the number of alternative routes that can supply private loads in order to decrease interruption cost.

$$\begin{aligned}
 & \text{minimize} \quad (\text{No. of Switch} \times C_{\text{Switch}}) + (\text{yr} \times \sum_{i=2}^{\text{No.ofLoadPoint}} P_{\text{unsupplied},i} \times IC_i) \\
 & \text{subject to} \quad \sum_{i=2}^{\text{No.ofLoadPoint}} P_{\text{supplied},i} \leq P_{\text{DG}} \\
 & \quad \sum_{i=2}^{\text{No.ofLoadPoint}} (P_{\text{supplied},i} + P_{\text{unsupplied},i}) \leq \text{TL}.
 \end{aligned} \tag{18.1}$$

where C_{Switch} is cost of switch, yr is the number of years for the investment plan, $P_{\text{unsupplied},i}$ is the unsupplied load (MW) at bus i , IC_i is the interruption cost of load at bus i , $P_{\text{supplied},i}$ is the supplied load at bus i , P_{DG} is the capacity of a DG connected to the network, and TL is the total load in the system. In addition, the location of switch must ensure to provide routes that can supply power to loads.

To estimate the annual interruption cost, we assume that a fault can occur with equal probability at 44 buses in one year. The algorithm finds the locations of switches such that when a fault occurs at any bus in the system, these switches can enable a configuration that preferentially distributes power to private loads. However, after supplying the private loads, if the remaining power is enough to supply other loads, those switches enable a configuration that also supplies other loads. Thus, the annual interruption cost will be the sum of the interruption costs due to possible single faults at any of the 44 buses. The interruption cost of private and public loads is assumed to be \$2,100 and \$0 per kWh, respectively. The investment plan for this analysis spans 10 years, and each NCS or NOS costs \$5,000. We use a genetic algorithm to search for the optimal switch placement.

To supply power to priority customers, the Flores distribution company should install more NCSs and NOSs. The possible locations for installing NCSs and NOSs in the system are shown in Fig. 18.3.

The resulting optimal number of switches to install in the system is 20, and their optimal locations are shown in Fig. 18.4. For the original system, the annual interruption cost is \$67,709. However, if we install those 20 switches, the interruption cost will significantly decrease to \$16,585 per year, as shown in Table 18.1. Even though the total cost of the original and modified system seems not considerably different in the 10 years of investment plan, in a long run, the interruption cost of modified system is lower than that of original system.

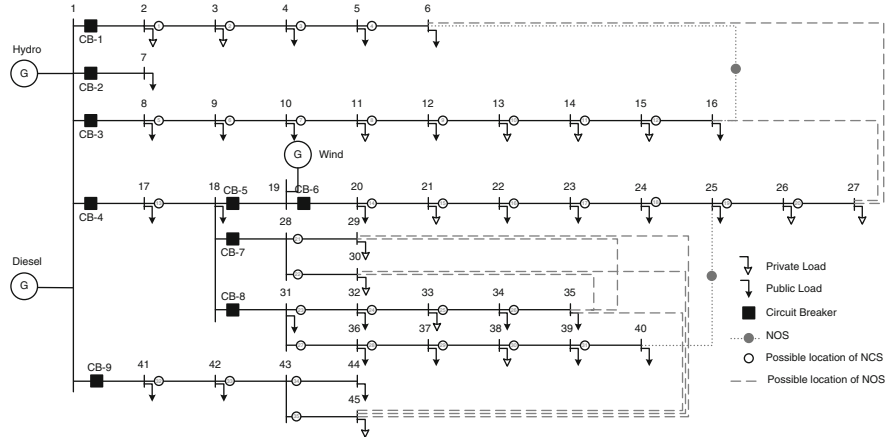


Fig. 18.3 A single line diagram of the distribution on the island of Flores with the locations of switches

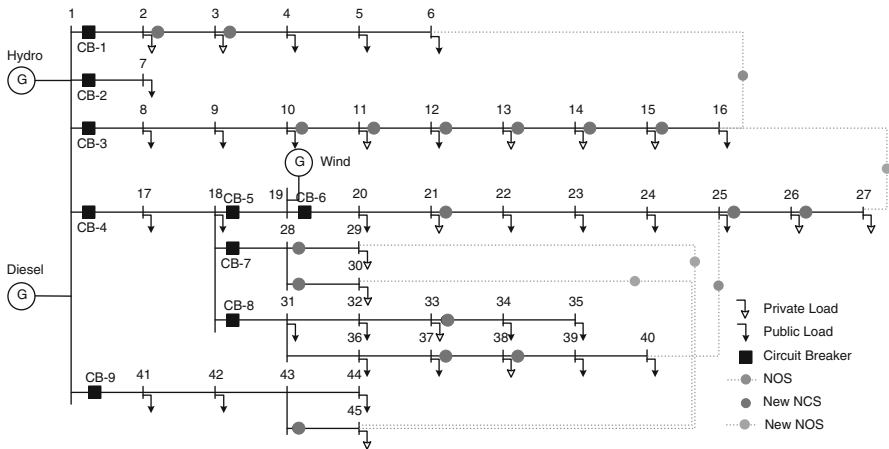


Fig. 18.4 The locations to install NCSs and NOSSs

Table 18.1 Comparison of total costs between the original and modified system

	Original system	Modified system
No. of installed switches	0	20
Switch cost	0	$20 \times \$5,000 = \$100,000$
Total interruption cost	$\$67,709/\text{year} \times 10 \text{ year} = \$677,090$	$\$16,585/\text{year} \times 10 \text{ year} = \$165,850$
Total cost	$\$677,090$	$\$265,850$

After installing NCSs and NOSSs at the optimal locations, the system operator can operate the NCSs and NOSSs to change the configuration of the system, if a fault occurs in a critical fault area, so that power can be provided to priority customers.

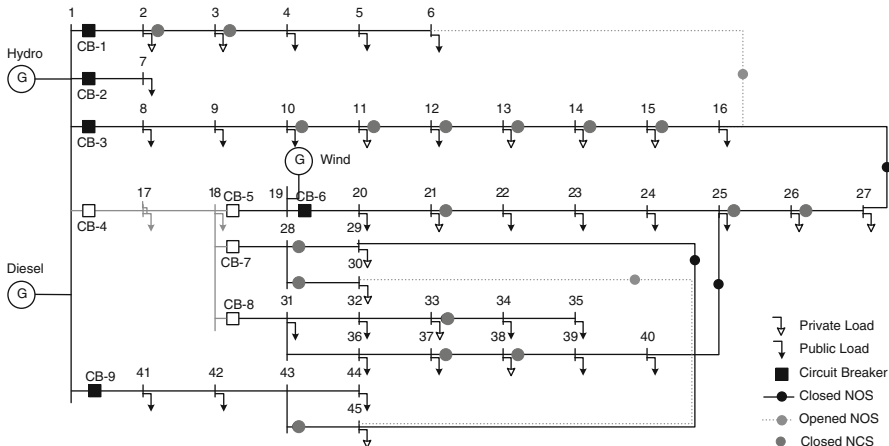


Fig. 18.5 The configuration of the Flores distribution system when the system has installed NCSs and NOSSs at optimal locations and a fault occurs in a critical area

As shown in Fig. 18.5, the system can close the NOSSs connecting between buses 16 and 27, buses 25 and 40, and buses 29 and 45. This configuration can provide power to most customers, except for the loads at buses 17 and 18, which are in the fault area [7].

18.4 Reserve Requirement for Differentiated Reliability of Service

In this section, we consider a possible method to reduce the reserve margin of central generation. The reserve margin of generation is the additional capacity that generation can provide when customers use more energy than the system normally supplies. Also, a high reserve margin is required for the high reliability of service. However, a high reserve margin of generation means that a utility needs to invest more money to expand the generation capacity. One means to decrease the reserve margin of central generation and improve the reliability of a system is to connect DG to the system. Moreover, DGs cooperating with demand response (DR) and reconfiguration can possibly improve the operation of the system.

To illustrate these new possibilities, we will show numerical examples of four possible solutions:

- I. Service provided by central generation
- II. Service provided by central generation with DR
- III. Service provided by central generation including DG
- IV. Service provided by central generation including DG with DR

In the Flores distribution system, the hydro and diesel power plants represent central generation, and the wind power plant represents DG. Economic dispatch is taken into account in this analyzes. For DR, we assume that public loads would agree to reduce their normal power usage by up to 80 % of their peak usage when a fault occurs and private loads would reduce their normal power usage by up to 20 %. Additionally, the solutions using DR, Solution III and Solution IV, will work well with a reconfiguration of the system by using NCSs and NOSs.

For each solution, we analyze the cases when the system loses central generation units as the following: (1) the system losing hydro generation, (2) the system losing diesel generation, and (3) the system losing both hydro and diesel generations.

18.4.1 Estimation of Reserve Margin Requirements

The generation on the island of Flores comes mainly from the diesel power plant. This power plant is reliable and has sufficient capacity to supply all loads on the island. However, the cost of generation is very high. On the island, the other generation options are hydro and wind. Although their generation costs are lower than that of diesel, they tend not to be reliable since they are intermittent energy resources. As a simplification, we will assume that all power plants are available whenever the system operator calls for power.

In Solutions I and II, when the system loses both central generation units, all customers are not supplied. On the other hand, in Solutions III and IV, DG can solve this problem. DG is used to supply power to customers when the system loses both central generation units. The amount of DG capacity depends on how much customers value reliability and are willing to pay for it. Furthermore, it should be noted that the generation cost of DG is lower than that of central generation. Thus, to meet the possible lowest generation cost, DG will be chosen to produce power during normal conditions.

Solution I: Service Provided by Central Generation with No DR

When the system loses one of its central generation units, another one should have a sufficient reserve margin to supply all customers in the system. Moreover, the generation unit that is still online should have enough capacity to cover the peak load.

According to the 2008 Flores load profile, the peak load was 1.978 MW. Thus, the hydro and diesel generation units should each have a capacity of at least 1.978 MW to cover the peak load and supply all customers when the other unit goes down. Without increasing capacity of central generation units, loss of one central generation unit, either the hydro or diesel plant, would interrupt electricity service to some customers.

Solution II: Service Provided by Central Generation with DR

Under normal conditions, the total capacity of both central generation units should at least cover the peak load of 1.978 MW. Both central generation units should have

Table 18.2 Summary of generation capacity, based on the load profile of the Flores distribution system, 2008, and assuming that all power plants will be available all the time

Solution	Capacity of hydro generation	Capacity of diesel generation	Capacity of wind generation	Total capacity on Island
I	1.978 MW	1.978 MW	—	3.956 MW
II	0.989 MW	0.989 MW	—	1.978 MW
III	—	—	1.978 MW	1.978 MW
IV	0.557 MW	0.557 MW	0.864 MW	1.978 MW

the same capacity of 0.989 MW so that when the system loses one of the central generation units, the other one is still able to supply half the customers. Moreover, according to the definition of DR, when a fault occurs in the system, all customers are required to reduce their energy usage. According to the 2008 Flores load profile, the peak load when applying DR was 0.864 MW, which is within the capacity of each central generation unit under normal conditions. Thus, the 0.989 MW capacity of each central generation unit would be sufficient to supply all customers under normal conditions and when the system loses one of the central generation units.

Solution III: Service Provided by Central Generation Including DG

In Solution III, if the system does not use DR and all customers want to be supplied, the capacity of DG will theoretically be an amount that covers the peak load of 1.978 MW. This will make the DG capacity sufficient to supply all customers in the system when the system loses both central generation units. In addition, since the generation cost of DG is lower than that of central generation, DG can be utilized to supply all customers under normal conditions without relying on central generation. However, this may not be practical since there are many other factors that are not taken into account, such as the uncertainty or reliability of DG in generating electricity.

Solution IV: Service Provided by Central Generation Including DG with DR

In Solution IV, if the system uses DR, the capacity of DG will decrease to 0.864 MW, which is the peak load when applying DR. In this solution, the system still relies on central generation since the system requires some power from central generation to supply customers under normal conditions. The capacity of each central generation unit is 0.557 MW.

The generation capacity, including the reserve margin for the 4 solutions, is summarized in Table 18.2. Solution IV—DGs collaborating with DR and reconfiguration—can decrease the reserve margin of central generation, and this solution seems to be the most practical. However, these numerical examples are based on the assumption that all power plants will be available all the time, which is not true in reality, of course. Also, it should be noted that these numbers are the minimum capacity of each generation and that they cover the peak load only in the year 2008.

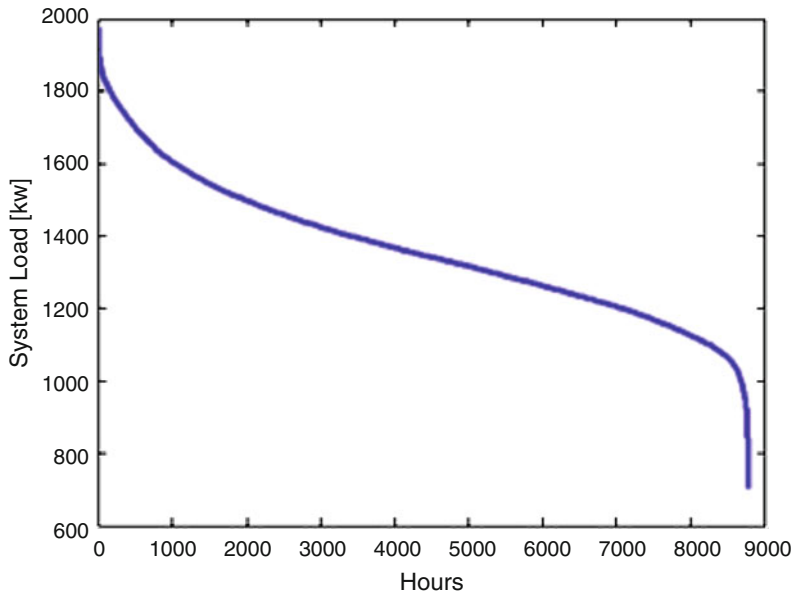


Fig. 18.6 The configuration of the Flores distribution system when the system has installed NCSs and NOSSs at optimal locations and a fault occurs in a critical area

18.4.2 Effect of DG Cost on Reserve Requirements

The strategy of the estimation of reserve margin will change if the generation cost of DG is higher than that of central generation. In the event that this happens, DG will be utilized to supply customers only during normal condition peak loads. Thus, the capacity of the central generation units should be estimated first. Based on the 2008 data for Flores, the total energy produced on the island was 11,600 MWh, and the peak load was 1.978 MW. Thus, we can calculate the load factor of the system as follows:

$$\text{LoadFactor} = \frac{\text{Total Energy 1 year (MWh)}}{\text{Peak Load (MW)} \times 8,760\text{h}} = \frac{11,600\text{MWh}}{1.978\text{MW} \times 8,760\text{h}} = 0.67 \quad (18.2)$$

We assume that the central generation should supply 90 % of overall loads. Thus, from the load duration curve in Fig. 18.6, the total capacity of both central generation units should cover the average power, 1.324 MW, while the capacity of DG will be 0.654 MW in order to supply peak load. However, the system may need to increase the capacity of DG to 0.864 MW, which is the peak load when applying DR, so that DG will have enough capacity to supply customers when both central generation units are disconnected from the system.

18.4.3 Impact of Intermittent Energy Resources on Generation and Energy Not Supplied Cost

In the estimation of the reserve margin, we consider that all power plants will be available all the time. However, in practice, hydro and wind are intermittent energy resources. Therefore, in this section, we will take the uncertainty of hydro and wind energy into account and study the impact of intermittent energy resources on generation and ENS cost. In this section, the capacities of the diesel, hydro, and wind power plants are 2.5 MW, 1.5 MW, and 0.6 MW, respectively. Moreover, according to the data for Flores in 2008, the hydro and wind power plants supplied high energy in winter and low energy in summer. Thus, the data from January 16 is chosen to represent when hydro and wind power plants supply high energy, while the data from July 15 is selected to represent when hydro and wind plants supply low energy. However, the hydro and wind power plants did not reach their maximum capacities for generating electricity. The costs of generation for diesel, hydro, and wind are \$180, \$88, and \$87, respectively. In addition, the interruption costs for public and private loads are \$0 and \$2,100 per kW, respectively.

The generation cost and ENS cost are estimated over a period of 30 days for each case, and they are also estimated when the prices of wind are \$87 and \$0. In addition, this can be done as in the previous section, creating four possible solutions: I. central generation, II. central generation with DR, III. central generation including DG, and IV. central generation including DG with DR. The hydro and diesel power plants represent central generation, and the wind power plant represents DG. The solutions serving DR—Solution III and Solution IV—are implemented by reconfiguring NCSs and NOSs. The results are shown in Tables 18.3 and 18.4.

Table 18.3 shows the generation cost, ENS cost, and the amount of ENS of Solutions I–IV when the hydro and wind power plants supply “high” energy. When the hydro power plant is disconnected from the system, all loads will be supplied by the diesel power plant, which has sufficient capacity. For this case, the generation costs of Solutions II–IV are better than that of Solution I. However, when the diesel power plant is disconnected from the system, the capacity of the hydro power plant is not enough to supply all customers, as shown in Solution I. Connecting DG to the system can increase the power to supply more loads, as shown in Solution III. Although the ENS of Solution III decreases from the ENS of Solution I, the generation cost of Solution III is higher than that of Solution I because there is the additional generation cost from DG if the wind price is \$87. Solution III would have been better off if the wind price had been \$0. For Solutions II and IV, both solutions are better than Solution I in terms of generation cost, ENS cost, and ENS. This is the result of applying DR. Applying DR reduces the power usage of all customers and then distributes the difference to customers who are willing to pay for it. In Solution IV, there is no ENS cost and ENS since applying DR decreases the power usage of all customers to within the capacity of the hydro and wind power plants. This enables all customers to have energy to use during the disconnection of the diesel power plant. In the case that both the hydro and diesel power plants are

Table 18.3 Hydro and wind power plants supply “high” energy

Disconnected generation	Solution I		Solution II		Solution III		Solution IV	
	Generation cost		Generation cost		Wind price	Wind price	Wind price	Wind price
					\$87	\$0	\$87	\$0
Hydro	\$183,891		\$80,292		\$163,221	\$143,884	\$59,622	\$40,286
Diesel	\$42,507		\$39,254		\$61,843	\$42,507	\$39,032	\$19,695
Both	\$0		\$0		\$19,337	\$0	\$19,337	\$0
	ENS cost	ENS (kWh)	ENS cost	ENS (kWh)	ENS cost	ENS (kWh)	ENS cost	ENS (kWh)
Hydro	—	—	—	—	—	—	—	—
Diesel	\$10 M	538,588	\$0	18,757	\$0	316,328	—	—
Both	\$846 M	1 M	\$677 M	446,069	\$379 M	799,357	\$210 M	223,809

Table 18.4 Hydro and wind power plants supply “low” energy

Disconnected generation	Solution I		Solution II		Solution III		Solution IV	
	Generation cost		Generation cost		Wind price	Wind price	Wind price	Wind price
					\$87	\$0	\$87	\$0
Hydro	\$187,002		\$81,651		\$186,293	\$185,629	\$80,941	\$80,278
Diesel	\$11,323		\$11,323		\$11,986	\$11,323	\$11,986	\$11,323
Both	\$0		\$0		\$663	\$0	\$663	\$0
	ENS cost	ENS (kWh)	ENS cost	ENS (kWh)	ENS cost	ENS (kWh)	ENS cost	ENS (kWh)
Hydro	—	—	—	—	—	—	—	—
Diesel	\$590 M	910,229	\$418,133	324,945	\$574 M	902,604	\$402 M	317,320
Both	\$860 M	1 M	\$688 M	453,615	\$844 M	1 M	\$672 M	445,990

disconnected from the system, we estimate the generation cost, ENS cost, and ENS when the system loses both power plants for 30 days. Installing DG and applying DR can help the system save a huge amount of money. Also, DG and DR improve the reliability of the system.

Table 18.4 shows the generation cost, ENS cost, and the amount of ENS of Solutions I–IV when the hydro and wind power plants supply “low” energy. When the hydro power plant is disconnected from the system, all loads will be supplied by the diesel power plant. This is similar to the result when the hydro and wind power plants supply “high” energy. The diesel power plant has a capacity large enough to supply all loads when the system loses the hydro power plant. However, when the diesel power plant is disconnected from the system, the power from the hydro power plant or even from the wind power plant is very small and will not be enough to supply all customers. In this case, the ENS cost and ENS are quite high. Applying DR would help defray the ENS cost and ENS, but not by much; the numbers are almost the same.

In the case that the hydro and diesel power plants are both disconnected from the system, connecting DG and applying DR will not help to supply many more customers. Scarce energy from the hydro and wind power plants would resemble when the system loses both the hydro and wind generation units.

18.5 Required Reconfiguration to Enable Differentiated Reliability

In the previous section, we estimate the possible reserve margin that would be sufficient to supply all customers when losing central generation units. Also, we mentioned that the use of DR should be coordinated with reconfiguring the system by using NCSs and NOSs. The reconfiguration is necessary in enabling differentiated reliability since it provides new routes to delivery power to end users. Importantly, if the capacity of generation is not adequate, the reconfiguration could disconnect some loads so that the limit power will be sufficient to supply to priority customers.

In this section, we will explain how the reconfiguration of the system can improve reliability service and how it enables differentiated reliability when the capacity of generation is not enough to all customers. Reconfiguration of the system allows customers to have more choices for their power service. Moreover, with advances in control, communication, and sensing technology, it has become possible to provide customers with differentiated levels of reliability. One way to provide differentiated levels of reliability is a deployment of NCSs and NOSs. During power outages, a utility can use NCSs and NOSs to reconfigure the networks in order to find a new route to supply priority customers.

To provide differentiated reliability options for customers, a utility may offer the customers different reliability insurance options [8]. The utility guarantees that these customers will be supplied according to the insurance option each one chooses. If the distribution utility is unable to supply the power laid out in the agreement to these customers due to an outage or an operational mistake, the distribution utility will compensate these customers. This compensation is defined as the customer's "interruption cost."

This methodology is based on optimal system reconfiguration that minimizes the interruption cost when guaranteeing a supply of power to priority customers as shown in (18.3). If the power supply is sufficient for all customers, the approach will find a configuration of distribution networks such that as many customers as possible are supplied. However, if the power supply is insufficient for all customers, the approach will seek a configuration that distributes power to priority customers. A genetic algorithm is developed to search for the optimal configuration for any given fault and DG capacity. The algorithm seeks to minimize the following objective function [7]:

$$\begin{aligned}
 & \text{minimize} \quad \sum_{i=2}^{\text{No. of Load Point}} P_{\text{unsupplied},i} \times IC_i \\
 & \text{subject to} \quad \sum_{i=2}^{\text{No. of Load Point}} P_{\text{supplied},i} \leq P_{\text{DG}} \\
 & \quad \sum_{i=2}^{\text{No. of Load Point}} (P_{\text{supplied},i} + P_{\text{unsupplied},i}) \leq \text{TL}.
 \end{aligned} \tag{18.3}$$

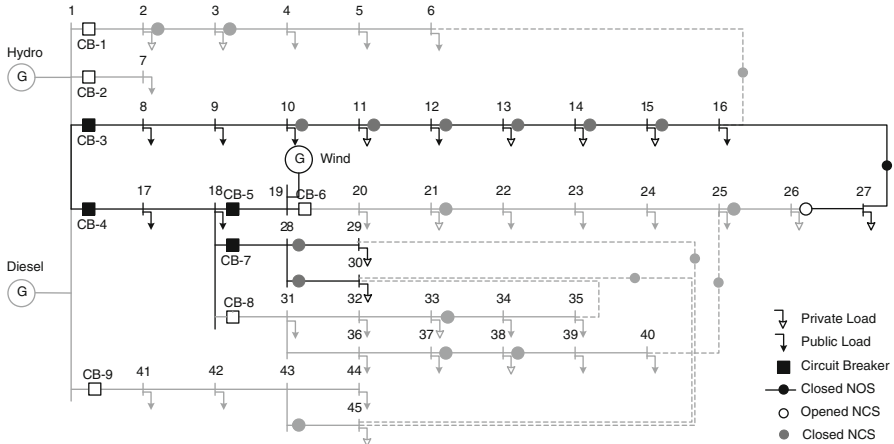


Fig. 18.7 Optimal configuration for winter load profile

where $P_{\text{un supplied},i}$ is the unsupplied load (in MW) at bus i , $P_{\text{supplied},i}$ is the supplied load at bus i , P_{DG} is the capacity of a DG connected to the network, and TL is the total load in the system. In addition, the optimal configuration must be a feasible configuration of distribution networks.

Examples of optimal configuration when the system loses both central generation units are shown in Figs. 18.7 and 18.8. The solid line is the route by which DG will deliver power to customers. The filled spots mean that the switch will be closed, and the empty spots mean that the switch will be open. In these examples, we give the capacity of DG as 0.7 MW. We select load profiles in both winter and summer to show the results. The total load during the winter is 1.688 MW, and the total load during the summer is 1.482 MW. The optimal configuration for the winter load profile is shown in Fig. 18.7. The total supplied load is 0.555 MW and the interruption cost for one hour is \$525. For the summer load profile, the optimal configuration is shown in Fig. 18.8. The total supplied load is 0.598 MW, and the interruption cost for one hour is \$495.

18.6 Conclusion

In this chapter we have considered the possibility of remote topology reconfiguration in a distribution system to ensure required reliability. First, for a given distribution system, an optimal placement of NOSs and NCSs is selected so that the cost of these switches combined with the infrastructure cost paid to customers by the utility is minimized. Next, given this new ability to reconfigure the system, several ways of providing reliable service are considered. In the island of Flores, it was found that without using wind power plant (DG) or increasing capacity of the hydro plant, loss of central diesel power plant would interrupt electricity service to

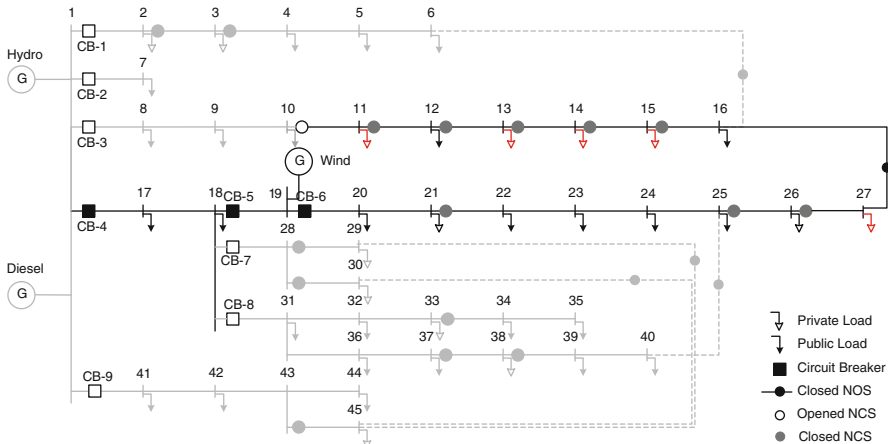


Fig. 18.8 Optimal configuration for summer load profile

some customers. However, a systematic reconfiguration of distribution system—to enable the use of DG and/or DR on the island—would facilitate differentiation for reliability of service. In particular, the private customers (including critical services, like hospitals, senior citizens) would be served by delivering power from a DG first. The remaining available power would be served to the other users.

In closing, we illustrate proof-of-concept implementation of differentiated reliability of service by means of remote distribution system reconfiguration. It is critical to have an off-line optimization algorithm for selecting the customers to be connected when central generation is lost.

References

1. R. Caldon, A. Stocco, R. Turri, Feasibility of adaptive intentional islanding operation of electric utility system with distributed generation. *Elec. Power Syst. Res.* **78**(12), 2017–2023 (2008)
2. P. Mahat, Z. Chen, B. Bak-Jensen, Review on islanding operation of distribution system with distributed generation, in *Proceedings of 2011 Power and Energy Society General Meeting*, 2011 IEEE 24–29 July pp. 1–8
3. Y. Zhang, M. Praca, M.Ilic, O.K. Tonguz, Toward smarter current relays for power grids, in *Proceedings of 2006 Power Engineering Society General Meeting*, 2006 IEEE
4. C.H. Lin, C.S. Chen, H.J. Chuang et al., Optimal switching placement for customer interruption cost minimization, in *Proceedings of 2006 Power Engineering Society General Meeting*, 2006 IEEE
5. A. Esteban, A. Alberto, Optimal selection and allocation of sectionalizers in distribution systems using fuzzy dynamic programming. *Energ. Power Eng.* **2**(4), 283–290 (2010)
6. A. Abiri-Jahromi, M. Fotuhi-Firuzabad, M. Parvania, M. Mosleh, Optimized sectionalizing switch placement strategy in distribution systems. *IEEE Trans. Power Delivery* **27**(1), 362–370 (2012)
7. S. Junlakarn, M. Ilic, Distribution system reliability options and minimizing utility liability. *IEEE Transa. Smart Grid* (in the process of submission)
8. E. Fumagalli, J.W. Black, I. Vogelsang, M. Ilic, Quality of service provision in electric power distribution systems through reliability insurance. *IEEE Trans. Power Syst.* **19**(3), 1286–1293 (2004)

Chapter 19

Transient Stabilization in Systems with Wind Power

Milos Cvetković, Kevin Bachovchin, and Marija Ilić

Potential of Nonlinear Fast Power-Electronically-Switched Storage

19.1 Transient Stabilization Problems in Systems with High Wind Penetration

The transient stability of today's electric power systems is an important and highly complex problem. With an increasing amount of power being supplied by unpredictable renewable energy sources, it has become extremely difficult to predict and prevent outages. In the case of a small power system, such as on Flores, high wind penetration can cause serious stability problems. The response of the system to large wind disturbances is governed by nonlinear dynamics. Therefore, it is very important to use adequate nonlinear control in order to ensure reliability under such circumstances.

Furthermore, efforts to increase the efficiency of the grid by operating closer to stability boundaries can cause the grid response to be unreliable in the case of unpredicted events. Building additional infrastructure, which only provides support in the rare cases of equipment failure and faults, is expensive. Also, operating the system suboptimally in order to guarantee stability or satisfy regulatory requirements is inefficient. An inexpensive and efficient solution would be to use existing power-electronically switched devices controlled by more advanced transient stabilizing algorithms. In case this is still insufficient, new fast controllers of storage devices and flywheels should be considered prior to building new transmission lines.

M. Cvetković (✉) • K. Bachovchin • M. Ilić

Department of Electrical and Computer Engineering, Carnegie Mellon University,
5000 Forbes Ave, Pittsburgh, PA 15213, USA

e-mail: mcvetkov@andrew.cmu.edu; kbachovc@andrew.cmu.edu; milic@ece.cmu.edu

Large disturbances and high energy faults are considered in transient stability studies. The system is said to be transiently stable if all its generators can preserve synchronism for a predefined set of disturbances. In other words, the mechanical frequencies of all the generators in a power system have to stay close to each other. Critical clearing time is defined as the longest duration of the fault in which the system can preserve stability.

Power electronic devices have great potential for stabilizing the system response to fast, unpredictable, high energy level disturbances. This chapter gives an overview of possible control designs for stabilization using power electronics and highlights their pros and cons. Flexible AC Transmission System (FACTS) devices are used to show the potential of power-electronically switched devices. These devices are located in the transmission part of the system. They are primarily used to redirect the flows of power if they are connected in series or to provide voltage support to the system if they are connected in shunt.

The main part of a power-electronically switched device is the reactive element: the capacitor and/or inductor. A connection with the grid is made through a set of interconnected thyristor switches. The fundamental characteristic of such a device is its ability to actively change its own equivalent impedance as seen from the network side. It is able to do so very quickly because the switching speed is in the range of a few kHz. The control logic will drive such a device to behave either as a current/voltage source or as a variable impedance. Regardless of the way the control is designed, the device is able to react in a fast and timely manner to any unpredicted major disturbance. For this reason, FACTS devices can improve reliability.

Flywheel energy storage systems are also considered for stabilization purposes. A flywheel energy storage system stores mechanical energy by accelerating a rotor. The flywheel accelerates to store energy and decelerates to supply energy to the grid. The direction of power is controlled using thyristor switches.

A fundamental difference between flywheels and FACTS is that the former stores active power while the latter stores reactive power. However, as will be shown later in this chapter, both can be used to stabilize the system in the event of disturbances. Flywheels are more appropriate for lengthy disturbances because they have a higher energy capacity than FACTS devices.

Sensing and communication play a significant role in achieving desirable control performance on these fast time scales. The controller needs to be updated frequently with accurate information. Phasor measurement units (PMUs) show a fast and reliable way to acquire needed information. Of course, locally implemented control has an advantage over global control. However, designing transient stability control for FACTS devices and flywheel energy storage systems using only local measurements is an interesting and challenging problem, which will be explained in subsequent sections.

19.2 The Flores Power System and High Energy Disturbances

19.2.1 Flores

The island of Flores is taken for demonstration purposes. The three-bus-reduced topology network of Flores introduced in Chaps. 15 and 16 is again used in this chapter. The same loading of the system is used as in Chap. 4. For completeness, the parameters of Flores are listed again in this section.

The forty-seven bus Flores system has been reduced to a three-bus system by using the standard network topology reduction method. The resulting three-bus equivalent is shown in Fig. 19.1. The only three preserved buses are the generator buses, bus 1 with a diesel generator, bus 2 with a wind generator, and bus 3 with a hydro generator.

The parameters of the three-bus system are given in per units in Table 19.1. The base values are $S_b = 10[\text{MVA}]$ and $V_b = 15[\text{kV}]$. The loads are represented as constant impedance loads.

19.2.2 Large Disturbances

Two types of large disturbances are considered in this chapter: high-energy wind perturbation and equipment failure. A high-energy wind power perturbation can be either a short-term high-magnitude wind power perturbation or a long-term low-magnitude wind power perturbation. A failure of the equipment is simulated as a short circuit

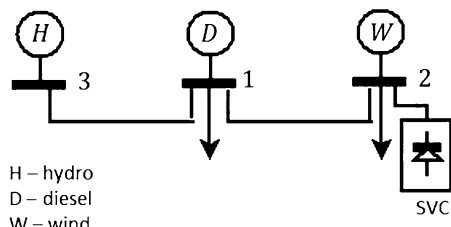


Fig. 19.1 Three-bus Flores equivalent system

Table 19.1 Three-bus system parameters

T. line.	From 3 to 1	From 1 to 2
$R[\text{pu}]$	0.04	0.3071
$L[\text{pu}]$	0.04	0.1695
$C_{ch}[\text{pu}]$	0.0080	0.00446
Load	Bus 1	Bus 2
$R[\text{pu}]$	7.8749	12.4954
$L[\text{pu}]$	2.3049	3.6506

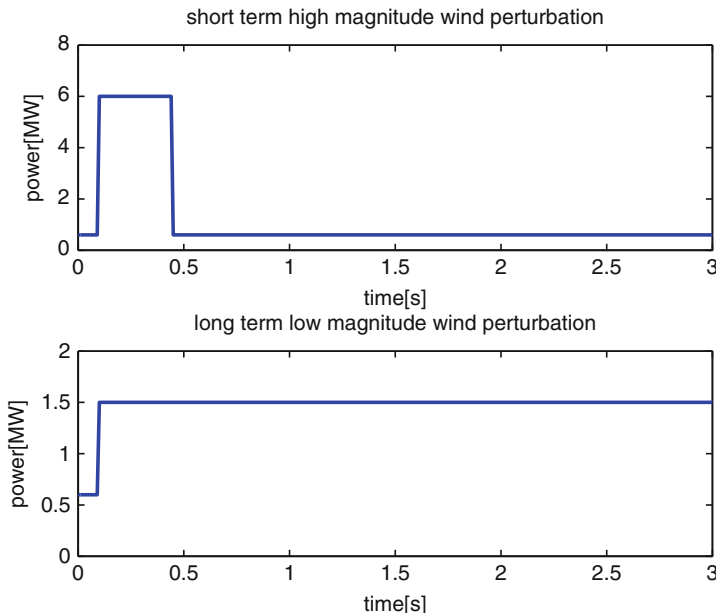


Fig. 19.2 Wind disturbances simulated in the Flores example

on either the hydro or the diesel power plant bus. Figures 19.2 and 19.3 show two wind power disturbances and two equipment failures.

All of the disturbances are large enough such that control actions have to be designed accordingly in order to preserve system stability. The small signal perturbation control and linearization methods described in Chaps. 15 and 16 are ineffective in stabilizing the system response to these large disturbances, so nonlinear modeling and nonlinear control techniques must be used.

19.3 Possible Ways of Meeting Transient Stability Requirements in Systems with High Wind Penetration

In today's systems, control of FACTS devices is implemented locally by linear controllers using linearized models [3] and is primarily used for voltage control and power transfer enhancement. This control is effective for the stabilization of small disturbances, but it generally fails to transiently stabilize large disturbances. The inaccuracy of the linearized model is unacceptable when the system is perturbed far away from its equilibrium.

No real-world attempts have been made yet to deploy a FACTS nonlinear controller for transient stabilization (or at least the authors of this chapter are not aware of any). The reason for this has been the lack of accurate sensing and

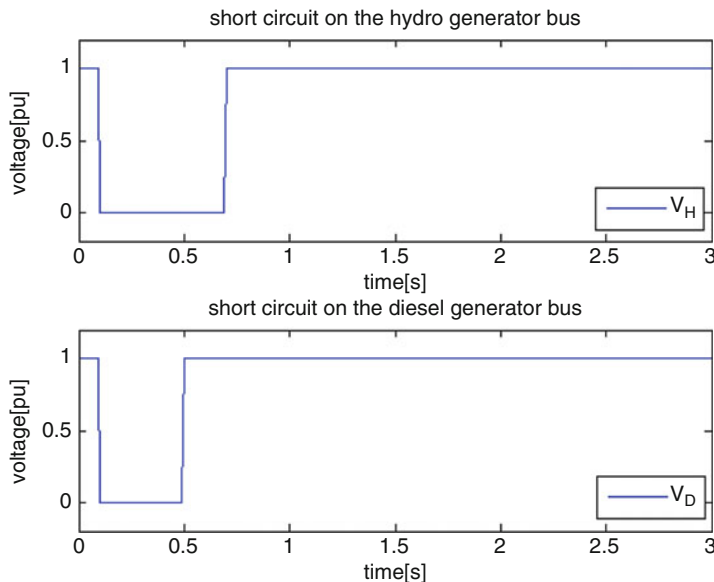


Fig. 19.3 Equipment failure simulated in the Flores example

communication so far. Therefore, the few theoretical nonlinear control designs that exist have never been actually implemented. Today, when technical achievements make transient stability control possible, some of the existing nonlinear control methods can be compared to the newly established ones.

One of the most interesting nonlinear controller designs, from a decade back, is presented in [1]. A Control Lyapunov Function (CLF) for the stabilization of high-magnitude oscillations is proposed. A controller designed according to this method relies on the minimization of an energy function. However, the controller uses nominal network topology and does not incorporate any information about the disturbance. Therefore, the region of attraction of the energy function is relatively small, compared to the energy level of large disturbances, and the controller does not perform transient stabilization well. A useful property of this energy function is that it allows decentralized control implementation.

A qualitatively new approach to stabilizing a power system using the energy function is introduced by the authors of this chapter in [2] and further explored in [4, 5]. An energy-based analysis shown in these earlier works leads to a FACTS controller which can perform well when dealing with the problem of transient stability. The fundamental difference between this approach and the one proposed in [2] is the control objective. In this case, the controller is not trying to reduce the entire increment of the system energy caused by the large disturbance. Instead, it is shifting the energy increment from some devices to others. Less strict requirements

on control will result in an increase of the region of attraction. Therefore, the controller will be able to keep synchronism between generators for a longer period of time.

On the other hand, a side effect of the control is a very rapid change of the states that are not directly controlled. In particular, the energy increment is moved from generators to FACTS devices and is temporarily stored there. Therefore, the currents in FACTS' inductors and voltages across FACTS' capacitors will increase rapidly. FACTS devices usually do not have any dissipative elements, and therefore, they cannot consume energy and cancel out a disturbance entirely. Eventually, their energy accumulation reaches their limits. Therefore, there exists an upper bound to the size of the disturbance FACTS devices are able to handle.

19.4 Transient Stabilization Using FACTS

This section explains how FACTS devices can be used in the stabilization of large disturbances on short time scales.

19.4.1 *FACTS as Low Energy Storage Devices*

An analysis of the fundamental physical processes driving the energy accumulation of FACTS is presented in this section. The goal is to show that FACTS can be used to store the energy changes caused by disturbances for short intervals.

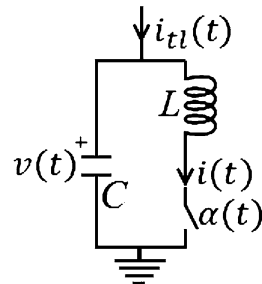
This goal requires a precise and multi-temporal dynamic model of FACTS. Time-varying phasors are used to capture the desired dynamics.

19.4.1.1 Time-Varying Phasor Model of the Static Var Compensator

Time-varying phasors can be used to model and capture transients of wires and transmission lines as well as the internal capacitors and inductors of FACTS devices. Time-varying phasors assume a constant frequency of the network, while the magnitude and the phase angle of the phasor vary with time. The time scale separation between the slowly changing network frequency and the fast voltage and current magnitude fluctuations allows us to remove the carrier and to consider only the dynamics of the phasor on short time scales. A formal derivation of the time-varying phasor dynamic models of different power-electronically switched devices is presented in [8] and [9]. The appendix shows the derivation of the time-varying phasor dynamic model of an SVC.

A shunt FACTS device, specifically a Static Var Compensator (SVC), is used in this chapter to show the potential of power-electronically switched devices to control large disturbances. Its structure is shown in Fig. 19.4 and its natural dynamic

Fig. 19.4 Static Var Compensator (SVC)



model in the time domain is given in (19.1). Variable α is the switching variable and the control input. It is equal to 1(0) if the switch is closed(open). Every value in between 1 and 0 can be considered based on the time interval during which the switch remains closed with respect to one full cycle of the electrical frequency:

$$\begin{aligned}\dot{v}(t) &= \frac{1}{C} (i_{tl}(t) - i(t)) \\ i(t) &= \frac{\alpha(t)}{L} v(t)\end{aligned}\quad (19.1)$$

The time-varying phasor model of the same device is given in (19.2). The phasors are given in Cartesian coordinates, and this coordinate system is referred to as the network reference frame. Letters D and Q are used to mark direct (real) and quadrature (imaginary) components of the phasor in the network reference frame:

$$\begin{aligned}\dot{V}_D(t) &= \frac{1}{C} (I_{ID}(t) - I_D(t)) + \omega V_Q(t) \\ \dot{V}_Q(t) &= \frac{1}{C} (I_{IQ}(t) - I_Q(t)) - \omega V_D(t) \\ \dot{I}_D(t) &= \frac{\alpha(t)}{L} V_D(t) + \omega I_Q(t) \\ \dot{I}_Q(t) &= \frac{\alpha(t)}{L} V_Q(t) - \omega I_D(t)\end{aligned}\quad (19.2)$$

19.4.1.2 SVC Energy Capacity

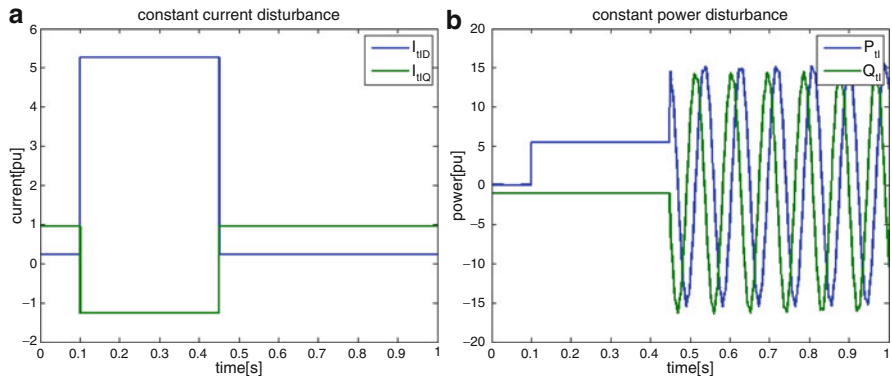
The energy accumulation potential of the SVC from Fig. 19.4 is illustrated using an SVC with the parameters given per unit in Table 19.2. The base values are $S_b = 10[\text{MVA}]$ and $V_b = 15[\text{kV}]$. Switching signal α remains constant throughout this section and its value is $\alpha = 0.5$.

Table 19.2 SVC parameters

	SVC
$C[\text{pu}]$	0.3
$L[\text{pu}]$	2.5

Table 19.3 Equilibrium of the SVC for given simulations

	Direct	Quadrature
$V_0[\text{pu}]$	0.9676	-0.2339
$I_0[\text{pu}]$	-0.4677	-1.9353
$I_t[\text{pu}]$	0.2341	0.9677

**Fig. 19.5** (a) Constant current and (b) constant power disturbance (plotted with respect to $S_b = 1[\text{MVA}]$ and $V_b = 15[\text{kV}]$)

The behavior of the SVC is investigated in two cases. In the first case, the SVC is modeled without dynamics. The capacitor and the inductor are represented as constant impedances, and currents and voltages change instantaneously. In the second case, the time-varying phasor dynamic model of the SVC is used, as expressed in (19.2).

At the beginning of simulations, the SVC is in equilibrium. The equilibrium values are given in Table 19.3.

The disturbance is modeled as the step change in the current of the transmission system, as shown in Fig. 19.5a. This is a constant current disturbance. The new current value is $I_{tID}^{\text{dist}} = 0.52719[\text{pu}]$ and $I_{tIQ}^{\text{dist}} = -0.12742[\text{pu}]$, and the disturbance lasts from $t = 0.1[\text{s}]$ to $t = 0.45[\text{s}]$. Figures 19.6a and 19.7a show the response of the SVC energy and its first derivative, respectively. The energy and its first derivative are calculated using the following equations:

$$\begin{aligned} v_{\text{svc}} &= \frac{1}{2}C(\tilde{V}_D^2 + \tilde{V}_Q^2) + \frac{1}{2}L(\tilde{I}_D^2 + \tilde{I}_Q^2) \\ \dot{v}_{\text{svc}} &= p_{\text{svc}} = C(\tilde{V}_D \dot{V}_D + \tilde{V}_Q \dot{V}_Q) + L(\tilde{I}_D \dot{I}_D + \tilde{I}_Q \dot{I}_Q) \end{aligned} \quad (19.3)$$

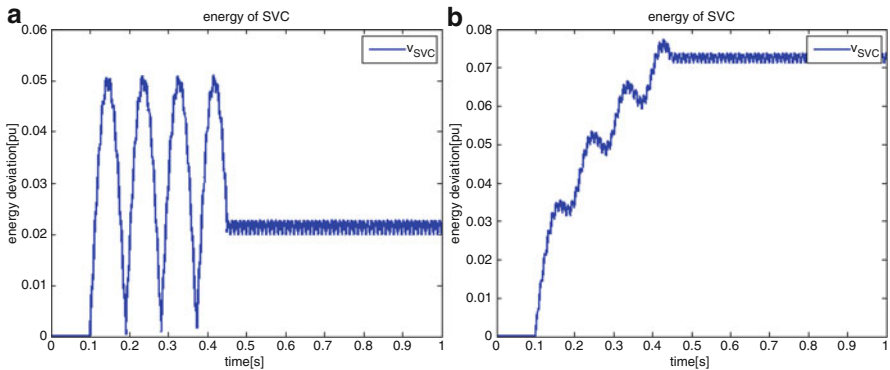


Fig. 19.6 SVC energy if the disturbance is (a) constant current or (b) constant power (plotted with respect to $S_b = 1[\text{MVA}]$ and $V_b = 15[\text{kV}]$)

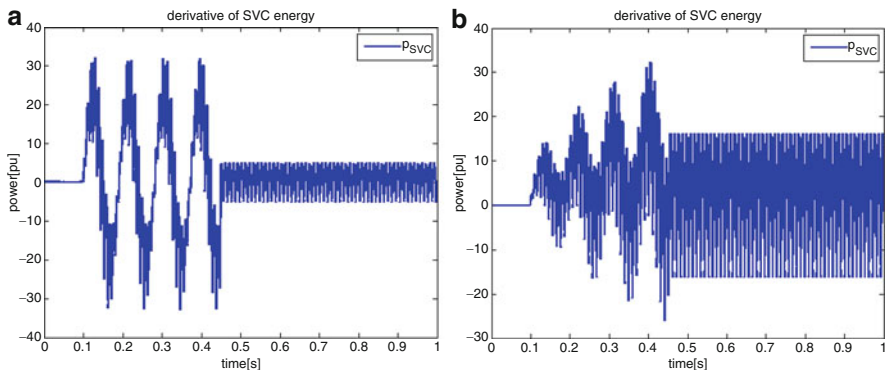


Fig. 19.7 SVC energy derivative if the disturbance is (a) constant current or (b) constant power (plotted with respect to $S_b = 1[\text{MVA}]$ and $V_b = 15[\text{kV}]$)

where the tilde symbol represents the deviation of the variable from its equilibrium, for example, $\tilde{V}_D = V_D - V_{D0}$.

If the SVC is modeled without dynamics, $\dot{v}_{\text{SVC}} = 0$ and v_{SVC} will have a sequence of discrete values. A different input current during the disturbance will mean that there is a different equilibrium and the energy of the SVC will be different. Indeed, the SVC energy is equal to zero if the disturbance is not present and higher than zero if the disturbance is present.

Figures 19.6a and 19.7a show that the behavior of the energy and its first derivative is much richer if the SVC is modeled using time-varying phasors.

The second important type of disturbance is a constant power disturbance. The real power input to the SVC is changed from zero to $P = 5.4[\text{MW}]$, while the reactive power input remains the same, as shown in Fig. 19.5b. The duration of the disturbance is the same as the duration of the constant current disturbance.

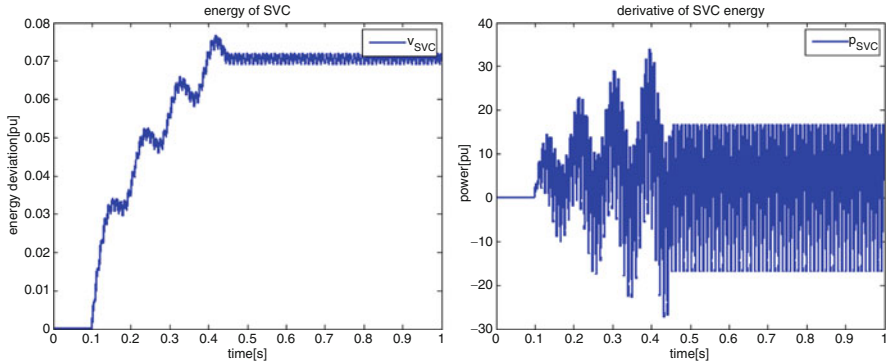


Fig. 19.8 SVC energy and its first derivative if the disturbance is $P = 5.4[\text{MW}]$ and $Q = 0[\text{MVar}]$ (plotted with respect to $S_b = 1[\text{MVA}]$ and $V_b = 15[\text{kV}]$)

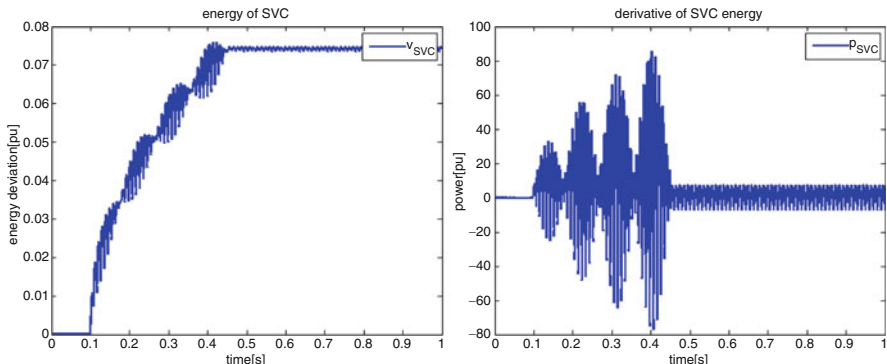


Fig. 19.9 SVC energy and its first derivative if the disturbance is $P = 5.4[\text{MW}]$ and $Q = 5.4[\text{MVar}]$ (plotted with respect to $S_b = 1[\text{MVA}]$ and $V_b = 15[\text{kV}]$)

A constant power disturbance will make the currents and voltages of the SVC vary in time even if the system is not modeled using the time-varying phasor dynamic model. The reason for this is simple. The LC circuit behaves like an oscillator, exchanging the additional energy between the inductor and the capacitor even after the disturbance has been cleared. Therefore, no equilibrium exists and a model which does not capture dynamics cannot be used. Figures 19.6b and 19.7b show the responses of the SVC energy and its first derivative.

A constant power disturbance can be both a real and a reactive power disturbance. Figures 19.8–19.10 show the behavior of the SVC energy and its first derivative for three different values of reactive power disturbance. One thing is clear: the reactive power disturbance does not affect the amount of energy accumulated in the SVC. However, there is no clear connection between the size of the reactive power disturbance and the oscillations in energy, or else that connection is highly nonlinear.

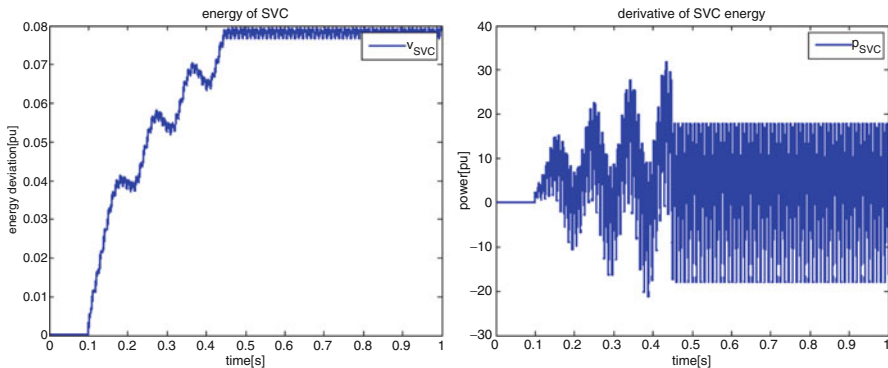


Fig. 19.10 SVC energy and its first derivative if the disturbance is $P = 5.4[\text{MW}]$ and $Q = -5.4[\text{MVar}]$ (plotted with respect to $S_b = 1[\text{MVA}]$ and $V_b = 15[\text{kV}]$)

The constant real power disturbance $P = 5.4[\text{MW}]$ ($Q = Q_0$) is used to show how the power of the disturbance and the size of the SVC affect the energy accumulation. The energy increment is shown in Fig. 19.11a. The corresponding SVC voltage is given in Fig. 19.12a. In the second scenario, the real power is increased from zero to $10.8[\text{MW}]$ for the same time period, and the energy response is shown in Fig. 19.11b while the corresponding SVC voltage is given in Fig. 19.12b. In the third case, the SVC inductor is changed to $L = 2[\text{pu}]$ (the disturbance is $5.4[\text{MW}]$), and the responses are shown in the same figures under (c).

The first thing one notices is that the SVC is actually able to store real power. However, the states of the SVC cannot reach an equilibrium. In other words, the SVC stores energy only in a limit cycle mode. This also is the main limitation of using the SVC as a storage device. The other power system states will have to cycle if the SVC is to be used as a storage device, and this is why its long-term usage may cause fluctuations in the network. However, on shorter time scales, in the case of large disturbances, these fluctuations might be desirable if they oppose instabilities.

The second important phenomenon is that if the magnitude of the power increases, the magnitudes of the accumulated energy and voltage also increase, but the waveforms remain the same. Therefore, the limit on how much energy the SVC can accumulate will be determined only by the characteristics of the material the SVC is made of. Thyristor switches are the most sensitive in this case and the entire equipment rating is based on their rating.

On the other hand, the size of the inductor and the capacitor will determine the shape of the waveform. In other words, it will determine the limit cycle and the trajectory of the SVC states. This trajectory is of high importance in determining how much a FACTS device can improve stability. However, the best possible choice for the size of the SVC inductor and capacitor depends on other system constants and cannot be found if the time constants of other devices are not considered. Therefore, it is a problem of high complexity and will be addressed in future work.

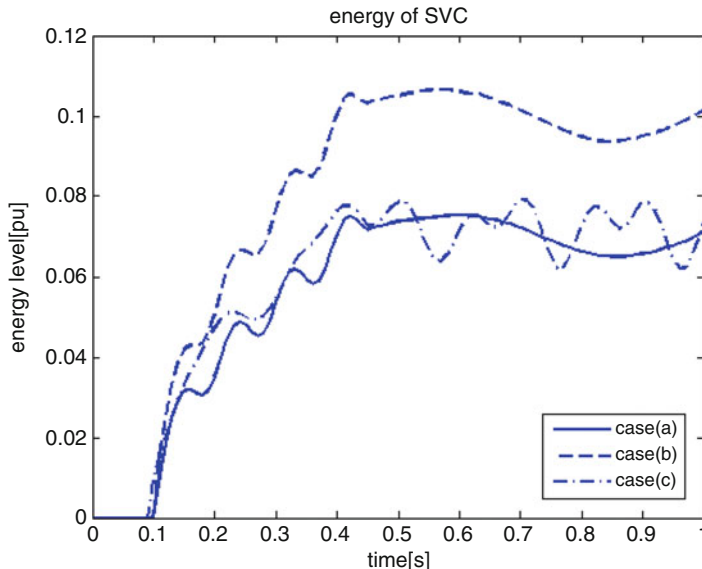


Fig. 19.11 Increment in the energy of SVC in response to (a) a disturbance power increment of 5.4[MW], (b) a disturbance power increment of 10.8[MW], (c) a disturbance power increment of 5.4[MW] when $L = 2[\text{PU}]$ (plotted with respect to $S_b = 1[\text{MVA}]$ and $V_b = 15[\text{kV}]$)

19.4.2 Nonlinear Multi-temporal Dynamic Model of a Power System

The fast dynamics of other devices (transmission lines, generator stator windings, constant impedance loads) has to be captured if the effects of FACTS are to be seen on the entire system. Time-varying phasors are used as a modeling tool for this purpose.

Time-varying phasors have rarely been deployed in the assessment of overall system stability. There are a few reasons for this. First, they increase the complexity of the dynamic model by adding dynamic states which would otherwise be considered algebraic. Second, the controllers for transient stabilization used in the past, such as the excitation system on synchronous generators, were not able to respond quickly enough to the error given by this model. Third, no real-time synchronized measurements on the fast time scales of kHz were available in the past. Today, the latter two technical issues have been overcome with the use of PMU sensing and power electronic controllers. The first issue can be resolved by using systematic model reduction once the controller has been designed. At any rate, the complexity of the model is an acceptable price for ensuring the stability of the power grid on all time scales and against very fast and large disturbances .

Time-varying phasors can benefit system modeling in another way. If the transmission grid is modeled using this concept, then the system model has an ordinary

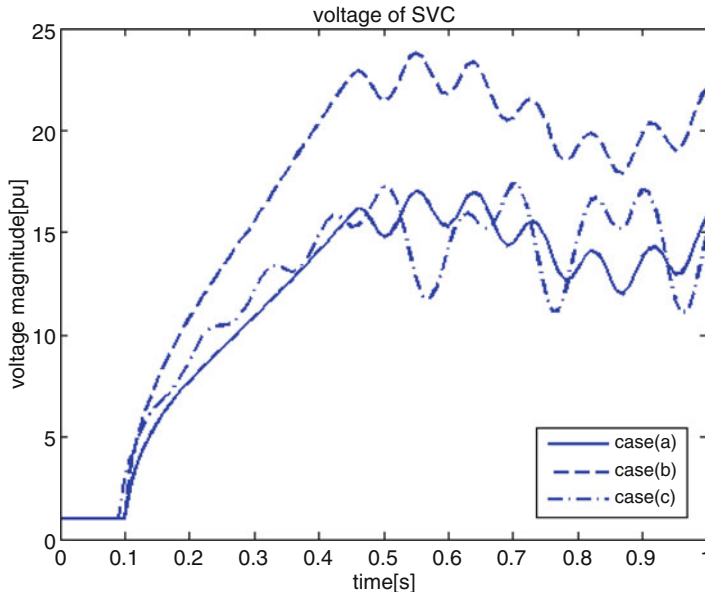


Fig. 19.12 Voltage of SVC in response to (a) a disturbance power increment of 5.4[MW], (b) a disturbance power increment of 10.8[MW], (c) a disturbance power increment of 5.4[MW] when $L = 2[\text{PU}]$ (plotted with respect to $S_b = 1[\text{MVA}]$ and $V_b = 15[\text{kV}]$)

differential equation (ODE) form, regardless of the load model one chooses. Using the traditional approach to modeling the transmission system involves algebraic equations, and the entire system model therefore has a differential algebraic equation (DAE) form. It is a well known fact that the variety of methodologies used to design a controller for a nonlinear ODE system model is much greater than for a DAE model. Therefore, the ODE model with time-varying phasors has an advantage over a DAE model when it comes to designing a controller for predictable performance.

Finally, time-varying phasors ensure the preservation of the system topology. Each of the time-varying phasor dynamic equations describes the dynamics of a certain physical device. Consequently, the need for network topology reduction disappears.

Incorporating the wind power plant model, taken from [6], with the time-varying phasor models of FACTS and wires yields (19.4):

$$\begin{aligned}\dot{\psi}_{d_i} &= -i_{d_i}r_{s_i} - v_{d_i} + \omega_s\psi_{q_i} \\ \dot{\psi}_{q_i} &= -i_{q_i}r_{s_i} - v_{q_i} - \omega_s\psi_{d_i} \\ \dot{\psi}_{D_i} &= -i_{D_i}r_{D_i} + (\omega_s - \omega_i)\psi_{Q_i}\end{aligned}$$

$$\begin{aligned}
\dot{\psi}_{Q_i} &= -i_{Q_i} r_{Q_i} - (\omega_s - \omega_i) \psi_{D_i} \\
\dot{\delta}_i &= \omega_i - \omega_s \\
\dot{\omega}_i &= \frac{1}{J_i} (T_{m_i} - T_{e_i}) \\
T_{e_i} &= \psi_{q_i} i_{d_i} - \psi_{d_i} i_{q_i} \\
[\psi_{d_i} \ \psi_{q_i} \ \psi_{D_i} \ \psi_{Q_i}]^T &= L_i * [i_{d_i} \ i_{q_i} \ i_{D_i} \ i_{Q_i}]^T
\end{aligned} \tag{19.4}$$

The synchronous machine model, taken from [7], is expressed in (19.5):

$$\begin{aligned}
\dot{\psi}_{d_i} &= -i_{d_i} r_{s_i} - v_{d_i} + \omega_s \psi_{q_i} \\
\dot{\psi}_{q_i} &= -i_{q_i} r_{s_i} - v_{q_i} - \omega_s \psi_{d_i} \\
\dot{\psi}_{f_i} &= -i_{f_i} r_{f_i} + v_{f_i} \\
\dot{\psi}_{D_i} &= -i_{D_i} r_{D_i} \\
\dot{\psi}_{Q_i} &= -i_{Q_i} r_{Q_i} \\
\dot{\delta}_i &= \omega_i - \omega_s \\
\dot{\omega}_i &= \frac{1}{J_i} (T_{m_i} - T_{e_i}) \\
T_{e_i} &= \psi_{q_i} i_{d_i} - \psi_{d_i} i_{q_i} \\
[\psi_{d_i} \ \psi_{q_i} \ \psi_{f_i} \ \psi_{D_i} \ \psi_{Q_i}]^T &= L_i * [i_{d_i} \ i_{q_i} \ i_{f_i} \ i_{D_i} \ i_{Q_i}]^T
\end{aligned} \tag{19.5}$$

L_i is the machine inductance matrix relating the flux linkages and the currents in the coils.

Rotor position in both generator models is described with respect to a reference angle δ_s . Angular frequency ω_s is the reference angular frequency. The angular frequency reference is chosen as the center of inertia reference. This concept is well known and can be found in the literature [14]. According to this concept, reference frequency can be found as the weighted sum of mechanical frequencies of all generators, (19.6):

$$\omega_s = \frac{\sum_i J_i \omega_i}{\sum_i J_i} \tag{19.6}$$

The ODE model of the interconnected system will not be presented here due to limited space. The derivation of the dynamic model using time-varying phasors and the model itself can be found in [2]. The equilibrium of the full dynamic model of the Flores power system is given in the appendix.

19.4.3 Energy-Based Transient Stabilization Control Using FACTS

The impact of FACTS on transient stability in response to high-energy fluctuations is only short term because of the devices' inability to dissipate energy. A FACTS device functions well as a short-term storage device which can accumulate energy for up to a few seconds, depending on its size, the size of the disturbance, the nominal conditions, and the inertia of the generators. During that period the inductors and capacitors of the FACTS device are being constantly filled with the energy created by the disturbance. Once the disturbance ends, the stored energy is returned back to the system in a gradual decrease of the FACTS energy level.

The control law which implements this action is based on a representation of the physical energy inside the system. A physical energy function is used to describe the energy level of all devices.

In the case of a physical state power system model, the energy function can be found by summing the energy expressions of all devices. The energy of a capacitor and the energy of an inductor are given using the following two expressions:

$$\begin{aligned} v_C &= \frac{1}{2}C(\tilde{V}_D^2 + \tilde{V}_Q^2) \\ v_L &= \frac{1}{2}L(\tilde{I}_D^2 + \tilde{I}_Q^2) \end{aligned} \quad (19.7)$$

The energy of a rotating machine is composed of the energy of rotation and the electromagnetic energy stored in the stator and rotor windings. The number of windings is n_L , while the generator inertia is denoted by J . The energy is given by the following expression:

$$v_{mach} = \frac{1}{2}J\tilde{\omega}^2 + \sum_{n_L} v_L \quad (19.8)$$

The energy function of all major devices in a power system can be represented using just these few energy expressions. Machines, lumped parameter represented transmission lines, FACTS, and loads represented as machines or impedances have similar energy expressions. These are also the devices considered in this study so far. The system energy function $v(x)$ is

$$\begin{aligned} v(x) &= \sum_i v_{C_i}(\tilde{V}_{iD}, \tilde{V}_{iQ}) + \sum_i v_{L_i}(\tilde{I}_{iD}, \tilde{I}_{iQ}) + \sum_i v_{rot_i}(\tilde{\omega}_i, \delta_i) \\ &= v_{em}(x) + v_{rot}(x) \end{aligned} \quad (19.9)$$

Here $v_{em}(x)$ represents the electromagnetic energy stored in inductors and capacitor, while $v_{rot}(x)$ represents the energy of the moving rotor.

Lyapunov theory offers steps for designing a controller that will minimize the energy of a disturbance. According to this theory, a candidate for the energy function of a closed-loop system $\dot{x} = f(x)$ is a function $v(x) > 0$ for which $\forall x \in M$ except in finite number of points x_0 in which $v(x) = 0$ where $\|x - x_0\| \leq M$. If it holds that $\dot{v}(x) < 0$ except in x_0 in which $\dot{v}(x) = 0$ the function $v(x)$ is an energy function.

Points x_0 do not necessarily have to be the equilibrium points. They can be a trajectory the system is trying to follow. This is the case with our proposed transient stabilizing controller. As already noted, FACTS devices cannot dissipate energy, and therefore the objective of its transient stabilizing controller should be to redirect energy so that the generators stay in synchronism as long as possible. This implies reshaping the energy function $v(x)$, keeping in mind that the function should still satisfy all conditions. The best way to achieve this is by controlling the first derivative of $v(x)$.

Observe that the energy function has two parts, one belonging to the electromagnetic energy of the inductors and capacitors v_{em} and the second belonging to the energy of rotation v_{rot} . The first part is controlled by FACTS, and its value should increase while FACTS accumulate the energy created by the disturbance.

The first derivative of the energy function is calculated as

$$\begin{aligned}\dot{v}(x) &= \dot{v}_{em}(x) + \dot{v}_{rot}(x) \\ &= \dot{v}_{diss}(x) + \dot{v}_{exch}(x) + \dot{v}_{acc}(x)\end{aligned}\tag{19.10}$$

Each of the terms in (19.10) has a functional meaning. The derivative of the energy of dissipation $\dot{v}_{diss}(x)$ shows the power of dissipation with respect to the equilibrium, and it is equal to

$$\begin{aligned}\dot{v}_{diss}(x) &= - \sum_i R_{tl_i} (I_{tl_{iD}} \tilde{I}_{tl_{iD}} + I_{tl_{iQ}} \tilde{I}_{tl_{iQ}}) \\ &\quad - \sum_i r_{s_i} (i_{d_i} \tilde{i}_{d_i} + i_{q_i} \tilde{i}_{q_i}) \\ &\quad - \sum_i r_{r_i} (i_{D_i} \tilde{i}_{D_i} + i_{Q_i} \tilde{i}_{Q_i}) \\ &\quad - \sum_i r_{f_i} i_{F_i} \tilde{i}_{F_i} \\ &\quad - \sum_i D_i \tilde{\omega}_i^2\end{aligned}\tag{19.11}$$

The exchange of energy between components is captured by the exchanged power $\dot{v}_{exch}(x)$, and it is equal to

$$\begin{aligned}\dot{v}_{exch}(x) &= - \sum_i v_{f_i} \tilde{i}_{F_i} \\ &\quad - \sum_i V_{iD} (\tilde{I}_{G_{iD}} + \sum_j \text{sgn}(d) \tilde{I}_{tl_{ijD}} - \tilde{I}_{L_{iD}})\end{aligned}$$

$$\begin{aligned}
& - \sum_i V_{iQ} (\tilde{I}_{G_{iQ}} + \sum_j \text{sgn}(d) \tilde{I}_{tl_{ijQ}} - \tilde{I}_{L_{iQ}}) \\
& + \sum_i \tilde{V}_{iD} (I_{G_{iD}} + \sum_j \text{sgn}(d) I_{tl_{ijD}} - I_{L_{iD}}) \\
& + \sum_i \tilde{V}_{iQ} (I_{G_{iQ}} + \sum_j \text{sgn}(d) I_{tl_{ijQ}} - I_{L_{iQ}})
\end{aligned} \tag{19.12}$$

where $d = 1$ if the direction of the current is into the bus and $d = -1$ if the direction of the current is out of the bus. The accumulation of energy inside the elements with memory is represented with $\dot{v}_{\text{acc}}(x)$, and it is equal to

$$\begin{aligned}
\dot{v}_{\text{acc}}(x) = & \sum_i L_{tl_i} (\tilde{I}_{tl_{iD}} I_{tl_{iQ}} - \tilde{I}_{tl_{iQ}} I_{tl_{iD}}) \\
& + \sum_i C_{\text{bus}_i} (\tilde{V}_{iD} V_{iQ} - \tilde{V}_{iQ} V_{iD}) \\
& + \sum_i L_{\text{svc}_i} (\tilde{I}_{\text{svc}_{iD}} I_{\text{svc}_{iQ}} - \tilde{I}_{\text{svc}_{iQ}} I_{\text{svc}_{iD}}) \\
& + \sum_i C_{\text{svc}_i} (\tilde{V}_{\text{svc}_{iD}} V_{\text{svc}_{iQ}} - \tilde{V}_{\text{svc}_{iQ}} V_{\text{svc}_{iD}}) \\
& + \sum_i (\psi_{q_i} \tilde{i}_{d_i} - \psi_{d_i} \tilde{i}_{q_i})
\end{aligned} \tag{19.13}$$

The goal of the control is to make sure that the power accumulated in these elements matches the power disturbances. If this happens, the entire disturbance energy will be accumulated in the electromagnetic elements and the rotational energy of the generators will be unaffected. Therefore, the control error signal $e(t)$ can be written as

$$e(t) = \dot{v}^{\text{ref}}(t) - \dot{v}_{\text{acc}}(t) = P^{\text{ref}}(t) - \dot{v}_{\text{acc}}(t) \tag{19.14}$$

For tracking purposes, the reference is taken to be the additional power created by the disturbance. In the case of wind fluctuations it is the difference between the expected and the actual wind power. In the case of a fault it is the power imbalance created by the fault.

The energy function control in its fundamental form requires a full state feedback. However, after analyzing the energy level of the different devices, it is noticed that the energy accumulated in the transmission lines is low. Therefore, the number of states required in the control algorithm can be reduced only to that number of states accumulating high amounts of energy. If this simplification is made, then the control law becomes the output feedback.

19.4.4 Communication Requirements and Control Limitations of FACTS

Based on the above proposed controller design, it is plausible to use FACTS devices to transiently stabilize system response to large disturbances. However, the implementation of this controller must be carefully considered, as discussed below.

19.4.4.1 Communication Requirements

The electromagnetic energy is mostly accumulated inside FACTS devices and large generator windings. Therefore, information about accumulated energy of these devices has to be transferred to the controllers on FACTS. As already stated, PMUs provide sensing fast enough to capture the relevant deviations of the generator states. The communication channels have to be fast enough in delivering this information to the controllers. A small analysis on how a delay in communication affects controller performance is given in [4].

It is desirable, in fast control applications such as this one, that the controllers be decentralized. Because they are based on the energy accumulation, the controllers do not need to communicate with each other. However, the energy accumulated in the generators has to be measured or estimated accurately at the location of the controller in order to make the controller completely decentralized. This is a topic that will be explored in future work.

19.4.4.2 Fundamental Limitations of FACTS Controllers

FACTS do not have any resistive or dissipative elements. Therefore, their effect in response to disturbances can only be temporary. This is the first and most important limitation.

The second limitation is the amount of energy FACTS devices are able to accumulate. This property correlates directly with the time interval during which the control is effective. The more energy FACTS is able to accumulate, the longer it will preserve system stability. The limitation on the energy accumulation of FACTS is determined by the maximum rating of the capacitor voltage and inductor current. Exact rating specifications remain an open question for future work.

19.4.5 Energy-Based Control of SVC in the Flores Power System

The SVC from Table 19.2 is placed on the wind generator bus in order to stabilize the system. With the controller on the SVC, the response of the system to the

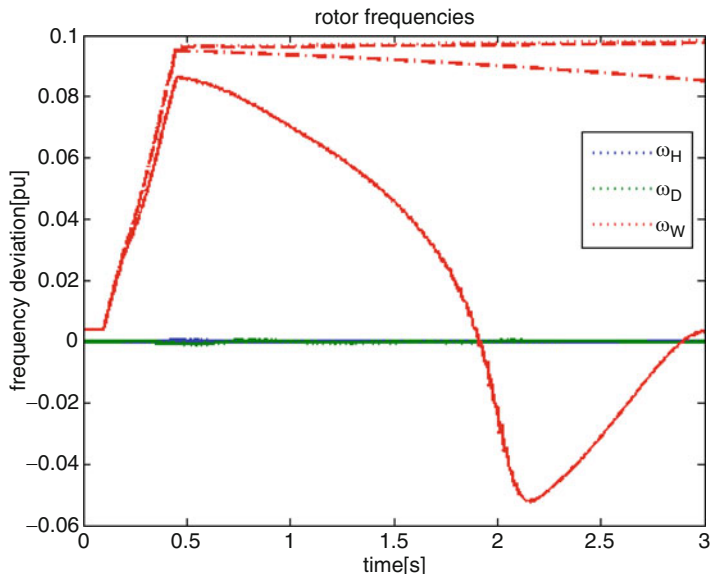


Fig. 19.13 Mechanical frequency of all generators in the system during a short-term high-magnitude wind perturbation: (a) dashed (without control on the SVC), (b) solid (with control on the SVC)

disturbances given in Figs. 19.2 and 19.3 is shown in the figures of this section. The control on the generator side is not the topic of this chapter, and therefore, the mechanical power inputs to all generators are taken as constants. The mechanical power of the wind turbine is an exception because it changes as the disturbance changes. The voltage on the hydro and diesel generators is controlled using the standard IEEE type 1 exciter with standard parameters. The exciter model is given in the Appendix.

19.4.5.1 SVC-Based Stabilization of High-Energy Wind Disturbances

Short-term high-magnitude wind power perturbation is simulated using a tenfold increase in the mechanical power input on the wind generator. Figure 19.13 shows a comparison of the mechanical frequencies of generators (a) without control on the SVC and (b) with control on the SVC. The uncontrolled case is unstable while control on the SVC improves the stability of the system.

It is interesting to show how the voltage magnitude of the three buses changes as a consequence of the control actions. Figure 19.14a shows high voltage spikes on the time scales which are not visible without time-varying phasors. The same fast voltage reaction to the SVC control actions helps improve the system stability. This observation can also be made by looking at the electrical power output of the three generators, shown in Fig. 19.14b.

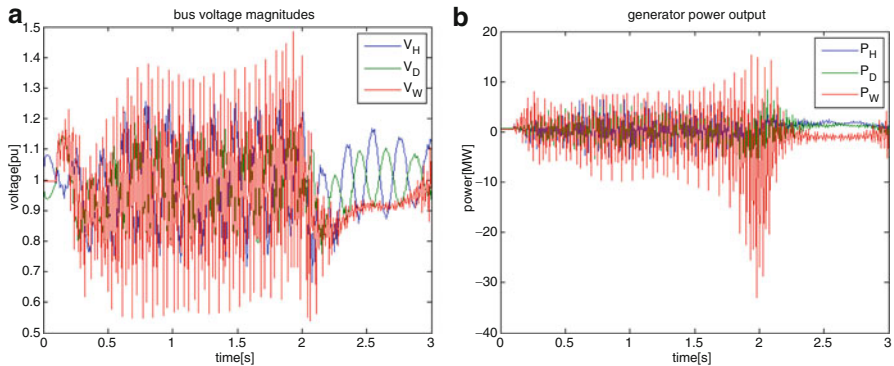


Fig. 19.14 (a) Voltage on the buses and (b) the electric power output of the generators if the system is controlled by the proposed energy-based controller

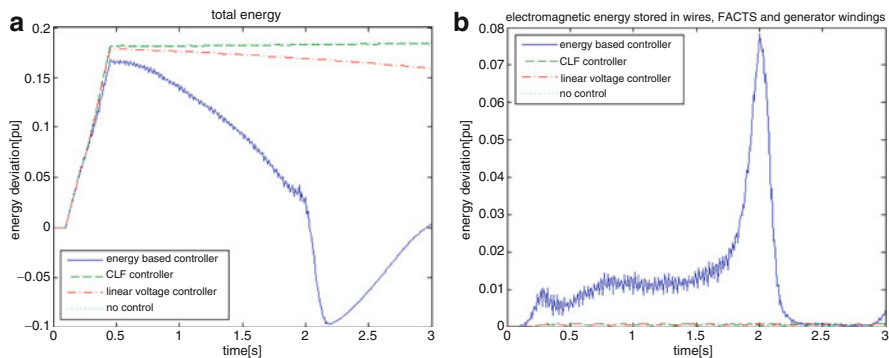


Fig. 19.15 (a) Total accumulated energy and (b) total accumulated electromagnetic energy in a system controlled by different controllers

The short-term high-magnitude wind power disturbance is further simulated to show the comparison of the control laws introduced in Sect. 19.3. Figure 19.15 shows both the total energy and the total electromagnetic energy accumulated in the system when different control laws are used. The total energy $v(x)$ is calculated using (19.9), while the total electromagnetic energy $v_{em}(x)$ is equal to the sum of the energies of all the electromagnetic elements in the system, including the transmission lines, FACTS, loads, and generator windings.

The difference between the accumulated electromagnetic energy, shown in Fig. 19.15b, in the case when the system is controlled by energy-based control, as opposed to the system being under other controls, is obvious. The accumulated electromagnetic energy is much higher in the first case. This is a consequence of the control law that tries to increase this energy, while at the same time reducing the energy accumulated in rotation.

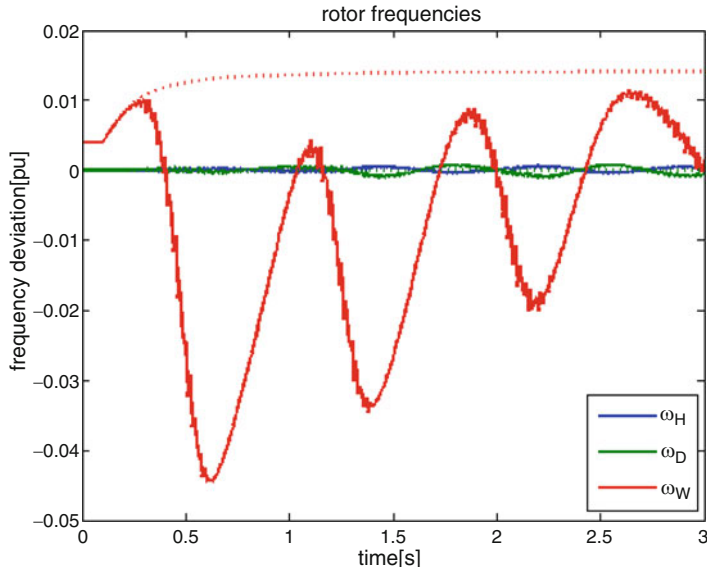


Fig. 19.16 Mechanical frequency of all generators in the system during a long-term low-magnitude wind power perturbation: (a) dashed (without control on the SVC), (b) solid (with control on the SVC)

The total system energy, shown in Fig. 19.15a, is lower in the case with an energy-based controller. The reason for this is the following. A high accumulation of electromagnetic energy means that high current and voltages exist. The higher these are, the bigger the dissipation is inside the resistive elements. Therefore, the total accumulated energy quickly decreases.

Long-term low-magnitude wind power perturbation is simulated using a two and a half-fold increase in the mechanical power input on the wind generator. The system slowly becomes unstable during this disturbance. Figure 19.16 shows the comparison of the mechanical frequencies of generators (a) without control on the SVC and (b) with control on the SVC. The uncontrolled case is clearly unstable. The frequency of all the generators is stabilized by using the proposed controller.

19.4.5.2 SVC-Based Stabilization of Large Disturbances Caused by Faults

The first major equipment failure is simulated as a short circuit on the hydro generator bus. Figure 19.17 shows the comparison of the mechanical frequencies of generators (a) without control on the SVC and (b) with control on the SVC. In both cases the frequency returns to equilibrium. By looking only at the frequency, it is not easy to conclude anything about the stability. Therefore, Fig. 19.18 shows how

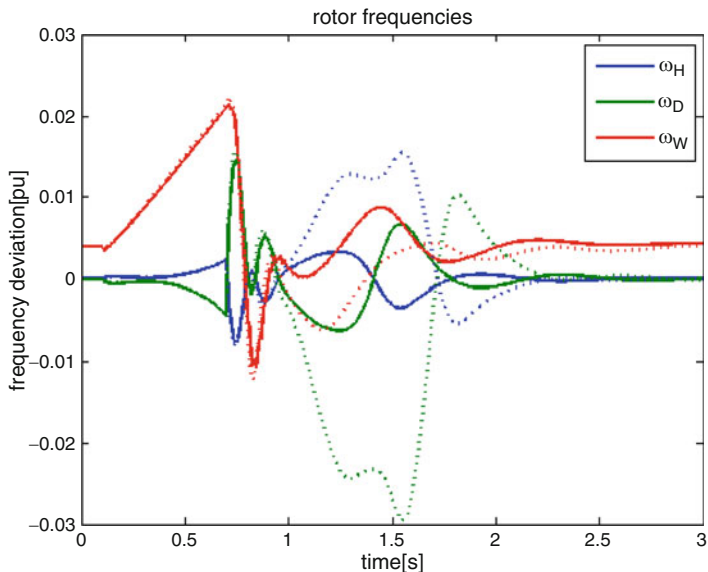


Fig. 19.17 Mechanical frequency of all generators in the system under a short circuit disturbance on the hydro generator bus: (a) dashed (without control on the SVC), (b) solid (with control on the SVC)

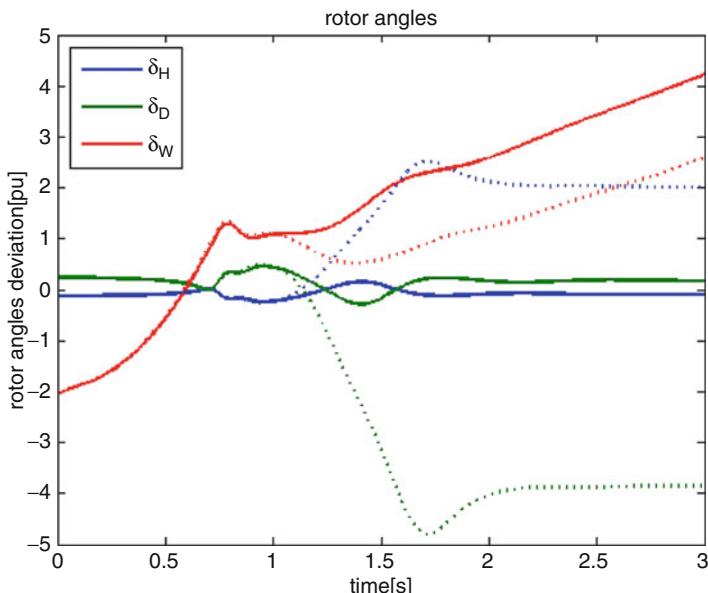


Fig. 19.18 Rotor angle deviation of all generators in the system under a short circuit disturbance on the hydro generator bus: (a) dashed (without control on the SVC), (b) solid (with control on the SVC)

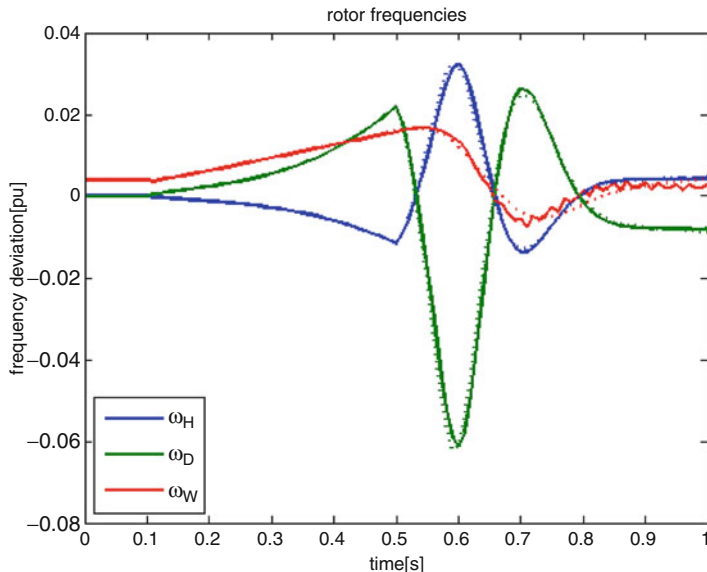


Fig. 19.19 Mechanical frequency of all generators in the system under a short circuit disturbance on the diesel generator bus: (a) dashed (without control on the SVC), (b) solid (with control on the SVC). The critical clearing time of the system has not been reached

the rotor angles behave during and after the fault. There is a very large difference between the uncontrolled and the controlled case. Clearly, the uncontrolled case is unstable.

Another interesting case can be considered. It is the one in which the transmission line between the diesel and the wind bus is removed, physically dividing the power system into two systems. The critical frequency belongs to the diesel generator in that case, and the controller on the SVC is helpless to prevent the instability. However, it can shape the wind frequency response before the system reaches its critical clearing time, as shown in Fig. 19.19.

Based on the above simulations, it can be concluded that FACTS devices can stabilize the system in response to high energy disturbances during time intervals when more conventional SVC control cannot. The size of the disturbance the FACTS devices are able to deal with will depend on their accumulation capacity.

19.5 Transient Stabilization Using Flywheels

Flywheel energy storage systems have several advantages compared to FACTS devices. Flywheels' ability to permanently store mechanical energy can help in system stabilization during disturbances. This section will first introduce the concept

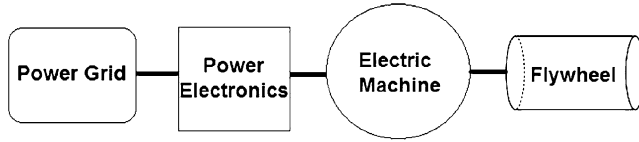


Fig. 19.20 Interface between the power grid and the flywheel

of sliding mode control applied to flywheels. Then using flywheels for stabilization in response to wind disturbances on the Flores system is analyzed. Stabilization using flywheels will first be analyzed by treating the wind generator as a pure disturbance and then by including the full dynamics of the entire system.

19.5.1 Introduction to Flywheel Energy Storage Systems

Flywheels are one of many mechanisms that can be used for storing energy. A flywheel energy storage system stores mechanical energy by accelerating a rotor, called the flywheel, to a very high speed. A flywheel energy storage system consists of the flywheel itself and the electric machine that the flywheel is connected to. When used in power system applications, high-speed power electronics will interface between the electric machine and the power grid as shown by Fig. 19.20. When the flywheel stores energy from the power grid, the electric machine acts as a motor, and the flywheel accelerates. Conversely when the flywheel supplies energy to the power grid, the electric machine acts as a generator and the flywheel decelerates. Flywheels can be used in many power systems applications, such as frequency stabilization, uninterruptible power supply, and reactive power control.

The amount of energy stored in the flywheel at any time is given by

$$W = 0.5J\omega^2 \quad (19.15)$$

where ω is the rotational velocity and J is the moment of inertia of the flywheel.

For a simple flywheel of radius r whose mass M is concentrated at the rim, the moment of inertia is simply

$$J = Mr^2 \quad (19.16)$$

When the flywheel is rotating, the tensile stress at the rim is

$$\sigma = \rho\omega^2r^2 \quad (19.17)$$

where ρ is the mass density of the flywheel.

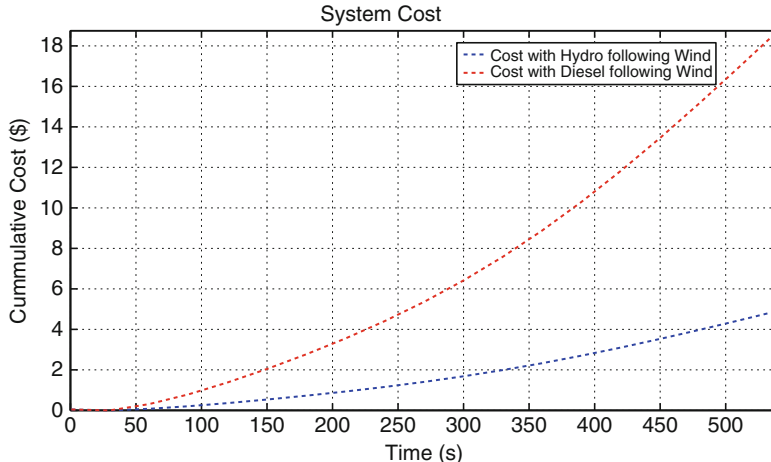


Fig. 19.21 Cost of energy storage systems: (1) hydrogen, (2) thermal, (3) flywheel, (4) compressed air-gas turbine, (5) underground pumped hydro, (6) advanced batteries, (7) advanced batteries with credit for dispersed siting [12]

The amount of energy a flywheel can store is determined by the maximum tensile stress the flywheel can withstand, which depends on the specific material used. The maximum energy the flywheel can store can be expressed as

$$W_{\max} = \frac{0.5M\sigma_{\max}}{\rho} \quad (19.18)$$

Due to this energy limitation, often an array of flywheels is used as opposed to one single flywheel.

It is of interest to compare flywheels to other storage devices. Other storage alternatives include chemical batteries, pumped hydro, thermal energy storage, hydrogen, and compressed air energy storage. One drawback to flywheels is that they typically have lower energy capacities than other storage alternatives as shown in Table 19.4 [12]. Also as Fig. 19.21 shows, flywheels are more costly than other storage alternatives for supplying a specific amount of power for a lengthy amount of time. For these reasons, other storage alternatives are more suitable than flywheels for large-scale power applications.

For small-scale applications, such as frequency regulation, flywheels have many benefits. Flywheels have an efficiency of around 85%, which is higher than for other storage alternatives in Table 19.4 [12]. This efficiency is measured by the percentage of the initial energy that is recovered when discharging immediately after charging. The main sources of loss are from windage, which can be reduced by running the flywheel in a vacuum, and from the bearings that support the flywheel, which can be reduced by using magnetic instead of mechanical bearings.

Table 19.4 Comparison of energy storage alternatives [12]

Type of storage	Efficiency (%)	Reasonable energy capacity (J)	Construction time (years)	Lifetime (years)	Number of cycles	Reverse time (s)
Flywheel	85	10^9	3	20	Unlimited	0.1
Batteries	80	Not constrained	2	10	500	0.01
Pumped hydro	80	10^{13}	8	50	Unlimited	10
Thermal	75	10^{11}	12	30	Unlimited	Tens of minutes
Hydrogen	50	10^{12}	3	25	Unlimited	360

Flywheels are very well suited for applications in which the power demand changes quickly because flywheels have an extremely small reverse time, which allows power to be delivered or consumed practically on demand. Among the energy storage types in Table 19.4, only chemical batteries have a reverse time as small as flywheels. Advantages of flywheels compared to chemical batteries are that they have twice the lifespan and they are not limited to a certain number of charge-discharge cycles. Finally flywheels are also environmentally benign.

19.5.2 Concept of Sliding Mode Control Applied to a Flywheel

Sliding mode control is a nonlinear variable structure control method where the feedback control law is not a continuous function of time, but rather switches from one continuous structure to another. Sliding mode control can be used to control the amount of electric torque supplied to a flywheel.

If the flywheel is connected to a permanent magnet synchronous machine (PMSM), the dynamic equations governing the flywheel energy storage system are [10]

$$T_e = J \frac{d\omega_f}{dt} + D\omega_f \quad (19.19)$$

$$v_{qs} = r_s i_{qs} + L \frac{di_{qs}}{dt} + \omega_f L i_{ds} + \omega_f \lambda_m \quad (19.20)$$

$$v_{ds} = r_s i_{ds} + L \frac{di_{ds}}{dt} - \omega_f L i_{qs} \quad (19.21)$$

$$T_e = \frac{N}{2} \lambda_m i_{qs} \quad (19.22)$$

The constant D is the damping coefficient of the flywheel and the electric machine associated with the rotational movement. Because flywheel energy storage systems typically operate in a vacuum, the damping coefficient is negligible, and it is assumed in this chapter that D is zero.

Table 19.5 Flywheel energy storage system parameters [10]

Moment of inertia J	0.63 kg m ²
Number of poles N	2
Back-EMF constant λ_m	5.95 V/krpm
Winding resistance r_s	8.17 mΩ
Winding inductance L	91.3 μH

When T_e is positive, the PMSM acts as a motor and the flywheel will accelerate. Conversely, when T_e is negative, the PMSM acts as a generator and the flywheel will decelerate.

The mechanical power P_{mech} delivered to the flywheel is

$$P_{\text{mech}} = T_e \omega_f \quad (19.23)$$

The flywheel energy storage system model can be represented in state-space form as follows:

$$\begin{aligned} \dot{x} &= Ax + Bu \\ y &= Cx \end{aligned} \quad (19.24)$$

where

$$\begin{aligned} x &= [i_{qs} \ i_{ds} \ \omega_f]^T \\ u &= [v_{qs} \ v_{ds}]^T \\ y &= [i_{qs} \ i_{ds} \ \omega_f]^T \end{aligned} \quad (19.25)$$

$$A = \begin{bmatrix} -r_s & -\omega_f & -i_{ds} - \frac{\lambda_m}{L} \\ \frac{r_s}{L} & -\frac{r_s}{L} & i_{qs} \\ \frac{P\lambda_m}{2J} & 0 & 0 \end{bmatrix} \quad (19.26)$$

$$B = \begin{bmatrix} \frac{1}{L} & 0 \\ 0 & \frac{1}{L} \\ 0 & 0 \end{bmatrix} \quad (19.27)$$

$$C = \begin{bmatrix} 1 & 0 & 0 \\ 0 & 1 & 0 \\ 0 & 0 & 1 \end{bmatrix} \quad (19.28)$$

The parameters used are specified in Table 19.5.

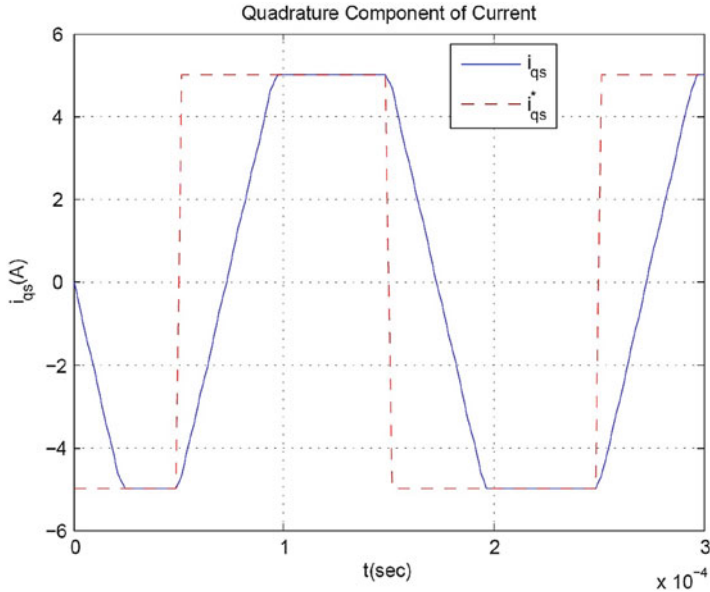


Fig. 19.22 Sliding mode control, i_{qs} response

In order to control the electric torque supplied by the PMSM, it is necessary to be able to control i_{qs} to a desired value. Sliding mode control can be used to drive i_{qs} and i_{ds} to the desired values by a fast switching of v_{qs} and v_{ds} . [11]

Let i_{qs}^* and i_{ds}^* denote the desired values of i_{qs} and i_{ds} . The switching function is then given by

$$s_{ds} = i_{ds}^* - i_{ds} \quad (19.29)$$

$$s_{qs} = i_{qs}^* - i_{qs} \quad (19.30)$$

The voltage inputs are then controlled by the following nonlinear control law:

$$v_{ds} = V_0 * \text{sign}\{s_{ds}\} \quad (19.31)$$

$$v_{qs} = V_0 * \text{sign}\{s_{qs}\} \quad (19.32)$$

where V_0 is a constant DC voltage. Thyristor switching in a bidirectional converter can be implemented in order to switch the values of v_{qs} and v_{ds} almost instantaneously.

For an example of sliding mode control, let $V_0 = 20$ V, $i_{ds}^* = 0$ A, and i_{qs}^* is -5 A from $0 < t < 0.5^{-4}$ s, 5 A from $0.5^{-4} < t < 1.5^{-4}$ s, -5 A from $1.5^{-4} < t < 2.5^{-4}$ s, and 5 A from $2.5^{-4} < t < 3.0^{-4}$ s. Initial conditions of all state variables are zero. Figures 19.22, 19.23, 19.24, and 19.25 show the time response of i_{qs} , i_{ds} , ω_f , and T_e , respectively.

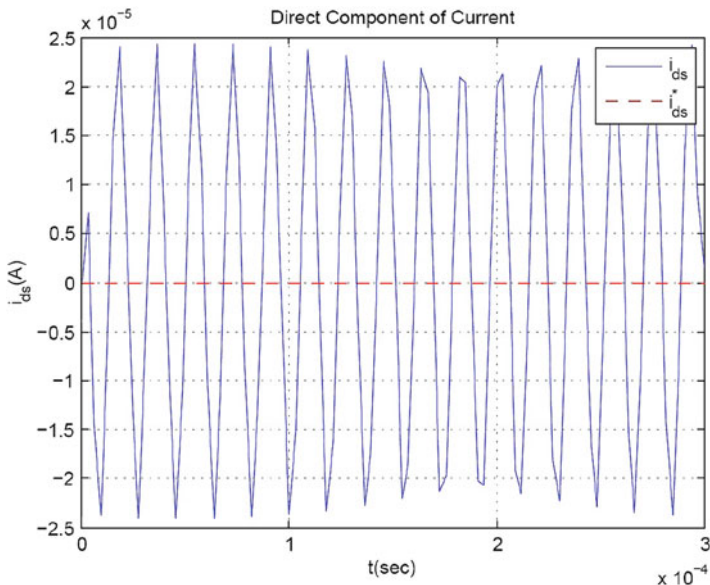


Fig. 19.23 Sliding mode control, i_{ds} response

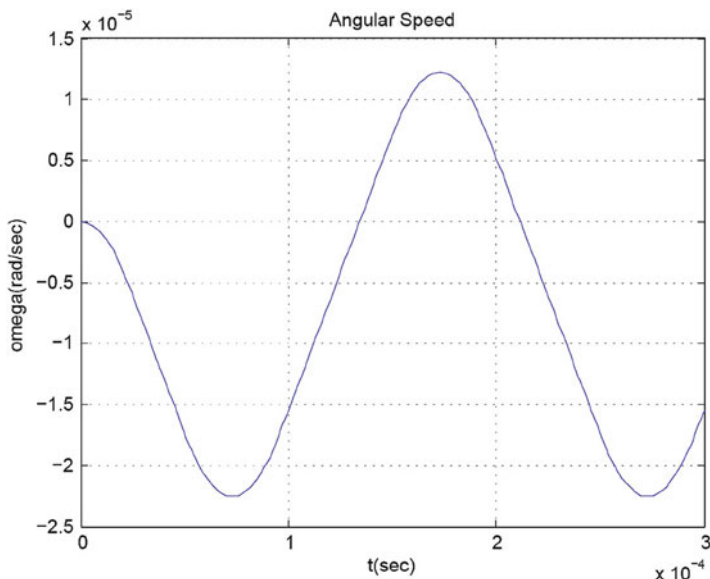


Fig. 19.24 Sliding mode control, ω response

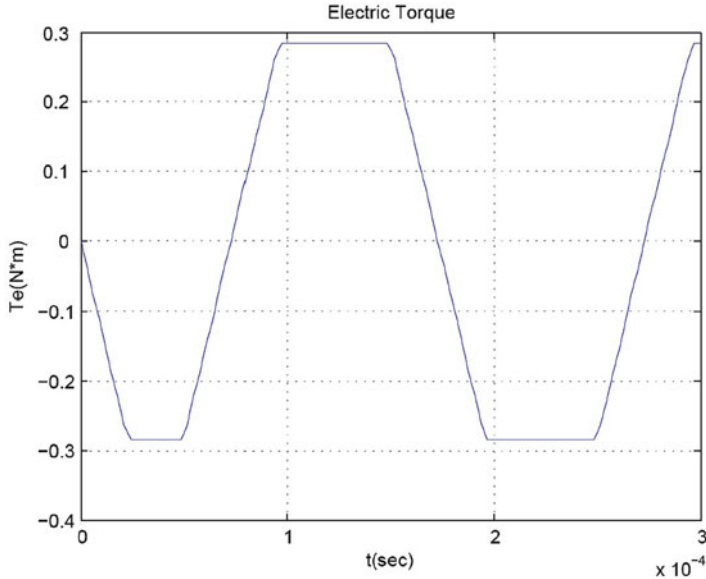


Fig. 19.25 Sliding mode control, electric torque response

As can be seen from the figures the desired values i_{qs}^* and i_{ds}^* are reached extremely quickly (on the order of 10^{-4} s) with sliding mode control. The response of the mechanical variable, ω_f , is much slower than the electrical variables. When i_{qs} is positive, ω_f increases while when i_{qs} is negative, ω_f decreases.

It should be noted that in order for s_{qs} to decay to zero, s_{qs} and the time derivative of s_{qs} must have opposite signs. Analogously, in order for s_{ds} to decay to zero, s_{ds} and the time derivative of s_{ds} must have opposite signs. Mathematically in order for these two conditions to be met, the DC voltage V_0 must be sufficiently large such that

$$V_0 > \left| \frac{Li_{ds}^*}{dt} + Ri_{ds} - L\omega_f i_{qs} \right| \quad (19.33)$$

$$V_0 > \left| \frac{Li_{qs}^*}{dt} + Ri_{qs} + L\omega_f i_{ds} + \lambda_0 \omega_f \right| \quad (19.34)$$

19.5.3 Sliding Mode Control Representing the Wind Generator as a Disturbance

We will now consider the Flores island system shown in Fig. 19.1. We will consider the two types of wind disturbance shown in Fig. 19.2. In this subsection, we will represent the wind generator as a pure disturbance while in the next subsection, we will include the full dynamics of the entire system.

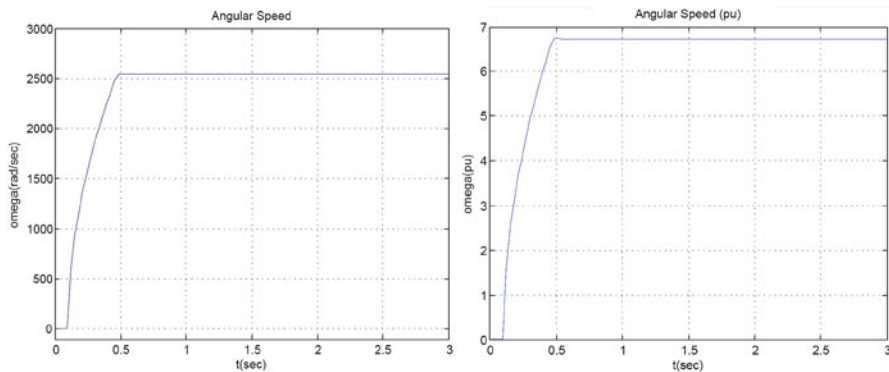


Fig. 19.26 Speed of the flywheel in response to a short wind disturbance

When treating the wind generator as a pure disturbance, the amount of power that should be supplied to the flywheel is determined by the deviation in the power output of the wind generator. If the power output of the wind generator is too high, then power should be supplied to the flywheel and the flywheel should accelerate. Alternatively, if the power output of the wind generator is too low, then power should be taken from the flywheel and the flywheel should decelerate.

For the short-term high-magnitude wind disturbance shown in Fig. 19.2, ΔP_{wind} is 5.4 per unit, or 5.4 MW from $t = 0.1$ s to $t = 0.45$ s. For the long-term high-magnitude wind disturbance, ΔP_{wind} is 0.9 per unit, or 0.9 MW after $t = 0.1$ s. The flywheel should be controlled to absorb the wind disturbance power:

$$P_{\text{fly}} = \Delta P_{\text{wind}} \quad (19.35)$$

The desired electric torque supplied to the flywheel is controlled by the sliding mode control. The torque will have to vary following the variations in speed of the flywheel in order to control the power supplied to the flywheel:

$$T_e^* = \frac{\Delta P_{\text{wind}}}{\omega_f} \quad (19.36)$$

Using this control, Figs. 19.26–19.29 show the response of the flywheel in response to the short disturbance. The responses are shown in both regular units and in the per unit system.

It can be seen that the flywheel stores energy and increases speed during the wind disturbance between $t = 0.1$ s and $t = 0.45$ s. Since the flywheel's speed is increasing, the electric torque decreases in order to maintain constant power delivery to the flywheel. By $t = 0.45$ s, the flywheel's speed has increased to around 2,500 rad/s. After $t = 0.45$ s, since the wind disturbance is over, the flywheel maintains a constant speed, and neither receives nor delivers power.

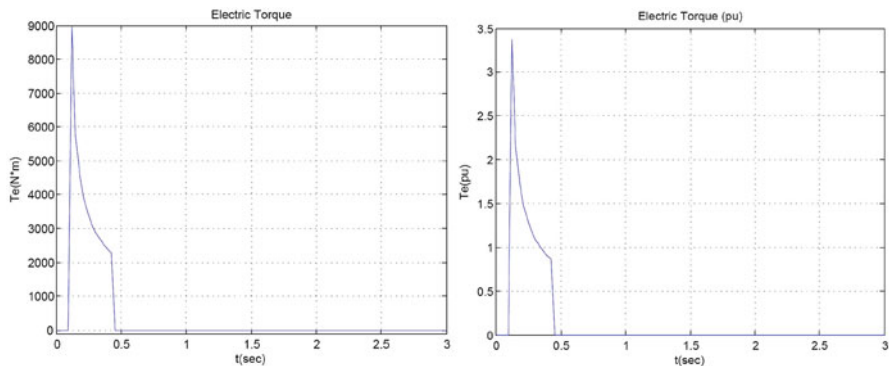


Fig. 19.27 Electric torque exerted on the flywheel in response to a short wind disturbance

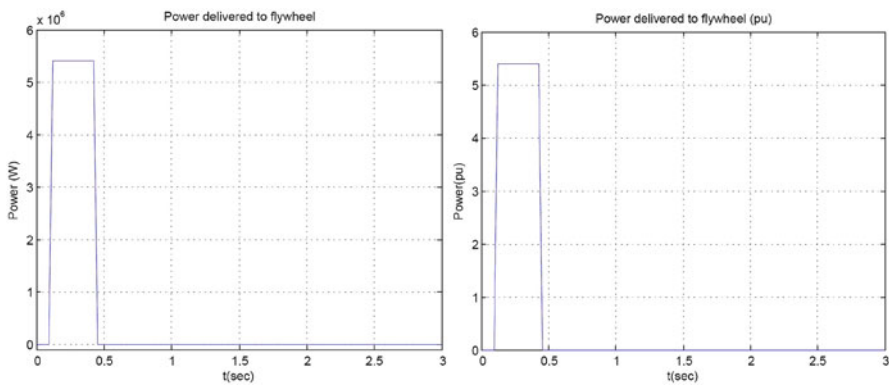


Fig. 19.28 Power delivered to the flywheel in response to a short wind disturbance

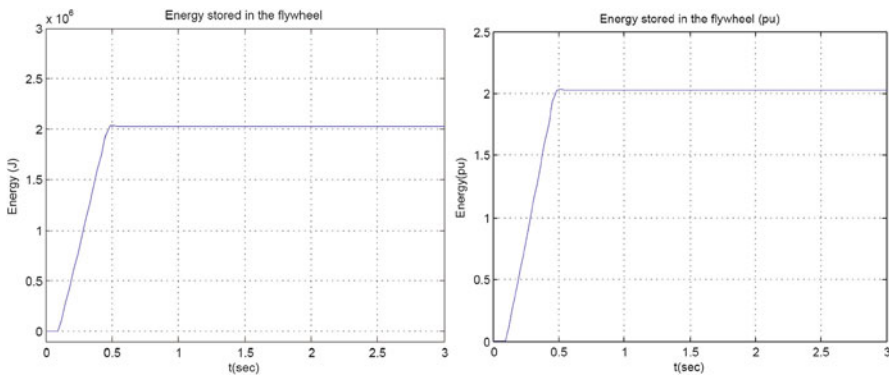


Fig. 19.29 Energy stored in the flywheel in response to short wind disturbance

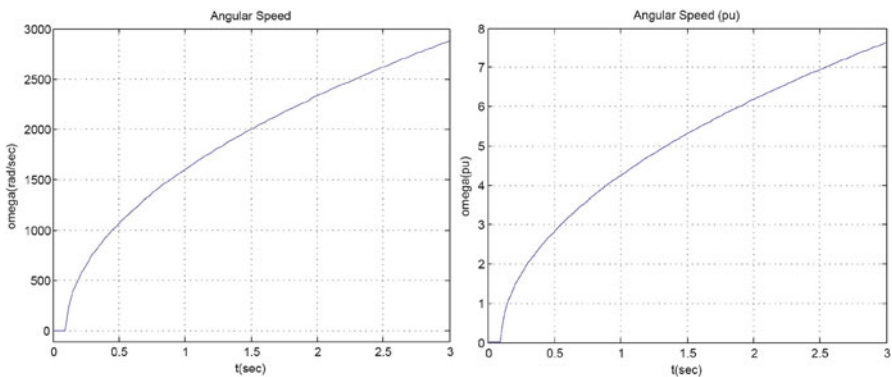


Fig. 19.30 Speed of the flywheel in response to a long wind disturbance

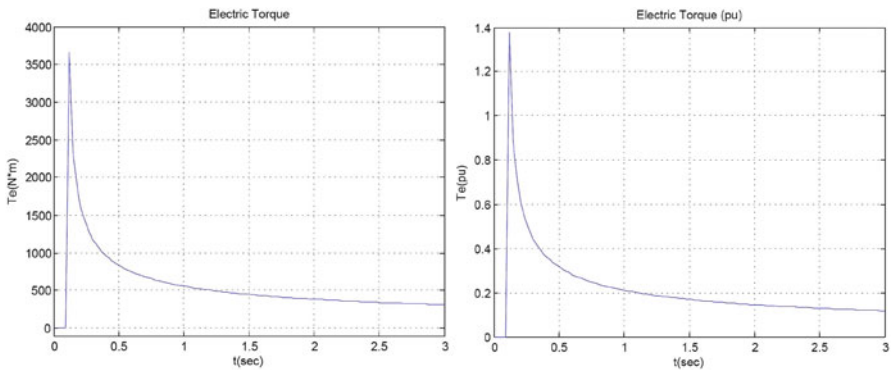


Fig. 19.31 Electric torque exerted on the flywheel in response to a long wind disturbance

Figures 19.30–19.33 show the response of the flywheel in response to the long disturbance. The responses are shown in both regular units and in the per unit system.

It can be seen that the flywheel is constantly accelerating after $t = 0.1$ s. Since the flywheel's speed is increasing, the electric torque decreases in order to maintain constant power delivery to the flywheel. By $t = 3$ s, the flywheel's speed has increased to around 2,900 rad/s.

There is, however, a limit to the length of a wind disturbance the flywheel can stabilize for, which is based on the maximum amount of energy the flywheel can store. Typically, the maximum amount of energy that the flywheel energy storage systems can store is around 10^9 J [12]. Therefore, for the long wind disturbance magnitude considered in this chapter, the flywheel could absorb power for around 1,000 s before the energy limit is reached.

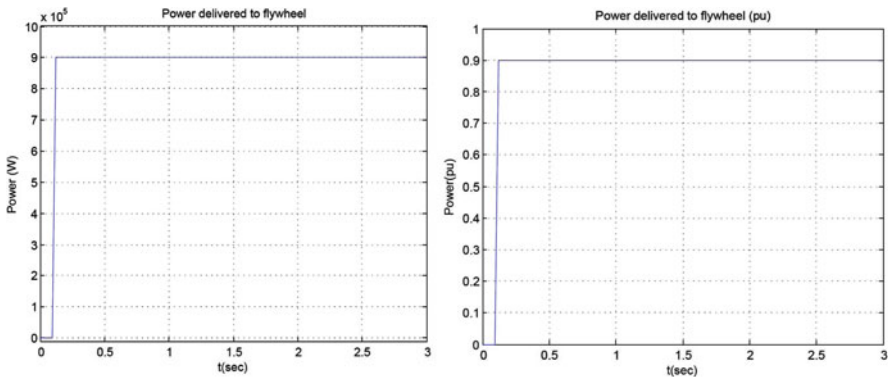


Fig. 19.32 Power delivered to the flywheel in response to a long wind disturbance

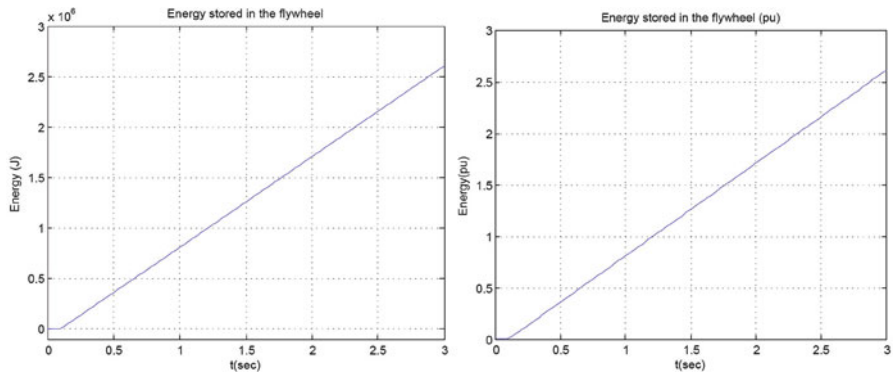


Fig. 19.33 Energy stored in the flywheel in response to a long wind disturbance

19.5.4 Sliding Mode Control Using the Full Dynamic Model of the Interconnected System

It is now of interest to combine the flywheel with the rest of the Flores power grid. Figure 19.34 illustrates this combination.

In the new power electronics design interfacing between the flywheel and the wind generator, there are four switches and two capacitors [13]. The four switches act as a bidirectional switch that controls the polarity of the small capacitor. The large capacitor is included in the design to ensure that the voltage across the wind generator remains close to constant even as the polarity of the small capacitor changes.

The four switches open and close at a very high frequency relative to the rest of the power grid. Therefore, two time scales will be used: t , which is the fast time scale, and τ , which is the slow time scale.

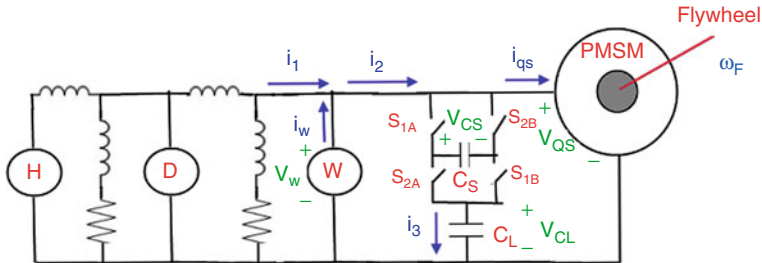


Fig. 19.34 Full diagram connecting the flywheel to Flores

When switches S_{1A} and S_{1B} are closed, the differential equation governing the voltage across the small capacitor is

$$i_3 = C_s \frac{dv_{cs}^+}{dt} \quad (19.37)$$

Alternatively, when switches S_{2A} and S_{2B} are closed, the differential equation governing the voltage across the small capacitor is

$$i_3 = -C_s \frac{dv_{cs}^-}{dt} \quad (19.38)$$

Using state-space averaging, the voltage across the small capacitor can be expressed in the slow time scale τ as follows:

$$\bar{v}_{cs}(\tau) = \frac{v_{cs}^+ t^+ + v_{cs}^- t^-}{t^+ + t^-} \quad (19.39)$$

For the flywheel, the direct component of the current through the stator windings i_{ds} is assumed to be zero for simplification. Therefore, the flywheel differential equations become

$$T_e = J \frac{d\omega_f}{d\tau} \quad (19.40)$$

$$v_{qs} = r_s i_{qs} + L \frac{di_{qs}}{dt} + \omega_f \lambda_m \quad (19.41)$$

Notice that the differential equation governing the electrical variable i_{qs} is in the fast time scale t , while the differential equation governing the mechanical variable is in the slow time scale τ .

There are several coupling equations connecting the state variables of the flywheel and the power electronics with the state variables of the rest of the system. The coupling equations are in the slow time scale τ .

The voltage across the wind generator, by Kirchoff's voltage law, is

$$v_w(\tau) = \bar{v}_{cs}(\tau) + v_{cl}(\tau) \quad (19.42)$$

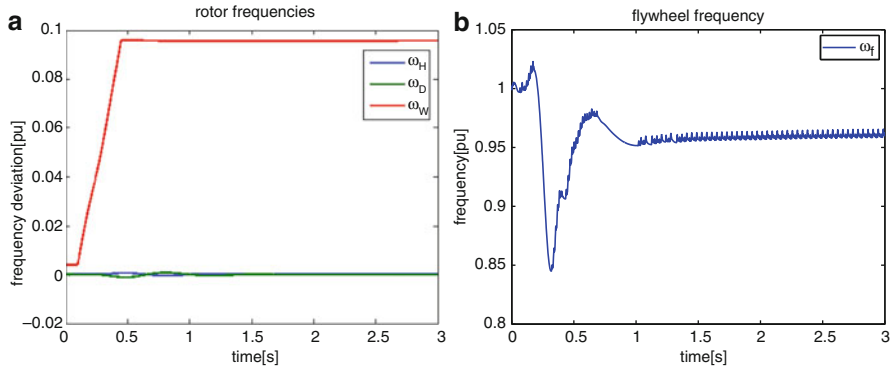


Fig. 19.35 Frequency of (a) the hydro, diesel, and wind generators, and (b) the flywheel, in the Flores system

Additionally, by Kirchoff's current law,

$$i_1(\tau) + i_w(\tau) = i_2(\tau) \quad (19.43)$$

$$i_2(\tau) = i_3(\tau) + i_{qs}(\tau) \quad (19.44)$$

The rest of the power system is modeled as explained in Sect. 19.4.2.

The first disturbance in Fig. 19.2, the short-term high perturbation of wind, is used in the following simulations. Figure 19.35a shows the frequencies of all three generators when the system is controlled using a flywheel. In order to make the nominal frequency of the flywheel 1 pu, the parameter λ_m is tuned to be 0.9644 pu. As can be noticed, the frequency of the wind generator does not drop. The reason for this is that the control logic behind the flywheel is based on stabilization, while the control logic of the FACTS devices is regulation based. In the case of the flywheel, the reference for the control is zero current flowing into the flywheel ($i_{qs}^* = 0$ A). Therefore, the flywheel does not try to accumulate the energy of the disturbance as the FACTS devices did.

Figure 19.35b shows the frequency of the flywheel. Figure 19.36 shows the response of the voltage of the three buses and the electrical power output of the three generators.

19.6 Conclusions

This chapter has shown the potential of power-electronically switched devices to stabilize a power system in response to disturbances. Since FACTS devices cannot permanently store energy, they can only stabilize the system for a limited amount of time. If longer-term stabilization is necessary, then flywheels are a good alternative.

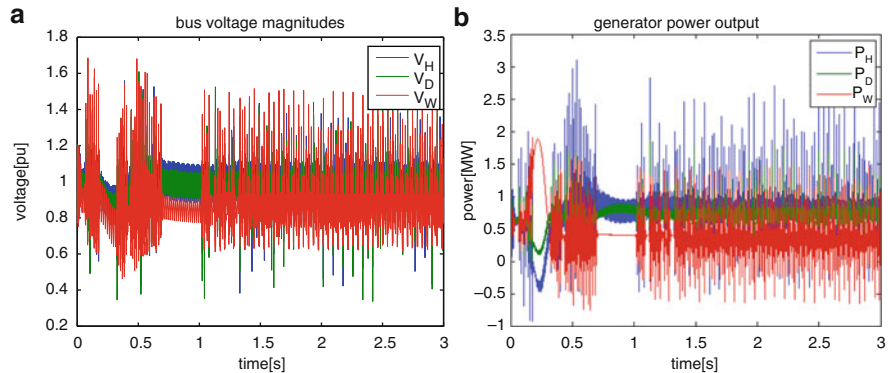


Fig. 19.36 (a) Voltage and (b) electrical power of the hydro, diesel, and wind generators in the Flores system controlled by flywheel

An open question remains concerning a systematic method for determining the specifications of the inductors and capacitors in FACTS devices needed to transiently stabilize a large disturbance of a given type. A fundamental understanding of the effects of very fast switching in the nonlinear dynamics of future electric energy systems will be addressed in future work.

Acknowledgments The authors would like to thank the ECE Sack Fellowship and the SRC Smart Grid Research Center for their financial support which made this work possible.

19.7 Appendix A

19.7.1 Derivation of SVC Time Varying Phasor Model

The derivation presented here is similar to the more strict and formal derivation of time varying phasor dynamic models introduced in [8] and [9]. SVC dynamic equations in time domain are given below while the SVC structure is shown in Fig. 19.4.

$$\begin{aligned}\dot{v}(t) &= \frac{1}{C} (i_{ll}(t) - i(t)) \\ i(t) &= \frac{\alpha(t)}{L} v(t)\end{aligned}$$

The equations can be rewritten using time varying phasor representation for each variable.

$$\begin{aligned}\frac{d}{dt}(V(t) \cos(\omega t + \theta(t))) &= \frac{1}{C} [I_{tl}(t) \cos(\omega t + \psi_{tl}(t)) \\ &\quad - I(t) \cos(\omega t + \psi(t))] \\ \frac{d}{dt}(I(t) \cos(\omega t + \psi(t))) &= \frac{\alpha(t)}{L} V(t) \cos(\omega t + \theta(t))\end{aligned}$$

After the trigonometric identities are introduced, carrier functions $\sin(\omega t)$ and $\cos(\omega t)$ can be removed by grouping the terms next to each of them. Dependence on time has been omitted for easier notation.

$$\begin{aligned}\frac{d}{dt}(V \cos \theta) &= \left[\frac{1}{C} (I_{tl} \cos \psi_{tl} - I \cos \psi) + \omega V \sin \theta \right] \\ \frac{d}{dt}(V \sin \theta) &= \left[\frac{1}{C} (I_{tl} \sin \psi_{tl} - I \sin \psi) - \omega V \cos \theta \right] \\ \frac{d}{dt}(I \cos \psi) &= \left[\frac{\alpha}{L} (V \cos \theta) + \omega I \sin \psi \right] \\ \frac{d}{dt}(I \sin \psi) &= \left[\frac{\alpha}{L} (V \sin \theta) - \omega I \cos \psi \right]\end{aligned}$$

The final form of the time varying phasor SVC dynamic model in Cartesian coordinates becomes

$$\begin{aligned}\dot{V}_D &= \frac{1}{C} (I_{tlD} - I_D) + \omega V_Q \\ \dot{V}_Q &= \frac{1}{C} (I_{tlQ} - I_Q) - \omega V_D \\ \dot{I}_D &= \frac{\alpha}{L} V_D + \omega I_Q \\ \dot{I}_Q &= \frac{\alpha}{L} V_Q - \omega I_D\end{aligned}$$

where subscripts D and Q indicate direct (real) and quadrature (imaginary) component of a phasor, respectively.

19.7.2 Flores System Equilibrium

All equilibrium values are given with respect to base power base $S_b = 10[\text{MVA}]$. The equilibrium values of the generator, shown in Table 19.6, are given using $V_b = 0.4[\text{kV}]$. Stator current I_{gs} is given in the network reference frame, while rotor damper I_{gr} and field winding I_{gf} currents are given in the rotor reference frame. The equilibrium values of the transmission system, shown in Table 19.7, are given using $V_b = 15[\text{kV}]$.

Table 19.6 Equilibrium of the generators of Flores power system

Generator	Hydro	Diesel	Wind
I_{gsD} [PU]	0.06643	0.06219	0.06916
I_{gsQ} [PU]	-0.00321	-0.02082	0.03340
I_{grD} [PU]	0	0	0.05735
I_{grQ} [PU]	0	0	0.02705
I_{gf} [PU]	-0.48134	-0.15584	NA
δ [rad]	-0.1270	0.2466	-2.0342
ω [PU]	1	1	1.004
V_r [PU]	1.1258	1.4855	NA
E_{fd} [PU]	0.9753	1.2397	NA
V_f [PU]	0	0	NA

Table 19.7 Equilibrium of the transmission system of Flores power system

Component	Real - D	Imag - Q
V_H [PU]	0.9724	-0.2201
V_D [PU]	0.9698	-0.2227
V_W [PU]	0.9676	-0.2339
$I_{l_{HD}}$ [PU]	0.06548	-0.00716
$I_{l_{DW}}$ [PU]	0.02056	0.02528
I_D [PU]	0.10580	-0.05924
I_W [PU]	0.06631	-0.03809
I_{svc} [PU]	-0.04677	-0.19353

19.7.3 Type I IEEE Exciter

Equations of the type 1 IEEE exciter used in this chapter are

$$\begin{aligned}\dot{V}_r &= -\frac{1}{T_A}V_r + \frac{K_A}{T_A} \left(V^{\text{ref}} - V - V_f \right) \\ \dot{E}_{fd} &= \frac{1}{T_E} \left(V_r - (K_E + S_E)E_{fd} \right) \\ \dot{V}_f &= -\frac{1}{T_F}V_f + \frac{K_F}{T_F} \dot{E}_{fd}\end{aligned}$$

where V_r , E_{fd} and V_f are the states of the exciter, V terminal voltage and $V^{\text{ref}} = 1$ [PU] the terminal voltage reference. The parameters of both exciters in Flores (on hydro and diesel generators) are the same, as shown in Table 19.8.

19.7.4 Dynamic Parameters of Generators

Generator data is given in Table 19.9 with respect to base power base $S_b = 10$ [MVA] and base voltage $V_b = 0.4$ [kV].

Table 19.8 Parameters of exciters

Parameter	Value
K_A [PU]	400
T_A [s]	0.02
K_E [PU]	1.3
T_E [s]	1
S_E [PU]	0.1667
K_F [PU]	0.03
T_F [s]	1

Table 19.9 Generator data

Generator	Hydro	Diesel	Wind
L_d [PU]	2.4	8.15	28.156
L_D [PU]	2.4	8.15	29.2
L_F [PU]	2.581	8.447	NA
L_q [PU]	1.437	8.15	28.156
L_Q [PU]	1.437	8.15	29.2
L_{ad} [PU]	2.038	7.556	27.075
L_{af} [PU]	2.038	7.556	NA
L_{df} [PU]	2.038	7.556	NA
L_{aq} [PU]	1.212	7.556	27.075
r_s [PU]	0.015	0.016	0.113
r_r [PU]	0.05	0.055	0.119
r_f [PU]	0.003	0.0031	NA
H [s]	2.159	1.133	0.233
D [PU]	0.02	0.005	0

References

1. M. Ghandhari, G. Andersson, I.A. Hiskens, Control Lyapunov functions for controllable series devices. *IEEE Trans. Power Syst.* **16**, 689–694 (2001)
2. M. Cvetkovic, M. Ilic, PMU based transient stabilization using FACTS, in *IEEE Power System Conference and Exposition*, March 2011
3. M. Noroozian, N.A. Petersson, B. Thorvaldson, A.B. Nilsson, C.W. Taylor, Benefits of SVC and STATCOM for electric utility application, in *IEEE PES Transmission and Distribution Conference and Exposition*, September 2003
4. M. Cvetkovic, M. Ilic, Nonlinear control for stabilizing power systems during major disturbances, in *IFAC World Congress*, August 2011
5. M. Ilic, M. Cvetkovic, K. Bachovchin, A. Hsu, Toward a systems approach to power-electronically switched T&D equipment at value, in *IEEE PES General Meeting*, July 2011
6. H.A. Pulgar-Painemal, P.W. Sauer, Dynamic modeling of wind power generation, in *North American Power Symposium*, October 2009
7. I. Boldea, *Synchronous Generators* (Taylor & Francis, London, 2006)
8. S.R. Sanders, J.M. Noworolski, X.Z. Liu, G.C. Vergheze Generalized averaging method for power conversion circuits. *IEEE Trans. Power Electron.* **6**(2), 251–259 (1991)
9. P. Mattavelli, G.C. Vergheze, A.M. Stankovic, Phasor dynamics of thyristor-controlled series capacitor systems. *IEEE Trans. Power Syst.* **12**, 1259–1267 (1997)
10. S. Talebi, B. Nikbakhtan, H.A. Toliyat, Analytical model-based analysis of high-speed Flywheel energy storage systems for pulsed power applications, in *Proceedings of ESTS 2009*, Baltimore, MD, 20–22 April 2009

11. V. Utkin, J. Guldner, J. Shi, *Sliding Mode Control in Electromechanical Systems* (Taylor & Francis, London, 1999)
12. A. Ter-Gazarian, *Energy Storage for Power Systems* (Institution of Engineering and Technology, London, 1994)
13. M. Cvetkovic, K. Bachovchin, M. Ilic, *A Power-Electronically-Controlled Switch Used for Advanced Control of Flywheels*, Provisional patent filing, Carnegie Mellon University, 22 Feb 2012
14. M.A. Pai, *Energy Function Analysis For Power System Stability* (Kluwer, Boston, 1989)

Part VII

Methods for Investing in New Technologies Under Uncertainties

Chapter 20

Generation Planning Under Uncertainty with Variable Resources

Audun Botterud, Noha Abdel-Karim, and Marija Ilić

20.1 Introduction

In this chapter we discuss generation expansion planning in systems with variable resources. The variability and uncertainty in renewable resources like wind and solar power pose new challenges from a long-term planning perspective. There is clearly a need to introduce cleaner sources of electricity generation for environmental reasons. However, at the same time, system reliability must be maintained while trying to minimize the total cost of meeting the electricity demand. We use a stochastic dynamic optimization model to analyze optimal expansion decisions considering uncertainty in wind power generation as well as future load. In a case study, we focus on the São Miguel Island and investigate how the uncertainty and variability in wind power and load impact optimal expansion decisions in the long run. We show that wind power is a cost-efficient expansion alternative on São Miguel, but that some dispatchable generation is also needed to compensate for the variability and uncertainty in wind power. We also analyze how demand response contributes to change the optimal portfolio of supply resources.

A. Botterud (✉)
Argonne National Laboratory, Argonne, IL 60439, USA
e-mail: abotterud@anl.gov

N. Abdel-Karim
Department of Engineering and Public Policy, Carnegie Mellon University,
5000 Forbes Ave, Pittsburgh, PA 15213, USA
e-mail: nabdelga@andrew.cmu.edu

M. Ilić
Department of Electrical and Computer Engineering, Carnegie Mellon University,
5000 Forbes Ave, Pittsburgh, PA 15213, USA
e-mail: milic@ece.cmu.edu

20.2 Modeling Framework

We build on the optimization model for generation expansion in electricity markets first proposed in [1, 2] and later expanded in [3]. The original model was inspired from real options theory for investments under uncertainty [4] and also from the theory of peak-load pricing [5]. We extend the model to consider wind power as an expansion candidate, and we represent the wind power variability in the system dispatch. Whereas the model developed in [1–3] was originally intended to analyze generation expansion decisions in restructured electricity markets, we now assume that the expansion decisions are made through centralized planning with the objective of maximizing social surplus in the system.

The generation expansion planning problem is formulated as a stochastic dynamic programming (SDP) problem. SDP has been used for generation expansion planning within the regulated industry in the past [6, 7], but typically for thermal or hydrothermal systems without consideration of variable renewable resources such as wind and solar energy. We differentiate between short- and long-term uncertainties in the generation expansion framework, as outlined below. We focus on generation expansion planning in this chapter. Detailed operational constraints and the impact of the transmission network are therefore not considered.

20.2.1 SDP Formulation with Short- and Long-Term Uncertainties

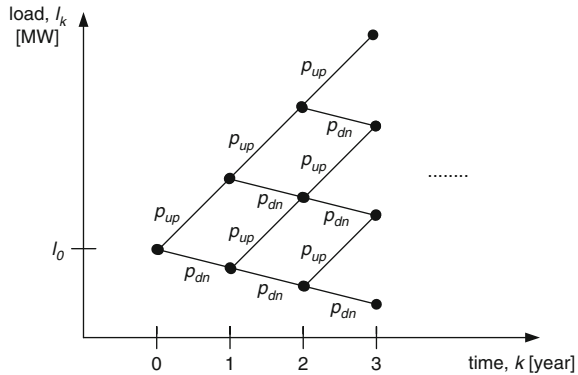
The overall problem for a centralized planner considering investing in new power generation can be stated as an optimization problem over a planning horizon of T years, as shown in (20.1)–(20.5). The objective is to maximize the sum of discounted social surplus over the planning horizon, considering supply costs and consumer benefits. We use a 1-year time resolution and assume that investments can only take place at the beginning of each year. In order to handle the value of a plant beyond the planning horizon, we adjust the investment costs according to its lifetime and the length of the planning period assuming a constant annuity. Hence, the termination payoff, g_T in (20.4), is simply the expected social surplus in the last period under the condition that no new investment is made:

$$J_0(x_0, l_0) = \max_{u_0, \dots, u_{T-1}, \omega_l} E \left\{ \sum_{k=0}^{T-1} [(1+r)^{-k} \cdot g_k(x_k, l_k, u_k, \omega_s)] + (1+r)^{-T} \cdot g_T(x_T, l_T, \omega_s) \right\} \quad (20.1)$$

$$x_{k+1} = x_k + u_{k-l+1} \quad (20.2)$$

$$l_{k+1} = l_k + \omega_{l,k} \quad (20.3)$$

Fig. 20.1 Illustration of discrete binomial representation of average annual load, l_k . p_{up} and p_{dn} are transition probabilities



$$g_T(x_T, l_T, \omega_s) = g_T(x_T, l_T, \omega_s | u_T = 0) \quad (20.4)$$

$$x_k \in \Omega_{x,k}, l_k \in \Omega_{l,k}, u_k \in \Omega_{u,k}, \omega_s \in \Omega_{\omega_s}, \omega_{l,k} \in \Omega_{\omega_{l,k}} \quad (20.5)$$

where

$J_0(x_0, l_0)$	Expected social surplus over planning period, period 0	[M\$]
$g_k(x_k, l_k, u_k, \omega_s)$	Expected net social surplus function, period k	[M\$/year]
$g_T(x_T, l_T, \omega_s)$	Termination surplus, period T	[M\$/year]
x_k	Total new capacity of wind and thermal power (state variable)	[MW]
l_k	Average annual load (state variable)	[MW]
u_k	New capacity of wind and thermal power (decision variable)	[MW]
ω_s	Short-term uncertainty (wind power and load)	
$\omega_{l,k}$	Long-term uncertainty (annual change in average load)	[MW]
r	Risk-adjusted discount rate	[%]
lt	Construction lead time	[years]
$\Omega_{x,l,u,\omega_s,\omega_l}$	Discrete feasible sets for $x, l, u, \omega_s, \omega_l$	

The short- and long-term uncertainties differ in respect to how they influence the optimal investment decision. The *long-term uncertainties* are correlated from year to year, and according to real options theory, there may be a value for the planner in waiting to see how these uncertainties unfold. This is because the future looks different depending on which state you move to from one year to the next. We represent the average annual load as a long-term uncertainty, since this will have an important impact on future generation costs. The average load is modeled as a binary Markov tree (Fig. 20.1). The model could be extended to also include other long-term uncertainties (e.g., fuel prices) with a similar representation, although this would increase the state space of the model.

In contrast to the long-term uncertainties, the *short-term uncertainties* in the model are not correlated from year to year. Hence, the planner has no incentive to wait for these uncertainties to be revealed. Availability of renewable resources, inflow to hydropower stations, unit outages, and weather-driven fluctuations in load

will typically be the most important short-term uncertainties influencing the system operation. We consider short-term uncertainties in wind power and load in this chapter. The short-term uncertainties will still influence the investment strategy, since they influence the dispatch and generation costs. Furthermore, different technologies are exposed to different levels of short-term risks. In our model we maximize the sum of expected social surplus over the planning horizon. The short-term uncertainties (ω_s) only have an effect on the net expected payoff function within the periods (g_k), while the long-term uncertainties (ω_l) influence the state transitions. The short- and long-term uncertainties are assumed to be uncorrelated.

Since the long-term uncertainty in load is represented as a discrete Markov tree and the annual expected payoffs are additive, we can solve the investment problem using SDP. We use a backward SDP algorithm with discrete time and states, as described in [8], to find the solution to the problem, based on the standard iterative Bellman equation in (20.6).

$$\begin{aligned} J_k(x_k, l_k) = \max_{u_k \in \Omega_{u_k}} & \left\{ g_k(x_k, l_k, u_k, \omega_s) \right. \\ & \left. + (1+r)^{-1} \cdot E_{\omega_{l,k}} [J_{k+1}(f(x_k, l_k, u_k, \omega_{l,k}))] \right\} \end{aligned} \quad (20.6)$$

The net expected payoff function in time step k , g_k , represents the annual social surplus from electricity generation. g_k depends on the installed capacity of different generation technologies, the load, and the expansion decisions at time step k . g_k is also a function of the short-term uncertainties in wind power and load, which influence the system dispatch as explained below.

20.2.2 Supply, Demand, and Dispatch Algorithm

Electricity supply is represented with an aggregate supply curve consisting of new and existing (old) generation technologies, as is illustrated in Fig. 20.2. The first step on the supply curve represents wind power, which has a low variable cost and uncertain availability. Hence, the length of the first step of the supply curve, $x'_{1,\text{new}}$, is a stochastic variable, which depends on the short-term uncertainty for wind power, as shown in (20.7). The short-term uncertainty in wind power consists of a set of discrete realizations of availability factors for wind power, rw' , for each of three demand subperiods within the year. The wind power availability for one realization, m , is given by

$$x'_{1,\text{new},k,m} = rw'_m x_{1,\text{new},k} = \begin{bmatrix} rw'_{m,1} \\ rw'_{m,2} \\ rw'_{m,3} \end{bmatrix} \cdot x_{1,\text{new},k} \quad (20.7)$$

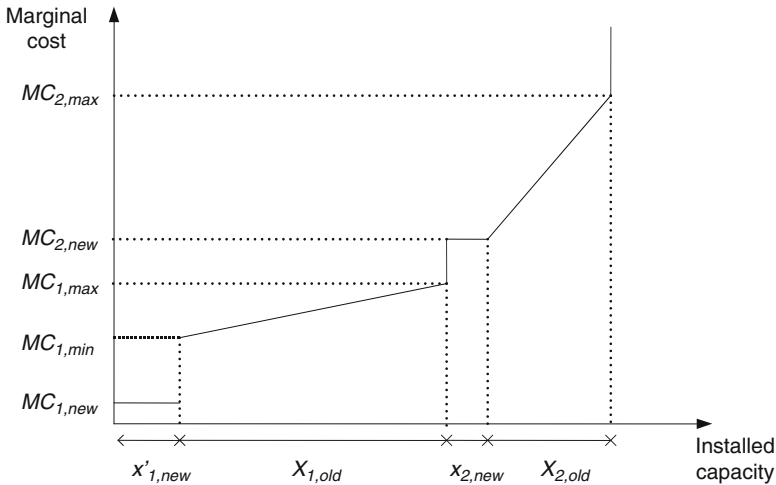


Fig. 20.2 Supply curve with old and new technologies. $x'_{1,new}$ represents wind power, with stochastic availability. $x_{2,new}$ represents peaking plants with fixed availability

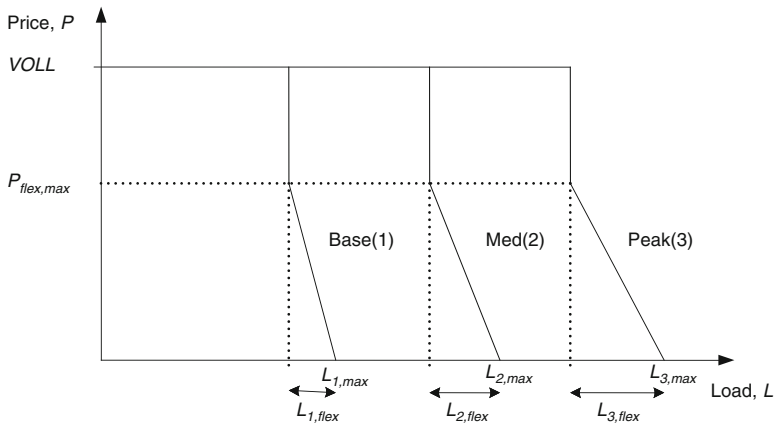


Fig. 20.3 Demand curves for the three subperiods. VOLL is value of lost load

The second step on the supply curve, $X_{1,old}$, represents baseload generation with low operating cost and a fixed capacity. The third and fourth steps of the supply curve consist of new and old capacity of dispatchable peaking generators, $x_{2,new}$ and $X_{2,old}$. Note that the old peaking capacity is assumed to have higher operating cost than the new technology, represented by the increasing marginal cost curve for $X_{2,old}$.

The annual demand is divided into three subperiods: base (1), medium (2), and peak demand (3), as illustrated in Fig. 20.3. A part of the demand within each sub period, $L_{i,flex}$, is assumed price responsive up to a certain price level, $P_{flex,max}$.

We assume a constant proportion between the maximum subperiod demands in the model, as described in (20.8). Furthermore, the price responsive parts of demand are fixed fractions of the maximum demands, i.e., $L_{\text{flex},k} = c_{L,\text{flex}} \times L_{\max,k}$, where $c_{L,\text{flex}}$ is a constant which applies to all three subperiods. Consequently, the demand curves for all three subperiods can be described by the state variable for load, l_k , in addition to the constant parameters for prices and loads. In the case study, we analyze the impact of varying the fraction of price flexible demand, $c_{L,\text{flex}}$:

$$L_{\max,k} = \begin{bmatrix} L_{1,\max,k} \\ L_{2,\max,k} \\ L_{3,\max,k} \end{bmatrix} = c_{L,\max} \cdot l_k = \begin{bmatrix} c_{L1,\max} \\ c_{L2,\max} \\ c_{L3,\max} \end{bmatrix} \cdot l_k \quad (20.8)$$

where

$L_{\max,k}$ Vector for maximum subperiod demand, period k [MW]
 $c_{L,\max}$ Vector for subperiod demand constants

Short-term uncertainty in demand is represented in an equivalent manner to the short-term uncertainty in wind power. The state variable for demand, l_k , is multiplied with a relative demand factor, rd' , as shown in (20.9). The relative demand factors follow a discrete probability distribution, which represents the deviations from the average demand in each subperiod. Hence, the relative demand factor represents both variability and uncertainty for demands within the subperiods. The subperiod demand constants, $c_{L,\max}$, combined with the discrete distributions for relative demand factors, rd' , give a representative probabilistic representation of the fluctuations in load over the course of the year:

$$l'_{k,n} = rd'_n \cdot l_k = \begin{bmatrix} rd'_{n,1} \\ rd'_{n,2} \\ rd'_{n,3} \end{bmatrix} \cdot l_k \quad (20.9)$$

We assume a merit order dispatch for the system, as illustrated in Fig. 20.4. This ensures that the system is dispatched to minimize the operating cost. Quantities and prices, which are equivalent to marginal costs, are calculated for each subperiod. Note that if there is insufficient generation capacity available to supply the fixed part of demand, load curtailment will take place. In contrast, in situations with surplus supply, wind curtailment may be necessary if the wind power generation is higher than the demand. The dispatch heuristic consists of a looping structure, which is repeated for each realization of the short-term uncertainties for wind and demand. The uncertainties in wind power and demand will cause horizontal shifts in the supply and demand curves, respectively. For each year, expected prices, quantities, costs, and the resulting social surplus are calculated over all combinations of the discrete realizations of the short-term uncertainties in wind power and demand.

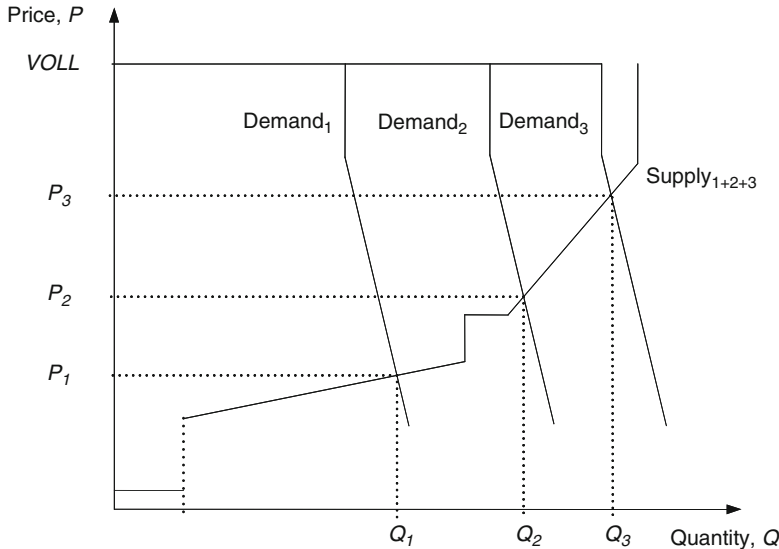


Fig. 20.4 Merit order dispatch in three subperiods with marginal prices P_1, P_2, P_3

The total expected social surplus over the year is used as the payoff, g_k , in the SDP expansion algorithm to find the optimal expansion strategy in the initial year, as explained above.

20.3 Case Study

We use the model to analyze generation expansion on São Miguel. The optimization model is used to find the optimal expansion decision at the beginning of each year with a 10-year planning horizon. We simulate the optimal expansion plan over a period of 20 years, assuming that the realized load growth equals the expected growth in the binomial tree for load (Fig. 20.1). The case study assumptions and results are presented below.

20.3.1 Assumptions

Parameters for supply and demand are summarized in Table 20.1. For supply, the existing generation fleet on São Miguel consists of geothermal power (40%), hydropower (4.5%), a small amount of power from biomass, and the remainder being met by heavy fuel oil generators, as explained in Chap. 4. There is no wind power installed on the island. In this chapter, we use the same assumption

Table 20.1 Supply and demand parameters for São Miguel

Supply	Value	Unit	Demand	Value	Unit
X_{old}	[0 72]	MW	VOLL	3500	\$/MWh
MC_{new}	[0 180]	\$/MWh	$P_{\text{flex,max}}$	350	\$/MWh
MC_{min}	[NA 185]	\$/MWh	$c_{L,\text{max}}$	[0.689 1.289 1.623]	
MC_{max}	[NA 215]	\$/MWh	$c_{L,\text{flex}}$	0.01 or 0.20	
ic_{new}	[2300 1000]	\$/kW	l_d	[4784 3000 1000]	Hours
Ω_μ	[0/9 0/5]	MW	l_{init}	28.52	MW
nt	[15 20]	Years	l_{growth}	2.7	MW/year
lt	[1 1]	Years	l_{sdv}	1.5	MW/year
r	5	% p.a.	p_u, p_{dn}	0.5	

Table 20.2 Levelized cost analysis of candidate power plants

	Wind power	Fuel oil		Unit
Capacity factor	46	20	50	%
Investment cost	55.0	50.4	20.2	\$/MWh
Operating cost	0.0	180.0	180.0	\$/MWh
Total cost	55.0	230.4	202.2	\$/MWh

as in previous chapters that geothermal, hydropower, and biomass are negative loads. Hence, the only existing technology modeled in the supply curve is fuel oil generators, assumed to have an operating cost of between 185 and 215 $$/\text{MWh}$, in line with assumptions in previous chapters. The two expansion alternatives are wind power and additional combustion turbines with fuel oil. We assume that the planner has the options to invest in 9 MW of wind power and/or 5 MW of fuel oil generation in each year. Of course, not investing at all is an additional option. Note that wind power, $x_{1,\text{new}}$, has a relatively high investment cost but zero operating cost. In contrast, fuel oil-fired generation, $x_{2,\text{new}}$, has a low investment cost, but very high operating cost. A simple levelized cost analysis of the two technologies is shown in Table 20.2. Wind power is assumed to have a capacity factor of 0.46, in line with the wind power data from Chap. 4. This is a very high capacity factor, indicating that the wind conditions are very good on São Miguel. The levelized cost calculation is done for different capacity factors for the fuel oil plant. This is a dispatchable plant, and its utilization is not known at the time the expansion decisions are made. Table 20.2 shows that for all capacity factors, the levelized cost for the fuel oil plant per kWh is much higher than for wind power. This is because of the high cost of fuel oil on the island. However, the availability of wind power is stochastic, whereas the combustion turbine is assumed to have a constant availability. The generation expansion model considers the differences in availability between the two technologies and factors this into the analysis to find the optimal expansion decisions.

The net load duration curve is shown in Fig. 20.5. The original load duration curve, before the non-dispatchable resources are subtracted, is also shown for

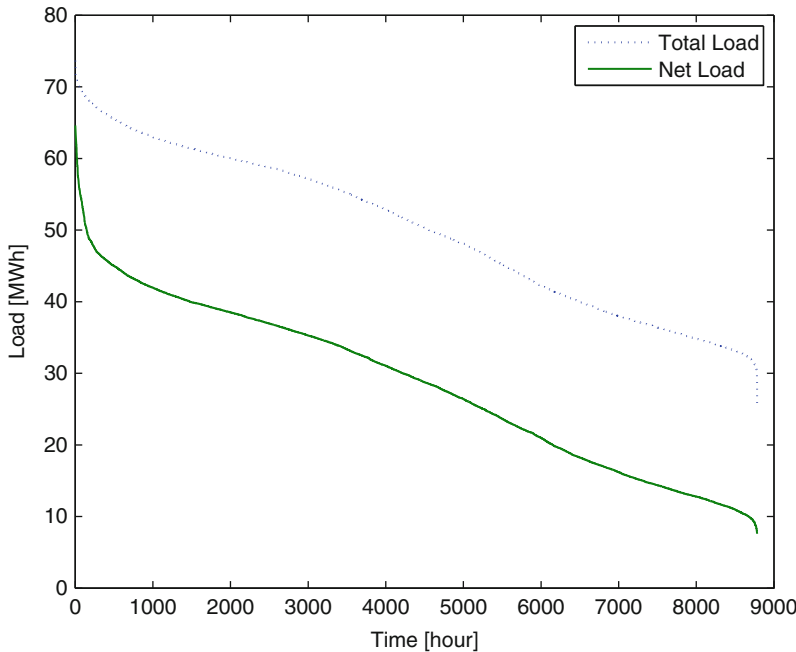


Fig. 20.5 Load duration curves (total and net load) for São Miguel in 2008

comparison. With the exception of the peaking hours, the difference between the two curves is relatively constant. This indicates that the generation from geothermal, hydro, and biomass mainly serves as baseload in the system. We use the net load duration curve to estimate parameters for the demand curve representation in the expansion model. The lengths of the base, medium, and peak demand sub periods are set to 4,784, 3,000, and 1,000 h accordingly. The subperiod demand constants, $c_{L,\max}$, in Table 20.1 are derived by taking the average of the loads in the three sub periods. The expected value and standard deviation of the annual load growth is estimated based on historical data from 2000 to 2008 [9]. In this period, the mean load grew on average 2.7 MW/year with a standard deviation of 1.5 MW/year. Hence, the parameters l_{growth} and l_{sdv} are set to 2.7 and 1.5, respectively (Table 20.1). The value of lost load is assumed to be 3,500 \$/MWh, and the highest price on the flexible part of the demand curve is set to 350 \$/MWh. In the case study, we use two different assumptions for the amount of flexible demand, i.e., that either 1 or 20% of the load is price responsive.

The short-term uncertainties in wind power and demand influence the expected dispatch and payoffs within each year. The probability distribution for the relative wind availability factors (Fig. 20.6) shows that the wind power resources are best in the medium demand subperiod, followed by the peak and base subperiods. For demand (Fig. 20.7), the base period has the widest range, which is expected since this is the longest subperiod and therefore covers a wider distribution of demands.

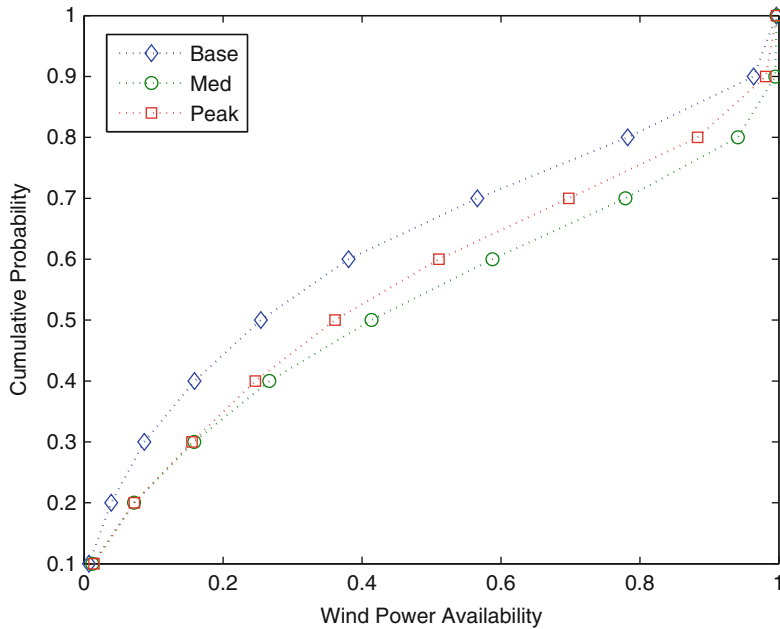


Fig. 20.6 Discrete distributions for relative wind availability factors, rw'

The distributions for the medium and peak periods are relatively similar, although the steep upper part of the net load duration curve (Fig. 20.5) is also reflected in the peak distribution. We assume that the demand and wind power uncertainties are independent. With 10 realizations of each uncertainty, the dispatch routine is run 100 times for each year, i.e., for each combination of load and wind power realizations. Note that both distributions remain constant in the expansion planning model. This is clearly a simplification, since load behavior is likely to change over time. Furthermore, the best wind resources are likely to be built first, and this would impact the wind availability for consecutive expansions. Geographical dispersion of wind power plants would also influence the distributions for the total wind resources on the island.

20.3.2 Results

We run the optimal expansion model for the time period 2008–2028. Expansion decisions are made at the beginning of each year based on a 10-year planning horizon. The simulated average load growth is assumed to follow the expected value of 2.7 MW/year. Below, we present results for optimal capacity expansion, the resulting dispatch of the different technologies, the amount of load and

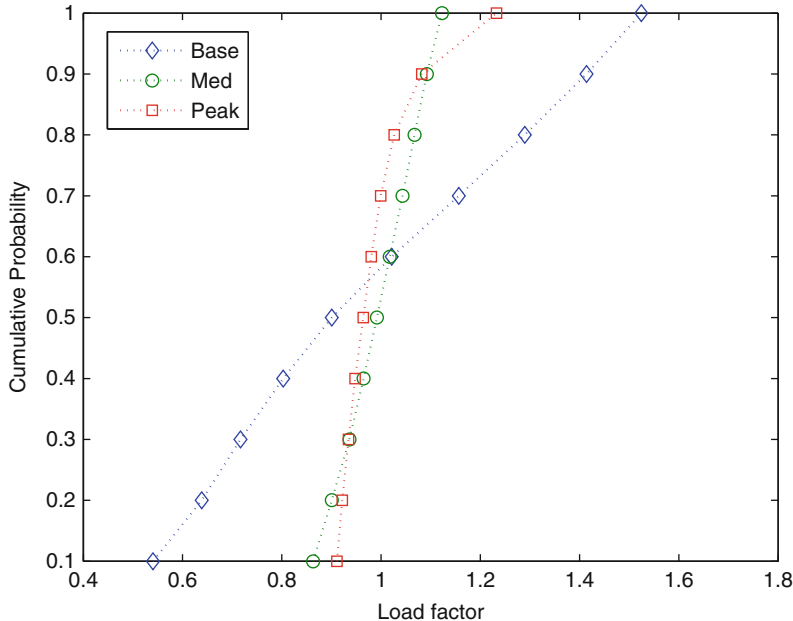


Fig. 20.7 Discrete distributions for relative demand factors, rd'

wind curtailment in the system, and the marginal costs in each of the demand subperiods, which in turn could be used for pricing purposes. We run two sets of simulations, i.e., with either 1% or 20% price responsive demand. Finally, we also conduct a sensitivity analysis of how the optimal generation expansion and curtailment levels change with the expected load growth.

Generation Expansion and Dispatch

The optimal expansion plan (Fig. 20.8) shows that the majority of the new capacity is wind power. The wind power expansion is driven by the low cost of wind power compared to fuel oil-fired power plants (Table 20.2). Most of the new fuel oil capacity is added in the last 10 years of the simulation period. At this point, additional thermal capacity is needed to compensate for the uncertainty and variability in wind power. In fact, with low demand response (DR1), the fuel oil capacity grows at about the same rate as the wind power capacity in the last 10 years. Increasing the amount of demand response (DR20) leads to lower capacity expansion overall, particularly for the fuel oil technology. Furthermore, the increase in thermal capacity occurs about 5 years later compared to DR1. This is because the price responsive demand acts a flexible and dispatchable resource, which reduces the need for dispatchable generation.

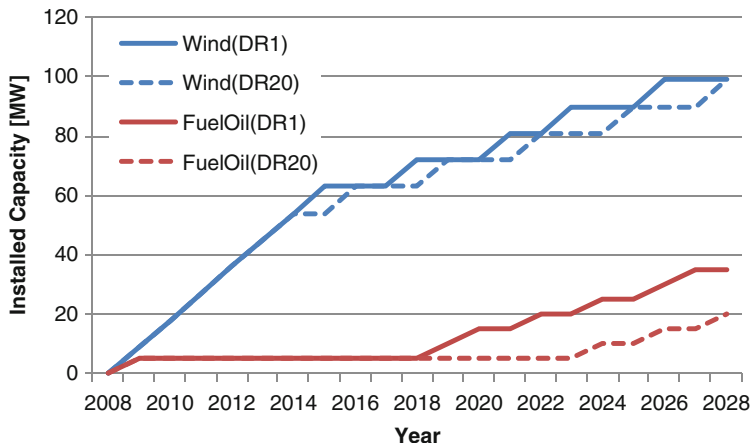


Fig. 20.8 Optimal expansion of wind power and fuel oil capacity with 1% (DR1) and 20% (DR20) demand response, 2008–2028

The resulting annual dispatch for all the generation technologies in the system is shown in Fig. 20.9. Geothermal and hydro generation is subtracted from the load, as explained above, and therefore has constant generation throughout the simulation period. Wind generation increases rapidly to meet between 35 and 40% of the total load in the system. The new fuel oil generation increases towards the end of the planning horizon. The main effect of increasing the demand response is that the total load decreases and also that less fuel oil generation is being dispatched. The higher demand response also allows for a slightly higher fraction of load being met by wind power.

Curtailment of Load and Wind Power

The short-term uncertainty in wind power must be compensated by flexible supply and demand resources in the system. The likelihood of being able to meet the fixed part of the demand increases by investing in more thermal capacity with constant availability. However, the more expansion of such resources, the less they are used. Hence, there is a trade-off between the investment cost of new capacity and the cost of curtailment in the system. The social surplus objective in the expansion model considers this trade-off in finding the optimal expansion plan. Figure 20.10 shows that load curtailment starts occurring a few years into the simulation period and eventually reaches a level of more than 5 GWh in the case with low demand response. This is close to 1% of the total fixed demand in the system. More demand response reduces the amount of load curtailment to about half, as the flexible part of the demand curve responds to high prices before load curtailment becomes necessary.

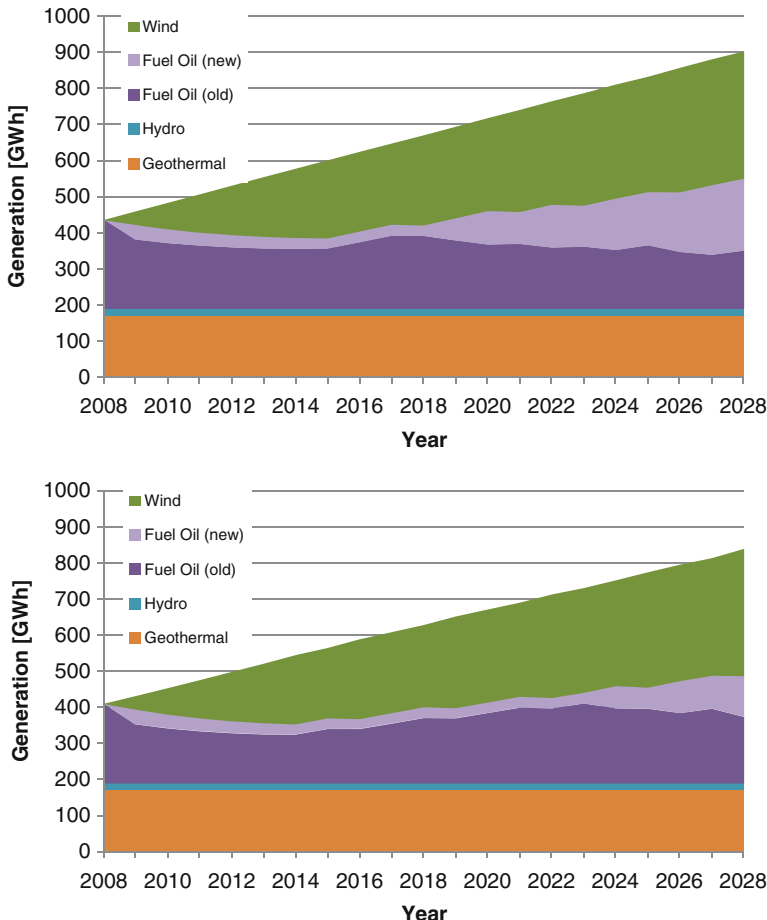


Fig. 20.9 Expected annual generation dispatch with 1% (*upper*) and 20% (*lower*) demand response, 2008–2028

Wind power is attractive from a cost perspective, given its low levelized cost. However, as the amount of installed wind capacity increases, there is a chance that wind power exceeds the load so that wind power curtailment becomes necessary.¹ In this case, there is a trade-off between meeting the load with cheap wind energy

¹In this expansion study, we assume that wind power alone can meet the demand when sufficient wind power is available. In reality, some thermal units may be required to stay online to provide certain ancillary services to the system. If so, wind curtailment would happen more frequently than under the assumptions used in this case study. The impact of more detailed operational constraints (e.g., unit commitment) on generation expansion with renewable resources is studied in more detail in [10, 11].

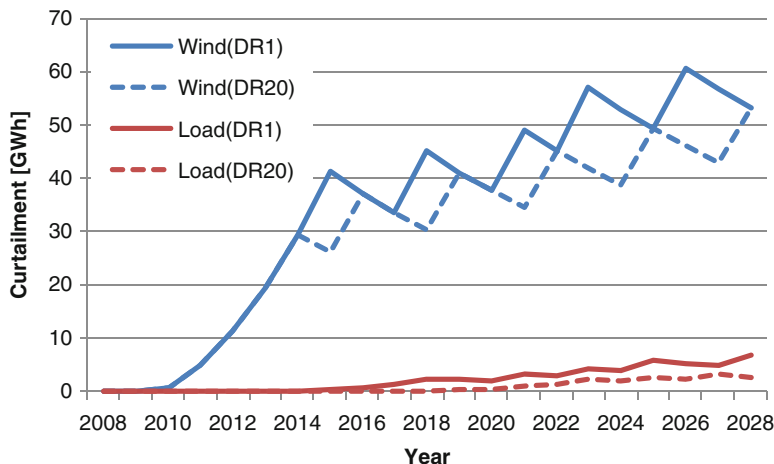


Fig. 20.10 Expected annual curtailment of load and wind power with 1% (DR1) and 20% (DR20) demand response, 2008–2028

and the need for curtailing the wind power in surplus situations. Figure 20.10 shows that wind power curtailment increases rapidly during the first 7–8 years of the simulation period. At this point the wind curtailment reaches approximately 16–17% of total dispatched wind generation, which appears to be an equilibrium level, as it stays at this level throughout the rest of the period. Demand response leads to slightly less wind power curtailment, since the pace of wind power expansion is a bit slower in this case (Fig. 20.8). Note that with the representation of demand response in the model, the dispatched load can only be reduced.²

The generation model considers the trade-offs discussed above and maximizes the sum of consumer and producer surpluses (i.e., the social surplus) over the short- and long-term uncertainties. An important finding from the analysis is that some curtailment of both load and wind power is optimal under the current assumptions. However, the optimal level of wind power curtailment is clearly much higher than the desired load curtailment, as shown in Fig. 20.10.

Marginal Costs of Generation (Prices)

We also analyze the impact of the optimal expansion plan on the marginal cost of generation. The marginal costs of generation in the subperiods can be interpreted as system prices and could possibly be used to determine dynamic rates or even for real-time pricing. Figure 20.11 shows that the prices are the same in all three demand

²An alternative demand representation, which allows for demand increase during low load periods through price response and/or load shifting, would contribute to reduce the level of wind power curtailment. Introduction of energy storage would have a similar effect by storing surplus wind energy for use during high loads.

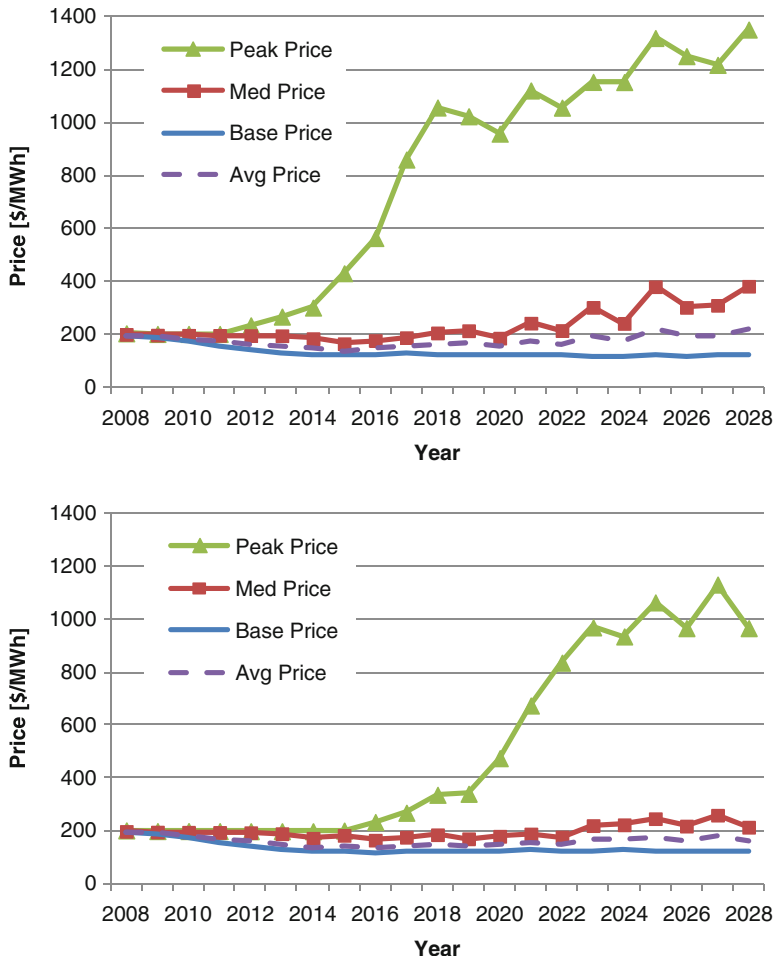


Fig. 20.11 Expected prices, or marginal cost of generation, with 1% (*upper*) and 20% (*lower*) demand response, 2008–2028

subperiods at the outset of the simulation period. This is because the original fuel oil generation ($X_{2,\text{old}}$) is always the marginal technology in the original system. The expansion of wind power leads to a significant reduction in the prices during the base period. At the same time, the peak price increases dramatically. This is because load curtailment starts occurring in the peak period during some realizations of the short-term uncertainty. The expected price is therefore influenced by the value of lost load (VOLL), assumed to be \$3,500/MWh. The average price during all subperiods remain at or below \$200/MWh. The main effects of more demand response are that the peak price increase occurs later and that the average price is lower towards the end of the simulation period.

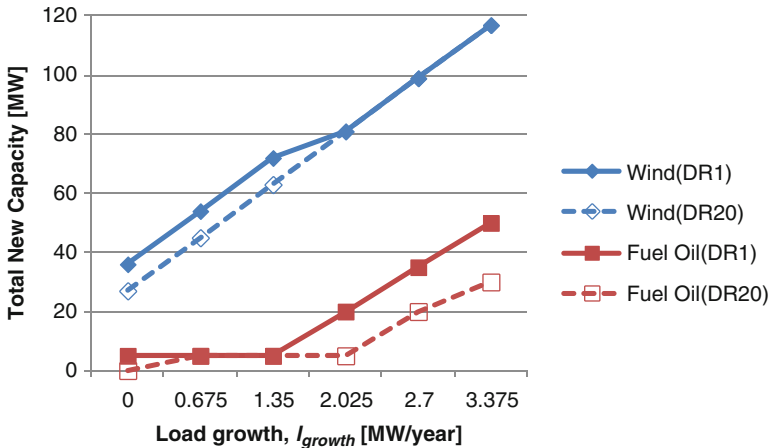


Fig. 20.12 Total expansion of wind power and fuel oil capacity for the period 2008–2028 with 1% (DR1) and 20% (DR20) demand response

Sensitivity Analysis: Load Growth

Finally, we investigate the impact of the annual load growth in the system, varying l_{growth} between 0 and 3.375 MW/year. Figure 20.12 shows that even with no load growth, it is optimal to invest in substantial amounts of wind power to reduce the overall cost of the electricity supply. The wind power capacity increases more or less as a linear function of load growth. In contrast, substantial expansion of fuel oil generation only takes place at the higher load growth levels. Demand response reduces the need for new capacity, particularly thermal generation. Figure 20.13 shows that wind curtailment takes place for all simulated load growths, whereas load curtailment only occurs for higher load growths as there is no load curtailment in the original system. Higher demand response leads to reductions in the curtailments of both wind power and load.

20.4 Conclusion

In this chapter we have used a stochastic dynamic optimization model to analyze generation expansion with variable resources. The case study of the São Miguel Island shows that wind power is an attractive investment alternative on this island, due to the low cost in comparison with thermal generation from fuel oil. However, some dispatchable thermal generation is still needed to compensate for the variability and uncertainty in wind power. The dispatch results show a significant curtailment of wind power during surplus conditions as the amount of wind power capacity increases. A small amount of load curtailment during scarcity situations

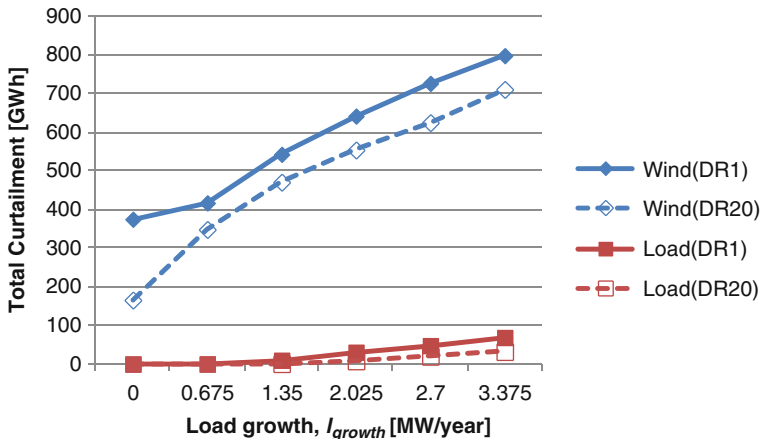


Fig. 20.13 Total expected curtailment of load and wind power for the period 2008–2028 with 1% (DR1) and 20% (DR20) demand response

is also optimal from a social surplus perspective. Furthermore, the change in the capacity mix leads to much higher differences between the marginal system costs during periods of high and low demand. Wind power brings down the marginal cost during low load periods, whereas scarcity situations with load curtailment lead to much higher expected marginal costs during peak-load periods. The average annual marginal costs remain relatively stable. The utility company and regulator would have to decide on how much of the increased price variability to pass on to end users. Our results show that an increase in the amount of price responsive demand from 1 to 20% of total demand has several advantages. A more flexible demand side leads to a large reduction in the need for new thermal generation capacity, as demand helps accommodate variability and uncertainty in wind power through its response to prices. More demand response also leads to less curtailment of wind power and load and to a slightly higher share of wind power in the overall system dispatch.

The generation expansion model used in this chapter focuses on the impact of long- and short-term uncertainties on the optimal investment decisions. The detailed operational constraints analyzed in previous chapters are not included in the expansion analysis. In future work, we are planning to improve the uncertainty representation by incorporating the decomposition methods for load and wind uncertainty from Chap. 6 into the SDP framework. We will also consider the impact of diversity in wind resources on the aggregate probability distribution for wind power. Furthermore, we will consider adding more operational constraints (e.g., unit commitment and operating reserves) into the dispatch algorithm, to better represent the operational impacts of variable generation on planning decisions for generation expansion.

Acknowledgments The generation expansion model used in this chapter was developed with funding in part from Industry's Innovation Fund at the Norwegian University of Science and Technology (NTNU).

References

1. A. Botterud, Long-term planning in restructured power systems: dynamic modelling of investments in new power generation under uncertainty. Ph.D. Thesis 2003:106, Norwegian University of Science and Technology, Trondheim, Norway, Dec 2003. <http://www.diva-portal.org/ntnu/theses/abstract.xsql?dbid=48>
2. A. Botterud, M.D. Ilić, I. Wangensteen, Optimal investments in power generation under centralized and decentralized decision making. *IEEE Trans. Power Syst.* **20**(1), 254–263 (2005)
3. G. Doorman, A. Botterud, Analysis of generation investments under different market designs. *IEEE Trans. Power Syst.* **23**(3), 859–867 (2008)
4. A.K. Dixit, R.S. Pindyck, *Investment Under Uncertainty* (Princeton University Press, Princeton, 1994)
5. M.A. Crew, C.S. Fernando, P.R. Kleindorfer, The theory of peak-load pricing: a survey. *J. Regul. Econ.* **8**, 215–248 (1995)
6. B.F. Hobbs, Optimization methods for electric utility resource planning. *Eur. J. Oper. Res.* **83**, 1–20 (1995)
7. B. Mo, J. Hegge, I. Wangensteen, Stochastic generation expansion planning by means of stochastic dynamic programming. *IEEE Trans. Power Syst.* **6**(2), 662–668 (1991)
8. D.P. Bertsekas, *Dynamic Programming and Optimal Control*, 2nd edn. (Athena Scientific, Nashua, NH, USA 2000)
9. F. Amorin, B. Palmintier, A. Pina, “Azores Green Islands: Looking at Demand,” Alliance for Global Sustainability, Annual Meeting, 2009.
10. B. Palmintier, M. Webster, Impact of unit commitment constraints on generation expansion planning with renewables, in *Proceedings of IEEE PES General Meeting*, Detroit, MI, Jul 2011
11. D.S. Kirschen, J. Ma, V. Silva, R. Bellhomme, Optimizing the flexibility of a portfolio of generating plants to deal with wind generation, in *Proceedings of IEEE PES General Meeting*, Detroit, MI, Jul 2011

Index

Symbols

ACE, 351
(AVRs), 306
(N-1) reliability criteria, 102, 104

A

AC (extended) optimal power flow (AC OPF), 78
AC OPF, 297, 306
AC OPF problem, 336
AC OPF-based scheduling, 308
AC power flow-based analyses, 308
AC XOPF, 307, 309, 331, 332
acceptable solutions, 67
adaptive control design, 39
Adaptive Load Management (ALM), 72, 225–228, 230, 231, 238, 239, 241
adaptive transient stabilization, 39
advanced meter infrastructures (AMIs), 58
advanced power system stabilizers (PSSs), 84
AGC, 347
aggregation of distributed users, 58
air-conditioning, 71, 240
ALM, 230
alternative relaxation of line flow, 324
Analysis, 309
annual emissions cost, 49
annual load profile, 317
annual T&D power delivery loss, 49
Appendix A, 309
approximate loss compensation, 77
approximate models of grid, 22
architecture-specific design of the IT, 56
architectures of energy systems, 56
area control error (ACE), 80, 351
asset utilization, 35, 308

Automated Frequency, 79

Automated voltage control (AVC), 80
Automatic Generation and Demand Control (AGDC), 367
Automatic Generation Control (AGC), 345, 351, 373

automatic generation control (AGC), 79

automation, 4, 48, 50, 63, 67, 308

average cost rule, 262

AVRs, 306

Azores Archipelago, 99, 102, 104, 105, 108–110, 113

B

batteries, 80
battery, 281, 282, 290
Bellman equation, 538
benchmark optimum, 26
better time-of-use (TOU), 229, 231
blackouts, 22, 36
bounds on achievable performance, 67
break-even point, 330
breaker connection, 311
breakeven wind power capacity, 317
brownouts, 51
bus voltage limits, 309
business stability, 53

C

capacitor banks, 79
capacity, 32
capacity cost, 33
capacity limits, 20
capacity-based cost-benefit analysis, 50
capital cost, 26

- capital cost of new investments, 49
 capital investment cost, 306
 center of inertia frequency, 413, 415–417
 central generation, 311
 central generation reserve, 87
 centralized, 70
 centralized industry, 75
 centralized SCADA, 75
 characteristics of the loads, 226, 228, 230
 choice, 60, 67, 73
 closed-loop system, 60
 collective choice rules, 53
 communications, 4, 36, 50
 complex dynamic systems, 39
 complex dynamical systems, 55
 complex electric grid, 57
 complex power network, 310
 complexity, 3, 65
 complexity of information exchange, 65
 computational complexity, 65
 computer algorithms, 40
 computer software, 4, 310
 computer-intensive algorithms, 75
 computer-supported decisions, 48
 conflicting performance objectives, 335
 conservative constraints, 17
 consumer, 33, 120–122, 127, 143, 305
 Contingencies, 86
 control, 50
 control areas, 22
 control center, 102, 105, 110
 control input, 85
 control/communications designs, 85
 controllable capacitor shunts, 332
 controllable capacitors, 310
 controllable equipment, 309
 controllable reactive power resources, 80
 controllable shunt capacitors, 306, 334
 controllable transformer, 334
 conventional power plants, 59, 84, 305
 convergence problems, 37
 coordinated decisions, 50
 coordination, 65
 core variables, 52, 53
 core- and second-order variables, 53
 corrective actions, 21, 87
 corrective resource management, 76, 79
 cost, 317
 cost of reconfiguration infrastructure, 87
 cost of uncertainties, 26
 cost reduction, 314
 cost savings, 73
 cost–benefit analysis, 36
 coupled real power-voltage model, 84
 coupled real-power voltage dynamic, 445, 457, 460, 466
 critical clearing time, 17
 critical contingencies, 20
 Critically Congested Lines, 323
 cumulative costs, 86
 cumulative frequency deviations, 80
 cumulative inefficiency, 26
 customer preferences, 50
 customer profiles, 23
 customers’ payments, 307
 customers’ tariffs, 72
- D**
- D-VAR, 409
 data repository of real-world, 48
 data-driven feed-forward look-ahead dispatch, 76
 data-driven operations, 47
 data-driven predictions, 48
 Day-Ahead Scheduling, 237, 245, 248–253, 255, 256, 258
 DC OPF, 306, 309
 DC power flow, 5
 decision tree, 76
 decision variables, 331
 decision-making objectives, 335
 decision-making tools, 308
 decomposition, 22
 decoupled real power-frequency model, 84
 deeper-level variables, 57
 deeper-order variables, 58
 delivery, 51
 Delivery loss minimization, 61
 delivery loss reduction, 76
 delivery losses, 77, 306, 314
 Delivery-related constraints, 54
 demand, 34
 demand bids, 73, 248, 250, 253
 demand function, 225, 228, 230, 238–240, 247, 250
 demand profiles, 307
 demand response, 23, 72
 demand-side management, 333
 DERs, 87
 devices, such as DC lines and Flexible AC Transmission Systems (FACTS), 333
 DFIG, 409, 411, 413, 425, 427, 432
 diesel, 126, 129, 130, 133, 134, 146
 diesel fuel, 73
 diesel power plants, 49, 307, 310
 differentiated reliability, 481, 487
 differentiated reliability of service, 87

- Direct Load Control (DLC), 71, 243
discipline boundaries, 62
discount rate, 31
Dispatch, 320
dispatch cost, 311
dispatch methods, 209, 213, 214, 217, 219–222
dispatchable equipment, 305
dispersed renewable generation, 65
distributed energy resources (DERs), 23, 65
distributed generation, 310
distributed generation (DG), 475, 476, 478, 482, 485
distributed look-ahead dispatch, 247
distributed model-predictive look-ahead dispatch, 70
distributed model-predictive manner, 65
distributed risk management, 93
distributed storage, 58
distribution factors, 20
distribution management systems (DMS), 23
distribution system technologies, 58
distribution system topology, 23
distribution systems, 87, 90
disturbances, 85
DLR sensors, 334
Droop Characteristics, 357
DYMONDS framework, 65
DYMONDS modules, 75
dynamic interactions, 88
dynamic investment, 91
dynamic line rating sensors (DLRs), 326
dynamic management, 89
dynamic monitoring and decision systems (DYMONDS), 47
dynamic monitoring and decision systems (DYMONDS) framework, 6
dynamic programming, 152, 281
dynamic security analysis, 17
Dynamical Model, 15
- E**
economic and policy incentives, 22
economic cost of certain constraint, 338
economic dispatch, 54, 61, 69, 261, 309, 331, 332
economic dispatch cost, 330
economic efficiency, 319, 328, 335
economic incentives, 33
Economic Outcomes, 317
economics, 56
economies of scope, 49
EDA, 144
effective control actions, 330
effective resource management, 331
efficiency, 54, 79, 310
efficiency loss, 36
efficient frontier of generators, 33
EHV/HV energy management system (EMS), 22, 23
elastic demand, 248, 250, 255
electric energy systems, 50
electric power system, 55, 113, 115, 117
electric vehicles, 58, 73, 273, 277
electrical characteristics, 317
electrical distances, 51, 84, 306, 353, 364, 393
electrical interactions, 84
electrical system characteristics, 68
Electricite de Azores (EDA), 87
electricity markets, 536
electricity price, 72, 279, 280, 282–284, 290
electricity service, 50, 307
electricity service interruptions, 87
electromagnetic energy stored, 84
electromagnetic subsystem, 448, 461
embedded automation, 66
embedded DYMONDS, 65
emergency, 63
emissions, 73, 273, 287, 289
energy resources, 52
energy balancing, 72
energy consumption, 119–122, 127
energy delivery, 54
energy delivery system, 52
energy function, 495, 505–507
energy needs, 72
energy resources, 309
energy storage devices, flywheels, 82
energy users, 52
energy-based control, 508, 510
energy-based controller, 511
Enhanced IT Methods, 79
Enhanced-AGC, 385
environmental costs, 73
environmental impact, 54
equal incremental condition, 262
equipment failures, 36
equipment outages, 51
estimated inefficiencies, 86
EVs, 273, 274, 278, 280, 282–284, 286–290
exchange, 93
expected annual variable fuel cost, 49
extended AC XOPF, 309
- F**
FACTS, 27, 409, 492, 494, 496, 505
Facts and flywheels, 90

FACTS control, 89
 family of models, 85
 fast disturbances, 83
 fast nonlinear control, 36
 fast storage, 15, 27, 87
 fast storage control, 51
 fast wind power fluctuations, 84
 fast-responding, 63
 fault, 17, 492
 fault-tolerant automation, 51
 faults, 87, 491, 492, 511
Feasible Power Delivery During Normal Operating Conditions, 76
 feasible power flow solution, 336
 feed-forward, 40
 feed-forward corrective, 87
 feed-forward scheduling, 80
 feed-in tariff rules, 307
 feed-in tariffs, 312
 feedback control, 15
 feeder, 311
Flexible Asset Utilization, 35
 flexible technologies, 306
 Flores electric power system, 310
 Flores Island, 99–101
 Flores Power System, 493, 504, 508
 flywheel, 379, 491, 492, 513, 514, 526
 forced equipment failures, 308
 forecast demand, 61, 80
 frequency, 81
 frequency bias, 351, 355
 frequency oscillations, 445, 446, 455, 462, 464, 465
 frequency regulation, 80, 81
 frequency regulation function, 80
 frequency stabilization, 81, 82
 frequency stabilization and regulation, 372, 373, 381, 382, 387–389, 392, 394, 395
 frequency-voltage dynamics, 410, 414
 fuel cost, 33
 fuel oil generators, 541, 542
 fully regulated governance system , 63

G

gas plants, 59
 gas power plants, 69
 generation, 63, 68
 generation and T&D reserves, 35
 generation cost, 308
 generation expansion planning, 535, 536
 generation O&M cost, 69
 generation output, 120
 generation reserves, 35

generation revenue, 315
 generation utilization factor, 63
 generation-cost functions, 305
 generators' revenues and profits, 307
 geothermal power, 318
 governance design, 59
 governance mechanisms, 59
 governance system, 52, 53, 62
 governor control, 445–447, 453, 456, 460, 461, 465
 governor gains, 84
Governor-Turbine-Generator (GTG), 355
 grid “congestion”, 307
 grid automation, 38
 grid congestion, 331
 grid FACTS device , 84

H

hardware limits, 324
 hidden assumptions, 17, 68
 hidden inefficiencies, 4, 20
 hidden inefficiency, 69
 hierarchical separation, 62
 high-cost hardware, 49
 high-energy tariffs, 61
 horizontal, 22
 horizontal scheduling, 4
 horizontally organized utilities, 22
 human-in-the-loop, 39
 hydropower, 49, 126, 129, 132, 134

I

impact of interruptions, 155, 156, 160
 impacts, 73
 incentives for voltage support, 338
 incremental (levelized) cost, 73
 incremental benefits, 337
 incremental wind power cost, 312
 Independent System Operator (ISO), 23
 individual components, 54
 indoor temperature dynamic equation, 242
 industry, 50
 industry stakeholders, 93
 industry standards, 62, 63, 81
 inefficiencies, 59
 inelastic demand, 59
 infinite power source, 23
 infrastructure complexity, 51
 innovating hardware, 53
 innovation, 4, 5
 innovation objectives, 52
 installed capacity, 32

- integrated cost management, 50
integrated resource planning, 63
interaction variables, 16, 58, 65
interactive decision making, 52, 67
interactive information exchange infrastructure, 68
interactive IT-enabled platform, 6
interactive planning, 91
interactive re-bundling, 67
interconnected power grid, 85
Interconnected Power System, 15
interconnection standards, 88
intermittent power, 50
intermittent resources, 68
internalization of the sub-objectives, 65
internalizing decision making, 65
intertemporal dependencies, 62, 63
Intra-Dispatch, 79, 346, 355
Intra-Dispatch Demand Response, 366
intra-dispatch imbalances, 80
intra-dispatch power deviations, 79
investment decisions, 26
investment options, 26
investment subproblem, 6
island community, 50
islanding, 475, 478
islands, 15, 68, 70, 310, 312, 318
IT enhancements, 67
IT infrastructure complexity, 65
IT solutions, 55
IT-enabled adaptation, 50
IT-enabled bidding information exchange, 92
IT-Enabled Corrective Resource Management, 86
IT-Enabled Demand, 71
IT-enabled governance system, 66
IT-enabled methods, 48
IT-enabled participation, 72
IT-enabled scheduling, 73
- J**
JIP, 35
JIT, 35
just-in-context (JIC), 41
just-in-place (JIP), 41, 50, 57
just-in-place generally, 63
just-in-time (JIT), 41, 50
just-in-time (JIT) adaptation, 3
- L**
lack of coordination, 59
lack of incentives, 310
- large disturbances, 492–496, 501, 502, 511, 527
large electrical distances, 306
large storage, 49
large wind, 491
large-scale wind power, 55
LCOE, 119, 130, 134, 136, 161
leadership, 53
learning, 56, 66
learning in complex network systems, 67
least-cost generation dispatch, 306
least-cost scheduling, 18
liability cost, 87
line flow limits, 319, 338
line flow proxy limit, 338
LMP, 337
LMPs, 332
load charges, 318
load curtailment, 540, 546, 548–551
load duration curve, 120, 122, 127
load factor, 63
load following, 80
load forecast, 172
load prediction, 75
load profile, 120–126, 128–132
load shifting, 231, 232, 234
load summer case, 320
load winter case, 320
load-following, 345
load-following cost, 81
load-following function, 80
load-following units, 69
loadability into large load areas, 332
local wind control, 84
locational marginal pricing (LMPs), 29, 307
long- and short-term economic efficiency, 306
long- and short-term social welfare, 307
long-run marginal, 91
long-run marginal cost, 33
Long-run marginal cost (LRMC), 74
long-term capacity, 90
long-term decisions, 50
long-term evolution, 50
long-term predictive models, 76
long-term scheduling, 231
long-term service cost, 47
long-term social welfare, 36, 318
long-term sustainability, 62
long-term uncertainties, 62, 536–538, 548
look-ahead, 67, 305
look-ahead decisions, 26
look-ahead dispatch, 209, 212–218, 221
look-ahead model-predictive, 69
look-ahead model-predictive dispatch, 69

look-ahead optimization, 239, 241, 243, 245
 loss minimization, 37, 309, 332
 loss of synchronism, 89
 low voltage photovoltaics, 330
 low-cost solutions, 49
 low-probability high-impact equipment outages, 86
 low-voltage buses, 323
 low-voltage line, 321

M

major substations, 87
 man-made electric power grids, 54
 man-made grid, 53, 57
 manage extreme voltage (MXV) function, 325
 management of extreme voltages, 309, 332
 marginal cost, 32
 market power, 269
 Markov model-based decision trees, 76
 Markov models, 173, 174
 Markov tree, 537, 538
 mathematical models, 57
 maximize extreme voltage (MXV), 336
 maximum loadability into large load areas, 309
 maximum power transfer, 332
 Mean hourly benefit per firm, 234
 measurements/data, 309
 merchandise surplus (MS), 315, 338
 micro-grids, 15
 microgrids, 312
 Mid- and Long-Term Stability, 359
 minimal coordination, 65, 67
 minimal downtime, 152
 minimal information exchange, 75
 minimum and maximum bus voltages, 308
 minimum electrical distance, 84
 minimum output power, 164
 mobile resources, 54
 mobility, 53
 model reduction, 57
 model verification, 39
 model-predictive decision making, 67
 model-predictive economic dispatch, 70
 Model-Predictive Look-Ahead Scheduling, 68
 most dominant problem, 335
 Most Effective Adjustments, 337
 MPC, 213, 214
 Multi-spatial Approach, 22
 multi-temporal characteristics of system demand, 6
 multi-temporal predictive wind power models, 76
 multi-temporal separation, 6

multilayered approach, 65
 multiple functionality, 337
 must-run power plants, 307

N

near real-time sensed data, 309
 near-real-time corrective actions, 79
 negative load, 50
 network congestion, 5, 61, 65
 network constraints, 77, 320
 Network power flow constraints, 334
 network-constrained dispatch, 310
 network-wide interactions, 84
 new candidate technologies, 33
 nodal prices p_i , 29
 nominal frequency, 80
 non-generation nodes, 314
 non-time-critical forced outages, 308
 nonlinear control, 491, 494, 495, 518
 nonlinear controller, 494, 495
 nonlinear optimization software, 37
 nonzero mean, 80
 normal conditions, 61
 normal operations, 308
 Normally Closed Switch (NCS), 475–480, 482, 485, 487, 488
 normally closed switches (NOCs), 87
 normally open switches (NOSSs), 87, 475–482, 485, 487, 488
 numerically robust, 332

O

O&M costs, 310
 O&M generation cost, 338
 O&M marginal cost, 307
 OBF (optimize branch flow) function, 336
 objectives of a smart grid, 52
 off-line simulations, 86
 OLTCs, 310
 on-line adjustments, 87
 on-line coordination, 22
 on-line corrective management, 63
 On-line decisions, 331
 on-line dispatch, 306
 on-line monitoring, 86
 On-line pricing, 337
 on-line scheduling, 340
 one fast storage flywheel, 49
 one-line diagram, 310
 onload tap-changing transformers (OLTCs), 79
 operations, 6, 68, 337
 operations subproblem, 62

- operations tasks, 68
operations-planning industry objective, 62
operations-planning problem, 26
operations-planning task under uncertainties, 67
operators, 50
optimal branch flows (OBF), 326
optimal generation investment, 6, 33
optimal generation mix, 33
optimal installed capacity, 33
optimal investment, 26, 91, 318
optimal investment condition, 33
optimal power schedule, 76
optimal real power generation, 307, 319
optimal schedules, 307
optimal technology selection, 6
optimal voltage, 307
optimal voltage profile, 319
Optimization, 309
optimization objectives, 331
optimization of voltages, 79
optimization sensitivities, 314, 323, 337
optimization sensitivities with respect to flows (OSFs), 323
optimization sensitivities with respect to line flow constraints (OSFs), 309, 332
optimization sensitivities with respect to reactive power constraints (OSQs), 309, 332
optimization sensitivities with respect to real power generation constraints (OSPs), 309, 332
optimization sensitivities with respect to voltage constraints (OSVs), 309, 332
optimized corrective, 17
optimizing hydropower, 70
- P**
Parameter identification, 39
peak load, 34, 121
peak-load pricing theory, 33
peak-shaving, 69, 153–155, 164, 169
peer-to-peer communications, 58
perfect information, 26, 67
performance metrics, 49, 310
performance objectives, 26, 62, 335
phase angle, 84
phase-angle regulators, 332
Phasor Measurement Units, 375, 387
physical delivery efficiency, 328
physical efficiency of delivery, 335
physical interaction variables, 57
physical network limits, 308
- physical processes, 57
planning, 6, 47, 90, 337
planning studies, 318
policy makers, 50
polluting diesel power, 70
poor quality of electricity service, 49
portfolio of wind power and responsive demand, 59
power delivery, 51, 79, 305
power delivery problems, 308
power electronics control of the wind power plant (DFIG), 84
power generated, 80
power imbalances, 51, 80
power plants, 69, 332
power transfers, 87, 309
power-electronically controlled fast storage, 88
power-electronically-switched, 492, 496, 526
pre-program set points, 307
predictability, 53
prediction models, 183, 207
predictions, 61, 63, 68, 69
predictive manner, 65
predictive models, 76
preferences, 72
preventing blackouts, 51
preventive approach, 86
price of power, 29
price sensitivity of demand, 239, 241
price-responsive demand, 59, 247
pricing rules, 306
pricing mechanisms, 307
pricing methods, 312
pricing wind power, 312
proactive decision, 62
probabilistic decision making, 76
productivity, 53
profits, 317
proof-of-concept IT framework, 48
Proportional Integral (PI) controllers, 80
proportional-integral (PI) governor controllers, 15
provable stabilization, 88
proven technologies, 34, 63
proxy line flow limit, 20
Proxy Line Flow Limits, 20
PSS, 410, 411, 414, 416, 417, 429, 432
- Q**
quadratic benefit function, 247
quality of service(QoS), 54
quasi-stationary, 355, 358

R

radial distribution network, 99, 105
ramp rate, 69, 130, 131, 134, 136, 305
ramp-rate-limited power plants, 61
reactive energy, 89
reactive power, 306
reactive power imbalances, 80
reactive power sources, 338
real options, 536, 537
real power generation limits, 309
real power line flow sensitivities, 20
real power sources, 338
real-power balancing, 346
Real-Time Adjustment, 237, 245, 246, 249, 252–255, 257, 258
reconfiguration, 87, 475, 476, 481–483, 487–489
reduced-order models, 26, 85
refrigeration, 71
refrigerators, 227–229, 237, 238
regulators, 50
regulatory rules, 63
relaxing prespecified limits, 326
Relaxing Voltage Limits for Reliability, 325
reliability, 56, 310
reliability standards, 86, 335
Reliable Operations, 86
reliable services, 62, 87
reliable solutions, 328
remote fast communications, 87
renewable resources, 306, 536, 537, 547
renewable technologies, 22
Residential energy consumption, 227
resource, 53
resource availability, 127, 133
resource system, 53
responsive demand, 59, 65
revenue, 317
ring distribution network, 104, 105, 108–110, 113
risk, 31
risk management problem, 31
robust software, 310
robustness, 51

S

second-order variables, 53
São Miguel Island, 110, 112
SCADA, 310
scaling up, 65
seasonality, 120
secure and reliable, 5
Secure Operations, 15

security-constrained economic dispatch (SCED), 20
security-constrained unit commitment (SCUC), 20
SEES sustainability objectives, 76
selection, 73
selective modal analysis, 425
self-organizing, 58
sensing, 50
sensors, 4
service providers, 62
service tariffs, 62
SES, 53
settlement costs, 315
short, 62
short-run marginal cost, 262
short-term economic efficiency, 319
short-term asset utilization, 49
short-term load states, 76
short-term operations, 28
short-term optimization, 26
short-term scheduling, 6
short-term uncertainties, 537, 538, 540, 543, 551
singularly perturbed form, 26
size, 53
sliding mode control, 516, 518, 520, 521, 524
small-signal instability, 84
small-signal stability, 412, 423, 425, 432, 445, 446, 454, 457, 460, 462, 465
small-signal unstable, 84
small-signal unstable equilibrium, 17
smart grids, 48, 49, 53, 309
smart meters, 58
smart reconfiguration, 90
smart systems, 56
social norms, 53
social surplus, 536, 538, 540, 541, 546, 551
socio-ecological energy systems (SEEs), 6, 48
socio-ecological systems (SES), 52
soft limits, 331
software technologies at value, 53
software tools, 310
solar, 337
solar power, 58, 275–277, 290, 330
solar power plants, 306
spatial, 65
spatial alignment, 63
spatial interactions, 57
spatial interdependencies, 57
spatial network-level constraints, 54
spot electricity markets, 29
stability problems, 87

stabilization, 79, 80
standard discrete-time, 26
standard state-space form, 84, 85
standby reserve, 63, 87
state variables, 85
state-of-art IT, 87
state-space-based real power-voltage model, 84
static optimization, 243
static Thevenin equivalent, 88
statistical characterization, 174, 176, 178
Steady-State Droop, 355
stochastic decision-making process, 91
stochastic dynamic programming, 536
stochastic optimal control, 26
stochastic optimization problem, 5
storage, 33, 63
strong coupling, 462
strongly coupled, 84, 85
sub-objectives, 66
suboptimality, 309
subsidy-free, 73
substations, 310
summer, 318
Summer Case, 324
sunk cost, 49
supervisory control data acquisition (SCADA), 15
sustainability, 53
sustainability analysis, 52
sustainable electric energy services, 6
sustainable electric power delivery, 61
sustainable electricity service, 48
sustainable energy services, 52, 59
sustainable performance, 57
sustainable SEES, 48
sustainable services, 58
SVC, 411, 425, 427, 432, 496, 497
switching curve law, 262
Switching equipment, 332
synchronism, 4
synchrophasors, 309
synchrophasors as sensors of fast measurements, 83
system, 15, 34, 69
system data, 68
system demand characteristics, 68
system efficiency, 54
System generation profit, 337
System generation revenue, 337
System load charges, 338
system load factor, 35
system objective, 308

system operators, 69, 73, 75, 310
system planners, 50
system users, 65
system-level performance, 60
system-level resource management, 310
system-wide performance, 75

T

T&D equipment, 306, 310
T&D power grid, 76
T&D system, 65
tariffs, 142–144
technology choice, 52
technology portfolio, 51
temporal, 65
Temporal Alignment, 68
temporal characteristics, 69
test-beds, 49
the consumers, 73
the role of smart grids, 52
thermal dynamics, 152, 154, 156, 164, 170
thermal limits, 332
thermal line constraint, 321
thermal line flow limits, 20, 308
thermal line limits, 307, 331
time criticality, 39
time error, 80
time horizon, 62
time-critical events, 89
time-of-use (ToU), 71, 73
time-varying phasors, 496, 502, 503
today's industry practice, 17
topology, 333
total social, 33
Tragedy of the Commons, 266
transfer capability (ATC), 17
transient stability, 491, 492, 494, 495, 505
transient stability assessment, 17
transient stabilization, 86, 87
transmission lines, 332

U

ubstation, 310
underutilization, 54
uninterrupted service, 86
unit commitment, 40, 68, 151, 153, 169, 262
units, 53
unserved load cost, 49
users, 58, 69
utilities, 50
utilization, 35

V

value of candidate technologies, 307

value of flexibility, 33

vertical, 22

volatility, 61

voltage collapse, 89

voltage dispatch, 305, 309

voltage optimization, 79, 305

voltage profile, 301, 306

Voltage Regulation, 79

voltage-controllable DERs, 79

voltage-controllable T&D, 76, 306

voltage-controlled equipment, 318

voltage-dispatchable equipment, 309

voltage-related system congestion, 79

voltages as real power generation, 79

W

weakly coupled, 85

wear-and-tear, 330, 375, 381, 383, 387, 389,

391, 394, 395, 409–411, 423, 425, 429,

430, 432

wear-and-tear costs, 82

weather, 331

welfare, 33

wind curtailment, 540, 545, 547, 548, 550

wind forecast, 50

wind gusts, 51

wind power, 58, 125–127, 129, 131–134,

136–144, 274, 276, 311, 337, 538,
540–551

wind power bids, 312

wind power capacity, 49

wind power curve, 137

wind power data, 68

wind power generation, 70

wind power tariffs, 318

wind prediction, 75

wind speed, 131, 136, 137

wind spill, 154, 156, 157, 159, 160,
162–170

winter, 318

Winter Case, 321

world, 337

worst-case approach, 21

worst-case contingency, 21

worst-case scenarios, 86, 306